This is to certify that the

dissertation entitled

In Vitro Depolymerization of Natural Insoluble Lignin in Aqueous Media by the Extracellular Peroxidases of Phanerochaete Chrysosporium

presented by

David Neil Thompson

has been accepted towards fulfillment
of the requirements for

Ph.D. degree in Chemical Engr.

Hans Goetzl
Major professor

Date Nov 11, 1994

IN VITRO DEPOLYMERIZATION OF NATURAL INSOLUBLE LIGNIN IN AQUEOUS MEDIA BY THE EXTRACELLULAR PEROXIDASES OF *PHANEROCHAETE CHRYSOSPORIUM*

Volume I

by

David Neil Thompson

A DISSERTATION

Submitted to
Michigan State University
in partial fulfillment of the requirements
for the degree of

DOCTOR OF PHILOSOPHY

Department of Chemical Engineering

1994

ABSTRACT

IN VITRO DEPOLYMERIZATION OF NATURAL INSOLUBLE LIGNIN IN AQUEOUS MEDIA BY THE EXTRACELLULAR PEROXIDASES OF *PHANEROCHAETE CHRYSOSPORIUM*

by

David Neil Thompson

The lignin peroxidases (LIPs) and manganese peroxidases (MNPs) of *Phanerochaete chrysosporium* have evoked worldwide interest because of their potential to degrade a wide range of xenobiotic compounds, to decolorize bleach plant effluents, and to be used in biopulping. LIPs and MNPs catalyze a wide range of reactions which are consistent with those necessary to depolymerize lignin; however, their ability to degrade the insoluble natural lignin polymer in aqueous media has not been demonstrated. This study investigates the roles of these enzymes in the *in vitro* depolymerization of an insoluble poplar lignin in aqueous media.

A small scale dialysis reactor was constructed and used to control veratryl alcohol and/or H_2O_2 concentrations in contact with the enzymes. Isolated poplar lignin was treated for 12 hours with LIPs and MNPs alone and in combination. After treatment, the residual solid lignin was analyzed by Fourier Transform Infrared Spectroscopy/Partial Least Squares Regression. Unique lignin-derived products formed were identified by gas chromatography/mass spectrometry (GC/MS) and subjected to structural analyses based on their mass spectra. Treatment with MNP alone darkened the residual solid lignin, slightly increased the mass of the solid, and produced measurable amounts of lignin-derived 2,6-dimethoxyhydroquinone and 2-methoxyhydroquinone, but effected no measurable change in lignin content. Treatment with LIP alone did not change the color of the solid, but slightly decreased the mass, produced significant amounts of lignin-derived *p*-hydroxybenzoic acid, and slightly decreased the lignin content. Finally, treatment with LIP and MNP together first darkened the solid and then lightened it back to its original color, decreased its mass by 11 %, decreased the lignin content by 8 %,

and gave compounds with molecular weights and mass spectra consistent with structures of oxidized lignin-derived products. Many of these products, however, were present in low concentrations (< 1 ppm in the concentrated extracts). LIPs and MNPs each may have the potential for limited degradation of insoluble lignin in aqueous media; however, these reults suggest that the main role of MNPs in lignin degradation is to increase the effectiveness of LIP-mediated degradation through modification of the lignin polymer. It is also clear that some method of control of H_2O_2 (and veratryl alcohol) concentrations in contact with the enzymes is necessary to achieve this degradation, and that longer reaction times are necessary for extensive degradation of the lignin polymer.

ACKNOWLEDGEMENTS

There are many people to whom I am indebted for assistance over the course of this project who deserve recognition; this work would not have been possible without their assistance. My deepest gratitude goes to my wife Vicki, whose love, support and encouragement kept me on track to finish. Special thanks go to both Bonnie Hames of the National Renewable Energy Laboratory for her expert analysis of the FTIR data and for her advice in matters of lignin chemistry, and to Jennifer Johnson for staying in late so many nights and weekends to run my seemingly endless supply of GC/MS samples. Thanks go to Nishant Rao and Dr. Elis M. Owens for general assistance in many areas over the course of the project. I would like to thank my advisor, Dr. Hans E. Grethlein, for his advice and support over the course of this project, and Dr. C.A. Reddy for lending his expertise in the lignin biodegradation area to the successful completion of this project. I wish to thank Dr. John R. Obst of the USDA Forest Products Laboratory for performing the acetylation and thioacidolysis tests on the isolated lignin substrate. I would also like to thank Dr. Michael H. Gold of the Oregon Graduate Institute of Science and Technology for his useful insights on the characterization of MNP-released products.

Finally, I wish to thank the NSF Center for Microbial Ecology, the Crop and Food Bioprocessing Center, and the Department of Chemical Engineering at Michigan State University for their financial support.

TABLE OF CONTENTS

LIST OF TABLES

LIST OF FIGURES

CHAPTER I: INTRODUCTION

Billions of tons of lignocellulose are produced annually in the biosphere (Tsao *et al.*, 1987). Were it not for the action of lignin degrading microorganisms, this biomass would be only partially decomposed due to the protective role played by lignin, a random phenylpropanoid polymer comprising 20-30% of the dry mass of woody plants (Boominathan and Reddy, 1992). While the carbon pool represented by lignin is an important renewable resource in its own right, most biomass conversion studies have focused on efficient recovery of carbohydrates from the two other major components of lignocellulosic materials, cellulose and hemicellulose. Cellulose and hemicellulose are comprised mainly of carbohydrates (glucose in cellulose and hemicellulose, and xylose, mannose, galactose, arabinose, and certain uronic acids in hemicellulose) joined by easily hydrolyzable bonds. This makes them prime candidates for use in commercial and industrial enterprises such as ethanol production, foods, etc. Lignin, on the other hand, is a highly complex heterogeneous aromatic polymer (see Figure 1.1), and therefore yields complex mixtures of aromatic products when degraded. Thus, lignin is not well suited for the economical production of industrial chemicals and fuels given the current process technology. In addition, the complex structure makes lignin difficult to degrade and therefore presents effective barriers to microbial degradation of lignocellulose and to chemical removal of lignin for paper production. In the pulp and paper industry, lignin removal is quite important and is a very energy intensive and expensive process (Michel *et al.*, 1991). Toxic effluents are produced by the various bleaching processes, which must be cleaned up prior to discharge. Clearly, chemical removal of lignin has major drawbacks which might be solved by the use of microbial delignifiers.

The major aerobic lignin degrading organisms are the white rot fungi (Boominathan and Reddy, 1992). Despite its high carbon content, lignin is unable to act as a carbon source for white rot fungi. White rot fungi also appear to degrade herbicides, pesticides, PCBs, polyaromatic hydrocarbons, and other xenobiotics

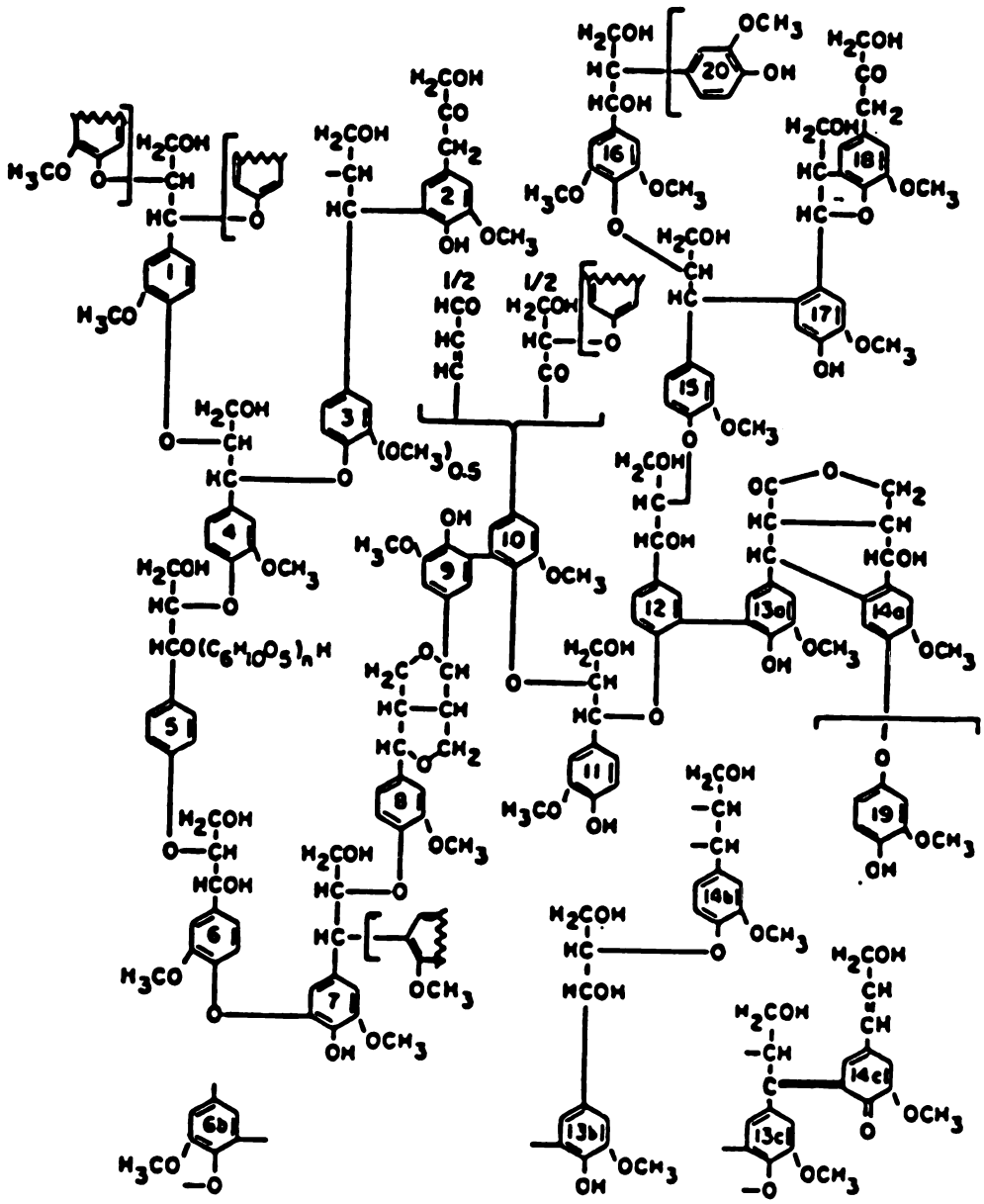

Figure 1.1: Representative structure for spruce lignin (Boominathan and Reddy, 1992).

(Boominathan and Reddy, 1992). Clearly, optimization of these processes for industrial use will in the end depend on which ligninolytic enzymes are most important in depolymerization of lignin, and the products which are formed. Reactions catalyzed by the ligninolytic enzymes of *Phanerochaete chrysosporium*, the best characterized white rot fungus, on soluble lignin model compounds have been fairly well characterized (Tien, 1987). However, rates of degradation of insoluble lignin are very slow compared to rates observed for these soluble substrates, and thus there is some question as to whether the results with soluble compounds can be extended to the results from insoluble substrates. To fully understand how lignin degradation occurs and what products to expect under optimized conditions, the *in vitro* mechanism of action of the ligninolytic enzymes on natural insoluble lignin must be determined (Tien, 1987). This information could then be used to develop industrial processes for *in vitro* removal of lignin by these enzymes, substantially decreasing the energy costs and the toxicity of plant effluents.

The broad goal of this study was to verify whether the extracellular ligninolytic enzymes of *P. chrysosporium* depolymerize water-insoluble natural lignin in completely aqueous media, an activity which has been suggested but not proven by the abilities of these enzymes to cleave lignin model dimers and to depolymerize synthetic lignins in aqueous organic media. Concentrated extracellular peroxidases of *P. chrysosporium* were incubated with insoluble lignin in a two-chambered reaction vessel, in the presence of O_2, H_2O_2, and veratryl alcohol and/or Mn(II), in tartrate buffer. One chamber of the reactor contained the insoluble lignin substrate and high levels of ligninolytic enzymes and was continuously supplied across a membrane with veratryl alcohol and/or H_2O_2 by diffusion from concentrated stock solutions in the second chamber. Insoluble lignin remaining after treatment with the ligninolytic enzymes was quantitatively recovered and any changes in lignin, carbohydrate, methoxyl, and phenolic hydroxyl contents were determined by Fourier Transform Infrared Spectroscopy (FTIR) combined with Partial Least Squares Regression. The soluble phase from the reactor was also recovered and

the major soluble products of lignin depolymerization were partially characterized by gas chromatography/mass spectrometry (GC/MS). Varying the culture conditions (Boominathan and Reddy, 1992) used for enzyme production enabled both families of ligninolytic enzymes (lignin peroxidases and manganese-dependent peroxidases) to be studied individually and in combination. This information was used to show that while LIPs and MNPs both appear to effect a very limited release of lignin-derived degradation products, the main role of MNP is to modify the insoluble lignin polymer, thereby increasing the effectiveness of LIP-mediated degradation.

This dissertation is divided into six chapters, including this first chapter (Introduction). A brief review of the relevant literature is presented in Chapter II, focusing on lignin structure, *in vivo* aerobic degradation of lignin by wood rotting fungi (major focus on the white rot fungi), the lignin degrading enzymes of the best characterized white rot fungus, *P. chrysosporium*, results of studies on *in vitro* degradation of lignin model compounds and synthetic lignins by lignin degrading enzymes, and methods for analyzing solid lignin and lignin degradation products. The rationale and approach for each part of the project are presented in Chapter III. Experimental and theoretical methods, and materials used are the subject of Chapter IV. The results of these experiments are presented in Chapter V and discussed in Chapter VI. Finally, pertinent equations, assays, computer programs, tabulated data, and FTIR and mass spectra not presented in the body of the text are presented in Appendices A-F.

CHAPTER II: LITERATURE SURVEY

The lignin biodegradation field is widely diverse, encompassing lignin structure, degradation by a wide variety of microorganisms, mechanisms of degradation of lignin by the various lignin-degrading enzymes, and the genetics of lignin degrading organisms. Many excellent reviews (Tsao *et al.*, 1987; Boominathan and Reddy, 1992; Tien, 1987; Fiechter, 1993; de Jong *et al.*, 1994; Evans *et al.*, 1994; Higuchi, 1993; Hadar *et al.*, 1993; Susmel and Stefanon, 1993; Reddy and D'Souza, 1994; Gold and Alic, 1993) have been published with some regularity on all these topics. Because there is so much information on lignin biodegradation available in the literature, a comprehensive literature review is not necessary and thus will not be done here; only areas directly contributing to this work will be presented. The areas included are lignin formation and substructure; aerobic lignin degradation by white rot fungi, specifically, *Phanerochaete chrysosporium*; the lignin peroxidases (LIPs) and manganese peroxidases (MNPs) of *P. chrysosporium*; mechanistic studies with LIPs and MNPs from *P. chrysosporium*; *in vitro* lignin and lignin substructure model compound degradation by the LIPs and MNPs of *P. chrysosporium*; and a brief overview of techniques used for the characterization of solid lignin and soluble lignin fragments.

2.1 Lignin Formation and Substructure

Lignin is a complicated, stereochemically complex, aromatic, heterogeneous renewable biopolymer that comprises 20-30% of the dry mass of woody plants. It is the second most abundant organic polymer in the biosphere and is relatively resistant to biodegradation (Ander and Eriksson, 1978; Crawford, R.L., 1981; Eriksson and Kirk, 1985; Higuchi *et al.*, 1983; Kirk and Farrell, 1987; Buswell and Odier, 1987). Since lignin occurs in close physical and chemical association with cellulose and hemicellulose, it limits access by polysaccharide-digesting enzymes to these plant polymers and is a major obstacle to the efficient economic conversion of lignocellulosic materials to feeds, fuels, and chemicals (Eriksson and Kirk, 1985; Buswell and Odier, 1987; Boominathan

and Reddy, 1992; Higuchi, 1990).

Lignin is formed by random free radical polymerization of sinapyl, coniferyl and coumaryl alcohols, which are synthesized from cinnamyl alcohol (ultimately derived from phenylalanine) in the plant (structures shown in Figure 2.1), to form a heterogeneous, optically inactive, cross linked, and highly polydisperse polymer of guaiacyl, syringyl and small amounts of p-hydroxyphenyl units (Kirk and Farrell, 1987). Gymnosperm lignins contain primarily guaiacyl units, while angiosperm lignins contain essentially equal amounts of guaiacyl and syringyl units; see Figure 2.2 for the structures of these base units. A typical formula for spruce lignin is presented in Figure 1.1 in the Introduction. The linkage types between the various lignin "monomers" have been fairly well characterized. The predominant type is the β-O-4 linkage, comprising about 40-60% of lignin linkages. The linkages in Figure 1.1 between the lignin monomers 1 and 4, 5 and 4, 5 and 6, 7 and 8, 13b and 14b, and 15 and 16, are of this type. Others include phenylcoumaran (6-12% of the total number of linkages; between lignin monomers 17 and 18), diarylpropane (5-10%; between lignin monomers 16 and 20), α-aryl ether linkages (6-8%; between lignin monomers 11 and 12), pinoresinol (less than 5%; between lignin monomers 8 and 9), biphenyl (5-10%; between lignin monomers 12 and 13a), and diphenyl ether (4-6%; between lignin monomers 6 and 7) (Boominathan and Reddy, 1992). This complicated polymer presents an effective deterrent to biodegradation of lignocellulose since any enzyme system utilized must be extracellular, nonspecific, and nonhydrolytic. The enzyme systems thus far discovered tend to rely on random free radical mediated lignin degradation (Crawford, R.L., 1981, Boominathan and Reddy, 1992), which will be discussed below.

2.2 Aerobic Lignin Degradation By White Rot Fungi

There is a considerable potential for the use of ligninolytic organisms or their enzymes in many processes of industrial importance, including biopulping and biobleaching of paper pulps (Eriksson and Kirk, 1985; Reid and Paice, 1994; Messner

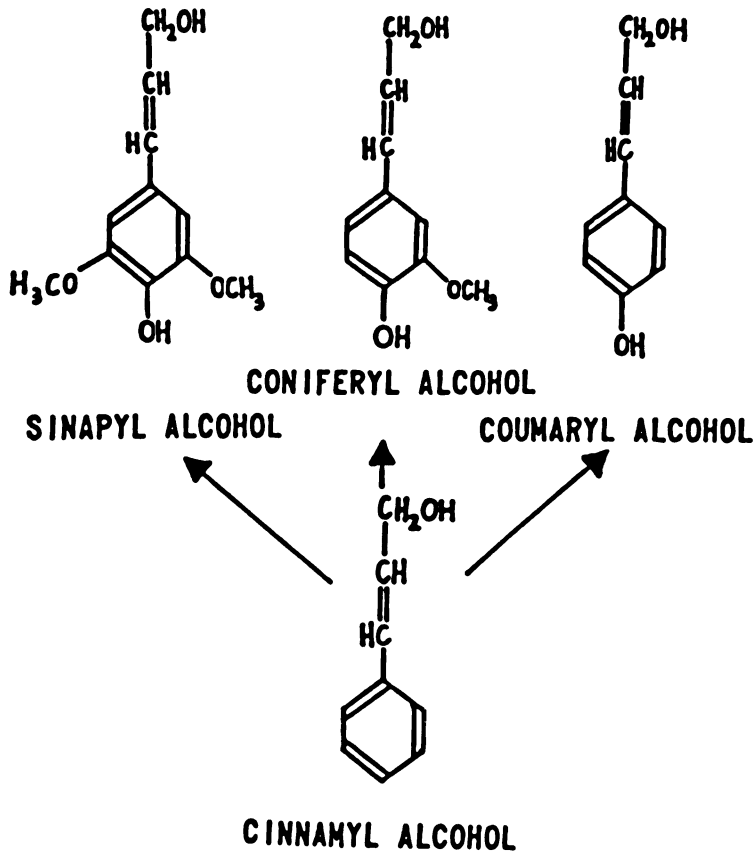

Figure 2.1: Precursor molecules used in biosynthesis of lignin (Boominathan and Reddy, 1992).

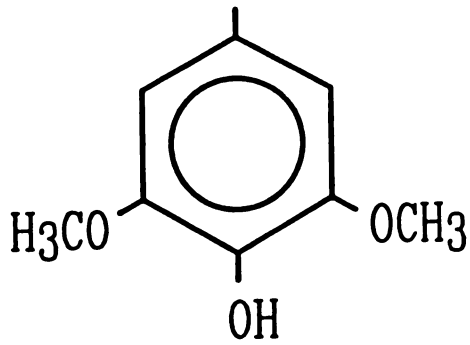

Syringyl substructure

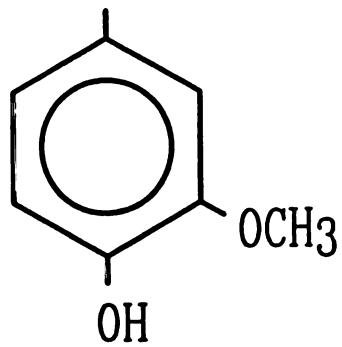

Guaiacyl substructure

Figure 2.2: Guaiacyl- and Syringyl-unit structures. The term guaiacyl- refers to the base structure 3-methoxy-4-hydroxy-, while syringyl- refers to 3,5-dimethoxy-4-hydroxy- substituted structures.

and Srebotnik, 1994), decolorization of bleached pulp effluents (Michel *et al.*, 1991, Boominathan and Reddy, 1992), biotransformation of lignin into aromatic chemical feedstocks and related applications (Eriksson, 1993). In view of the ecological and industrial importance of lignin biodegradation, there has been much interest in recent years on lignin degradation by white rot fungi because these organisms rapidly and completely degrade lignin to CO_2 and H_2O (Crawford, R.L., 1981; Kirk and Farrell, 1987; Tien, 1987; Higuchi, 1990; Boominathan and Reddy, 1992; Fiechter, 1993). Many fungi, including the white rot fungi (de Jong *et al.*, 1992; Orth *et al.*, 1993; Hatakka, 1994), degrade lignin. Brown rot (Kirk *et al.* 1975; Haider and Trojanowski, 1980) and soft rot (Haider and Trojanowski, 1980; Kirk, 1984; Kirk and Cowling, 1984) fungi, as well as some bacteria (Antai and Crawford, 1981; Crawford, D.L. *et al.*, 1982; McCarthy and Broda, 1984) have also been shown to degrade lignin aerobically (lignin is not degraded to any great extent anaerobically (Kirk and Farrell, 1987)), but the major lignin degrading organisms have been found to be the white rot fungi (Boominathan and Reddy, 1992). Since this study will focus on the extracellular peroxidases produced by a white rot fungus, only white rot fungi will be treated in detail here.

White rot basidiomycetes have been found to degrade lignin more rapidly and extensively than other microbial groups that have been studied. Their apparent mode of attack is to grow into the lumens of cell walls, where they secrete extracellular enzymes, including cellulases, hemicellulases, and peroxidases. It has been shown, using electron microscopic techniques, that lignin degradation takes place at some distance from the hyphae and that lignin is progressively removed from the lumens as degradation proceeds (Blanchette, 1984; Blanchette and Reid, 1986; Otjen and Blanchette, 1986; Ruel and Barnoud, 1985). While these fungi do not utilize the lignin as a growth substrate, the removal of the protective lignin barrier opens up the structure of the carbohydrate matrix so that near complete degradation of the lignocellulose is possible (Blanchette *et al.*, 1989). Cellulose and hemicellulose serve as the substrates for growth and other

metabolic functions. Ligninolytic enzymes are produced by the fungus during secondary metabolism as a result of carbon and/or nitrogen limitation in wood. These factors indicate that lignin depolymerization is likely to be a rate limiting step in the mineralization (degradation to CO_2) of lignocellulose.

The best studied of the white rot fungi is *Phanerochaete chrysosporium* (Boominathan and Reddy, 1992). This organism lends itself well to lignin biodegradation studies because of a number of factors. There is already a wide base of knowledge on its physiology, molecular biology, biochemistry, and genetics (Boominathan and Reddy, 1992; Reddy, 1993; Reddy and D'Souza, 1994). It can be reproducibly grown on chemically defined media. The fungus produces both conidia (asexual spores) and basidiospores (sexual spores), so culture maintenance and stability are greatly simplified. More importantly, however, the fungus grows rapidly in agitated cultures, produces substantial levels of extracellular peroxidases relative to peroxidase production by other white rot fungi, and rapidly degrades lignocellulose (Boominathan and Reddy, 1992). The following sections will describe *P. chrysosporium* and its lignin degrading system (LDS).

2.3 The Lignin Degrading System of *P. chrysosporium*

P. chrysosporium is known to degrade lignin extensively and rapidly and has been the organism of choice for lignin degradation studies in most laboratories worldwide. This fungus has also evoked worldwide interest because of the potential of its ligninolytic system in degrading a variety of toxic xenobiotic compounds from the environment such as PCBs (Bumpus *et al.*, 1985), benzo(a)pyrenes (Sanglard *et al.*, 1986), di- and trichlorophenols (Valli and Gold, 1991; Joshi and Gold, 1993), dioxins (Valli *et al.*, 1992a), and dinitrotoluene (Valli *et al.*, 1992b). Consequently, knowledge is rapidly accumulating on the physiology, biochemistry, and molecular biology of the lignin-degrading system of this organism. Although lignin is rapidly mineralized by *P. chrysosporium*, the lignin itself is of little significance as a carbon source for this

organism (as with other white rot fungi), and a suitable cosubstrate such as cellulose, hemicellulose or glucose must be present for lignin degradation to occur (Kirk *et al.*, 1976; Kirk and Farrell, 1987; Buswell and Odier, 1987; Buswell, 1991). The ligninolytic enzymes of *P. chrysosporium*, as with other white-rot fungi, are produced during secondary metabolism triggered by limitation of nutrients such as carbon and/or nitrogen.

P. chrysosporium produces two families of extracellular peroxidases, designated lignin peroxidases (LIPs) and manganese-dependent peroxidases (MNPs) (Kirk and Farrell, 1987; Buswell, 1991) and several H_2O_2 producing enzymes as major components of its lignin-degrading enzyme system. At least six LIP isoenzymes and 4 MNP isoenzymes have been described (Tien, 1987; Gold *et al.*, 1989; Dass and Reddy, 1990; Boominathan and Reddy, 1992). Average molecular weights of the two families are 41 and 46 kDa, respectively (Boominathan and Reddy, 1992). Each isoenzyme is a glycoprotein which possesses one mole of iron protoporphyrin IX per mole of enzyme and obligately requires H_2O_2 for activity. MNPs, in addition to these characteristics, also require Mn(II) (Gold *et al.*, 1989; Boominathan and Reddy, 1992). These enzyme families are discussed below.

2.3.1 Lignin Peroxidases (LIPs)

LIPs are glycosylated heme proteins (molecular weight 38,000 to 46,000). They are obligately dependent on H_2O_2 for activity, and have been shown to catalyze the oxidative cleavage of β-O-4 linkages (the most abundant linkage in the lignin polymer), C_α-C_β linkages, and β-1 linkages in lignin substructure model compounds. LIPs have also been shown to depolymerize the water-insoluble synthetic lignin polymer when solubilized in organic solvents, and to catalyze demethoxylation of ring structures, produce ethylene from KTBA (2-keto-4-thiomethylbutyric acid), and decolorize the polymeric dyes Poly-R and Remazol blue, which have some structural similarities to the lignin polymer (Kirk and Farrell, 1987; Buswell, 1991; Tien and Kirk, 1984; Andersson

et al., 1985). Reactions typical of those found to be catalyzed by LIP on lignin model compounds are shown in Figure 2.3 (Boominathan and Reddy, 1992). LIP activity is conveniently assayed by measuring the oxidation of veratryl alcohol (VA) to veratraldehyde (Tien and Kirk, 1984). VA also stimulates LIP activity *in vivo* (Shimada *et al.*, 1981; Tien and Kirk, 1984; Faison *et al.*, 1986; Harvey *et al.*, 1986; Hammel and Moen, 1991; de Jong *et al.*, 1994).

At least six heme proteins (H1, H2, H6, H7, H8, and H10) with LIP activity are seen in Fast Protein Liquid Chromatography (FPLC) profiles of *P. chrysosporium* strain BKMF-1767 (Dass and Reddy, 1990; Kirk *et al.*, 1986a; Kirk *et al.* 1986b) cultures grown in nitrogen-limited media although other investigators have reported observing as many as 15 isoenzymes (Leisola *et al.*, 1987). A typical FPLC profile for an acetate buffered, agitated culture of *P. chrysosporium* is shown in Figure 2.4 (Boominathan and Reddy, 1992). The LIP isoenzymes H2, H6, H8, and H10 constitute the major LIPs in both static and agitated cultures of *P. chrysosporium* (Kirk *et al.*, 1986b; Leisola *et al.*, 1987; Dass and Reddy, 1990). The optimum pH for LIP activity is 2.5, although the enzymes are not very stable at this pH (Tien, 1987; Boominathan and Reddy, 1992). Detailed investigation of LIP isoenzymes has shown that each isoenzyme is encoded by a separate *lip* gene (Boominathan and Reddy, 1992; Gaskell and Cullen, 1993; Reddy and D'Souza, 1994). H1 and H2 have been shown to be nearly identical (Tien, 1987; Boominathan and Reddy, 1992; Reddy and D'Souza, 1994). H7 and H8 were shown to be similar to each other and to H1 and H2, but different in that they lacked at least two major peptides (Tien, 1987; Boominathan and Reddy, 1992). H6 and H10 have been shown to be most similar to H7 and H8 (Tien, 1987; Boominathan and Reddy, 1992). The V_{max}/K_m (productive binding rate) for H_2O_2 is essentially the same for all the isoenzymes, while the binding constants (K_m) vary markedly. A broader range of V_{max}/K_m and K_m were observed for the reducing substrates (methoxylated aromatics and lignin substructure models) of the LIP isoenzymes (Tien *et al.*, 1986). Thus, the

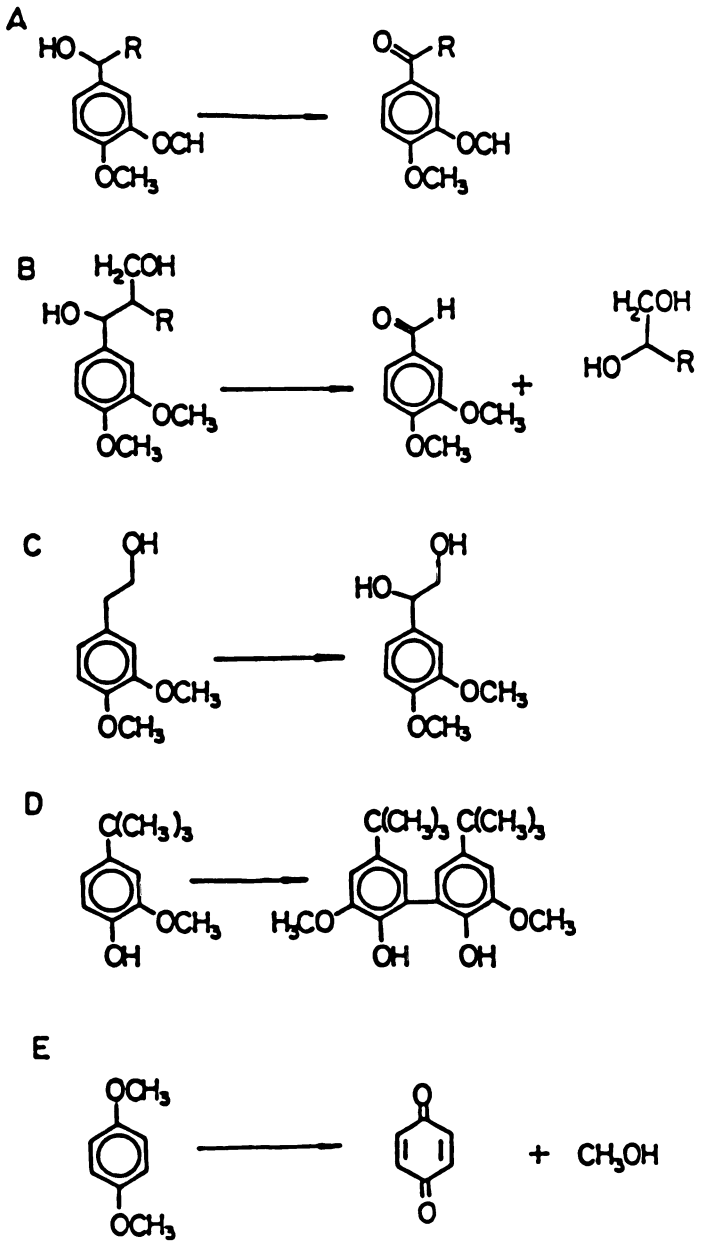

Figure 2.3: Typical reactions catalyzed by *Phanerochaete chrysosporium* lignin peroxidase (Boominathan and Reddy, 1992).

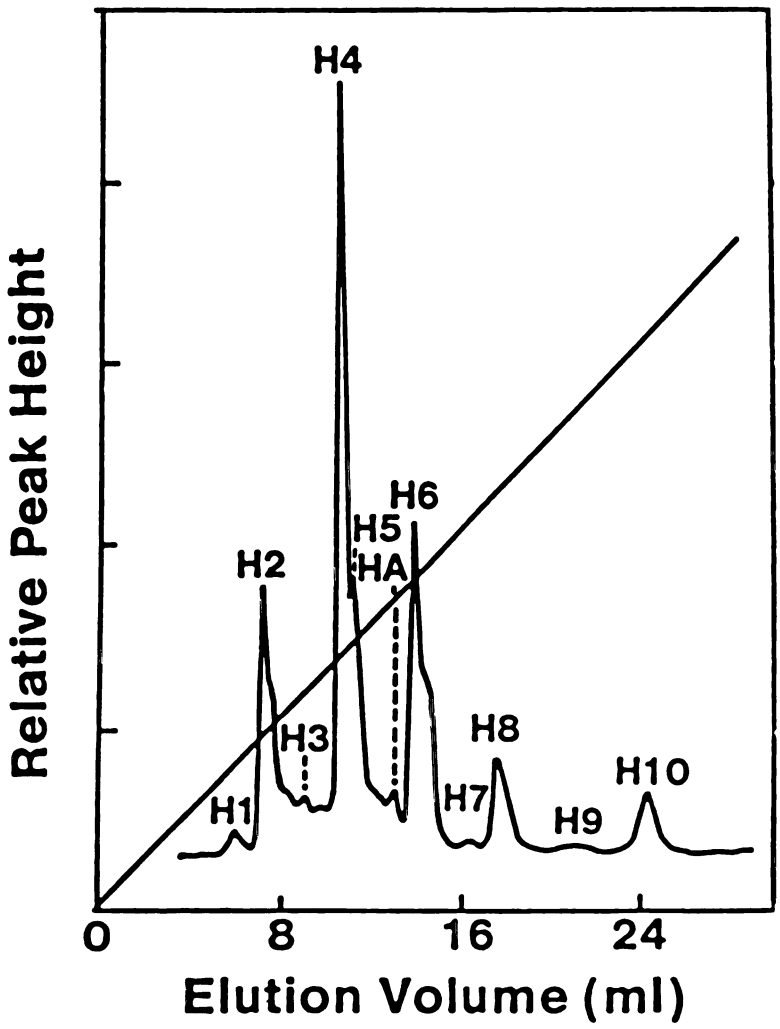

Figure 2.4: Typical FPLC profile of the extracellular peroxidases of *Phanerochaete chrysosporium* grown in acetate buffered, agitated culture (Boominathan and Reddy, 1992).

isoenzymes are quite similar in some respects but also somewhat different in their preferred substrates (Tien *et al.*, 1986; Leisola *et al.*, 1987; Dass and Reddy, 1990).

Studies done with lignin substructure models have shown that LIPs, operate by a free radical generating mechanism (Hammel *et al.*, 1985; Kersten *et al.*, 1985; Gold *et al.*, 1989). Steady-state kinetic studies with VA have indicated a ping-pong mechanism in which the LIP heme is first oxidized by H_2O_2, and the oxidized heme then reacts with VA to form veratraldehyde (Tien *et al.*, 1986; Gold *et al.*, 1989; Harvey *et al.*, 1993; de Jong *et al.*, 1994). H_2O_2 was found to competitively inhibit binding of VA to the enzyme, and to irreversibly inactivate the enzyme at high relative concentrations (Tien *et al.*, 1986). Since VA is normally produced by this fungus under secondary metabolic conditions (Shimada *et al.*, 1981; Faison *et al.*, 1986; Liebeskind *et al.*, 1990), it has been suggested that LIP may catalyze the oxidation of VA to a cation radical which is then free to diffuse into the lignin matrix and react with oxidizable lignin bonds (Harvey *et al.*, 1986; Cui and Dolphin, 1991; Hammel and Moen, 1991; Harvey *et al.*, 1993; Schoemaker *et al.*, 1994; de Jong *et al.*, 1994). ESR spectroscopy studies (Kersten *et al.*, 1985) have indicated that some LIP-generated free radicals are stable enough to diffuse away from the active site of the enzyme; this does not, however, completely rule out physical accessibility of the lignin to the enzyme as a rate limiting factor (Tien, 1987; Daniel *et al.*, 1989; Blanchette *et al.*, 1989). Physical accessibility of the substrate to cellulases has been shown to be the rate limiting factor in the hydrolysis of cellulose (Thompson *et al.* 1992); it is probable that this limitation affects other enzyme systems as well (Tien, 1987).

2.3.2 Manganese Peroxidases

MNPs are also glycosylated heme proteins (average molecular weight 46,000) and are obligately dependent on H_2O_2 for activity. In addition, MNPs require Mn(II) for activity, and catalyze the oxidation of Mn(II) to Mn(III) which in turn oxidizes phenols to phenoxy radicals (Glenn and Gold, 1985; Paszczynski *et al.*, 1985; Gold *et al.* 1989;

Gold and Alic, 1993). MNPs have been shown catalyze a number of oxidations of aromatic compounds. The dyes Poly B-411 and Poly R-481 are decolorized by oxidation by MNP (Glenn and Gold, 1985). Higher molecular weight chlorolignins are also degraded by MNPs (Lackner *et al.*, 1991). MNPs have been shown to partially depolymerize synthetic lignin (Wariishi *et al.*, 1991), to cleave α-carbonyl lignin model dimers (Tuor *et al.*, 1992), and to degrade a wide range of phenolic environmental contaminants (Valli and Gold, 1991; Valli *et al.*, 1992a; Valli *et al.*, 1992b; Joshi and Gold, 1993). In addition, MNPs have been shown to be the limiting factor in the decolorization of kraft bleach plant effluent (BPE) by continuous cultures of *P. chrysosporium* (Michel *et al.*, 1991), although Ferrer *et al.* (1991) found that lignin peroxidase also decolorized kraft BPE if the LIP was immobilized. MNP activity is assayed by measuring the oxidation of Phenol Red dye (Kuwahara *et al.*, 1984) or by measuring the conversion of Mn(II) to Mn(III) in the presence of tartrate (Paszczynski *et al.*, 1988).

At least four heme proteins, H3, H4, H5, and H9 (see Figure 2.4) with MNP activity have been described in nitrogen-limited agitated or static cultures of *P. chrysosporium* strain BKMF-1767 (Kirk *et al.*, 1986b; Glenn and Gold, 1985; Paszczynski *et al.*, 1985; Kuwahara *et al.*, 1984) although other investigators have reported observing as many as 6 or more isoenzymes (Leisola *et al.*, 1987). The MNP isoenzyme H4 constitutes the major MNP in both static and agitated cultures of *P. chrysosporium* (Dass and Reddy, 1990). MNP activity is stimulated by the addition of an α-hydroxy acid such as malonate, tartrate, lactate, etc. as a chelator (Glenn *et al.*, 1986; Wariishi *et al.*, 1988). In acetate-buffered cultures at 37°C, fungal production of LIP is suppressed and MNP production is enhanced by addition of 40-100 ppm Mn(II) (Bonnarme and Jeffries, 1990; Brown *et al.*, 1990). Similarly, MNP production can be eliminated by the omission of Mn(II) from the medium (Bonnarme and Jeffries, 1990). The catalytic cycle of MNPs is similar to that of LIPs, except that Mn(II) is oxidized to

Mn(III) by the MNP, and the Mn(III) in turn oxidizes the substrate molecule. A comparison of the catalytic cycles of LIP and MNP is shown in Figure 2.5. Kinetic studies on the oxidation of Mn(II) by MNP and hydrogen peroxide have indicated that the stoichiometry is 2 Mn(II) oxidized per H_2O_2 consumed, that the catalysis occurs via a typical peroxidase ping-pong mechanism similar to that of LIP, and that an organic acid chelator (such as malonate, lactate, tartrate, etc.) must be present to stabilize the Mn(III) that is formed and to efficiently remove it from the active site of the MNP (Wariishi *et al.*, 1989a; Aitken and Irvine, 1990; Wariishi *et al.*, 1992). Perez and Jeffries (1992; 1993) found that both Mn(II) and organic acid chelators were important in regulating not only the expression of both LIPs and MNPs, but also their activity. They found that in whole cultures when high levels of Mn were present along with a suitable chelator, some depolymerization of a synthetic lignin occurred, but the bulk of the depolymerization did not occur until the Mn eventually precipitated out as MnO_2 and LIPs were expressed. In addition, they found that lignin mineralization was most efficient at low Mn concentrations. This led them to conclude that MNPs catalyze an initial modification of lignin, preparing it for further degradation by LIPs (Perez and Jeffries, 1992; Perez and Jeffries, 1993).

2.4 Mechanistic Studies Of Lignin Degradation

2.4.1 Water-soluble Lignin Substructure Models

In vitro mechanistic studies with LIP H8 have shown that in the presence of H_2O_2, LIP will catalyze C_α-C_β cleavage, oxidation of benzylic alcohols, β-aryl ether cleavage, loss of methoxyl groups, and aromatic ring opening (Kirk and Farrell, 1987; Boominathan and Reddy, 1992; Tien, 1987; Gold *et al.*, 1989; Tien *et al.*, 1986; Kersten *et al.*, 1985; Hammel *et al.*, 1985). The mechanism of C_α-C_β cleavage of lignin model compounds is shown in Figure 2.6 (Tien, 1987). Using lignin model compounds, MNPs have been shown to catalyze, through the generation of Mn(III), the cleavage of phenolic β-1 dimers (Gold *et al.*, 1989) and α-carbonyl lignin model dimers (Tuor *et al.*, 1992),

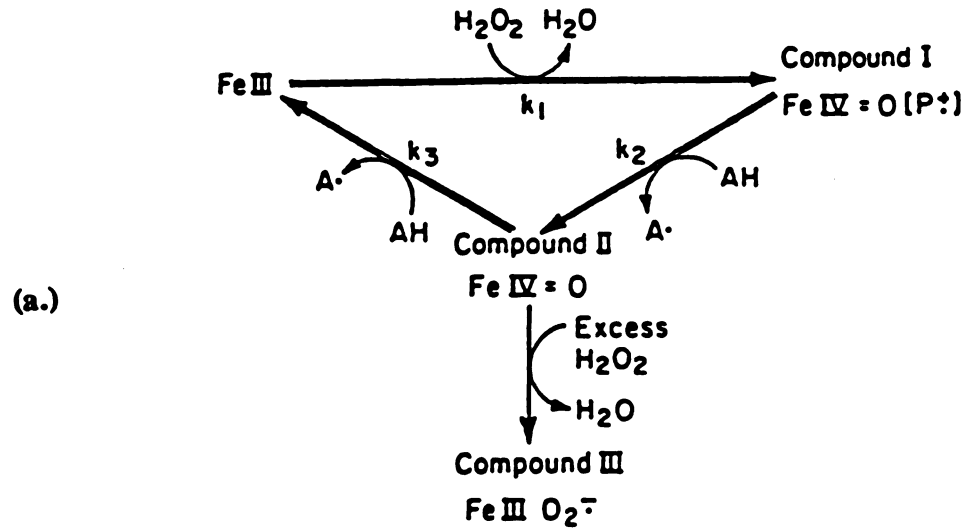

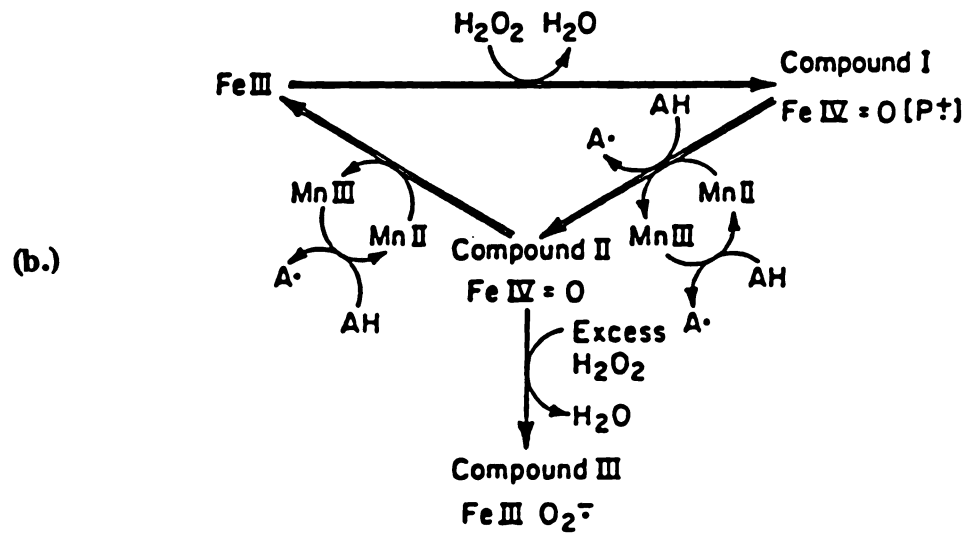

Figure 2.5: Comparison of the LIP and MNP catalytic cycles. **(a.)** LIP catalytic cycle, and **(b.)** MNP catalytic cycle (Gold *et al.*, 1989).

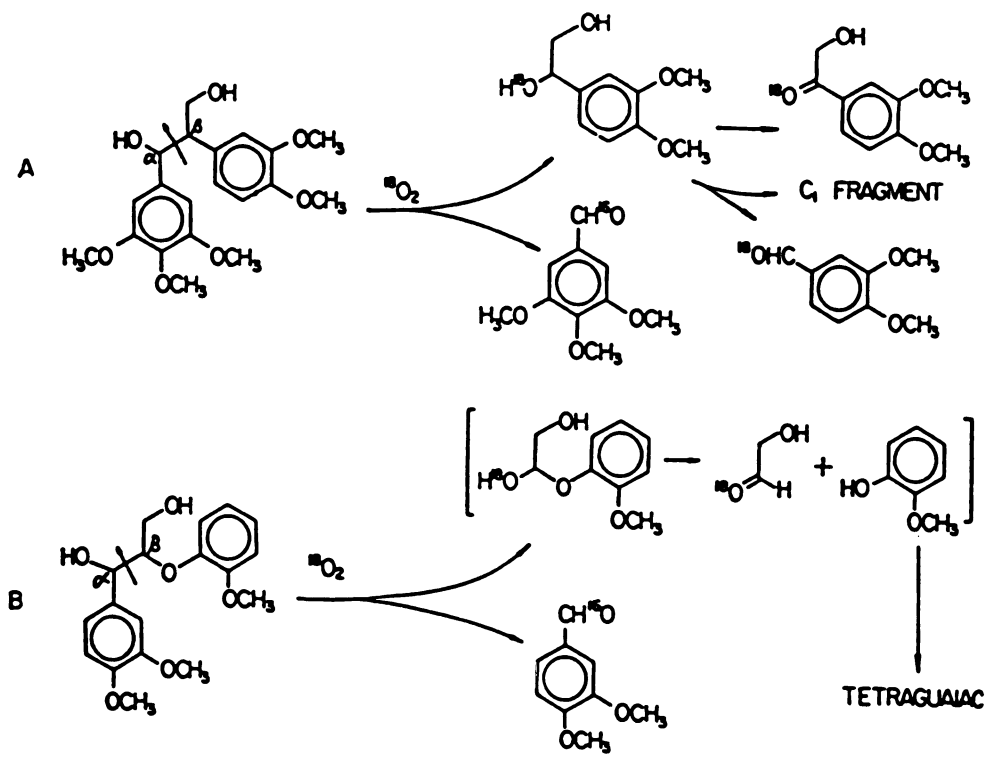

Figure 2.6: The mechanism of C_α-C_β cleavage by LIP for two types of lignin model dimers: **A.** β-1 linked dimer, and **B.** β-O-4 linked dimer (Tien, 1987).

alkyl-phenyl cleavage, and C_α-C_β cleavage (Wariishi *et al.*, 1989b; Wariishi *et al.*, 1991). These reactions are consistent with the types of bond breakages necessary to release monomers from polymeric lignin (Tien, 1987; Boominathan and Reddy, 1992; Gold and Alic, 1993), leading to the lignin degradation roles assigned to both LIPs and MNPs.

At present, there are at least two theories on the putative roles of LIPs and MNPs in lignin degradation. Perez and Jeffries (1990; 1992; 1993), in studies with soluble ^{14}C-labelled synthetic lignins, suggested that MNPs perform the initial steps of lignin depolymerization, but that LIPs are necessary for further degradation of the polymer to low molecular weight products, and for complete mineralization. Boyle *et al.* (1992), however, in a study with ^{14}C-lignin labelled wood, found evidence that LIPs played the main role in lignin solubilization and MNPs were important in subsequent CO_2 production. Haemmerli *et al.* (1986) demonstrated that at least in some cases, LIP catalyzes polymerization of solubilized isolated lignin fragments and not depolymerization, and that the polymerization was enhanced by the addition of VA. This led them to conclude that LIPs are not directly involved in the depolymerization of lignin. However, these studies were done under conditions of low O_2 and at extremely low H_2O_2 and VA levels relative to LIP. This may result in anaerobic free radical coupling reactions due to both the low O_2 and the lowered levels of cation radicals generated from H_2O_2. Sarkanen *et al.* (1991) also indicated that LIPs are not involved directly in the depolymerization of lignin, but may either play a role in detoxification of lower molecular weight phenolic fragments released by MNPs, or may directly enhance the susceptibility of polymeric lignin toward depolymerization by another enzyme through the introduction of suitable functional groups.

2.4.2 Synthetic Polymeric Lignins

Most of the studies on degradation of water-insoluble naturally occurring lignocellulosic substrates have focused on total CO_2 production by cultures of the whole

organism (*P. chrysosporium* or other white rot fungi) (Kirk and Farrell, 1987; Buswell and Odier, 1987; Buswell, 1991; Boominathan and Reddy, 1992). There is a wealth of information on LIP and MNP catalyzed reactions using water-soluble, lower molecular weight lignins and lignin substructure models; however, very little has been done with water-insoluble polymeric lignin substrates until the recent studies of Hammel and Moen (1991), Hammel *et al.* (1993), and Wariishi *et al.* (1991). The reasons behind this reluctance to use a water-insoluble, high molecular weight natural lignin are not trivial: (1) the rates of *in vivo* depolymerization of water-insoluble lignin are orders of magnitude slower than rates seen with water-soluble lignins and model compounds; (2) maintenance of a steady supply of H_2O_2 at levels which will not inactivate the enzyme, yet sustain the reaction is difficult; and (3) analytical techniques for the rapid characterization of partially degraded solid substrate are not readily accessible (Tien, 1987). Hammel and Moen (1991) presented the first direct evidence for the *in vitro* depolymerization of synthetic guaiacyl-syringyl lignin. They demonstrated the partial solubilization of a $^{14}C_{\beta}$-labelled synthetic hardwood lignin partially soluble in 9:1 sodium acetate (pH 4.5)/N,N-dimethylformamide, in the presence of LIP, H_2O_2, and VA. LIP and H_2O_2 were continuously added slowly to a stirred dispersion of lignin in the presence of VA (by means of a peristaltic pump). Products with molecular weights as low as 170 were detected and 25-30 % of the radiolabel originally present was converted to volatile products. In experiments where LIP or H_2O_2 were omitted, no evidence of depolymerization was found. Moreover, little discernible lignin depolymerization was observed in reactions lacking VA. Since the majority of intermonomer linkages in lignin occur through C_{β} of the propyl sidechain (Adler, 1977; Ander and Eriksson, 1978; Higuchi, 1990), the extensive volatilization of ^{14}C from a $^{14}C_{\beta}$-labelled lignin can only occur if the sidechain is broken (Hammel and Moen, 1991). Thus, these results clearly indicate the peroxidative alkyl side-chain cleavage of the synthetic lignin in the presence of LIP, H_2O_2, and VA.

Hammel *et al.* (1993), in further investigations using the system described above, again found that LIP depolymerized synthetic lignins, but only if the lignin was dispersed in an organic solvent. Veratryl alcohol was also required; ligninolysis was most effective when VA was added at 375 μmoles/liter of reaction, with H_2O_2 present in limiting amounts. Increases of VA above this amount gave little change in the extent of lignin depolymerization. LIP was found to degrade highly methylated (derivatized) phenolic lignin as well as phenolic lignin, but MNP was only effective with phenolic lignin. Conclusions from this study were: (1.) organic cosolvents are preferred for *in vitro* lignin depolymerization studies; (2.) H_2O_2 should be present as limiting substrate, and preferably at concentrations less than 100 μM; (3.) VA is required for protection of the LIP from H_2O_2-mediated inactivation, and also as a one-electron redox shuttle to promote LIP catalyzed oxidations; (4.) lignin concentrations should be low; and (5.) O_2 is absolutely required to prevent free radical coupling reactions, which lead to polymerization rather than depolymerization.

Olsen *et al.* (1991), in a recent European Patent Application, described a process in which water-insoluble paper pulp is treated *in vitro* with mixtures of LIPs, MNPs, and xylanases in the presence of H_2O_2, VA, Mn(II), lactate, and O_2. Measurements of pulp brightness and Kappa number for the treated material versus controls (in which no enzymes were added) indicated that extensive delignification had occurred. This is the first direct evidence of *in vitro* delignification of a water-insoluble polymeric lignin from a natural source (as opposed to synthetic lignin), although during the pulping process it is likely that the lignin in the pulp was modified enough that it no longer closely resembled lignin as it occurs undisturbed in wood. In this study, H_2O_2 was generated in the reaction vessel by glucose oxidase, while VA was added intermittently. Ranges of enzymatic activities and reagent concentrations to achieve maximum delignification were presented in the preferred embodiment of the patent. These ranges are presented in Table 4.2 (Chapter IV) rather than here, since they were used in the design of

experiments for this study.

Wariishi *et al.* (1991) recently demonstrated that a purified MNP also catalyzes the depolymerization of ^{14}C-labelled synthetic guaiacyl as well as guaiacyl-syringyl lignins in 3% DMF in water. Reactions were carried out under an atmosphere of 100% O_2 at 37°C, pH 4.5, 200 μM Mn(II), and with an H_2O_2 generating system consisting of 2.5 mM glucose and 0.025 Units of glucose oxidase. Gel permeation profiles showed significant depolymerization of the various synthetic lignins, indicating involvement of MNPs in lignin depolymerization. The major product released from the syringyl lignin was identified as 3,5-dimethoxy-1,4-benzoquinone, with much smaller amounts of 3,5-dimethoxy-1,4-dihydroxybenzene and syringaldehyde. Tuor *et al.* (1992) also identified the quinone and hydroquinone structures above in a study of the oxidation of phenolic arylglycerol β-aryl ether lignin model compounds; again, the quinone was present in much higher concentrations than the hydroquinone form. It was found that in the presence of O_2 or Mn(III), the hydroquinone form was spontaneously oxidized to the quinone form, accounting for the low concentrations of the hydroquinone (M.H. Gold, personal communication). Based on these studies, pathways for C_α-C_β cleavage, C_α-oxidation, and alkyl-phenyl cleavage of lignin by MNP were proposed; these pathways are presented in Figures 2.7 and 2.8. They concluded that MNP oxidized C_α-oxo-substituted substructures as well as C_α-C_β substructures, leading to the depolymerization of lignin.

2.5 Techniques for Characterization of Lignin

Lignin chemistry is a complex, ill-defined field due to the heterogeneous aromatic structure of lignin (Sarkanen and Ludwig, 1971). Most early techniques for lignin characterization relied on oxidative degradation of the lignin or acid hydrolysis of the aliphatic sidechains in lignin, followed by characterization of the aromatic products released, and formulation of probable intermonomer linkages based on the functional groups and side chains present in the products (Sarkanen and Ludwig, 1971). More

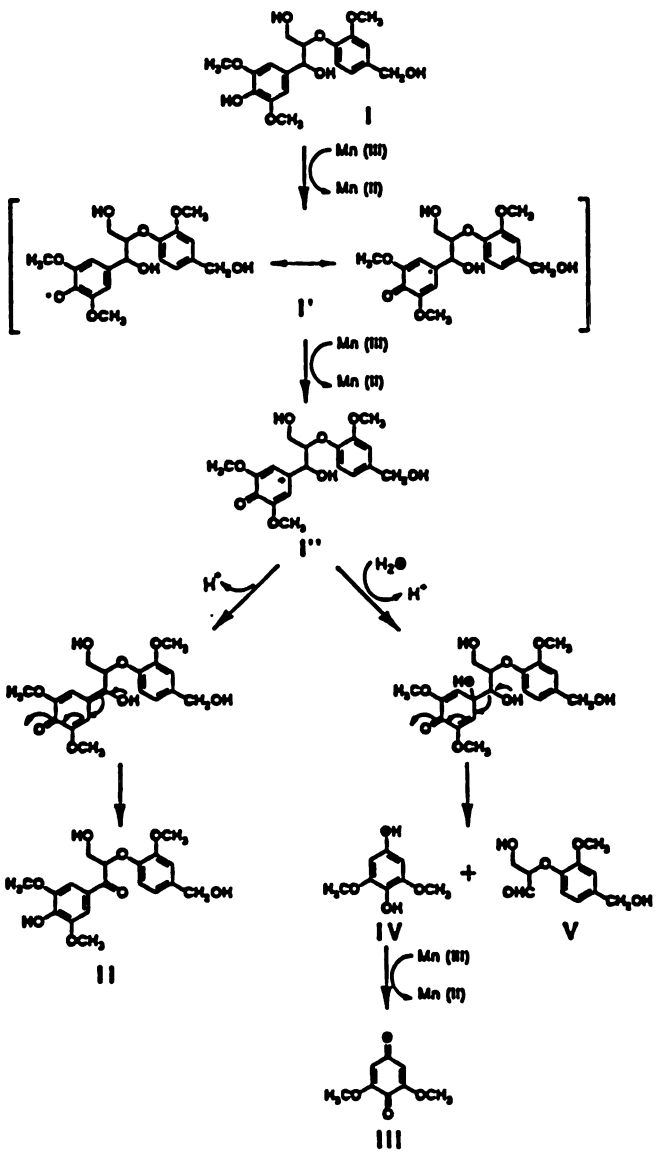

Figure 2.7: The mechanism of alkyl-phenyl cleavage of a lignin-model dimer by MNP and C_α-oxidation. Solid "O" refers to oxygen atom derived from ^{18}O in labelled water (Tuor *et al.*, 1992).

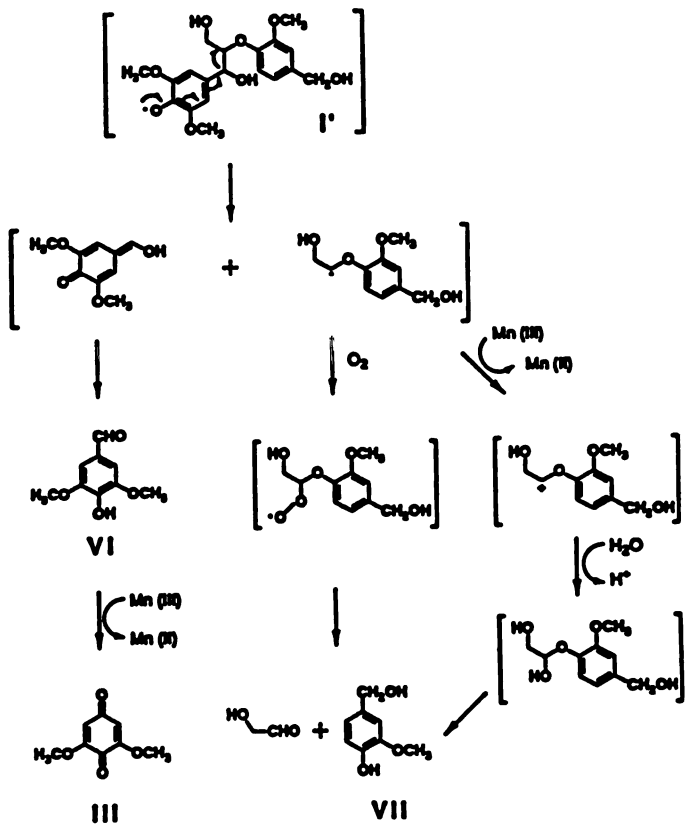

Figure 2.8: The mechanism of C_α-C_β cleavage of a lignin model dimer by MNP (Tuor *et al.*, 1992).

recent developments, such as Fourier Transform Infrared Spectroscopy (FTIR) have allowed nondegradative characterization of lignin, although interpretation of the spectra in terms of the actual lignin structure are difficult. Pyrolysis-Gas Chromatography/Mass Spectrometry (Pyrolysis-GC/MS), although still a degradative technique, has gained in popularity in recent years due to its nonoxidative method of depolymerization, yielding lignin-derived products that are not significantly more oxidized than they occur in the polymeric lignin. Finally, ^{13}C Nuclear Magnetic Resonance (NMR) of both solubilized and solid lignins has proven to be a useful technique in characterizing the structure and intermonomer linkages in lignin. These techniques will be briefly reviewed below.

2.5.1 Chemical Techniques

The three major degradative chemical techniques for lignin characterization are potassium permanganate oxidation (Sarkanen and Ludwig, 1971; Tanahashi and Higuchi, 1988; Gellerstedt, 1992), nitrobenzene oxidation (Sarkanen and Ludwig, 1971; Tanahashi and Higuchi, 1988), and thioacidolysis (Obst, 1982; Tanahashi and Higuchi, 1988; Rolando *et al.*, 1992). Each technique releases lignin monomers by different mechanisms, resulting in different functional group changes, which are used to predict the original linkage types in the lignin. Detailed descriptions of procedures for these techniques and specific results from studies using them are beyond the scope of this review; rather, only the general information which can be gained from each technique and the advantages and disadvantages of each will be given.

Potassium permanganate oxidation has been used for quite a number of years in the characterization of lignin samples; the initial publication describing the procedure was published in 1936 (Freudenburg *et al.*, 1936). This technique involves the selective degradation of all aliphatic sidechains directly attached to aromatic rings in lignin with potassium permanganate, resulting in a mixture of aromatic syringyl- and guaiacyl-derived carboxylic acids. The amounts and identities of each acid, usually determined by HPLC or GC/MS, provide information as to the frequency of occurrence of each

aromatic ring substitution pattern and the amounts of different types of intermonomer linkages (Gellerstedt, 1992). The biggest drawback of permanganate oxidation is that lignin monomers which do not contain free phenolic hydroxyl groups cannot be analyzed by this method, so the information gained represents only a small fraction of the total lignin structures. Sample size is preferentially on the order of 10-100 mg calculated as lignin (Gellerstedt, 1992); therefore, if quantitative replicate analyses are required, relatively large lignin samples (up to 300 mg calculated as lignin) are needed.

Nitrobenzene oxidation, first reported by Freudenberg *et al.* (1940) releases aromatic aldehydes and carboxylic acids from lignin. High yields of vanillin, and vanillin and syringaldehyde are obtained from gymnosperm and angiosperm lignins, respectively (Tanahashi and Higuchi, 1988). In addition, large amounts of p-hydroxybenzaldehyde are obtained from grass lignin. The determination of each aldehyde present, usually by GC/MS, in the oxidation mixture provides information that is useful in the chemical characterization of the lignin. Carboxylic acids produced from the corresponding aldehydes by the Cannizaro reaction (Tanahashi and Higuchi, 1988) decrease the yields of the aldehydes, and should be included in the aldehyde totals. This method has been one of the most useful in providing information for the phylogenetic and taxonomic classification of woody plants. Sample sizes of 60 mg of wood meal or 15 mg of lignin (both extractive-free) are necessary for good quantitative results.

Thioacidolysis is but one of a number of hydrolysis techniques, including ethanolysis, acidolysis, thioacidolysis, and thioacetolysis, commonly used for the characterization of lignin (Tanahashi and Higuchi, 1988). These techniques cleave the alkyl-aryl ether linkages (the most common intermonomeric bonds in lignin) to form syringyl- and guaiacyl-derived lignin monomers which can be quantified and used to determine, among other things, the syringyl and guaiacyl contents of the lignin (Obst, 1982; Tanahashi and Higuchi, 1988; Rolando *et al.*, 1992). Acidolysis and thioacidolysis are used to determine arylglycerol-β-aryl ether linkages in lignin (Tanahashi and Higuchi,

1988) through characterization of the γ-methyl isomers of β-oxy-p-coumaryl alcohol derivatives released from the lignin. Compared to acidolysis, thioacidolysis gives greater yields of less complex monomers, especially from hardwoods, which makes the resulting monomeric composition of hydrolyzable structures in the lignin more reliable. Relatively little (20 mg) of sample is needed for either technique (Obst, 1982; Tanahashi and Higuchi, 1988; Rolando *et al.*, 1992), but complete chemical characterization of the lignin is not possible by this technique (or by any of the techniques above); rather, information from this and all of the above techniques is necessary for complete characterization of the lignin. The biggest drawback to chemical characterization of lignin through the use of these degradative techniques, then, is that a large amount (400 mg or more) of sample would be needed to get complete, reliable results.

2.5.2 Pyrolysis-GC/MS

Pyrolysis-GC/MS, with the advances in GC/MS analysis in recent years, has gained in popularity because it yields lignin-derived products that are not significantly more oxidized than they occur in the polymeric lignin. Within the last 15 years, a wealth of information on lignin monomeric products has been generated using pyrolysis combined with electron-impact GC/MS (Martin *et al.*, 1979; Philp *et al.*, 1982; Fullerton and Franich, 1983; Saiz-Jimenez and de Leeuw, 1984; Faix *et al.*, 1987; Pouwels and Boon, 1987; Boon *et al.*, 1987; Genuit *et al.*, 1987; Faix *et al.*, 1988; Sjostrom and Reunanen, 1990; Faix *et al.*, 1990a; Faix *et al.*, 1990b; van der Hage *et al.*, 1993).

Since the structure of lignin is so complicated, many different degradation products are possible using any degradative technique. The mass spectra of the lignin-derived products found in these studies should be useful in identifying oxidative lignin degradation products, since the more stable molecular fragments (containing the aromatic moiety and substituents attached directly to the ring) produced by electron impact mass spectrometry should be similar whether the aliphatic side chains are oxidized or not. The most complete studies on pyrolysis-GC/MS of lignins have been done by Faix and co-

workers (1987; 1988; 1990a; 1990b; Genuit *et al.*, 1987), in which they determined the mass spectra of hundreds of previously unmeasured compounds derived from lignin, including substituted guaiacyl and syringyl alcohols, aldehydes, and ketones; catechols, aliphatic-substituted phenols, and many others. It was found in these studies that there are key mass fragments that can be assigned to certain lignin-related structures: m/z 107 is typical for alkylated phenols, m/z 137 and 167 are key fragments for alkylated guaiacyl- and syringyl- structures, respectively, and m/z 151 and 181, in general, indicate a carbonyl-group at the α-carbon of the propyl side chain in guaiacyl- and syringyl-structures, respectively (Faix *et al.*, 1990a; Faix *et al.*, 1990b). The masses of these fragments change with degree of substitution beyond the base syringyl and guaiacyl structures (Faix *et al.*, 1990b). As little as 100 μg of lignin can be used for pyrolysis-GC/MS (Faix *et al.*, 1990a). One disadvantage of using pyrolysis-GC/MS for routine lignin analysis is that it requires very expensive equipment which is dedicated solely to that task, making it unavailable to most researchers. In addition, the mass spectra obtained from pyrolysis-GC/MS may be of limited use to some lignin degradation studies; since derivatization of the volatile products is not possible, matching of spectra obtained is then limited to nonderivatizable products.

2.5.3 ^{13}C NMR of Solubilized and Solid Lignin

^{13}C NMR has been used extensively to characterize lignin structure, with both acetylated and other solubilized lignins, and with the development of cross-polarization magic angle spinning (CPMAS or CP/MAS; Yannoni, 1982), solid lignins. Each case will be briefly described below.

Liquid-state ^{13}C NMR has been used both qualitatively and quantitatively to characterize solubilized lignins. Qualitative liquid ^{13}C NMR has been successfully used to differentiate between lignins from hardwoods and softwoods (Nimz *et al.*, 1981), to identify degradation products of lignin degraded *in vivo* by *Phanerochaete chrysosporium* (Chua *et al.*, 1982; Chen *et al.*, 1982), to compare the importance of syringyl and

guaiacyl units in Poplar lignin (Lapierre *et al.*, 1982; Lapierre and Monties, 1984), to study the structure of Kraft lignins (Kringstad and Morck, 1983; Morck *et al.*, 1986), and to compare the structure of a synthetic lignin to a milled wood lignin isolated from spruce wood (Evliya, 1989). Quantitatively (quantified by integration of the peaks in the NMR spectrum), it has been used to determine hardwood syringyl to guaiacyl ratios (Obst and Ralph, 1983), methoxyl to aryl ratios (Obst and Landucci, 1986) in hardwoods, to estimate total hydroxyl content in milled wood lignin from spruce and in a synthetic lignin (Robert and Brunow, 1984), and to quantify C_α-C_β bonds present in spruce wood decayed by *Phanerochaete chrysosporium* (Robert and Chen, 1989). Clearly, Liquid-State ^{13}C NMR is a powerful tool for the characterization of lignins that can be solubilized. The main drawback to using Liquid-State ^{13}C NMR is that it has a very low sensitivity, which makes necessary the use of large amounts of lignin in order to get relatively concentrated samples, and a long duration of analysis (in the instrument) is required in order to get clear peaks for minor, but important structures (Lapierre and Monties, 1984). In addition, only lignin samples that are of low enough molecular weight to be solubilized can be analyzed with this technique.

Solid-State ^{13}C NMR utilizing CP/MAS has been used in several structural studies of solid lignin isolated from spruce wood (Fleming and Bolker, 1980; Bartuska *et al.*, 1980), intact lodgepole pine wood (Kolodziejski *et al.*, 1982; Taylor *et al.*, 1983), and residual Kraft lignin (Leary *et al.*, 1988), with mixed results. This technique can be used to determine differences in functional group contents between related lignin samples (Taylor *et al.*, 1983), but it remains to be seen whether truly quantitative results can be obtained due to the lack of sharpness and separation of peaks in the NMR spectrum. The Solid State ^{13}C NMR technique using CP/MAS has the advantage over Liquid-State ^{13}C NMR that the molecular weight of the lignin to be analyzed is not limited by solubility; however, sample sizes remain large (0.4 cm^3 sample volume; Kolodziejski *et al.*, 1982; Taylor *et al.*, 1983) and analysis times are very long (1-4 hours per sample; Taylor *et*

al., 1983). In short, both ^{13}C NMR techniques require large samples and long analysis times to get good results, a strong disadvantage if sample size is limited.

2.5.4 Spectrophotometric Techniques

The spectrophotometric techniques most commonly used for lignin analysis are Ultraviolet (UV) and Fourier Transform Infrared Spectroscopy (FTIR), due to the reproducible absorbance maxima exhibited within relatively narrow wavelength ranges by aromatic rings and functional groups attached to them. Characterization of lignin by UV and FTIR spectroscopy depends completely on the assignment of absorbances at various wavelengths to specific functional groups, usually identified through studies of the absorbances of model compounds (Sarkanen and Ludwig, 1971). The use of UV and FTIR spectroscopy for lignin characterization will be discussed below.

The major use for UV spectroscopy in lignin characterization is in the determination of the lignin content of woods and isolated lignins (Fergus *et al.*, 1969; Bagby *et al.*, 1973; Boutelje and Eriksson, 1982; Saka *et al.*, 1982; Janshekar *et al.*, 1981; Boutelje and Eriksson, 1984), since the aromatic rings in lignin absorb intensely at 280 nm, while cellulose and hemicellulose are transparent to UV in this region (Sarkanen and Ludwig, 1971). Some functional group contents can also be estimated with this method, including carboxylic acid content (Sarkanen and Ludwig, 1971) and phenolic hydroxyl content (Yang and Goring, 1980; Boutelje and Eriksson, 1984). Clearly, this method could be potentially useful for the characterization of lignins, but it cannot be used to completely characterize lignin since the aliphatic sidechains in the lignin cannot be measured by UV (Sarkanen and Ludwig, 1971).

IR spectroscopy has been useful in determining differences between lignins from different sources, and between lignins from the same source but isolated by different methods (Sarkanen and Ludwig, 1971). Comparison of absorbances at the various maxima in the range of 4000-700 wavenumbers ($1/\lambda$, cm^{-1}), which can be attributed to various functional groups and lignin bonds (identified by inspecting IR spectra of lignin

model monomers and dimers (Sarkanen and Ludwig, 1971)), gives important information about differences in the chemical and structural makeup of the lignin. These IR band assignments are shown in Table 2.1 (Faix, 1992). Lignin does not have to be soluble to be used in IR studies (Sarkanen and Ludwig, 1971), making the technique quite useful in studies of whole, insoluble isolated lignins (and not just organic solvent-soluble extracts).

With the development of FTIR, which allows for much faster and accurate measurement and analysis due to the ability to quickly measure and average a large number of scans (Griffiths and de Haseth, 1986), methods have been developed for the quantitative measurement of functional group compositions of lignins using FTIR and Beer's Law (Sarkanen and Ludwig, 1971), and various mathematical methods (Schultz *et al.*, 1985; Schultz and Glasser, 1986; Fuller *et al.*, 1988a; Fuller *et al.*, 1988b; Hames *et al.*, 1991). The first method to be developed employed was Diffuse Reflectance FTIR (DRIFT FTIR; Schultz *et al.*, 1985; Schultz and Glasser, 1986) and empirical regression methods. In DRIFT FTIR, the FTIR spectrum of the solid lignin sample is determined by measuring the spectrum of IR radiation reflected from the lignin (1:40 in powdered KBr) using a complex system of mirrors; the method is made quantitative by integrating the spectral peaks corresponding to each functional group and applying an empirical relationship derived using linear regression on data obtained from chemical measurements of functional group contents (Schultz and Glasser, 1986). Normally, FTIR spectra of solid samples are measured with the lignin (finely ground) dispersed in a KBr pellet (or wafer) (Sarkanen and Ludwig, 1971; Griffiths and de Haseth, 1986); DRIFT FTIR was found to offer the advantage that the spectral baseline was more stable than those obtained with KBr pellets, allowing for more accurate measurements of peak areas. Good correlations were obtained for phenolic hydroxyl content, hydrolysis ratio, methoxyl content, aromatic hydrogen content, and condensation ratio (Schultz and Glasser, 1986). The advantages to DRIFT FTIR were that sample preparation was

Table 2.1: Band assignments in the mid-infrared region for non-derivatized guaiacyl- (G), guaiacyl/syringyl- (GS), and hydroxyphenyl/guaiacyl/syringyl-type (HGS) milled wood lignins. Band intensities are in parenthesis. (Adapted from Faix, 1992).

Table 2.1

Wavenumbers (cm^{-1})		Band origin, short comments	Maxima at cm^{-1}, % absorbance (% A) from standard spectra					
Baseline (Abs.=0)	Range of Maxima		Spruce MWL		Beech MWL		Bamboo MWL	
			cm^{-1}	% A	cm^{-1}	% A	cm^{-1}	% A
from 3695								
	3412-3460	O - H stretch	3412	(58)	3460	(49)	3428	(45)
to 3042								
from 3042								
	3000-2842	C - H stretch in methyl and methylene groups	3000	(5)	3000	(7)	3002	(6)
			2937	(24)	2940	(22)	2942	(22)
			2879	(15)	2880	(12)	2879	(11)
			2840	(12)	2840	(12)	2840	(11)
to 2782								
from 1800								
	1738-1709	C = O stretch in unconjugated ketones, carbonyls and in ester groups (frequently of carbohydrate origin); conjugated aldehydes and carboxylic acids absorb around and below 1700 cm^{-1}	1722	(11)	1735	(18)	1709	(45)
	1655-1675	C = O stretch in conjugated p-subst. aryl ketones; strong electronegative substituents lower the wavenumber	1663	(29)	1658	(23)		
	1593-1605	Aromatic skeletal vibrations plus C = O stretch; S > G; G condensed > G etherified	1596	(46)	1593	(54)	1601	(75)
	1505-1515	Aromatic skeletal vibrations; G > S	1510	(95)	1505	(60)	1511	(77)
	1460-1470	C - H deformations; asym. in - CH_3 and - CH_2 -	1464	(60)	1462	(63)	1462	(68)
	1422-1430	Aromatic skeletal vibrations combined with C - H in-plane deformations	1423	(53)	1422	(53)	1423	(56)
	1365-1370	Aliphatic C - H stretch in CH_3, not in OMe; phen. OH	1367	(33)	1367	(27)		
	1325-1330	S ring plus G ring condensed; (ie., G ring substituted in position 5)	1326	(38)	1329	(48)	1329	(57)
	1266-1270	G ring plus C = O stretch	1269	(100)	1266	(48)	1267	(80)
	1221-1230	C - C plus C - O plus C = O stretch; G condensed > G etherified	1221	(70)	1227	(67)	1229	(81)
	1166	Typical for HGS lignins; C = O in ester groups (conj.)					1166	(71)
	1140	Aromatic C - H in plane deformation; typical for G units; whereby G condensed > G etherified	1140	(78)				
	1128-1125	Aromatic C - H in-plane deformation (typical for S units); plus secondary alcohols plus C = O stretch			1126	(100)	1127	(100)
	1086	C - O stretch in *secondary alcohols* and aliphatic ethers	1086	(45)				
	1030-1035	Aromatic C - H in-plane deformation, G > S; plus C - O deform. in primary alcohols; plus C = O stretch (unconj.)	1032	(76)	1033	(54)	1032	(58)
	966-990	- HC = CH - out-of-plane deform. (trans)						
	915-925	C - H out-of-plane; aromatic	919	(5)	925	(20)		
	853-858	C - H out-of-plane in position 2, 5, and 6 of G units	858	(11)				
	834-835	C - H out-of-plane in position 2 and 6 of S, and in all positions of H units			835	(10)	834	(26)
	817-832	C - H out-of-plane in positions 2, 5, and 6 of G units			817	(8)		
to 780								

relatively easier than pressing KBr pellets, the baseline was relatively level, and fewer problems were introduced by moisture-related noise (Schultz and Glasser, 1986). The only major drawback to this method, it was concluded, was that the DRIFT cell had a relatively low throughput (IR radiation reaching the detector) versus pellet-based FTIR measurement (Schultz and Glasser, 1986). Despite the ease of sample preparation, KBr pellet measurements are generally preferred over DRIFT measurements because the reproducibility of the band width, in addition to the intensity, for DRIFT measurements is about four times less than those obtained with KBr pellets (Griffiths and de Haseth, 1986). There is no reason to expect, however, that the empirical relationships derived (Schultz and Glasser, 1986) could not be used for Pellet FTIR spectra.

Partial Least Squares Regression (PLS) of FTIR spectra, the second method and the more accurate of the two (Faix, 1992), has proven useful in accurately predicting functional group contents in lignins (Fuller *et al.*, 1988a; Fuller *et al.*, 1988b; Hames *et al.*, 1991). The PLS technique was developed in response to the observation that single IR absorbance peak areas could not fully account for all absorbances for a particular functional group, and thus could not fully account for the contents of single functional groups (Fuller *et al.*, 1988a; Fuller *et al.*, 1988b; Hames *et al.*, 1991). When combined with a new, faster and easier method of producing high quality KBr pellets (Breneman *et al.*, 1989), this technique offers an excellent alternative with few drawbacks to the DRIFT method (Hames *et al.*, 1991). When the PLS method was calibrated with chemical analysis data from a large number of milled wood lignins, good correlations were obtained for methoxyl content, methoxyl to aryl ratio (Hames *et al.*, 1991), lignin and carbohydrate compositions, and phenolic hydroxyl content (B. Hames, Personal Communication). This technique requires only 1.5 mg of lignin sample (1:200 in a KBr wafer), which makes it quite useful when sample availability is limited (Hames *et al.*, 1991).

2.6 GC/MS and LC/MS Techniques for Characterization of Soluble Lignin Fragments

Mass spectrometry is a useful tool in the identification of unknown compounds. When combined with a separation technique such as gas or liquid chromatography, the result is a powerful system for the separation and characterization of products in complex mixtures. GC/MS is one of the more powerful tools in the analysis of complex mixtures, due to its ability to separate mixtures and to obtain high-quality mass spectra which can be used to identify the compounds without isolating them (Sedgwick and Hindenlang, 1988; Evershed, 1989). GC/MS is sensitive in the detection of nanogram quantities of compounds, making it extremely useful in detecting major as well as minor products in complex mixtures (Sedgwick and Hindenlang, 1988; Evershed, 1989). Derivatization methods for nonvolatile compounds (Blau and King, 1978; Kim *et al.*, 1989) as well as lignin-like compounds (Drawert and Leupold, 1976; Salomonsson *et al.*, 1978; Hoffmann and Sweetman, 1987; Hyatt, 1989) to make them volatile and/or stable for GC analysis have been well characterized.

Many studies have been done on the lignin-derived products present in spent bleach liquor and Kraft liquor, with the identification of a wide range of phenolic lignin-derived acids, aldehydes, and alcohols (Lindstrom and Osterberg, 1984; Osterberg and Lindstrom, 1985a; Osterberg and Lindstrom, 1985b; Van der Klashorst, 1988; Niemela, 1988a; Niemela, 1988b; Niemela, 1989). In addition, GC/MS has seen extensive use in characterizing soluble lignin-derived and lignin-like products (Concin *et al.*, 1983; Fritz and Moore, 1987; Umezawa and Higuchi, 1988; Chen, 1988; Pometto and Crawford, 1988a; Katayama *et al.*, 1989; Wariishi *et al.*, 1991; Valli and Gold, 1991; Valli *et al.*, 1992a; Valli *et al.*, 1992b; Joshi and Gold, 1993). Most studies have used different derivatization procedures (or no derivatization at all), so matching of spectra is often not possible; however, the structures of the lignin-derived products identified in these studies are useful in providing a starting point for determination of molecular

structures in the analysis of mass spectra from compounds derivatized by a different procedure. Many of the products seen with pyrolysis-GC/MS are either identical or very similar to those found in the lignin degradation studies which used GC/MS to characterize soluble products, for example syringaldehyde, vanillic acid, coniferaldehyde, etc., so the fragmentation rules outlined above for lignin-derived products should also hold for the soluble product studies (Concin *et al.*, 1983; Fritz and Moore, 1987; Umezawa and Higuchi, 1988; Chen, 1988). The main drawback to using GC/MS for soluble product identification is that only products of molecular weight of about 600 and below can be analyzed, because anything much larger than that is not likely to be volatilized, even with derivatization (Sedgwick and Hindenlang, 1988; Evershed, 1989). For products below molecular weight 600, however, GC/MS provides an excellent tool for identifying (and roughly quantifying through GC peak integration) trace quantities of unknowns in complex mixtures.

Liquid chromatography combined with mass spectrometry (Hartley and Buchan, 1979; Pometto and Crawford, 1988b; Catlow and Rose, 1989; Budde *et al.*, 1990) is emerging as a method of analysis for products which are either of too high a molecular weight to be volatilized by GC, or which decompose at the temperatures required for volatilization. Relatively little has been done in the analysis of lignin derived products using LC/MS or HPLC/MS, although Hartley and Buchan (1979) in a study on HPLC of lignin-derived products, were able to detect as little as 100 ng of various lignin-derived monomers using UV detection. It remains to be seen whether LC/MS or HPLC/MS will become competitive with GC/MS in the characterization of soluble lignin-derived monomers, due to difficulties in technical interfacing of the instruments (Evershed, 1989).

CHAPTER III: RESEARCH GOALS AND STRATEGIES

The broad goals of this study were: (1) to verify whether the extracellular ligninolytic enzymes of *P. chrysosporium* depolymerize a water-insoluble lignin from a natural source which was not significantly different from lignin as it occurs in the lignocellulosic matrix; (2) to determine the differences in how the two classes of peroxidases, lignin peroxidases (LIPs) and manganese peroxidases (MNPs) depolymerize lignin; and (3) to identify soluble products whose release could be used to follow the rate of lignin depolymerization, in order to determine whether the macroporous structure of lignocellulose limits its accessibility to the ligninolytic enzymes. The specific objectives of the proposed study were to: (1) demonstrate whether any soluble lignin-derived products are released from lignin by LIPs and/or MNPs, and, if so, their identities; (2) determine whether any significant modification of the solid lignin occurs due to the action of LIPs and/or MNPs; (3) characterize the major soluble products which are formed so that in the future, a method by which measurement of these products may be used to determine rates of lignin depolymerization could be developed; and, (4) determine the roles of lignin peroxidases (LIPs) and manganese peroxidases (MNPs) in *in vitro* depolymerization of insoluble lignin polymer.

This study was composed of five separate parts dealing with engineering design and optimization, modelling, lignin chemistry, microbiology and biochemistry, and analytical chemistry. These parts were combined in the development of a simple, inexpensive reactor system for the *in vitro* degradation of insoluble natural lignin by extracellular peroxidases, which has not previously been proven to occur (Tien, 1987; Boominathan and Reddy, 1992). This chapter is provided as a preliminary discussion about why and how each part of the project was approached, and how each part fits together into the whole. A flow chart indicating the general strategy for the work is presented in Figure 3.1.

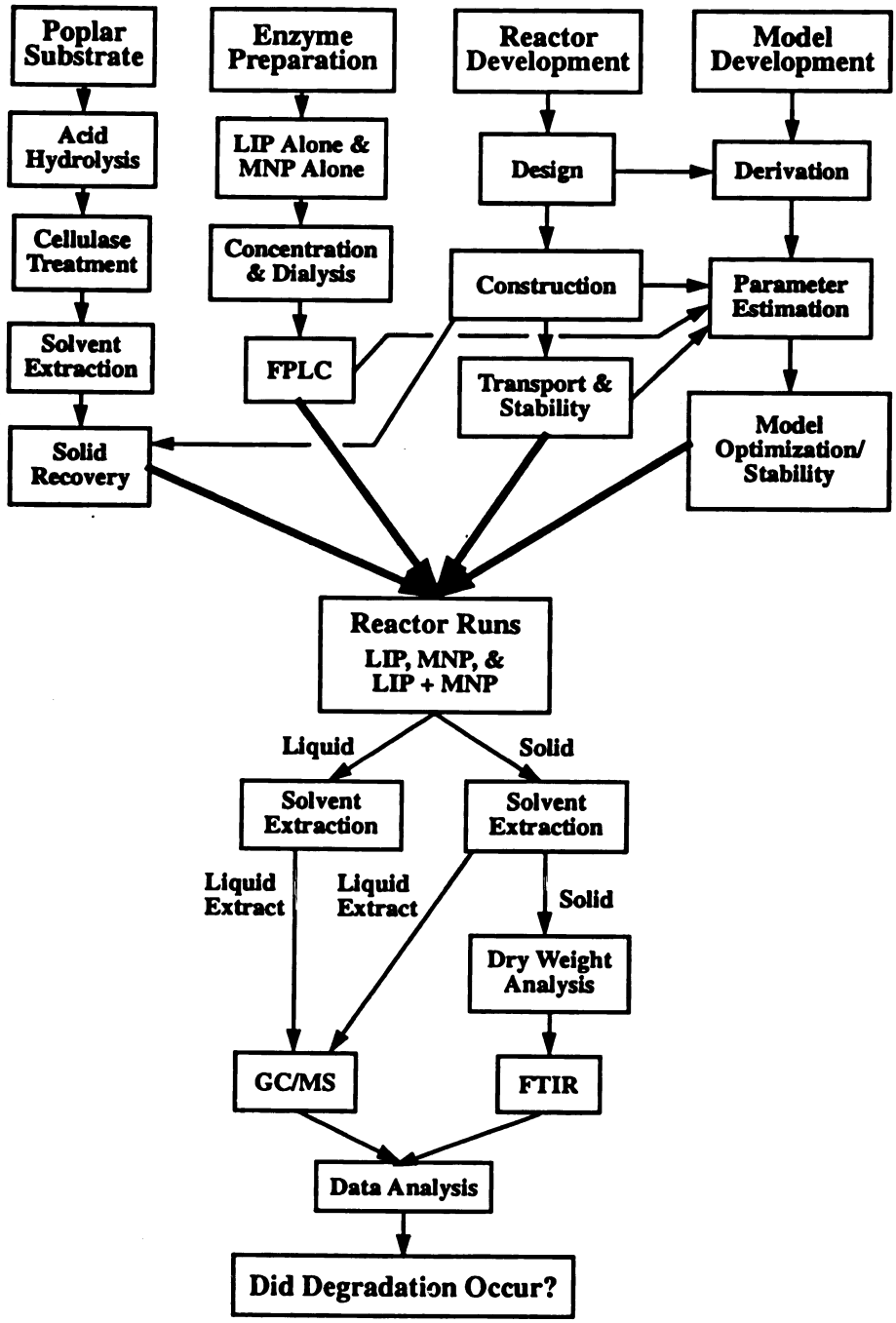

Figure 3.1: Flowchart indicating the strategy for this study and how each part contributes to other the parts. All steps in the top half of the figure contribute directly to the design, development, and operation of the reactor for the *in vitro* lignin degradation experiments.

3.1 Hypotheses

The hypotheses for this study were: (1.) That a relatively simple and inexpensive reactor system could be developed which could maintain reactant and enzyme concentrations at levels optimal for the action of LIPs and MNPs of *P. chrysosporium*; (2.) That *in vitro* lignin depolymerization would be achieved by one or the other of these enzymes, using a high molecular weight, water-insoluble lignin isolated from a natural source instead of low molecular weight synthetic lignins used in previous studies; (3). That the extracellular ligninolytic enzymes of *P. chrysosporium* (LIPs and MNPs) are both involved in the depolymerization of insoluble natural lignin; and (4.) That MNPs modify the high molecular weight, insoluble lignin polymer, making it a better substrate for the LIPs, which then depolymerize the lignin by release of low molecular weight fragments.

3.2 Research Strategies

3.2.1 Choice of Substrate

The insoluble substrate chosen for these studies was an insoluble lignin isolated from ground poplar wood flour (*Poplus*) obtained through the NSF Center for Microbial Ecology at Michigan State University (see Chapter IV). The desired substrate was one essentially free of cellulose and hemicellulose so that masking of lignin absorbances by cellulose and hemicellulose absorbances would not occur when FTIR was used to characterize the solid lignin (carbohydrates absorb IR radiation in same region as lignin).

3.2.2 *In vivo* vs *In vitro* Depolymerization of Insoluble Lignin

Previous studies with soluble lignin model compounds have suggested that LIPs and MNPs depolymerize lignin; however, no evidence directly linking these activities to depolymerization of unmodified insoluble lignin in aqueous media has been reported. *In vivo* depolymerization of lignin (by the fungus), while technically much easier to accomplish, would not supply the necessary data on soluble product formation since these compounds would be further metabolized by the fungus. *In vitro* depolymerization of

lignin by lignin peroxidases has been achieved with partially soluble synthetic lignin (see Chapter II), and with insoluble lignocellulose when H_2O_2 was supplied transiently by glucose oxidase. However, these studies have relied on detection of ^{14}C-containing compounds being solubilized. In this study, the *in vitro* experiments were chosen to provide direct evidence of lignin depolymerization by following changes in the chemical composition of the insoluble lignin and the major soluble products formed.

3.2.3 Choice of Reactor System

The system chosen for the *in vitro* reaction studies on insoluble lignin was a small dialysis reactor. The reactor was operated such that the concentration of H_2O_2 in contact with the enzymes would not be difficult to control. This is necessary because high H_2O_2 concentrations inactivate the enzymes, and because consumption of H_2O_2 by oxidation of lignin is very slow relative to rates of consumption in the oxidation of VA. The reasons for this choice of reactor system are discussed below.

A number of important points were considered in the design of this study (refer to Chapter II for discussions of these topics): (1) H_2O_2 and VA are required for the degradation of lignin by LIP; (2) H_2O_2 inactivates the enzymes over time; (3) H_2O_2 competitively inhibits the oxidation of VA to veratraldehyde, a reaction which is necessary for stabilization of LIP activity against inactivation by H_2O_2; (4) the peroxidases of *P. chrysosporium* are difficult to obtain in large quantities, so only fairly small quantities of enzyme would be available; and (5) degradation of insoluble lignin has been shown to be very slow as compared to the rapid reaction rates observed with lignin model compounds and with synthetic lignins in aqueous organic solvents. Thus, large amounts of enzyme relative to the amount of lignin present were used in order to shorten the time needed to see chemical changes in the lignin and production of soluble lignin-derived products, and small amounts of lignin were used so that less enzyme would be needed. Finally, the multiple roles of VA in the culture and the adverse effects of high H_2O_2 concentrations on enzyme activity necessitated the development of a feasible

method for control of the concentrations of H_2O_2 and VA in contact with the enzyme, since without this control, depolymerization would likely not occur (Olsen *et al.*, 1991; Hammel *et al.*, 1993).

Three methods were considered: (1) supply of H_2O_2 by enzymatic generation from glucose by glucose oxidase and metered addition of VA; (2) metered addition over time of both H_2O_2 and VA; and (3) transient supply of H_2O_2 and VA by transport processes across a membrane. The main drawback to Method 1 is that, glucose oxidase is most active near pH 5 (Olsen *et al.*, 1991), while LIP is nearly inactive at this pH (LIP is most active at pH 2.5 (but least stable)) (Boominathan and Reddy, 1992). Thus, using Method 1 would mean that longer reaction times would be necessary to see any chemical change in the insoluble lignin. If Method 2 were chosen (as done by Hammel *et al.*, 1991 and Hammel *et al.*, 1993), the reaction mixture would be significantly diluted over the course of the run, which would only serve to lengthen reaction times by decreasing the amount of reaction per unit volume of the solution. With Method 3, the rates of supply and consumption could be regulated by adding concentrated, small volume pulses of H_2O_2 and VA to the reactant reservoir and LIP and/or MNP to the reaction chamber, without significantly increasing the volume of the reaction mixture (volume increases over 12 hours of reaction were kept to 8 %, 10 %, and 16 % of the initial volume of the reaction mixture for MNP alone, LIP alone, and LIP + MNP; see Chapter IV). Thus, the dialysis reactor was chosen.

3.2.4 Choice of Reaction Conditions

A recent patent application (Olsen *et al.*, 1991) described a process in which insoluble paper pulp was treated *in vitro* with a mixture of xylanases, MNPs, and LIPs. In this process, H_2O_2 was supplied transiently by glucose oxidase. The rates of depolymerization were still very slow, however, because glucose oxidase operates best around pH 5, while the lignin peroxidase optimum is 2.5. The pH was chosen to be 3.5 for this study, as a tradeoff between enzyme stability and good activity. The reaction

temperature was chosen as 37 °C since the fungus also grows well at this temperature. Reactant concentrations in contact with the enzyme were chosen by maintaining the levels within ranges specified in the patent described above.

3.2.5 Choice of Solid Measurement Technique

It was decided early on that chemical changes in the insoluble lignin polymer would be measured by FTIR combined with Partial Least Squares Regression (PLS). Solid-state ^{13}C-NMR using CP/MAS was available, but this technique requires relatively large amounts of sample, and long analysis times (and would thus be very expensive). Chemical techniques, while inexpensive, would require large amounts of sample for complete analysis. Finally, UV spectroscopy simply would not have provided enough information on the chemical composition of the solid lignin to make a supportable case that depolymerization or modification had occurred.

FTIR equipment for the measurements was readily available through the Michigan Biotechnology Institute, Lansing, MI. In addition, the KBr pellet FTIR/PLS technique required only 1.5 mg of dried sample per run, so sufficient sample (20 mg would be treated) would be available for replicate measurements. The use of isolated lignin instead of lignocellulose, as described above, circumvents the problem of masking of lignin peaks by cellulose and hemicellulose. Any changes in spectral peak areas relative to untreated insoluble lignin could then be determined by peak deconvolution and integration using the PLS technique developed at the National Renewable Energy Laboratory (NREL, Golden, CO) (Hames *et al.*, 1991).

3.2.6 Choice of Liquid Measurement Technique

Gas Chromatography/Mass Spectrometry (GC/MS) has been widely used for the characterization soluble lignin degradation products in complex mixtures, and was thus well suited for this study. GC/MS analysis was readily available through the MSU-NIH Mass Spectrometry Facility at Michigan State University. Pyrolysis-GC/MS has been successfully employed on a variety of lignocellulose and lignin samples, but the

proce

availa

comp

Thus,

procedure is both time-consuming and expensive, in addition to not being readily available at Michigan State University. Volatilization of low molecular weight phenolic compounds by derivatization, as would be necessary for the GC/MS is also well studied. Thus, GC/MS was chosen to characterize soluble lignin-derived products.

CHAPTER IV: MATERIALS AND METHODS

4.1 Substrate

The water-insoluble lignin substrate for this study was isolated from a hybrid poplar grown at the Kellogg Biological Station for the Center for Microbial Ecology at Michigan State University. The clone (*Poplus eugeneii*) is a hybrid between *Poplus nigra* and *Poplus deltoides* and has been designated *Poplus* × *euramericana*. The harvested poplar was ground in a Wiley mill to about 60 mesh before isolating the lignin for use as substrate in biodegradation studies. The lignin isolation was carried out in three steps: (1) Dilute acid hydrolysis in a plug flow reactor; (2) Treatment with cellulase; and (3) Exhaustive extraction at 37 °C with increasingly polar solvents and subsequent rehydration. These steps are described in the following sections.

4.1.1 Acid Hydrolysis Pretreatment

Dilute acid hydrolysis pretreatment of Native (untreated) poplar was performed in a high temperature plug flow reactor system as described by Allen *et al.* (1983). A schematic of the reactor system used (MBI High Temperature Flow Reactor, Michigan Biotechnology Institute, Lansing, MI) is shown in Figure 4.1. The reactor is fed from a 20 L feed tank by a Moyno pump (moving cavity positive displacement pump, Robbins-Myer, Springfield, OH) with 18 stages, which was designed to handle slurries at up to 1650 psig and flow rates from 1 to 8 L/min. The reactor is constructed of 0.5" o.d. stainless steel tubing with 0.048" wall thickness, with a total reactor volume of 190.1 mL. High temperatures are attained by the injection of steam through a series of drill holes near the inlet of the reactor. A 1 mm orifice is located near the end of the reactor at which the reaction mixture is flashed from reactor pressure and temperature to atmospheric pressure (and 100 °C). The remaining steam is then condensed and the pretreated slurry collected at the reactor outlet. Temperature is controlled by steam addition, and residence time is controlled by mass flow rate of the slurry in conjunction with steam addition. Operating pressure is typically about 50 psi above the steam

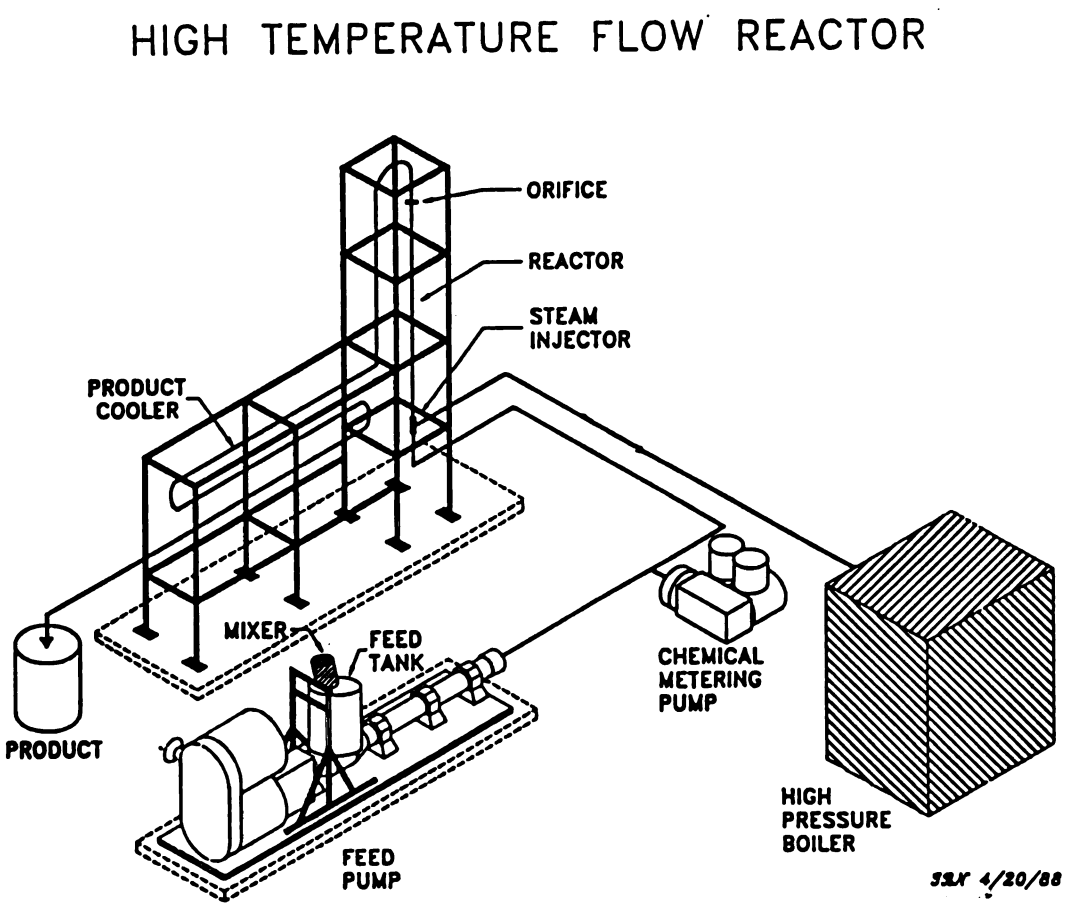

Figure 4.1: Schematic diagram of the MBI High Temperature Flow Reactor.

saturation pressure at the desired reactor temperature.

The pretreatment was carried out at 220 °C on a 5.0 % (w/v) slurry, with the addition of 1.0 wt. % H_2SO_4. The nominal residence time for the pretreatment was 7.3 seconds. The pretreated slurry was then washed free of acid and solubilized compounds by filtration with distilled water, collected and stored at 4 °C as a wet filter cake.

4.1.2 Cellulose Removal

Water-insoluble isolated lignin containing little carbohydrates was prepared from the pretreated poplar by cellulolytic hydrolysis. The enzymatic hydrolysis was carried out in stoppered 250 mL Erlenmeyer flasks with crude cellulase powder from *Trichoderma reesei* (Rutgers C30, U.S. Army Natick Research and Development Center, Natick, MA) with a reported cellulase activity of 0.38 FPU/mg enzyme powder (0.408 FPU/mg dry enzyme powder). In addition, the cellulase, which has very low levels of β-glucosidase, was supplemented with Novozym TN 188, a liquid β-glucosidase from *Aspergillus niger* (Novo Industries, Denmark) with a β-glucosidase activity of 588 Units/mL. The β-glucosidase was added in order to minimize cellobiose accumulation, which inhibits the cellobiohydrolase activity of the *T. reesei* cellulase complex (Marsden and Gray, 1986). Hydrolysis was performed at the optimum conditions (Marsden and Gray, 1986) of 50.0 °C and pH 4.80. The reaction mixture, preheated to 50 °C by the time of enzyme addition, consisted of citrate buffer (50 mM, pH 4.80), Rutgers C30 cellulase (40.8 FPU/g substrate), Novozym TN 188 β-glucosidase (40.8 Units/g substrate), and 4 % (w/v) oven-dried equivalent of wet substrate. Sodium azide is normally used as preservative in this procedure, but none was added since azides bind irreversibly to the heme group of lignin peroxidase (Tien, 1987), and the final lignin residue was to be used for lignin peroxidase and manganese peroxidase degradation studies.

Reaction was carried out at 200 rpm in a shaker bath. Homogeneous 2 mL samples were withdrawn at various times and quenched by adding 10 μL of 72 % H_2SO_4

(this stops the reaction by precipitating the cellulase). The samples were then neutralized with a scoop of $PbCO_3$ (powder, Sigma), the insoluble $PbSO_4$ was removed by filtration, and the glucose concentration was measured by HPLC with a BioRad HPX-87P Carbohydrate column. Glucose yield from the enzymatic hydrolysis was calculated as the percent of potential glucose in the original sample which was formed as a result of the hydrolysis:

$$\%\,Yield = \frac{grams\ glucose\ formed}{grams\ potential\ glucose} \times 100 \qquad (4\text{-}1)$$

Hydrolysis was continued until no increase in yield was measured in consecutive samples (about 48 hours). At the end of the enzymatic hydrolysis, the slurries from all flasks were combined and the solids collected by filtration on Whatman GF/D glass fiber filter paper. The filter cake was resuspended in distilled water, acidified with 50 mM H_2SO_4 (to precipitate the cellulase) and washed free of acid and cellulase by filtration with 1 M NaCl, until the pH was once again neutral and no protein was detected in the filtrate, as measured by the Bradford Method (Bradford, 1976).

4.1.3 Solvent Extraction of Isolated Lignin

Solvent extraction of the lignin isolated by enzymatic hydrolysis was carried out in order to remove small molecular weight lignin fragments, if any, produced during the initial pretreatment in the plug flow reactor; this was expected to leave a high molecular weight, completely water-insoluble lignin residue which resembled lignin as it occurs in the lignocellulose matrix. The extractions were carried out sequentially on a 10 gram (dry weight) batch of lignin which was initially saturated with water. Each extraction step was carried out in a reagent bottle with 100 mL of solvent per gram dry weight of lignin. The bottle was secured on its side (capped with a teflon lined cap) on a rotary shaker platform at 37 °C and 400 rpm for 30-40 minutes per extraction step. Three extraction solvents with increasing polarities (chloroform, ethyl acetate, and methanol) were used in consecutive extractions. The insoluble lignin was collected after each step

by filtration on Whatman GF/C glass fiber filter paper. Extraction with each solvent or solvent mixture was determined to be complete when the solvent after extraction was colorless and had no absorbance at 280 nm (absorbance maximum for aromatic rings). The order and number of extraction steps are shown in Table 4.1. About 3.6 % of the dry weight of the solid was removed as extractable material in these steps (see Chapter V).

4.1.4 Measurement of Substrate Compositions

Carbohydrate and lignin compositions were determined using the Quantitative Saccharification Method of Saeman *et al.* (1945). In this procedure, lignocellulosic samples were subjected first to hydrolysis with 72 % H_2SO_4 at 30 °C for one hour and subsequently with 4 % H_2SO_4 at 121 °C for one hour in an autoclave. The remaining insoluble portion was defined as Klasson lignin with extractives and ash. The liquor from the hydrolysis was measured for carbohydrates by HPLC, using a BioRad HPX-87P Carbohydrate column. The procedure was as follows.

To begin, 200.0 $\pm$ 20.0 mg of ground, oven-dried sample was weighed, to the nearest 0.1 mg, into an 18×150 mm test tube. Two milliliters of 72 % (w/w) H_2SO_4 were then added and the mixture was mixed thoroughly with a glass stir-rod (which was left in the tube). The sample was then placed in a 30 °C water bath for one hour and was mixed with the stir rod at 10, 20 and 40 minutes. At the end of one hour, the sample was transferred quantitatively to a 500 mL Erlenmeyer flask using 28 mL of distilled water per 1 mL of 72 % H_2SO_4 originally used (56 mL of distilled water). The flask was then covered with aluminum foil and autoclaved for one hour at 121 °C. The acid insoluble portion was quantitatively collected by filtration on a tared 30 mL coarse porosity fritted gooch crucible to which a 1.2 μm porosity Whatman GF/C glass fiber filter paper disk had been added to improve the filtration rate and recovery of small particles. Subsequent drying of the insoluble portion to constant weight in a 105 °C oven, cooling in a desiccator and weighing yielded the mass of Klasson lignin with

Table 4.1: Order of solvent extractions performed on the C-AH lignin residue. Extractions were carried out consecutively on a single 10 g sample of the residue.

Extraction No.	Weight of lignin (g)	Solvent 1	Solvent 2	Volume Ratio (1:2)	Total Volume
1	10.00	$CHCl_3$	EtOAc*	1:1	1 L
2	10.00	$CHCl_3$	EtOAc	1:1	1 L
3	10.00	$CHCl_3$	EtOAc	1:1	1 L
4	10.00	$CHCl_3$	EtOAc	1:1	1 L
5	10.00	$CHCl_3$	CH_3OH	1:2	1 L
6	10.00	$CHCl_3$	CH_3OH	1:2	1 L
7	10.00	$CHCl_3$	CH_3OH	1:2	1 L
8	10.00	$CHCl_3$	CH_3OH	1:2	1 L
9	10.00	CH_3OH	---	100 %	1 L
10	10.00	CH_3OH	DI H_2O	3:1	1 L
11	10.00	CH_3OH	DI H_2O	1:1	1 L
12	10.00	CH_3OH	DI H_2O	1:3	1 L
13	10.00	DI H_2O	---	100 %	1 L
14	10.00	DI H_2O	---	100 %	1 L
15	10.00	DI H_2O	---	100 %	1 L
16	10.00	DI H_2O	---	100 %	1 L
17	10.00	DI H_2O	---	100 %	1 L
18	10.00	DI H_2O	---	100 %	2 L

* EtOAc = Ethyl Acetate

extractives and ash. The liquor from the hydrolysis was quantitatively diluted with distilled water to 100.00 ± 0.08 mL in a volumetric flask. Twenty milliliters of this solution were then stored in a leak-proof polyethylene bottle at 4 °C for further analysis.

Determinations of the carbohydrate concentrations in the diluted hydrolysis liquor were made by HPLC using a BioRad HPX-87P column. Degassed HPLC-grade water (from a Millipore deionizing system) was used as eluent. Conditions for the chromatography were 0.500 mL/min and 70 °C. The column system consisted of carbohydrate deashing system (BioRad, Holder Cat. No. 125-0139, Cartridges Cat. No. 125-0118) and a GC620 Guard Column System (Interaction Chemicals) which contained a lead-based ion-exchange resin similar to that of the chromatography column. Samples were prepared by first neutralizing 3 mL with a scoop of $PbCO_3$ (powder form, Fisher Scientific), centrifuging for 3 min at 14,000 rpm and filtering the supernatant through a 0.45 μm syringe filter into an autoinjector vial.

Concentrations determined by HPLC were corrected for recovery losses incurred during the high temperature step by performing an additional experiment to determine the recoveries of the various wood sugars when subjected to this step in monomer form. In this recovery experiment, solid samples containing all five wood sugars were subjected to the autoclave step of the procedure and then treated as normal lignocellulosic samples. The fractional recoveries were then defined as:

$$R_i = \frac{m_{i,f}}{m_{i,i}} \qquad (4\text{-}2)$$

where R_i is the fractional recovery of sugar i, $m_{i,f}$ is the mass of sugar i recovered from the experiment (measured by HPLC), and $m_{i,i}$ is the mass of sugar i initially present in the sample.

In addition, in polymeric form, wood carbohydrates are present as anhydro-monomers, so to complete the material balance, the mass of each sugar must be

multiplied by a "polymerization factor", as defined below:

$$F_i = \frac{(MW_i - MW_w)}{MW_i} \tag{4-3}$$

where F_i is the polymerization factor for sugar i, MW_i is the molecular weight of sugar i, and MW_w is the molecular weight of water.

For any wood sugar, then, the potential amount in the original sample, expressed as a percent, is:

$$P_i = \frac{10C_i}{WR_i} \tag{4-4}$$

where P_i is the percent potential sugar i, C_i is the diluted liquor concentration (g/L) of sugar i, and W is the mass of original lignocellulosic sample (g). R_i is used as defined in equation (4-2); note that R_i must be between 0 and 1. It should also be noted that since the P_i values are based on the masses of their free sugars and not their anhydro-forms, the material balance need not sum to 100 % or less. The carbohydrate contents, expressed in their anhydro- forms (for example, glucan instead of glucose), are then:

$$P_{M,i} = P_i F_i \tag{4-5}$$

where $P_{M,i}$ is the percent potential sugar monomer i, and F_i and P_i are as defined in the above equations, respectively. The values of $P_{M,i}$, then, must sum to 100 % or less. When combined with the percent lignin with extractives and ash, calculated by dividing the mass of the acid insoluble fraction by the initial sample mass and multiplying by 100 %, these values complete the material balance (neglecting uronic acid content and recovery errors).

4.2 Enzyme Preparation

LIP and MNP enzymes used in this study were isolated from the extracellular fluid from nitrogen-limited shake flask cultures of *Phanerochaete chrysosporium*, strain BKM-F-1767 (ATCC 24725) obtained from the laboratory of Dr. C.A. Reddy, Department of Microbiology and Public Health, Michigan State University.

4.2.1 Culture Maintenance

Stock cultures were maintained (Tien and Kirk, 1988) on malt agar extract slants, pH 4.5, at 4 °C. The malt agar media contained 2 % (w/v) agar (Difco Bactoagar), 1 % (w/v) malt extract (Difco), 55.5 mM glucose, 14.70 mM KH_2PO_4, 4.057 mM $MgSO_4$, 6.66 mM L-asparagine, 2.81 μM thiamine hydrochloride, 1 % (w/v) malt extract, 0.2 % (w/v) peptone (Difco), and 0.2 % (w/v) yeast extract (Difco). The slant cultures were subcultured every 4 to 6 months by adding 3 mL of sterile water to the old slant, scraping the surface of the agar to suspend the conidiospores, and inoculating a new slant with one loopful of the suspension. The new slant was then incubated for 4 to 5 days at 37 °C and then stored at 4 °C.

Frozen conidiospore stocks were prepared for inoculation of stationary starter cultures. This was done by adding 3 mL of sterile water to a stock slant, scraping the surface of the agar to suspend the conidiospores, and plating out 0.2 mL of the suspension onto a plate containing identical media. After incubation for 4 to 6 days at 37 °C, conidiospores were harvested by adding 5 mL of sterile water to the plate and scraping the surface of the agar to suspend the conidiospores. The conidial suspension was then filtered through sterile glass wool to remove mycelia, and the absorbance at 650 nm was measured (1 OD is equivalent to 5×10^6 conidiospores/mL). The suspension was then diluted to 15-20 OD with sterile water, dispensed to sterile culture tubes, and frozen at -20 °C.

4.2.2 Culture Conditions

Enzyme production runs were carried out, using aseptic techniques, at 37 °C in agitated acetate-buffered, nitrogen-limited culture with glucose as carbon source as described by Tien and Kirk (1988). The defined culture medium contained 1.09 mM diammonium tartrate as the nitrogen source and 55.5 mM glucose as the carbon source. The media also contained 14.70 mM KH_2PO_4, 5.90 mM $MgSO_4$, 0.900 mM $CaCl_2$, 2.81 μM thiamine hydrochloride, 0.5 g/L Tween 80 (not added in stationary starter cultures), 20.0 mM acetate (pH 4.50) and 0.4 mM veratryl alcohol (VA). The following trace elements were also added: 0.500 mM nitriloacetate trisodium salt, 1.20 mM NaCl, 25.2 μM $FeSO_4$, 53.0 μM $CoCl_2$, 24.3 μM $ZnSO_4$, 4.37 μM $CuSO_4$, 1.48 μM $AlK(SO_4)_2$, 11.3 μM H_3BO_3, and 2.89 μM Na_2MoO_4. Depending on the enzyme mixture desired, Mn(II) was added (as $MnSO_4$) to the shake flask cultures in various amounts, as follows: (1) LIPs only, no Mn(II) added (denoted "D5NoMn"); and (2) MNPs only, 100.0 ppm of Mn(II) added (denoted "D4HiMn"). The starter cultures always contained 11.5 ppm of Mn(II) (Tien and Kirk, 1988).

4.2.3 Enzyme Production Procedure

Stationary starter cultures were begun by measuring 75 mL of sterile media into a sterile 1500 mL Fernbach flask and inoculating to 0.15 OD with frozen conidiospore stock (prepared as described above) and gently mixing, taking care not to splash the thin layer of liquid onto the sides of the flask. The flasks were then stoppered with a sterile stopper of glass wool covered with cheesecloth, sealed with three layers of parafilm to prevent excessive evaporation, and incubated for 24-48 hours at 37 °C. The mycelial mat produced was then homogenized in a sterile homogenizer cup (Cat. No. 6301 0001 0C, Virtis, Gardiner, NY) and used as inoculum for the shake flask culture.

To begin a shake flask culture, 81 mL of sterile media containing the desired Mn(II) concentration were dispensed into sterile 250 mL rubber stoppered Erlenmeyer flasks. 9 mL of homogenized mycelia from the starter culture were then added to the

flask. The headspace (160 mL) was flushed initially and then every 24 hours with pure oxygen for approximately 3 minutes at a flow rate of 1 L/min. The flasks were agitated at 175 rpm on a rotary shaker table (New Brunswick Gyrotory G-10) with an eccentricity of 2.5 cm. The cultures were harvested either on day 4 or day 5, depending on the enzyme mixture being produced and the level of enzyme activity on that day: (1) LIPs only, day 5 (D5NoMn); and (2) MNPs only, day 4 (D4HiMn). Only one run (70 flasks) was necessary for the D4HiMn cultures, since the MNP activity was about 3 times the expected levels. For the D5NoMn cultures, however, the LIP activity was about 30 % of the expected levels, and many flasks produced significant levels of MNP, probably due to contaminating Mn(II) present in the distilled (tap) water. Thus, future D5NoMn culture media was made up with deionized/distilled water from a Millipore deionizing filter system. The LIP levels were still low, however, so seven sets of 70 flasks each were run. Each flask was assayed on day 5 for MNP activity, and only flasks containing less than 100 U/L of MNP (by MNP Assay #1) were kept. All remaining flasks were combined and stored for later concentration.

The extracellular fluid (EF) from each type of culture was collected and stored frozen at -20 °C until all production runs for the desired enzyme were completed. The bottles of EF were then thawed and filtered through wet cheesecloth to remove extracellular polysaccharides (precipitated due to freezing). The EF was then concentrated by ultrafiltration in two steps. The first step was done with an Amicon Model S1-10 Spiral-Wound Ultrafiltration Cartridge with a PM membrane (10,000 MWCO) in order to reduce the volume of the EF from 6.3 L to about 300 mL for the D4HiMn EF, and from 40 L to about 300 mL for the D5NoMn EF. The 300 mL remaining for each case were then concentrated to 20-30 mL in a 500 mL batch ultrafiltration apparatus (Amicon), also with a 10,000 MWCO PM-type membrane, and using N_2 gas at 60 psig as driving force for the ultrafiltration. Both concentrates were then dialyzed twice at a ratio of 4000 mL of buffer per 20-30 mL of concentrate (133:1)

using 6000-8000 MWCO dialysis tubing (Cat No. 132703, Spectrum Medical Industries, Los Angeles, CA). The first dialysis was done with 10 mM sodium acetate at pH 7.0, while the second was with 5 mM phosphate buffer, pH 6.0 (better for storage of the enzyme). Aliquots of the dialyzed concentrates were then pipetted to Eppendorf tubes, capped, and stored frozen at -20 °C for future use in kinetic studies, temperature and pH stability studies, FPLC profiles, and *in vitro* reactor runs.

4.2.4 Enzyme Activity Assays

LIP activity was determined by spectrophotometrically measuring the rate of formation of veratraldehyde from veratryl alcohol at pH 2.5, room temperature (23 °C) and at a wavelength of 310 nm as described by Tien and Kirk (1988). One U/L of LIP activity is then defined as one μmole of veratraldehyde formed per liter per minute at these conditions, using an extinction coefficient of 9300 M^{-1} cm^{-1}. A detailed description of this assay is given in Appendix A (LIP Assay).

MNP activity was measured as described by Kuwahara *et al.* (1984) and Michel *et al.* (1991) at 30 °C, pH 4.5, and a wavelength of 610 nm. The reaction time was 4 minutes, and sample volumes of 20 or 40 μL were used. To stop the reaction, 40 μL of 2 N NaOH were added, bringing the total volume to 1.06 or 1.08 mL, depending on the sample volume. One U/L is then defined as one μmole of phenol red oxidized per liter per minute, using an extinction coefficient (Michel *et al.*, 1991) of 4460 M^{-1} cm^{-1}. A detailed description of this assay is given in Appendix A (MNP Assay #1).

MNP was also assayed by following the oxidation of phenol red at room temperature and a wavelength of 530 nm. In this assay (Olsen *et al.*, 1991), instead of letting the reaction go for 4 minutes and then stopping it with NaOH, which changes the color for measurement at 610 nm, the absorbance change is transiently measured at 530 nm. For this assay, one U/L is defined as an increase of one absorbance unit per minute per liter of sample volume. A detailed description of this assay is given in Appendix A (MNP Assay #2). Measurement of MNP by this assay was necessary to determine

Mn(II) concentrations for the *in vitro* studies (described later). Measurement of identical samples with both assays gave a relationship of 2.08 U (MNP Assay #2) per 1 U (MNP Assay #1).

4.2.5 FPLC Profiles

LIP and MNP isoenzyme profiles for each enzyme mixture were determined by FPLC with a Pharmacia FPLC System (Pharmacia, Piscataway, NJ). The system consisted of a Liquid Chromatography Controller LCC-500 Plus, two P-500 pumps, a mixer, Motor Valve MV-7, Mono Q Column, Single Path Monitor UV-1, and Fraction Collector FRAC-100. The chromatography was performed at 23 °C, a flowrate of 1 mL/min, a pH 4.5 sodium acetate gradient from 10 mM to 1 M, and a column loading of 200 μg of protein. Profiles were monitored by the absorbance at 409 nm (maximum absorbance wavelength for the heme group) with a chart recorder over the course of the run. Fractions were collected and assayed for LIP and MNP activity in order to assign each peak in the FPLC chromatogram. Percentages of each isoenzyme were determined using peak areas. Since no on-line data system was available to store the chromatograms, peak areas were measured by cutting out the peaks on a copy of the chart recorder printout and weighing them.

4.3 *In vitro* Reactor System

A small-scale reactor system for the *in vitro* treatment of water-insoluble lignin with lignin peroxidases and manganese peroxidases was developed which was designed to regulate the concentrations of H_2O_2 and veratryl alcohol (VA) in contact with the peroxidases over long periods of time (6 to 12 hours). A number of important points were considered in the development of the reactor; they are restated here for convenience: (1) H_2O_2 and VA are required for the degradation of lignin by LIP (Tien, 1987; Boominathan and Reddy, 1992; de Jong *et al.*, 1994); (2) H_2O_2 inactivates the enzyme over time (Tien, 1987; Hammel *et al.*, 1993; de Jong *et al.*, 1994); (3) H_2O_2 competitively inhibits the oxidation of VA to veratraldehyde (Tien *et al.*, 1986); (4) the

peroxidases of *P. chrysosporium* are difficult to obtain in large quantities, so only small amounts of enzyme would be available for use; and (5) degradation of insoluble lignin has been shown to be very slow as compared to the oxidation rates for water-soluble lignin model compounds (Tien, 1987). The system developed was a small dialysis reactor which would transiently supply H_2O_2 and VA to the reaction at controllable rates (see Chapter III for the rationale behind this choice). This system is described below.

The dialysis reactor which was constructed for the *in vitro* lignin degradation experiments is depicted in Figures 4.2 and 4.3. The reactor was constructed in two halves, held together at a ground glass joint by a metal pinch-type clamp (Cat. No. C6121-2, Baxter Scientific, McGaw Park, IL). Both chambers of the reactor (Side A, reactant reservoir, and Side B, reaction chamber) were constructed with a sampling port for addition of pulses and recovery of solutions. The sampling ports were threaded so that they could be closed with open-hole vial caps sealed with teflon-faced rubber septa. The two chambers were separated by a 6000-8000 MW cutoff (pores smaller than LIP or MNP enzymes and lignin particles) dialysis membrane (Spectra/Por Dialysis Discs, No. 132478, Spectrum Medical Industries, Los Angeles, CA) with an average wet membrane thickness of 61.36 μm (measured). The volume of each chamber was approximately 2.0 mL, with an 0.5300 cm diameter opening between the chambers, giving an area available for transport of 0.2206 cm^2. A reactor holder was crafted from a No. 13 rubber stopper so that the reactor would fit snugly into a 125 mL Erlenmeyer flask clamp on the platform of a reciprocal shaker for agitation perpendicular to the plane of the membrane. The headspace (about 1 mL) of Side B was set up to be continuously flushed with humidified 100% O_2 through an 18 gauge needle inserted through the septum, and vented to the atmosphere through another 18 gauge needle; the O_2 was humidified at 37 °C by bubbling it through water and then the flow was metered to the reactors with variable area rotameters (Cat No. L-03216-00, Cole Parmer, Niles, IL). Also note that the reactor halves were silanized (Watson, 1985) prior to use to prevent

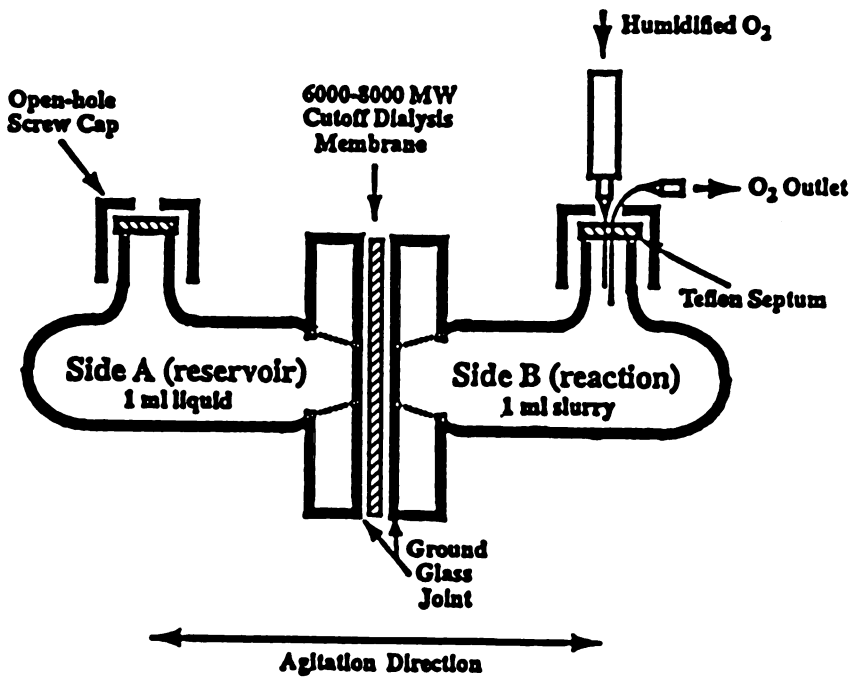

Figure 4.2: Schematic diagram of the dialysis reactor.

Figure 4.3: Photograph of an assembled dialysis reactor and its component parts.

binding of compounds released from lignin to the glass (a precaution for later GC/MS analysis).

4.4 Control Scheme for Dialysis Reactor

In order to maintain peroxide and VA concentrations in contact with the enzymes in side B, it was necessary to develop a predictive control scheme which determined peroxide and VA concentrations adjustments for Side A (necessary because of the small volume of the system). A mass balance was derived for each species involved, and the balances were joined into a control model and solved. The processes included in the balances included: (1) H_2O_2, VA, Mn(II), and Mn(III) (chelated with tartrate) transport across the membrane from Side A; (2) Rates of consumption of H_2O_2, VA, Mn(II), and Mn(III) in Side B due to reaction; (3) Rates of loss of H_2O_2 and VA due to decomposition at 37 °C and pH 3.50; and (4) Rates of loss of LIP and MNP activity due to decomposition at 37 °C and pH 3.50. These processes are dealt with in this section.

4.4.1 Species Transport

The transport of H_2O_2, VA, Mn(II), and Mn(III) across the dialysis membrane was treated as simple diffusion in a modified diaphragm cell (Cussler, 1986). Although diaphragm cells should be vertical in orientation (horizontal membrane) (Cussler, 1986), preliminary transport experiments in the dialysis reactor (vertical membrane) indicated that the transport of H_2O_2, VA, and Mn(II) could be described by simple diffusion (see Chapter V). Note that while diaphragm cells usually do not contain free headspace (Cussler, 1986), the dialysis reactor system used here does have about 1 mL of headspace in each side (see above).

The transport rate equations for diffusion of H_2O_2, VA, Mn(II), and Mn(III) across the membrane from Side A to Side B are (see Appendix B for derivation)

$$\frac{dC_A}{dt} = -\frac{D^{eff}_A}{lV_A}(C_A - C_B) \qquad \text{(B-4)}$$

and

$$\frac{dC_B}{dt} = \frac{D^{eff}A}{lV_B}(C_A - C_B) \qquad \text{(B-5)}$$

where C_i denotes concentration (mM) in side *i*, t is time (min), V_i is the chamber volume for side *i* (mL), *l* is the membrane thickness (cm), A is the membrane area available for transport (cm^2), and D^{eff} is the effective diffusion coefficient (cm^2/min).

Combining equations (B-4) and (B-5) and solving gives

$$\ln\left(\frac{C_A - C_B}{C_{A_o} - C_{B_o}}\right) = -\gamma D^{eff} t \qquad \text{(B-11)}$$

where

$$\gamma = \frac{A}{l}\left(\frac{1}{V_A} + \frac{1}{V_B}\right) \qquad \text{(B-10)}$$

Knowledge of the cell measurements, initial concentrations, and concentrations at a certain time into the experiment allows calculation of D^{eff}.

Experiments were performed to determine the values of the effective diffusion coefficients (D^{eff}) for H_2O_2, Mn(II), and Mn(III), and the dependence of D^{eff} for VA on concentration. In the first set of experiments, the transport of H_2O_2 across the membrane was measured with various driving forces over 10-12 minutes. $[H_2O_2]_A$ was varied from 50 mM to 5000 mM, while $[H_2O_2]_B$ remained constant at 8 mM. Four 10 μL samples were taken from Side B over the time range, and assayed for H_2O_2 by following the decolorization of Remazol Blue dye (to completion) by Horseradish Peroxidase (Type II, Sigma) using a set of H_2O_2 standards (calibrated with the absorbance at 230 nm with an extinction coefficient of 81 $M^{-1}cm^{-1}$ (Pick and Keisari, 1980)) to calculate concentrations. This assay is described in detail in Appendix A (H_2O_2 Assay). The data were then used

with equation (B-8) to calculate an average D^{eff} for H_2O_2.

In an analogous set of experiments, $[Mn(II)]_A$ was varied from 50 mM to 2000 mM, with $[Mn(II)]_B$ constant at 0 mM. Twenty microliter samples were withdrawn from Side A each hour over a 6 hr period, and $[Mn(II)]_A$ concentrations in these samples were measured by titration with EDTA (Harris, 1982; Clesceri *et al.*, 1989). $[Mn(II)]_B$ concentrations were calculated by difference. These data were then used with equation (B-8) to calculate an average D^{eff} for Mn(II).

Because Mn(III) is a relatively strong oxidizing agent (Glenn *et al.*, 1986), it does not remain as free Mn(III) in water (two Mn(III) atoms dismute to Mn(II) + Mn(IV)), but must be chelated to remain at that oxidation state (Glenn *et al.*, 1986; Wariishi *et al.*, 1992). Since the buffer to be used in the *in vitro* lignin degradation experiments was tartrate, and tartrate is a better chelator of Mn(III) than lactate (Wariishi *et al.*, 1992), it was decided to omit lactate from future reaction mixtures and to determine the diffusion coefficient of the Mn(III)-tartrate complex. Preliminary experiments, supported by published evidence on Mn(III)-chelate stability (Wariishi *et al.*, 1992), indicated that the Mn(III)-tartrate complex was not stable enough at 37 °C to allow for delayed concentration measurements. Since no on-line method of measuring the Mn(III)-tartrate complex concentration in the reactor was available, it was decided instead to estimate the effective diffusion coefficient of the Mn(III)-tartrate complex. The available literature indicated that Mn(III) has a coordination number of 6 (Mellor, 1979), and that tartrate binds to manganese ions as depicted in Figure 4.4 (Bell, 1977). This indicated that two tartrate molecules bind per Mn(III) atom. In addition, the bonds between each tartrate and the Mn(III) atom are planar (Ramakrishnan and Maroor, 1988). This information was used, with the software package Polygraf (Molecular Simulations, Inc., Burlington, MA) to find a likely energetic minimum for [Mn(III)-$tart_2$] in water. The structure of the predicted chelate complex is shown in Figure 4.5, with several measurements of the diameter of the complex. The center atom is the Mn(III), and the shaded area

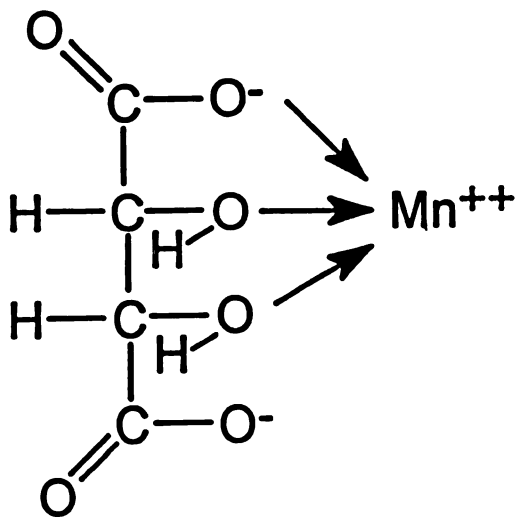

Figure 4.4: Mechanism of binding between a single tartrate molecule and a manganese ion in water (Bell, 1977).

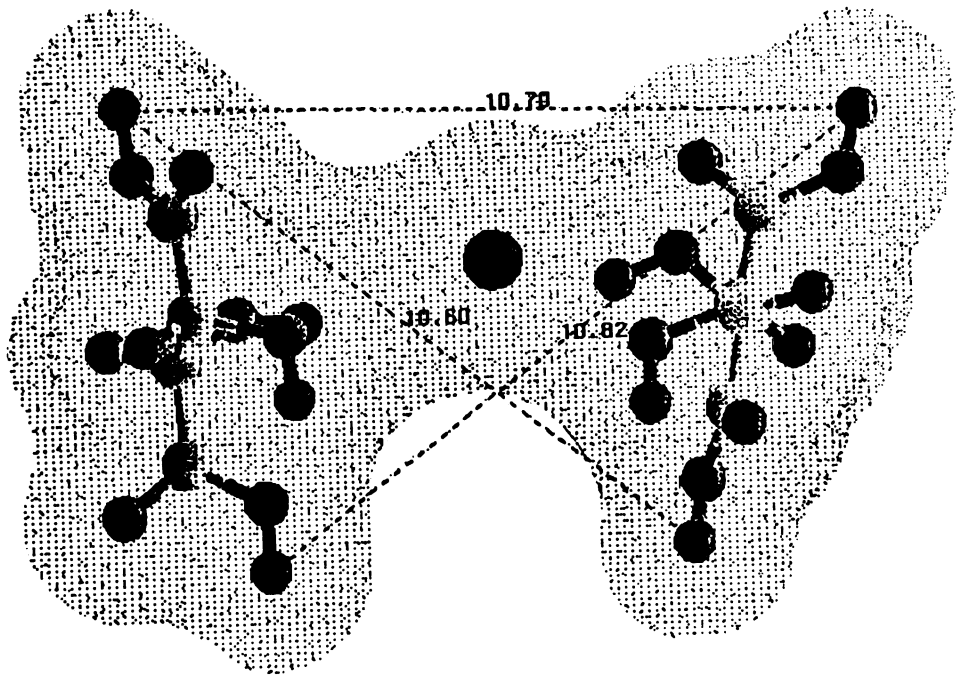

Figure 4.5: Graphical representation of the structure of an [Mn(III)-tart$_2$] complex as predicted by the molecular modelling software Polygraf (Molecular Simulations Inc., Burlington, MA).

surrounding the complex represents the charge density surface. The effective diffusion coefficient of [Mn(III)-tart$_2$] was then calculated from the average diameter of the chelate complex (rms average, 10.71 Å), the effective radius of Mn(II) in water (Bell, 1977) assuming that it is in a high spin state (Nicholls, 1974), and the measured effective diffusion coefficient for Mn(II). This was done by assuming that the ratio of the two effective diffusion coefficients was proportional to the inverse ratio of their radii, the result obtained by ratioing the Stokes-Einstein Equations (Bird *et al.*, 1960) for each species.

In the next set of experiments, the transport of VA across the membrane was measured with various driving forces over 10-12 minutes in a manner identical to that used for H_2O_2. $[VA]_A$ was varied from 50 mM to 2500 mM (the maximum $[VA]_A$ is lower than the maximum $[H_2O_2]_A$ because above 2500 mM, the transport did not increase much with an increase with concentration), while $[VA]_B$ remained constant at 10 mM. Four 10 μL samples were taken from Side B over the time range, and assayed for VA by measuring the total absorbance change (reaction completion) by LIP in an assay modified from the LIP Assay (Appendix A) using a set of VA standards to calculate concentrations. This assay is described in detail in Appendix A (VA Assay). The data were then used with equation (B-8) to calculate a value of D^{eff} for VA at each $[VA]_A$. The D^{eff} vs $[VA]_A$ data were then statistically fit using PEAKFIT (Jandel Scientific) to equation (B-6). To demonstrate the effect of concentration on viscosity, the viscosity of solutions of VA ranging from 0 to 2500 mM were measured in a capillary tube viscometer. A statistical fit of the viscosity (μ) vs [VA] data using PEAKFIT gave an exponential relationship (see Chapter V) which is consistent with relationships given in the literature (Bird *et al.*, 1960). This relationship was inserted into the Stokes-Einstein Equation (Bird *et al.*, 1960) to yield a concentration dependent effective diffusion coefficient for VA. The concentration-time data from the experiments were then fit by trial and error to the diffusion equation with concentration-dependent diffusion

coefficient. An additional exponential term was necessary to obtain a good fit to the data, and this was assumed to be the effect of molecular aggregation of VA molecules (relatively hydrophobic) in water, effectively increasing the molecular diameter of VA in water; therefore an additional term representing an exponential dependence of molecular aggregate radius was added to the Stokes-Einstein expression. This point is discussed in more detail in Chapter V.

Experiments were also conducted with H_2O_2 and VA together to see if the increased viscosity of the solution due to higher VA concentrations had an effect on D^{eff} for H_2O_2. The experiments were identical to those for H_2O_2 described above, except that the solution contained VA at various concentrations from 50 mM up to 2500 mM (both sides). $[H_2O_2]_A$ was varied from 50 mM to 5000 mM, and samples were measured with Horseradish Peroxidase as described in Appendix A (H_2O_2 Assay). No effect of solution viscosity was found on the effective diffusion coefficients for H_2O_2 or Mn(II). The actual concentrations of H_2O_2 and VA used in Side B during reactor runs (see Chapter V) were much less than 8 mM and 10 mM (the Side B concentrations used in the transport experiments), respectively; however, since the driving force (concentration in Side A minus concentration in Side B) was very large compared to the concentration in Side B, this difference was neglected.

4.4.2 Kinetics of Veratryl Alcohol Oxidation by LIP

The reactions for oxidation of veratryl alcohol to veratraldehyde by LIP, as proposed by Tien *et al.* (1986), are

$$H_2O_2 + Cpd0 \xrightarrow{k_1} CpdI + H_2O \qquad (4\text{-}6)$$

$$H_2O_2 + CpdI \underset{k_{-2}}{\overset{k_2}{\rightleftharpoons}} CpdI\text{-}H_2O_2 \qquad (4\text{-}7)$$

$$VA + CpdI \xrightarrow{k_3} CpdII\text{-}VA\cdot \qquad (4\text{-}8)$$

whe

and

pin:

of th

deri

Taki

To e

exce

inhib

appr

inhib

plots

Case

Case

$$CpdII\text{-}VA\cdot \xrightarrow{k_4} VA_{ox} + Cpd0 \qquad (4\text{-}9)$$

where Cpd0, CpdI and CpdII represent the different oxidation states of the LIP heme, and VA_{ox} is veratraldehyde (Tien *et al.*, 1986). These kinetics represent two substrate ping-pong kinetics with competitive inhibition by the first substrate and two-step reaction of the second (Tien *et al.*, 1986; Tien, 1987). The rate equation for these kinetics, derived in Appendix C, is

$$v=\frac{k_1k_3k_4[LIP]_o[H_2O_2][VA]}{k_3k_4[VA]+k_1k_3[H_2O_2][VA]+k_1k_4[H_2O_2](1+\frac{[H_2O_2]}{K_I})} \qquad (C\text{-}11)$$

Taking the reciprocal and canceling like terms gives

$$\frac{[LIP]_o}{v} = \frac{1}{k_1[H_2O_2]} + (1+\frac{[H_2O_2]}{K_I})(\frac{1}{k_3[VA]}) + \frac{1}{k_4} \qquad (4\text{-}10)$$

To evaluate the kinetic rate constants, 3 separate cases are needed: (1) Vary $[H_2O_2]$ with excess VA, and $[H_2O_2] << K_I$, so that [VA] is approximately constant and there is no inhibition; (2) Vary [VA] with excess H_2O_2, and $[H_2O_2] << K_I$, so that $[H_2O_2]$ is approximately constant and there is no inhibition; and (3) Vary [VA] with several inhibitory excess H_2O_2 concentrations. Then the data are plotted on double reciprocal plots and the kinetic constants determined as follows.

Case 1:

$$slope = \frac{1}{k_1}$$
$$intercept = (\frac{1}{k_3[VA]_o} + \frac{1}{k_4}) \qquad (4\text{-}11)$$

Case 2:

$$slope = \frac{1}{k_3}$$
$$intercept = (\frac{1}{k_1[H_2O_2]_o} + \frac{1}{k_4}) \qquad (4\text{-}12)$$

Case 3:

$$slope = \frac{1}{k_3}\left(1 + \frac{[H_2O_2]}{K_I}\right)$$
$$intercept = \left(\frac{1}{k_1[H_2O_2]_o} + \frac{1}{k_4}\right) \quad (4\text{-}13)$$

Plotting the slopes from Case 3 versus the peroxide concentrations then gives a line with

$$slope = \frac{1}{k_3 K_I}$$
$$intercept = \frac{1}{k_3} \quad (4\text{-}14)$$

Experiments were performed for each of the cases listed above, using LIP alone (D5NoMn LIP), which contained a small amount of MNP. The experiments were done spectrophotometrically in quartz cuvets at 37 °C in 20 mM tartrate buffer, pH 3.50. To do this, the spectrophotometer was moved into the 37 °C room since it did not have a temperature controlled sample chamber. Experiments were performed as follows: (1) the spectrophotometer was blanked at 310 nm with distilled water; (2) 100 μL of a solution containing H_2O_2 and VA were added to an empty quartz cuvet (at concentrations which would give the desired final concentrations when diluted to 1100 μL); (3) 1000 μL of concentrated, dialyzed LIP, diluted to the desired activity, was added to the cuvet; (4) the cuvet contents were immediately mixed by placing a piece of parafilm over the cuvet and inverting several times; and (5) the absorbance at 310 nm was measured for 1 minute with a chart recorder at 2 cm/min and 2 to 100 mV (0.02 to 1.0 OD full scale). The initial rate of veratraldehyde formation (mM/min) was then calculated from the recorder trace using an extinction coefficient (Tien *et al.*, 1986) of 9300 M^{-1} cm^{-1}. From equation (C-10), this was the negative of the veratryl alcohol and H_2O_2 consumption rates (stoichiometry of 1:1 (Tien *et al.*, 1986)). The rates were then plotted on double reciprocal plots as described above and the kinetic rate constants were determined. For Case 1, $[H_2O_2]$ was varied from 1 to 2000 μM, with $[VA]_o$ at 50 mM. LIP activities of

78.45 and 199.8 U/L were used to demonstrate that the rate of consumption was directly proportional to the enzyme activity. For Case 2, [VA] was varied from 10 to 100 μM, with [H_2O_2] at 200 and 500 μM, and [LIP] at about 200 U/L. For Case 3, [VA] was varied from 10 to 1000 μM, and [H_2O_2] was varied from 500 to 2000 μM, with [LIP] at about 200 U/L.

4.4.3 Kinetics of Mn(II) Oxidation by MNP

The reactions for oxidation of Mn(II) to Mn(III) by MNP are (Wariishi *et al.*, 1989a)

$$MNP + H_2O_2 \xrightarrow{k_5} MNPI + H_2O \qquad (4\text{-}15)$$

$$MNPI + Mn(II) \xrightarrow{k_6} MNPII + Mn(III) \qquad (4\text{-}16)$$

$$MNPII + Mn(II) \xrightarrow{k_7} MNP + Mn(III) \qquad (4\text{-}17)$$

$$Mn(III) + AH \xrightarrow{k_8} Mn(II) + A\cdot \qquad (4\text{-}18)$$

where MNP, MNPI and MNPII represent the different oxidation states of the MNP heme, AH represents an oxidizable compound, and A· is the oxidized (free radical) compound (Wariishi *et al.*, 1989a). The first three reactions represent a two substrate peroxidase ping-pong mechanism (Wariishi *et al.*, 1989a; Wariishi *et al.*, 1992), while the third reaction is independent of MNP and has been shown to be second order (Wariishi *et al.*, 1992). Note the 2:1 stoichiometry for Mn(II) oxidized per H_2O_2 consumed. It was shown (Wariishi *et al.*, 1992) that α-hydroxy acids stimulate the third reaction step by facilitating the release of the Mn(III) from the active site of the enzyme, and then stabilizing the Mn(III) while it diffuses to the oxidizable substrate for the fourth reaction (Wariishi *et al.*, 1992). Several α-hydroxy acids were evaluated in this role in the oxidation of 2,6-dimethoxyphenol (Wariishi *et al.*, 1992), and the five most efficient

chelators were assigned as (listed as chelator {Relative reaction rate}): Malonate {100} ⟩ Malate {99} ⟩ Tartrate {93} ⟩ Lactate {83} ⟩ Oxalate {42}. Since the LIP Alone experiments were to take place in tartrate buffer (and the LIP kinetics were measured in tartrate buffer), it was decided that tartrate would be used in all MNP experiments as well. This decision does not affect the rate of step 4 very much, as shown in the relative efficiencies above.

The rate equation for these kinetics (rate of formation of Mn(III)), also derived in Appendix C, is

$$v = \frac{2k_5k_6k_7[MNP]_o[H_2O_2][Mn(II)]}{k_6k_7[Mn(II)]+k_5(k_6+k_7)[H_2O_2]} - k_8[Mn(III)][AH] \qquad (4\text{-}19)$$

Another assay for MNP measures the oxidation of Mn(II) to Mn(III) in tartrate buffer (Paszczynski *et al.*, 1988). This assay (hereafter referred to as MNP Assay #3), was not used in these studies for general measurement of MNP activity because it is an extremely fast reaction and thus is not well suited for accurate repetitive measurement of a large number of samples. In this assay, which encompasses only the first three reactions above, if no oxidizable substrate is added, reaction 4 does not occur, and k_5, k_6, and k_7 can be estimated. Dropping the term for reaction 4, taking the reciprocal and canceling like terms gives

$$\frac{[MNP]_o}{v} = \frac{1}{2k_5[H_2O_2]} + \left(\frac{k_6+k_7}{2k_6k_7}\right)\frac{1}{[Mn(II)]} \qquad (4\text{-}20)$$

Note that values for k_6 and k_7 cannot be determined if all three reactions are considered, since they cannot be separated in the second term. This point is dealt with in the following section.

To evaluate the kinetic rate constants, only one case was needed, since k_6 and k_7 cannot be explicitly evaluated. In this case, $[H_2O_2]$ was varied in the presence of excess

Mn(II) and tartrate. The data were then plotted on a double reciprocal double reciprocal plot and the kinetic constants determined as follows.

$$slope = \frac{1}{2k_5}$$
$$intercept = \frac{k_6+k_7}{2k_6k_7[Mn(II)]} \qquad (4\text{-}21)$$

k_5 was calculated from the slope as shown above, while the best that could be done for k_6 and k_7 is to calculate the ratio $(k_6+k_7)/(k_6k_7)$. In all of the kinetic experiments performed for this enzyme, [Mn(II)] was 2 mM. Defining a new parameter, Ψ, as

$$\Psi = \frac{k_6 + k_7}{k_6k_7} \qquad (C\text{-}21)$$

the y-intercept becomes

$$intercept = \frac{\Psi}{2[Mn(II)]} \qquad (4\text{-}22)$$

which can be used to solve for Ψ. Inserting $(k_6+k_7)\Psi$ into the kinetic equation for k_6k_7, and noting that [Mn(II)] in the kinetic experiments was always 2 mM, yields the form of the equation which was used in the reactor model:

$$v = \frac{2k_5[MNP]_o[H_2O_2][Mn(II)]}{[Mn(II)]+4k_5\Psi[H_2O_2]} - k_8[Mn(III)][AH] \qquad (C\text{-}23)$$

Experiments were performed for each source of MNP, D5NoMn MNP, designated MNP_a, and D4HiMn MNP, designated MNP_b. The kinetic rate constant k_5 and the parameter Ψ for each case were then designated k_{5a} and Ψ_a, and k_{5b} and Ψ_b, respectively. The experiments were done spectrophotometrically in quartz cuvets at 37 °C in 20 mM tartrate buffer, pH 3.50. To do this, the spectrophotometer was moved

into the 37 °C room since it did not have a temperature controlled sample chamber. Experiments were performed as follows: (1) the spectrophotometer was blanked at 238 nm with 1 mL of reaction mix, containing the desired activity of MNP, 2 mM $MnSO_4$, and 20 mM tartaric acid, pH 3.50; (2) 100 μL of H_2O_2 were added to an empty quartz cuvet (at concentrations which would give the desired final concentrations when diluted to 1100 μL), and the cuvet was placed in the spectrophotometer; (3) 1000 μL of reaction mix (described in (1) above) were added to the cuvet; (4) the absorbance at 238 nm was measured for 30-45 seconds with a chart recorder set at 20 to 100 cm/min and 20 to 500 mV (0.2 to 5.0 OD full scale). The initial rate of Mn(III) formation in mM/min (Mn(III) present as Mn(III)-tartrate chelate complex, which absorbs at 238 nm) was then calculated from the recorder trace using an extinction coefficient (Paszczynski *et al.*, 1988) of 6500 M^{-1} cm^{-1}. The rates were then plotted on a double reciprocal plot as described above and the kinetic rate constant k_5 and the parameter Ψ were determined. For MNP_a, $[H_2O_2]$ was varied from 38.62 to 481.5 μM, with $[Mn(II)]_o$ at 2 mM, and for MNP_b, $[H_2O_2]$ was varied from 10.59 to 544.7 μM, also with $[Mn(II)]_o$ at 2 mM. MNP_a was present at 1000 U/L for measurement of its kinetic parameters, while MNP_b was present at 3160 U/L in its experiments (both using MNP Assay #1).

The value of k_8 was estimated from values published previously (Wariishi *et al.*, 1992). This was done because k_8 for each substrate will be different, and the substrate for the reactor studies was to be lignin; no values for k_8 for lignin bonds have been (or are likely to ever be) measured due to the complexity of lignin. Since the lignin to be used was known to be of a very high molecular weight, and was insoluble in water, but the compound for which the value of k_8 was published (vanillyl alcohol, molecular weight 154) was water-soluble, it was likely that the k_8 value for the lignin bonds would be much lower than that for vanillyl alcohol. It was thus assumed that the lignin value of k8 would be smaller by the ratio of the molecular weights of the two (vanillyl alcohol/lignin). Since no directly measured value of molecular weight was obtainable for

the lignin used in this study due to its complete insolubility in lignin solvents (see Chapter V), an estimate was needed for the molecular weight (MW). At this point, the assumption was made that since the MW of the highest MW lignin that is still amenable to gel permeation chromatography (ie. soluble in lignin solvents but not water) is 10^5 g/mole (Connors *et al.*, 1980), the lignin used in this study must have a higher MW because it was not soluble in these solvents (see Chapter V). Therefore, the MW of the lignin used in this study was estimated (somewhat arbitrarily) to be one order of magnitude higher, ie. 10^6 g/mole. The base lignin monomer is a substituted C_9 unit (Sarkanen and Ludwig, 1971) as shown in Figure 4.6. Molecular formulas for the "average" monomer in Beech and Birch lignins (also hardwoods) have been determined to be (Sarkanen and Ludwig, 1971) $C_9H_{8.05}O_{2.70}(OCH_3)_{1.41}$ and $C_9H_{9.03}O_{2.77}(OCH_3)_{1.58}$, respectively; the average of these two formulas gives $C_9H_{8.45}O_{2.73}(OCH_3)_{1.50}$, which gives a calculated "average" monomer molecular weight of 206.9 g/mole. Assuming that there are an average of 2 oxidizable bonds per monomer (Sarkanen and Ludwig, 1971), and that few (arbitrarily assumed to be on the order of 10 % based on observations from cellulose accessibility studies (Thompson *et al.*, 1992)) of the lignin bonds are accessible to the enzyme (Blanchette *et al.*, 1989), the concentration of oxidizable lignin bonds for 20 mg of lignin in 1 mL of water (reactor run levels) is 193.3 mM. These values were used, along with an estimated molecular weight (see Chapter V) to estimate k_6.

4.4.4 Stability of H_2O_2 and VA

The stability of H_2O_2 at the desired reactor run conditions was measured for various initial concentrations of H_2O_2 by making up the desired H_2O_2 solution in 20 mM tartrate buffer, pH 3.50, and incubating at 37 °C in a test tube on the reciprocal shaker at 350 spm (strokes per minute). Samples were taken at various times over a 24 hour period and the concentration measured. H_2O_2 concentrations were measured by absorbance at 230 nm using an extinction coefficient of 81 M^{-1} cm^{-1} (Pick and Keisari, 1980). VA was assumed to be stable because of its aromatic structure (VA is

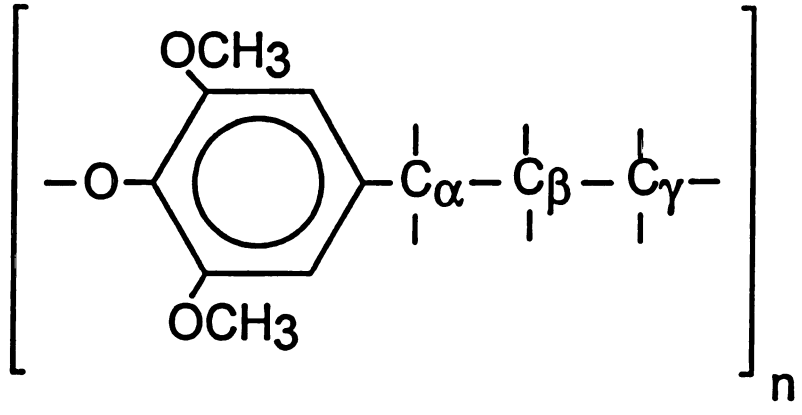

Figure 4.6: The general structure of a syringyl- phenylpropane unit in lignin (Adapted from Sarkanen and Ludwig (1971)). Intermonomer linkages occur generally through the oxygen at position 4 of the ring and through C_α, C_β, and C_γ.

3,4-dimethoxy benzyl alcohol).

4.4.5 Stability of LIP and MNP

LIP and MNP stability at pH 3.50 and 37 °C were measured by placing 3 mL of concentrated, dialyzed extracellular fluid containing LIPs and low levels of MNPs (D5NoMn) or MNPs (D4HiMn) at various levels of activity into test tubes and incubating them for 8 hours at 350 spm on the reciprocal shaker. Samples (0.55 mL) were taken at various times and the enzyme activities were determined using the LIP Assay and MNP Assay #1 (see Appendix A).

Statistical fits of the enzyme activity decay data were obtained by sequentially fitting the data to increasing order (zero order, first order, etc.) decay models (Bailey and Ollis, 1986). The simplest decay model which gave a good fit of the data was used for each enzyme. Only the final forms of the decay rate equations are presented here; see Chapter V for more detail. The final forms of the LIP and MNP decay rates are:

LIP (sum of zero order and first order):

$$\frac{d[LIP]}{dt} = -(k_{d_1} + k_{d_2}[LIP]) \qquad (4\text{-}23)$$

MNP (first order):

$$\frac{d[MNP]}{dt} = -k_d[MNP] \qquad (4\text{-}24)$$

4.5 Dialysis Reactor Model

The reactor system was modelled to provide a predictive control scheme in order to maintain the reactant concentrations in Side B (reaction chamber) within the ranges specified by Olsen *et al.* (1991). Physical processes included in the model were: (1) H_2O_2, VA, Mn(II), and [Mn(III)-tart$_2$] transport across the membrane; (2) The kinetics of H_2O_2 and VA consumption by LIP; (3) The kinetics of H_2O_2 and Mn(II) consumption by MNP (from both enzyme sources); (4) The kinetics of Mn(III) consumption through

oxidation of lignin bonds (and the rate of production of Mn(II) from this reaction); and (5) The stabilities of LIP, MNP, H_2O_2, and VA at pH 3.50, 37 °C, and 350 spm agitation rate. The rate of consumption of H_2O_2 in lignin oxidation catalyzed by LIP was assumed to be small relative to the rate of consumption in oxidation of VA (Tien, 1987), and thus was ignored. By experiment, H_2O_2 and VA were found to be stable over a 24 hour period at pH 3.50, 37 °C, and 350 spm agitation rate (see Chapter V), and thus it was not necessary to include these processes in the model. Mn(II) was assumed to be stable since it is oxidized very quickly to Mn(III) by MNP (Wariishi *et al.*, 1989b; Wariishi *et al.*, 1992) and thus would not be present long enough for stability to be a concern, so it was also left out of the model. Lastly, [Mn(III)-tart$_2$] was assumed to be stable enough to diffuse to a lignin bond and react (Wariishi *et al.*, 1992). The equations for each process combined into material balances and were used to develop an unsteady state model for Side B (derived in Appendices B and C). This model is presented below.

4.5.1 Unsteady State Balances on Side B

A mass balance for Side B for any species *i*, at constant volume, gives

$$\frac{dC_{i_B}}{dt} = \left(\frac{dC_{i_B}}{dt}\right)_{Transport} - \left(\frac{dC_{i_B}}{dt}\right)_{Reaction} \qquad (4\text{-}25)$$

Inserting the proper terms for each species, H_2O_2, VA, Mn(II), and [Mn(III)-tart$_2$] gives the equations shown below (following page):

A. H_2O_2:

$$\frac{d[H_2O_2]_B}{dt} = \frac{D^{eff}_{H_2O_2}A}{lV_B}([H_2O_2]_A - [H_2O_2]_B)$$

$$- \frac{k_1k_3k_4[LIP]_B[H_2O_2]_B[VA]_B}{k_3k_4[VA]_B + k_1k_3[H_2O_2]_B[VA]_B + k_1k_4[H_2O_2]_B(1+\frac{[H_2O_2]_B}{K_I})}$$

$$- \frac{k_{5_a}[MNP_a]_B[H_2O_2]_B[Mn(II)]_B}{[Mn(II)]_B + 4k_{5_a}\psi_a[H_2O_2]_B}$$

$$- \frac{k_{5_b}[MNP_b]_B[H_2O_2]_B[Mn(II)]_B}{[Mn(II)]_B + 4k_{5_b}\psi_b[H_2O_2]_B} \qquad (4\text{-}26)$$

B. VA:

$$\frac{d[VA]_B}{dt} = \frac{D^{e}_{VA}A}{\beta V_B}(e^{-\beta[VA]_B} - e^{-\beta[VA]_A}) \qquad (4\text{-}27)$$

$$- \frac{k_1k_3k_4[LIP]_B[H_2O_2]_B[VA]_B}{k_3k_4[VA]_B + k_1k_3[H_2O_2]_B[VA]_B + k_1k_4[H_2O_2]_B(1+\frac{[H_2O_2]_B}{K_I})}$$

C. Mn(II):

$$\frac{d[Mn(II)]_B}{dt} = \frac{D^{eff}_{Mn(II)}A}{lV_B}([Mn(II)]_A - [Mn(II)]_B)$$

$$- \frac{2k_{5_a}[MNP_a]_B[H_2O_2]_B[Mn(II)]_B}{[Mn(II)]_B + 4k_{5_a}\psi_a[H_2O_2]_B}$$

$$- \frac{2k_{5_b}[MNP_b]_B[H_2O_2]_B[Mn(II)]_B}{[Mn(II)]_B + 4k_{5_b}\psi_b[H_2O_2]_B}$$

$$+ k_8[Mn(III)\text{-}tart_2]_B[Lignin]_B \qquad (4\text{-}28)$$

D. Mn(III):

$$\frac{d[Mn(III)-tart_2]_B}{dt} = \frac{D^{eff}_{Mn(III)tart_2}A}{lV_B}([Mn(III)-tart_2]_A - [Mn(III)-tart_2]_B)$$
$$+ \frac{2k_{5_a}[MNP_a]_B[H_2O_2]_B[Mn(II)]_B}{[Mn(II)]_B + 4k_{5_a}\Psi_a[H_2O_2]_B}$$
$$+ \frac{2k_{5_b}[MNP_b]_B[H_2O_2]_B[Mn(II)]_B}{[Mn(II)]_B + 4k_{5_b}\Psi_b[H_2O_2]_B}$$
$$- k_8[Mn(III)-tart_2]_B[Lignin]_B \qquad (4\text{-}29)$$

In all cases, k_1, k_3, k_4, and K_l are D5NoMn LIP kinetic constants, k_{5a} and Ψ_a (= $\{k_{6a} + k_{7a}\}/\{k_{6a}k_{7a}\}$) are D5NoMn MNP ($MNP_a$) kinetic constants, k_{5b} and Ψ_b (= $\{k_{6b} + k_{7b}\}/\{k_{6b}k_{7b}\}$) are D4HiMn MNP ($MNP_b$) kinetic constants, β (= $\alpha + 1/a_l$) depends on VA viscosity and aggregate radius, k_8 is the rate constant for consumption of Mn(III) in the oxidation of lignin bonds, and the other variables are as described earlier. For a complete definition and explanation of these variables, refer to the model derivation in Appendices B and C.

4.5.2 Initial Conditions

At time zero, the concentrations of H_2O_2 and VA are set at their maximum values as defined by Olsen *et al.* (1991). The concentrations of H_2O_2 and VA in Side A are then set so that the initial rates of consumption of both H_2O_2 and VA are slightly higher than their initial rates of supply. This effectively drives the concentrations of H_2O_2 and VA in Side B down into their respective ranges. Since the rates of consumption of H_2O_2 and VA will follow the reactant in lower concentration, their rates of supply must be maintained close to one another. In addition, the concentrations of H_2O_2 and VA in Side B must be maintained within narrow ranges (see Table 4.2) which are dependent on the LIP and MNP activities as specified by Olsen *et al.* (1991). Since D^{eff} for H_2O_2 is much larger than D^{eff} for VA, the rate of supply of H_2O_2 can be expected to decrease much

Table 4.2: Optimal conditions for *in vitro* delignification of paper pulp by a mixture of xylanases and the LIPs and MNPs of *P. chrysosporium* (Olsen *et al.*, 1991).

Parameter	Conditions	Cases
Buffer	15-25 mM Tartrate	All
pH	3.0 to 5.0	All
Tween 80	0.01 to 0.05 %	All
Lactate	Add @ 1.0 to 10.0 mM	MNP, LIP+MNP
Lignocellulose	2 to 10 % (w/v)	All
H_2O_2	Maintain @ 0.005 to 0.1 mM	All
VA	Maintain @ 0.005 to 0.6 mM	LIP, LIP+MNP
Mn(II)	Add @ 0.1 to 0.50 mM	MNP, LIP+MNP
LIP	Add @ 15 to 30 U/g	LIP, LIP+MNP
MNP	Add @ 35 to 100 U/g	MNP, LIP+MNP

more rapidly than the rate of supply of VA. The volume of the reactor chambers is not large enough to allow constant rates of supply without concentration adjustment over time; thus, to keep the concentrations of H_2O_2 and VA in Side B within their respective ranges, pulses of concentrated H_2O_2, VA, LIP, and MNP must be added in order to maintain the rates of supply and consumption. During attempts to determine the initial rates, it was noted that the rates of supply had to be set at values lower than the rate of consumption or else one of the reactants would accumulate rapidly (normally VA). Therefore the initial conditions were set generally as

$$\begin{aligned} \left(\frac{d[VA]_B}{dt}\right)_{Transport} &= f_1 \left(\frac{d[VA]_B}{dt}\right)_{Reaction} \\ \left(\frac{d[H_2O_2]_B}{dt}\right)_{Transport} &= f_2 \left(\frac{d[H_2O_2]_B}{dt}\right)_{Reaction} \end{aligned} \qquad (4\text{-}30)$$

where f_1 and f_2 are fractions. Olsen *et al.* (1991) suggested ranges of LIP and MNP activity and corresponding ranges of H_2O_2 and VA concentrations which they found were optimum for *in vitro* degradation of paper pulp. By using their criteria, we can define three constants β_1, δ, and ϵ such that

$$\begin{aligned} [H_2O_2]_{B_{max}} &= \beta_1 [LIP]_{B_o} \\ [VA]_{B_{max}} &= \delta [LIP]_{B_o} \\ [Mn(II)]_{B_{max}} &= \epsilon([MNP_o]_{B_o} + [MNP_h]_{B_o}) \end{aligned} \qquad (4\text{-}31)$$

These equations are solved for Side B concentrations, inserted into the initial conditions above, and solved for $[H_2O_2]_A$ and $[VA]_A$. The final forms of the equations for $[H_2O_2]_A$ and $[VA]_A$ are (following page):

$$[VA]_A = -\frac{1}{\beta}\ln\{e^{-\beta\delta[LIP]_{B_o}} \qquad (4\text{-}32)$$

$$+ \frac{k_1k_3k_4\beta_1\delta\beta lV_B[LIP]^2_{B_o}}{D^o_{VA}A\{k_3k_4\delta + k_1k_3\beta_1\delta[LIP]_{B_o} + k_1k_4\beta_1(1+\frac{\beta_1[LIP]_{B_o}}{K_I})\}}\}$$

and

$$[H_2O_2]_A = \beta_1[LIP]_{B_o} \qquad (4\text{-}33)$$

$$- \frac{k_1k_3k_4\beta_1\delta lV_B[LIP]^2_{B_o}}{D^{eff}_{H_2O_2}A\{k_3k_4\delta + k_1k_3\beta_1\delta[LIP]_{B_o} + k_1k_4\beta_1(1+\frac{\beta_1[LIP]_{B_o}}{K_I})\}}$$

$$- \frac{k_{5_a}\beta_1\epsilon lV_B[LIP]_{B_o}[MNP_a]_{B_o}([MNP_a]_{B_o}+[MNP_b]_{B_o})}{D^{eff}_{H_2O_2}A\{\epsilon([MNP_a]_{B_o}+[MNP_b]_{B_o})+4k_{5_a}\Psi_a\beta_1[LIP]_{B_o}\}}$$

$$- \frac{k_{5_b}\beta_1\epsilon lV_B[LIP]_{B_o}[MNP_b]_{B_o}([MNP_a]_{B_o}+[MNP_b]_{B_o})}{D^{eff}_{H_2O_2}A\{\epsilon([MNP_a]_{B_o}+[MNP_b]_{B_o})+4k_{5_b}\Psi_b\beta_1[LIP]_{B_o}\}}$$

Choosing the LIP, MNP_a, and MNP_b activities then sets the initial conditions for the model.

4.5.3 FORTRAN Model Simulation

The model presented above was numerically solved by computer using a fourth-order Runge-Kutta-Gill predictor-corrector method (Finlayson, 1980) with a time step of 0.1 minutes for LIP alone or 0.01 minutes for MNP alone and for LIP + MNP. The program, RKG.FOR, is listed in Appendix D, with definitions of the variables preceding the program. Initial conditions were set as described above. The program was used as a predictor/corrector to construct a control scheme for each enzyme and the mixture (LIP + MNP), as follows. Starting with the initial conditions, the model was solved step-wise

until conditions (H_2O_2 and VA concentrations and/or LIP and MNP activities) in Side B warranted adjustment of the supply and consumption rates or enzyme activities. Program output included pulse (reagent additions to Side A or enzyme additions to Side B) times, volumes, and concentrations necessary to maintain Side B levels of reactants and enzymes within their prescribed ranges. The pulse times and concentrations were optimized for each LIP and/or MNP activity and enzyme source by using a shooting method to choose the best values of adjustable model parameters (see Appendix D). The optimization algorithm is presented in Figure 4.7. The conditions chosen for reaction/transport rate adjustments (through adjustment of $[H_2O_2]_A$, $[VA]_A$, $[LIP]_B$, $[MNP]_B$, or combinations of these), and the actions taken to correct the rates are given below. For the first case ((1a)) below, the conditions for concentration adjustments are explained in both verbal and mathematical terms; for subsequent cases, only the mathematical shorthand is used. All fractions used below are named identically to the variables used in RKG.FOR.

(1) LIP Alone:

(a) If the VA concentration in Side B exceeds a predefined fraction *brange* of its maximum, ie. $[VA]_B \geq brange \times [VA]_{Bmax}$, and the LIP in Side B is above a certain predefined fraction *lrange* of its initial (absolute time zero) activity, ie. $[LIP]_B > lrange \times [LIP]_{Bo}$, where $[VA]_{Bmax} = 0.6$ mM, and $[LIP]_{Bo} = 1000$ U/L, then $[H_2O_2]_A$ is adjusted such that

$$\left(\frac{d[H_2O_2]_A}{dt}\right)_{transport} = delta\left(\frac{d[VA]_A}{dt}\right)_{transport} \qquad (4\text{-}34)$$

where *delta* $\rangle$ 1. For a constant pulse concentration, RKG.FOR calculates the pulse volume necessary to adjust the H_2O_2 concentration in Side A.

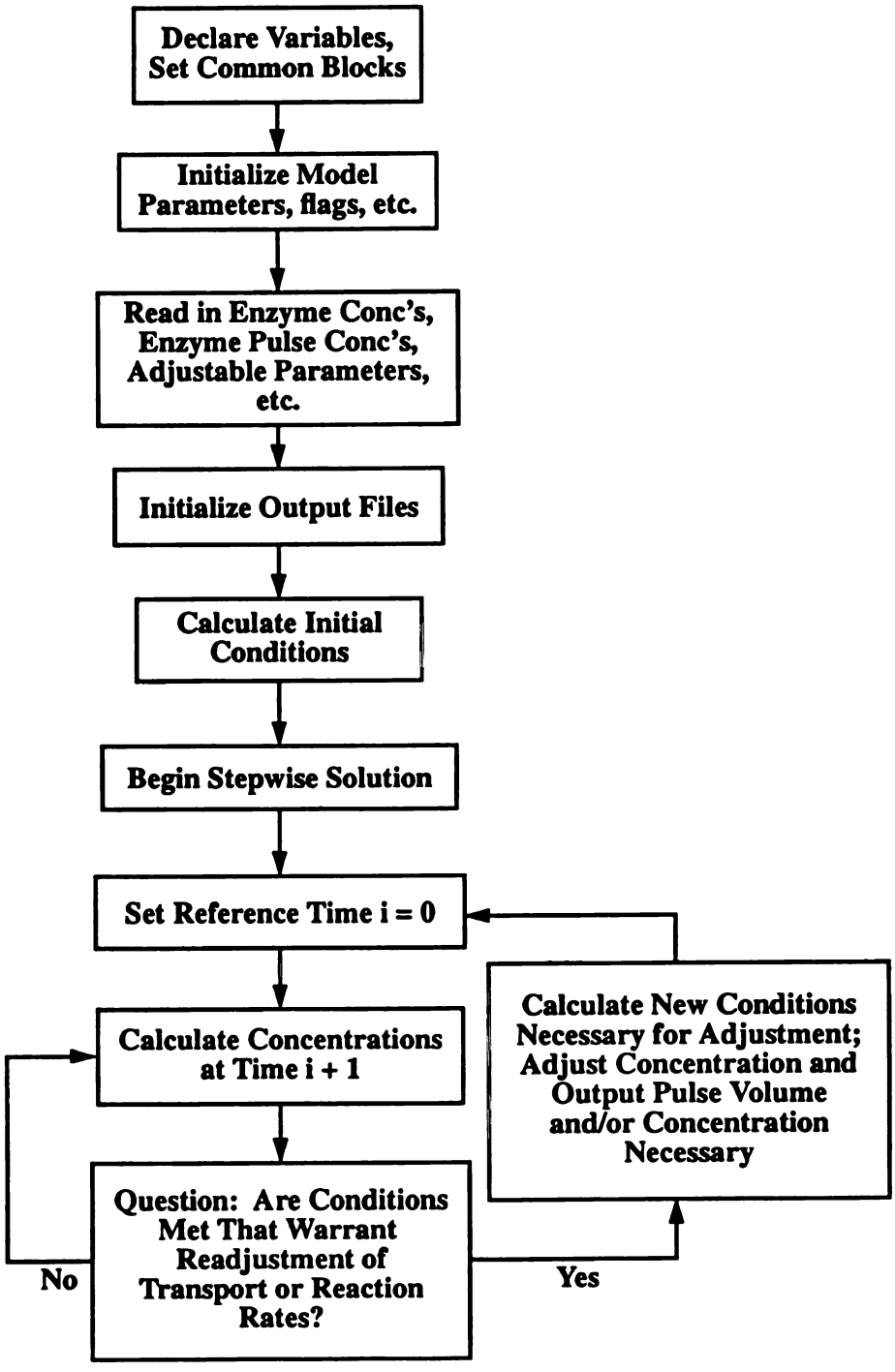

Figure 4.7: Flowchart representation of the solution strategy used by the reactor model program RKG.FOR.

(b) If ($[VA]_B \geq$ *brange*$\times[VA]_{Bmax}$) and ($[LIP]_B \leq$ *lrange*$\times[LIP]_{Bo}$), then $[H_2O_2]_A$ and $[VA]_A$ are adjusted such that

$$\left(\frac{d[H_2O_2]_A}{dt}\right)_{transport} = g_2\left(\frac{d[H_2O_2]_B}{dt}\right)_{reaction}$$
$$\left(\frac{d[VA]_A}{dt}\right)_{transport} = g_1\left(\frac{d[VA]_B}{dt}\right)_{reaction} \qquad (4\text{-}35)$$

where g_1 and g_2 are analogous to f_1 and f_2 in the initial conditions. The two equations, which depend on LIP activity, are solved for $[H_2O_2]_A$, and $[VA]_A$, for a constant volume (20 μL), constant concentration (5000 U/L) LIP pulse to Side B. For a constant pulse volume of 40 μL, RKG.FOR calculates the Side A pulse concentrations of H_2O_2 and VA necessary to satisfy the above rate conditions.

(c) Time delays in pulse addition: The computer simulation can change Side A concentrations instantaneously. This is not physically possible, so a pulse time delay was programmed into the solution, as follows: (i) Pulse $[H_2O_2]_A$ alone, remove pulse volume from Side A, and 3 time steps (0.3 min) later add identical volume at pulse concentration to Side A (keeps volumes of Side A and Side B equal); (ii) Pulse $[H_2O_2]_A$, $[VA]_A$, and $[LIP]_B$, remove 20 μL from Side A, 3 time steps later add 40 μL of Side A pulse solution to Side A, and 4 time steps later (0.4 min) add 20 μL of LIP pulse solution. The net volume increase (both sides) in this case is 20 μL.

(2) LIP + MNP:

(a) If ($[VA]_B \geq$ *brange*$\times[VA]_{Bmax}$), but ($[LIP]_B \rangle$ *lrange*$\times[LIP]_{Bo}$) and ($[MNP]_B \rangle$ *mrange*$\times[MNP]_{Bo}$) where *mrange* is a fraction, $[MNP]_{Bo}$ is the MNP activity at absolute time zero, and all other variables are as above, then $[H_2O_2]_A$ is adjusted such that

$$\left(\frac{d[H_2O_2]_A}{dt}\right)_{transport} = delta\left(\frac{d[VA]_A}{dt}\right)_{transport} + \left(\frac{d[H_2O_2]_B}{dt}\right)_{MNP\ reaction} \qquad (4\text{-}36)$$

where *delta* $\rangle$ 1. This condition is analogous to (1a) above.

(b) If ($[VA]_B \geq brange \times [VA]_{Bmax}$) and ($[LIP]_B \leq lrange \times [LIP]_{Bo}$), but ($[MNP]_B \rangle mrange \times [MNP]_{Bo}$), then $[H_2O_2]_A$ and $[VA]_A$ are adjusted such that

$$\left(\frac{d[H_2O_2]_A}{dt}\right)_{transport} = g_2\left(\frac{d[H_2O_2]_B}{dt}\right)_{LIP\ reaction}$$
$$\left(\frac{d[VA]_A}{dt}\right)_{transport} = g_1\left(\frac{d[VA]_B}{dt}\right)_{LIP\ reaction} \qquad (4\text{-}37)$$

where g_1 and g_2 are analogous to f_1 and f_2 in the initial conditions. This case is analogous to (1b) above.

(c) If ($[VA]_B \geq brange \times [VA]_{Bmax}$), but ($[LIP]_B \rangle lrange \times [LIP]_{Bo}$) and ($[MNP]_B \leq mrange \times [MNP]_{Bo}$), then $[H_2O_2]_A$ is adjusted exactly as in (2a) above, and MNP_b is added to Side B. This condition is also analogous to (1a) above.

(d) If ($[VA]_B \geq brange \times [VA]_{Bmax}$) and ($[LIP]_B \leq lrange \times [LIP]_{Bo}$), and ($[MNP]_B \leq mrange \times [MNP]_{Bo}$), then $[H_2O_2]_A$ and $[VA]_A$ are adjusted such that

$$\left(\frac{d[H_2O_2]_A}{dt}\right)_{transport} = g_3\left(\frac{d[H_2O_2]_B}{dt}\right)_{LIP\ reaction}$$
$$\left(\frac{d[VA]_A}{dt}\right)_{transport} = g_1\left(\frac{d[VA]_B}{dt}\right)_{LIP\ reaction} \qquad (4\text{-}38)$$

where g_3 is not equivalent to g_2. Both LIP and MNP_b are added for this case. This case is analogous to (2b) above.

(c) Time delays in pulse addition: Pulse delays for these cases are: (i) Pulse $[H2O2]_A$ alone, remove pulse volume from Side A, and 30 time steps (0.3 min) later add identical volume at pulse concentration to Side A (keeps volumes of Side A and Side B equal); (ii) Pulse $[H_2O_2]_A$, $[VA]_A$, and $[LIP]_B$, remove 20 μL from Side A, 30 time steps later add 40 μL of Side A pulse solution to Side A, and 40 time steps later (0.4 min) add 200 μL of LIP pulse solution; (iii) Pulse $[H_2O_2]_A$ and $[MNP_b]_B$, add 20 μL of Side A pulse solution to Side A, and 40 time steps later add 20 μL of MNP_b pulse solution to Side B; (iv) Pulse $[H_2O_2]_A$, $[VA]_A$, $[LIP]_B$, and $[MNP_b]_B$, remove 20 μL from Side A, 30 time

steps later add 40 μL of Side A pulse solution to Side A, and 40 times steps later add 20 μL of LIP + MNP_b pulse solution to Side B. The volume increase in this case is 20 μL.

(3) MNP Alone (No VA is Present):

(a) If ($[H_2O_2]_B \geq \{[H_2O_2]_{Bmin} + arange \times ([H_2O_2]_{Bmax} - [H_2O_2]_{Bmin})\}$) but ($[MNP]_B \rangle$ $mrange \times [MNP]_{Bo}$), where *arange* is a fraction, $[H_2O_2]_{Bmin}$ = 0.005 mM, $[H_2O_2]_{Bmax}$ = 0.1 mM, and $[MNP]_{Bo}$ is the MNP activity at absolute time zero, then $[H_2O_2]_A$ is adjusted such that

$$[H_2O_2]_A = f_3[H_2O_2]_{A_o} \qquad (4\text{-}39)$$

where f_3 is an empirical fraction, and $[H_2O_2]_{Ao}$ is the Side A concentration of H_2O_2 at absolute time zero. Note that $[Mn(II)]_B$ decreases over time since none is initially added to Side A. The kinetic rate of consumption then also decreases, and so f_3 must decrease with each consecutive pulse; arbitrarily it was made to decrease linearly. Also note that this is a completely empirical approach for this case. For a constant pulse concentration, RKG.FOR calculates the Side A pulse concentration of H_2O_2, at constant pulse volume of 20 μL, necessary to satisfy the above rate conditions.

(b) If ($[H_2O_2]_B \leq \{[H_2O_2]_{Bmin} + arange \times ([H_2O_2]_{Bmax} - [H_2O_2]_{Bmin})\}$) and ($[MNP]_B \leq$ $mrange \times [MNP]_{Bo}$), then $[H_2O_2]_A$ is adjusted such that

$$[H_2O_2]_A = f_3 f_4 [H_2O_2]_{A_o} \qquad (4\text{-}40)$$

where f_3 is as above and f_4 is an additional empirical fraction which accounts for rate changes when MNP is later added to Side B. This is also a completely empirical approach to control of this case.

(c) Time delays in pulse addition: Pulse time delays for this case are: (i) Pulse $[H2O2]_A$ alone, remove pulse volume from Side A, and 40 time steps (0.4 min) later add identical volume at pulse concentration to Side A (keeps volumes of Side A and Side B equal); (ii) Pulse $[H_2O_2]_A$ and $[MNP]_B$, add 20 μL of Side A pulse solution to Side A,

and 40 time steps later (0.4 min) add 20 μL of MNP pulse solution. The net volume increase (both sides) in this case is 20 μL.

4.5.4 Perturbation Analysis of Model Parameters

In order to determine the stability characteristics of the reactor simulation with respect to the accuracy of the measured model parameters, an additional FORTRAN program was developed. This program, named PERTURB.FOR, and listed in Appendix D, accepts the pulse time/volume/concentration output from RKG.FOR, and solves the model using this data. 95 % Confidence Intervals were calculated for each measured model parameter (ie. effective diffusion coefficients, kinetic constants, etc.) using linear regression (if data were fit to obtain the values), or elementary statistics (Taylor, 1982) using the Normal Distribution. In order to simplify calculations for the linear regression, a FORTRAN program using matrix algebra was written to perform the operations (LINREG.FOR, listed in Appendix D). The Side B reactant and enzyme profiles using the measured model parameters +/- their 95 % Confidence Intervals were calculated in order to find the parameters which had the greatest effect on the stability of the model solutions, and how much error in their measurement was possible before the model solution no longer stayed within the prescribed concentration limits. This perturbation analysis provided no information on how the reactor was to be run, ie. reactant concentrations, pulses, etc., but served merely as a tool to get a feel for the more important measured parameters and the necessary degree of accuracy in their measurement. This information would be helpful in designing similar systems in the future.

4.6 *In vitro* Treatment of Lignin in the Reactor

Treatment of insoluble lignin with LIPs and/or MNPs was carried out in the dialysis reactor at 37 °C, 2 % (w/v) solids, approximately 50 U/g of LIP and/or 2800 U/g of MNP (by MNP Assay #1) in 20 mM tartrate buffer, pH 3.50. This pH was chosen as a tradeoff between LIP activity and MNP activity (see Figure 4.8 (Michel,

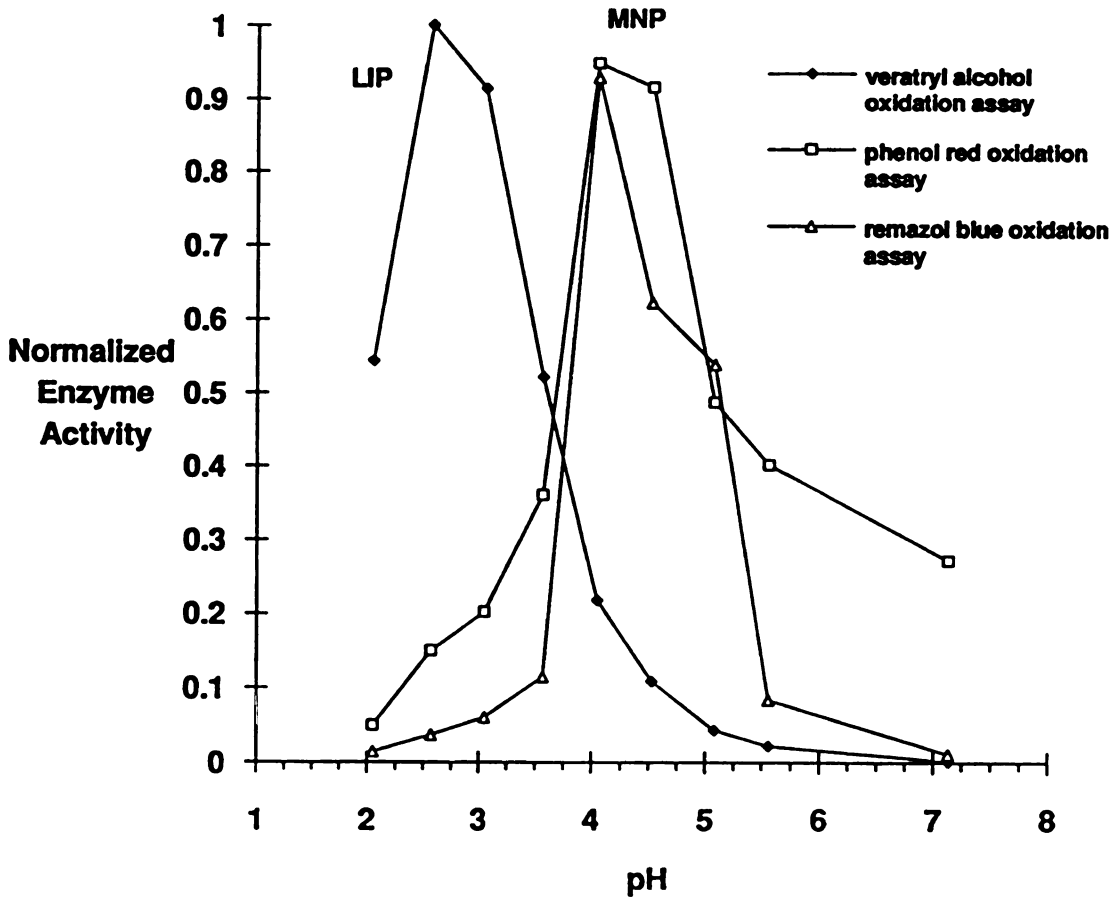

Figure 4.8: Variation of LIP and MNP activities with pH of the system (Michel, 1991).

1991)). The initial liquid volume in both sides was 1 mL. Initial concentrations of H_2O_2 and VA in Side A were determined for given LIP, MNP, or LIP + MNP activities using RKG.FOR (described above). When MNP was included in the run, enough Mn(II) for a final Side B concentration of 0.1 mM was added first to a tube containing the MNP enzyme, a stoichiometric amount of H_2O_2, and 20 mM tartrate buffer, pH 3.50, in order to convert it to [Mn(III)-$tart_2$] prior to starting the reaction. This made the reaction rates easier to control since by far the highest rate of consumption of H_2O_2 is in the initial conversion of Mn(II) to [Mn(III)-$tart_2$]. Note that lactate was not added to any reactor run since tartrate is a better chelator of Mn(III) than lactate (Wariishi *et al.*, 1992), and that Mn(II) was added only to Side B (none added to Side A). The maximum and minimum values of $[H_2O_2]_B$, $[VA]_B$, and $[Mn(II)]_B$ were determined from the ranges reported by Olsen *et al.* (1991), and are presented in Table 4.2 above. Side B concentrations of H_2O_2, VA, and Mn(II) were set at the maximum values specified by Olsen *et al.* (1991) (Table 4.2). Runs were carried out as described below.

4.6.1 Reactor Run Procedure

Before starting a reactor run, the LIP and MNP activities in the stored enzyme were measured using the LIP Assay and MNP Assay #1 (MNP activity then converted to MNP Assay #2 units for calculation of initial conditions; see Appendix A). The amount of stored enzyme to add to Side B was then calculated for the desired LIP level. If LIP or MNP were to be run alone, the pulse times and concentrations were already determined known from prior optimization of RKG.FOR for those conditions and enzyme levels. However, when LIP and MNP were present in the run, the ratio of MNP_a (present in small amounts with the D5NoMn LIP) and MNP_b (concentrated D4HiMn) was calculated and RKG.FOR was run and optimized for those conditions prior to starting the run, in order to determine the pulse profiles. This was done because the kinetic constants for the two MNP sources were different due to their differing isoenzyme profiles (refer to FPLC profiles in Chapter V). The Side A pulse solutions (ie. H_2O_2

alone and H_2O_2 with VA if LIP was run alone) and Side B pulse solution (ie. LIP pulse for a LIP alone run) were then made.

The time zero Side A solution, containing the desired levels of H_2O_2 +/- VA in 20 mM tartrate buffer, pH 3.50, was made by adding the necessary volumes of fresh concentrated stock reagents and distilled water to give 1 mL total volume of solution at the desired concentrations. Stock reagents included: (1) 7.37 M H_2O_2 (Sigma); (2) 6.60 M VA (Aldrich, 96 wt % VA in water); (3) 125 mM Tartaric Acid, pH 3.50; (4) 2 mM H_2O_2, made fresh daily; (5) 8 mM H_2O_2, made fresh daily; (6) 500 mM H_2O_2, made fresh daily; (7) 40 mM VA, made fresh daily; and (8) 4 mM $MnSO_4$, made fresh each month. The time zero Side B solution, containing the desired levels of H_2O_2 +/- VA +/- Mn(II)) in tartrate buffer, pH 3.50, was made in a similar manner, except that the volume was made up to 1 mL minus the necessary volume of stored enzyme (see above for exception in the case of MNP presence in the run). Concentrations were such that when diluted to 1 mL with the stored enzyme, the desired Side B levels would be present. Initial solutions were oxygenated at 37 °C with pure, humidified O_2 at a flowrate of 2 mL/min for 10 minutes by bubbling the gas through the solutions in Eppendorf tubes; the solutions then remained at 37 °C for about 5 to 10 minutes before being added to the reactor. While the starting solutions were being oxygenated, 20.0 mg dry weight of wet insoluble lignin were measured into Side B. A (wet) membrane was then placed in the reactor joint, the two halves of the reactor clamped together, and the joint sealed with a double layer of parafilm.

To begin the reactor run, the initial Side A solution (1 mL) was pipetted into Side A. Next, the initial Side B solution (1 mL minus the necessary volume of stored enzyme or MNP/[Mn(III)-$tart_2$] mixture) was pipetted into Side B, and the necessary volume of stored enzyme (or MNP/[Mn(III)-$tart_2$]) mixture, which contained the MNP, immediately added. The sample ports were then capped (teflon face of septa facing reaction mixture), and agitation was begun (350 spm, perpendicular to the membrane). Pulses were added

to Side A and/or Side B when predicted to be necessary by RKG.FOR optimization, as described above. Pulses to Side A were added by pipet after removal of the cap and septum (cap and septum were replaced after the pulse was completed). Pulses to Side B (always enzyme only) were added through the septum using a glass microliter syringe (Hamilton Co., Reno, NV). When the reaction had proceeded for the desired amount of time, the shaker was turned off and the reactors removed from the 37 °C room for recovery of the Side A and Side B solutions. The pulse profiles (predicted by RKG.FOR) for the LIP alone (50 U/g), MNP alone (2800 U/g), and LIP + MNP (50 U/g LIP and 2800 U/g total MNP) are presented in Tables 4.3 through 4.5. While these pulse profiles are results of the model, they are presented here because they were used to make up and add pulses in the actual reactor runs. Please refer to Chapter V for the Side A and Side B concentration profiles predicted by the model; the pulse profiles listed in Tables 4.3-4.5 and the concentration profiles were simultaneously generated by RKG.FOR, and as such, the concentration profiles are the direct result of using the pulse profiles listed.

Controls for each case were run in which one or more components of the reaction mixture were left out. These controls were carefully chosen in order to screen out compounds originating from sources other than the lignin. These controls (presented in tabular form in Tables 4.6 through 4.8) included: (1) Enzyme(s) + reagents (H_2O_2 +/- VA +/- Mn(II)) + O_2 + buffer (no lignin), hereafter referred to as L^- control, to screen out products of oxidation of VA by LIP, and/or products from the action of [Mn(III)-$tart_2$] on MNP solution contaminants; (2) Enzyme(s) + lignin + O_2 + buffer (no reagents), designated R^-, to screen out compounds produced by the action of any protein or compound present in the enzyme mixture(s) other than the peroxidase enzymes (LIP and/or MNP); (3) Lignin + reagents + O_2 + buffer (no enzyme(s)), designated E^-, to screen out compounds arising purely from the action of the reagents on the lignin or low molecular weight compounds still present in the lignin;

Table 4.3: Pulse profiles predicted by RKG.FOR for the LIP Alone enzyme case. Pulse volumes and concentrations are listed for both Side A and Side B.

	Side A			Side B			
Pulse	Side A	Pulse Conc's		Side B	Pulse Enzyme Activity		
time (min)	Pulse Vol (μL)	$[H_2O_2]$ (mM)	[VA] (mM)	Pulse Vol (μL)	[LIP] (U/L)	$[MNP_a]$ (U/L)	$[MNP_b]$ (U/L)
63.50	9.26	1000.0	0.0	0.00	0.0	0.0	0.0
121.20	40.00	406.7	857.4	20.00	5000.0	0.0	0.0
184.90	9.55	1000.0	0.0	0.00	0.0	0.0	0.0
243.60	40.00	419.4	876.1	20.00	5000.0	0.0	0.0
308.30	9.95	1000.0	0.0	0.00	0.0	0.0	0.0
368.20	40.00	432.4	895.3	20.00	5000.0	0.0	0.0
434.00	10.33	1000.0	0.0	0.00	0.0	0.0	0.0
494.80	40.00	443.6	911.7	20.00	5000.0	0.0	0.0
561.70	10.69	1000.0	0.0	0.00	0.0	0.0	0.0
623.60	40.00	454.5	926.0	20.00	5000.0	0.0	0.0
691.60	11.03	1000.0	0.0	0.00	0.0	0.0	0.0

Table 4.4: Pulse profiles predicted by RKG.FOR for the MNP Alone enzyme case. Pulse volumes and concentrations are listed for both Side A and Side B.

	Side A			Side B			
Pulse time (min)	Side A Pulse Vol (μL)	Pulse Conc's $[H_2O_2]$ (mM)	[VA] (mM)	Side B Pulse Vol (μL)	Pulse Enzyme Activity [LIP] (U/L)	$[MNP_a]$ (U/L)	$[MNP_b]$ (U/L)
21.90	15.24	150.0	0.0	0.00	0.0	0.0	0.0
61.44	13.47	150.0	0.0	0.00	0.0	0.0	0.0
102.15	13.14	150.0	0.0	0.00	0.0	0.0	0.0
143.61	20.00	86.5	0.0	20.00	0.0	0.0	250000.0
182.66	12.62	150.0	0.0	0.00	0.0	0.0	0.0
230.06	13.07	150.0	0.0	0.00	0.0	0.0	0.0
278.41	12.62	150.0	0.0	0.00	0.0	0.0	0.0
327.35	20.00	83.9	0.0	20.00	0.0	0.0	250000.0
373.72	11.91	150.0	0.0	0.00	0.0	0.0	0.0
428.15	12.05	150.0	0.0	0.00	0.0	0.0	0.0
482.74	20.00	80.1	0.0	20.00	0.0	0.0	250000.0
534.28	11.14	150.0	0.0	0.00	0.0	0.0	0.0
593.34	11.06	150.0	0.0	0.00	0.0	0.0	0.0
651.47	20.00	72.6	0.0	20.00	0.0	0.0	250000.0
705.19	9.81	150.0	0.0	0.00	0.0	0.0	0.0

Table 4.5: Pulse profiles predicted by RKG.FOR for the LIP + MNP enzyme case. Pulse volumes and concentrations are listed for both Side A and Side B.

	Side A			Side B			
Pulse	Side A	Pulse Conc's		Side B	Pulse Enzyme Activity		
time (min)	Pulse Vol (μL)	$[H_2O_2]$ (mM)	[VA] (mM)	Pulse Vol (μL)	[LIP] (U/L)	$[MNP_a]$ (U/L)	$[MNP_b]$ (U/L)
59.12	10.09	1000.0	0.0	0.00	0.0	0.0	0.0
115.53	40.00	249.1	272.0	20.00	5000.0	4493.4	0.0
153.75	20.00	409.4	0.0	20.00	0.0	0.0	250000.0
218.32	40.00	327.2	534.0	20.00	5000.0	4493.4	0.0
266.50	20.00	443.9	0.0	20.00	0.0	0.0	250000.0
335.08	40.00	342.1	471.5	20.00	5000.0	4493.4	0.0
398.94	40.00	320.9	330.8	30.00	3333.3	2995.4	163671.3
471.35	40.00	347.7	330.5	30.00	3333.3	2995.4	163671.3
553.45	10.21	1000.0	0.0	0.00	0.0	0.0	0.0
626.24	40.00	368.2	445.5	30.00	3333.3	2995.4	163671.3
719.08	40.00	378.2	322.8	30.00	3333.3	2995.4	163671.3

Table 4.6: List of reactor components present in each experiment performed for the LIP Alone enzyme case (Base = Base Case; L^- = No lignin control; R^- = No reagent control; E^- = No enzyme control; AE = Autoclaved enzyme control; and ER^- = No enzyme, no reagent control). A "+" indicates the presence of the component in the Side B reaction mixture.

Case	LIP	lignin	H_2O_2	VA	O_2	Buffer
Base	+	+	+	+	+	+
L^-	+		+	+	+	+
R^-	+	+			+	+
E^-		+	+	+	+	+
AE	(+)*	+	+	+	+	+
ER^-		+			+	+

* Enzyme present but inactive.

Table 4.7: List of reactor components present in each experiment performed for the MNP Alone enzyme case (Base = Base Case; L^- = No lignin control; R^- = No reagent control; E^- = No enzyme control; AE = Autoclaved enzyme control; and ER^- = No enzyme, no reagent control). A "+" indicates the presence of the component in the Side B reaction mixture.

Case	MNP	lignin	H_2O_2	Mn(II)	O_2	Buffer
Base	+	+	+	+	+	+
L^-	+		+	+	+	+
R^-	+	+			+	+
E^-		+	+	+	+	+
AE	(+)*	+	+	+	+	+
ER^-		+			+	+

* Enzyme present but inactive.

Table 4.8: List of reactor components present in each experiment performed for the LIP + MNP enzyme case (Base = Base Case; L^- = No lignin control; R^- = No reagent control; E^- = No enzyme control; AE = Autoclaved enzyme control; and ER^- = No enzyme, no reagent control). A "+" indicates the presence of the component in the Side B reaction mixture.

Case	LIP	MNP	lignin	H_2O_2	VA	Mn(II)	O_2	Buffer
Base	+	+	+	+	+	+	+	+
L^-	+	+		+	+	+	+	+
R^-	+	+	+				+	+
E^-			+	+	+	+	+	+
AE	(+)*	(+)*	+	+	+	+	+	+
ER^-			+				+	+

* Enzyme present but inactive.

(4) Autoclaved enzyme(s) + reagents + O_2 + buffer (inactive enzyme(s)), designated AE, to screen out products arising from the action of free (non-enzyme-bound) heme and reagents on the lignin; and (5) Lignin + O_2 + buffer (no enzyme(s) or reagents), designated ER^-, to screen out low molecular weight compounds already present in the lignin. The samples (liquid and solid) from these controls were treated in exactly the same manner as the cases in which all components of the reaction mixtures were present (hereafter referred to as the "base cases," or "BCs"), with the following exceptions in the pulse profiles: (1) No lignin controls: No exceptions -- identical pulses and times to base case; (2) No reagent controls: Same pulse volumes and times as base case, but reagent pulses replaced with distilled water (enzyme pulses identical to base case); (3) No enzyme controls: Pulse times and volumes identical to base case, but reagent pulses equal to initial reagent concentrations (maximum in concentration control ranges), and enzyme pulses replaced with distilled water; (4) Autoclaved enzyme controls: Pulse times and volumes identical to base case, but reagent pulses equal to initial reagent concentrations (maximum in concentration control ranges), and enzyme pulses replaced with autoclaved enzyme pulses (solutions made up with volumes of autoclaved enzyme solution identical to the amount of active enzyme solution used in the base case); and (5) Lignin only controls: Pulse times and volumes identical to base case, but all pulses replaced with distilled water.

4.6.2 Recovery of Liquid and Solid Fractions

After the reaction was stopped, the solution from Side A was removed with a Pasteur pipet and frozen at -20 °C in a silanized glass test tube for further analysis (Note that all glassware to come into contact with the samples from the reactor run on was silanized as a precaution for the GC/MS analysis (see above)). The slurry in Side B was transferred with a dry, silanized Pasteur pipet into a dry, tared, silanized (Watson, 1985) glass conical vial (Cat. No. B7797-2, Baxter Scientific, McGaw Park, IL) and centrifuged for 10 minutes at 4000 rpm. The supernatant was transferred to a silanized

glass test tube and frozen at -80 °C for future analysis by GC/MS. Side B of the reactor was washed consecutively with 1 mL of distilled water to quantitatively recover solids remaining in the reactor. A simple recovery experiment (using isolated lignin in the reactor) indicated about 95% recovery of solids by this procedure. These wash volumes were added to the conical vial and centrifuged; the supernatants from the reactor washes were discarded. After all the lignin had been transferred from the reactor to the conical vial, the lignin pellet was washed by centrifugation in the conical vial five times with 2 mL of 1 M NaCl to remove the enzyme(s), and then five times with 2 mL of distilled water to remove the NaCl. The lignin pellet, still in the conical vial, was then suspended in 1 mL of distilled water, capped (teflon-lined septum) and stored frozen at -80 °C for further analysis.

4.7 GC/MS Analysis of Solubilized Compounds

Chloroform and ethyl acetate extracts of the liquid and solid fractions from each run were derivatized with *N,O*-bis-(trimethylsilyl)-trifluoroacetamide (BSTFA; Supelco) and analyzed (as the TMS ethers) by Gas Chromatography/Mass Spectrometry (GC/MS). Sample analysis procedures are described below.

4.7.1 Sample Preparation

All samples were prepared using reagent-grade chloroform and ethyl acetate, and were contacted only with silanized (Watson, 1985) glassware. Latex gloves were worn at all times during sample handling. Once extracted, the GC/MS samples were stored at -20 °C, and were allowed to sit no longer than 24 hours before analysis to guard against unwanted loss of products due to volatilization over time. Liquid and solid extracts were prepared as follows.

The recovered liquid fractions from each experiment were removed from the -80 °C freezer and thawed. The liquid was then transferred to a silanized 1/2 dram vial (Cat. No. 60910-L, Kimble) and the approximate volume noted. An equal volume of chloroform was added to the vial using a glass pipet. The rubber septum in the vial cap

was replaced with a teflon-faced rubber septum (Cat. No. 73048, Alltech Associates, Deerfield, IL) taking care not to touch the septum with bare hands. The vial, containing liquid phase from the reactor and an equal volume of chloroform, was capped and shaken vigorously 3 times for 15 seconds each time. The vial was then uncapped and the chloroform (bottom layer) was transferred with a silanized Pasteur pipet as quantitatively as possible to another silanized 1/2 dram vial, which was then capped (also with teflon-faced septum). This procedure was repeated 2 more times, and the three chloroform extracts were mixed together in the silanized collection vial. The entire procedure was then repeated in an identical manner except that ethyl acetate was used as extraction solvent instead of chloroform (ethyl acetate is the top layer in these extractions). The ethyl acetate and chloroform extracts were not mixed but were analyzed separately.

The recovered solid fractions from each experiment were removed from the -80 °C freezer (still in their tared conical glass vials) and thawed. The thawed slurries (slurried with 1 mL of distilled water before freezing for storage) were then centrifuged for 10 minutes at 4000 rpm and the supernatant discarded. One mL of chloroform was then added to the conical glass vial, and the vial was capped (same cap as for storage, with same teflon-lined septum), mixed by vortexing, and placed on its side on a reciprocal shaker, parallel to the direction of shaking, at 37 °C. The mixture was shaken vigorously (450 spm) for 15 minutes. The vial was then removed from the shaker and centrifuged for 10 minutes at 4000 rpm to separate the solid lignin and the chloroform. The chloroform was then pipetted from the conical vial using a silanized glass Pasteur pipet and transferred to a silanized 1/2 dram vial (same type as used above) with a teflon-faced rubber septum in the vial cap. The extraction procedure was repeated once more with chloroform, and then twice with ethyl acetate. As with the liquid extracts, the chloroform extracts were mixed together as were the ethyl acetate fractions, but the chloroform and ethyl acetate extracts were kept separate. The extracted solids were then washed, still in the tared conical glass vials, by centrifugation (as before) 5 times with

2 mL of distilled water to displace any remaining extraction solvents, and stored frozen at -80 °C under 1 mL of distilled water for future FTIR analysis.

At this point, 20 μL of 51 ng/μL 2-chloro-5-trifluoromethylbenzoic acid (Aldrich) in ethyl acetate were added to each vial containing solvent extracts of the samples using a clean glass microliter syringe. This compound was added as an internal standard and was used because of its similarity in structure to expected lignin degradation products, and also because it would have a clearly recognizable mass spectrum due to the chlorine molecule. A separate sample containing only the internal standard was also prepared with each set of samples by adding 20 μL of the internal standard to 1800 μL of ethyl acetate, and treating the standard as a normal sample in future steps. In addition, one sample was prepared (one time only) containing the 20 μL of the internal standard, 20 μL of a solution containing 49.2 ng/μL syringaldehyde (Aldrich), 49.6 ng/μL syringic acid (Aldrich), and 53 ng/μL vanillic acid (Aldrich) in ethyl acetate, and 1800 μL of ethyl acetate (hereafter referred to as STD Mix), since these compounds were expected to be released from the lignin due to enzyme activity. The liquid and solid extracts were then concentrated with a light stream of nitrogen (manifold made of 90% glass, 10% Nalgene tubing) to about 200 μL. The sample vials were then capped and delivered to the Mass Spectrometry Facility where they were stored no longer than 24 hours at -20 °C before analysis. Before analysis, the samples were concentrated to dryness (just) under a light stream of nitrogen (stainless steel/teflon manifold) and 20 μL of BSTFA in pyridine (Supelco) were added using a clean glass microliter syringe. The vials were then capped and heated for 30 minutes at 60 °C to derivatize the samples. After derivatization, the samples were allowed to cool (capped) in the sand bath and were then analyzed by GC/MS.

4.7.2 Sample Measurement

Samples were run by Jennifer Johnson at the NIH Mass Spectrometry Facility at Michigan State University using a JEOL AX 505 double focussing magnetic sector mass

spectrometer and equipped with an HP5890 gas chromatograph (GC). The capillary GC column was interfaced directly to the ion source via a heated inlet; ionization was achieved by electron impact at 70 eV. Separation was achieved with a 30 m DB5-MS capillary GC column (5 % phenyl methyl silicone; J & W, Folsom, CA) with an inside diameter of 0.32 mm and a film thickness of 0.25 nm for the MNP only samples, and with a 30 m DB-1 capillary GC column (SPB-1, Supelco) for the LIP only and LIP + MNP samples. The samples (2 μL) were volatilized for GC using a temperature program as follows: Hold for 2 minutes at 100 °C; increase to 320 °C at 10 °C/min; hold for 5 minutes at 320 °C. Mass data for m/z from 45-600 were collected at a scan rate of 1 scan/second for 25 minutes. In the early samples (MNP Only samples), the mass spectral data were recorded starting at 2 minutes into the run in order to avoid swamping the detector with the solvent front; in later samples (LIP Only, LIP + MNP, and STD Mix samples), this initial waiting time before data collection was 3.75 minutes. This caused retention time data from the later runs to be slower than the earlier runs by 50-75 scans (ie. the internal standard came out in the scan range 545-555 in the earlier runs, but in the scan range 490-500 in the later runs). Datafiles from each run were stored on optical disk for future analysis.

4.7.3 GC/MS Data Analysis

The GC/MS data were analyzed initially by comparing the Total Ion Chromatograms (TICs) for each extract with those of the corresponding extracts from the controls. Assuming that the partition coefficient for a particular compound was the same in different samples (a reasonable assumption), the concentrations in corresponding extracts should be directly comparable. The TICs from each sample, each containing 100 or more separate peaks, were printed out with identical x-axes (retention time/scan number) and the chromatograms from different samples were lined up and searched for peaks that were present in the base case but not in the controls, and then for peaks that were present in the base case in at least 3 times the concentration that they were in the

controls (concentrations compared by ratioing the peak height of the unknown to the peak height of the internal standard in that sample). Any peaks not meeting these criteria were not considered to be peaks of interest and were barred from future consideration.

Peaks remaining after the first set of comparisons, were checked (again using the TICs) versus other extracts from the same base case. If the peak was present in the other base case extract, but was not marked as a peak of interest in that base case (meaning that it was in at least one control for that base case at a similar concentration), it was discarded. Finally, the mass spectra for the peaks of interest were obtained, and if the peaks of interest appeared in lower concentrations in the controls of that extract, compared with the mass spectra of the corresponding peaks in the controls. If the peaks of interest did not appear in any of the controls, the major ions in its mass spectrum were searched for in the corresponding extracts of the controls. The mass spectra of the unknowns remaining were checked to make sure that they were even molecular weight (compounds containing only C, H, and O, such as lignin, cannot have an odd molecular weight), that they were not fatty acids (TMS ethers of fatty acids have characteristic mass peaks (Dr. D.A. Gage, Personal Communication) at M^+, M^+-15 (100%), and 117, 129 or 132, and 145), that they were not hydrocarbons present due to contamination from contact with rubber (ie. from syringe seals, septa, etc.; Hamming and Foster, 1972; McLafferty, 1973), and that they were not likely to be GC column bleed (large mass peaks at 207, 221, and 355 (Dr. D.A. Gage, Personal Communication)). Any peaks not passing these tests were discarded.

The remaining peaks were then integrated, and their concentrations estimated using the calibration for the internal standard for each standard. This concentration is not exact, but is only a ball-park estimate since the calibration (proportionality between concentration and peak area) will be different for each compound, but not substantially.

The NIST and Wiley mass spectral databases were searched for matches to the mass spectra of the unknowns. Unfortunately, only two matches were found since there

are not many TMS-derivatized compounds that have been submitted to the databases, relative to non-derivatized compounds; analyses of the mass spectra were then completed by hand.

4.8 FTIR Analysis of Remaining Solid Lignin

A pellet Fourier Transform Infrared spectrum (FTIR) was measured for all base cases and controls that contained lignin. Measurements were performed with a Perkin-Elmer Model 1600 FT-IR Spectrophotometer (Perkin Elmer, Norwalk, CT) with a DTGS detector; the instrument was supplied by Michigan Biotechnology Institute (MBI, Lansing, MI). Desiccated IR-grade KBr was used as pellet medium; a KBr background spectrum was subtracted from each FTIR spectrum measured. The procedure is described below.

4.8.1 Sample Preparation

The solid samples, after extraction with chloroform and ethyl acetate, were removed from the -80 °C freezer, the vials covered with a piece of dry, tared 10 μm polyethylene mesh, and lyophilized to dryness (48 hours). The vials, with mesh, were then weighed and the lignin recovered from the reactor run was calculated by weight difference. The mesh was then discarded, and the dry solid lignin was stored under desiccation for FTIR analysis. Samples were dried and weighed just prior to FTIR analysis in order to minimize interference in the FTIR analysis from adsorbed water.

Pellets for FTIR analysis were pressed at room temperature (23 °C) using a 12 ton Carver press (Model C, Fred S. Carver, Inc., Menomonee Falls, WI) and a pair of 13 mm pellet dies (Cat. No. 0016-001, Model 129, SpectraTech, Stamford, CT). Pellets were pressed from sample and KBr ground and mixed in a Wig-L-Bug grinder/mixer (Model 3110B, Crescent Dental Mfg. Co., Lyons, IL).

To press a pellet, 1.5 $\pm$ 0.1 mg of dry lignin were measured into a dry, tared plastic 0.5" x 1" (d x l) Wig-L-Bug vial (Cat. No. 3111, Crescent Dental Mfg. Co., Lyons, IL). Next, 298.5 $\pm$ 0.5 mg of desiccated spectral grade KBr were added to the

vial (for a background spectrum, only 300 mg of KBr was added to the vial). An unused, dry, tared plastic ball pestle (Cat. No. 3112, Crescent Dental Mfg. Co., Lyons, IL) was then added and the mixture ground/mixed on the Wig-L-Bug for 1 minute. The powdered KBr/lignin mixture was then transferred to the dies. The vial, cap, and ball pestle, which contained residual sample and KBr, were immediately placed in the desiccator and later weighed to determine the pellet mass. Assuming the mixture was completely homogeneous, this gave the mass of lignin sample per pellet. The die was quickly assembled and placed into the Carver press. A vacuum line was attached to the die to continuously evacuate the pellet chamber during the pellet pressing operation. The pellet material was pressed in a four step process: (1) The material was compressed to 5000 psi and the pressure quickly released; (2) The material was compressed to 10000 psi and the pressure quickly released; (3) The material was compressed to 15000 psi and the pressure held at 15000 psi for 2 minutes; and (4) The pressure was slowly released to zero. The newly pressed pellet was then quickly removed from the die, placed in a glass vial, and stored under desiccation (no longer than 24 hours) for spectral measurement.

4.8.2 Sample Measurement

Transmission FTIR spectra of the pellets averaged from 50 scans were measured from 4000 to 700 cm^{-1} with 2 cm^{-1} resolution using a Perkin Elmer Model 1600 Fourier Transform Infrared Spectrophotometer (1600 Series FTIR, Perkin Elmer, Norwalk, CT) equipped with a DTGS detector (cesium iodide window). Samples were measured using strong apodization, and with the Jacquinot stop in place. At all times, the sample chamber was continuously purged with moisture-free, CO_2-free N_2 to keep the moisture and CO_2 at undetectable levels. The transmission spectra were then converted to absorbance spectra, which were then converted to ASCII format and transferred to an IBM compatible PC. The FTIR spectra were analyzed by Bonnie Hames of the Analytical Chemistry Group, National Renewable Energy Laboratory (NREL, Golden,

CO) using a Partial Least Squares (PLS) regression technique developed for this type of analysis (Hames *et al.*, 1991) and calibrated with milled wood lignins from various sources (Hames *et al.*, 1991). The spectra were analyzed for carbohydrate and lignin content, methoxyl content per C_9 unit (methoxyl:aryl ratio), and phenolic hydroxyl content per C_9 unit. Syringyl to guaiacyl ratios were calculated from the predicted methoxyl:aryl ratios. A four factor regression model was used for the PLS analysis of the lignin and carbohydrate contents, while five factor models were used for both the methoxyl content analysis and the phenolic hydroxyl content analysis by PLS (Hames *et al.*, 1991).

CHAPTER V: RESULTS

5.1 Substrate Composition

The compositions of the untreated (native) poplar substrate, acid pretreated (AH) poplar, the cellulase-treated acid pretreated (C-AH) poplar, and the extracted residual (EC-AH) lignin (final substrate for the reactor runs) are presented in Table 5.1. All components were present in the native poplar at levels consistent with this type of hardwood (Grous *et al.*, 1986), with 58.4 % carbohydrates and 25.4 % lignin. Pretreatment in the flow reactor at 220 °C with 1 % H_2SO_4 resulted in a residue with a composition similar to that obtained with mixed hardwood (90 % birch, 10 % maple) in an earlier study (Thompson *et al.*, 1992), increasing the carbohydrate content to 63.8 % and the lignin content to 29.3 %. After treatment with saturating levels (Thompson, 1989) of cellulase, the C-AH residue was reduced to 9.3 % carbohydrates and 78.1 % lignin. Finally, the extractions with increasingly polar solvents at 37 °C yielded a final substrate (EC-AH) which contained 74.5 % lignin and 12.2 % carbohydrates (this indicates an extractives content of at least 3.6 % in the C-AH residue).

The resulting lignin substrate was subjected to several tests in an attempt to justify the assumption that it was similar to naturally occurring lignin. First, several known lignin solvents (Sarkanen and Ludwig, 1971) were used to try to solubilize the residue so that a molecular weight distribution could be obtained by gel permeation chromatography. Solvents tried included dioxane, dimethylformamide (DMF), and various aqueous solutions of the two, as follows: (1.) 100 % dioxane; (2.) dioxane:water at 9:1, 3:1, and 1:1; (3.) 100 % DMF; (4.) DMF:water at 9:1 and 1:1; (5.) dioxane:DMF at 1:1; and (6.) dioxane:DMF:water at 1:1:2. In all cases, no lignin was solubilized as determined by measuring the absorbance of the liquid phase at 280 nm (absorbance maximum of the aromatic ring) (Sarkanen and Ludwig, 1971). A sample of the lignin was then sent to Dr. John R. Obst, at the USDA Forest Products Research Laboratory in Madison, WI for further analysis. Dr. Obst is an expert in the field of

Table 5.1: Compositions of the poplar substrate and each residue at each step of the lignin isolation procedure as measured by the Quantitative Saccharification technique (Saeman *et al.*, 1945).

Component	Native Poplar (%)	AH Poplar (%)	C^{-}AH Poplar (%)	EC^{-}AH Poplar (%)
Glucan	42.9	62.9	8.1	10.1
Xylan	13.8	0.9	0.9	1.1
Galactan	0.1	ND*	0.3	1.0
Arabinan	0.6	ND	ND	ND
Mannan	1.0	ND	ND	ND
Lignin**	25.4	29.3	78.1	74.5
SUM+	83.8	93.1	87.4	86.7

* ND = None Detected

** Includes Klasson lignin, extractives, and ash.

+ Not equal to 100 % due to recovery errors and unknown uronic acid content.

lignin characterization, and routinely performs standard tests to determine properties of lignins. Acetylation (Sarkanen and Ludwig, 1971) of the lignin was performed in order to make it more soluble in the lignin solvents; however, even after acetylation, the lignin was still completely insoluble in all lignin solvents tried (J.R. Obst, Personal Communication). One possible explanation for this marked insolubility of the lignin was that the β-O-4 ether bonds in the lignin, which form the crosslinks between the various monomers, were highly condensed during the pretreatment at 220 °C, causing the lignin to be insoluble (J.R. Obst, Personal Communication). This possibility was tested by Dr. Obst using thioacidolysis (Obst, 1982; Rolando *et al.*, 1992), a degradative technique which releases substituted syringyl and guaiacyl monomers from the lignin (which can be analyzed as groups based on the differences in their basic structures; see Chapter II). If the recoveries of syringyl and guaiacyl monomers per unit mass of the isolated lignin were much less than the values obtained for the native wood lignin, then a high degree of condensation would be confirmed. The relative yield of syringyl thioacidolysis monomer product was 78 % of that of the native wood lignin, while the yield of the guaiacyl product was 87 % of that of the native wood lignin. The syringyl to guaiacyl ratios for the isolated lignin and the native wood lignin were 1.02 and 1.15, respectively, which are not significantly different. This indicates that, although a small amount of condensation occurred during pretreatment, the final isolated lignin was at the very least similar to native lignin in both absolute monomer contents, ratio of monomer types, and frequency of intact interunit linkages (β-O-4 ether bonds). This leads to the conclusion (J.R. Obst, Personal Communication) that the low molecular weight lignin fragments present in the native, AH, and C$^-$AH lignins, which are the substrates normally used in lignin degradation studies (Tien, 1987), were extracted in the final isolation step, leaving a very high molecular weight lignin (EC$^-$AH).

5.2 LIP and MNP Production

Due to the low levels of LIP (1/10 to 1/4 of the 250 U/L normally obtained in our laboratory with the identical isolate of *P. chrysosporium* (Dosoretz and Grethlein, 1991)) and the presence of relatively high levels of MNP in the extracellular fluid collected from these cultures, many more production runs were necessary than was originally intended. Each flask was assayed for MNP before harvest, and any flask which contained more than 100 U/L of MNP (by MNP Assay #1) was discarded; this helped to minimize the final amount of contaminating MNP in the final D5NoMn enzyme. The bottles of extracellular fluid (EF) collected from each of the D5NoMn enzyme production runs were combined and assayed for LIP and MNP; LIP activity was around 75 U/L, while about 100 U/L of MNP activity was detected. The EF was concentrated and dialyzed, and assayed again for LIP and MNP activity, and for total protein before storage; LIP activity was found to be 9,900 U/L, MNP was present at about 16,000 U/L, and the total protein concentration was 192.0 μg/mL. At this protein concentration, assuming all of the protein is LIP or MNP, the specific activities of LIP and MNP were 51.56 and 83.33 U/mg total protein, respectively (note the different definitions of one Unit (U) of enzyme activity for each). A sample of the EF was subjected to FPLC; the FPLC profile is presented in Figure 5.1. The trace is the absorbance at 409 nm, which is the absorbance maximum for the heme group, while the diagonal line represents the sodium acetate gradient (10 Mm to 1 M) used to elute the proteins. Each isoenzyme (H#) labeled was assigned by the position at which it eluted on the salt gradient. The enzyme activity present in each peak was verified by assaying fractions collected during the FPLC run. The isoenzymes H1, H2, HA, H6, H7, H8, and H10 are lignin peroxidases, while H3 (not present or masked by H2), H4, H5, and H9 are manganese peroxidases. The small peak eluting between H3 and H4 is also a manganese peroxidase, but is not assigned a designation in the literature, and so is not designated here. The D5NoMn concentrate was dispensed to tubes (0.3 mL/tube) and

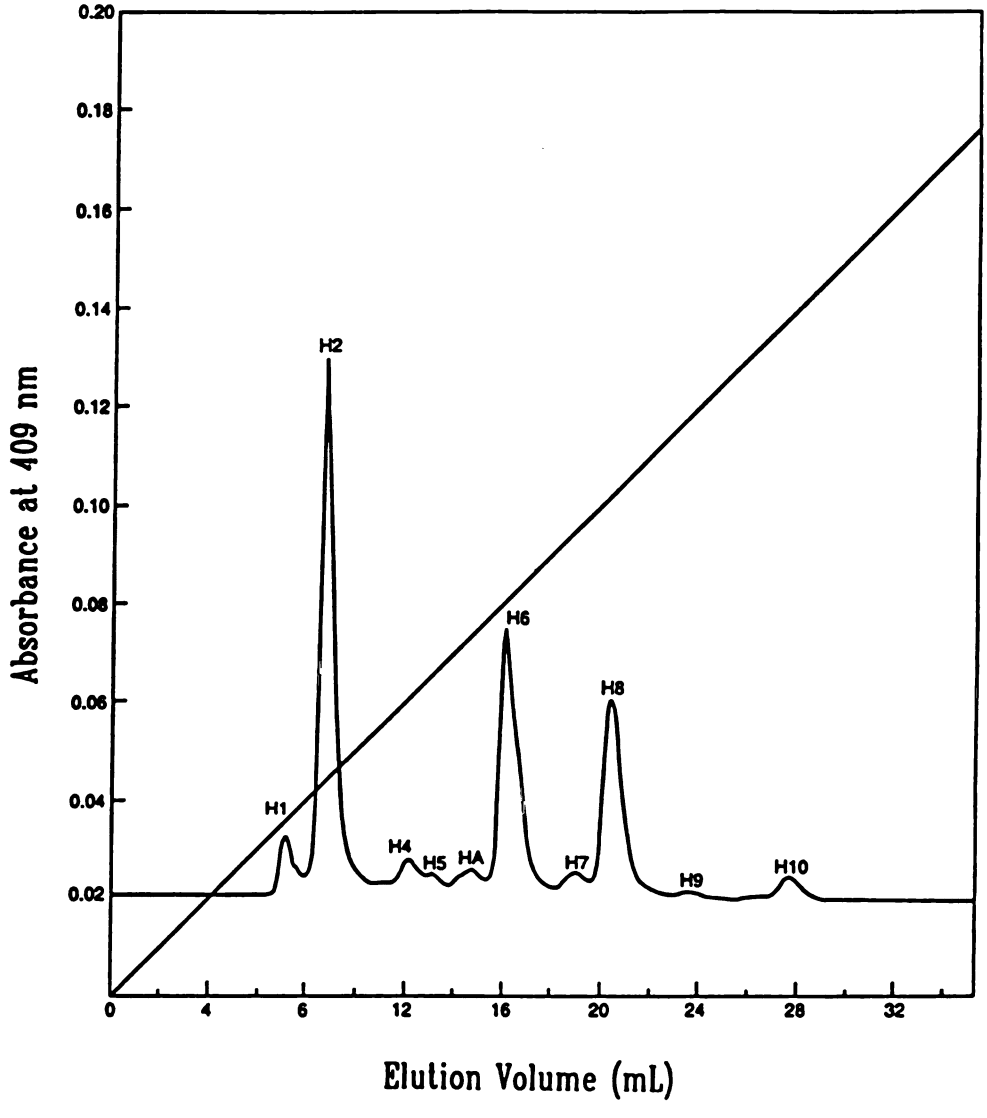

Figure 5.1: FPLC profile of the concentrated, dialyzed D5NoMn extracellular fluid. The peaks designated H1, H2, HA, H6, H7, H8, and H10 are lignin peroxidases, while H4, H5, and H9 are manganese peroxidases. The diagonal line represents the sodium acetate gradient (10 mM to 1 M) used to elute the proteins.

frozen for future use.

The MNP activity level produced in the D4HiMn run was higher than expected; three runs were planned, but only one was necessary because the MNP activity from the single run was about three times higher than expected (about 9700 U/L in the D4HiMn run versus a normal (Dosoretz and Grethlein, 1986) level of about 3000 U/L). The EF was concentrated and dialyzed, and the concentrate was assayed for LIP, and dilutions of the concentrate were assayed for MNP (using MNP Assay #1) and for total protein. No LIP activity was detected in the D4HiMn EF concentrate, MNP activity was present at about 560,000 U/L, and the total protein concentration was 1265.5 μg/mL. The specific activity of the MNP was then calculated (see assumption above) to be 442.5 U/mg total protein. The FPLC profile of the D4HiMn concentrate is presented in Figure 5.2. The trace and diagonal line are as before. Fractions were collected during the run and assayed for LIP and MNP activity, as above, and the results used with the retention time to assign the isoenzyme identities. Note that HA, H6, H7, and H8 are assigned solely based on their retention times, as there was no detectable LIP activity in the fractions collected at these retention times; the presence of LIP activity in the D4HiMn concentrate was confirmed in reactor runs using the D4HiMn concentrate, through the presence of veratraldehyde formed from veratryl alcohol present in the concentrate (discussed in the reactor run section). The small peak eluting between H3 and H4 was found to correspond with that seen above (it is an MNP).

A mixture of the D5NoMn and D4HiMn concentrates which was equivalent to that used in the reactor run containing both LIPs and MNPs, was also analyzed by FPLC; the FPLC profile is shown in Figure 5.3. Isoenzymes were assigned as above. In order to determine how much of the heme protein eluting was LIP and MNP isoenzymes, the FPLC profiles of each sample above were integrated and the peak areas used to estimate percentages of each enzyme class; the results are presented in Table 5.2. Since H2 and H3 coeluted (for some retention times) in the mixture, the ratio of H2 to

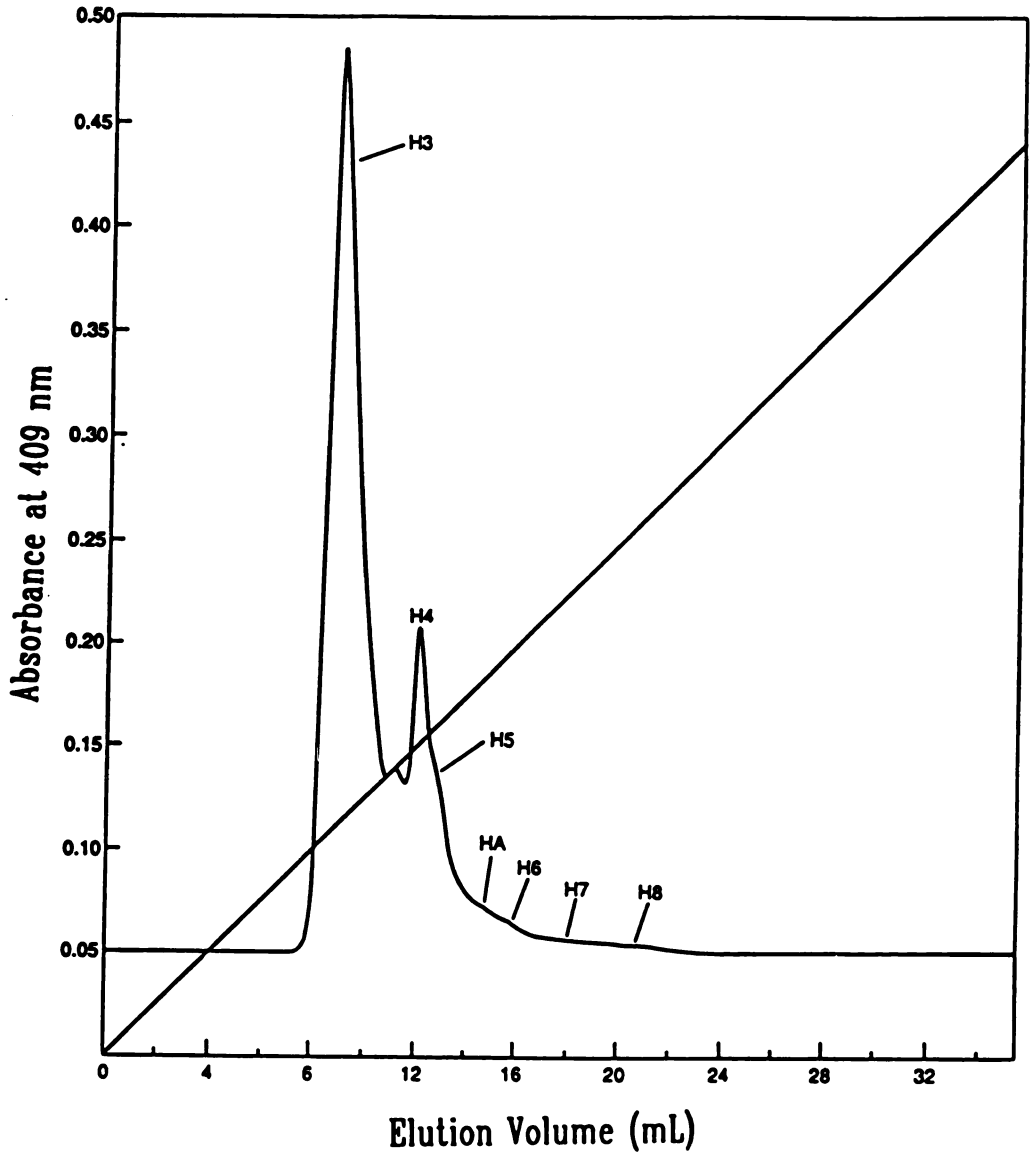

Figure 5.2: FPLC profile of the concentrated, dialyzed D4HiMn extracellular fluid. The peaks designated HA, H6, H7, and H8 are lignin peroxidases, while H3, H4, and H5 are manganese peroxidases. The diagonal line represents the sodium acetate gradient (10 mM to 1 M) used to elute the proteins.

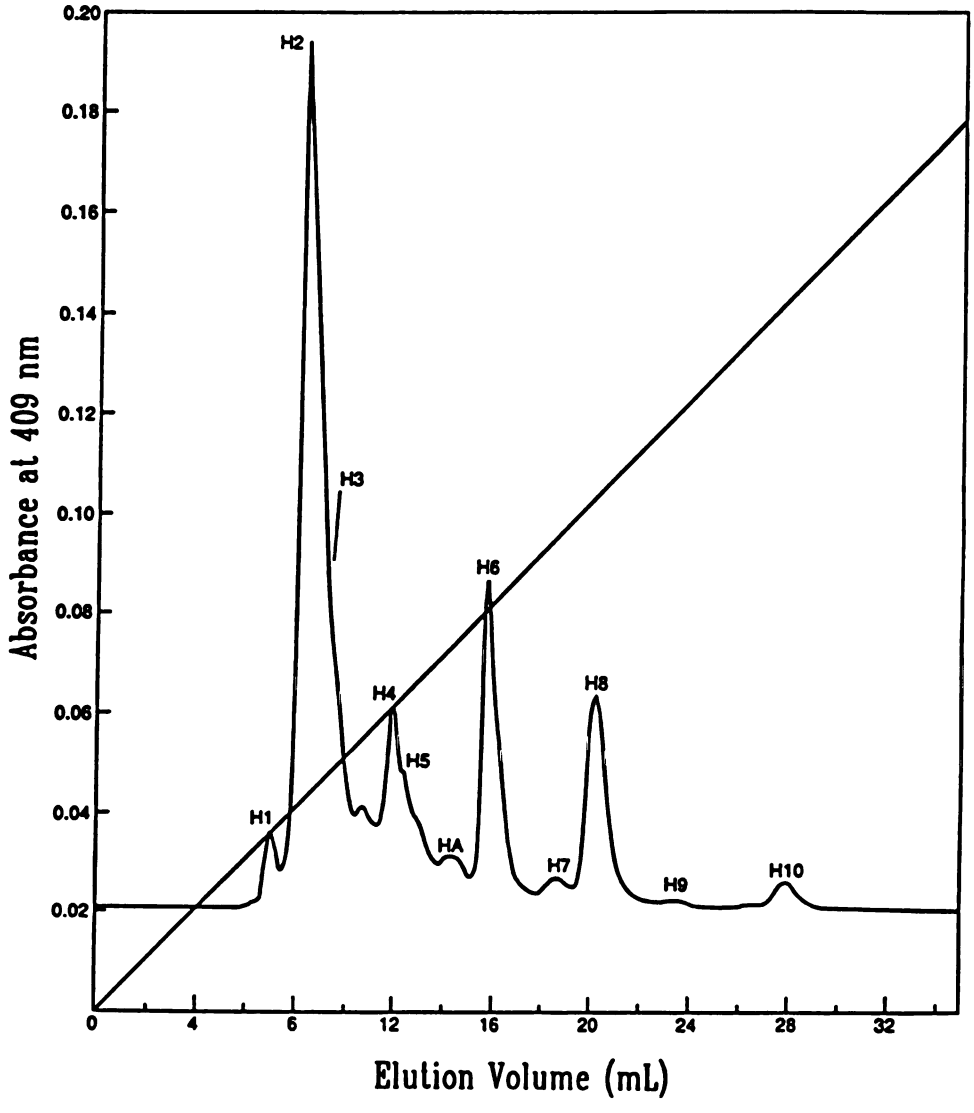

Figure 5.3: FPLC profile of the D5NoMn/D4HiMn extracellular fluid mixture used for mixed enzyme reactor runs. The peaks designated H1, H2, HA, H6, H7, H8, and H10 are lignin peroxidases, while H3, H4, H5, and H9 are manganese peroxidases. The diagonal line represents the sodium acetate gradient (10 mM to 1 M) used to elute the proteins.

Table 5.2: Isoenzyme compositions and overall LIP and MNP compositions of the D5NoMn and D4HiMn extracellular fluid (concentrated and dialyzed) and the D5NoMn/D4HiMn mixture. Percentages were determined from peak areas in the FPLC profiles and represent percentage of total heme protein.

Isoenzyme	D5NoMn (%)	D4HiMn (%)	Mixture (%)
H1	4.5	0.0	2.8
H2	36.8	0.0	22.8
H3	0.0	67.5	26.5
H7*	0.7	7.1	3.4
H4	3.7	14.7	9.9
H5	1.7	4.8	2.9
HA	2.9	1.8	3.0
H6	24.8	2.2	13.1
H7	2.9	1.3	1.8
H8	20.1	0.7	11.2
H9	0.1	0.0	0.8
H10	1.9	0.0	1.8
total	100.0	100.0	100.0
LIP	93.8	6.0	56.5
MNP	6.2	94.0	43.5

* This peak has not been designated, but is an MNP isoenzyme.

H1 in the D5NoMn FPLC profile was used to determine H2, and H3 was calculated by difference; this was possible since H1 and H2 were not present in the D4HiMn concentrate.

5.3 Species Transport

Before using the pseudo steady state assumption to calculate the effective diffusion coefficients for each species, the unsteady state case was solved using a constant diffusion coefficient. The determination of effective diffusion coefficients for H_2O_2, Mn(II), [Mn(III)-$tart_2$], and VA are dealt with in the following sections.

5.3.1 H_2O_2 and Mn(II)

The partial differential equation for membrane diffusion with a constant diffusion coefficient is (Cussler, 1986)

$$\frac{\partial C}{\partial t} = D\frac{\partial^2 C}{\partial x^2} \tag{5-1}$$

where C is concentration, t is time, x is distance through the membrane, and D is the diffusion coefficient. Nondimensionalizing by defining

$$f = \frac{C}{C_o} = \frac{C}{C_{A_o}+C_{B_o}}$$
$$\xi = \frac{x}{l} \; ; \; \tau = \frac{Dt}{l^2} \tag{5-2}$$

where C_{Ao} and C_{Bo} are the initial concentrations in Sides A and B, respectively and l is the membrane thickness, the equation becomes

$$\frac{\partial f}{\partial \tau} = \frac{\partial^2 f}{\partial \xi^2} \tag{5-3}$$

The boundary conditions are

$$at \; \xi = 1, \; (\frac{\partial f}{\partial \tau})_{\xi=1} = -(\frac{Al}{V_B})(\frac{\partial f}{\partial \xi})_{\xi=1}$$
$$at \; \xi = 0, \; (\frac{\partial f}{\partial \tau})_{\xi=0} = +(\frac{Al}{V_B})(\frac{\partial f}{\partial \xi})_{\xi=0} \tag{5-4}$$

The initial condition and steady state are

$$\begin{aligned} &\textit{I.C: at } \tau = 0, f = 0 \textit{ for } 0 < \xi < 1 \\ &\textit{Steady State: as } \tau \to \infty, \; f \to \frac{1}{2} \end{aligned} \tag{5-5}$$

Solving by separation of variables (Kreyszig, 1988) and defining

$$f = \frac{1}{2} + g(\xi,\tau) \tag{5-6}$$

the solution is

$$\begin{aligned} f(\xi,\tau) = \frac{1}{2} + \sum_{i=1}^{\infty} a_i e^{-\lambda_i^2 \tau}\{\cos(\lambda_i \xi) - \frac{\lambda_i}{\beta}\sin(\lambda_i \xi)\} \\ (\frac{\lambda_i^2 - \beta^2}{2\beta\lambda_i})\tan\lambda_i = 1 \end{aligned} \tag{5-7}$$

where $\beta=(Al)/V_B$, a_i is given by

$$a_j = \frac{h_1^o Z_j(1) + h_0^o Z_j(0) + \beta\int_0^1 h_\xi^o Z_j d\xi}{Z_j^2(1) + Z_j^2(0) + \beta\int_0^1 Z_j^2 d\xi} \tag{5-8}$$

and

$$\begin{aligned} h_\xi^o &= f(\xi,0) - \frac{1}{2} \\ Z_j &= \cos(\lambda_i \xi) - \frac{\lambda_i}{\beta}\sin(\lambda_i \xi) \end{aligned} \tag{5-9}$$

and the other parameters are as previously defined. Note that β in this equation is not related to the β in the reactor balances (Chapter IV).

The effective diffusion coefficient estimated from the concentration-time data for H_2O_2 using equation (B-11) (this uses the pseudo steady state assumption to estimate the diffusion coefficient) was used with this equation, along with the reactor measurements (see Chapter IV) to determine the time needed to reach steady state. The solution, for times up to 2 minutes, are plotted in Figure 5.4; steady state was achieved in only

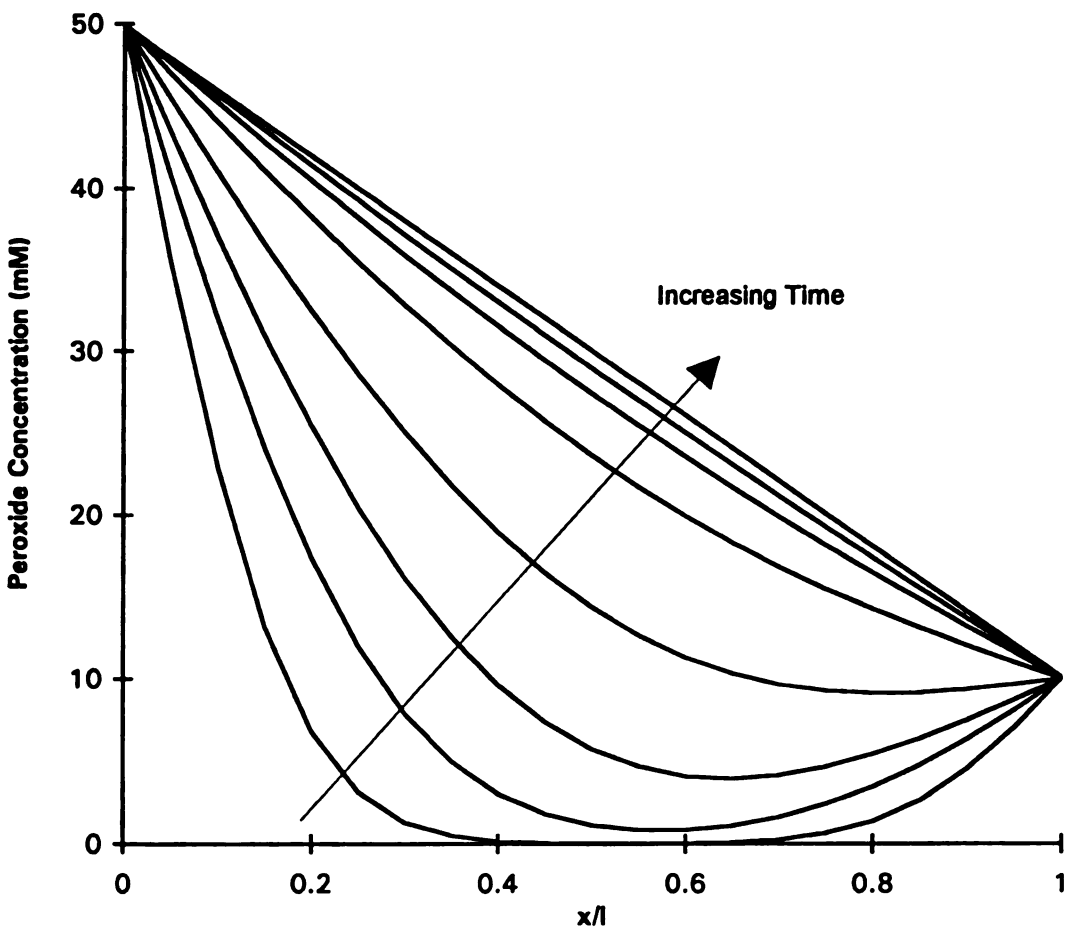

Figure 5.4: Solution of the unsteady state diffusion equation for diffusion through the membrane of the dialysis reactor for H_2O_2 using a value of 1.80×10^{-4} cm^2/min for the diffusion coefficient. Shown are the concentration profiles within the membrane with dimensionless distance for 0.002, 0.005, 0.010, 0.020, 0.040, 0.060, 0.080, and 0.500 minutes.

30 seconds. The diffusion coefficient used was 1.80×10^{-4} (cm^2/min), and was calculated by averaging the solution of equation (B-11) evaluated at each time point, and using all diffusion experiments for H_2O_2 (different initial $[H_2O_2]_{A_o}$ in each run). Order-of-magnitude changes in the diffusion coefficient had relatively little effect, increasing or decreasing the time to reach steady state by a minute or so each way. The measured effective diffusion coefficient for Mn(II) was on the same order of magnitude as that for H_2O_2, so the equation was solved only for H_2O_2. Therefore, the pseudo steady state approximation was used to estimate the diffusion coefficients of H_2O_2 and Mn(II), but using data from all the experiments (different $[H_2O_2]_{A_o}$ and not just single time points.

In order to do this for H_2O_2, equation (B-5) was solved to give $[H_2O_2]_B$ as a function of time, and this expression was solved for time to yield

$$lhs = t = -\left(\frac{lV_B}{2D^{eff}_{H_2O_2}A}\right) \ln\left\{\frac{\frac{1}{2}([H_2O_2]_{A_o}+[H_2O_2]_{B_o})-[H_2O_2]_B}{\frac{1}{2}([H_2O_2]_{A_o}-[H_2O_2]_{B_o})}\right\} \qquad (5\text{-}10)$$

where "lhs" stands for the "left-hand-side" of the equation, and is actually the "time" calculated from each concentration measurement. The data from all transport experiments for H_2O_2 were combined, the value of "lhs" calculated for each concentration/time point, and the resulting data were plotted versus the actual experimental time at which the data were taken. Using a shooting method, values for D^{eff} were chosen, the value of "lhs" was calculated, and the resulting data set was fitted versus actual time values using linear regression. The value of D^{eff} which gave the best fit to the data was chosen as the true value of D^{eff} for H_2O_2; this value was determined to be 1.700×10^{-4} cm^2/min, with an r^2 of 0.968. The final iteration of the shooting method, with the best fit to the data, is presented in Figure 5.5.

In the case of Mn(II), the concentration in Side B was too low to measure by titration with EDTA (see Chapter IV), so $[Mn(II)]_A$ was measured and used to calculate

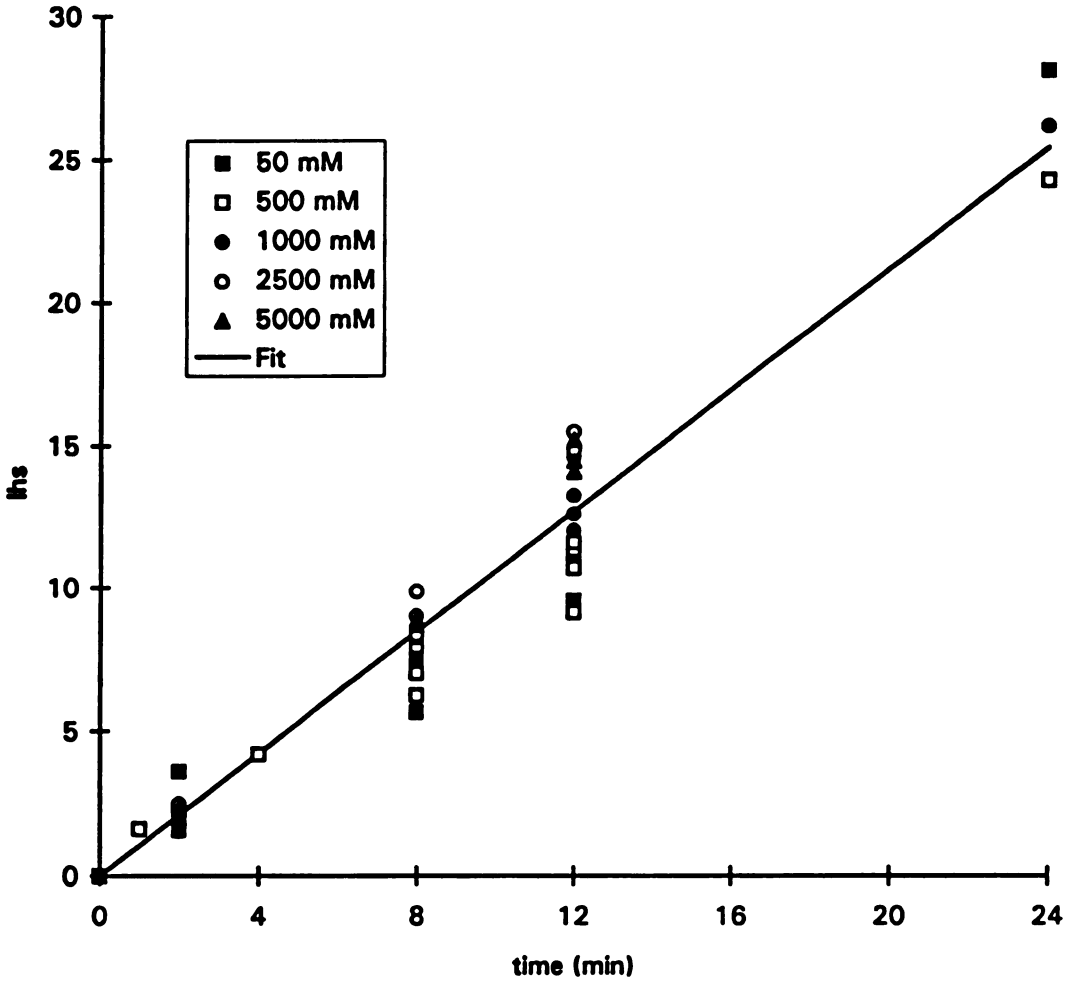

Figure 5.5: The final iteration values of lhs versus time for the determination of D^{eff} for H_2O_2. Initial $[H_2O_2]_A$ concentrations for each data set are listed in the legend box. r^2 for the fit was 0.968.

the effective diffusion coefficient for Mn(II). When equation (B-4) is solved for $[Mn(II)]_A$ instead of $[MN(II)]_B$, it gives

$$lhs = -D^{eff}_{Mn(II)}t = \left(\frac{lV_A}{2A}\right) \ln\left\{\frac{2[Mn(II)]_A}{[Mn(II)]_{Ao}+[Mn(II)]_{Bo}} - 1\right\} \qquad (5\text{-}11)$$

This equation is analogous to equation (5-10) above, except that "lhs" is equal to the effective diffusion coefficient multiplied by time and not just equal to time. This equation was solved in a manner identical to that described above for H_2O_2; the final iteration is presented in Figure 5.6. The best fit value of D^{eff} for Mn(II) was 1.319×10^{-4} cm^2/min, with an r^2 of 0.999.

5.3.2 Veratryl Alcohol

The effective diffusion coefficient for VA was also estimated initially using equation (B-11), even though it was found to depend on [VA], as shown in Figure 5.7. To include to variation of D^{eff} for VA with VA concentration, equation (5-7) above was solved using both the highest and lowest values for D^{eff} for VA estimated from equation (B-11) (at the highest and lowest $[VA]_A$, respectively; see Figure 5.7). The estimated highest and lowest values for D^{eff} for VA were 4.37×10^{-5} and 1.00×10^{-5} cm^2/min, respectively. The solution for each value of D^{eff} for VA used are shown in Figures 5.8 and 5.9; the times required to reach steady state were 30 seconds and 2 minutes, respectively. Since the value of D^{eff} for VA was not expected to exceed these bounds (a reasonable assumption), it was decided to use the steady state approximation for VA diffusion, also.

The form of the VA diffusion equation used in the reactor model is derived in Appendix B. The diffusion coefficient was found to depend exponentially on VA concentration due to solution viscosity effects and to the effect of increasing radius of molecular aggregates in solution (see Chapter IV for a discussion of this point). The dependence of solution viscosity on VA concentration is shown in Figure 5.10; this

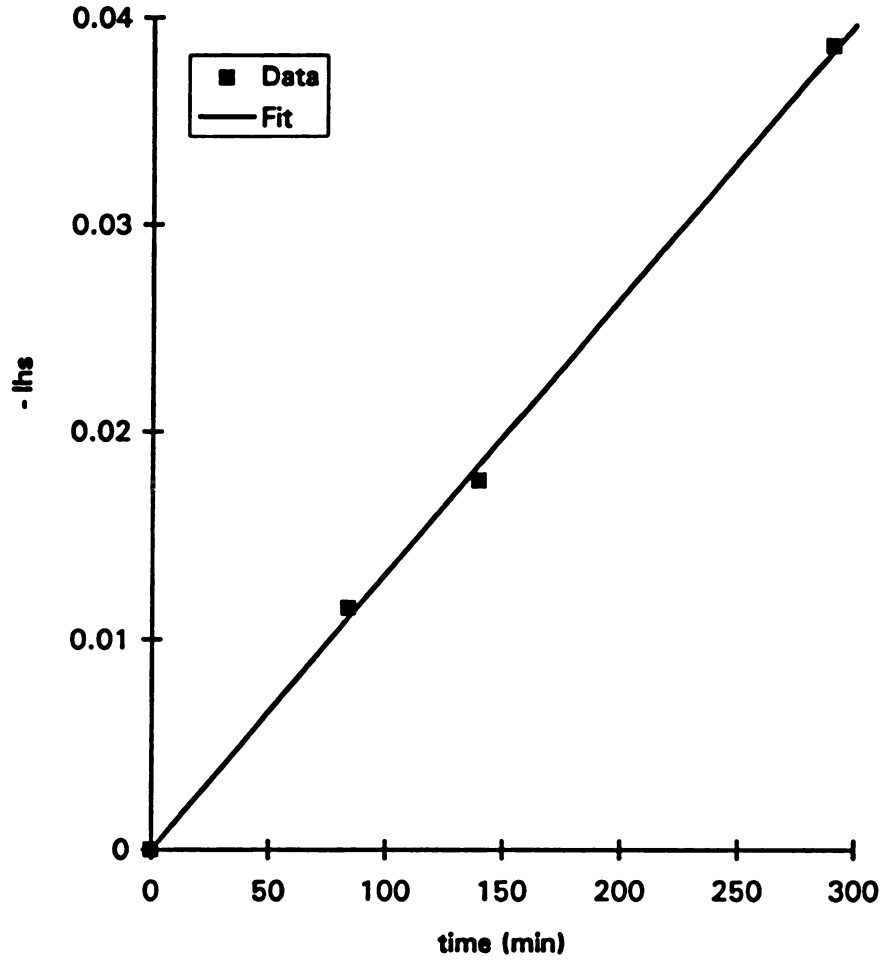

Figure 5.6: The final iteration values of -lhs versus time for the determination of D^{ef} for Mn(II). r^2 for the fit was 0.999.

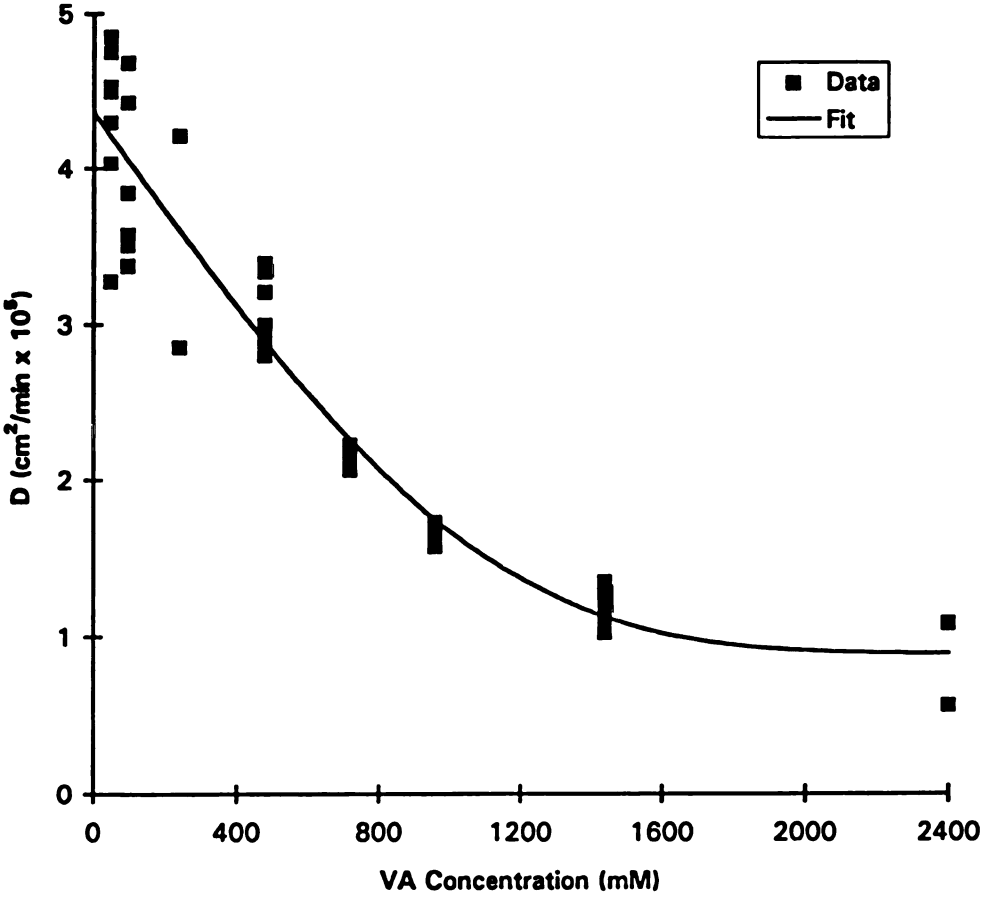

Figure 5.7: Effective diffusion coefficient for VA calculated from the $[VA]_B$ versus time data assuming that D^{eff} for VA was independent of concentration and that steady state could be assumed. The data were fit using PEAKFIT to the equation

$$D_{VA}^{eff} = a_o + a_1 \exp(a_2 \exp\{-\frac{[VA]_A}{a_3}\} - a_4) \qquad (5\text{-}12)$$

Values of a_o, a_1, a_2, a_3, and a_4 were found to be 8.865×10^{-6}, 3.213×10^{-6}, -1.051, -1134.8, and -3.435, respectively. r^2 for the fit was 0.928.

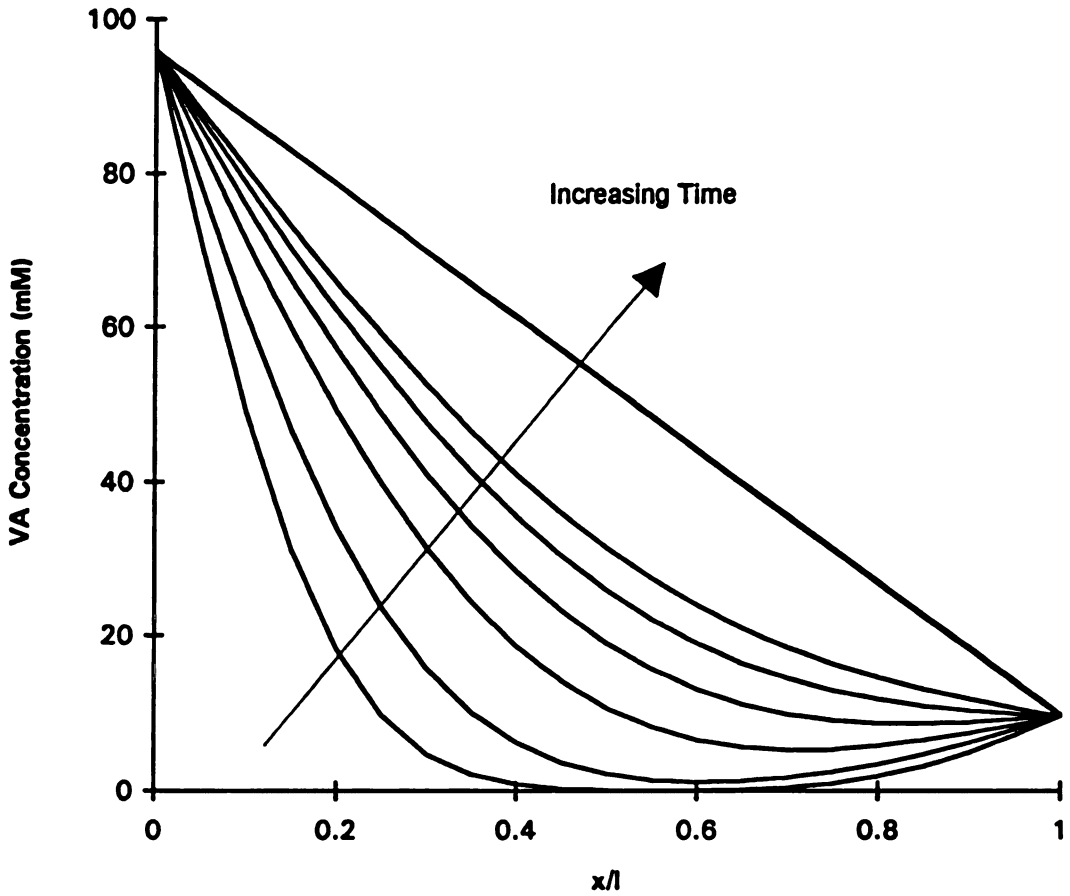

Figure 5.8: Solution of the unsteady state diffusion equation for diffusion through the membrane of the dialysis reactor for VA using a value of 4.37×10^{-5} cm^2/min for the diffusion coefficient. Shown are the concentration profiles within the membrane with dimensionless distance for 0.010, 0.020, 0.040, 0.060, 0.080, 0.160, 0.500, and 2.00 minutes.

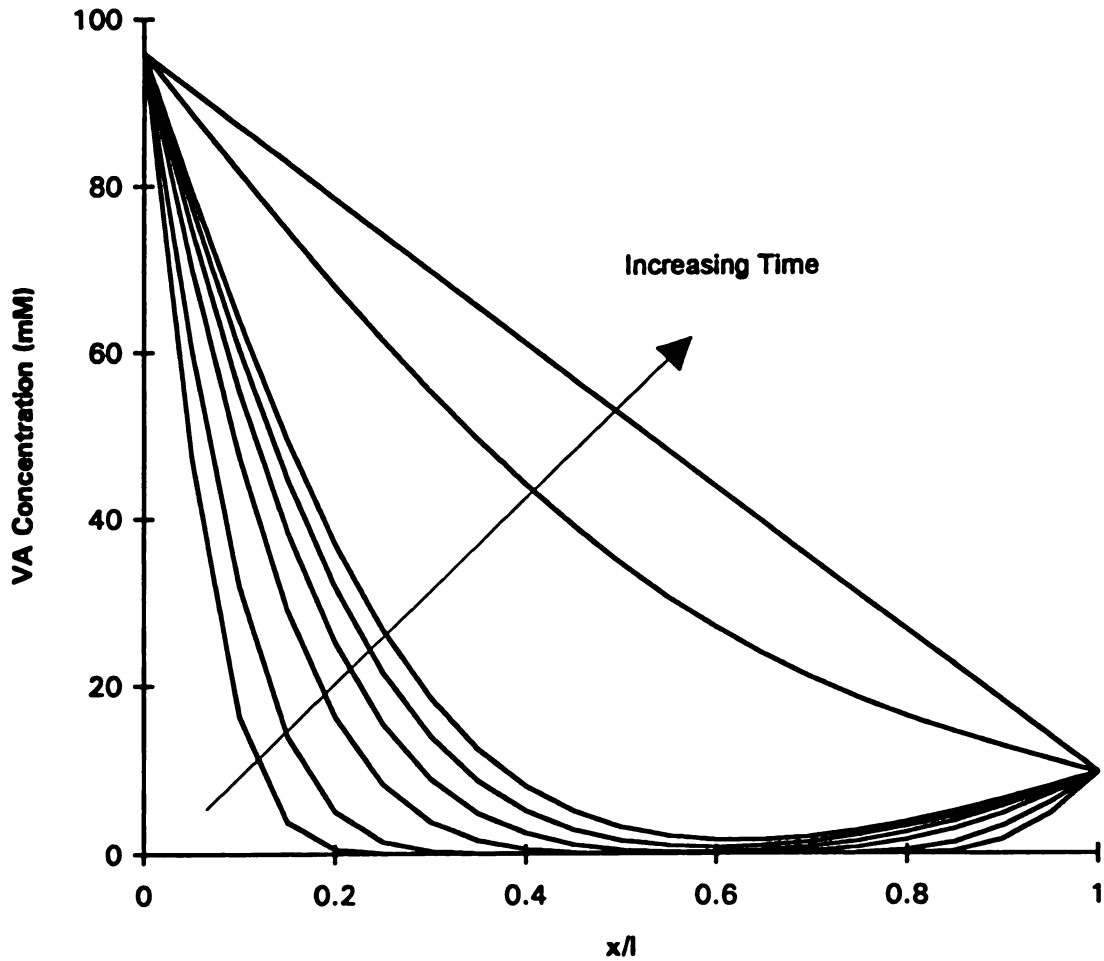

Figure 5.9: Solution of the unsteady state diffusion equation for diffusion through the membrane of the dialysis reactor for VA using a value of 1.00×10^{-5} cm^2/min for the diffusion coefficient. Shown are the concentration profiles within the membrane with dimensionless distance for 0.010, 0.020, 0.040, 0.060, 0.080, 0.160, 0.500, and 2.00 minutes.

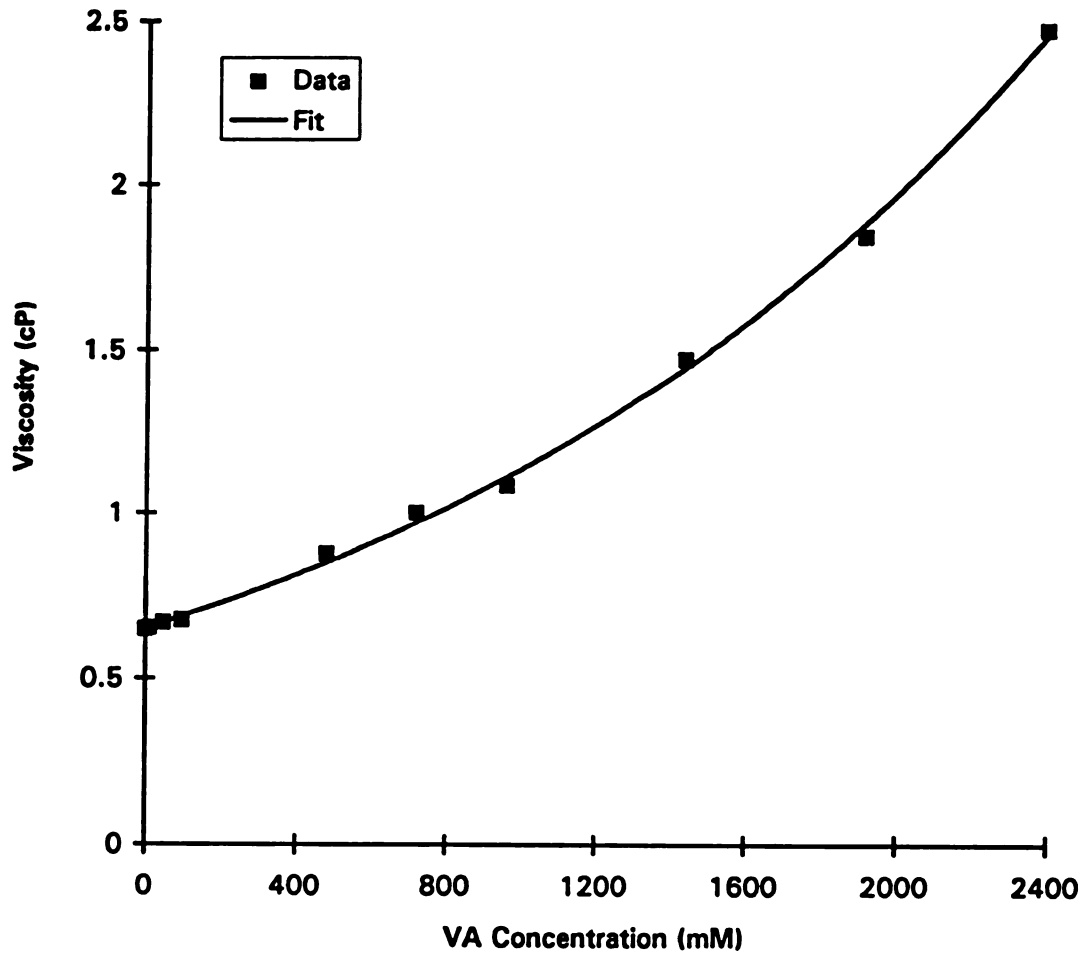

Figure 5.10: Variation of the viscosity of aqueous VA solutions with [VA], and the exponential viscosity fit determined using PEAKFIT. r^2 for the fit was 0.999.

dependence is clearly exponential (μ^o = 0.6529 cP, α = 5.532 × 10^{-4} mM^{-1}, r^2 = 0.999), which is supported by common viscosity-concentration relationships published in the literature (Bird *et al.*, 1960). Equation (B-12) was used, with the value of μ determined from the fit depicted in Figure 5.10, to determine the best values of D^o and a_1 (a_1 is the additional exponential term due to aggregate radius effects, and was necessary to obtain a good fit to the data; see Chapter IV), where

$$D_{VA}^{eff} = D^o e^{-(\alpha + a_1^{-1})[VA]} \qquad \text{(B-7)}$$

Equation (B-12) was solved for D^ot (again named "lhs"); lhs then depended only on D^o, while the right-hand-side of the equation depended only on a_1. To find the best values for D^o and a_1, a value of a_1 was chosen and lhs was calculated for each concentration-time data point. The values were then plotted versus the time at which the data were originally taken, and the best fit slope was determined using linear regression (the slope is equal to D^o). This was repeated over a wide range of values of a_1. At each value of a_1, the total residual error for the fit was calculated; these values were then plotted versus a_1, and the "true" values of D^o and a_1 were chosen at the point where the residual error was minimized. The method broke down at concentrations above 720 mM VA, so data above the value were excluded; this probably occurred because the Stokes-Einstein equation, which was used to derive the final form of the diffusion coefficient (including the exponential dependence on aggregate radius), is only valid for dilute solutions (Bird *et al.*, 1960). The plot of "lhs" versus time used to estimate the best fit values for D^o and a_1 (minimum total residual error) is shown in Figure 5.11. The values of D^o and a_1 were determined to be 4.494 × 10^{-5} cm^2/min and 600 mM, respectively; r^2 for the fit was 0.986. Using this value of a_1, the dependence of VA molecular aggregate radius was calculated; this relationship is plotted in Figure 5.12. The aggregate radius at infinite dilution was calculated from the y-intercept of this plot, and was found to be 46.5 Å. This value seems to be unusually high, considering that the molecular weight of VA

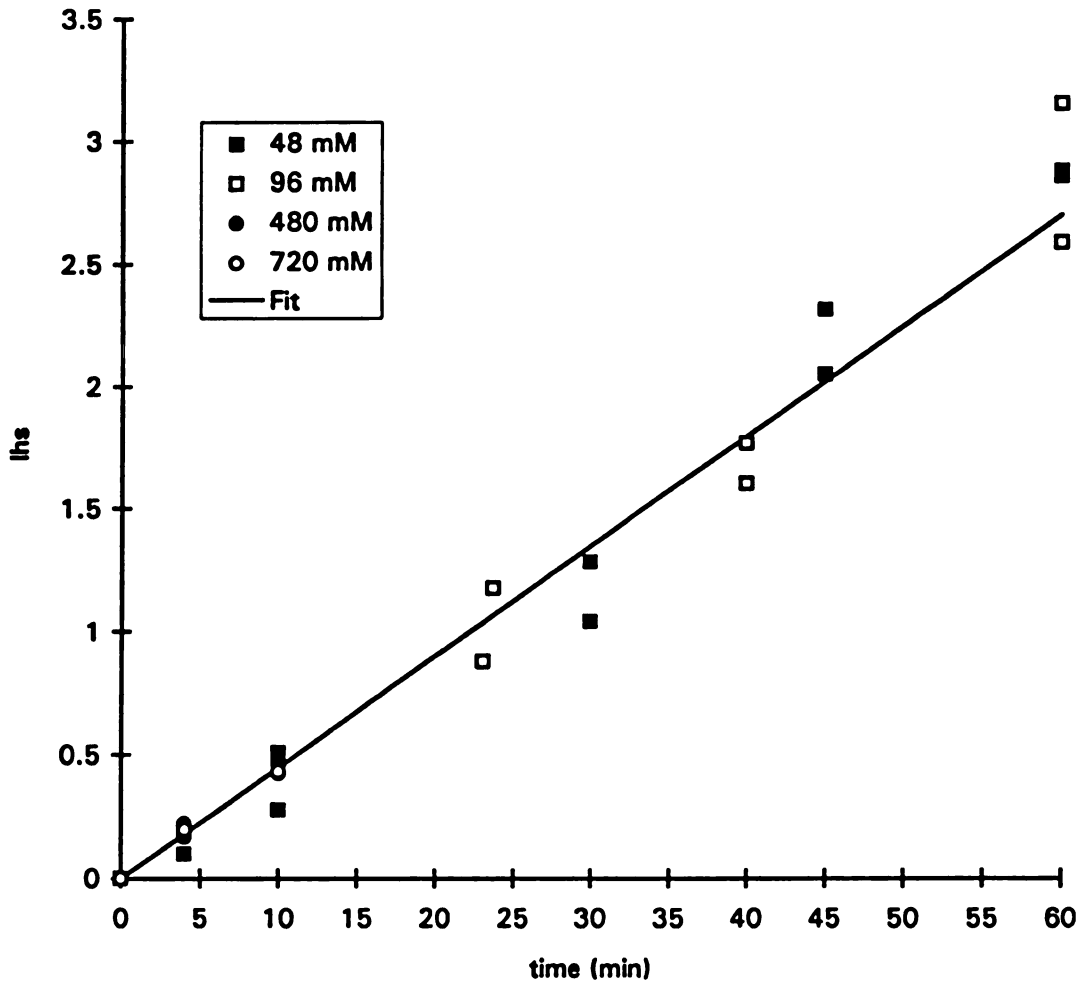

Figure 5.11: The final iteration values of lhs versus time for the determination of D^o and a_1 for the concentration dependence of D^{ef} for VA. Initial $[VA]_A$ concentrations for each data set are listed in the legend box. r^2 for the fit was 0.986.

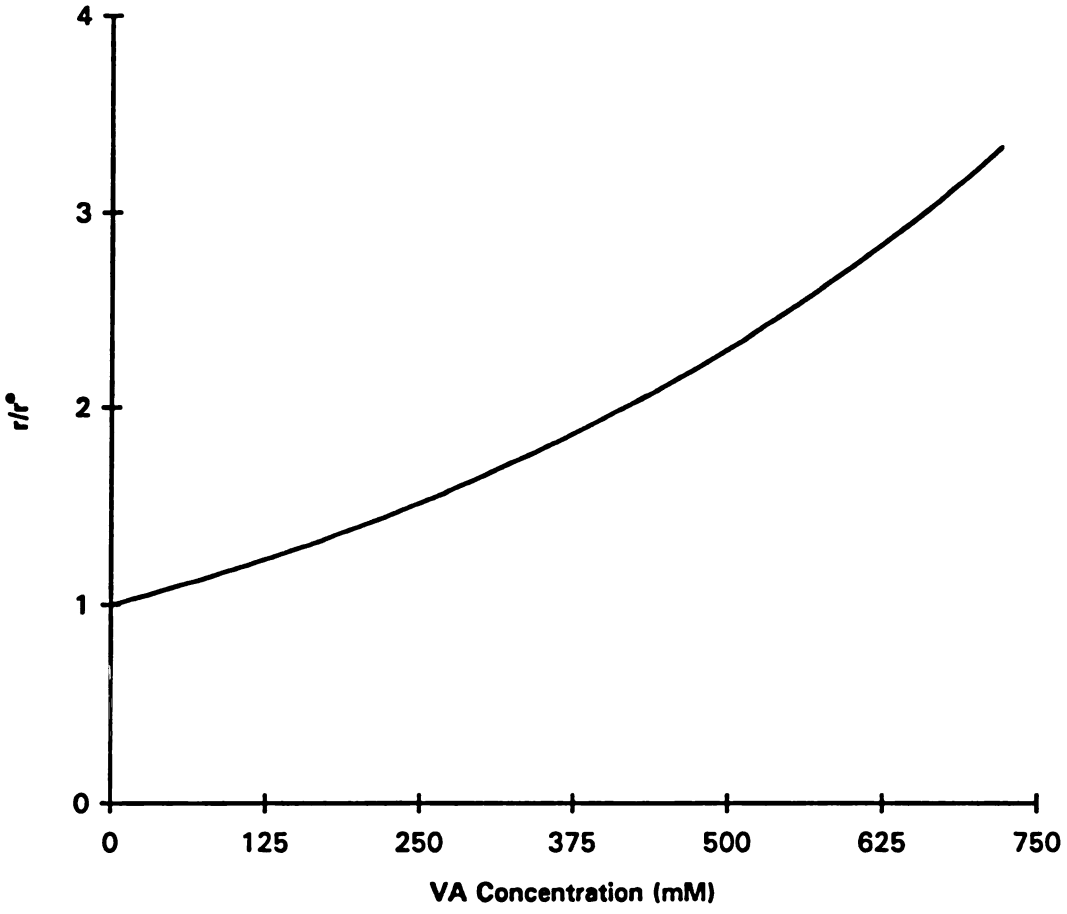

Figure 5.12: Predicted variation of VA aggregate radius with the concentration of VA, determined using the value of a_1 calculated in the determination of D^{dl} for VA.

is only 168 g/mole, and that the molecule is essentially planar (VA is 3,4-dimethoxy benzyl alcohol). Perhaps this indicates that the additional exponential term needed to get a good fit to the data was not entirely attributable to aggregate radius (or even not at all); since this question is beyond the scope of this project, it will not be discussed further here.

5.3.3 [Mn(III)-tart$_2$]

Since [Mn(III)-tart$_2$] was not stable enough to take samples and store them for later analysis, and since no simple way of measuring its concentration on-line was available, the Stokes-Einstein equation was used to estimate the value of D^{eff} for [Mn(III)-tart$_2$] from the value of D^{eff} measured for Mn(II). Assuming that Mn(II) is in a high spin state (Nicholls, 1974), its radius is 82 pm. In water, Mn(II) is coordinated with 6 water molecules in octahedral coordination (Mellor, 1979), but these water molecules are constantly exchanging with other water molecules as the ion diffuses through the bulk liquid. Thus, the effective diameter of the [Mn(II)-6H_2O] was assumed to be simply the diameter of the Mn(II) ion. Assuming that the viscosity of dilute solutions of [Mn(III)-tart$_2$] and [Mn(II)-6H_2O] are the same (equal to the viscosity of water), ratioing the Stokes-Einstein equations evaluated for each species yields the relationship

$$\frac{D^{eff}_{[Mn(III)\text{-}tart_2]}}{D^{eff}_{[Mn(II)\text{-}6H_2O]}} = \frac{r_{[Mn(III)\text{-}6H_2O]}}{r_{[Mn(III)\text{-}tart_2]}} \qquad (5\text{-}13)$$

Using the measured value of D^{eff} for Mn(II), the estimated radius of the [Mn(III)-tart$_2$] complex (see Chapter IV), and the diameter of Mn(II) listed above, D^{eff} for [Mn(III)-tart$_2$] was calculated to be 2.020×10^{-5} cm^2/min.

5.4 Kinetics of VA Oxidation by LIP

Recorder traces from the LIP kinetic experiments were converted to numerical data using an extinction coefficient of 9300 M^{-1}cm^{-1}, the chart speed, and the full scale OD to yield rate versus concentration data for each case described in Chapter IV. The

reciprocals of each data point were calculated and plotted in a Lineweaver-Burk arrangement (double reciprocal plot), which was then used to calculate the kinetic constants. Each case treated is described in turn below.

5.4.1 Case 1: Excess VA, $[H_2O_2]/K_I \approx 0$.

The Lineweaver-Burk plot for this case is presented in Figure 5.13. [LIP] for this case was 155.7 U/L, with [VA] at 52.08 mM; $[H_2O_2]$ was varied from 9.628 to 1905 μM. The increase in [LIP]/v at low values of $1/[H_2O_2]$ is typical for competitive inhibition (Bailey and Ollis, 1986). The data (not including the points where competitive inhibition was influencing the reaction rate (ie. where [LIP]/v increased as $1/[H_2O_2]$ decreased) were fitted to a line using linear regression; the slope and intercept were 46.58 min(U/L) and 799.5 min(U/L)/mM, with an r^2 of 0.939. The value of k_1 (calculated from the slope) was then 2.147×10^{-2} $(\text{min(U/L)})^{-1}$. The value of the intercept was kept for future use in estimating k_4 (see below).

5.4.2 Case 2: Excess H_2O_2, $[H_2O_2]/K_I \approx 0$.

The Lineweaver-Burk plot for Case 2 is presented in Figure 5.14. [LIP] for this case was again 155.7 U/L, with $[H_2O_2]$ at 192.3 μM; [VA] was varied from 20.00 to 579.1 μM. The concentration of H_2O_2 in this case was not in excess over the entire range of the [VA] used in the measurements; this was because competitive inhibition by H_2O_2 began to affect the rate in the range 400-500 μM $[H_2O_2]$. Thus, a lower concentration of H_2O_2 was used to make sure that no inhibition was taking place; at any rate, the lowered $[H_2O_2]$ did not affect the linearity of the Lineweaver-Burk plot (see Figure 5.14). The data were fitted to a line using linear regression; the slope and intercept were 130.3 min(U/L) and 944.5 min(U/L)/mM, with an r^2 of 0.996. The value of k_3 (calculated from the slope) was then 7.676×10^{-3} $(\text{min(U/L)})^{-1}$. The value of the intercept was kept for future use in estimating k_4 (see below).

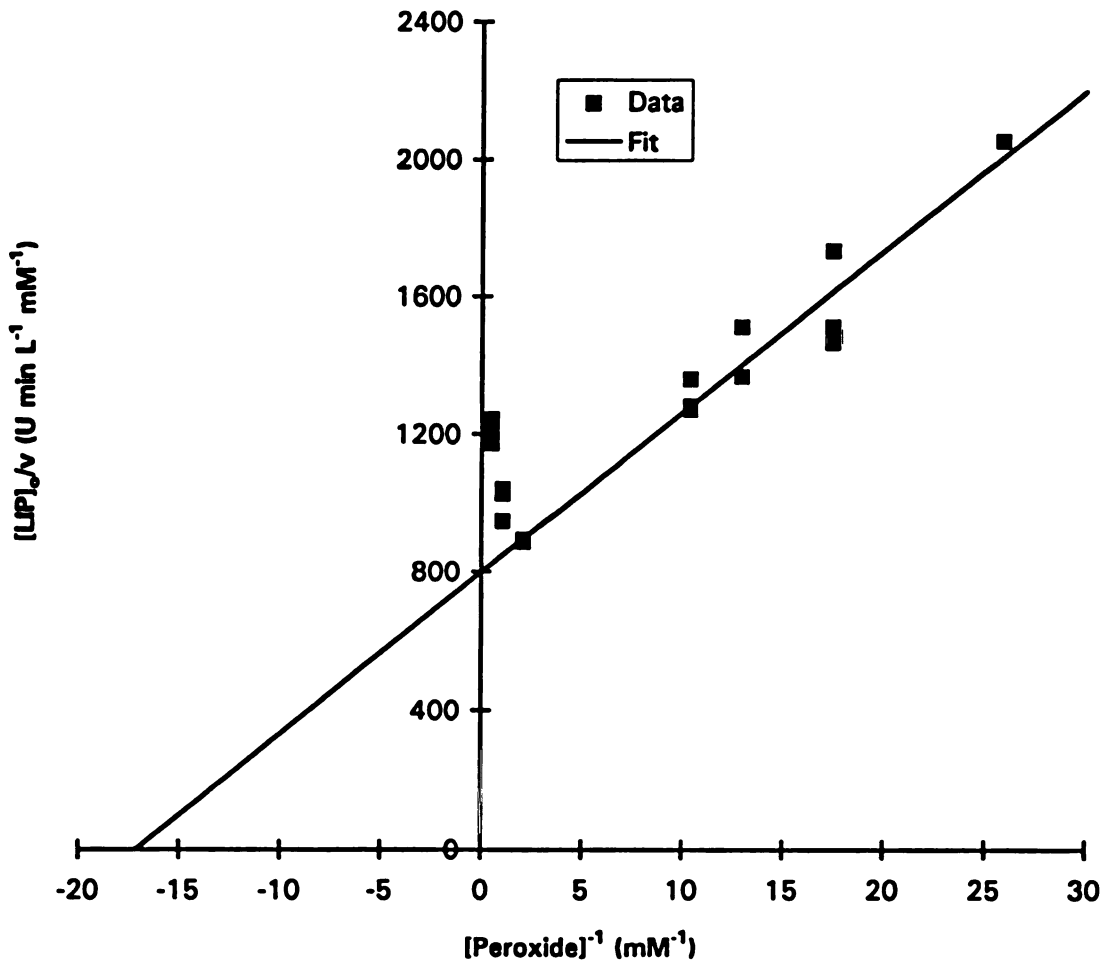

Figure 5.13: Lineweaver-Burk plot for Case 1 (excess VA) of the LIP/VA kinetic experiments. r^2 for the fit was 0.939.

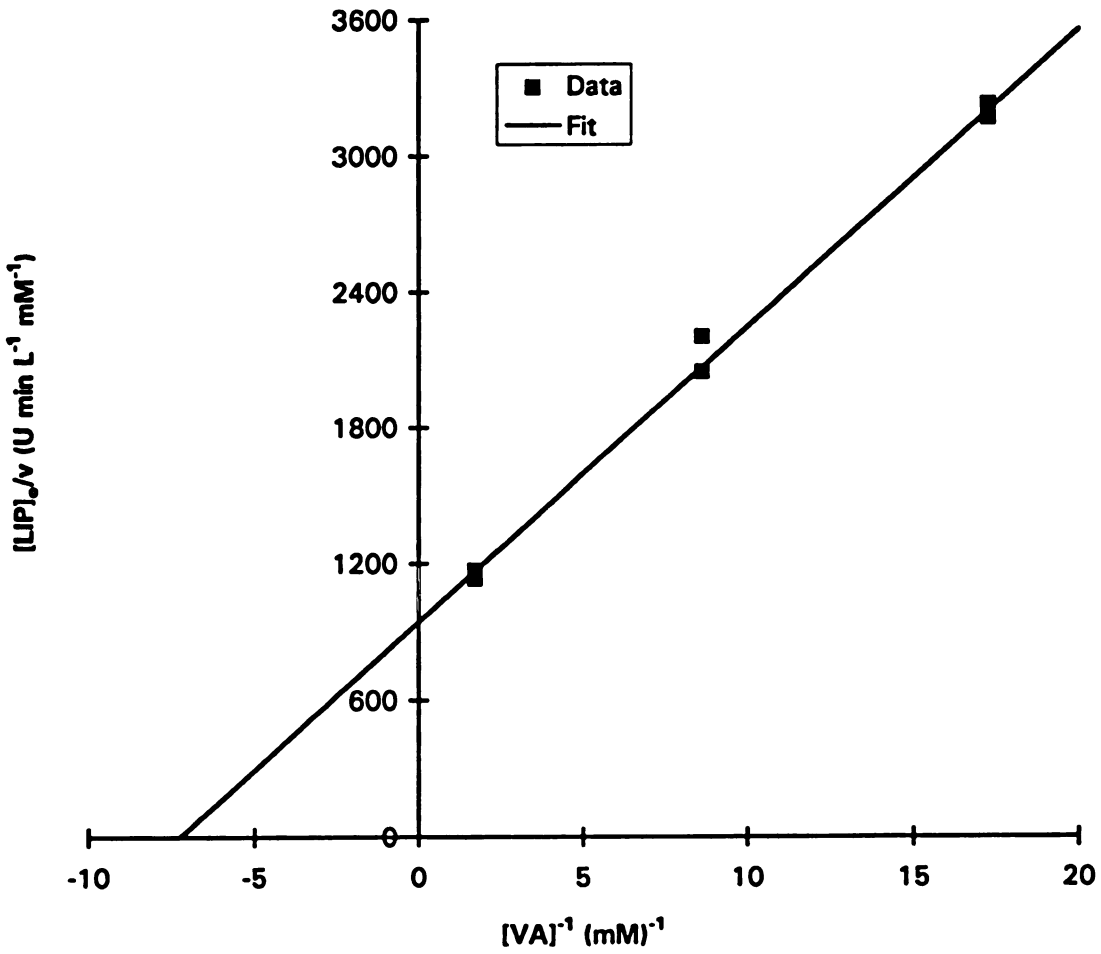

Figure 5.14: Lineweaver-Burk plot for Case 2 (excess, noninhibiting H_2O_2) of the LIP/VA kinetic experiments. r^2 for the fit was 0.996.

5.4.3 Case 3: Excess H_2O_2, $[H_2O_2] \approx K_I$

The Lineweaver-Burk plot for Case 3 is presented in Figure 5.15; each line represents a separate experiment with a different $[H_2O_2]$. [LIP] for this case was again 155.7 U/L. Complete experiments were done with $[H_2O_2]$ at 481.5, 940.4, 1428, and 1905 μM, respectively; [VA] was varied in each from 57.91 to 579.1 μM. Each set of data was fitted to a line using linear regression; the slopes, intercepts, and values of r^2 for each are presented in Table 5.3. For true competitive inhibition, all four lines should intercept the y-axis at the same point; indeed, an analysis of variance of the intercepts of the lines indicated no statistical difference in the intercepts (data not shown). The values of the intercepts from Figure 5.15 were kept for future use in estimating k_4 (see below). The slopes were plotted versus $[H_2O_2]$; this is shown in Figure 5.16; r^2 for this plot is 0.929, with a slope of 23.85 min(U/L)/mM and a y-intercept of 117.3 min(U/L). Another value for k_3, 8.527×10^{-3} $(\text{min(U/L)})^{-1}$, was estimated from the y-intercept of this plot and averaged with the value of k_3 calculated from Case 2 above. The averaged value of k_3 was used, with the slope of Figure 5.16, to calculate K_I. The averaged value of k_3 was found to be 8.101×10^{-3} $(\text{min(U/L)})^{-1}$, and the value of K_I was found to be 4.918 mM. At this point, two estimates of k_3 were known, one estimate of k_1 was known, and there were six equations relating k_4 to either k_1 or k_3. A value for k_4 was calculated from each intercept equation, using both values of k_3 (to get two estimates for k_4) and the single estimate of k_1; this gave seven estimates of k_4. The seven values were averaged, and any values more than two standard deviations away from the mean were dropped (only one estimate was dropped). The "true" value of k_4, 1.246×10^{-3} mM(min(U/L)^{-1} was then calculated as the average of the remaining six estimates. To summarize, the values of the LIP kinetic constants k_1, k_3, k_4, and K_I were found to be 2.147×10^{-2} $(\text{min(U/L)})^{-1}$, 8.101×10^{-3} $(\text{min(U/L)})^{-1}$, 1.246×10^{-3} mM(min(U/L)^{-1}, and 4.918 mM, respectively.

Table 5.3: Slopes, intercepts, and r^2 for the statistical fits of the LIP/VA kinetic data for Case 3 (inhibiting H_2O_2).

$[H_2O_2]$ (μM)	slope (U min/L)	y-intercept (Umin/L mM)	r^2
481.5	130.5	886.1	0.991
940.4	140.0	858.3	0.955
1428	145.6	861.5	0.995
1905	166.4	817.9	0.994

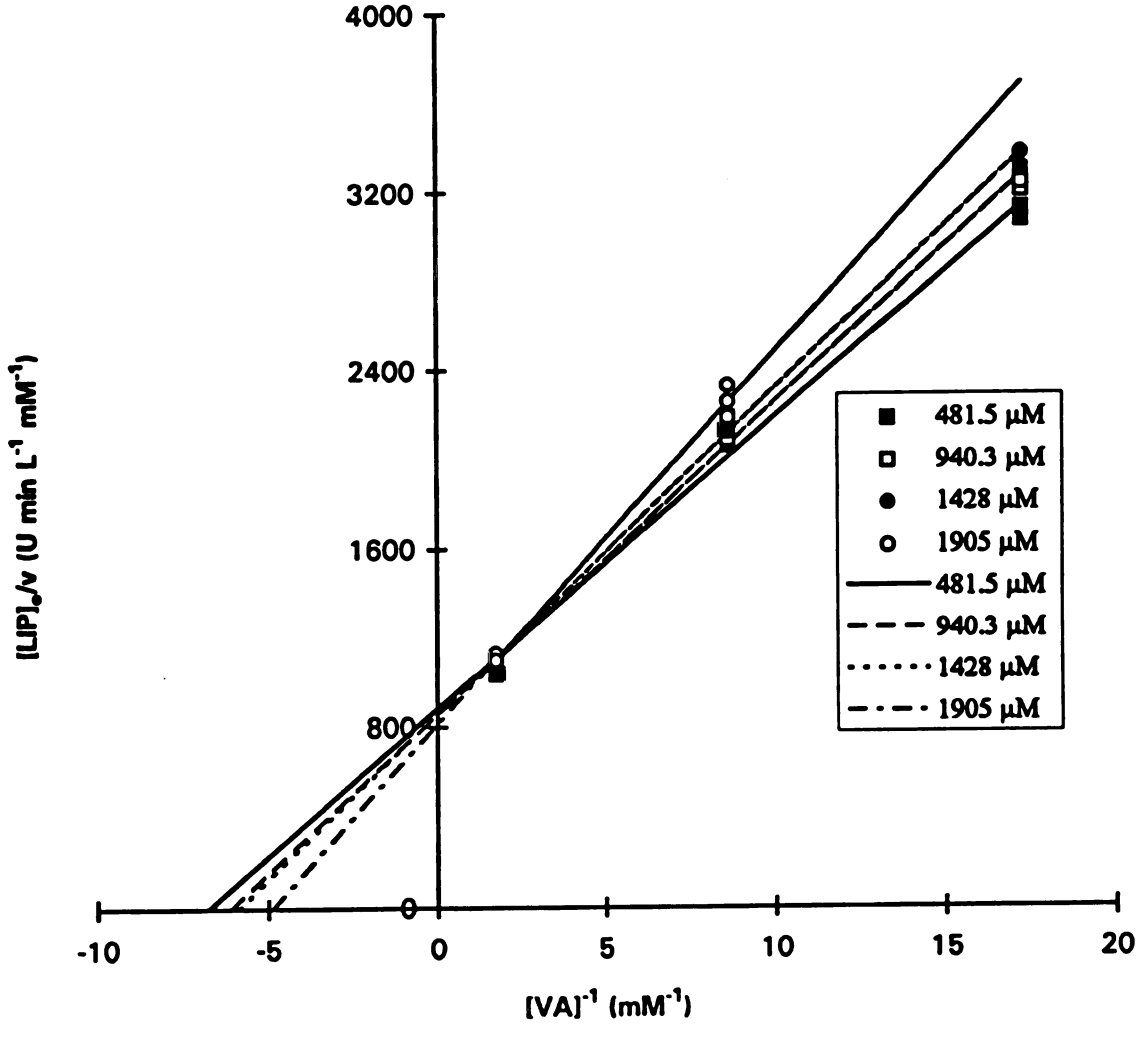

Figure 5.15: Lineweaver-Burk plot for Case 3 (excess, inhibiting H_2O_2) of the LIP/VA kinetic experiments. The intercepts are not statistically different within 95 % confidence, indicating competitive substrate inhibition. H_2O_2 concentrations are listed in the legend box, along with the corresponding fits.

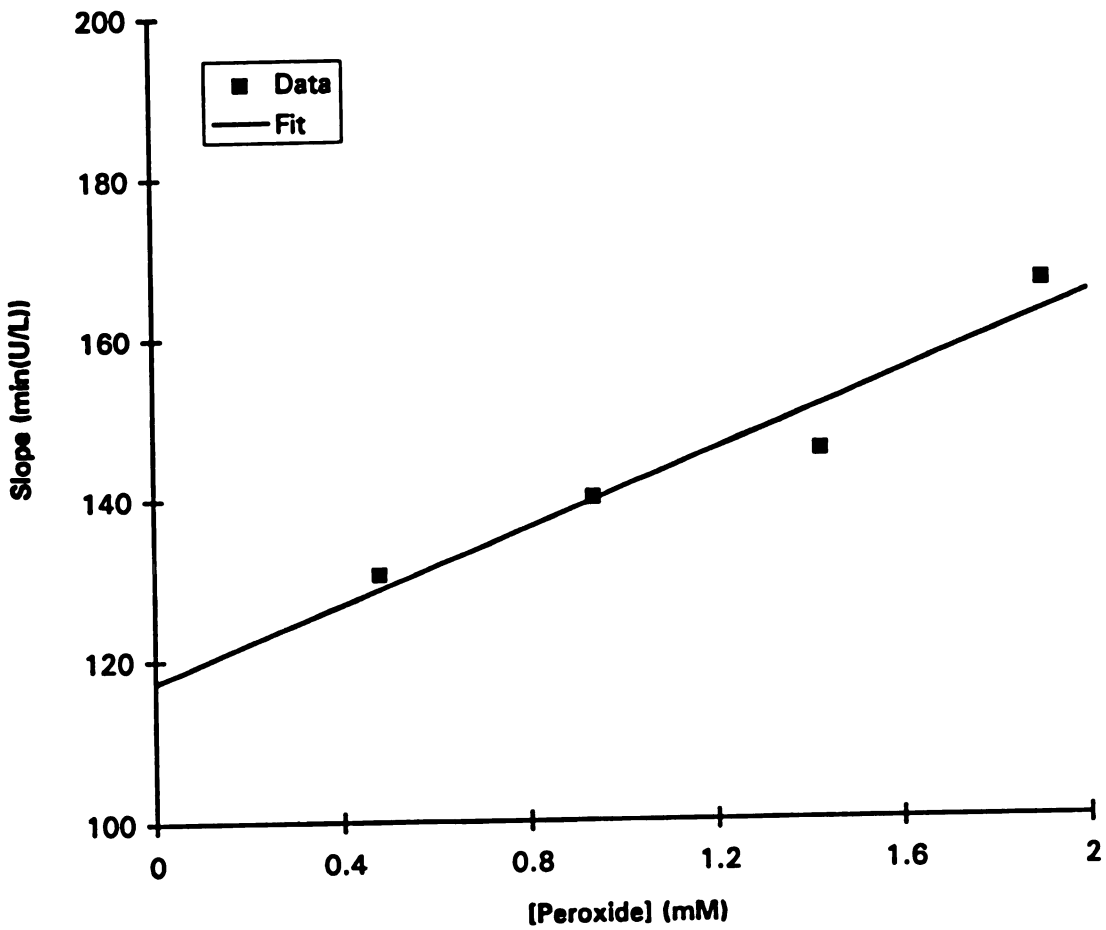

Figure 5.16: Secondary slope plot for Case 3 (excess, inhibiting H_2O_2) of the LIP/VA kinetic experiments. r^2 for the fit was 0.929.

5.5 MNP/Mn(II) and Mn(III) Kinetics

Recorder traces from the MNP kinetic experiments were converted to numerical data using an extinction coefficient of 6500 $M^{-1}cm^{-1}$, the chart speed, and the full scale OD to yield rate versus concentration data for each source of MNP described in Chapter IV. The reciprocals of each data point were calculated and plotted in a Lineweaver-Burk arrangement as for the LIP kinetics (Case 1), which was then used to calculate the kinetic constants. The kinetic rate constant for [Mn(III)-$tart_2$] reduction through the oxidation of lignin bonds was estimated from literature data, combined with several assumptions. Each case is described in turn below.

5.5.1 Kinetics of Mn(II) Oxidation by D5NoMn MNP (MNP_a)

The Lineweaver-Burk plot for MNP_a is presented in Figure 5.17. [MNP] for this case was 1000 U/L (by MNP Assay #1), with [Mn(II)] at 2.000 mM; [H_2O_2] was varied from 38.62 to 481.5 μM. The data were fitted to a line using linear regression; the slope and intercept were 76.15 min(U/L) and 745.8 min(U/L)/mM, with an r^2 of 0.938. The value of k_{5a} (calculated from the slope) was then 6.566×10^{-3} $(min(U/L))^{-1}$, and the value of Ψ_a (calculated from the intercept) was found to be 2983 min(U/L)/mM.

5.5.2 Kinetics of Mn(II) Oxidation by D4HiMn MNP (MNP_b)

The Lineweaver-Burk plot for MNP_b is presented in Figure 5.18. [MNP] for this case was 3160 U/L (by MNP Assay #1), with [Mn(II)] at 2.000 mM; [H_2O_2] was varied from 10.59 to 544.7 μM. The data were fitted to a line using linear regression; the slope and intercept were 98.25 min(U/L) and 584.2 min(U/L)/mM, with an r^2 of 0.959. The value of k_{5b} (calculated from the slope) was then 5.089×10^{-3} $(min(U/L))^{-1}$, and the value of Ψ_b (calculated from the intercept) was found to be 2337 min(U/L)/mM. Note that the kinetic constants for MNP_a and MNP_b are different -- this is because the MNP from each source is made up of different relative amounts of the various MNP isoenzymes H3, H4, H5, and H9. Each isoenzyme has its own k_5 and Ψ values, and the values measured are in effect "averaged" over all the isoenzymes.

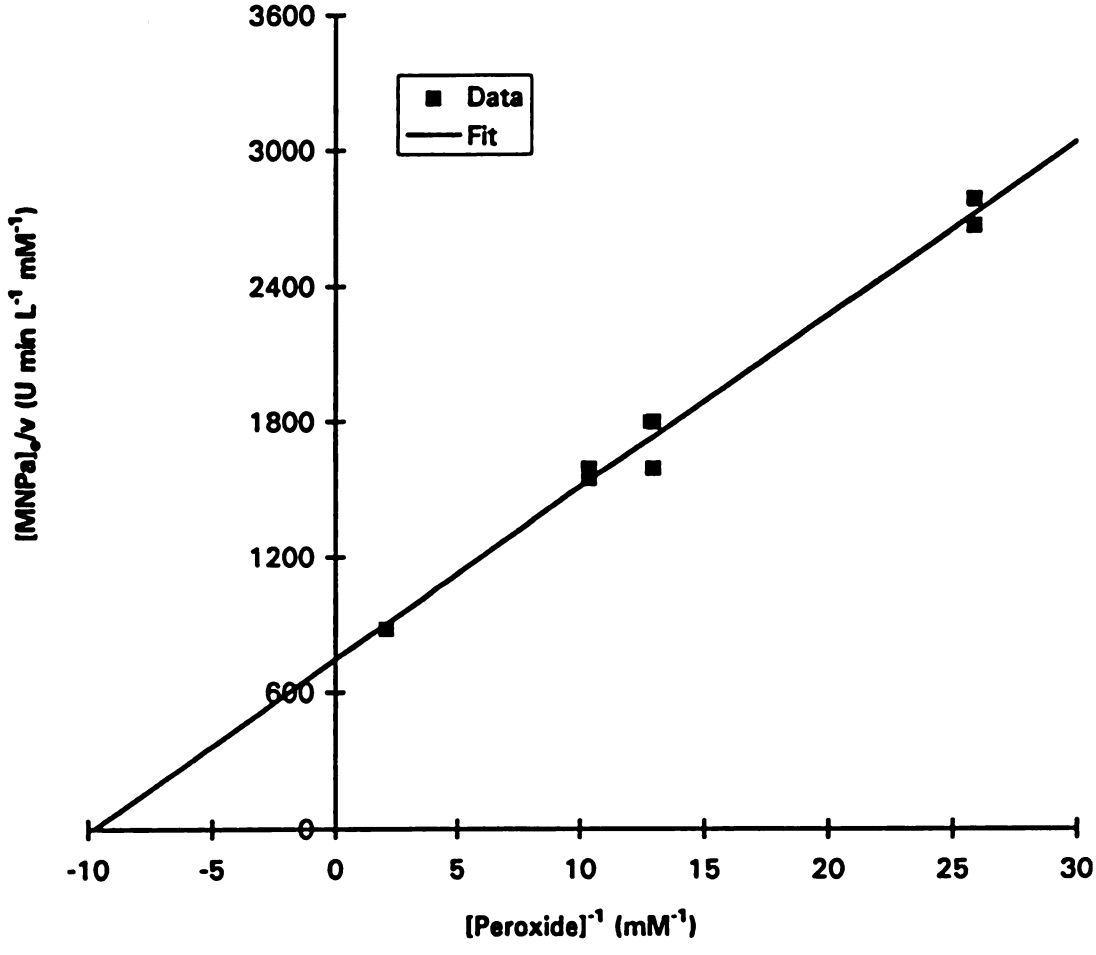

Figure 5.17: Lineweaver-Burk plot for the MNP/Mn(II) kinetic experiments (excess Mn(II)) using D5NoMn MNP (MNP_a). r^2 for the fit was 0.938.

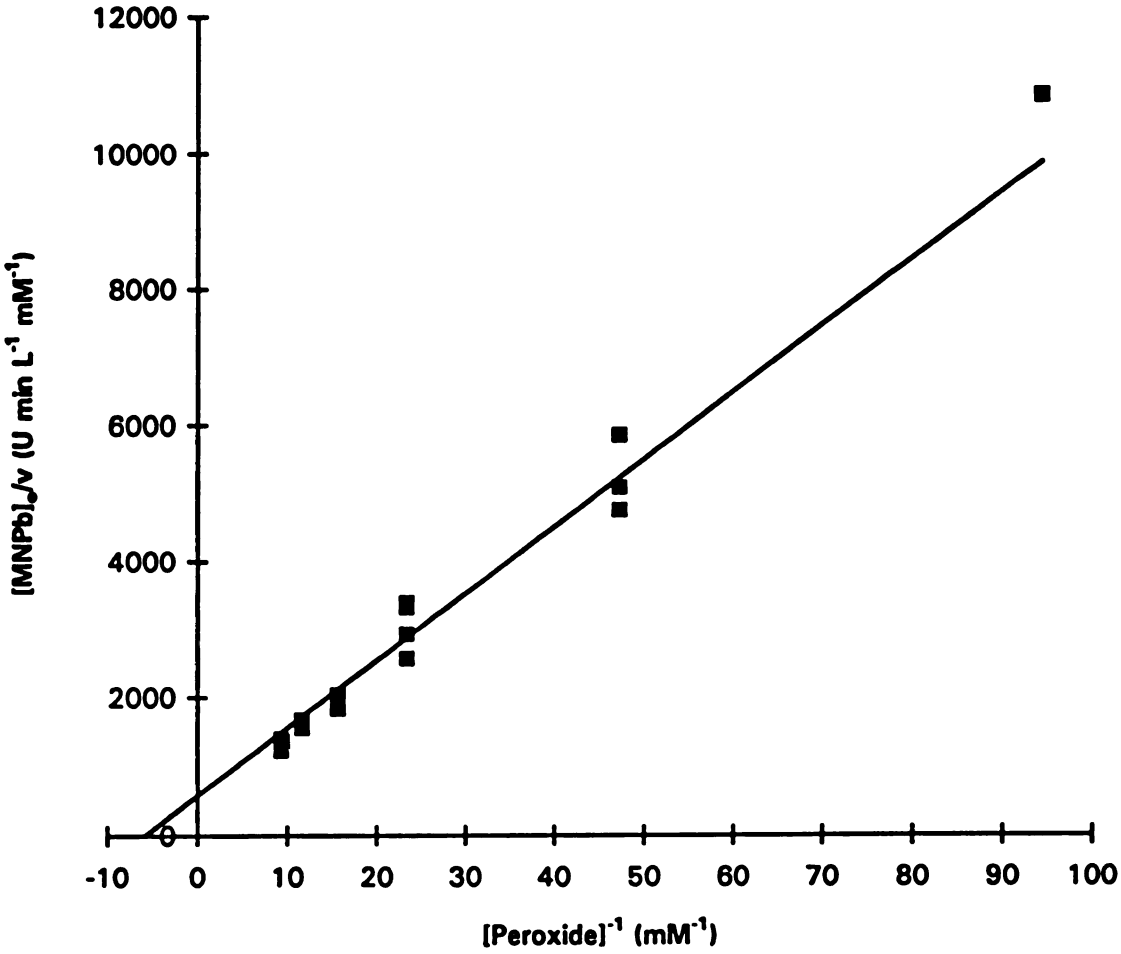

Figure 5.18: Lineweaver-Burk plot for the MNP/Mn(II) kinetic experiments (excess Mn(II)) using D4HiMn MNP (MNP_b). r^2 for the fit was 0.959.

5.5.3 Kinetics of [Mn(III)-tart$_2$] Reduction

As described in Chapter IV, the value of k_8 was estimated from values published previously (Wariishi *et al.*, 1992). This was done because k_8 for each substrate will be different, and the substrate for the reactor studies was lignin, a randomly polymerized phenylpropanoid polymer; no values for k_8 for lignin bonds have been (or are likely to ever be) measured due to this complexity. The final value of k_8 (the same value of k_8 is used for both MNP sources since the reduction of [Mn(III)-tart$_2$] does not depend on MNP activity) was estimated from the value given by Wariishi *et al.* (1992) for vanillyl alcohol. The reaction was found to be second order, with k_4 (my k_8) equal to 720 $mM^{-1}min^{-1}$. Multiplying the value of k_8 for vanillyl alcohol by approximately the ratio of the molecular weights (the ratio of the molecular weights is 1.54×10^{-4}; 1×10^{-4} was used) gives a value of 7.2×10^{-2} $mM^{-1}min^{-1}$ for k_8. Since vanillyl alcohol is soluble in water but the lignin used is not, the value of k_8 was decreased by another order of magnitude to account for the time it would take for the [Mn(III)-tart$_2$] complex to diffuse to a lignin bond in order to oxidize it, giving a final value of 7.2×10^{-3} $mM^{-1}min^{-1}$ for k_8. This was the value used in the reactor simulation. Using this number in the model, along with the estimated initial concentration of lignin bonds (193.3 mM), it was predicted that the lignin bonds would be about 50 % oxidized over the course of a 24 hour run (this predicted value is completely arbitrary, but seemed to be supported by visual observations of the lignin after 6 and 12 hours of treatment in the reactor -- MNP alone caused a lignin color change which darkened over time). Of all terms in the model, this term contains the most assumptions.

5.6 Stabilities of H_2O_2 and VA at 37 °C, pH 3.50, and 350 spm

The stability of H_2O_2 was determined by incubation at 37 °C, pH 3.50, and 350 spm, and measuring the H_2O_2 concentration in samples taken over a 24 hour period. The results are shown in Figures 5.19a and 5.19b. H_2O_2 was found to be completely stable over this period. This result would not be all that surprising for VA, which is expected

(a.)

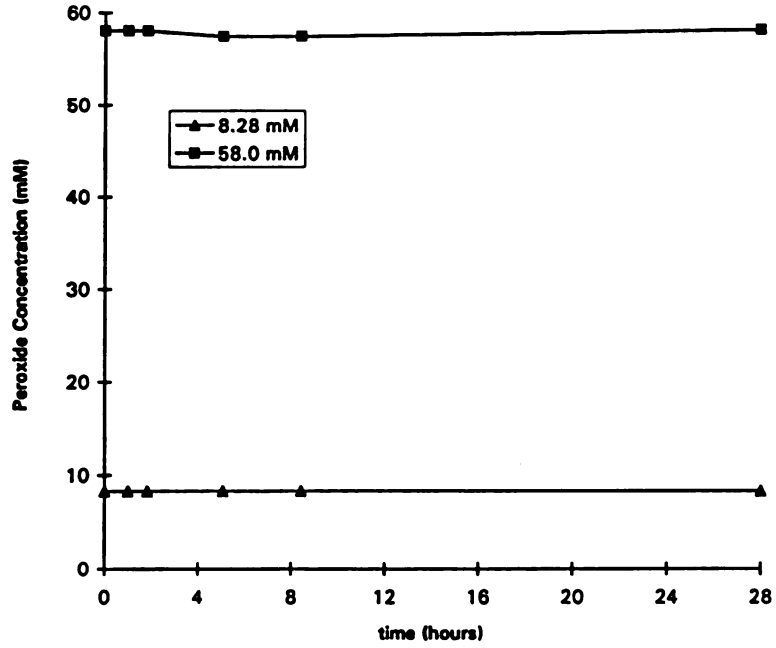

(b.)

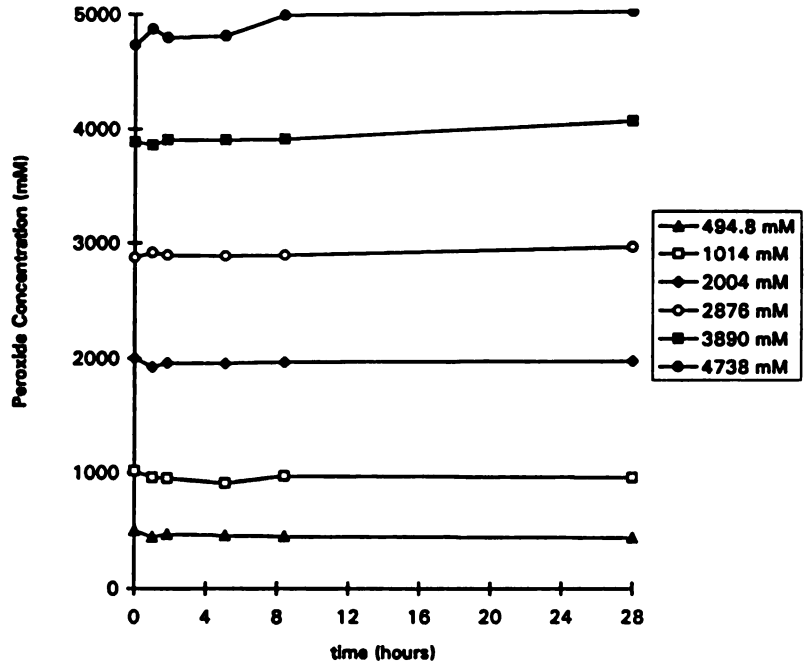

Figure 5.19: Variation of the concentration of H_2O_2 with time in the H_2O_2 stability experiments at 37 °C, pH 3.50, and 350 spm agitation, for: (a.) Low initial H_2O_2 concentrations, and (b.) High initial H_2O_2 concentrations.

to be somewhat stable due to its aromatic structure; in fact, VA was assumed to be stable at 37 °C. For H_2O_2, however, it was somewhat of a surprise. The experiment was repeated with the same result; a probable explanation for this stability is that the stock H_2O_2 (Sigma) must be stabilized in some way. This presumption is supported by the fact that the entire lab staff has been using the same 500 mL bottle of H_2O_2 (stored at 4 °C) for at least 6 years and the concentration of H_2O_2 in this bottle has only dropped from 9.71 M to 7.37 M over this period.

5.7 Stability of D5NoMn LIP at 37 °C, pH 3.50, and 350 spm

The [LIP] versus time data obtained from the LIP stability experiments was fitted to various simple decay models, including first order (exponential) decay, second order decay, and third order decay, using linear regression. None of these models gave a very good fit to the data (data not shown). The next models tried were sums of the three simple decay models; the best fit at all initial [LIP] levels was obtained by a zero order plus first order decay model, suggesting that LIP activity decay is due to two processes, rather than just one (ie. decay due to pH may have one mechanism, while decay due to temperature has another mechanism). Since further exploration of this point was beyond the scope of this project, no further research was done on this point, but the zero order plus first order decay model was used in the reactor model since it described the data well. The decay constants $k_{d,l1}$ and $k_{d,l2}$ were determined as follows.

Equation (4-23) was solved for [LIP] and rearranged to give

$$-\ln\left(\frac{\frac{[LIP]}{[LIP]_o} + \frac{k_{d,l_1}}{k_{d,l_2}[LIP]_o}}{\frac{k_{d,l_1}}{k_{d,l_2}[LIP]_o} + 1}\right) = k_{d,l_2} t \qquad (5\text{-}14)$$

where $[LIP]_o$ is the initial LIP activity and the other parameters are as previously defined. The left-hand-side of the equation was defined as "lhs," and lhs was plotted versus time

to obtain a fit to the experimental data. There are an infinite number of combinations of $k_{d,l1}$ and $k_{d,l2}$ which will satisfy this equation, so $k_{d,l2}$ was chosen to be on the order of magnitude of the decay constants determined for the MNP enzymes (10^{-2} to 10^{-3}); this was an arbitrary choice, and was done because both were first order (exponential) decay constants for similar types of enzymes. A value was chosen for $k_{d,l1}$, then, which would allow a value of $k_{d,l2}$ that was in the order of magnitude range above; $k_{d,l2}$ was then chosen, the data were fitted using linear regression, and the slope gave a new estimate for $k_{d,l2}$. The value of $k_{d,l1}$ was chosen initially so that the first estimate of $k_{d,l2}$ was exactly equal to the decay constant calculated for MNP_b (see below); this value was determined by trial and error using a shooting method. The final iteration for this method, with $k_{d,l1}$ equal to 19.16 (U/L)/hr, and $k_{d,l2}$ equal to 1.867×10^{-2} hr^{-1}, is shown in Figure 5.20 ($r^2 = 0.962$). The goodness of fit to the [LIP] versus time data is shown in Figure 5.21.

5.8 Stabilities of D5NoMn and D4HiMn MNPs at 37 °C, pH 3.50, and 350 spm

The same method was used to find the correct decay models for MNP_a and MNP_b as was used for the LIP above. Both MNP_a and MNP_b decay rates were found be adequately predicted using a simple first order (exponential) decay. The decay constants were determined by linearizing the solution to the first order decay equation (by taking the logarithm of both sides) and fitting the data to a line using linear regression; this procedure is a well known method and so it will not be shown here. The goodness of the fits, however, is demonstrated in Figures 5.22 and 5.23 for MNP_a and MNP_b, respectively. The decay constants $k_{d,Ma}$ and $k_{d,Mb}$, corresponding to MNP_a and MNP_b, respectively, were found to be 5.168×10^{-3} hr^{-1} and 2.535×10^{-2} hr^{-1} (the MNP_a seems to be more stable than the MNP_b). The correlation coefficients (r^2) for the linear fits were 0.978 and 0.830 for MNP_a and MNP_b, respectively.

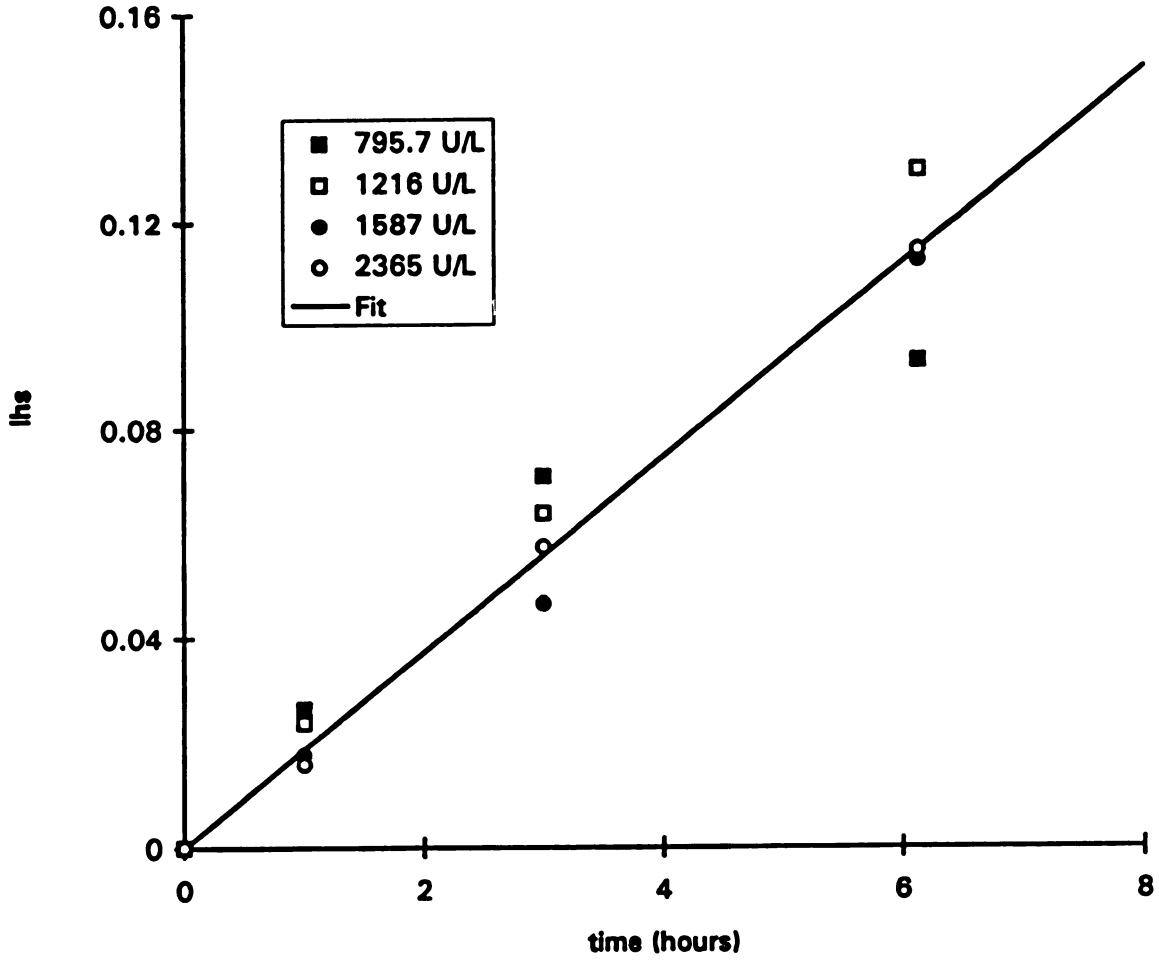

Figure 5.20: lhs versus time for the determination of $k_{d,L1}$ and $k_{d,L2}$ for LIP stability. Initial LIP levels are listed in the legend box. r^2 for the fit was 0.962.

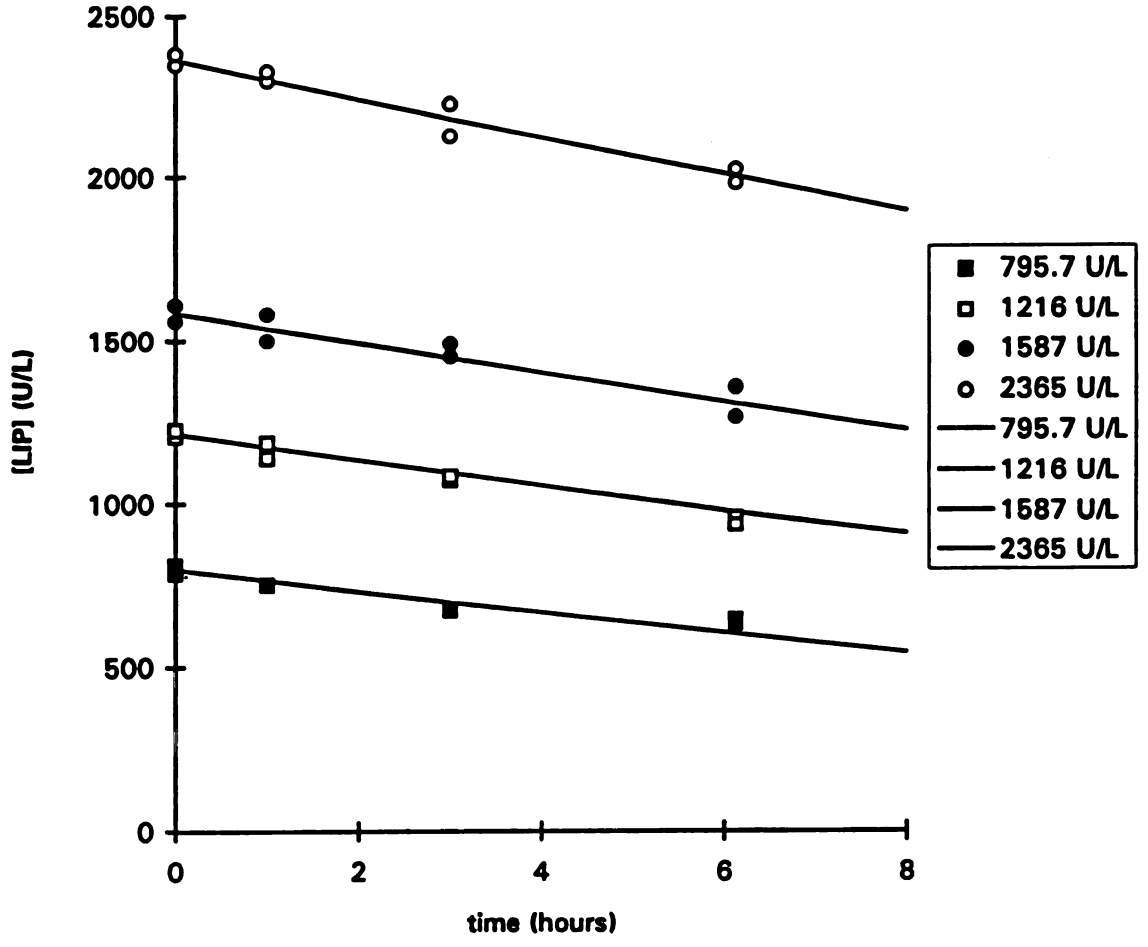

Figure 5.21: Plot of [LIP] (U/L) versus time for the LIP stability experiments at 37 °C, pH 3.50, and 350 spm agitation. The curves shown are the predicted values from the fit to zero order plus first order decay. Initial LIP levels are indicated in the legend box.

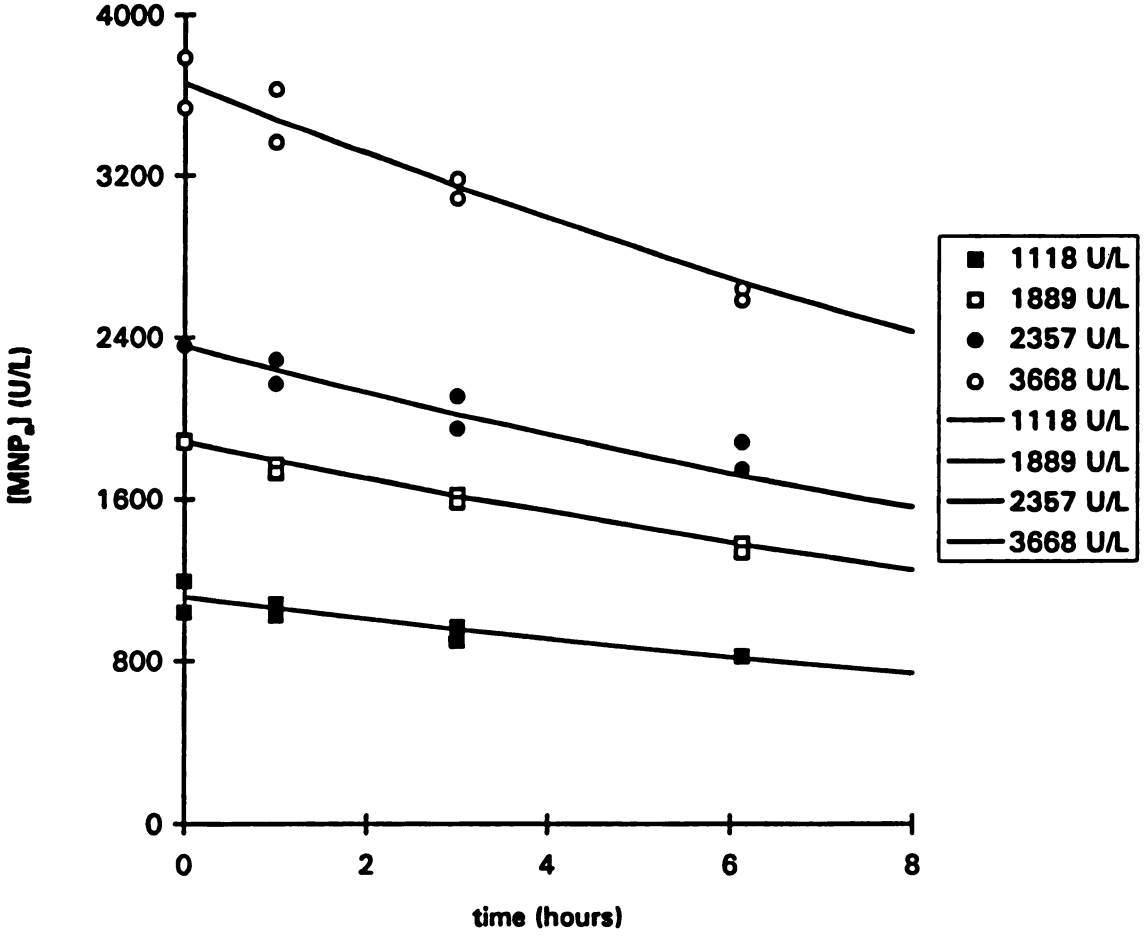

Figure 5.22: Plot of [MNP] (U/L) versus time for the MNP_a stability experiments at 37 °C, pH 3.50, and 350 spm agitation. The curves shown are the predicted values from the fit to a simple first order decay model (r^2 of 0.978). Initial MNP levels are indicated in the legend box.

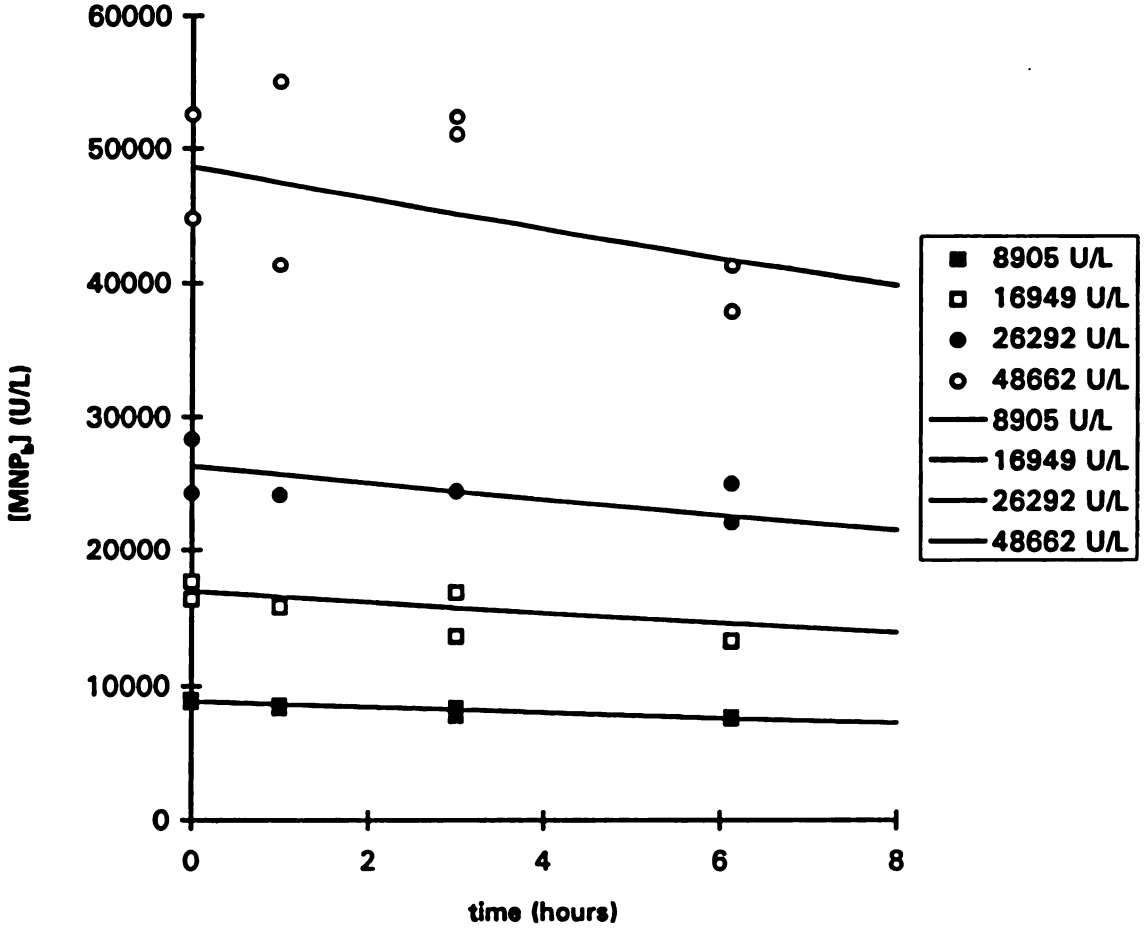

Figure 5.23: Plot of [MNP] (U/L) versus time for the MNP_b stability experiments at 37 °C, pH 3.50, and 350 spm agitation. The curves shown are the predicted values from the fit to a simple first order decay model (r^2 of 0.830). Initial MNP levels are indicated in the legend box.

5.9 Dialysis Reactor Model -- Run Simulations

The reactor model simulation program, RKG.FOR, was run and optimized for each enzyme mixture (LIP alone, MNP alone, and LIP + MNP), for 20 mg of lignin, 1 mL total initial volume in each side of the reactor, and using the concentration ranges specified by Olsen *et al.* (1991). The concentrations, volumes, and times of pulse additions are listed in Tables 4.3 through 4.5 in Chapter IV.

5.9.1 LIP Only

The H_2O_2 and VA concentration profiles for Side B are shown in Figures 5.24 and 5.25; refer to Table 4.3 for the pulse profiles for Sides A and B. The dashed lines in Figures 5.24 and 5.25 are the minimum and maximum concentrations specified by Olsen *et al.* (1991), and the curves are the concentrations of H_2O_2 and VA in Side B for each figure, respectively. The sharp vertical changes in H_2O_2 concentration in Figure 5.24 correspond to the sudden drops in VA concentration in Figure 5.25, and are due to additions of H_2O_2 to Side A to adjust the transport rate of H_2O_2 to Side B in such a way that the consumption rate of VA in Side B will increase. The variations in H_2O_2 concentration are small, with the average concentration at about 15 μM. VA concentrations vary much more because the value of the effective diffusion coefficient for VA is about an order of magnitude smaller than that for H_2O_2; thus, VA transport rates do not drop as fast as H_2O_2 transport rates. The average VA concentration in Side B over the course of the run was about 360 μM.

The Side B LIP activity profile is shown in Figure 5.26; activity is maintained near the initial value of 1000 U/L for the entire course of the run through enzyme additions to Side B. The variation of the concentration of lignin bonds in Side B is shown in Figure 5.27. Note that the only decreases are due to dilutions caused by enzyme addition to Side B. This result occurs because the consumption of H_2O_2 due to oxidation of lignin bonds was neglected since it was assumed to be small relative to the rate of oxidation of VA. Thus, no oxidation of lignin bonds is predicted by the model.

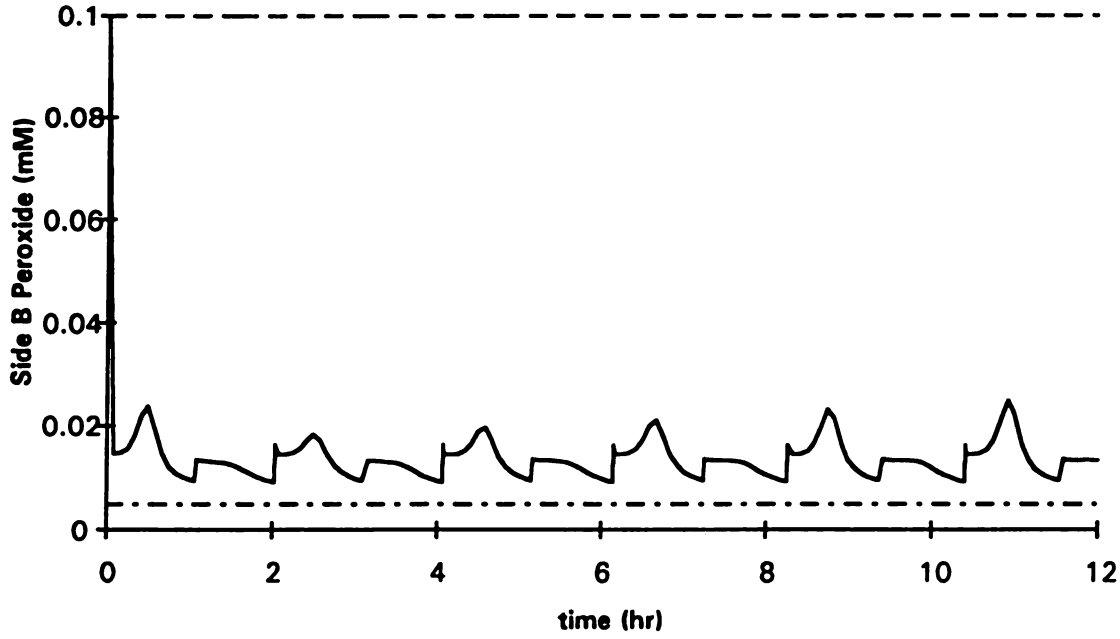

Figure 5.24: $[H_2O_2]_B$ variation with time predicted by RKG.FOR using the pulse profile listed in Table 4.3 (LIP Alone enzyme case). The upper and lower dashed lines indicate the allowed range of $[H_2O_2]_B$.

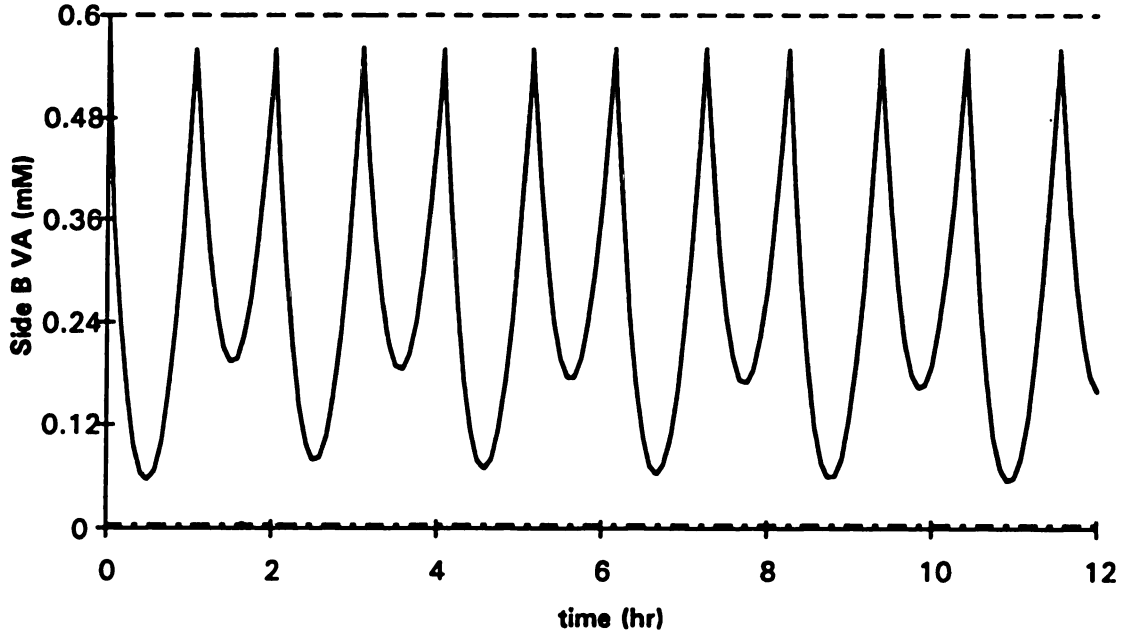

Figure 5.25: $[VA]_B$ variation with time predicted by RKG.FOR using the pulse profile listed in Table 4.3 (LIP Alone enzyme case). The upper and lower dashed lines indicate the allowed range of $[VA]_B$.

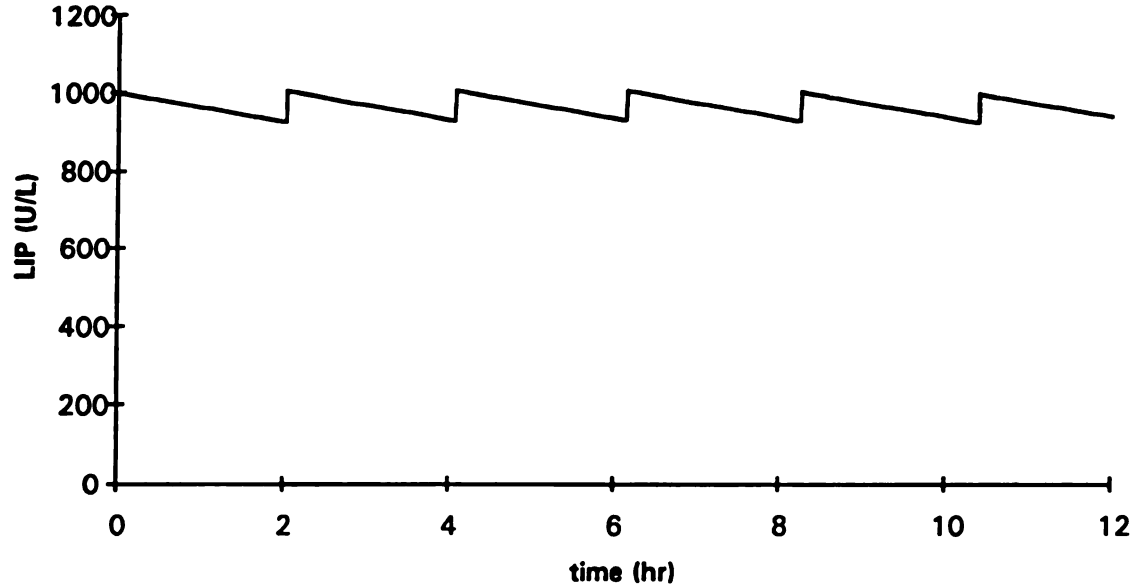

Figure 5.26: $[LIP]_B$ variation with time predicted by RKG.FOR using the pulse profile listed in Table 4.3 (LIP Alone enzyme case).

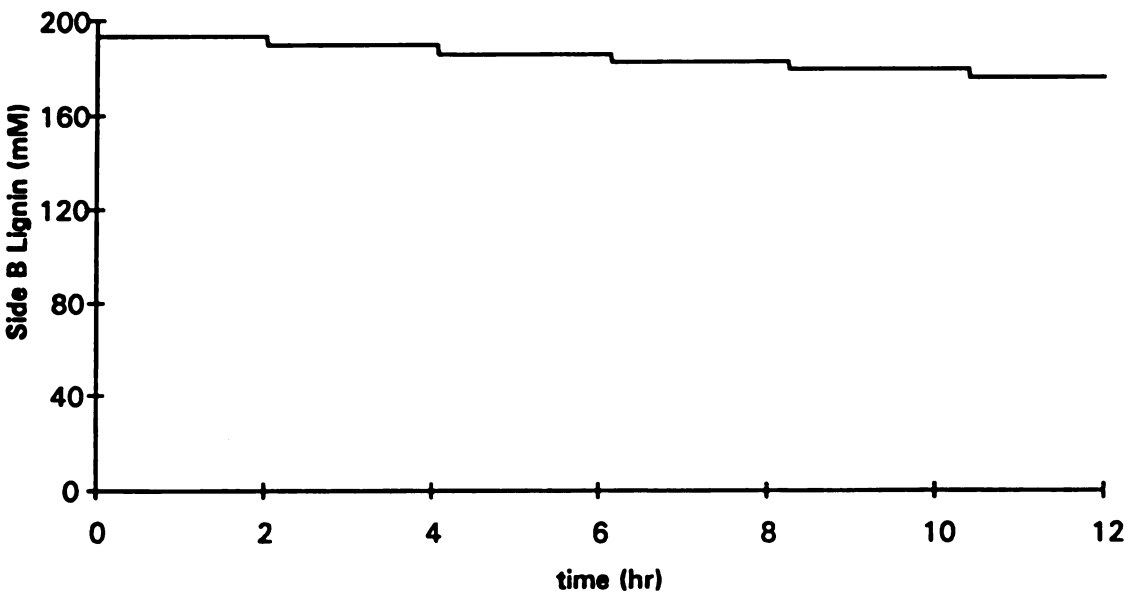

Figure 5.27: $[Lignin]_B$ variation with time predicted by RKG.FOR using the pulse profile listed in Table 4.3 (LIP Alone enzyme case). Because use of H_2O_2 to oxidized lignin is neglected in the model, the only changes in $[Lignin]_B$ occur because of dilution due to pulses.

Figures 5.28 and 5.29 depict the H_2O_2 and VA concentration profiles in Side A (reservoir). The sharp increases in each correspond to additions of each respective reagent to Side A, while the small drops in VA concentration are due to dilution (addition of H_2O_2 but not VA). Finally, Figure 5.30 shows the variation of the rates of supply and consumption of H_2O_2 and VA for Side B (solid line is VA transport rate, dashed lines are VA consumption (large + small dashes), H_2O_2 supply (small dashes) and H_2O_2 consumption (large dashes)). The supply rate of H_2O_2 and the consumption rates of both H_2O_2 and VA are practically identical, which is why they are difficult to tell apart in Figure 5.30. This behavior occurs because of the following: Since H_2O_2 is in much lower concentration than VA, it limits the consumption rates of both (1:1 stoichiometry); however, the H_2O_2 supply rate is used to adjust the H_2O_2 consumption rate. The net result is the key to how this control method works -- by making sure that the supply and consumption rates of H_2O_2 and VA do not deviate very far from one another.

5.9.2 MNP Only

The H_2O_2 concentration profile for Side B is shown in Figure 5.31; refer to Table 4.4 for the pulse profiles for Sides A and B. The dashed lines in Figure 5.31 again represent the minimum and maximum concentrations specified by Olsen *et al.* (1991), and the curve is the concentration of H_2O_2 in Side B. The sudden sharp increases in H_2O_2 concentration in Figure 5.31 are due to additions of H_2O_2 to Side A (upward adjustment of transport rate of H_2O_2 to Side B). The variations in H_2O_2 concentration are larger for this case, with the average concentration at about 40 μM. The concentration profiles for Mn species in Sides A and B are shown in Figures 5.32a and 5.32b, respectively. Note that no Mn was initially added to Side A -- both [Mn(III)-$tart_2$] (solid curve) and Mn(II) (dashed curve) increased in Side A over time from zero to about 28 μM and 2 μM, respectively, which is consistent with this fact. Mn(II) concentration in Side B is relatively constant at about 2-3 μM, while [Mn(III)-$tart_2$] drops from the initial value of 100 μM to about 65 μM over 12 hours.

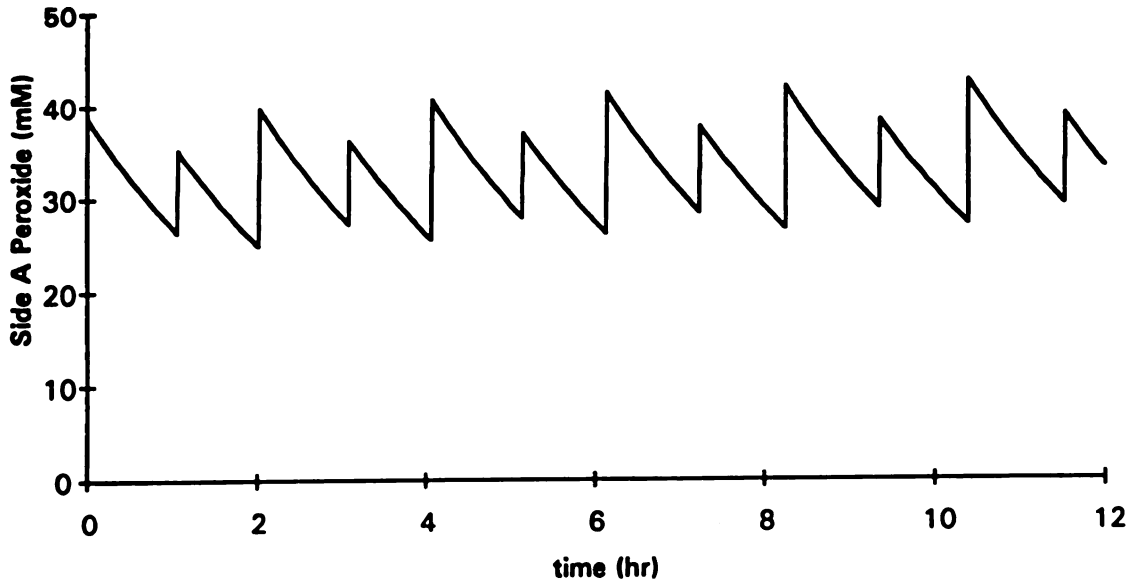

Figure 5.28: Plot of $[H_2O_2]_A$ with time (LIP Alone enzyme case) predicted by RKG.FOR to be necessary to maintain $[H_2O_2]_B$ and $[VA]_B$ within the desired ranges.

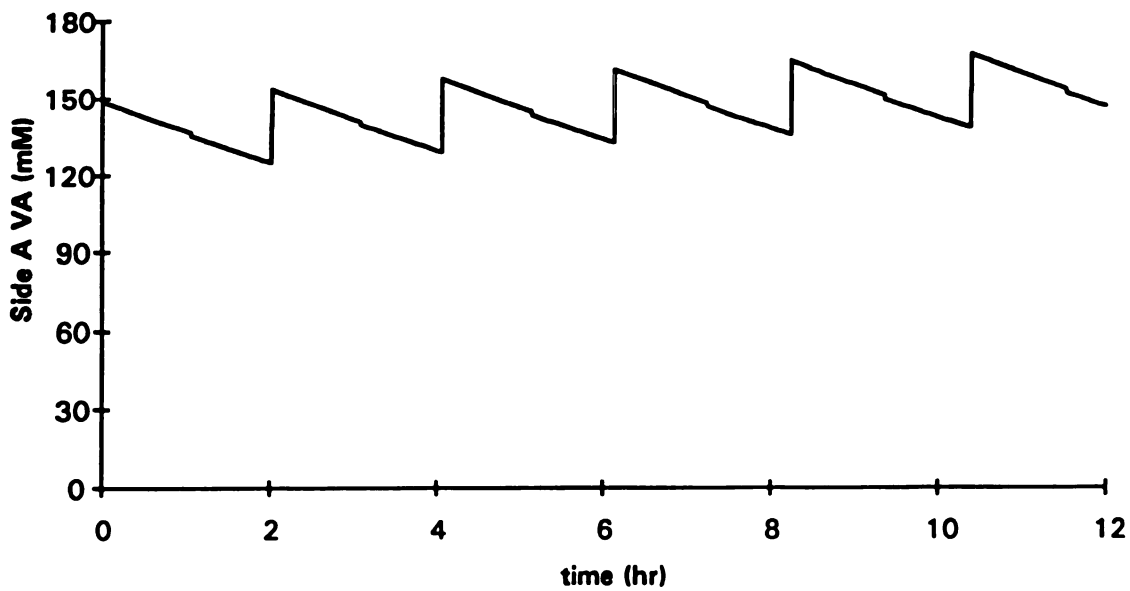

Figure 5.29: Plot of $[VA]_A$ with time (LIP Alone enzyme case) predicted by RKG.FOR to be necessary to maintain $[H_2O_2]_B$ and $[VA]_B$ within the desired ranges.

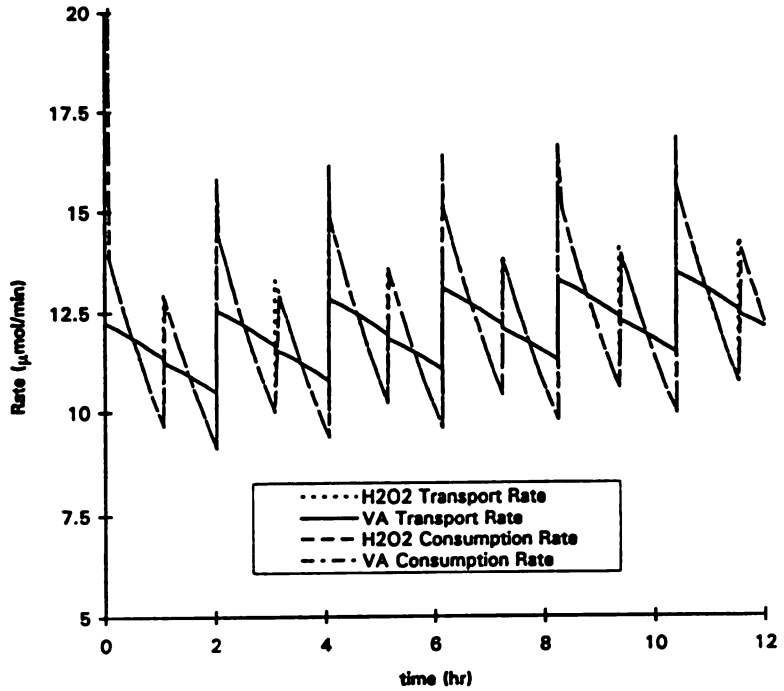

Figure 5.30: Variation of the transport and consumption rates of H_2O_2 and VA in Side B (LIP Alone enzyme case). The line type for each is listed in the legend box. The rates are maintained closely to one another to attenuate the levels of H_2O_2 and VA in Side B.

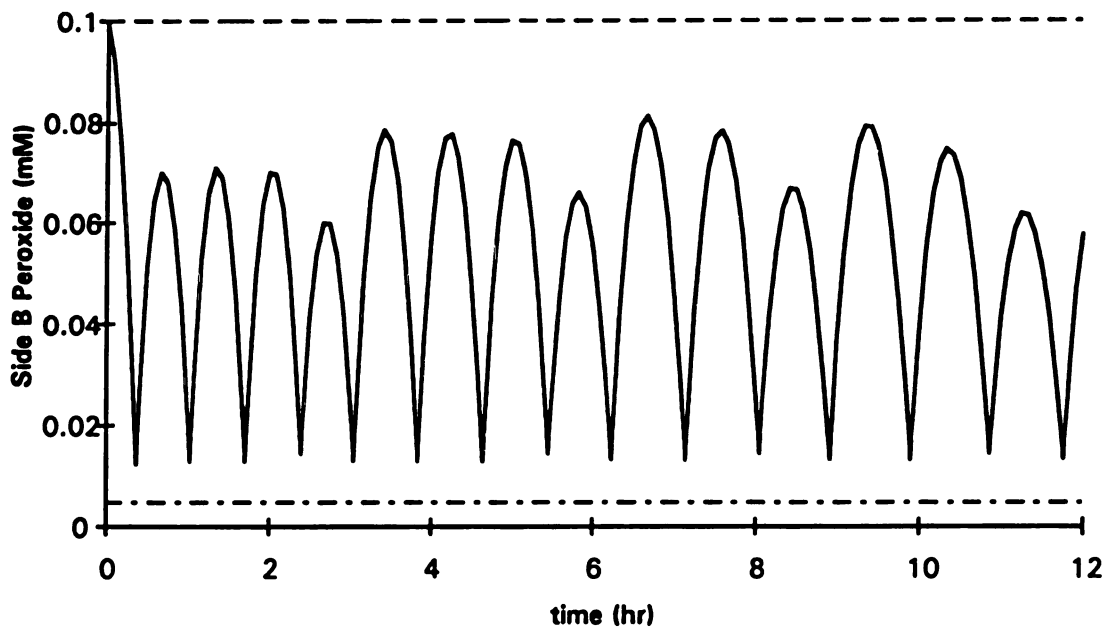

Figure 5.31: $[H_2O_2]_B$ variation with time predicted by RKG.FOR using the pulse profile listed in Table 4.4 (MNP Alone enzyme case). The upper and lower dashed lines indicate the allowed range of $[H_2O_2]_B$.

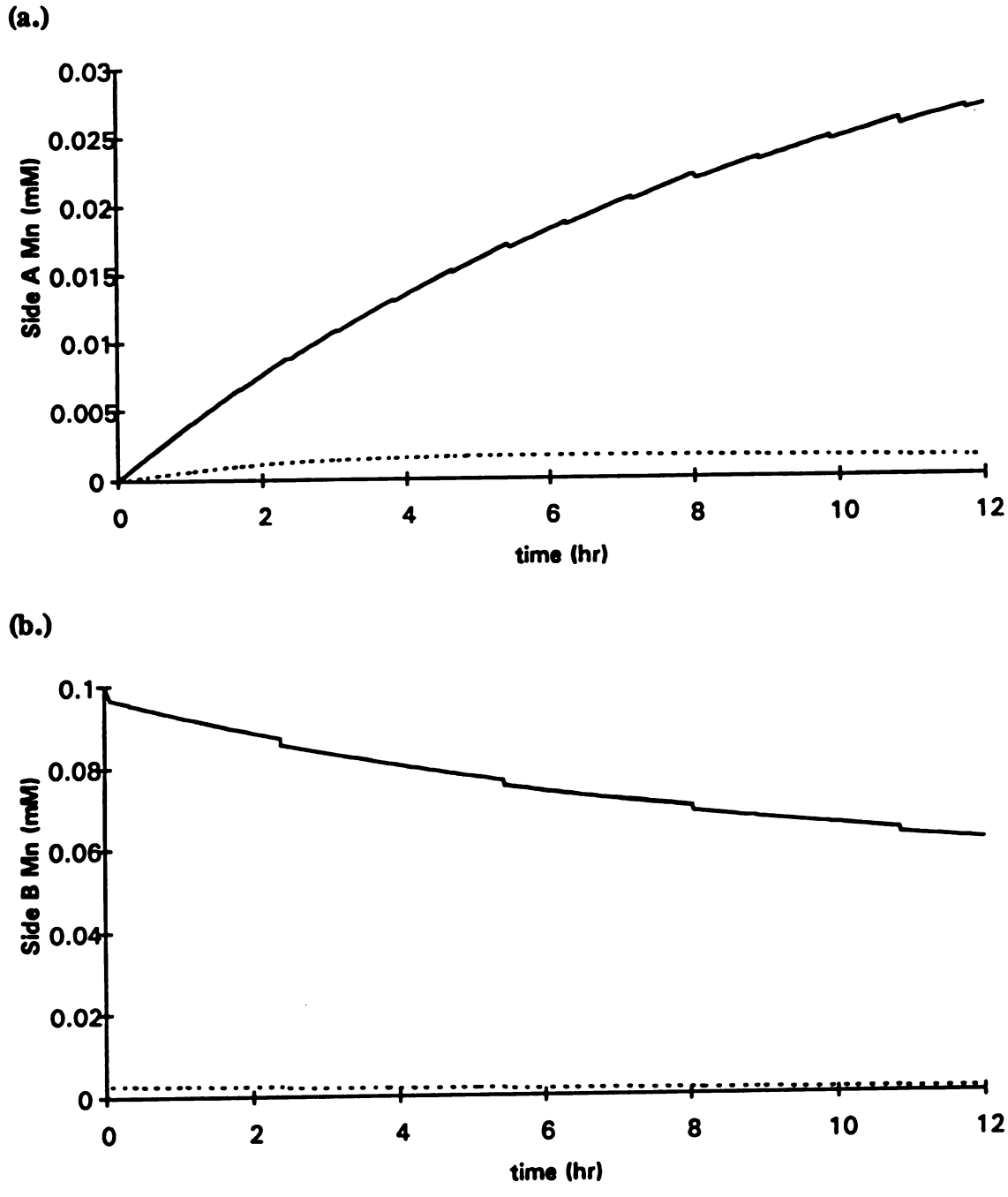

Figure 5.32: Variation of Mn species with time predicted by RKG.FOR using the pulse profile listed in Table 4.4 (MNP Alone enzyme case). (a.) $[Mn(II)]_A$ (dashed curve) and $[Mn(III)\text{-}tart_2]_A$ (solid curve), and (b.) $[Mn(II)]_B$ (dashed curve) and $[Mn(III)\text{-}tart_2]_B$ (solid curve).

The MNP activity profile in Side B is shown in Figure 5.33; activity is maintained near the initial value of 56000 U/L for the entire course of the run as for LIP above. The variation of the concentration of lignin bonds in Side B is shown in Figure 5.34. The sharp drops in the otherwise smooth decline in lignin bond concentration (due to oxidation by [Mn(III)-$tart_2$]) are due to dilution when MNP is added to Side B.

Figure 5.35 shows the H_2O_2 concentration profile in Side A (reservoir). The sharp increases again correspond to additions of H_2O_2. Finally, Figure 5.36 shows the variation of the rates of supply and consumption of H_2O_2 in Side B (solid line is consumption rate, dashed line is supply rate). Figure 5.36 again shows how the control method for this case works -- by making sure that the supply and consumption rates of H_2O_2 are maintained close to one another.

5.9.3 LIP + MNP

The H_2O_2 and VA concentration profiles for Side B are shown in Figures 5.37 and 5.38; refer to Table 4.5 for the pulse profiles for Sides A and B. These figures are analogous to Figures 5.24 and 5.25 for the LIP alone case above. The average H_2O_2 and VA concentrations are about 8 μM and 340 μM, respectively, neglecting the spike in H_2O_2 concentration at about 11 hours. This spike was unavoidable and appeared to be a cumulative effect due to the adjustment of LIP and MNP activities at the same time; since the H_2O_2 concentration stayed within the bounds set by Olsen *et al.* (1991), the H_2O_2 spike was ignored. The concentration profiles for Mn species in Sides A and B are shown in Figures 5.39a and 5.39b, respectively. Again, note that no Mn was initially added to Side A -- both [Mn(III)-$tart_2$] (solid line) and Mn(II) (dashed line) increased over time to about 25 μM and 2 μM, respectively. Mn(II) concentration in Side B is relatively constant at about 1-2 μM, while [Mn(III)-$tart_2$] drops to about 60 μM over 12 hours. These figures are analogous to Figures 5.32a and 5.32b for MNP alone (above).

The Side B LIP activity profile is shown in Figure 5.40; activity is maintained near the initial value of 1000 U/L for the entire course of the run. The MNP activity

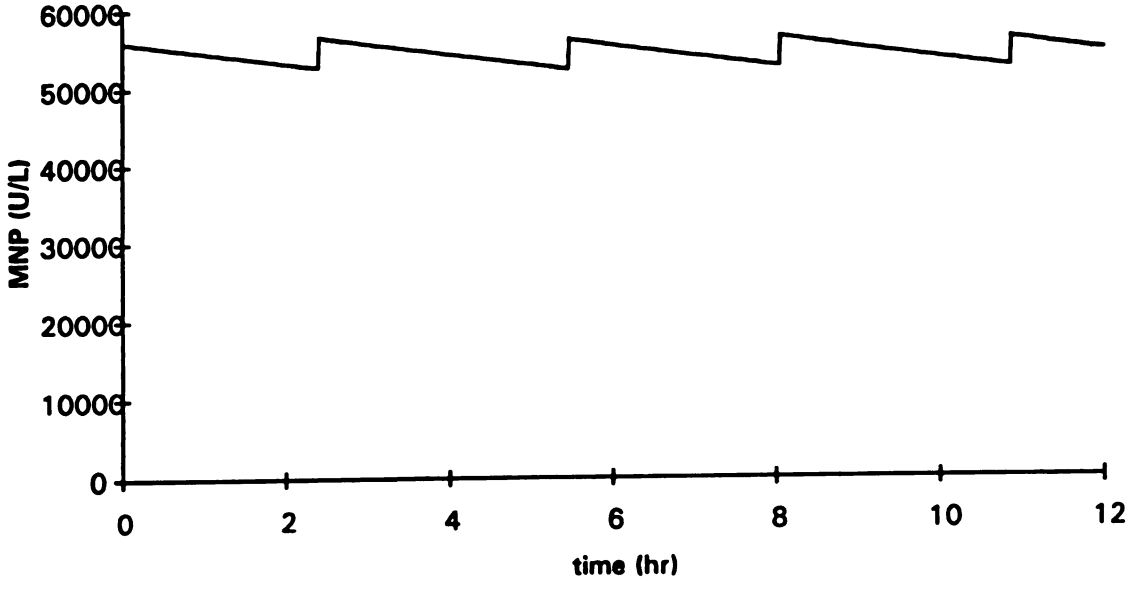

Figure 5.33: $[MNP_s]_B$ variation with time predicted by RKG.FOR using the pulse profile listed in Table 4.4 (MNP Alone enzyme case).

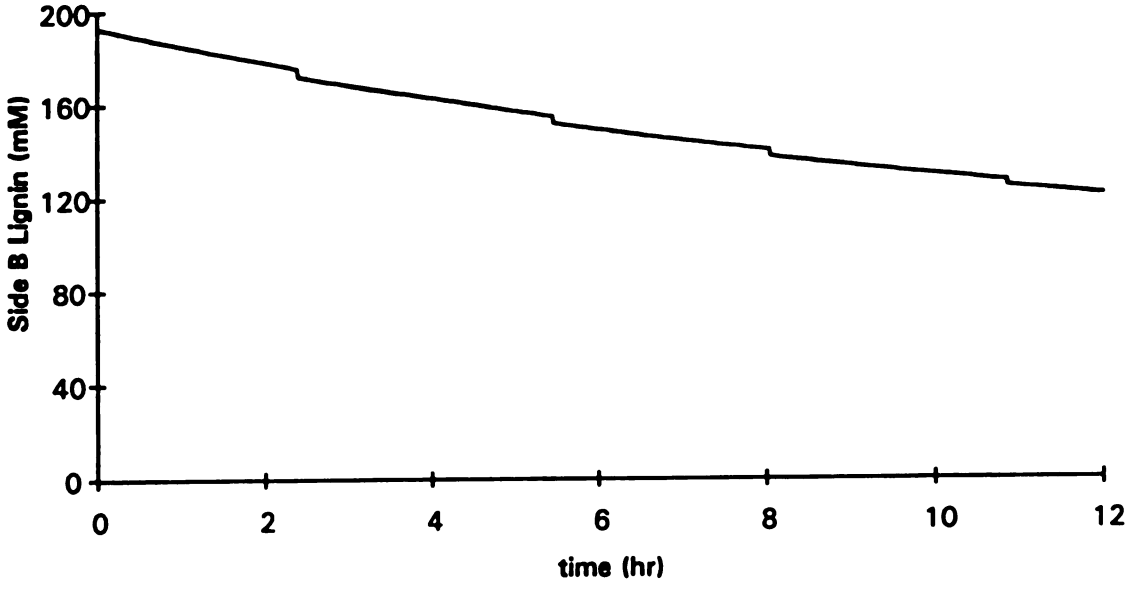

Figure 5.34: $[Lignin]_B$ variation with time predicted by RKG.FOR using the pulse profile listed in Table 4.4 (MNP Alone enzyme case). Changes in $[Lignin]_B$ occur because of both oxidation by $[Mn(III)\text{-}tart_2]$ and by dilution due to pulses.

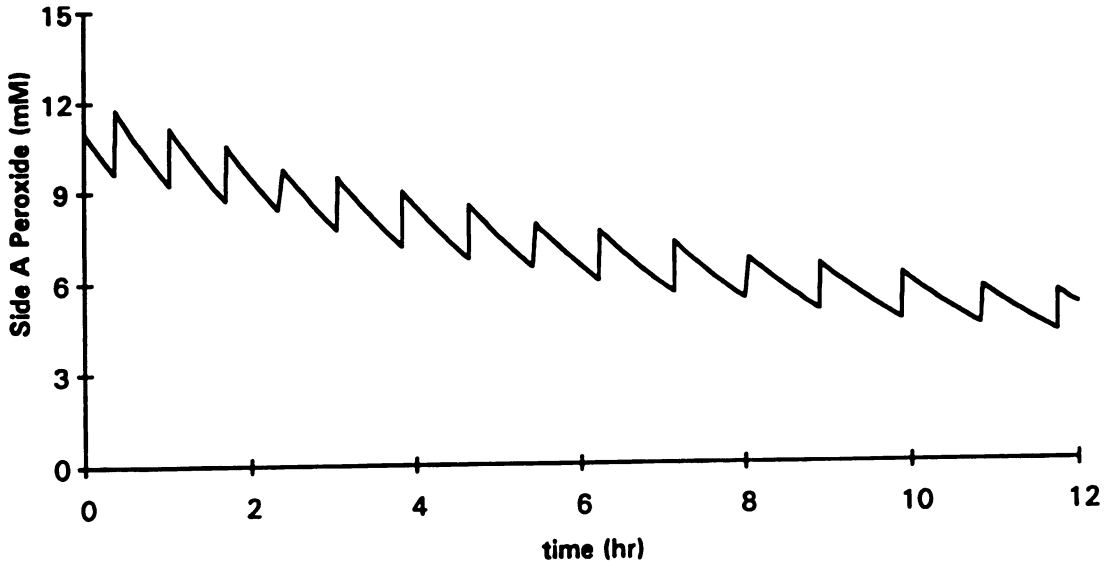

Figure 5.35: Plot of $[H_2O_2]_A$ with time (MNP Alone enzyme case) predicted by RKG.FOR to be necessary to maintain $[H_2O_2]_B$ the desired range.

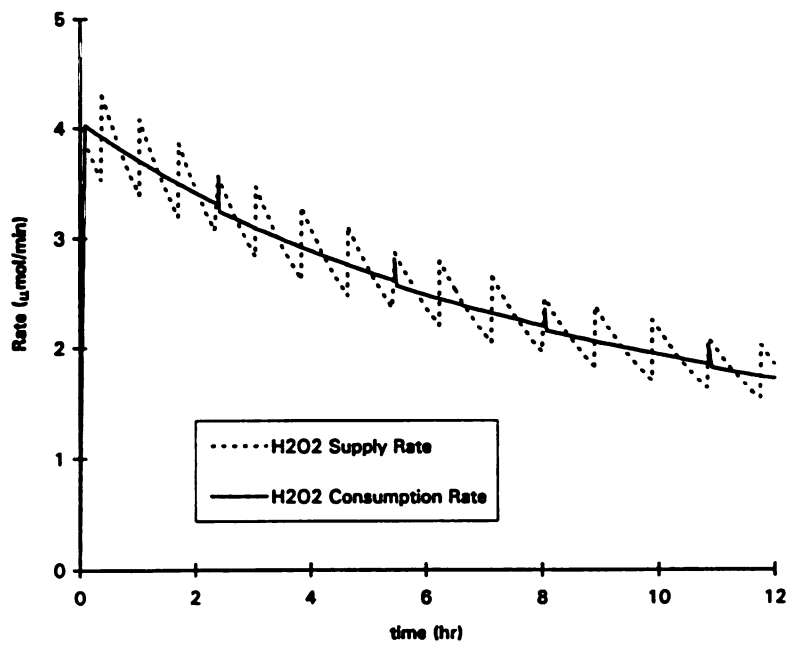

Figure 5.36: Variation of the transport and consumption rates of H_2O_2 in Side B (MNP Alone enzyme case). The line type for each is listed in the legend box. The rates are maintained closely to one another to attenuate the levels of H_2O_2 in Side B.

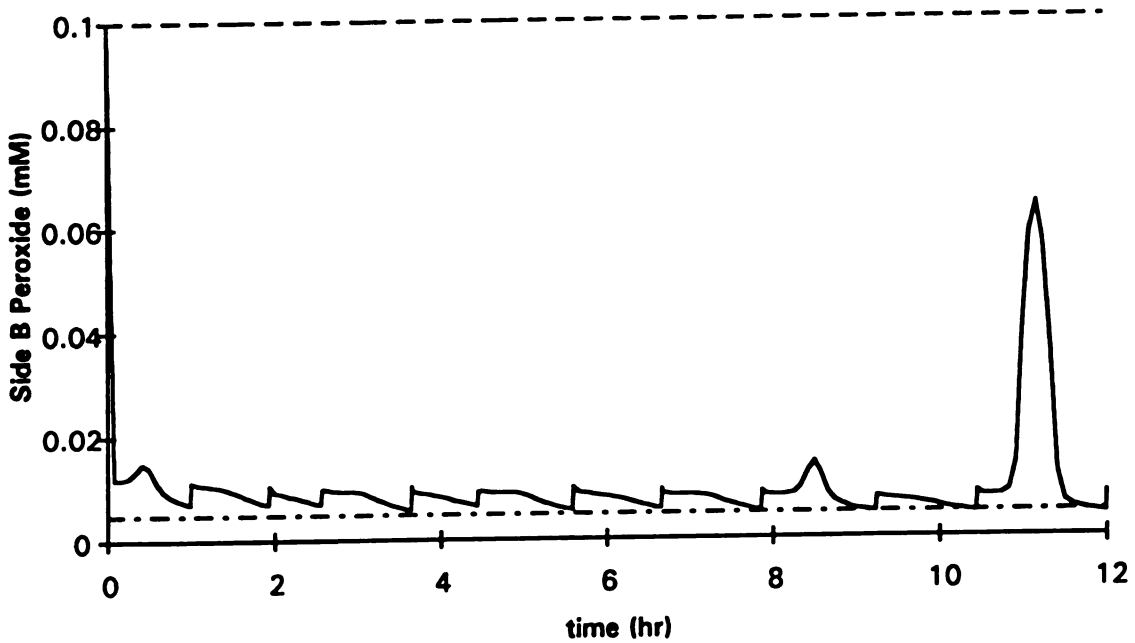

Figure 5.37: $[H_2O_2]_B$ variation with time predicted by RKG.FOR using the pulse profile listed in Table 4.5 (LIP + MNP enzyme case). The upper and lower dashed lines indicate the allowed range of $[H_2O_2]_B$.

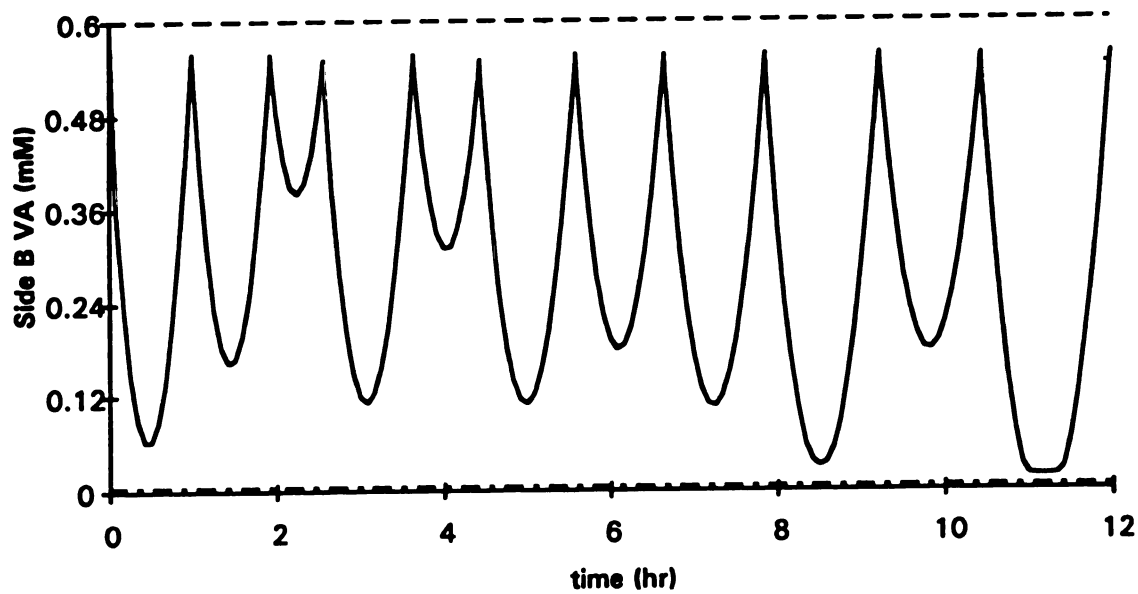

Figure 5.38: $[VA]_B$ variation with time predicted by RKG.FOR using the pulse profile listed in Table 4.5 (LIP + MNP enzyme case). The upper and lower dashed lines indicate the allowed range of $[VA]_B$.

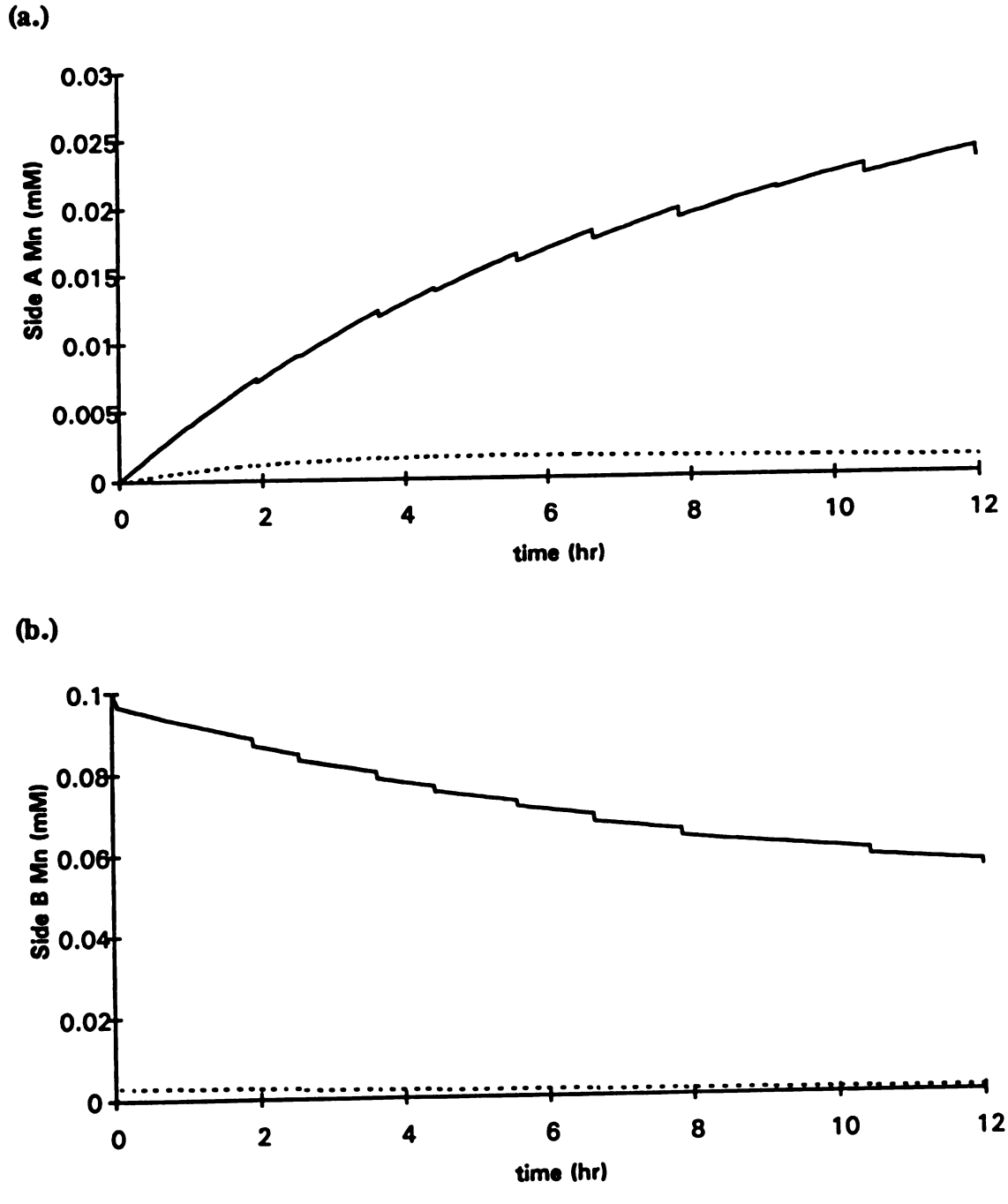

Figure 5.39: Variation of Mn species with time predicted by RKG.FOR using the pulse profile listed in Table 4.5 (LIP + MNP enzyme case). (a.) $[Mn(II)]_A$ (dashed curve) and $[Mn(III)\text{-}tart_2]_A$ (solid curve), and (b.) $[Mn(II)]_B$ (dashed curve) and $[Mn(III)\text{-}tart_2]_B$ (solid curve).

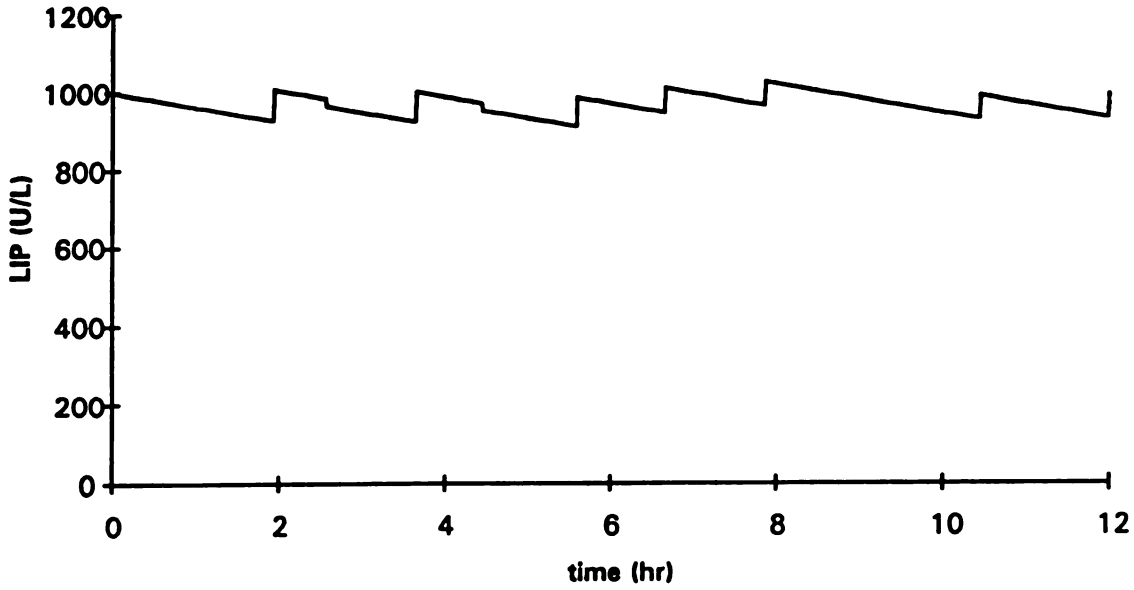

Figure 5.40: $[LIP]_B$ variation with time predicted by RKG.FOR using the pulse profile listed in Table 4.5 (LIP + MNP enzyme case). The sudden sharp drops are due to MNP addition without adding LIP.

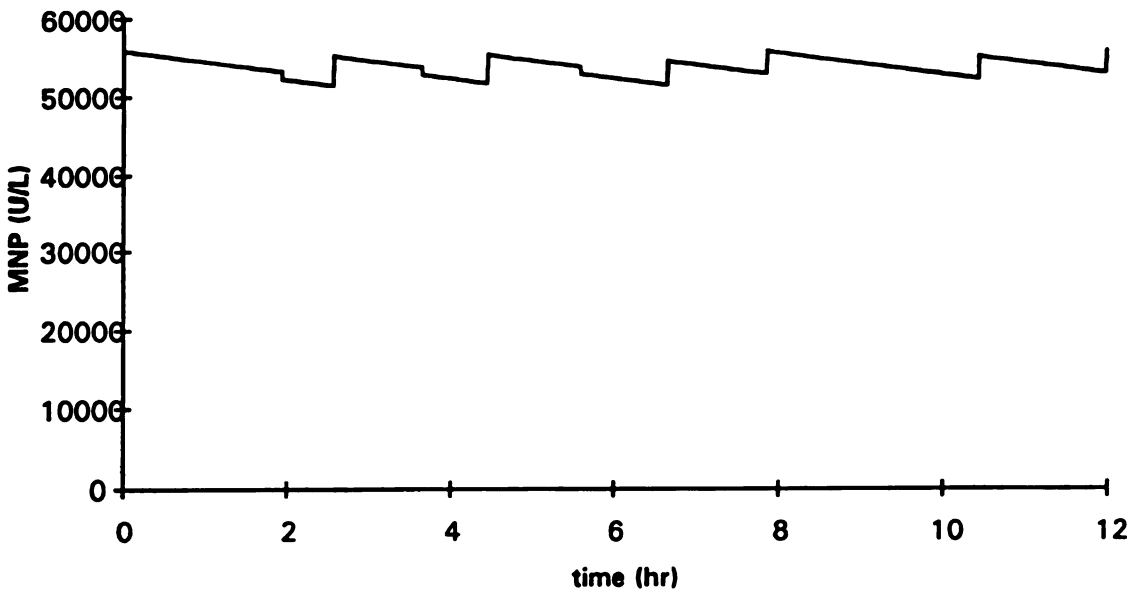

Figure 5.41: Total $[MNP]_B$ variation with time predicted by RKG.FOR using the pulse profile listed in Table 4.5 (LIP + MNP enzyme case). The sudden sharp drops are due to LIP addition without adding substantial amounts of MNP (small amounts of MNP_a are added).

profile in Side B is shown in Figure 5.41; activity is maintained near the initial value of 56000 U/L for the entire course of the run as for LIP above. For both enzymes, the very small sharp drops in concentration are due simply to dilution when one enzyme is added but not the other. The variation of the concentration of lignin bonds in Side B is shown in Figure 5.42; as above, the sharp drops in the otherwise smooth decline in lignin bond concentration (due to oxidation by [Mn(III)-$tart_2$]) are due to dilution when LIP and/or MNP are added to Side B.

Figures 5.43 and 5.44 depict the H_2O_2 and VA concentration profiles in Side A (reservoir). The sharp increases in each again correspond to additions of each respective reagent to Side A, while the small drops in VA concentration are due to dilution (addition of H_2O_2 but not VA).

Finally, Figure 5.45 shows the variation of the rates of supply and consumption of H_2O_2 and VA for Side B (solid line is VA transport rate, dashed lines are VA consumption (large + small dashes), H_2O_2 supply (small dashes) and H_2O_2 consumption (large dashes)). The supply and consumption rates of H_2O_2 are higher than those for VA because there is an additional consumption of H_2O_2 by MNP; however, the consumption rate of VA is at all times parallel to that for H_2O_2, indicating that H_2O_2 is still being used to control the rates of supply and consumption and thus the concentrations in Side B. H_2O_2 supply and consumption rates are again identical, and thus they are difficult to tell apart in Figure 5.45. In any case, the net result is that the control method works by making the supply and consumption rates of H_2O_2 and VA vary proportionately.

5.10 Dialysis Reactor Model -- Perturbation Analyses

Since the model was not tested by running the reactor and measuring concentration-time profiles for each species due to the large amounts of enzymes which would be required (one complete reactor run for each time point), it was decided that the model solutions would be tested for stability by setting the model parameters (one at a time) equal to the upper and lower bounds of their confidence intervals, respectively.

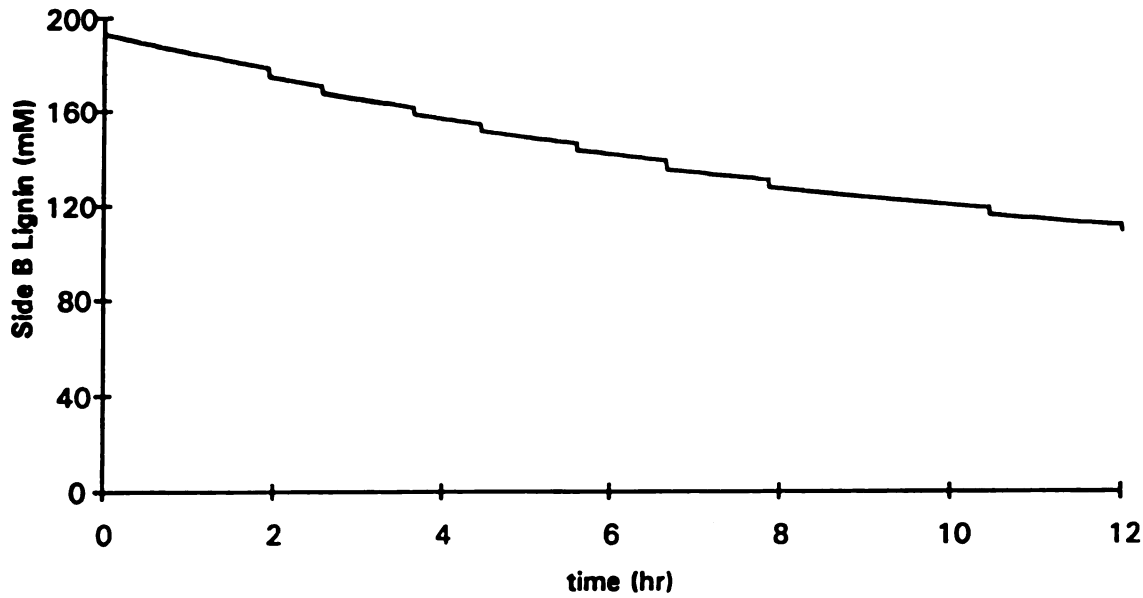

Figure 5.42: $[Lignin]_B$ variation with time predicted by RKG.FOR using the pulse profile listed in Table 4.5 (LIP + MNP enzyme case). Changes in $[Lignin]_B$ occur because of both oxidation by $[Mn(III)\text{-}tart_2]$ and by dilution due to pulses.

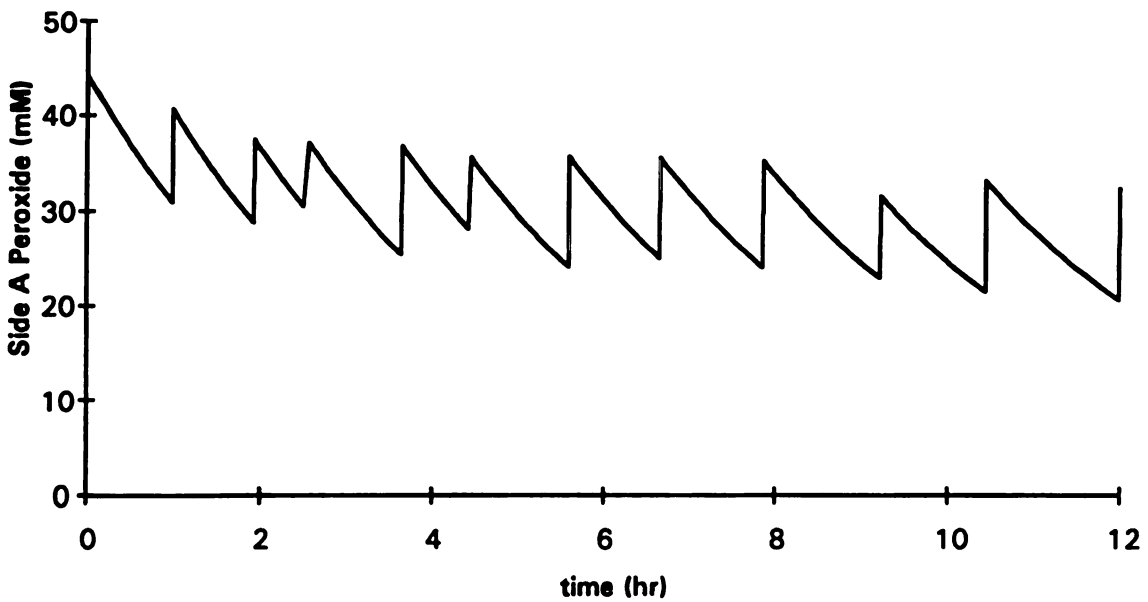

Figure 5.43: Plot of $[H_2O_2]_A$ with time (LIP + MNP enzyme case) predicted by RKG.FOR to be necessary to maintain $[H_2O_2]_B$ and $[VA]_B$ within the desired ranges.

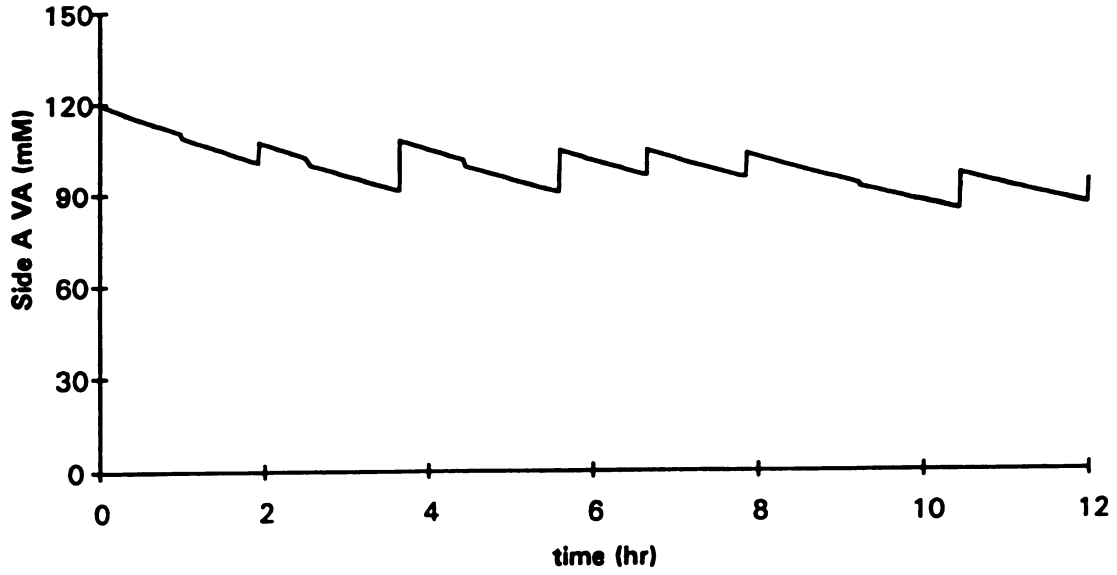

Figure 5.44: Plot of $[VA]_A$ with time (LIP + MNP enzyme case) predicted by RKG.FOR to be necessary to maintain $[H_2O_2]_B$ and $[VA]_B$ within the desired ranges.

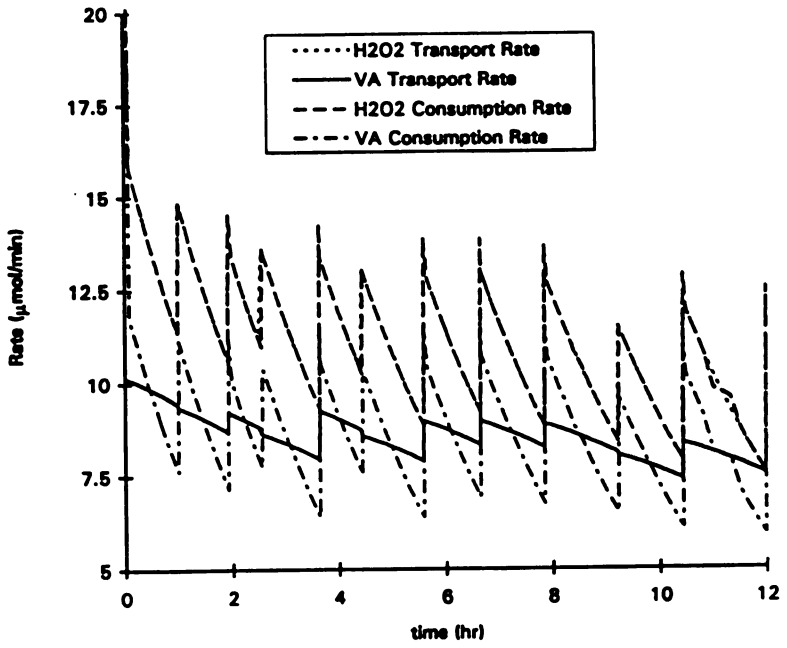

Figure 5.45: Variation of the transport and consumption rates of H_2O_2 and VA in Side B (LIP + MNP enzyme case). The line type for each is listed in the legend box. The rates of H_2O_2 supply and consumption are above those for VA due to the additional consumption of H_2O_2 by MNP. The rates are maintained closely to one another to attenuate the levels of H_2O_2 and VA in Side B.

The RKG.FOR pulse profile results for each enzyme case were used with the program PERTURB.FOR, and with the upper and lower bounds of the 95 % Confidence Intervals for each model parameter, to determine which parameters were most likely to cause the model's predictions for H_2O_2 and VA concentrations to exceed the limits set forth by Olsen *et al.* (1991). These studies are presented below.

5.10.1 Confidence Intervals on Model Parameters

The confidence intervals on each reactor parameter and measured constant were determined as described in Chapter IV. The results are summarized in Table 5.4; Table 5.4 may also be used here as a summary of model constants, since all are listed together there. Many of the confidence intervals were plus/minus less than 5 % of the value of the constant; however, some were much higher. The confidence intervals (CI) for the LIP and MNP kinetic constants were the largest, since they were calculated from reciprocals of slopes and intercepts calculated by linear regression (this is also why they are not centered on the value of the constant, but are skewed). The largest CI was that for K_I, at $\pm$ 87%. The CIs for $k_{d,Mb}$, at $\pm$ 23 %, and $k_{d,L1}$, at + 33 %, -17 %, were also quite large, reflecting the larger amount of scatter in the original data used in determining each constant. The results of the perturbation studies for each case are combined below, since the model parameters affected all three cases in the same ways.

5.10.2 Perturbation Analyses

The results of the perturbation analyses are presented in Table 5.5 for LIP alone, in Table 5.6 for LIP + MNP, and in Table 5.7 for MNP alone. The case in each listed as "base" is the case in which the parameters were used as measured (no perturbation). Values presented are the maximum and minimum concentrations of $[H_2O_2]_B$ and $[VA]_B$ reached over the course of the perturbation run ($t > 0$), using first the lower end of the 95 % confidence interval of each model parameter, and then the higher end, instead of the measured model parameter. Since the values of k_s and D^{eff} for [Mn(III)-tart$_2$] were assumed, it was not possible to determine 95 % confidence intervals for them. Thus,

Table 5.4: Measured values of the physical parameters experimentally determined for use in the reactor model RKG.FOR and their 95 % Confidence Intervals (listed as ± percentages of their values).

Parameter	Units	Value	95 % C.I. - %	95 % C.I. + %
$D^{eff}(H_2O_2)$	cm^2/min	1.700E-04	3.53	3.53
D° (VA)	cm^2/min	4.494E-05	2.98	2.98
D^{eff} (Mn(II))	cm^2/min	1.319E-04	3.79	3.79
a_1	mM	600.0	33.20	16.33
a_2*	mM	1807.7	3.13	3.13
k_1	$[min(U/L)]^{-1}$	2.147E-02	15.28	21.98
k_3	$[min(U/L)]^{-1}$	8.101E-03	8.63	17.71
k_4	$mM[min(U/L)]^{-1}$	1.246E-03	5.78	5.78
K_I	mM	4.918	87.01	87.01
k_{5a}	$[min(U/L)]^{-1}$	6.566E-03	20.82	35.68
k_{5b}	$[min(U/L)]^{-1}$	5.089E-03	9.90	12.36
ψ_a	--	2983.2	28.25	28.25
ψ_b	--	2336.8	43.85	43.85
$k_{d,L1}$	$(U/L)hr^{-1}$	19.16	17.22	32.93
$k_{d,L2}$	hr^{-1}	1.867E-02	7.28	7.28
$k_{d,Ma}$	hr^{-1}	5.168E-03	5.65	5.65
$k_{d,Mb}$	hr^{-1}	2.535E-02	23.04	23.04
A	cm^2	0.2206	2.58	2.58
l	cm	6.136E-03	5.39	5.39
LIP:				
V_{Bo}	cm^3	1.00	1.33	1.33
V_{Ao}	cm^3	1.00	1.52	1.52
MNP:				
V_{Bo}	cm^3	1.00	1.23	1.23
V_{Ao}	cm^3	1.00	1.67	1.67
LIP+MNP:				
V_{Bo}	cm^3	1.00	1.25	1.25
V_{Ao}	cm^3	1.00	1.51	1.51

* $a_2 = \alpha^{-1}$

Table 5.5: Maximum and minimum concentrations of H_2O_2 and of VA in the LIP Alone enzyme case predicted by PERTURB.FOR to be reached in Side B when each parameter measured for the model (first column) was used at the lower (1st and 2nd columns under $[H_2O_2]_B$ and under $[VA]_B$) and upper (3rd and 4th columns under $[H_2O_2]_B$ and under $[VA]_B$) bounds of its 95 % Confidence Interval. The pulse profiles used were those determined by RKG.FOR with the measured values of the parameters.

	$[H_2O_2]_B$				$[VA]_B$			
	- 95 % CI		+ 95 % CI		- 95 % CI		+ 95 % CI	
Parameter	Max.	Min.	Max.	Min.	Max.	Min.	Max.	Min.
Base	0.025	0.009	0.025	0.009	0.561	0.056	0.561	0.056
a_1	2.855	0.015	0.016	0.009	0.309	0.029	1.560	0.138
a_2	0.076	0.009	0.022	0.009	0.545	0.036	0.630	0.061
A	0.812	0.009	0.024	0.009	0.513	0.030	1.578	0.058
l	0.025	0.009	1.602	0.009	2.790	0.060	0.469	0.029
V_{Bo}	0.027	0.009	0.023	0.009	0.563	0.053	0.559	0.058
V_{Ao}	0.022	0.009	0.036	0.009	0.601	0.062	0.533	0.044
$D^{eff}(H_2O_2)$	0.015	0.009	0.639	0.010	1.334	0.232	0.326	0.031
$D^{o}(VA)$	1.465	0.010	0.016	0.009	0.335	0.030	2.331	0.202
D^{eff}(Mn(II))	0.025	0.009	0.025	0.009	0.561	0.056	0.561	0.056
k_1	0.028	0.011	0.022	0.008	0.564	0.059	0.559	0.052
k_3	0.027	0.009	0.022	0.009	0.561	0.057	0.561	0.053
k_4	0.025	0.009	0.024	0.009	0.561	0.056	0.561	0.055
K_I	0.025	0.009	0.025	0.009	0.561	0.056	0.561	0.056
k_{5a}	0.025	0.009	0.025	0.009	0.561	0.056	0.561	0.056
k_{5b}	0.025	0.009	0.025	0.009	0.561	0.056	0.561	0.056
ψ_a	0.025	0.009	0.025	0.009	0.561	0.056	0.561	0.056
ψ_b	0.025	0.009	0.025	0.009	0.561	0.056	0.561	0.056
k_{dL1}	0.024	0.009	0.027	0.009	0.561	0.054	0.561	0.057
k_{dL2}	0.024	0.009	0.025	0.009	0.561	0.055	0.561	0.056
k_{dMa}	0.025	0.009	0.025	0.009	0.561	0.056	0.561	0.056
k_{dMb}	0.025	0.009	0.025	0.009	0.561	0.056	0.561	0.056
k_s (10 %)	0.025	0.009	0.025	0.009	0.561	0.056	0.561	0.056
k_s (50 %)	0.025	0.009	0.025	0.009	0.561	0.056	0.561	0.056
k_s (x 10)	0.025	0.009	0.025	0.009	0.561	0.056	0.561	0.056
k_s (x 10^2)	0.025	0.009	0.025	0.009	0.561	0.056	0.561	0.056
D^{eff}([Mn(III)-$tart_2$]):								
= D^{eff}(Mn(II))	0.025	0.009	0.025	0.009	0.561	0.056	0.561	0.056
= 50 %	0.025	0.009	0.025	0.009	0.561	0.056	0.561	0.056
= x 5	0.025	0.009	0.025	0.009	0.561	0.056	0.561	0.056

Table 5.6: Maximum and minimum concentrations of H_2O_2 and of VA in the LIP + MNP enzyme case predicted by PERTURB.FOR to be reached in Side B when each parameter measured for the model (first column) was used at the lower (1st and 2nd columns under $[H_2O_2]_B$ and under $[VA]_B$) and upper (3rd and 4th columns under $[H_2O_2]_B$ and under $[VA]_B$) bounds of its 95 % Confidence Interval. The pulse profiles used were those determined by RKG.FOR with the measured values of the parameters.

	$[H_2O_2]_B$				$[VA]_B$			
	- 95 % CI		+ 95 % CI		- 95 % CI		+ 95 % CI	
Parameter	Max.	Min.	Max.	Min.	Max.	Min.	Max.	Min.
Base	0.015	0.005	0.015	0.005	0.559	0.046	0.559	0.046
a_1	1.215	0.008	0.012	0.005	0.318	0.018	0.978	0.114
a_2	0.020	0.005	0.014	0.005	0.551	0.025	0.587	0.067
A	0.440	0.005	0.032	0.005	0.606	0.017	1.084	0.035
l	0.080	0.005	0.839	0.006	1.715	0.029	0.654	0.017
V_{Bo}	0.234	0.005	0.012	0.005	0.514	0.017	0.819	0.087
V_{Ao}	0.014	0.005	0.021	0.005	0.614	0.065	0.531	0.024
$D^{eff}(H_2O_2)$	0.011	0.005	0.516	0.006	1.280	0.254	0.311	0.017
$D^{o}(VA)$	0.963	0.007	0.012	0.005	0.331	0.017	1.696	0.180
$D^{eff}(Mn(II))$	0.015	0.005	0.015	0.005	0.561	0.049	0.559	0.044
k_1	0.017	0.006	0.013	0.004	0.561	0.049	0.557	0.043
k_3	0.016	0.005	0.014	0.005	0.559	0.047	0.559	0.045
k_4	0.015	0.005	0.015	0.005	0.559	0.047	0.559	0.046
K_I	0.015	0.005	0.015	0.005	0.559	0.046	0.559	0.046
k_{Sa}	0.015	0.005	0.015	0.005	0.559	0.046	0.559	0.046
k_{Sb}	0.015	0.005	0.015	0.005	0.559	0.045	0.560	0.047
ψ_a	0.015	0.005	0.015	0.005	0.560	0.049	0.559	0.045
ψ_b	0.013	0.005	0.169	0.005	0.765	0.084	0.511	0.017
$k_{d,L1}$	0.015	0.005	0.015	0.005	0.559	0.046	0.559	0.048
$k_{d,L2}$	0.015	0.005	0.015	0.005	0.559	0.046	0.559	0.047
$k_{d,Ma}$	0.015	0.005	0.015	0.005	0.559	0.046	0.559	0.046
$k_{d,Mb}$	0.015	0.005	0.015	0.005	0.568	0.056	0.559	0.036
k_s (10 %)	1.141	0.008	0.011	0.005	0.325	0.018	1.895	0.213
k_s (50 %)	6.223	0.016	0.009	0.004	0.196	0.027	6.710	0.513
k_s (x 10)	12.37	0.028	0.008	0.001	0.073	0.027	36.06	1.269
k_s (x 10^2)	13.92	0.038	0.010	0.001	0.061	0.027	46.06	1.311
D^{eff}([Mn(III)-tart$_2$]):								
= $D^{eff}(Mn(II))$	0.015	0.005	0.070	0.005	0.647	0.064	0.557	0.018
= 50 %	0.014	0.005	0.858	0.006	1.926	0.070	0.523	0.017
= x 5	0.014	0.004	3.295	0.008	2.944	0.074	0.354	0.022

Table 5.7: Maximum and minimum concentrations of H_2O_2 and of VA in the MNP Alone enzyme case predicted by PERTURB.FOR to be reached in Side B when each parameter measured for the model (first column) was used at the lower (1st and 2nd columns under $[H_2O_2]_B$ and under $[VA]_B$) and upper (3rd and 4th columns under $[H_2O_2]_B$ and under $[VA]_B$) bounds of its 95 % Confidence Interval. The pulse profiles used were those determined by RKG.FOR with the measured values of the parameters.

	$[H_2O_2]_B$				$[VA]_B$			
	- 95 % CI		+ 95 % CI		- 95 % CI		+ 95 % CI	
Parameter	Max.	Min.	Max.	Min.	Max.	Min.	Max.	Min.
Base	0.093	0.013	0.093	0.013	0.000	0.000	0.000	0.000
a_1	0.093	0.013	0.093	0.013	0.000	0.000	0.000	0.000
a_2	0.093	0.013	0.093	0.013	0.000	0.000	0.000	0.000
A	0.084	1E-04	0.206	0.044	0.000	0.000	0.000	0.000
l	0.350	0.082	0.076	1E-04	0.000	0.000	0.000	0.000
V_{Bo}	0.288	0.029	0.089	1E-04	0.000	0.000	0.000	0.000
V_{Ao}	0.093	1E-04	0.121	0.014	0.000	0.000	0.000	0.000
$D^{eff}(H_2O_2)$	0.081	2E-04	0.221	0.055	0.000	0.000	0.000	0.000
D°(VA)	0.093	0.013	0.093	0.013	0.000	0.000	0.000	0.000
D^{eff}(Mn(II))	0.093	0.010	0.093	0.013	0.000	0.000	0.000	0.000
k_1	0.093	0.013	0.093	0.013	0.000	0.000	0.000	0.000
k_3	0.093	0.013	0.093	0.013	0.000	0.000	0.000	0.000
k_4	0.093	0.013	0.093	0.013	0.000	0.000	0.000	0.000
K_I	0.093	0.013	0.093	0.013	0.000	0.000	0.000	0.000
k_{5a}	0.093	0.013	0.093	0.013	0.000	0.000	0.000	0.000
k_{5b}	0.093	0.013	0.093	0.013	0.000	0.000	0.000	0.000
ψ_a	0.093	0.013	0.093	0.013	0.000	0.000	0.000	0.000
ψ_b	0.088	1E-04	0.252	0.030	0.000	0.000	0.000	0.000
$k_{d,L1}$	0.093	0.013	0.093	0.013	0.000	0.000	0.000	0.000
$k_{d,L2}$	0.093	0.013	0.093	0.013	0.000	0.000	0.000	0.000
$k_{d,Ma}$	0.093	0.013	0.093	0.013	0.000	0.000	0.000	0.000
$k_{d,Mb}$	0.093	0.002	0.093	0.013	0.000	0.000	0.000	0.000
k_s (10 %)	1.298	0.125	0.061	1E-04	0.000	0.000	0.000	0.000
k_s (50 %)	6.892	0.255	3E-04	1E-04	0.000	0.000	0.000	0.000
k_s (x 10)	13.69	0.389	3E-04	1E-04	0.000	0.000	0.000	0.000
k_s (x 10^2)	15.42	0.420	9.684	1.483	0.000	0.000	0.000	0.000
D^{eff}([Mn(III)-tart$_2$]):								
= D^{eff}(Mn(II))	0.093	1E-04	0.146	0.013	0.000	0.000	0.000	0.000
= 50 %	0.092	1E-04	0.989	0.018	0.000	0.000	0.000	0.000
= x 5	0.092	1E-04	3.655	0.054	0.000	0.000	0.000	0.000

instead of using confidence intervals for k_8 and D^{eff} for [Mn(III)-tart$_2$], perturbation analyses were run as follows: (1.) k_8 at $\pm$ 10 %, $\pm$ 50 %, $\times$ 10, and $\times$ 100; and (2.) D^{eff} for [Mn(III)-tart$_2$] at $\pm$ 50 %, $\times$ 5, and then at $\pm$ the 95 % Confidence Interval for D^{eff} for Mn(II) ($\pm$ 3.79 %). Comparison of the concentration values listed in Tables 5.5-5.7 with the concentration range limits for $[H_2O_2]_B$ and $[VA]_B$ (minimum of 0.005 mM for both H_2O_2 and VA, maximum of 0.1 mM for $[H_2O_2]_B$, and maximum of 0.6 mM for $[VA]_B$) (Olsen *et al.*, 1991) indicates the model parameters which are most likely to cause erroneous model predictions because of errors in measurement.

The model is quite sensitive, in general, to the reactor design parameters A, l, and V_{Bo}, but is only sensitive to V_{Ao} in the case of VA; the values of A and l were measured with calipers and were thus as accurate as possible, while volumes were measured with Pipetman pipets, and are thus limited to the accuracy of the pipets. Both of the measured values of effective diffusion coefficients, as well as the constants for the VA diffusion coefficient, when varied at the upper and lower bounds of their confidence intervals, cause the model predictions for one or another component to exceed the specified limits; this is surprising, since the confidence intervals were relatively narrow (largest at $\pm$ 3.8 %). The model is insensitive to all enzyme stability parameters, as well as to LIP kinetic constants, k_5 for both MNPs, and Ψ_a; even the $\pm$ 87 % confidence interval for K_I caused little change in the model predictions. Of the kinetic parameters, only Ψ_b seems to have much of an effect on model stability, probably since there is so much MNP_b present in the runs (Ψ_a has little effect since it is a minor component). When the effective diffusion coefficient for [Mn(III)-tart$_2$] is varied at the limits for D^{eff} for Mn(II), $[H_2O_2]_B$ only slightly exceeds the upper limit; however, if the assumed value for D^{eff} for [Mn(III)-tart$_2$] is much farther than that from its assumed value, large errors in model predictions occur. Finally, the model is extremely sensitive to the value of k_8. Even just a 10 % variation in k_8 causes $[H_2O_2]_B$ to exceed its maximum value of 0.1 mM by nearly 1300 %. The conclusion from this exercise is that the parameters over which

there can be little control in the accuracy of measurement cause the greatest variations in the model predictions, with the exception of the diffusion coefficients.

5.11 Treatment of Lignin in Dialysis Reactor

Base cases and controls were run for each enzyme mixture as described in Chapter IV, using the pulse profiles determined by RKG.FOR (listed in Chapter IV). The initial conditions (concentrations, etc.) for each run are listed in Tables 5.8a and 5.8b. Refer to Chapter IV for the definitions of the acronyms used for each case. Table 5.9 lists the initial, final, and corrected final (corrected for 95 % recovery of solids) masses of lignin for each reactor run. Since no enzyme activity (active enzyme plus all of the required reagents) was present in any control which contained lignin, the error of the lignin recovery for each case was calculated as the variance of all controls combined (all cases); the average corrected percent recovery of lignin from the reactor control runs was found to be 99.5 % $\pm$ 6.2 %. The uncertainty indicated is for 90 % confidence assuming the data are from a Normal Distribution. A 90 % confidence level (mean $\pm$ 1.64s) was used because the interval encompasses all but one data point, that for the MNP E^- control, which is only 0.2 % below the interval. Comparing the base case recoveries for each enzyme with the average recovery for the controls indicates that the lignin recovery from the LIP alone run was not statistically different from the controls, the MNP alone run slightly *increased* the mass of the lignin, and the LIP + MNP run released 10.3 % of the lignin.

Photographs of the solid lignin were taken (after extraction for the GC/MS, but before lyophilization) in order to compare appearance of the base case (BC) lignin with that of its controls. The lignin samples from the LIP alone runs are shown in Figure 5.46; samples are, from left to right: Base Case (BC), No reagent control (R^-), No LIP control (E^-), Autoclaved LIP control (AE), and No LIP, No reagent control (ER^-). Only a slight color change is seen in the BC versus the controls (all controls are identical), if any, which is consistent with the lignin recovery data above.

Table 5.8a: Initial (time zero) lignin and enzyme levels in Side B of the reactor for each Base Case and its controls.

Enzyme(s)	Case	Lignin (mg)	[LIP] (U/L)	[MNP_a] (U/L)	[MNP_b] (U/L)
LIP	BC	22.8	1000.0	898.7	0.0
LIP	L⁻	0.0	1000.0	898.7	0.0
LIP	R⁻	23.1	1000.0	898.7	0.0
LIP	E⁻	22.9	0.0	0.0	0.0
LIP	AE	23.1	ND*	ND	0.0
LIP	ER⁻	22.9	0.0	0.0	0.0
LIP+MNP	BC	22.8	1000.0	898.7	55101.3
LIP+MNP	L⁻	0.0	1000.0	898.7	55101.3
LIP+MNP	R⁻	22.8	1000.0	898.7	55101.3
LIP+MNP	E⁻	23.1	0.0	0.0	0.0
LIP+MNP	AE	23.0	ND	ND	ND
LIP+MNP	ER⁻	23.0	0.0	0.0	0.0
MNP	BC	22.8	ND	0.0	56000.0
MNP	L⁻	0.0	ND	0.0	56000.0
MNP	R⁻	23.0	ND	0.0	56000.0
MNP	E⁻	22.8	0.0	0.0	0.0
MNP	AE	22.9	ND	0.0	ND
MNP	ER⁻	23.1	0.0	0.0	0.0

* ND = None Detected

Table 5.8b: Initial (time zero) H_2O_2 and VA concentrations in Sides A and B of the reactor and Mn(II) in Side B for each Base Case and its controls.

Enzyme(s)	Case	$[H_2O_2]_{Ao}$ (mM)	$[VA]_{Ao}$ (mM)	$[H_2O_2]_{Bo}$ (mM)	$[VA]_{Bo}$ (mM)	$[Mn(II)]_{Bo}$ (mM)*
LIP	BC	38.84	149.1	0.100	0.600	0.000
LIP	L˙	38.84	149.1	0.100	0.600	0.000
LIP	R˙	0.000	0.000	0.000	0.000	0.000
LIP	E˙	0.100	0.600	0.100	0.600	0.000
LIP	AE	0.100	0.600	0.100	0.600	0.000
LIP	ER˙	0.000	0.000	0.000	0.000	0.000
LIP+MNP	BC	44.37	119.9	0.100	0.600	0.100
LIP+MNP	L˙	44.37	119.9	0.100	0.600	0.100
LIP+MNP	R˙	0.000	0.000	0.000	0.000	0.000
LIP+MNP	E˙	0.100	0.600	0.100	0.600	0.100
LIP+MNP	AE	0.100	0.600	0.100	0.600	0.100
LIP+MNP	ER˙	0.000	0.000	0.000	0.000	0.000
MNP	BC	11.00	0.000	0.100	0.000	0.100
MNP	L˙	11.00	0.000	0.100	0.000	0.100
MNP	R˙	0.000	0.000	0.000	0.000	0.000
MNP	E˙	0.100	0.000	0.100	0.000	0.100
MNP	AE	0.100	0.000	0.100	0.000	0.100
MNP	ER˙	0.000	0.000	0.000	0.000	0.000

* Added as [Mn(III)-$tart_2$].

Table 5.9: Initial (time zero) and final (12 hour) mass of lignin present, and the final lignin mass as a percentage of the initial for each Base Case and its controls.

Enzyme(s)	Case	Initial Lignin (mg)	Recovered Lignin (mg)	Final Lignin (mg)*	Final Lignin (% of initial)
LIP	BC	22.8	21.2	22.3	97.8
LIP	R⁻	23.1	22.2	23.4	101
LIP	E⁻	22.9	20.5	21.6	94.3
LIP	AE	23.1	21.6	22.7	98.3
LIP	ER⁻	22.9	22.3	23.5	103
LIP+MNP	BC	22.8	19.3	20.3	89.0
LIP+MNP	R⁻	22.8	21.6	22.7	99.6
LIP+MNP	E⁻	23.1	22.9	24.1	104
LIP+MNP	AE	23.0	22.5	23.7	103
LIP+MNP	ER⁻	23.0	21.6	22.7	98.7
MNP	BC	22.8	22.9	24.1	106
MNP	R⁻	23.0	22.9	24.1	105
MNP	E⁻	22.8	20.1	21.2	93.0
MNP	AE	22.9	21.0	22.1	96.5
MNP	ER⁻	23.1	21.7	22.8	98.7

* Corrected for 95 % recovery.

Figure 5.46: Photograph of the lignin recovered from the LIP Alone enzyme runs, still in the conical vials, and under 1 mL of distilled water. From left to right: Base Case, No reagent control (R^-), No LIP control (E^-), Autoclaved LIP control (AE), and No reagent, no LIP control (ER^-).

The lignin samples for the MNP alone runs are presented in Figures 5.47a (6 hour treatment) and 5.47b (12 hour treatment); sample order is as in Figure 5.46. There is a definite darkening of the lignin from the base case versus the controls, which are all identical in color. The darker color is definitely not due to precipitation of MnO_2, since the L^- control (which contained MNP, H_2O_2, and Mn(II), but no lignin) did not form a precipitate. The color change is consistent with the formation of quinone structures (a known MNP reaction) in the solid lignin (from the aromatic rings) since quinones in lignin are, in general, darker in color than phenolics (B. Hames, Personal Communication), quinone formation by oxidation of lignin is a known reaction in lignin chemistry (Sarkanen and Ludwig, 1971), and quinone formation from lignin model dimers is a reaction known to be catalyzed by MNP (Wariishi *et al.*, 1991; Tuor *et al.*, 1992). This is also consistent with the lignin recovery data above, since oxidation of the lignin by the MNP without significant release of products would increase the mass of the lignin. The base case lignin from the 12 hour treatment may be slightly darker than that for the 6 hour treatment, but not significantly.

Finally, the lignin samples from the LIP + MNP runs are presented in Figure 5.48; again, the order is identical to that used above. There is little change in the color of the base case lignin versus the controls (again, all identical); however, observation of the color of the lignin while in the reactor during the run revealed that the color of the LIP + MNP base case lignin darkened considerably over the first 4 to 6 hours of reaction, and then lightened in color over the remainder of the reaction time. This suggests that the MNP first modified the solid lignin by oxidation and the LIP released lignin fragments from this modified lignin, leaving a final solid lignin that was relatively indistinguishable in appearance from the initial lignin. This is also supported by the lignin recovery data presented above, since the LIP + MNP case was the only case to show lignin removal in the base case. Finally, this result, combined with that for the MNP alone runs for 6 and 12 hours, suggest that the MNP was only active for the first

(a.)

(b.)

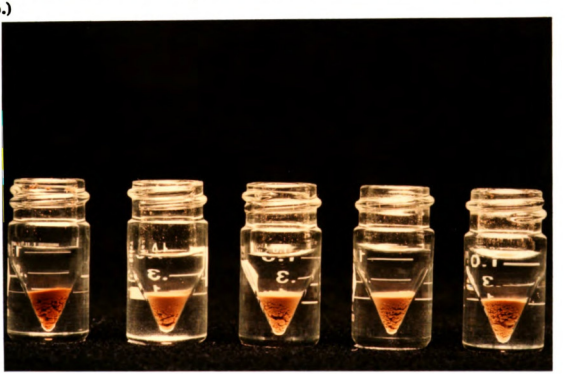

Figure 5.47: Photographs of the lignin recovered from the MNP Alone enzyme runs, still in the conical vials, and under 1 mL of distilled water. From left to right: Base Case, No reagent control (R-), No MNP control (E-), Autoclaved MNP control (AE), and No reagent, no MNP control (ER-). **(a.)** 6 hour treatment time; and **(b.)** 12 hour treatment time.

Figure 5.48: Photograph of the lignin recovered from the LIP + MNP enzyme runs, still in the conical vials, and under 1 mL of distilled water. From left to right: Base Case, No reagent control (R'), No LIP, no MNP control (E'), Autoclaved LIP, autoclaved MNP control (AE), and No reagent, no LIP, no MNP control (ER').

6 hours of the run, perhaps indicating that the enzyme may have been inactivated due to excessive H_2O_2 accumulation in Side B (due to breakdown of the model predictions over a 6 hour period).

5.12 FTIR/PLS Analysis of Peroxidase Treated Solid Lignin

KBr pellets containing about 1.5 mg of dried, extracted lignin from the reactor runs were pressed and FTIR spectra for each were measured. The spectral data files were saved on disk for future analysis, and sent to Bonnie Hames, an Associate Chemist in the Chemical Conversion Research Branch at the National Renewable Energy Laboratory (NREL, Golden, CO). The data were subjected to PLS analysis (Hames *et al.*, 1991) to determine whether changes had occurred in the lignin and/or carbohydrate compositions, methoxyl contents, or phenolic hydroxyl contents as a result of treatment with the peroxidase enzymes alone and in combination. Calibration of the methods was by chemical measurement of these parameters for a range of milled wood lignins (Hames *et al.*, 1991). Pellet lignin concentrations and the order of measurement of the FTIR spectra are listed in Table 5.10.

The transmission spectrum of the KBR background pellet is shown if Figure 5.49. The peaks in the spectrum in the range 1800-1000 cm^{-1} are due to a contaminant, perhaps some oil from the surface of the die which was used to press the pellet (a new die, which was assumed to be clean, was used). The spectrum of the background pellet was subtracted from the spectra of all of the sample pellets to remove absorbances from the sample pellet medium. The spectra were analyzed by PLS for methoxyl content with this background and also with an uncontaminated background spectrum obtained at NREL since this is the region which most affects the predictions of aromatic methoxyl content (Faix, 1992; B. Hames, Personal Communication); no significant change in the predictions occurred by using the uncontaminated background spectrum, indicating that the contaminant had little or no effect on the predictions of the PLS technique (B. Hames, Personal Communication). Therefore, in order to eliminate any errors

Table 5.10: Lignin concentrations in the KBr pellets used to measured the FTIR spectra of each Base Case and its controls. The order of measurement indicates the order in which the IR spectrum of each pellet was measured, and is used to indicate which spectra were measured more closely in time.

Sample	Pellet Lignin Concentration (%)	Order of Measurement
LIP Only		
BC	0.4995	11
R$^-$	0.4997	12
E$^-$	0.4665	13
AE	0.4993	14
ER$^-$	0.5326	15
LIP + MNP		
BC	0.4636	6
R$^-$	0.4665	7
E$^-$	0.4660	8
AE	0.4670	9
ER$^-$	0.4662	10
MNP Only		
BC	0.5576	1
R$^-$	0.3069	2
E$^-$	0.4696	3
AE	0.4659	4
ER$^-$	0.4988	5

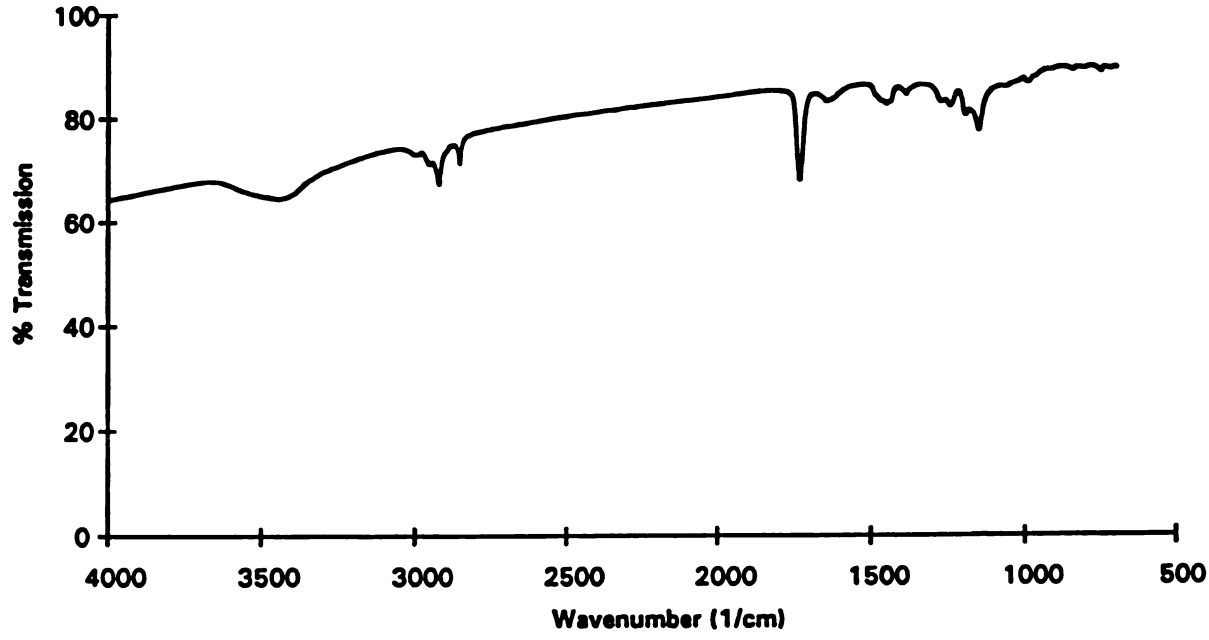

Figure 5.49: Transmission FTIR spectrum from 4000-700 wavenumbers for the KBr background pellet.

introduced into future PLS analyses due to discrepancies in the KBr backgrounds obtained here and at NREL, PLS analyses were conducted using the spectra ratioed with the background measured when the pellets were measured.

The FTIR absorbance spectra of the three base case (BC) lignins and their ER$^-$ controls are presented in Figure 5.50 (LIP Only BC and its ER$^-$ control), Figure 5.51 (LIP + MNP BC and its ER$^-$ control), and Figure 5.52 (MNP Only BC and its ER$^-$ control); the remainder of the spectra are presented in Appendix F in Figures F.1 through F.9. The appearances of these spectra are typical for lignins (Schultz *et al.*, 1985; Schultz and Glasser, 1986; Hames *et al.*, 1991). Not many differences are seen by visual comparison of the spectra, but minor differences in FTIR spectra often indicate major differences in structure (Sarkanen and Ludwig, 1971).

Initial PLS analysis of the sample spectra for lignin and carbohydrate contents indicated that the spectra would have to be normalized because the maximum absorbance in each spectrum did not proportionally correspond with the known solid lignin concentrations in the pellet as is predicted by Beer's Law (Griffiths and de Haseth, 1986); possible causes for this will be discussed below. In addition, it appeared that the total absorbance fluctuated with time (which makes the order of pellet measurement important), probably due to a decrease in the energy output of the FTIR instrument over time. To minimize the effect of this problem, all of the spectral files were normalized so that the absorbance at a reference peak was proportional to the known solid lignin concentration in the pellets; the reference peak was chosen as the absorbance peak at 1125.5 cm^{-1}, which is due in large part to the aromatic C-H in-plane deformation of syringyl units (Faix, 1992) and is the highest peak in all of the spectra. This peak was chosen because only insignificant differences (regardless of background used) were seen in the methoxyl contents of all the samples when they were analyzed previously to determine the effect of the contaminant in the background pellet; thus, this peak seemed to be an ideal choice for normalization because it is due in large part to the absorbance

(a.)

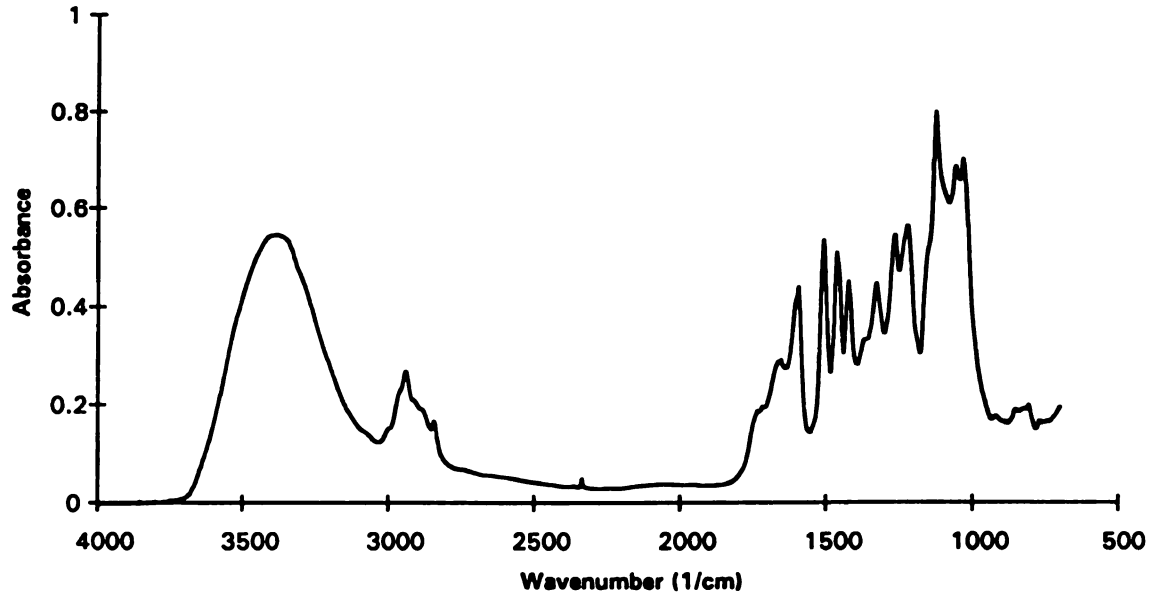

(b.)

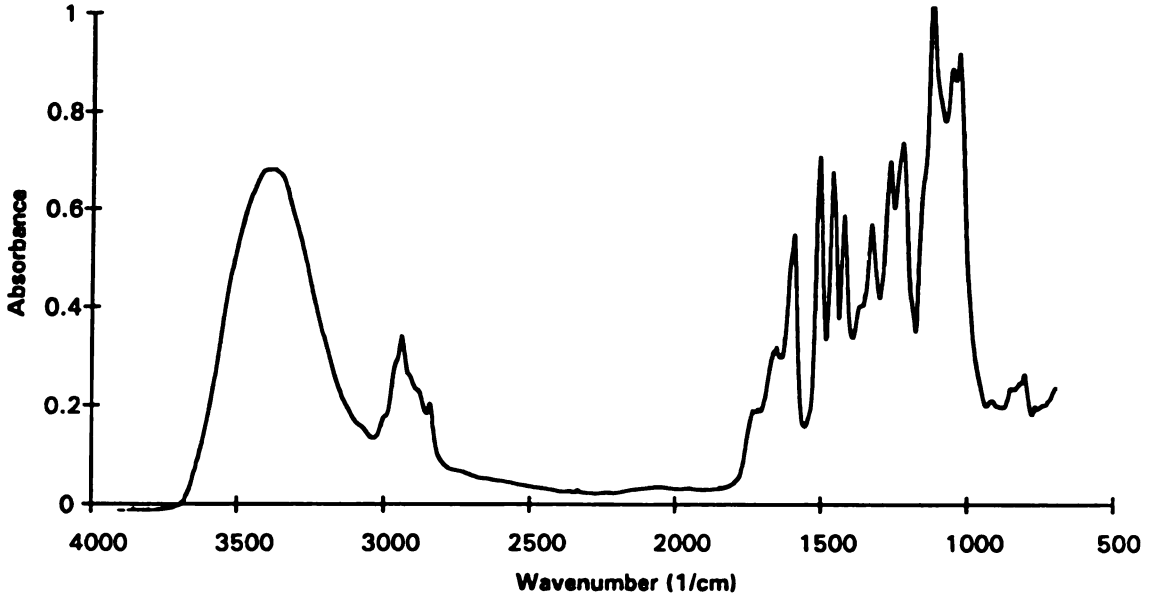

Figure 5.50: FTIR absorbance spectra for (a.) LIP Alone BC lignin after treatment for 12 hours; and (b.) No reagent, no LIP control (ER$^-$) lignin after treatment for 12 hours.

(a.)

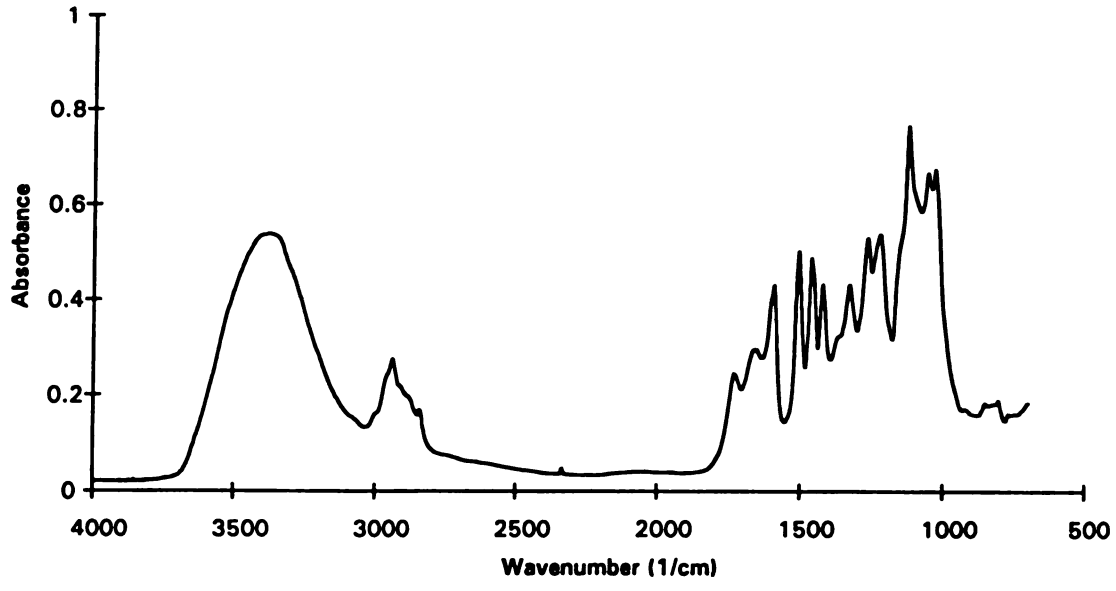

(b.)

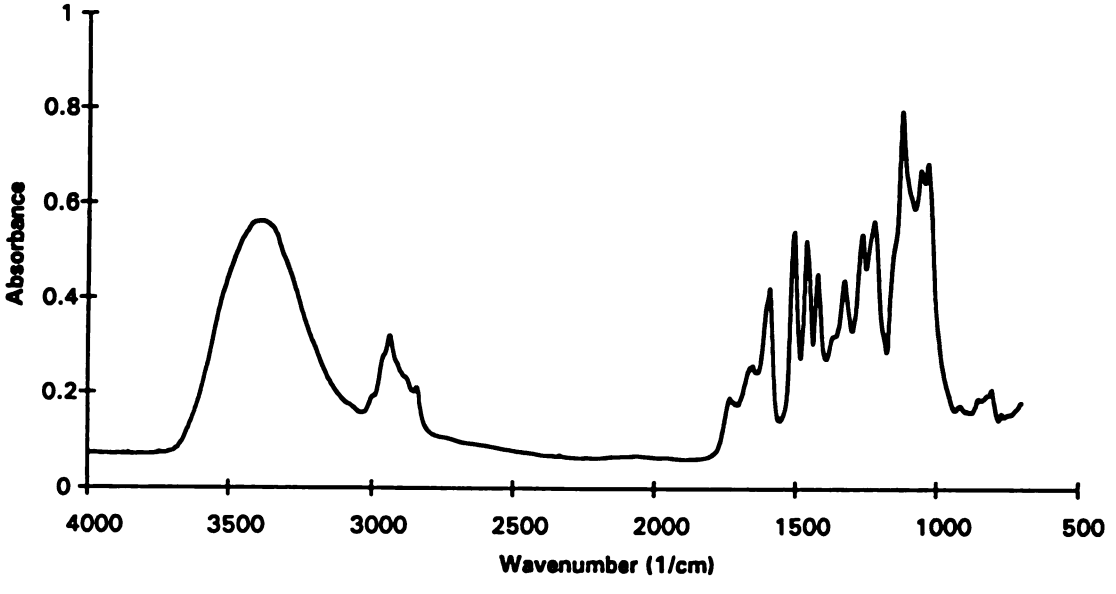

Figure 5.51: FTIR absorbance spectra for (a.) LIP + MNP BC lignin after treatment for 12 hours; and (b.) No reagent, no LIP, no MNP control (ER^-) lignin after treatment for 12 hours.

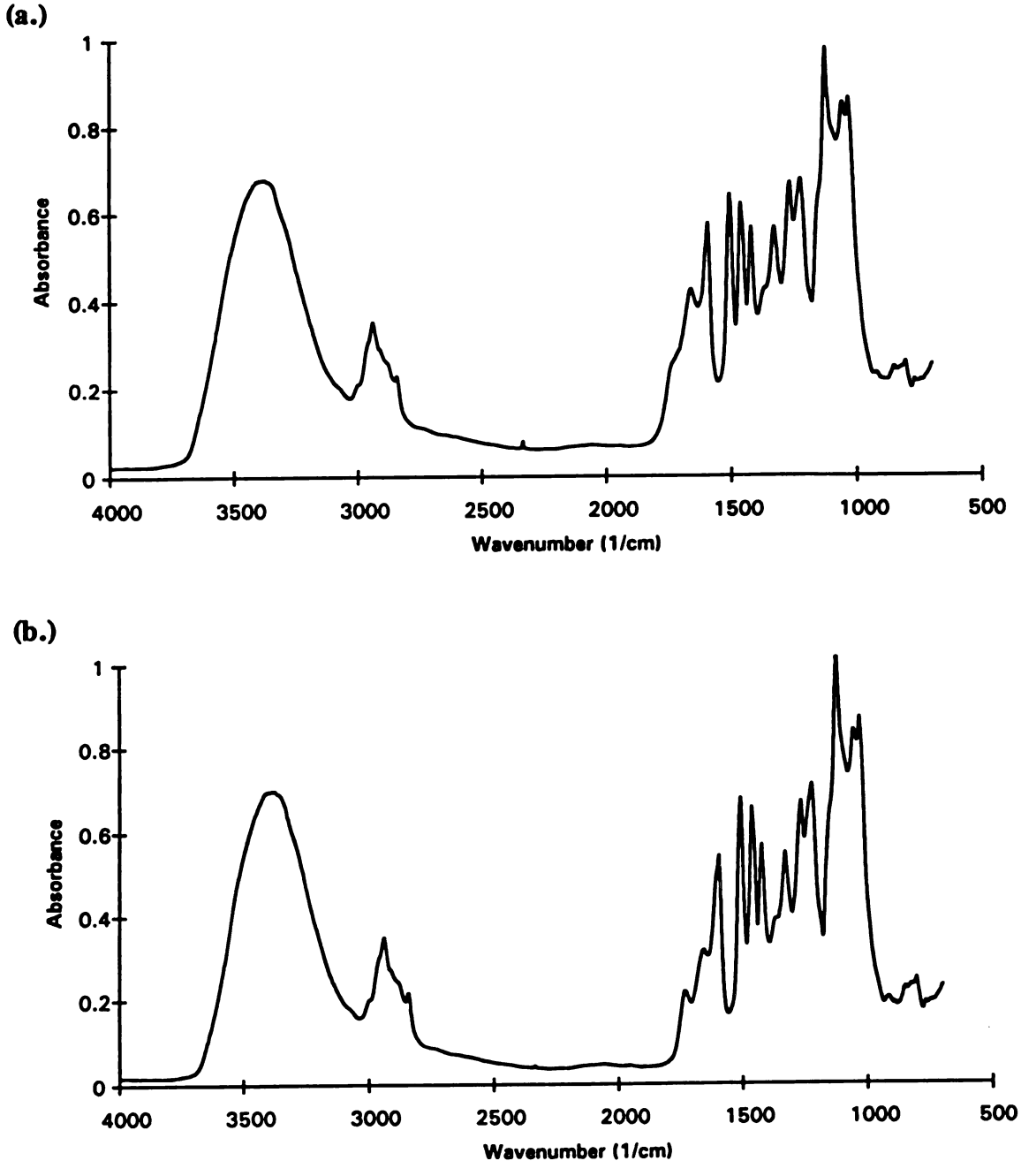

Figure 5.52: FTIR absorbance spectra for (a.) MNP Alone BC lignin after treatment for 12 hours; and (b.) No reagent, no MNP control (ER^-) lignin after treatment for 12 hours.

of aromatic methoxyl groups (B. Hames, Personal Communication; Faix, 1992).

The results of the PLS analysis of the concentration-normalized spectra for lignin and carbohydrate contents are given in Table 5.11. Lignin contents are ± 3.60 %, carbohydrate contents are ± 7.00 %, and the r^2 for each of these analyses are 0.9689 and 0.9205, respectively. The uncertainties in the carbohydrate analyses are much too large to allow the predicted contents to be useful; this is not surprising since the PLS program output indicated that the carbohydrate data were outside the calibration range. Milled wood lignins (lower molecular weight lignin fragments extracted with dioxane), which were used to calibrate the PLS technique, typically contain a fairly high amount of carbohydrates, while this lignin has little carbohydrate present, most of which is likely to be covalently linked to the lignin based on the inability to remove it with saturating levels of cellulase. The specific results presented in Table 5.11 will be discussed below, but first it is useful to look at trends in the lignin content predictions for the controls (between enzyme cases).

The predictions of lignin contents are consistent within each set of controls, but they are not consistent between the control sets (none of the controls contained all of the necessary components for enzyme activity so their lignin contents should be very close to one another). It should be noted here that the chemically measured lignin and carbohydrate contents of the starting material (see Section 5.1) were 74.5 % and 12.2 %, respectively. There is a still an increase in the predicted lignin contents of the controls between sets with the order of measurement (increasing time of analysis) of the FTIR spectra of the sample pellets. Thus, the normalization did not fully account for the time dependence of the absorbed intensity; this indicates that either there must have been some sort of difference in the way the samples from each set were handled (ie. number of times they were frozen at -80 °C and thawed before analysis for photos, extraction, etc., how long they stayed frozen, etc.), or the energy output of the FTIR instrument simply decreased too much over time to allow a consistent amount of IR radiation to

Table 5.11: Lignin and carbohydrate contents for the lignin recovered from the reactor runs for each Base Case and its controls, as predicted by the FTIR/PLS technique (Hames *et al.*, 1991). The standard errors of the predictions and the r^2 for the calibrations of the methods with milled wood lignins are listed at the bottom of each column.

Sample/ Case	Lignin Content (%)	Carbohydrate Content (%)
LIP Only		
BC	68.25	14.45
R⁻	71.86	11.74
E⁻	76.14	6.71
AE	71.76	11.43
ER⁻	76.89	5.29
LIP + MNP		
BC	60.26	23.25
R⁻	68.46	16.69
E⁻	67.88	18.11
AE	68.27	16.32
ER⁻	67.41	17.60
MNP Only		
BC	67.05	12.58
R⁻	64.74	21.06
E⁻	65.00	19.58
AE	67.50	17.43
ER⁻	66.20	19.14
Std. Error	3.60	7.00
r^2	0.9698	0.9205

reach the detector. The second explanation is the more likely of the two, since the desiccant for the window of the detector on the FTIR instrument at MBI was near the end of its useful life and needed to be replaced (Richard Turk, MBI, Personal Communication); this would certainly cause a decrease in the amount of energy reaching the detector over time because it would allow fogging of the detector window with moisture from the air. The desiccant should have been replaced before measuring the samples; however, a replacement was not readily available, and time constraints prohibited waiting for one. Nonetheless, since the samples within each enzyme case were measured consecutively and closely together in time, they can still be compared with a high degree of confidence (B. Hames, Personal Communication). The bottom line for this is that it limits the use of this data to internal comparisons only, ie. comparisons of one experiment in a given set to another one in its set. Comparisons based on actual lignin contents between sets may not be made accurately with this data (this warning applies to the lignin and carbohydrate determinations only, because no such trends were seen with the other PLS analyses) (B. Hames, Personal Communication).

The lignin and carbohydrate contents predicted for the LIP only BC are 68.25 % ± 3.60 % and 14.45 % ± 7.00 %, respectively, with average contents in the controls of 74.16 % ± 5.46 % (mean ± 2s, 95 % confidence) and 8.79 % ± 6.56 %, respectively. The carbohydrate predictions will not be considered, given the lower bound of their uncertainty range is very near zero. The lignin content predictions, however, are useful with a high degree of confidence (B. Hames, Personal Communication). Within the uncertainty ranges of the controls in Table 5.11, there is only a small decrease in lignin content for the LIP only BC versus the controls; this is completely consistent with the solid lignin dry weight analysis results given above, indicating that if LIP alone did release lignin from the solid, it was not an amount significant enough to see an effect with these methods.

The lignin and carbohydrate contents predicted for the MNP only BC are 67.05

% ± 3.60 % and 12.58 % ± 7.00 %, respectively, with average contents in the controls of 65.86 % ± 2.52 % and 19.30 % ± 2.98 %, respectively. No lignin appears to have been released by MNP alone; the lack of lignin removal by MNP alone is completely consistent with the lignin dry weight recovery analysis presented above, which found a slight increase in the mass of solid recovered from the reactor.

Finally, the lignin and carbohydrate contents predicted for the LIP + MNP BC are 60.26 % ± 3.60 % and 23.25 % ± 7.00 %, respectively, with average contents in the controls of 68.01 % ± 0.92 % and 17.18 % ± 1.64 %, respectively. The lignin content of the BC is clearly lower than that of its controls, even considering the extreme values in the uncertainty ranges; this result is again completely consistent with the lignin dry weight recovery from the reactor run, indicating that lignin removal occurred when both enzymes were present and active.

The PLS predictions for the methoxyl content per C_9 unit for the concentration-normalized spectra are presented in Table 5.12. The standard error in the predictions is ± 0.03, with an r^2 for the analysis of 0.9935. The values and averages for the controls for each case (uncertainties estimated as above) are as follows: (1.) LIP Alone BC: 1.32 ± 0.03, Controls: 1.34 ± 0.03 (95 % confidence); (2.) LIP + MNP BC: 1.33 ± 0.03, Controls: 1.34 ± 0.03; and (3.) MNP Alone BC: 1.31 ± 0.03, Controls: 1.35 ± 0.03. Thus, there was no change in the methoxyl content for any enzyme case, indicating that if lignin was removed for any of the enzyme BCs, the removal was homogeneous with respect to the amounts of syringyl (2 methoxyls per unit) and guaiacyl (1 methoxyl per unit) units.

Unfortunately, the PLS analysis for phenolic hydroxyl contents was not successful. The phenolic hydroxyl PLS calculation is calibrated, as with the other programs, with milled wood lignins, which are not generally expected to have lower than 0.70 OH groups per aromatic unit (the lower end of the calibration range for the milled wood lignins used to calibrate the PLS method; B. Hames, Personal Communication);

Table 5.12: Methoxyl contents of the lignin recovered from the reactor runs for each Base Case and its controls, as predicted by the FTIR/PLS technique (Hames *et al.*, 1991). The standard error of the prediction and the r^2 for the calibration with milled wood lignins are listed at the bottom of the column.

Sample/ Case	Methoxyl Content Per C_9 Unit
LIP Only	
BC	1.32
R'	1.35
E'	1.34
AE	1.35
ER'	1.32
LIP + MNP	
BC	1.33
R'	1.34
E'	1.33
AE	1.33
ER'	1.36
MNP Only	
BC	1.31
R'	1.36
E'	1.36
AE	1.34
ER'	1.33
Std. Error	0.03
r^2	0.9935

this is because milled wood lignins are smaller (dioxane-extractable) lignin fragments, and are expected to have a significant number of free phenolic hydroxyls on the end units of the lignin polymer (recall that the most common intermonomer lignin bond is the β-O-4 ether linkage, which uses up the ring-bound oxygens para- to the aliphatic side chain which otherwise would remain as hydroxyls). The r^2 for the calibration of this PLS method is 0.988. The predicted phenolic hydroxyl contents for all samples were 0.00 ± 0.07 OH groups per aromatic unit, which is well below the calibration range. The only conclusion that can be drawn from the phenolic hydroxyl analysis, then, is that the phenolic hydroxyl contents are below 0.70 OH groups per aromatic unit. This, in turn, indicates that all of the lignin samples are highly polymeric, which is supported by the fact that at least the starting material was completely insoluble in any lignin solvent. This also indicates that if any significant degradation of the lignin occurred, it must have occurred near the free phenolic ends of the lignin polymer so as not to increase the free phenolic hydroxyl content.

5.13 GC/MS Analysis of Solubilized Compounds

The mass spectrum of the internal standard (2-chloro-5-trifluoromethylbenzoic acid (mono-TMS ether)) is presented in Figure 5.53. Note the clear presence of chlorine in the mass spectrum evidenced by the $^{35}Cl/^{37}Cl$ natural abundance isotope patterns for the fragments at m/z 281, 237, 207, and 179. The peak eluted from the DB5-MS column in the early samples (MNP Only runs) at about 8'15" (scan number 550), and eluted from the DB-1 column in the later samples (LIP Only, LIP + MNP, and STD Mix) at about 7'30" (scan number 500). This peak was used during the comparison of Total Ion Chromatograms (TICs) from the BCs and their controls both as an internal standard for approximate quantitation, and as a reference peak to correct for small differences in retention times among the Base Case extracts and the extracts from the controls.

The controls which were run for each enzyme case (LIP Alone, MNP Alone, and

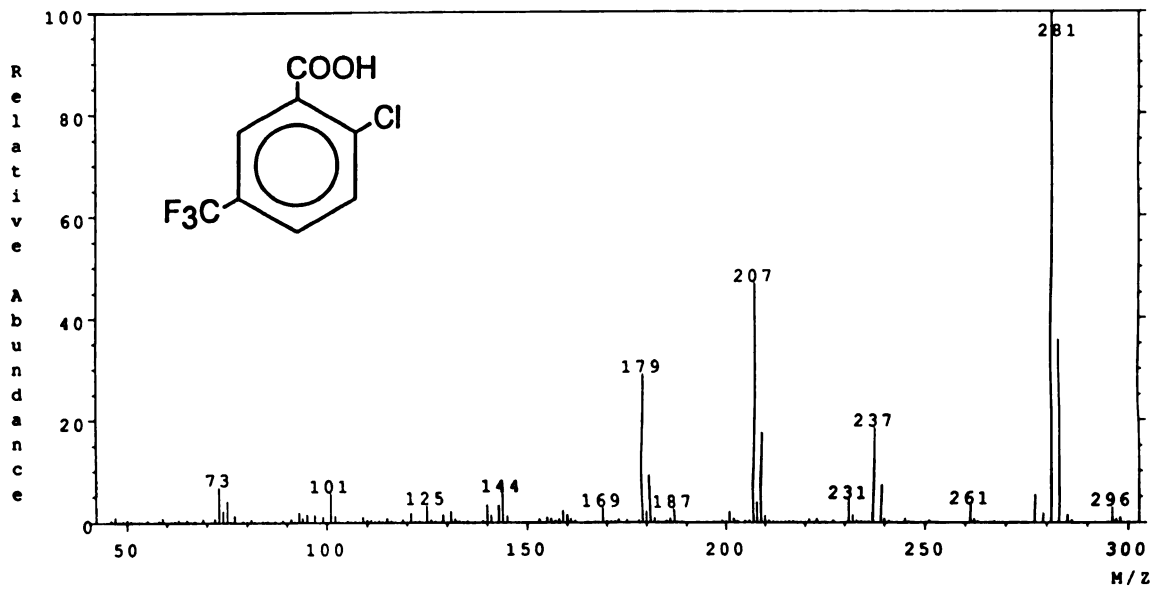

Figure 5.53: Electron-impact mass spectrum of the internal standard, 2-chloro-5-(trifluoromethyl)-benzoic acid (mono-TMS derivative). The spectrum was obtained from scan 499 (7'28") after elution from the DB-1 GC column. The background subtraction was the average of scans 495 and 501.

LIP + MNP; see Tables 4.6-4.8) were designed specifically to screen out products which were not released from the lignin by the activities of the peroxidase enzymes when all necessary reagents were present. These controls included: (1) L^- Control: Enzyme(s) + reagents (H_2O_2 +/- VA +/- Mn(II)) + O_2 + buffer, to screen out products of oxidation of VA by LIP, and/or products from the action of [Mn(III)-$tart_2$] on MNP solution contaminants; (2) R^- Control: Enzyme(s) + lignin + O_2 + buffer, to screen out compounds produced by the action of any protein or compound present in the enzyme mixture(s) other than the peroxidase enzymes (LIP and/or MNP); (3) E^- Control: Lignin + reagents + O_2 + buffer, to screen out compounds arising purely from the action of the reagents on the lignin or on low molecular weight extractives still present in the lignin; (4) AE Control: Autoclaved (inactive) enzyme(s) + reagents + O_2 + buffer, to screen out products arising from the action of free (non-enzyme-bound) heme (in the presence of H_2O_2); and (5) ER^- Control: Lignin + O_2 + buffer, to screen out low molecular weight compounds (extractives) already present in the lignin. The samples (liquid and solid) from these controls were handled and analyzed by GC/MS in exactly the same manner as the Base Cases (BCs: Enzyme(s) + reagents + lignin + O_2 + buffer). In addition, separate samples of the internal standard (in ethyl acetate) were analyzed by GC/MS to screen out contaminants in the stock supply of the internal standard (20 μL of which was added to each extract before concentration). Thus, any peak (compound) found in a BC extract which was unique to the BC could only be a compound released from the lignin by the active enzyme(s) in the presence of their required reagents. The mass spectra from the peaks remaining after comparison of the TICs of the BC extracts with those of the extracts of the controls were analyzed to determine whether structures consistent with lignin-derived products could be elucidated for the compounds. For all spectra except ones which were matched with spectra in the NIST or Wiley databases, or matched with published spectra, a general approach was taken due to the fact that many of the compounds were in very low concentrations

(concentrations estimated from the proportionality constant with peak area for the internal standard) and their mass spectra contained peaks which were due to noise. This procedure is described below.

5.13.1 Structural Analysis Procedure

The first step in structure determination was to identify the molecular ion (aromatic compound generally have high abundance molecular ions). The next step was to determine how many TMS ethers were formed with free hydroxyl or carboxyl groups present in the compound (loss of 1, 2, and 3 $Si(CH_3)_3$ groups gives characteristic peaks in the mass spectrum at 73, 147, and sometimes 221, respectively, indicating the degree of derivatization and the minimum number of oxygens) from the mass spectrum. It was assumed that the compounds were lignin-derived based on their absence in the controls (which were carefully planned to eliminate products which were not lignin-derived products released by peroxidase activity) and a separately run sample of the internal standard, and therefore could only contain C, H, and O atoms, so the molecular ion had to be an even number. Note that the addition of *n* TMS ethers (MW 73) to the compound does not change the fact that the compound must be even molecular weight, since a hydrogen atom is lost for each TMS ether formed. Any peaks with clearly odd molecular weight molecular ions were discarded. It should be noted here that no TMS-derivatized compounds were seen which did not have a clear molecular ion, but had a clear M^+-15 peak, corresponding to the loss of a methyl group from a TMS ether (this type of spectrum would appear to indicate an odd molecular weight). It was then assumed that the lignin-derived products would retain their ring structure, whether in the aromatic or quinone forms. Next, possible molecular formulas were determined by choosing a number of carbons (6 or higher) and oxygens (1 to 10 for derivatized molecular weights 400 and below, 1 to 15 if higher) and calculating the number of hydrogens necessary to complete the molecular weight. Any molecular formulas with less than 1 hydrogen or $2n + 2$ (where n is the number of carbons) or more hydrogens

(completely saturated hydrocarbons have 2n + 2 hydrogens) were discarded. Any molecular formula which did not contain at least as many oxygens as the number of TMS groups was discarded. The number of rings plus double bonds (hereafter referred to as "r+db") (McLafferty, 1973) were then calculated as half of the difference between the number of hydrogen atoms in a completely saturated hydrocarbon (2n + 2) and the number of hydrogens in the molecular formula (ie. for benzene, C_6H_6, r+db is (2 × 6 + 2 - 6) ÷ 2 = 4 r+db, or 1 ring and 3 double bonds). Any possibilities with less than 4 r+db (could not be aromatic or quinone structures) were discarded. Next, the degree of saturation and number of oxygens were examined. Any formula which did not have at least 2 oxygens per C_9 unit were discarded (an inspection of Figure 1.1 will validate this), and any formula which had significantly fewer hydrogens than the number of carbons was discarded (eg. $C_{17}H_4O_6$, which is typical of highly unsaturated naphtha-based structures, but not lignin-derived compounds). The remaining formulas (usually 2 to 4 per molecular weight possibility) were considered to be viable possibilities and structures were considered using the molecular formula and number of r+db, and assuming that the base unit for any of the compounds would be a six membered ring with 1 to 3 carbon-carbon double bonds and with at least 2 substitutions to the ring (no lignin-derived monomer should have any less; see Figure 1.1). If the number of carbons was higher than 10 and the molecular weight was such that it was clear from the number of r+db that the compound contained only a single ring, carbons were generally added to the aliphatic side chain (up to 3), and then to the hydroxyl at position 4 of the ring (ie. occurring via a β-O-4 intermonomer bond), and finally, through an ether linkage to the β-carbon of the propyl side chain (ie. occurring via an additional β-O-4 or β-1 linked intermonomer bond). Any formulas for which these constraints were not possible were discarded. Any structures which, in general, did not conform to the great majority of these constraints were discarded. The structures were then compared with the mass spectra obtained for that peak from the sample analysis. Any structures which contained

groups which could not possibly be accounted for by mass losses in the mass spectrum were discarded, unless the noise level in the mass spectrum was high enough to mask low level ion fragments; this yielded the final set of structural possibilities. The results of these analyses are presented in this section, starting with the LIP Only enzyme case. The procedure will be described in detail only for the first unknown compound; only the results of the procedure will presented for later spectra. Note that in the following sections, since there were four extracts analyzed per reactor run (ie. BC and each control except for the L^- controls, in which there were only 2), each extract will be dealt with separately. The extracts will be referred to with shorthand notation to save space, as follows: (1.) Chloroform extract of liquid phase, L-C; (2.) Ethyl acetate extract of liquid phase, L-EA; (3.) Chloroform extract of solid, S-C; and (4.) Ethyl acetate extract of solid phase, S-EA. Finally, note that when concentration estimates are given, they are estimates of the concentrations in the unconcentrated extracts. Since the initial volumes of the extracts before concentration ranged from about 1500-1900 μL, concentration to dryness and the addition of 25 μL of BSTFA would make the final (concentrated; value measured by integration of the TIC) values of concentration from about 56 to 76 times higher than in the unconcentrated extracts. The estimated concentrations are given for the unconcentrated extracts since this allows comparison of concentrations between different extracts from a single sample, and also between extracts from other reactor runs.

5.13.2 LIP Only Reactor Runs

As an example of the GC output obtained for the LIP Only BC and control samples, the TIC for the LIP Only S-EA extract is shown in Figure 5.54; the L-C or L-EA chromatograms are not shown because the large amount of VA present (about 3225 ppm from addition to the reactor, while this method accurately detects 1-70 ppm) causes the y-scale (abundance) to be so large that no other peaks are seen in the complete TIC. Close to 200 clear peaks are present in this chromatogram, although some are not clear

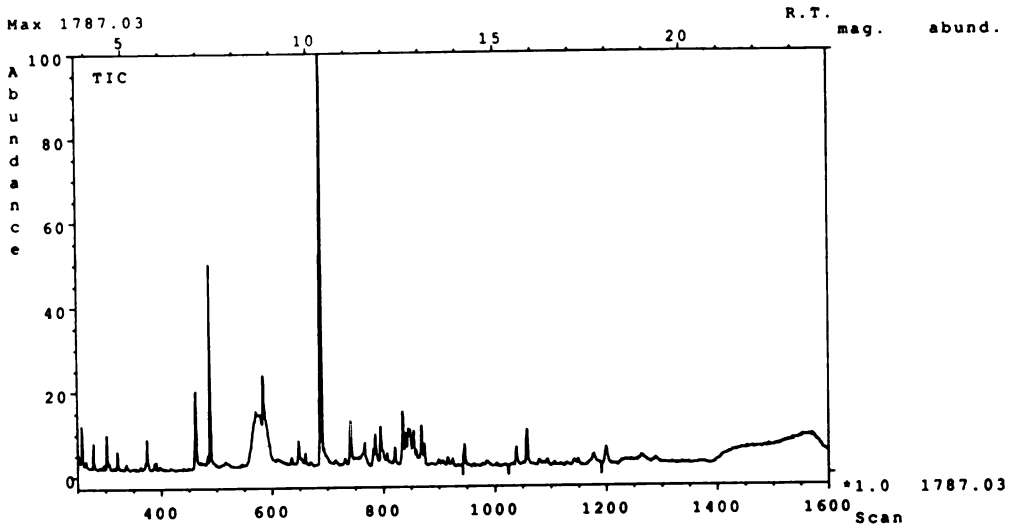

Figure 5.54: Total Ion Chromatogram (TIC) for the ethyl acetate extract of the LIP Alone Base Case solid phase over the scan range 250-1600 (3'44" to 23'58").

even here because of the scale. The peak at about scan 495 (7'49") is the internal standard, while the peaks at scans 595 (8'53") and 695 (10'24") were identified using authentic standards (both from Aldrich) as veratraldehyde and veratryl alcohol; their spectra are presented in Figures 5.55a and 5.55b, respectively. Syringaldehyde (scan 795, 11'54"), vanillic acid (scan 857, 12'50"), and syringic acid (scan 953, 14'16") were identified in all samples (controls included) with the exception of the L⁻ control extracts, indicating that the compounds were present in the lignin itself as extractives, although at very low concentrations (at or below 0.1 ppm in the unconcentrated extracts) for all except syringaldehyde, which was as high as 0.25 ppm in some control samples (unconcentrated extracts); they were also identified by authentic standards (all from Aldrich), and their spectra are presented in Figures 5.56a-c, respectively. Syringaldehyde was present in much higher concentrations in the control extracts than in the BC extracts; this point will be dealt with in the MNP Only section below. Finally, 3,5-dimethoxyhydroquinone (scan 786, 11'46"; correctly named 2,6-dimethoxy-hydroquinone, but referred to here as 3,5- to illustrate its relationship to the syringyl-structure) and 3-methoxyhydroquinone (scan 673, 10'04"; correctly, 2-methoxy-hydroquinone, use of 3- refers to guaiacyl- structure) were also identified in the mixtures, but comparison with published spectra for these compounds (Wariishi *et al.*, 1989a; Valli *et al.*, 1992b). 2,6-dimethoxyhydroquinone was present in all samples (although much more was present in the BC extracts, while 2-methoxyhydroquinone was present only in the ethyl acetate extract of the liquid phase from the BC. Their spectra are presented in Figures 5.57a and 5.57b.

The peaks for all extracts for the LIP Alone BC which were not eliminated by comparison with the chromatograms of the controls and the standard alone are presented, with concentration estimates (concentrations in the unconcentrated extracts), in Table 5.13. None of these peaks (or their spectra) were present in any extract from any of the controls, indicating their probable origin as lignin-derived. Note that no unique peaks

(a.)

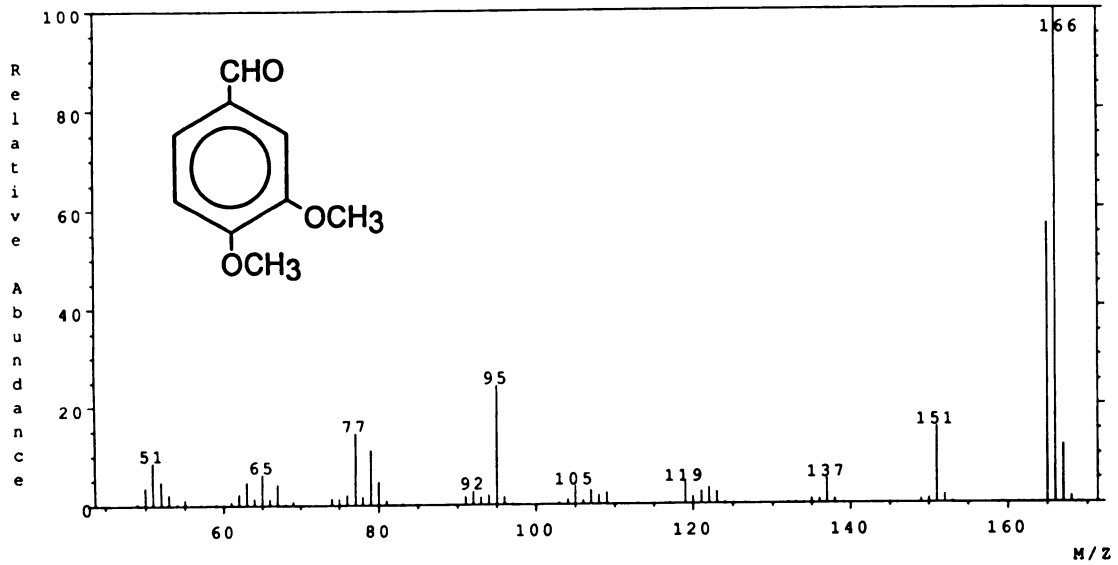

(b.)

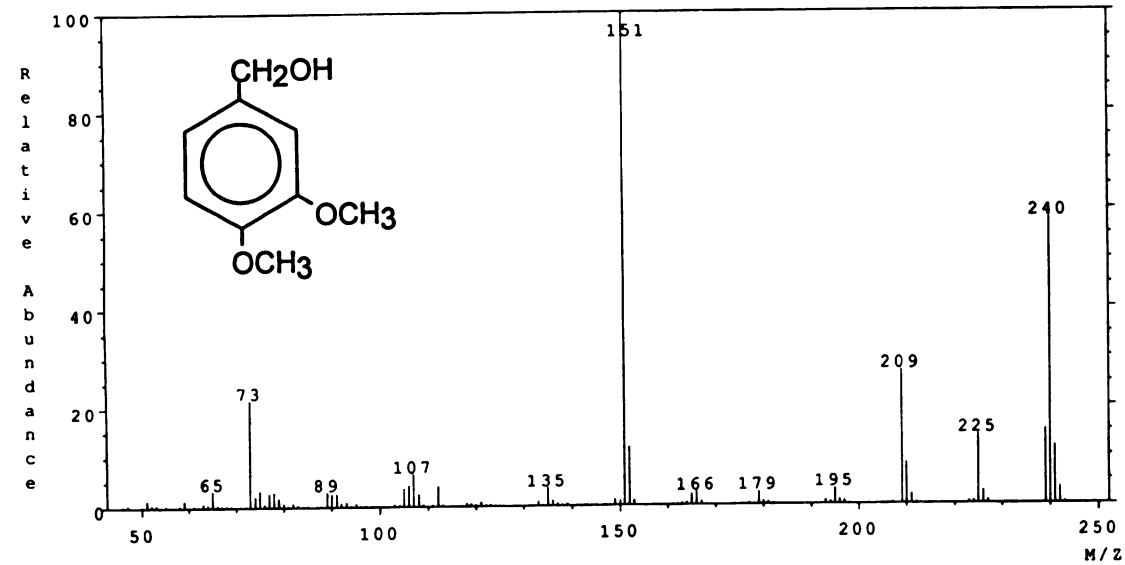

Figure 5.55: Electron-impact mass spectra of: **(a.)** Veratraldehyde; and **(b.)** Veratryl Alcohol (mono-TMS derivative). The spectra were obtained from scans 604 (9'02") and 697 (10'26"), respectively, after elution from the DB-1 GC column. The background subtractions were from scans 591 and 689.

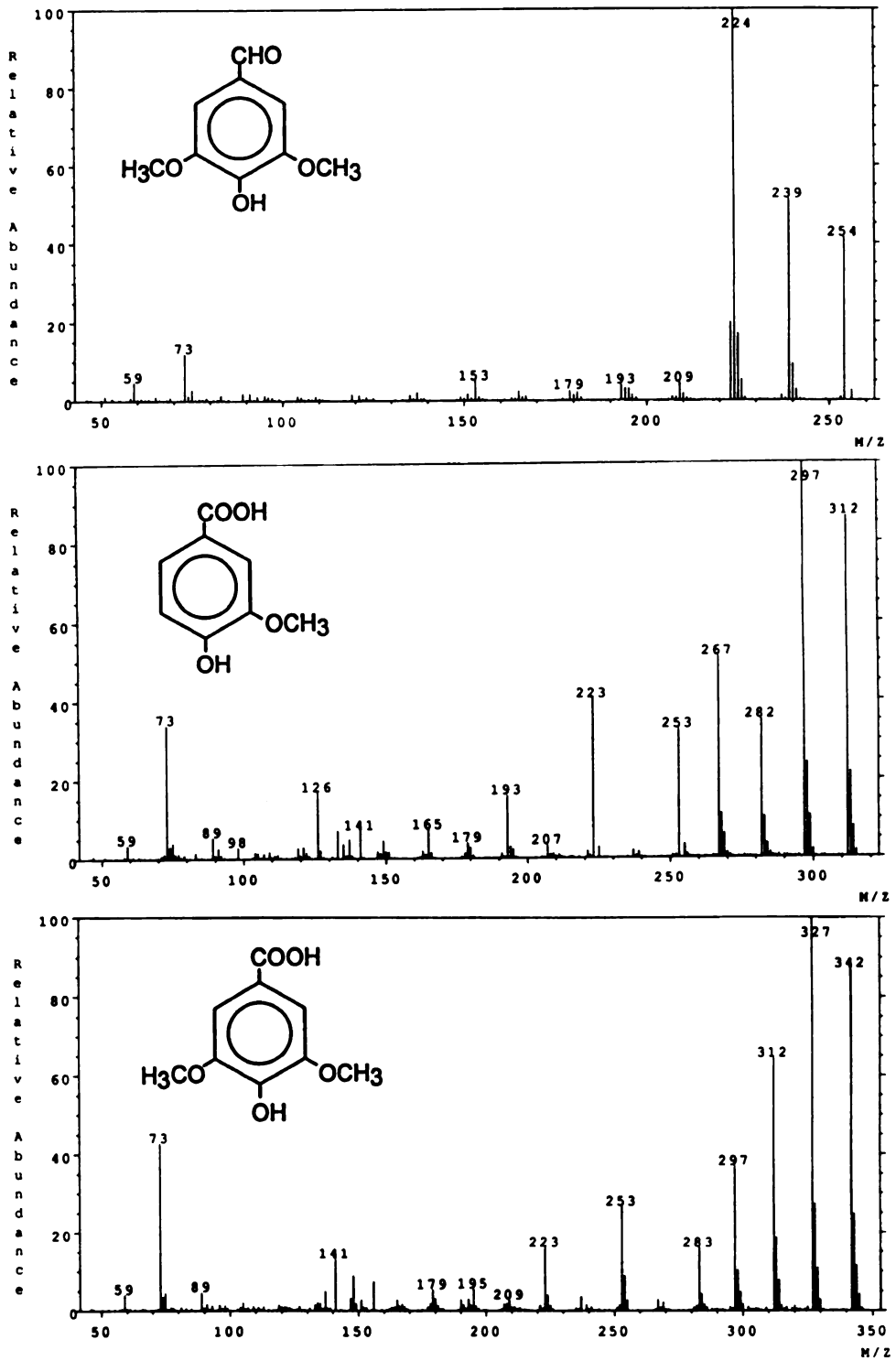

Figure 5.56: Electron-impact mass spectra of: **(a.)** Syringaldehyde (mono-TMS derivative); **(b.)** Vanillic Acid (di-TMS derivative); and **(c.)** Syringic Acid (di-TMS derivative). The spectra were obtained from scans 795 (11'54"), 857 (12'50"), and 953 (14'16"), respectively, after elution from the DB-1 GC column. The background subtractions were the averages of scans 790 and 799, 852 and 860, and 947 and 956, respectively.

(a.)

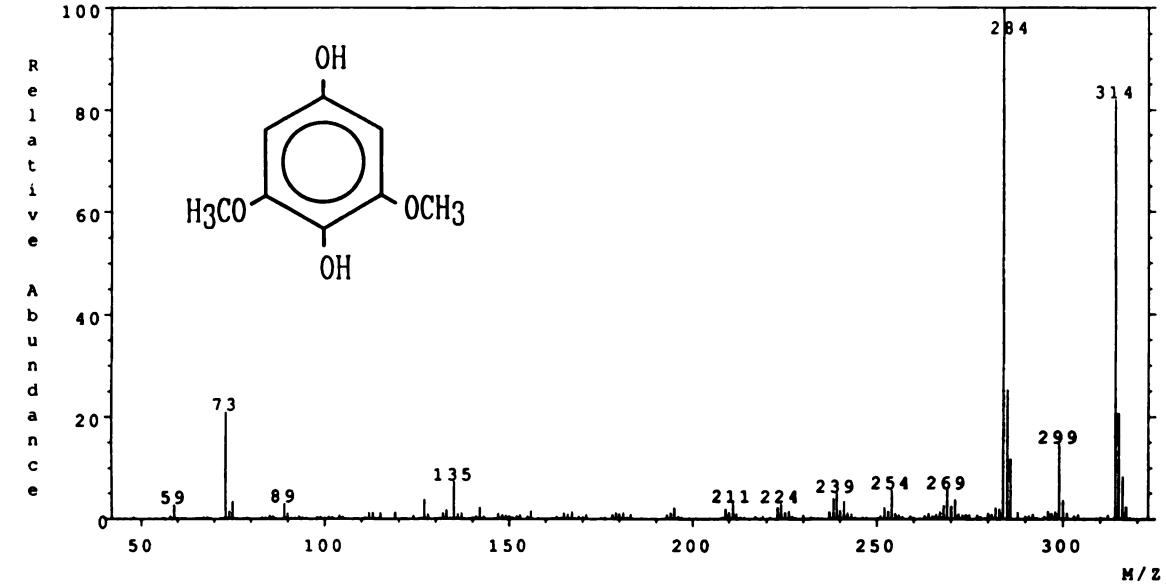

(b.)

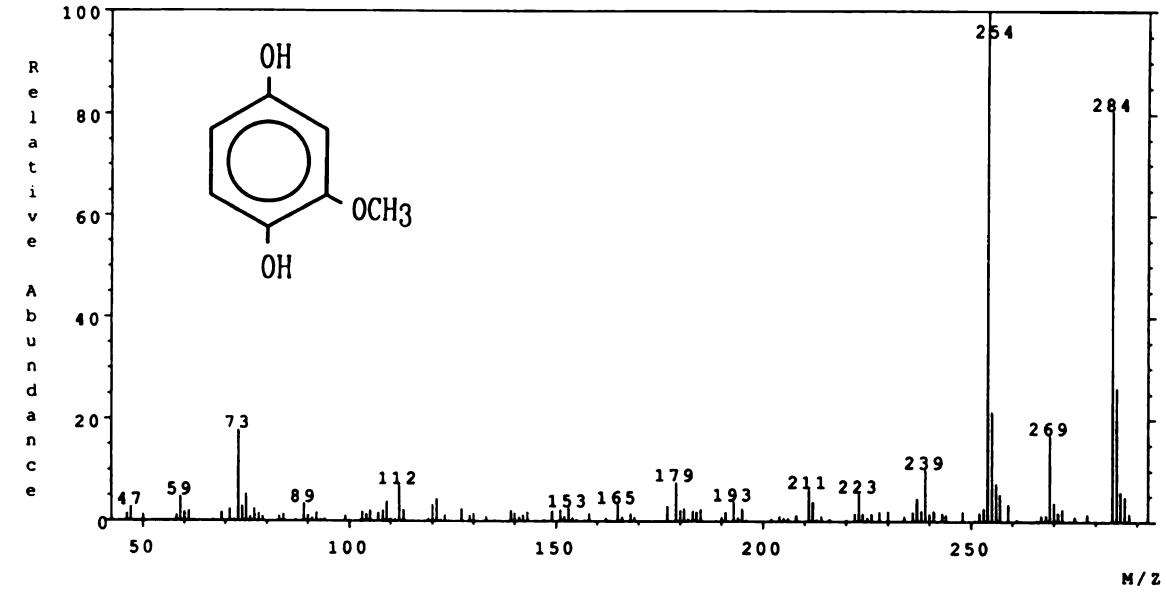

Figure 5.57: Electron-impact mass spectra of: (**a.**) 2,6-dimethoxyhydroquinone (di-TMS derivative; matched with that of Wariishi *et al.* (1989a)); and (**b.**) 2-methoxy-hydroquinone (di-TMS derivative; matched with that of Valli *et al.* (1992b)). The spectra were obtained from scans 860 (12'52") and 744 (11'08"), respectively, after elution from the DB5MS GC column. The background subtraction for (**a.**) was from scan 858, and for (**b.**) was from the average of scans 742 and 746.

Table 5.13: Peaks in the LIP Alone BC extracts selected for structural analysis by comparing the Total Ion Chromatograms of the BC extracts with the corresponding extracts of its controls. The identity of the compound is listed if known; if not, the possible molecular formulas (based on the molecular weight determined from the mass spectrum) are listed.

Extract	Scan No.	RT+	Est. Conc. (ng/μL)	Derivatized M.W. (g/mole)	No. TMS Groups	Identity if known
L-C	1069	16'00"	0.0256	370?	2?	Unknown
L-EA	544	8'08"	0.1656	182	0	$C_9H_{10}O_4$ or $C_{10}H_{14}O_3$
L-EA	600	8'59"	0.8820	226	1	$C_7H_6O_4$ or $C_8H_{10}O_3$
L-EA	673	10'04"	0.1209	284	2	2-methoxyhydroquinone*
L-EA	745	11'10"	0.0925	282	2	p-hydroxybenzoic acid**
L-EA	752	11'15"	0.9226	256	0	$C_9H_{12}O_4$

+ Retention time with DB-1 GC column and 3.75 min solvent hold.

* Identified by comparison with spectrum of Valli et al. (1992b).

** Identified by comparison with spectrum in NIST database.

were found in the S-C and S-EA extracts; one unique peak was identified in the L-C extract, and four unique peaks were identified in the L-EA extract (2-methoxy-hydroquinone was not unique to the BC, but was also present in all of the controls).

5.13.2.1 Peaks In The LIP Alone BC L-C Extract

The mass spectrum for the lone unique peak identified in the L-C extract of the LIP Alone BC at scan 1069 (16'00") is presented in Figure 5.58a, and the TIC and mass chromatograms for fragments of masses 370, 327, 239, and 151 over the scan range 1040-1080 are presented in Figure 5.58b (the mass chromatogram indicates the abundances in the TIC of fragments of the given masses -- a peak in the mass chromatogram of a fragment that corresponds with a peak in the TIC indicates that that mass is truly part of the spectrum). The maximum abundances for each mass in the mass chromatogram are listed to the right of each mass plot. While this spectrum is clearly too noisy to identify the compound, the high abundance of mass 151 in the spectrum suggests a lignin-derived origin (Faix, 1990b). The compound may be molecular weight 370, but it clearly contains the mass 151 fragment, as evidenced by the mass chromatogram.

5.13.2.2 Peaks In The LIP Alone BC L-EA Extract

a. Scan 544

The mass spectrum for the peak in the L-EA extract at scan 544 (8'08") is presented in Figure 5.59a; its mass chromatogram and the TIC is presented in Figure 5.59b over the scan range 500-600. This spectrum is much cleaner than the previous spectrum for the L-C peak, owing to its higher concentration; this is the peak for which the structure analysis method will be demonstrated.

This compound does not contain any free hydroxyls or carboxylic acid groups, as evidenced by the absence of a peak of mass 73 (if the compound is derivatized at all, it should have a peak of substantial abundance at mass 73). At first inspection, it does not even seem to be lignin-derived, since it contains only an very small peak at mass

(a.)

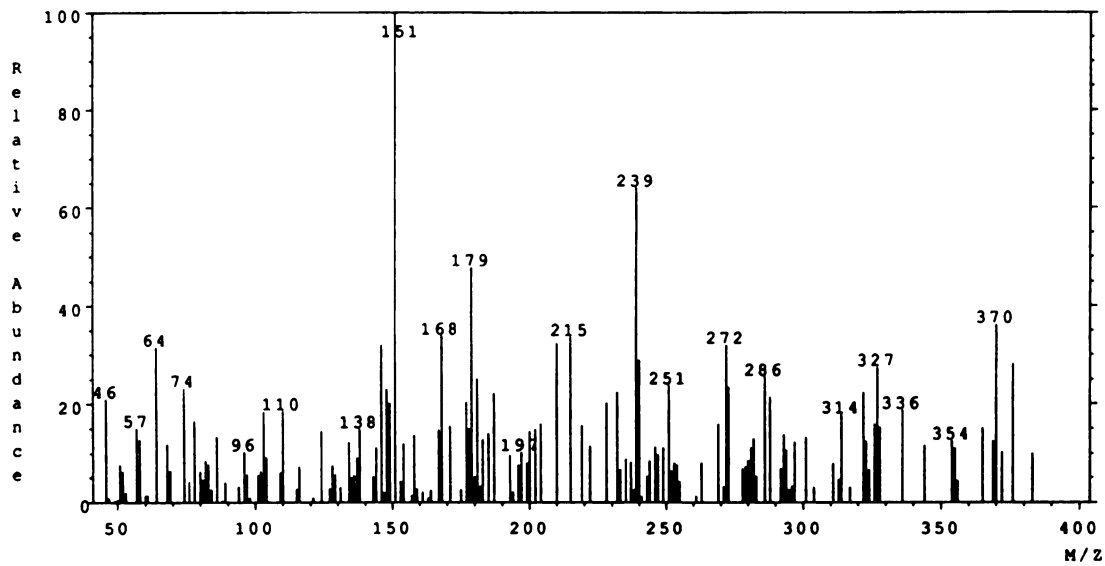

(b.)

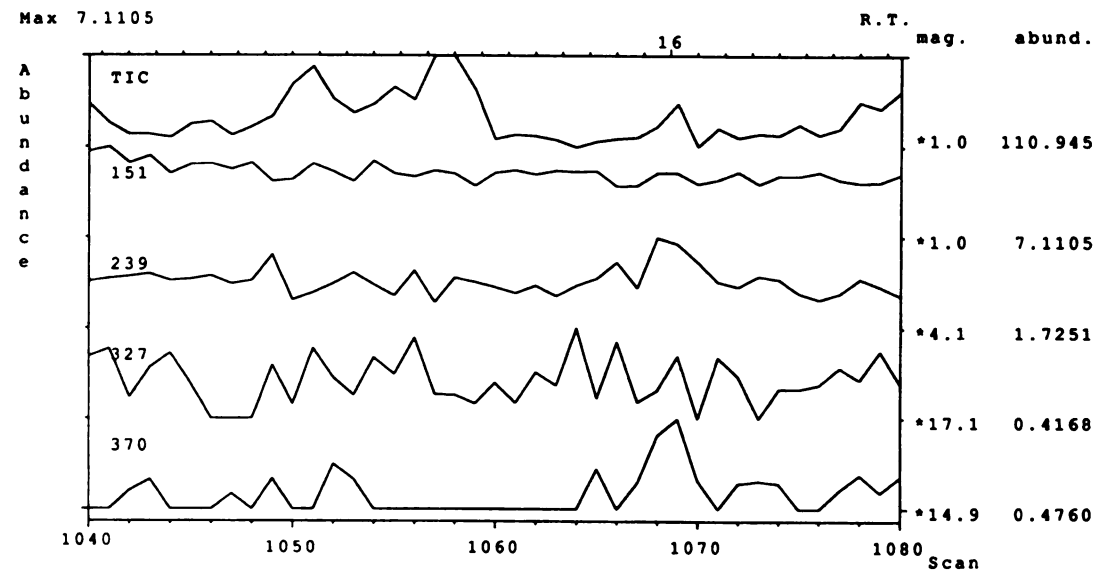

Figure 5.58: **(a.)** Electron-impact mass spectrum obtained from scan 1069 (background average of scans 1067 and 1070) of the TIC from the LIP Alone BC L-C extract; and **(b.)** TIC and mass chromatograms for ions of mass 151, 239, 327, and 370 over the scan range 1040-1080.

(a.)

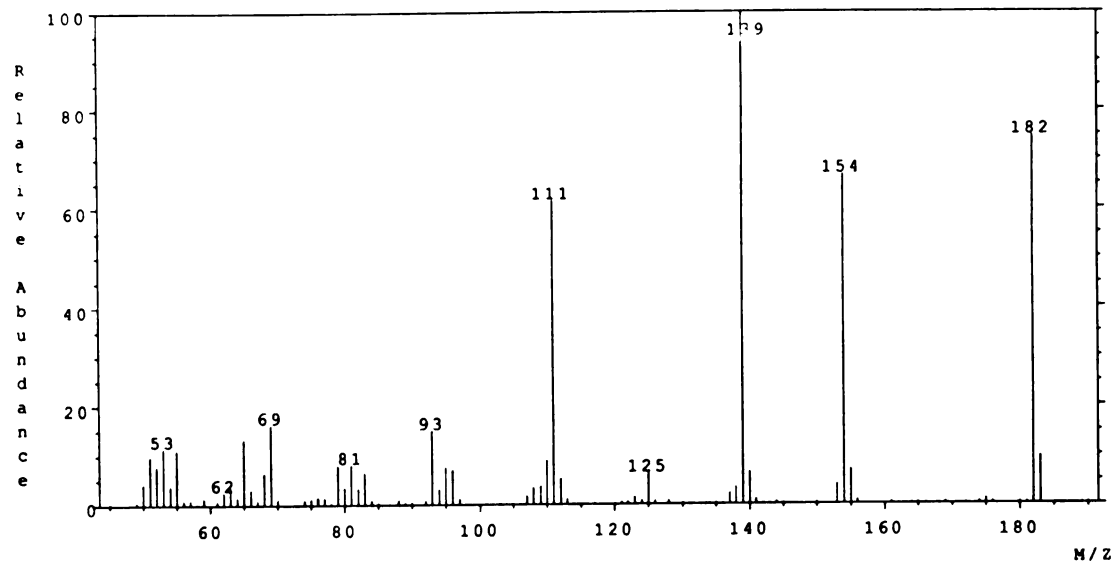

(b.)

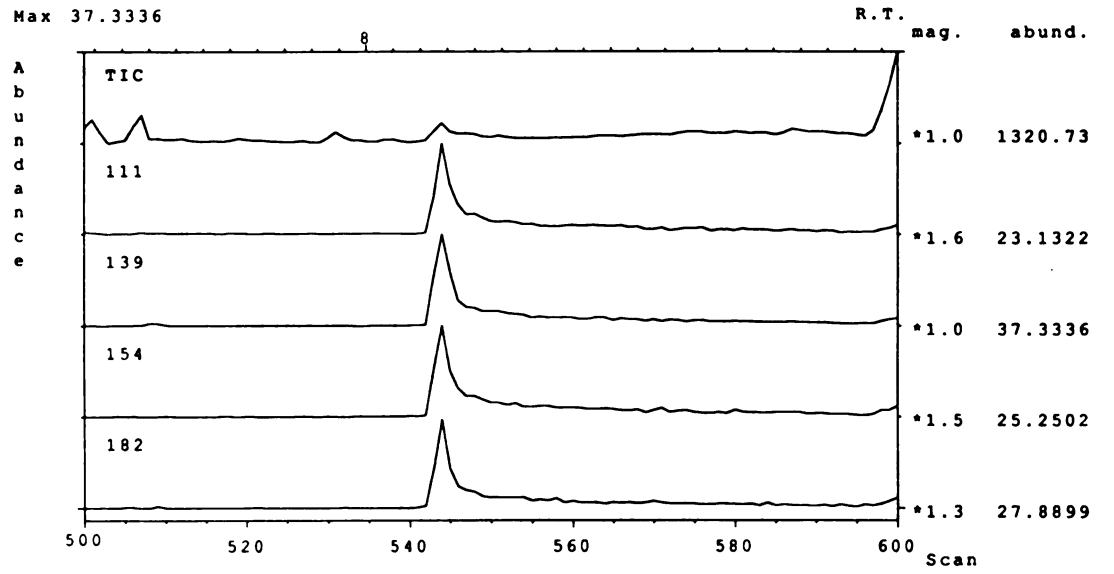

Figure 5.59: **(a.)** Electron-impact mass spectrum obtained from scan 544 (background average of scans 542 and 547) of the TIC from the LIP Alone BC L-EA extract; and **(b.)** TIC and mass chromatograms for ions of mass 111, 139, 154, and 182 over the scan range 500-600.

107. Comparison with the spectrum of underivatized syringaldehyde (Figure 5.60), obtained from the NIST database, shows striking similarities; namely, the peaks at 139, 111, 93, 79, 69, 65, etc. Closer examination of the spectrum of scan 544 indicates a very small (almost unnoticeable) peak at mass 167.

Molecular formulas possible for this compound, which is molecular weight 182 and does not form TMS ethers, are (r+db in braces): $C_7H_2O_6$ {7}, $C_8H_6O_5$ {6}, $C_9H_{10}O_4$ {5}, $C_{10}H_{14}O_3$ {4}, $C_{11}H_{18}O_2$ {3}, $C_{11}H_2O_3$ {11}, $C_{12}H_{22}O$ {2}, $C_{12}H_6O_2$ {10}, and $C_{13}H_{10}O$ {9}. The formulas $C_7H_2O_6$, $C_{11}H_2O_3$, and $C_{12}H_6O_2$ have simply too high a degree of unsaturation to be viable choices as lignin-derived products; thus, they were discarded. The formulas $C_{11}H_{18}O_2$, $C_{12}H_{22}O$ have fewer than 4 r+db and so could not be aromatic or quinone structures, and were thus discarded. The formula $C_{13}H_{10}O$ has too few oxygens to be a lignin-derived product, so it was discarded. Finally, the formula $C_8H_6O_5$, while initially seeming to be valid, is too unsaturated (too many r+db for the number of carbons) given the high number of oxygens and the limitation that it must contain a di- or tri-substituted six-membered aromatic or quinone ring. Thus, $C_8H_6O_5$ was discarded. That left only $C_9H_{10}O_4$ and $C_{10}H_{14}O_3$ for further consideration. The mass spectrum indicated the presence of a carbonyl group (loss of 28, from 182 to 154), a methyl group (15 loss from 154 to 139), or possibly a methoxyl group (31 loss from 154 to 123). The compound has no free hydroxyls and no free carboxylic acid groups. If the compound is aromatic, it is not likely to have an aldehyde at C_α, because completely underivatized aromatic compounds that contain aldehydes at C_α generally have a characteristically high abundance fragment at $M^+ - 1$, corresponding to loss of the hydrogen atom linked to the carbonyl group of the aldehyde (McLafferty, 1973; for a demonstration of this point, refer to the spectra of veratraldehyde and underivatized syringaldehyde presented in Figures 5.55b and 5.60, respectively), and this compound does not. Thus the carbonyl group indicated in the mass spectrum must either be from an aldehyde somewhere other than C_α of an aromatic ring, from a keto group, or from

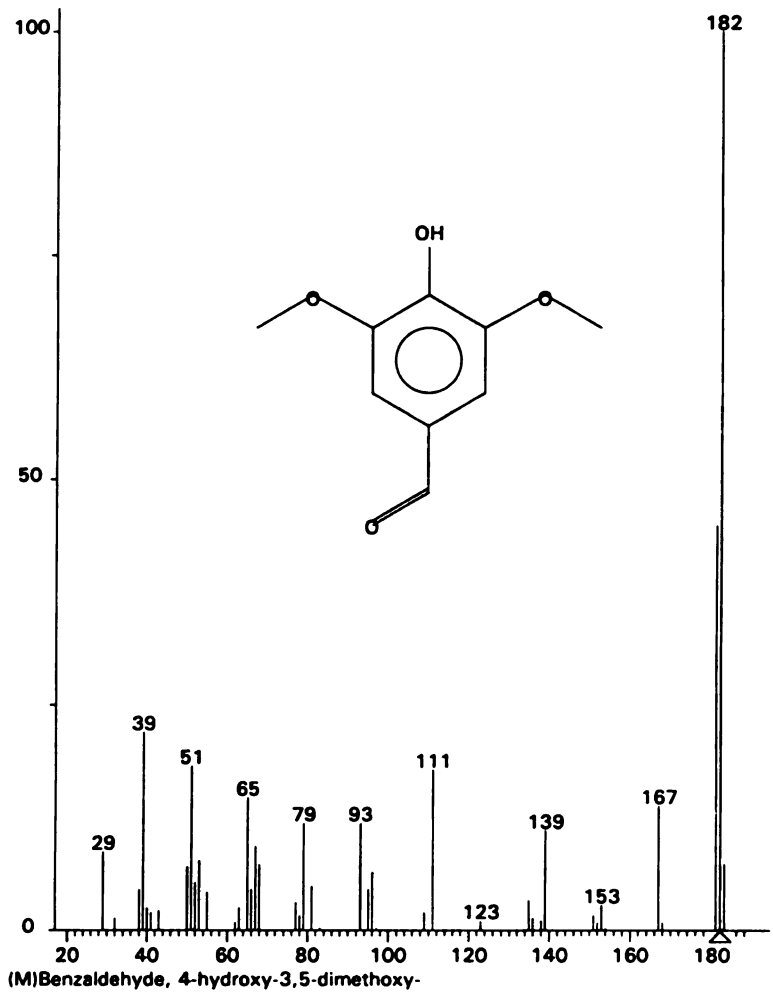

Figure 5.60: Electron-impact mass spectrum of underivatized syringaldehyde obtain from the NIST database (provided for comparison with Figure 5.59a).

an ester group. Possible structures are presented in Figure 5.61 for both molecular formulas; unfortunately, none of these compounds were found to be commercially available, so matching with an authentic standard is not possible unless the compounds are synthesized.

Structure I seems a likely candidate, since it resembles a syringyl unit and the lack of aromaticity in the ring could cause the aldehyde fragment loss of 1 mass unit not to appear; it might also explain the similarity of the mass spectrum to that of underivatized syringaldehyde (see Figure 5.60). Structure II is not likely, due to the partial unsaturation of the ring while containing two oxo- groups on the ring; in addition, it is not likely that oxidative release of a compound containing an unoxidized methyl ketone at C_α would occur from lignin through the activity of LIP (Hammel *et al.*, 1985). The stability of structure III is questionable; it is most likely not stable since the ring is saturated. Structures IV and V contain a methylene-dioxy ring, possibly formed by condensation during the lignin isolation step in the flow reactor (it is well established that these structures form in lignin at high temperatures (Sarkanen and Ludwig, 1971)); it is possible that these compounds would be stable due to the stabilizing effect of the additional ring, but it is probably more likely that more stable resonance forms of these compounds would be formed by elimination of the aliphatic side chains to form quinone structures. Structure VI is not likely because it contains a completely unoxidized side chain; this is inconsistent with the known mechanism of C_α-C_β cleavage of lignin model dimers by LIP (Hammel *et al.*, 1985), which leaves both carbon atoms at the cleavage site oxidized. Structures VII and VIII are unlikely, since formation of quinone-like structures with both C-1 and C-4 saturated is likely to be energetically unfavorable if the starting compound is aromatic (Dr. Douglas Gage, Personal Communication). In addition, the unoxidized methyl ketone at C_α is unlikely to be a product of oxidative degradation (see comments for structure II). Finally, structure IX is unlikely not only because of the unoxidized ethyl ether, but also because of the lack of an aliphatic side

$C_9H_{10}O_4$

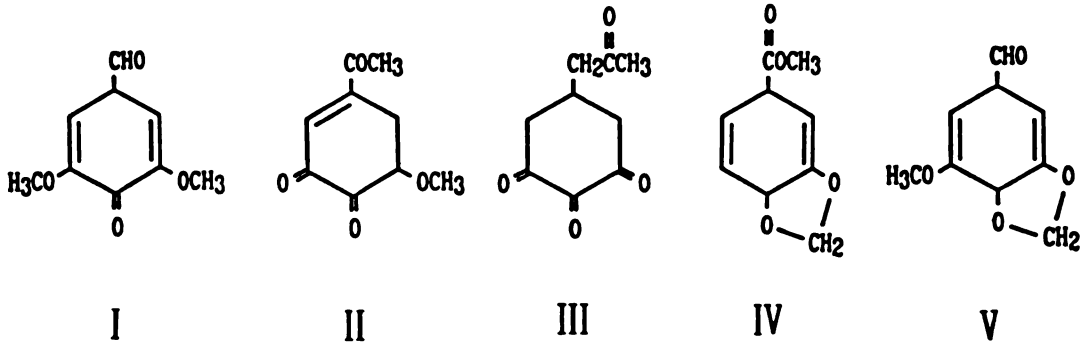

I II III IV V

$C_{10}H_{14}O_3$

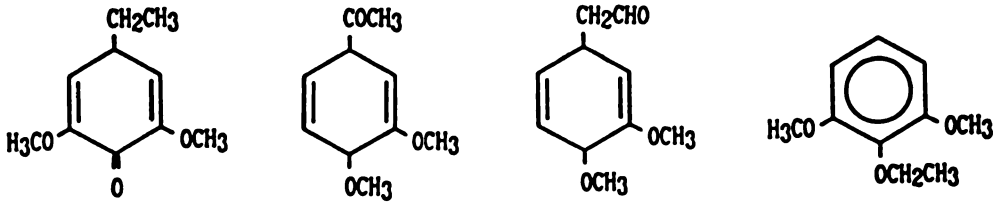

VI VII VIII IX

Figure 5.61: Proposed lignin-derived structures for the compound with mass spectrum shown in Figure 5.59a.

chain (or a hydroxyl group where it used to be; this is not possible because the compound does not form a TMS ether). Thus, structure I is the most likely candidate of the structures proposed. For the remainder of the peaks analyzed below, please refer to the preceding analysis for the general methodology in the structure elucidation procedure.

b. Scan 600

The mass spectrum of scan 600 (8'59") in the L-EA extract is presented in Figure 5.62a and the TIC and mass chromatograms for fragments 226, 211, 183, and 153 are presented in Figure 5.62b. The spectrum contains the lignin peaks 107, 151, 167, and 181, indicating the probability that it is a syringyl-type structure; it is present in a relatively high concentration (see Table 5.13). The compound contains one TMS-derivatizable group, and probably contains two methoxyl groups due to the presence of 181, 167, and 151 mass fragments (181 and 151 are for syringyl-type structures, 167 is for guaiacyl-type). Possible molecular formulas {r+db} are $C_7H_6O_4$ {5} and $C_8H_{10}O_3$ {4}. Proposed structures are presented in Figure 5.63. Structure X, 3-hydroxy-5-methoxy-benzoquinone, is quite likely given the confirmed presence of 3,5-dimethoxy-hydroquinone since it could be formed by demethoxylation and oxidation to the quinone by LIP (both known LIP catalyzed reactions (Tien, 1987; Boominathan and Reddy, 1992)). Structure XII is also quite likely and could arise from a guaiacyl unit, and is probably more likely than structure X given the presence of the mass fragments 151, 167, and 181, which include C_α, in the mass spectrum. Of these compounds, only structure XI, 2,6-dimethoxyphenol (and positional isomers) are available commercially (Aldrich); this structure, however, is the least likely of the three (see discussion above for compound IX). Structure XI, 2,6-dimethoxyphenol, and the isomers 3,4-dimethoxyphenol and 3,5-dimethoxyphenol were purchased from Aldrich and GC/MS of the samples was done with the DB-1 GC column. The 2,6-isomer eluted in scan 536 (8'01"), the 3,5-isomer eluted in scan 625 (9'21"), and the 3,4-isomer eluted in scan 598

(a.)

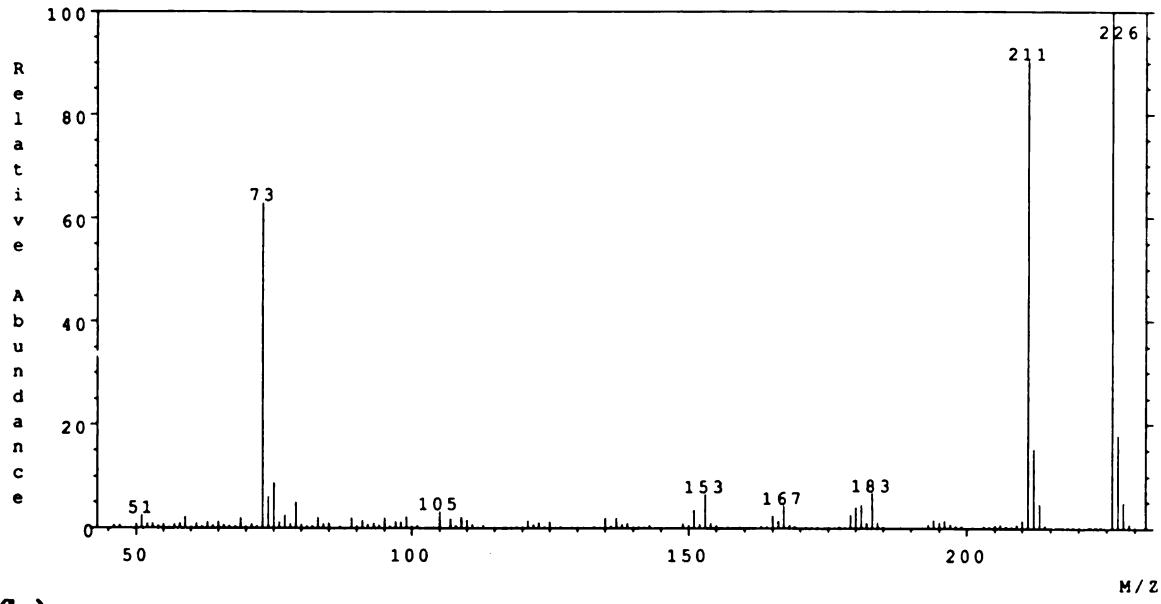

(b.)

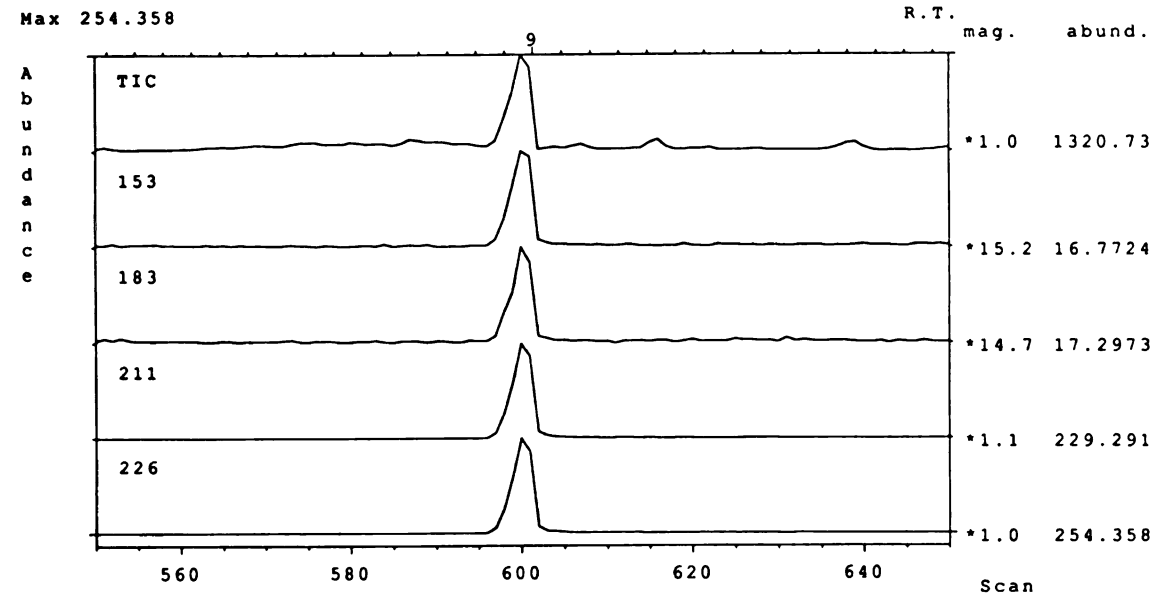

Figure 5.62: **(a.)** Electron-impact mass spectrum obtained from scan 600 (background average of scans 596 and 602) of the TIC from the LIP Alone BC L-EA extract; and **(b.)** TIC and mass chromatograms for ions of mass 153, 183, 211, and 226 over the scan range 550-650.

$C_7H_6O_4$

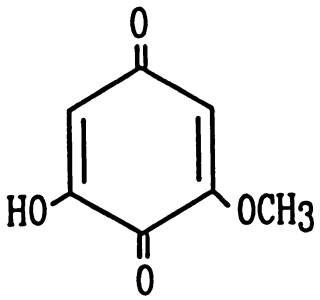

X

Aromatic ring not possible.

$C_8H_{10}O_3$

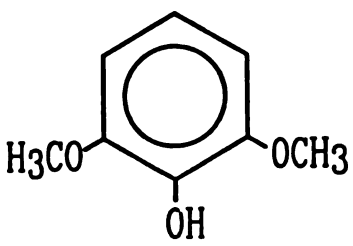

XI

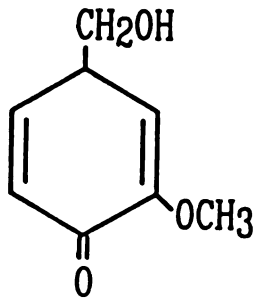

XII

Figure 5.63: Proposed lignin-derived structures for the compound with mass spectrum shown in Figure 5.62.

(8'57"); their mass spectra are shown in Figures F.10 through F.12 (Appendix F), respectively. The mass spectrum shown in Figure F.12 and the retention time of that peak match those of scan 600, so the compound eluting in scan 600 is 3,4-dimethoxyphenol. It is difficult to imagine how a 3,4-methoxy-substituted product could arise from lignin, but veratryl alcohol was found as an extractive in the lignin (see MNP alone case below), and this peak was unique to the BC extracts (not present in the L control extracts. Thus, this 3,4-dimethoxyphenol could not have come from added veratryl alcohol, but must be a product of the methoxylation of a guaiacyl- subunit by LIP (a known LIP reaction; Boominathan and Reddy, 1992).

c. Scan 673

The mass spectrum of scan 673 (10'04") in the L-EA extract was presented previously in Figure 5.57b. This product was identified as 2-methoxyhydroquinone by comparison with a published spectrum (Valli *et al.*, 1992b), and arises from guaiacyl-type structures. Its formation is consistent with published mechanisms of the action of LIP (Boominathan and Reddy, 1992).

d. Scan 745

The mass spectrum of scan 745 (11'10") in the L-EA extract is presented in Figure 5.64a. It was identified as p-hydroxybenzoic acid by comparison with a reference spectrum in the NIST database; the reference spectrum is presented in Figure 5.64b. This compound was purchased (Aldrich) and GC/MS was run using the DB-1 GC column; the authentic standard eluted in scan 744 (11'08"), and its mass spectrum is shown in Figure F.13 (Appendix F). This product is clearly a lignin degradation product, as it has been reported as a product of *in vivo* degradation of spruce wood by *P. chrysosporium* (Chen and Chang, 1982).

e. Scan 752

The mass spectrum of scan 752 (11'10") in the L-EA extract is presented in Figure 5.65a, and the TIC and mass chromatograms for the fragments 256,151, 137, and

(a.)

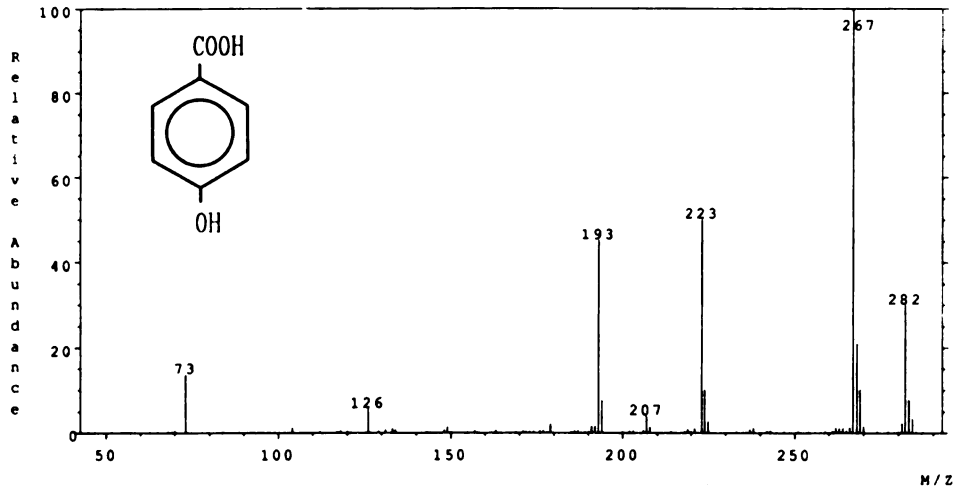

(b.)

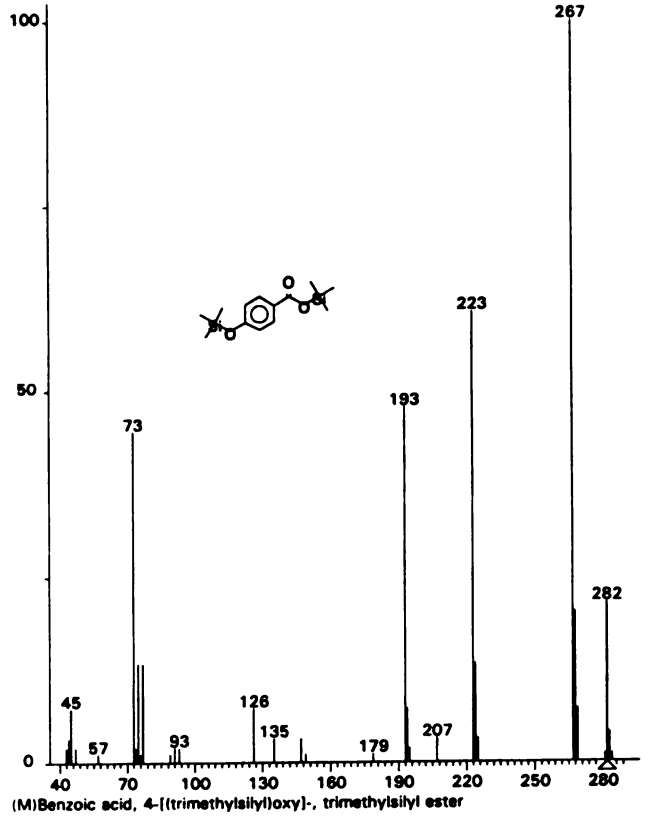

Figure 5.64: (a.) Electron-impact mass spectrum obtained from scan 745 (background average of scans 740 and 748) of the TIC from the LIP Alone BC L-EA extract. This compound was identified as p-hydroxybenzoic acid by comparison the reference spectrum of the authentic compound shown in (b.) (obtained from the NIST database).

(a.)

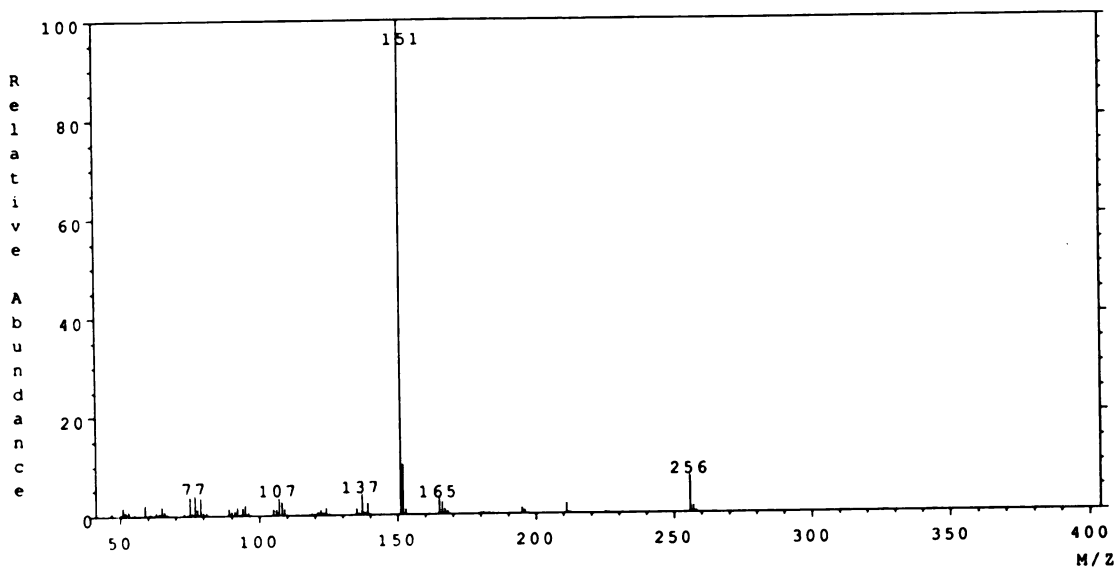

(b.)

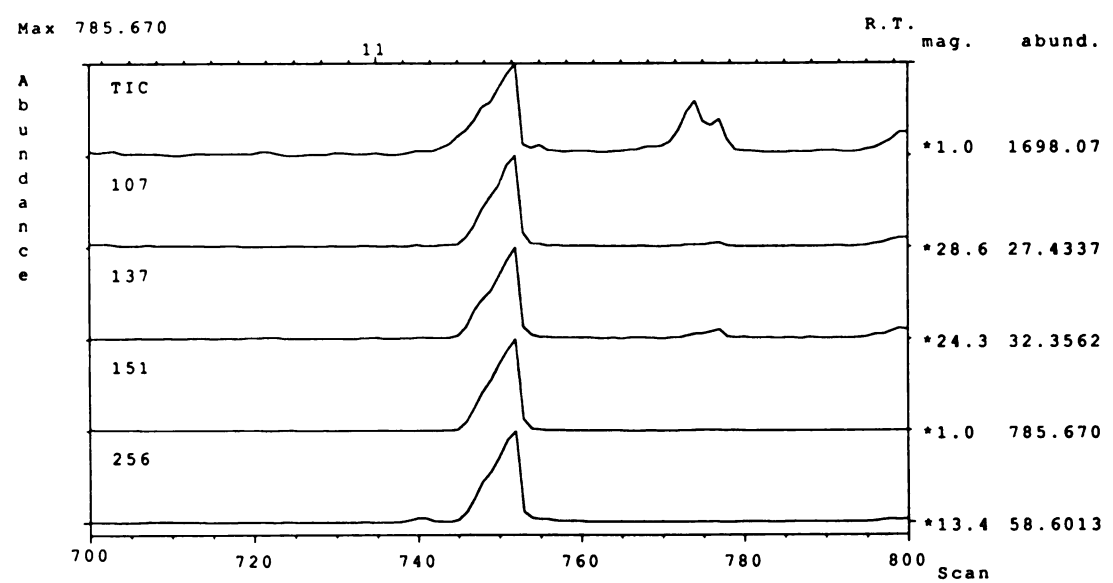

Figure 5.65: **(a.)** Electron-impact mass spectrum obtained from scan 752 (background average of scans 745 and 754) of the TIC from the LIP Alone BC L-EA extract; and **(b.)** TIC and mass chromatograms for ions of mass 107, 137, 151, and 256 over the scan range 700-800.

107 are presented in Figure 5.65b. The compound does not seem to be derivatized (no 73 fragment); however, the loss of 90 mass units from the molecular ion (256) suggests the loss of the group $HOSi(CH_3)_3$, and so the compound probably does contain a TMS ether which is probably attached to an aliphatic side chain (TMS ethers of phenols do not usually lose the phenolic oxygen with the TMS (Dr. Douglas Gage, Personal Communication). This compound is present in substantial amounts (see Table 5.13), so it is possible that it arose from veratryl alcohol; however, it was not present in the L- control extracts, indicating that it is probably lignin derived. The peaks in the spectrum at 107 (aliphatic substituted phenol), 137 (aliphatic substituted guaiacyl) and 151 (carbonyl at C_α) (Faix *et al.*, 1990b) also indicate that it probably lignin-derived. Possible molecular formulas (1 derivatizable group) are $C_8H_8O_5$ {5} and $C_9H_{12}O_4$ {4}. $C_8H_8O_5$ has too many oxygens to allow an aromatic or quinone structure, leaving $C_9H_{12}O_4$. An aromatic structure is not possible for this last formula (too many r+db for the number of oxygens). The possible structures are presented in Figure 5.66. Structure XIII is possible, but it the energetics of formation of this compound are questionable (see discussion of structures VII and VIII above. Structure XIV is possible, and appears to be the best choice of the proposed structures, since it is possible that a rearrangement of XIV could occur in the instrument to account for the peak at 151 (carbonyl at C_α). None of these structures are commercially available.

5.13.3 LIP + MNP Reactor Runs

As an example of the GC output obtained for the LIP + MNP BC and control samples, the TIC for the LIP + MNP BC L-EA extract is shown in Figure 5.67. The peak at about scan 490 (7'44") is the internal standard, the peaks at scans 595 (8'53") and 695 (10'23") are veratraldehyde and veratryl alcohol; syringaldehyde is at scan 789 (11'49"), vanillic acid is at scan 859, 12'59"), syringic acid is at scan 948 (14'11"), and 2,6-dimethoxyhydroquinone is at scan 786 (11'46"); 2-methoxyhydroquinone was not found in any of the samples. See above for spectra and identification methods for these

$C_9H_{12}O_4$

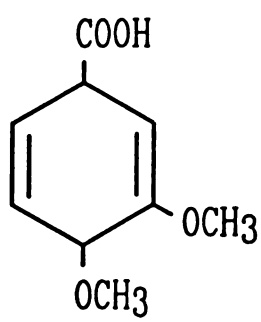

XIII

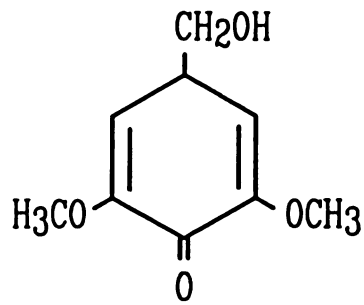

XIV

Figure 5.66: Proposed lignin-derived structures for the compound with mass spectrum shown in Figure 5.65.

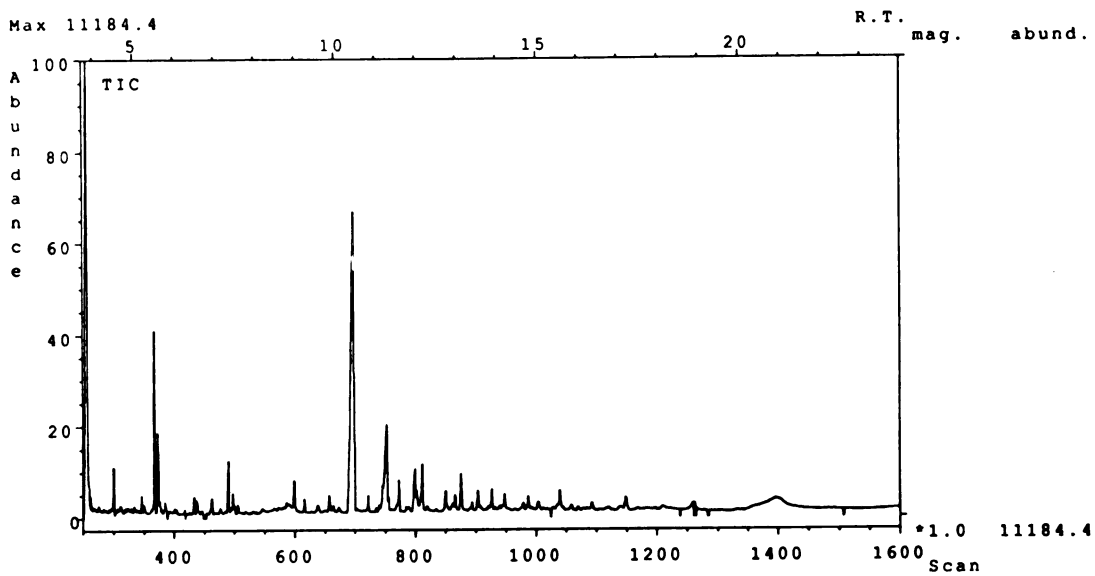

Figure 5.67: Total Ion Chromatogram (TIC) for the LIP + MNP BC L-EA extract over the scan range 250-1600 (3'44" to 23'58").

compounds.

The peaks for all extracts for the LIP + MNP BC which were not eliminated by comparison with the chromatograms of the controls and the standard alone are presented, with concentration estimates (concentrations in unconcentrated extracts), in Table 5.14. In the L-EA BC extract, scan 426 was unique; scan 987 appeared in the following cases: BC: 0.1933 ng/μL; L^- control, was not present; R^- control, 0.0067 ng/μL; E^- control, 0.0249 ng/μL; AE control, 0.0405 ng/μL; and ER^- control, 0.0361 ng/μL. In the S-C BC extract, scan 620 appeared at 0.0532 ng/μL and in the R^- control at 0.0065 ng/μL, but was absent in all other extracts; scan 834 appeared in the following cases: BC: 0.0450 ng/μL; no L^- control since this is a solid extract; R^- control, was not present; E^- control, 0.0054 ng/μL; AE control, 0.0112 ng/μL; and ER^- control, 0.0080 ng/μL. Finally, in the S-EA extract, both peaks were unique. The implications of the presence of the compounds in the controls at substantially lower concentrations will be discussed with each compound.

5.13.3.1 Peaks In The LIP + MNP BC L-EA Extract

a. Scan 426

The mass spectrum for the peak in the L-EA extract at scan 426 (6'22") is presented in Figure 5.68. This compound occurs in fairly low concentration, and its spectrum is not very clean; nonetheless, the molecular ion is evident at mass 280. The compound is derivatized, but it is not clear whether once or twice. With one and two derivatizable groups, the possible molecular formulas are {r+db}: $C_{10}H_8O_5$ {7}, $C_{11}H_{12}O_4$ {6}, and $C_{12}H_{16}O_3$ {5} (one TMS), and $C_8H_8O_2$ {5} (two TMS). The possible structures for both cases are presented in Figure 5.69. It is quite likely that structure XV could be released from lignin that has been thermally treated (see comments for structures IV and V above) given the methylene-dioxy ring and the resemblance to sinapic acid. Structures XVI and XVII are also quite possible, as products of the release of oxidized coniferyl alcohol and its acid form. Structure XVIII is sinapyl aldehyde, and again, is a likely

Table 5.14: Peaks in the LIP + MNP BC extracts selected for structural analysis by comparing the Total Ion Chromatograms of the BC extracts with the corresponding extracts of its controls. The identity of the compound is listed if known; if not, the possible molecular formulas (based on the molecular weight determined from the mass spectrum) are listed.

Extract	Scan No.	RT+	Est. Conc. (ng/μL)	Derivatized M.W. (g/mole)	No. TMS Groups	Identity if known
L-EA	426	6'22"	0.0235	280	1	$C_{10}H_8O_5$, $C_{11}H_{12}O_4$, or $C_{12}H_{16}O_3$
					2	$C_8H_8O_2$
L-EA	987	14'47"	0.1933	400	1	$C_{17}H_{12}O_7$, $C_{18}H_{16}O_6$, $C_{19}H_{20}O_5$, or $C_{20}H_{24}O_4$
					2	$C_{11}H_{12}O_7$, $C_{12}H_{16}O_6$, or $C_{13}H_{20}O_5$
					3	$C_7H_4O_6$, $C_8H_8O_5$, or $C_9H_{12}O_4$
S-C	620	9'17"	0.0532	308	1	$C_{12}H_{12}O_5$, $C_{13}H_{16}O_4$, or $C_{14}H_{20}O_3$
					2	$C_9H_8O_3$ or $C_{10}H_{12}O_2$
S-C	834	12'29"	0.0450	372	2	$C_{11}H_{16}O_5$ or $C_{14}H_{12}O_5$
					3	$C_6H_4O_5$ or $C_7H_8O_4$
S-EA	809	12'07"	0.0252	356	2	$C_{10}H_{12}O_5$ or $C_{11}H_{16}O_4$
					3	$C_7H_8O_3$
S-EA*	986	14'46"	0.0551	400	1	$C_{17}H_{12}O_7$, $C_{18}H_{16}O_6$, $C_{19}H_{20}O_5$, or $C_{20}H_{24}O_4$
					2	$C_{11}H_{12}O_7$, $C_{12}H_{16}O_6$, or $C_{13}H_{20}O_5$
					3	$C_7H_4O_6$, $C_8H_8O_5$, or $C_9H_{12}O_4$

+ Retention time with DB-1 GC column and 3.75 min solvent hold.

* This compound is identical to that in scan 987 (14'47") of the L-EA BC extract for this enzyme case.

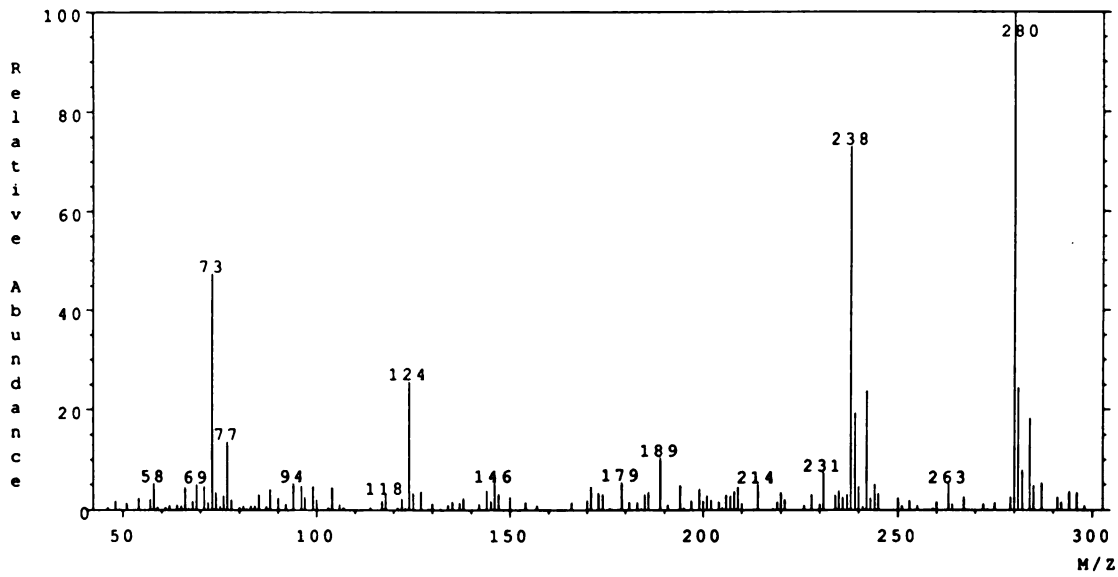

Figure 5.68: Electron-impact mass spectrum obtained from scan 426 (background scan 428) of the TIC from the LIP + MNP BC L-EA extract.

1 TMS

$C_{10}H_8O_5$

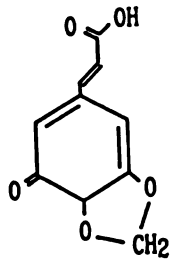

XV

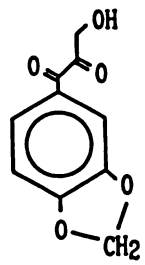

XVI

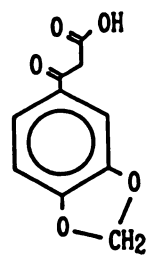

XVII

$C_{11}H_{12}O_4$

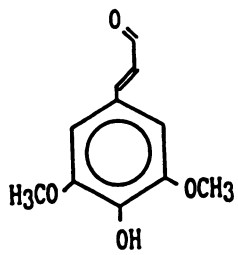

XVIII

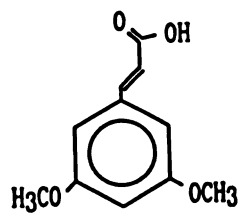

XIX

$C_{12}H_{16}O_3$

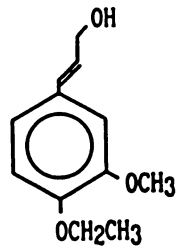

No quinone structures possible.

XX

2 TMS

$C_8H_8O_2$

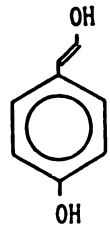

XXI

Figure 5.69: Proposed lignin-derived structures for the compound with mass spectrum shown in Figure 5.68.

product of lignin depolymerization. Structure XIX is 3,5-dimethoxycinnamic acid; it is doubtful that this compound could be released from lignin by an oxidative degradation due to the lack of a hydroxyl or ether at position 4 of the ring. Structure XX is unlikely because the ethyl group in the ether linkage to position 4 of the ring is not oxidized. Isomers of structure XX are possible, but with only one derivatizable oxygen, they would still be unlikely candidates. Structure XXI is unlikely since it is not probable that the hydroxyl on the side chain would remain as a hydroxyl group, but would probably be more stable as an aldehyde (both of the oxygens are required to be derivatized). Of these compounds, only 3,5-dimethoxycinnamic acid is commercially available (Aldrich). This compound and its 3,4-isomer were purchased and analyzed by GC/MS using the DB-1 GC column; the 3,5-dimethoxycinnamic acid eluted in scan 1021 (15'17"), while the 3,4-isomer eluted in scan 1021 (15'16") (different samples were used for each; see Figures F.14 and F.15 for the mass spectra, respectively), and thus the compound eluting in scan 426 cannot be one of these. Thus, there are still at least four viable structures that are possible: structures XV, XVI, XVII, and XVIII.

b. Scan 987

The mass spectrum for the peak in the L-EA extract at scan 987 (14'47") is presented in Figure 5.70. An excellent spectrum was obtained for this compound. This compound occurs in fairly high concentration in the L-EA BC extract, and also occurs in lower concentration in all but the L^{-} extract, indicating its definite origin as lignin-derived. The concentration of this compound in the BC extract is nearly 5 times the highest occurrence in the controls (AE control), indicating that it is released from the lignin by the LIP and/or MNP enzymes as well as being a minor extractive in the EC^{-}AH lignin substrate. It is not clear whether this compound contains 2 or 3 TMS etherified groups, as there are only small mass peaks present at 147 and 221, but it definitely has at least 1 derivatizable group. In addition, the mass peaks 107, 137, 151, and 167 clearly indicate a lignin origin. The large separation of the base peak at mass 223 and

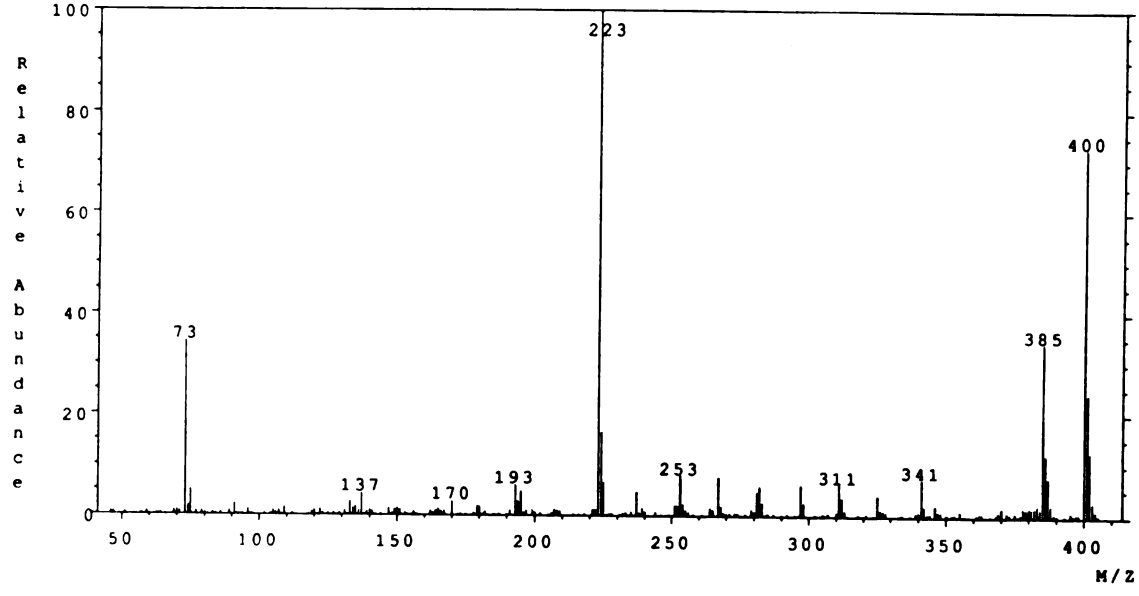

Figure 5.70: Electron-impact mass spectrum obtained from scan 987 (background scan 983) of the TIC from the LIP + MNP BC L-EA extract.

the molecular ion at mass 400 suggests that the compound is a dimer (but does not prove it). Based on the observance of peaks 223 and 253 in the spectra of TMS-derivatized syringic and vanillic acid (see Figures 5.56b and 5.56c), which are formed by loss of $OSi(CH_3)_3$ from the α-carboxylic acids for each, structures for these mass fragments were proposed; these are presented in Figure 5.71. These assignments are analogous to the assignment of 151 and 181 to α-carbonyl guaiacyl and syringyl structures by Faix *et al.* (1990b), respectively. Possible molecular formulas {r+db} are: (a) 1 TMS: $C_{17}H_{12}O_7$ {12}, $C_{18}H_{16}O_6$ {11}, $C_{19}H_{20}O_5$ {10}, and $C_{20}H_{24}O_4$ {9}; (b) 2 TMS: $C_{11}H_{12}O_7$ {6}, $C_{12}H_{16}O_6$ {5}, and $C_{13}H_{20}O_5$ {4}; and, (c) $C_8H_8O_5$ {5} and $C_9H_{12}O_4$ {4}. Structural possibilities are presented in Figure 5.72a for 1 TMS and 5.72b for 2 and 3 TMS. Of the structures containing one derivatizable group, only XXV is an unlikely candidate for a an oxidative lignin degradation product because of the unoxidized side chains at C-1 of both of the rings; XXII - XXV are quite likely to be degradation products since they all have about the right degree of oxidation, and contain β-O-4 linkages (XXII and XXIV) or α-carbonyl linkages (XXIII; the original bond would be an α-aryl ether linkage -- oxidation of C_α would be expected if the side chain of the right-hand monomer in XXIII were cleaved between C_α and C_β by LIP (Hammel *et al.*, 1985)). Assuming that the assignment of the mass fragments 223 and 253 are correct, only XXIII should give both of these fragments, making it the best possibility for a singly-derivatized dimer. All of the twice-derivatized structures (XXVI - XXVIII) are also likely to arise from oxidative lignin degradation; all three structures should give a fragments of mass 223 and 253. Structure XXVI could arise from C_α-C_β cleavage of two intermonomer β-O-4 linkages. Structure XXVII is identical to a product released *in vitro* from a phenolic β-aryl ether lignin model dimer by MNP (Tuor *et al.*, 1992). One might expect that there might be an unsaturation in the side chain of XXVIII if it had come from lignin, but that is not enough evidence to discard it. Structures containing three derivatizable groups, XXIX and XXX (4-hydroxy-homovanillyl alcohol), are again likely degradation products

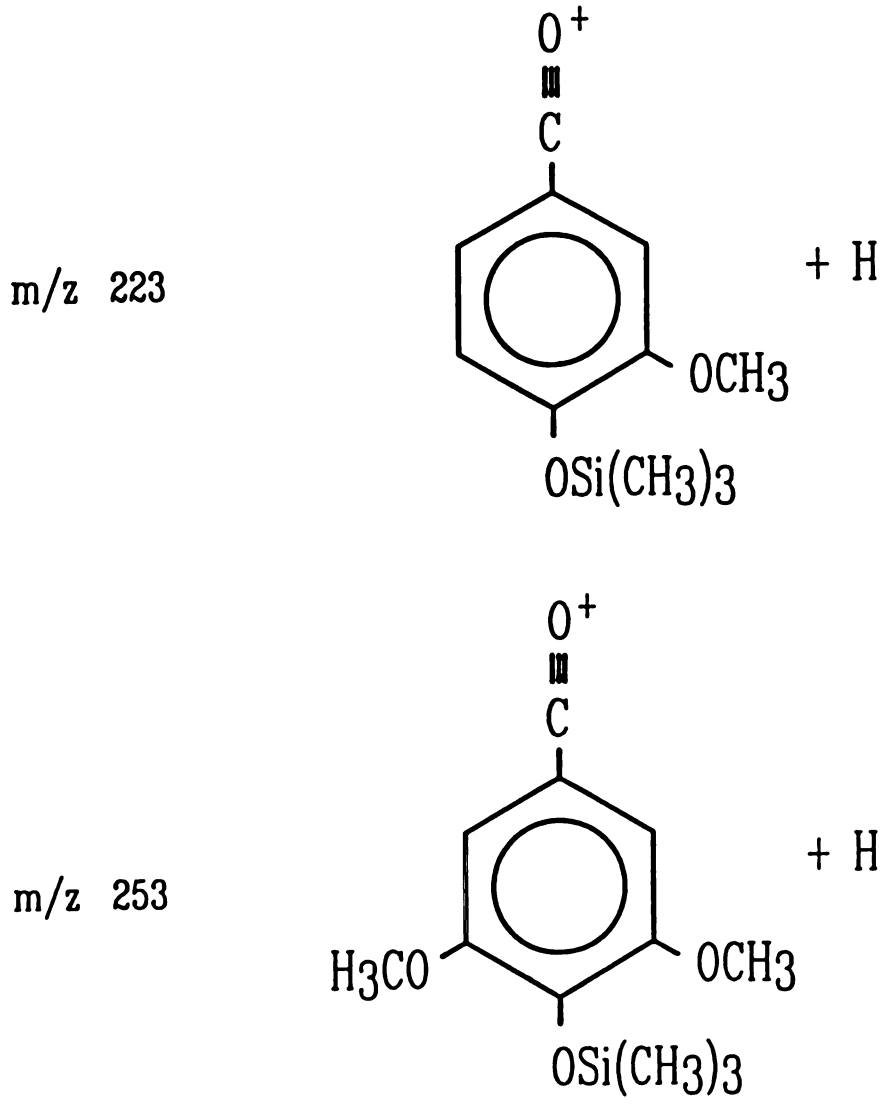

Figure 5.71: Proposed lignin-derived ion fragments of masses 223 and 253, formed by loss for $OSi(CH_3)_3$ from an α-carboxylic acid with guaiacyl- and syringyl-type structures, respectively.

1 TMS

$C_{17}H_{12}O_7$

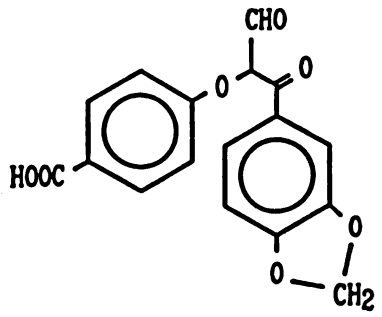

XXII

$C_{18}H_{16}O_6$

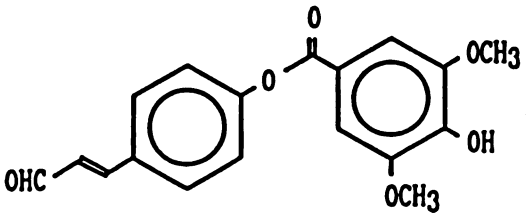

XXIII

$C_{19}H_{20}O_5$

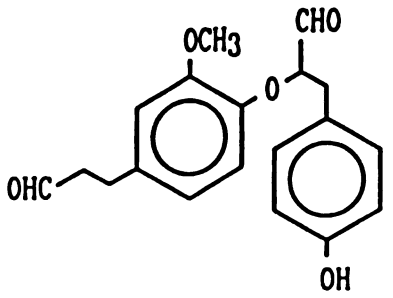

XXIV

$C_{20}H_{24}O_4$

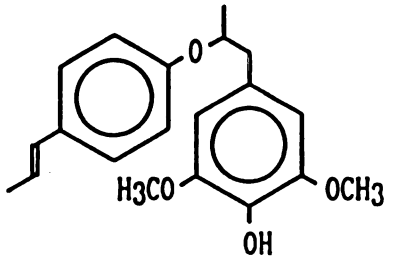

XXV

Figure 5.72: Proposed lignin-derived structures for the compound with mass spectrum shown in Figure 5.70. (a.) Structures which form mono-TMS derivatives.

2 TMS

$C_{11}H_{12}O_7$ 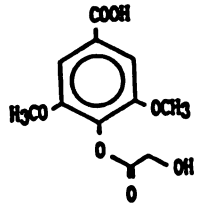 XXVI

$C_{12}H_{16}O_6$ 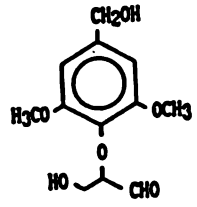 XXVII

$C_{13}H_{20}O_5$ 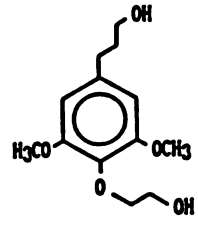 XXVIII

3 TMS

$C_8H_8O_5$ 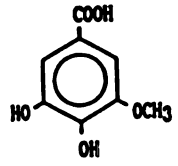 XXIX

$C_9H_{12}O_4$ 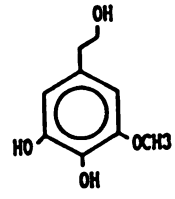 XXX

Figure 5.72b: Proposed lignin-derived structures for the compound with mass spectrum shown in Figure 5.70. **(b.)** Structures which form di- or tri-TMS derivatives.

of lignin; however, neither of these should give both 223 and 253 mass fragments. Based on the assumption of the 223 and 253 mass fragments, then, XXIX and XXX are not likely possibilities. Not surprisingly, none of the mono- or di-TMS-derivatized compounds are commercially available; in addition, notwithstanding their relative structural simplicity, structures XXIX and XXX also appear to not be commercially available. In summary, structures XXII - XXIV and XXVI-XXVIII are all likely possibilities which seem to fit the mass spectral evidence.

5.13.3.2 Peaks In The LIP + MNP BC S-C Extract

a. Scan 620

The mass spectrum for the peak in the S-C extract at scan 620 (9'17") is presented in Figure 5.73. A relatively clean spectrum of this compound was obtained, although it is not possible to distinguish whether the compound is derivatized twice or just once. The compound is an aliphatic substituted phenol based on the peak at mass 107. In the S-C BC extract, scan 620 appeared at 0.0532 ng/μL and in the R^- control at 0.0065 ng/μL (concentration 8.2 times higher in the BC than in this control), and was absent in all other extracts of the controls and other BC extracts. This suggests perhaps that it is a product of some enzyme in the extracellular fluid other than one of the peroxidases, which has greater activity in the presence of H_2O_2, VA, or Mn(II)/Mn(III). It should appear in the L^- control if it were simply a product of purely chemical oxidation due to the high O_2 levels present; in any case, it will be treated as a product of interest and dealt with in Chapter VI. Possible molecular formulas are {r+db}: $C_{12}H_{12}O_5$ {7}, $C_{13}H_{16}O_4$ {6}, $C_{14}H_{20}O_3$ {5} (one TMS); and $C_9H_8O_3$ {6} and $C_{10}H_{12}O_2$ {5} (two TMS). Possible structures for both one and two TMS-derivatizable groups are presented in Figure 5.74. Of these structures, only 4-coumaric acid (XXXV) is commercially available (Aldrich). Structure XXXI is probably not likely due to the lack of complete conjugation in the ring. Structure XXXII, if this were an LIP or MNP catalyzed reaction, would not be probable due to the unoxidized ethylene group at position 4 of the

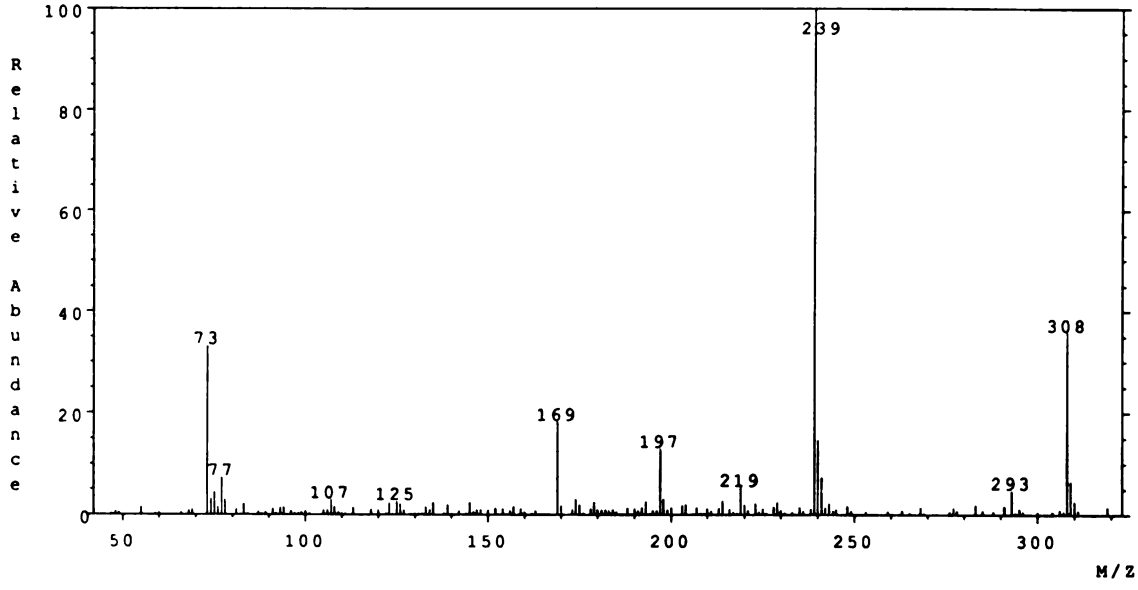

Figure 5.73: Electron-impact mass spectrum obtained from scan 620 (background scan 618) of the TIC from the LIP + MNP BC S-C extract.

1 TMS

$C_{12}H_{12}O_5$

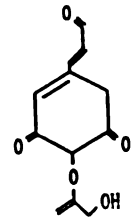

XXXI

$C_{13}H_{16}O_4$

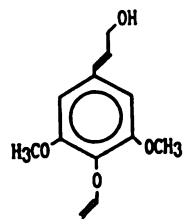

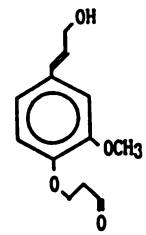

XXXII XXXIII

$C_{14}H_{20}O_3$

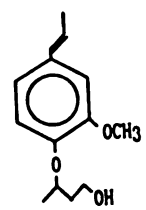

XXXIV

2 TMS

$C_9H_8O_3$

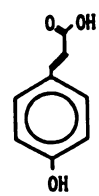

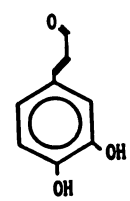

XXXV XXXVI

$C_{10}H_{12}O_2$

XXXVII

Figure 5.74: Proposed lignin-derived structures for the compound with mass spectrum shown in Figure 5.73, including structures which form mono- or di-TMS derivatives.

ring. Structure XXXIII would be a very likely possibility, as would structures XXXIII, XXXV (4-coumaric acid), and XXXVI (3,4-dihydroxy cinnamaldehyde). Structures XXXIV and XXXVII, however, are not likely to be lignin-derived products due to the presence of 4-carbon chains, and in XXXIV, to the unoxidized side chain. Structure XXXV, 4-coumaric acid (or 4-hydroxycinnamic acid) was purchased from Aldrich, as well as its isomer 3-coumaric acid; these authentic standards were analyzed by GC/MS using the DB-1 GC column. The 4-hydroxy isomer eluted in scan 975 (14'36"), while the 3-hydroxy isomer eluted in scan 926 (13'52"); their mass spectra are presented in Figures F.16 and F.17 (Appendix F), respectively. Neither the retention times nor the mass spectra match those of the peak eluting in scan 620; thus, only structures XXXIII and XXXVI were kept as possible structures.

b. Scan 834

The mass spectrum for the peak in the S-C extract at scan 834 (12'29") is presented in Figure 5.75. This compound appeared in the BC at 0.0450 ng/μL, in the E^- control at 0.0054 ng/μL, in the AE control at 0.0112 ng/μL, and in the ER^- control at 0.0080 ng/μL, but not in any other control. Since the concentration in the BC extract is 4 times the highest occurrence in any control, this compound is thus a compound which is a low level extractive in the EC^-AH lignin substrate, but can also be formed by LIP or MNP activity. The compound contains at least two TMS-derivatizable groups; it may not contain three, due to the lack of a peak at 221, but the peak at 221 does not always occur when three TMS groups are present; in addition, the odd isotope pattern on the molecular ion (372) indicates a large amount of silicon present (Dr. Douglas Gage, Personal Communication). Therefore, the three TMS case will also be treated. Possible molecular formulas are {r+db}: $C_{11}H_{16}O_5$ {4} and $C_{14}H_{12}O_5$ {9} (two TMS); and $C_7H_8O_4$ {4} (three TMS). Possible structures are presented in Figure 5.76 for both cases. Structures XXXVIII and XXXIX are both very likely candidates, given the structure of lignin; structures XL and XLI are also both quite possible, and XLII

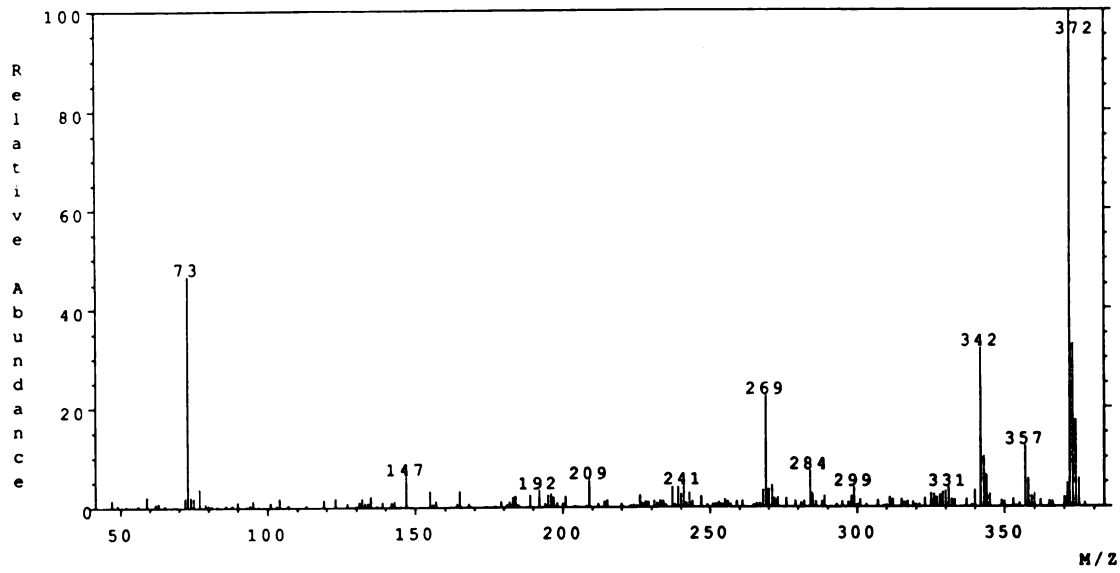

Figure 5.75: Electron-impact mass spectrum obtained from scan 834 (background average of scans 831 and 836) of the TIC from the LIP + MNP BC S-C extract.

2 TMS

$C_{11}H_{16}O_5$

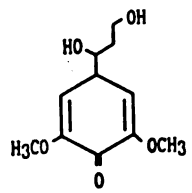

XXXVIII

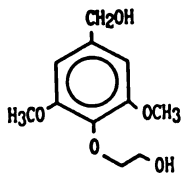

XXXIX

$C_{14}H_{12}O_5$

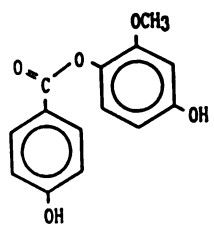

XL

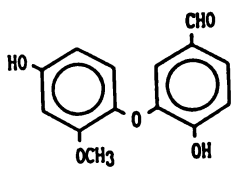

XLI

3 TMS

$C_7H_8O_4$

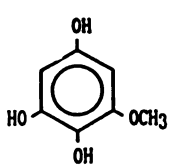

XLII

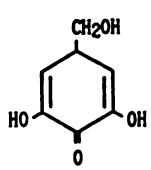

XLIII

Figure 5.76: Proposed lignin-derived structures for the compound with mass spectrum shown in Figure 5.75, including structures which form di- or tri-TMS derivatives.

(2,3,5-trihydroxy-anisole) and XLIII could arise from the oxidative degradation of lignin. Therefore, none of the structures proposed can be eliminated, since all could reasonably be formed during an oxidative degradation of lignin. None of the compounds in Figure 5.76 were found to be commercially available.

5.13.3.3 Peaks In The LIP + MNP BC S-EA Extract

a. Scan 809

The mass spectrum for the peak in the S-C extract at scan 809 (12'07") is presented in Figure 5.77. This compound was unique to this extract of the LIP + MNP BC (appeared in none of the controls), indicating its origin as an enzyme-released lignin product. This compound contains at least two TMS-derivatizable groups, and probably three, not only because of the peak at 221 (which may just be noise due to the lack of isotope peaks), but also because of the odd isotope pattern on the molecular ion (356) (see analysis of previous peak). The compound occurred in relatively low concentration, contributing to the fair amount of noise in the mass spectrum. The spectrum contains the 253 fragment, but it is unclear whether it could be from the same source (an α-carboxylic acid); in addition, the spectrum does not contain the 223 fragment, which it should if it is a syringyl structure (a syringyl-type α-carboxylic acid should contain both peaks if the assignment of the fragments is correct (refer to the mass spectrum of syringic acid in Figure 5.56c)). Possible molecular formulas are {r+db}: $C_{10}H_{12}O_5$ {5} and $C_{11}H_{16}O_4$ {4} (two TMS); and $C_7H_8O_3$ {4} (three TMS). Possible structures are presented in Figure 5.78. None of these compounds were found to be commercially available. Structures XLIV, XLV, XLVI (hydrosinapyl alcohol), and XLVII are all reasonable possibilities for lignin-derived oxidation products. Structure XLVIII could come from veratryl alcohol oxidation by LIP, but if this peak were this compound, the peak should have been present in the L^- controls, and it was not; therefore the peak either cannot be this compound, or the compound is produced from guaiacyl units but not from veratryl alcohol. It is well known that the major product of oxidation of veratryl alcohol

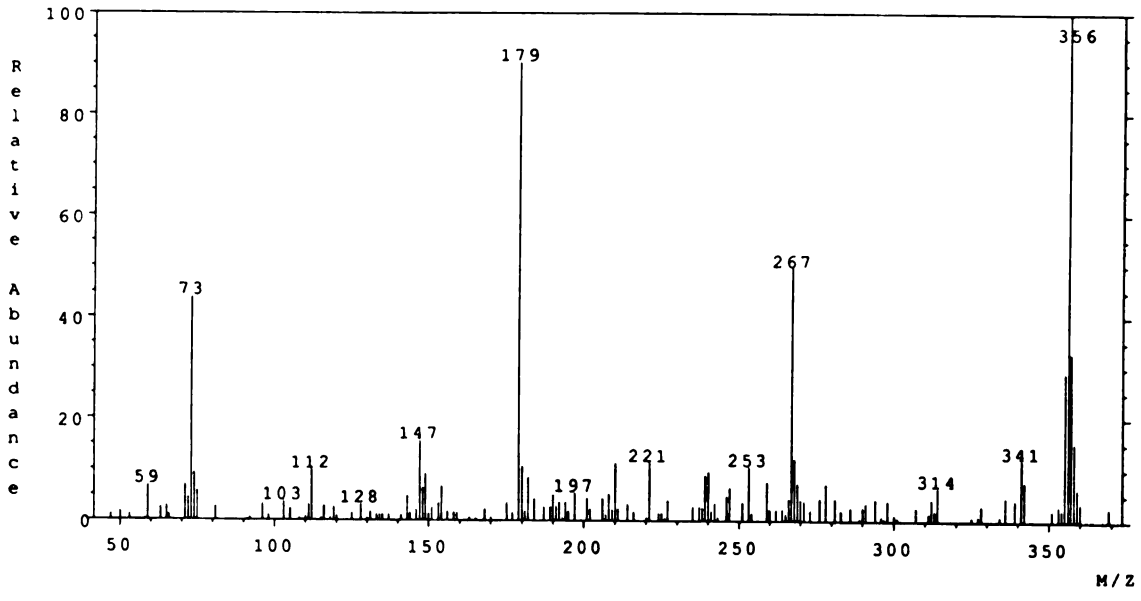

Figure 5.77: Electron-impact mass spectrum obtained from scan 809 (background average of scans 807 and 811) of the TIC from the LIP + MNP BC S-EA extract.

2 TMS

$C_{10}H_{12}O_5$

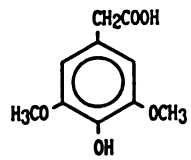

XLIV

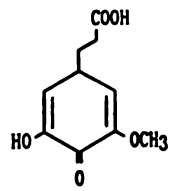

XLV

$C_{11}H_{16}O_4$

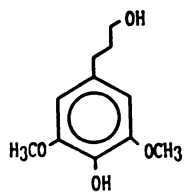

XLVI

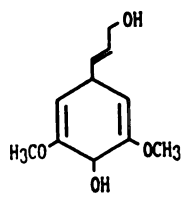

XLVII

3 TMS

$C_7H_8O_3$

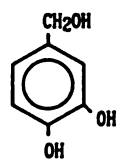

XLVIII

Figure 5.78: Proposed lignin-derived structures for the compound with mass spectrum shown in Figure 5.77, including structures which form di- or tri-TMS derivatives.

by LIP is veratraldehyde (Haemmerli *et al.*, 1987; Schmidt *et al.*, 1989); it is unknown whether this compound is produced in appreciable amounts, so the structure was retained as a possibility. Thus, all of the structures XLIV - XLVIII are reasonable possibilities for lignin-derived degradation products.

b. Scan 986

The mass spectrum for the peak in the S-C extract at scan 986 (14'46") is presented in Figure 5.70; it is identical to that found in the L-EA extract. This compound was found in the S-EA BC extract at 0.0551 ng/μL, and in the E^- control at 0.0044 ng/μL; it is probable, based on the results for the L-EA extract that it was present in the other controls also, but evidently at levels low enough to be undetectable. Refer to the treatment of scan 987 in the L-EA BC extract for this peak.

5.13.4 MNP Alone Reactor Runs

As an example of the GC output obtained for the MNP Alone BC and control samples, the TIC for the MNP Only L-C extract is shown in Figure 5.79. The peak at about scan 550 (8'14") is the internal standard; note that the retention times are different for this case because a different GC column and solvent hold time was used. The peaks at scans 652 (9'45") and 767 (11'29") are veratraldehyde and veratryl alcohol; VA was not added to the reaction mixture, so this VA has to have come either from the lignin or from the enzyme solution. It is known that the D4HiMn MNP contained about 6 % LIP (as total protein), so since VA and H_2O_2 were both present, the presence of veratraldehyde is not surprising. VA was added to the *P. chrysosporium* cultures in the enzyme production runs (to stimulate enzyme production); it is likely, then, that this VA was carried along through the concentration and dialysis steps, perhaps bound to the enzyme proteins. In the L-C extract, VA occurred in all of the extracts (BC and controls) in the following amounts (concentrations in the unconcentrated extracts): (a) BC, 2.748 ng/μL; (b) L^- control, 0.0215 ng/μL; (c) R^- control, 0.2633 ng/μL; (d) E^- control, 0.0463 ng/μL; (e) AE control, 2.107 ng/μL; and (f) ER^- control,

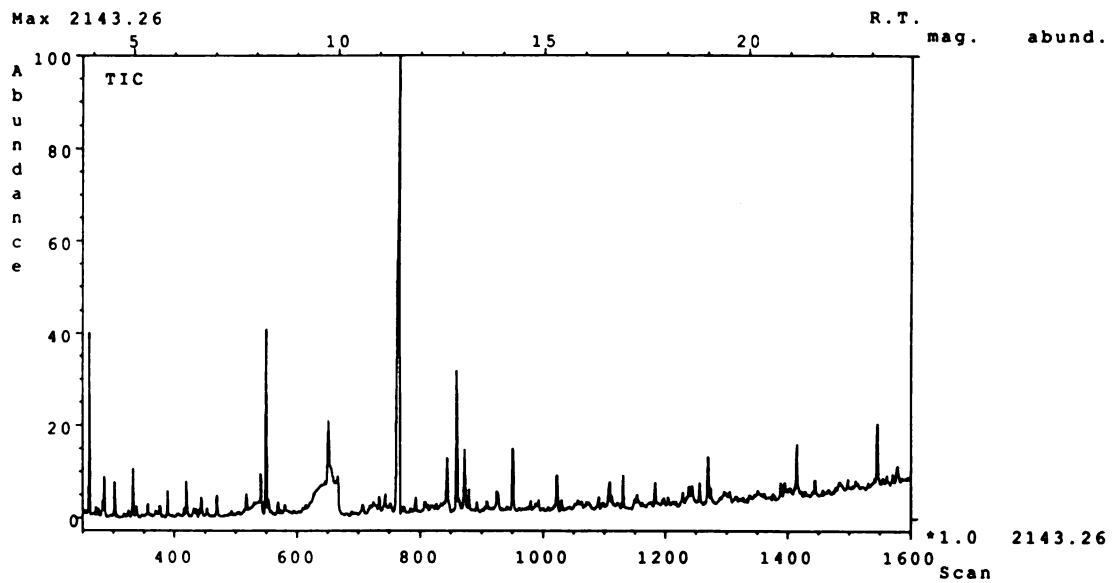

Figure 5.79: Total Ion Chromatogram (TIC) for the MNP Alone BC L-C extract over the scan range 250-1600 (3'44" to 23'58").

0.0683 ng/μL. The other extracts contained different amounts of VA relative to the L-C extracts, but the relative amounts for each reactor run (BC and controls) within an extract group were as above. These results confirm that most of the VA was bound to or entrained in the enzyme protein, and that enzyme activity in the presence of lignin caused the release of this VA, and also that a small amount of VA is present as an extractive in the lignin itself. This is because: (1.) The presence of only low levels of VA in the L^- control, when combined with the fact that the E^- control and the ER^- control also had only low levels of VA, indicates that the lignin contains a small amount of VA as an extractive, and that little VA is released from the enzyme when lignin or H_2O_2 are not present; (2.) The R^- control had a slightly higher VA level, indicating that the presence of reagents (H_2O_2) is required in addition to lignin for the bulk of the VA to be released from the enzyme; (3.) The fact that the AE control had high levels of VA (nearly as high as the BC), which could have been released by disruption of the enzyme structure, when combined with the high levels of VA present in the BC, indicates that the VA is bound to the enzyme and that the presence of both lignin and H_2O_2 are required for the release of the VA from the enzyme. It is probable that the LIP present (low level) in the D4HiMn MNP was the enzyme which bound the VA, since VA is a substrate for LIP.

The peak at scan 863 (12'55") is syringaldehyde, vanillic acid is at scan 925 (13'57"), syringic acid is at scan 1023 (15'19"), 3,5-dimethoxy-hydroquinone is at scan 860 (12'52"), and 2-methoxy-hydroquinone is at scan 744 (11'08"). See above for spectra and identification methods for these compounds. In all of the control extracts (all extracts from all control runs (except for the L^- controls) for both the MNP Alone runs and the LIP + MNP runs), the concentration of syringaldehyde was substantially (3 times or more) higher than the concentration of 3,5-dimethoxyhydroquinone, which is known to be formed from syringaldehyde (Wariishi *et al.*, 1989b; Tuor *et al.*, 1992). In the BC extracts, the ratios had switched; the hydroquinone was present in quantities high enough that more hydroquinone was present than the extractive levels of

syringaldehyde could account for. A rough mass balance over all of the extracts for the MNP Alone BC and the control with the highest concentrations of both compounds, using concentrations estimated from the internal standard's proportionality with peak area (ball-park estimate), indicated that nearly 2 moles of hydroquinone were present for every mole of syringaldehyde lost, indicating that some of the hydroquinone had to be formed from syringyl structures released from the lignin. What is odd about the presence of the hydroquinone, though, is that the major product of this reaction is 3,5-dimethoxy-1,4-benzoquinone (one additional oxidation step) and the hydroquinone is usually a minor product and is not generally produced in quantities greatly exceeding that of the quinone (Wariishi *et al.*, 1989b; Tuor *et al.*, 1992); the quinone was <u>not</u> found in any of the samples (an authentic spectrum of the quinone has been published by Tuor *et al.*, 1992; the TICs were searched for the major ion fragments in this spectrum: {170 (M^+ + 2, 12.5 %), 168 (M^+, 59.8), 125 (17.1), 80 (50.0), 69 (100)}). The most probable explanation for this fact is that the quinone form is extremely volatile, even at room temperature (Dr. M.H. Gold, Personal Communication), and would almost certainly have evaporated when the extracts were concentrated to dryness before derivatization for GC/MS. The hydroquinone is not especially stable in an oxidizing environment and easily converts to the quinone in the presence of Mn(III), and so should not be present in very high amounts (Dr. M.H. Gold, Personal Communication). Since the derivatizations were done in 1/2 dram vials at 60 °C and the total liquid volume was only 25 μL, it is likely that any of the quinone remaining after concentration of the sample (very little) would wind up stuck to the sides of the vial near the top, and not in the sample. Therefore, the observation of the presence of the hydroquinone in the samples at a given concentration leads to the conclusion that the quinone must have been there in much higher concentrations (Dr. M.H. Gold, Personal Communication). Since there is already more than enough hydroquinone present to account for the decrease in syringaldehyde concentration in the controls versus the BC, this additional quinone could

only have been formed from the lignin (Dr. M.H. Gold, Personal Communication). In order to test whether this was true also for the 2-methoxyhydroquinone, vanillin (vanillyl aldehyde) was purchased (Aldrich) and analyzed by GC/MS using the DB-1 GC column to get a reference spectrum. The vanillin eluted the column in scan 649 (9'43"); the mass spectrum of vanillin is shown in Figure F.18 (Appendix F). Further analysis indicated that the 2-methoxyhydroquinone could be accounted for simply by extractable vanillin, since the concentration of vanillin was significantly higher than that of the 2-methoxyhydroquinone in all samples.

The peaks for all extracts for the MNP Alone BC which were not eliminated by comparison with the chromatograms of the controls and the standard alone are presented, with concentration estimates (concentrations in the unconcentrated extracts), in Table 5.15. In the L-C BC extract, three unique peaks were identified, one of which was identical to that in scan 834 of the S-C extract of the LIP + MNP BC. In the L-EA BC extract, one unique peak was found, in addition to the compound found in scan 987 of the LIP + MNP BC L-EA extract. One unique peak was found in the S-C extract; one unique peak was found in the S-EA extract, in addition to the compound in scan 987 of the LIP + MNP BC L-EA extract. These peaks are analyzed below.

5.13.4.1 Peaks In The MNP Alone BC L-C Extract

a. Scan 909

The mass spectrum for the peak in the L-C extract at scan 909 (13'36") is presented in Figure 5.75; it is identical to that found in scan 834 (12'29") of the LIP + MNP BC S-C extract. This compound was found in the S-EA BC extract at 0.0249 ng/μL, but not in any of the controls; it is probable, based on the results for the LIP + MNP BC L-EA extract that it was present in other controls also, but evidently at levels low enough to be undetectable. Its presence in the MNP Only enzyme case indicates that it is an MNP-released product. Refer to the treatment of scan 834 in the S-C BC extract for this peak.

Table 5.15: Peaks in the MNP Alone BC extracts selected for structural analysis by comparing the Total Ion Chromatograms of the BC extracts with the corresponding extracts of its controls. The identity of the compound is listed if known; if not, the possible molecular formulas (based on the molecular weight determined from the mass spectrum) are listed.

Extract	Scan No.	RT+	Est. Conc. (ng/μL)	Derivatized M.W. (g/mole)	No. TMS Groups	Identity if known
L-C*	909	13'36"	0.0249	372	2	$C_{11}H_{16}O_5$ or $C_{14}H_{12}O_5$
					3	$C_6H_4O_5$ or $C_7H_8O_4$
L-C	1030	15'25"	0.0445	342	2	$C_9H_{10}O_5$ or $C_{10}H_{14}O_4$
					3	$C_6H_6O_3$
L-C	1444	21'37"	0.0498	526	1	$C_{24}H_{22}O_9$
					2	$C_{20}H_{14}O_8$ or $C_{21}H_{18}O_7$
					3	$C_{15}H_{18}O_7$ or $C_{16}H_{22}O_6$
					4	$C_{11}H_{10}O_6$ or $C_{12}H_{14}O_5$
L-EA	682	10'12"	0.0358	290?	2?	Unknown**
L-EA#	1062	15'54"	0.1499	400	1	$C_{17}H_{12}O_7$, $C_{18}H_{16}O_6$, $C_{19}H_{20}O_5$, or $C_{20}H_{24}O_4$
					2	$C_{11}H_{12}O_7$, $C_{12}H_{16}O_6$, or $C_{13}H_{20}O_5$
					3	$C_7H_4O_6$, $C_8H_8O_5$, or $C_9H_{12}O_4$
S-C	1498	22'26"	0.0988	552	1	$C_{25}H_{20}O_{10}$, $C_{26}H_{24}O_9$, or $C_{27}H_{28}O_8$
					2	$C_{19}H_{20}O_{10}$ or $C_{20}H_{24}O_9$
					3	$C_{16}H_{16}O_8$, $C_{17}H_{20}O_7$, or $C_{18}H_{24}O_6$
S-EA	437	6'32"	0.0189	318	1	$C_{14}H_{14}O_4$ or $C_{15}H_{18}O_3$
S-EA#	1063	15'55"	0.0902	400	1	$C_{17}H_{12}O_7$, $C_{18}H_{16}O_6$, $C_{19}H_{20}O_5$, or $C_{20}H_{24}O_4$
					2	$C_{11}H_{12}O_7$, $C_{12}H_{16}O_6$, or $C_{13}H_{20}O_5$
					3	$C_7H_4O_6$, $C_8H_8O_5$, or $C_9H_{12}O_4$

+ Retention time with DB5-MS GC column and 2.00 min solvent hold.

* This compound is identical to that in scan 834 (12'29") of the S-C BC extract for the LIP + MNP enzyme case.

** The noise level in the mass spectrum for this peak is too high to identify the molecular ion with a high degree of certainty.

This compound is identical to that in scan 987 (14'47") of the L-EA BC extract for the LIP + MNP enzyme case.

b. Scan 1030

The mass spectrum for the peak in the L-C extract at scan 1030 (15'25") is presented in Figure 5.80a and the TIC and mass chromatograms for masses 342, 327, 297, and 254 over the scan range 980 to 1080 are presented in Figure 5.80b. This peak was unique to the MNP Alone L-C BC extract. The derivatized molecular weight of this compound is 342, and it contains at least one TMS-derivatizable group. Based on the molecular weight, it was thought that this might be syringic acid which is also molecular weight 342 and elutes the column near this retention time; however, syringic acid was located in this sample at scan 1023 (15'19"), and so is also in the TIC and mass chromatograms given in Figure 5.80b (it is the large peak just to the left of the peak at 1030). Thus, this compound is not syringic acid, but may resemble it due to the appearance of many of the same ion fragments (refer to Figure 5.56c for the mass spectrum of syringic acid). The compound contains 2 or 3 derivatizable groups (the case for only 1 derivatizable group was checked; no lignin derived structures were possible). The peak at 223 mass units suggests a guaiacyl-type structure. Possible molecular formulas are {r+db}: $C_9H_{10}O_5$ {5} and $C_{10}H_{14}O_4$ {4} (two TMS); and $C_6H_6O_3$ {4}. The possible structures for both cases (excluding syringic acid for $C_9H_{10}O_5$ {5} (2 TMS)) are presented in Figure 5.81. All of the structures (XLIX - LVI) for two TMS are possible lignin-derived compounds; there is only one possibility for 3 TMS, 1,2,4-trihydroxybenzene, which is available from Aldrich (none of the isomers are not likely to be lignin-derived). None of the other compounds were found to be commercially available. Of these compounds, structure XLIX most resembles a guaiacyl structure released oxidatively from lignin, while structure LII most resembles a syringyl-type structure (because it is) and also resembles syringic acid; the presence of an M^+ - 90 fragment (252) also supports this structure. Finally, structure LVII (1,2,4-trihydroxybenzene) is not supported by the mass spectrum -- it is difficult to imagine how this molecule could lose a fragment of mass 15 from its molecular ion (except from the

(a.)

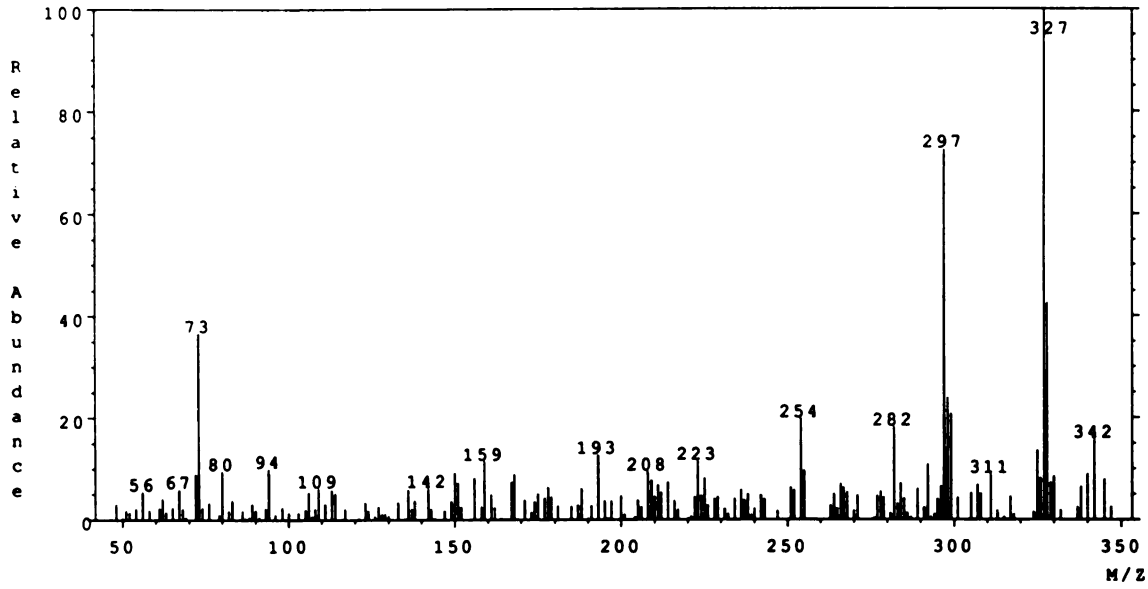

(b.)

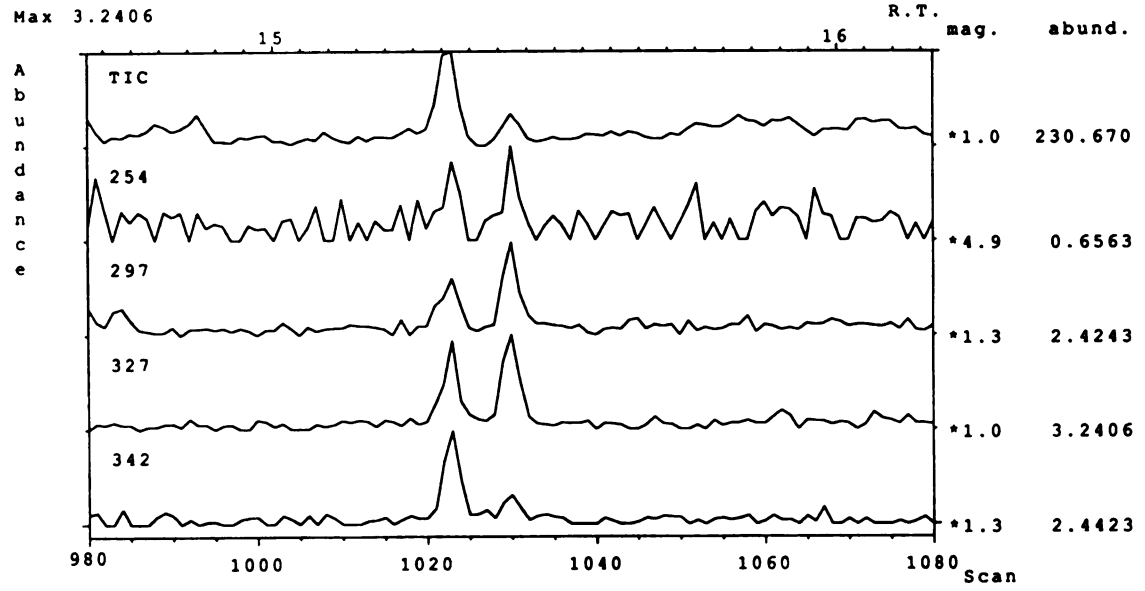

Figure 5.80: (a.) Electron-impact mass spectrum obtained from scan 1030 (background average of scans 1027 and 1033) of the TIC from the MNP Alone BC L-C extract; and (b.) TIC and mass chromatograms for ions of mass 254, 297, 327, and 342 over the scan range 980-1080.

2 TMS

$C_9H_{10}O_5$

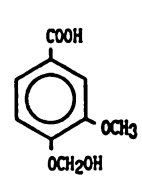

XLIX

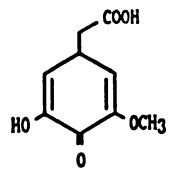

L

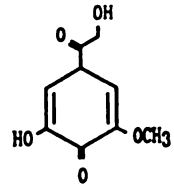

LI

$C_{10}H_{14}O_4$

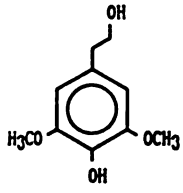

LII

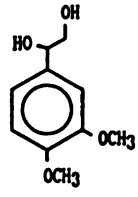

LIII

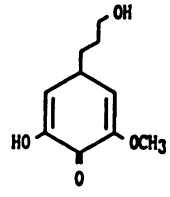

LIV

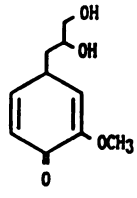

LV

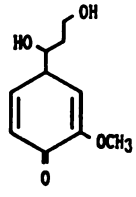

LVI

3 TMS

$C_6H_6O_3$

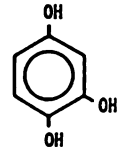

LVII

Figure 5.81: Proposed lignin-derived structures for the compound with mass spectrum shown in Figure 5.80, including structures which form di- or tri-TMS derivatives.

TMS groups), or have a fragment of mass 223. This compound was purchased (Aldrich) and analyzed by GC/MS using the DB-1 GC column; it eluted the column in scan 732 (10'52"), and its mass spectrum is shown in Figure F.19 (Appendix F). Neither the retention time nor the mass spectrum matches that of scan 1030, so scan 1030 cannot be this compound. While the other structures cannot be ruled out based on this (noisy) spectrum, structures XLIX and LII seem to be the most likely candidates because they are syringyl- guaiacyl-type structures which could likely be released from lignin.

c. Scan 1444

The mass spectrum for the peak in the L-C extract at scan 1444 (21'37") is presented in Figure 5.82; this peak was unique to the MNP Alone L-C BC extract. This compound is very large (derivatized molecular weight of 526), and is probably a dimer or trimer based on its low volatility (late retention time). This compound is present in low concentration (0.0498 ng/μL), which accounts for the fair amount of noise in the mass spectrum. There is a peak at mass 436 (M^+ - 90), suggesting an α-carboxylic acid is present; in addition, the isotope pattern on the molecular ion suggests a fair amount of Si is present. Based on its molecular weight, this compound could contain up to five derivatizable groups; it was found during analysis that no lignin-derived products were possible for the case of 5 TMS-derivatizable groups. Possible molecular formulas are {r+db}: $C_{24}H_{22}O_9$ {14} (one TMS; others are probably possible, but based on the isotope pattern on the molecular ion, 1 TMS is not probable); $C_{20}H_{14}O_8$ {14} and $C_{21}H_{18}O_7$ {13} (two TMS); $C_{15}H_{18}O_7$ {7} and $C_{16}H_{22}O_6$ {6} (three TMS); and finally, $C_{11}H_{10}O_6$ {7} and $C_{12}H_{14}O_5$ {6}. Possible structure are presented in Figure 5.83. Structure LVIII is unlikely due to the unoxidized sidechain fragment attached to the para oxygen on ring 1 (left-land ring). Structure LIX is quite likely if the compound arose from an end group in the lignin. Structure LX may not be exist; it was assumed that the hydroxyl group of the enol at C_γ of the sidechain of ring 2, which in the authentic compound would exist as an aldehyde, was derivatizable. The same is true for the enols present in structures

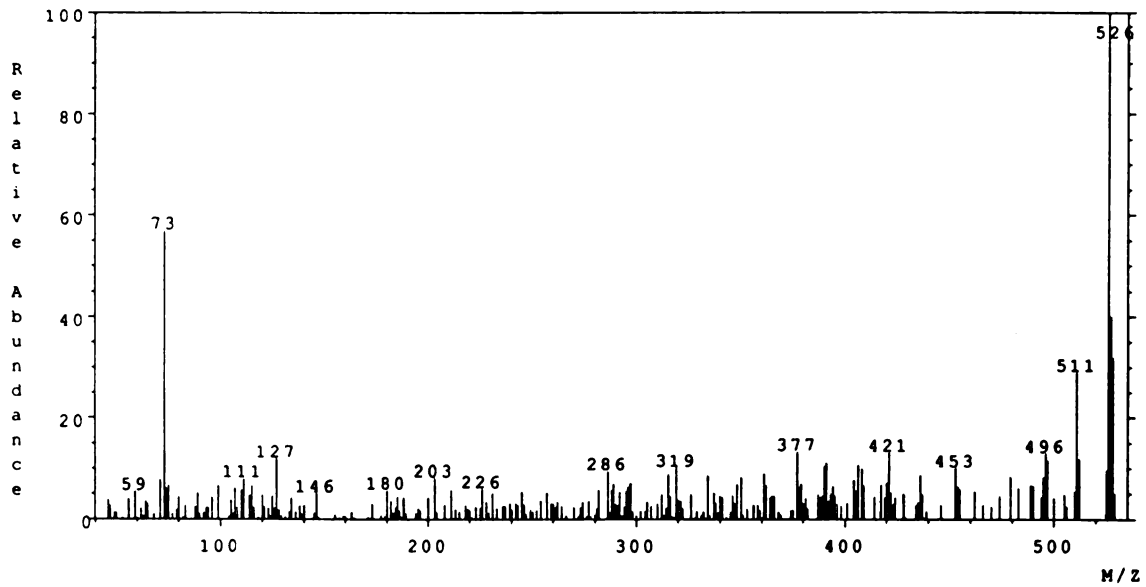

Figure 5.82: Electron-impact mass spectrum obtained from scan 1444 (background average of scans 1442 and 1447) of the TIC from the MNP Alone BC L-C extract.

1 TMS

$C_{24}H_{22}O_9$

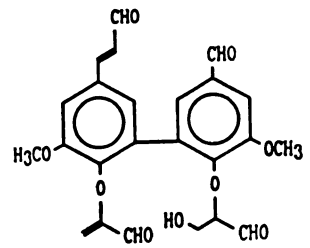

LVIII

2 TMS

$C_{20}H_{14}O_8$

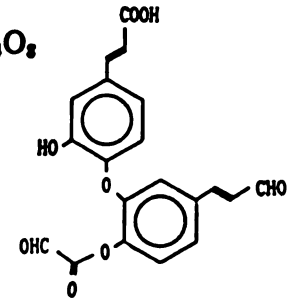

LIX

$C_{21}H_{18}O_7$

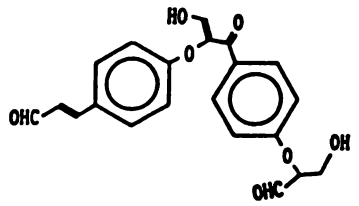

LX

3 TMS

$C_{15}H_{18}O_7$

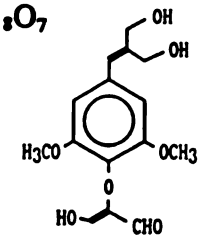

LXI

$C_{16}H_{22}O_6$

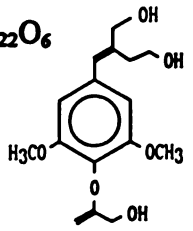

LXII

4 TMS

$C_{11}H_{10}O_6$

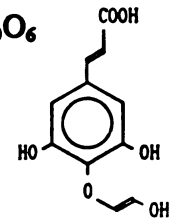

LXIII

$C_{12}H_{14}O_5$

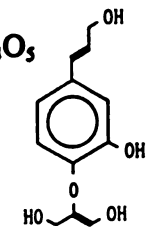

LXIV

Figure 5.83: Proposed lignin-derived structures for the compound with mass spectrum shown in Figure 5.82, including structures which form mono-, di-, tri- or tetra-TMS derivatives.

LXI, LXIII, and LXIV. Note that the aliphatic side chains in structures LXI and LXII could arise from a pinoresinol linkage. Thus, of the structures proposed, LIX seems to be the most likely to arise from an oxidative degradation of lignin. None of these compounds are commercially available. Note that most of these structures contain enolic hydroxyls -- it could be that one of the rings in the dimer is a ring-opened product, which would allow more possibilities for molecular formula (no ring-opened possibilities were considered).

5.13.4.2 Peaks In The MNP Alone BC L-EA Extract

a. Scan 682

The mass spectrum for the peak in the L-EA extract at scan 682 (10'12") is presented in Figure 5.84; this peak was unique to the MNP Alone BC L-EA extract. While this compound is in higher concentration (0.0358 ng/μL) than some compounds for which clean spectra were obtained, this peak was in a very noisy region of the chromatogram, so a clean spectrum was not possible. This compound is then tagged as an unknown of possible molecular weight 290, and with two TMS-derivatizable groups.

b. Scan 1062

The mass spectrum for the peak in the L-EA extract at scan 1062 (15'54") is presented in Figure 5.70; it is identical to that found in the LIP + MNP BC L-EA extract in scan 987 (14'47"). This compound was found in the L-EA BC extract at 0.1499 ng/μL, but not in any other controls; it is probable, based on the results for the LIP + MNP BC L-EA extract that it was present in the other controls also, but evidently at levels low enough to be undetectable. Refer to the treatment of scan 987 in the LIP + MNP BC L-EA extract for this peak.

5.13.4.3 Peaks In The MNP Alone BC S-C Extract

a. Scan 1498

The mass spectrum for the peak in the S-C extract at scan 1498 (22'26") is presented in Figure 5.85; this peak was unique to the MNP Alone S-C BC extract. This

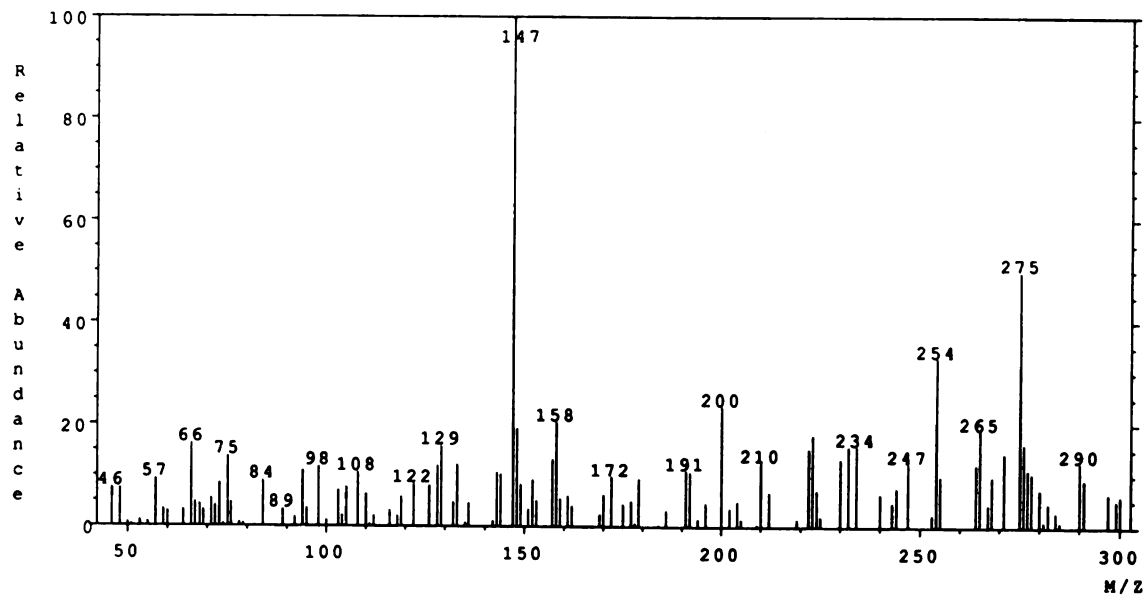

Figure 5.84: Electron-impact mass spectrum obtained from scan 682 (background scan 681) of the TIC from the MNP Alone BC L-EA extract.

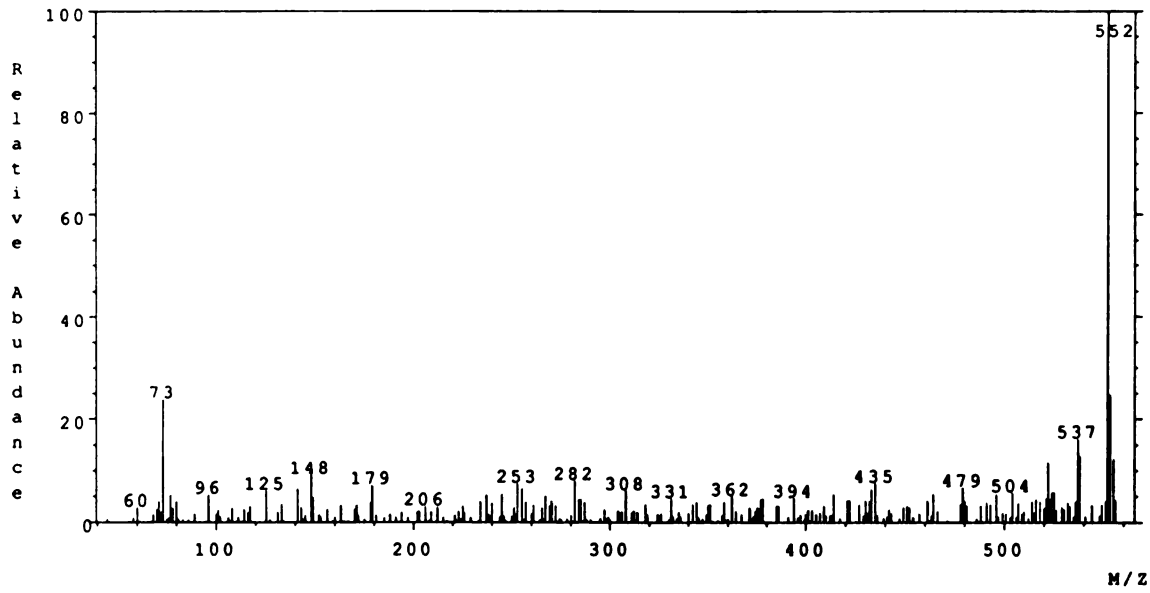

Figure 5.85: Electron-impact mass spectrum obtained from scan 1498 (background average of scans 1496 and 1500) of the TIC from the MNP Alone BC S-C extract.

compound is another probable dimer or trimer of derivatized molecular weight 552. The compound contains at least one and can have as many as 3 TMS-derivatizations (4 and 5 TMS are not structurally possible for a lignin-derived product). This compound contains both 223 and 253 mass fragments, suggesting guaiacyl- and/or syringyl-type structures are present. The peak at mass 462 (which could be noise), may suggest an α-carboxylic acid. The compound was found in fairly substantial (comparatively) concentration of 0.0988 ng/μL. Possible molecular formulas are {r+db}: $C_{25}H_{20}O_{10}$ {16}, $C_{26}H_{24}O_9$ {15}, and $C_{27}H_{28}O_8$ {14} (one TMS); $C_{19}H_{20}O_{10}$ {10} and $C_{20}H_{24}O_9$ {9} (two TMS); and $C_{16}H_{16}O_8$ {9}, $C_{17}H_{20}O_7$ {8}, and $C_{18}H_{24}O_6$ {7}. Possible structures are presented in Figure 5.86a (one TMS), Figure 5.86b (two TMS), and Figure 5.86c (three TMS). None of these compounds are commercially available; note that the proposed structures for this compound are not exclusive of other possibilities (nor is this true for any other peak analyzed) due to isomers, etc. The monomers in structure LXV are linked by one β-O-4 linkage (originally β-O-4, now oxidized) and one diphenyl ether linkage; this is a reasonable lignin-derived product. Structure LXVI is linked by one diphenyl ether linkage and one (now oxidized) α-aryl ether linkage, and is another reasonable lignin-derived product. Structure LXVII is linked by two β-O-4 linkages; this structure may not be a candidate due to the lack of oxidation in the side chains. Structures LXVIII and LXIX are linked by an α-aryl ether bond (now oxidized), and are both reasonable lignin-derived products. Structure LXX is linked by a β-O-4 linkage, and is a reasonable possibility, as well as are a number of possible isomers of this structure. Structure LXXI looks odd at first glance, but inspection of the linkage between monomers 3 and 2, and monomers 13c and 14c in Figure 1.1 will provide the source of the extra side chain at position 5 of the ring; it is unknown whether this type of structure would be formed in an oxidative degradation of lignin. Structure LXXII is another reasonable lignin-derived product, and is linked by a diphenyl ether bond. Structure LXXIII is linked by an intact α-aryl ether linkage and could arise from C_α-C_β

1 TMS

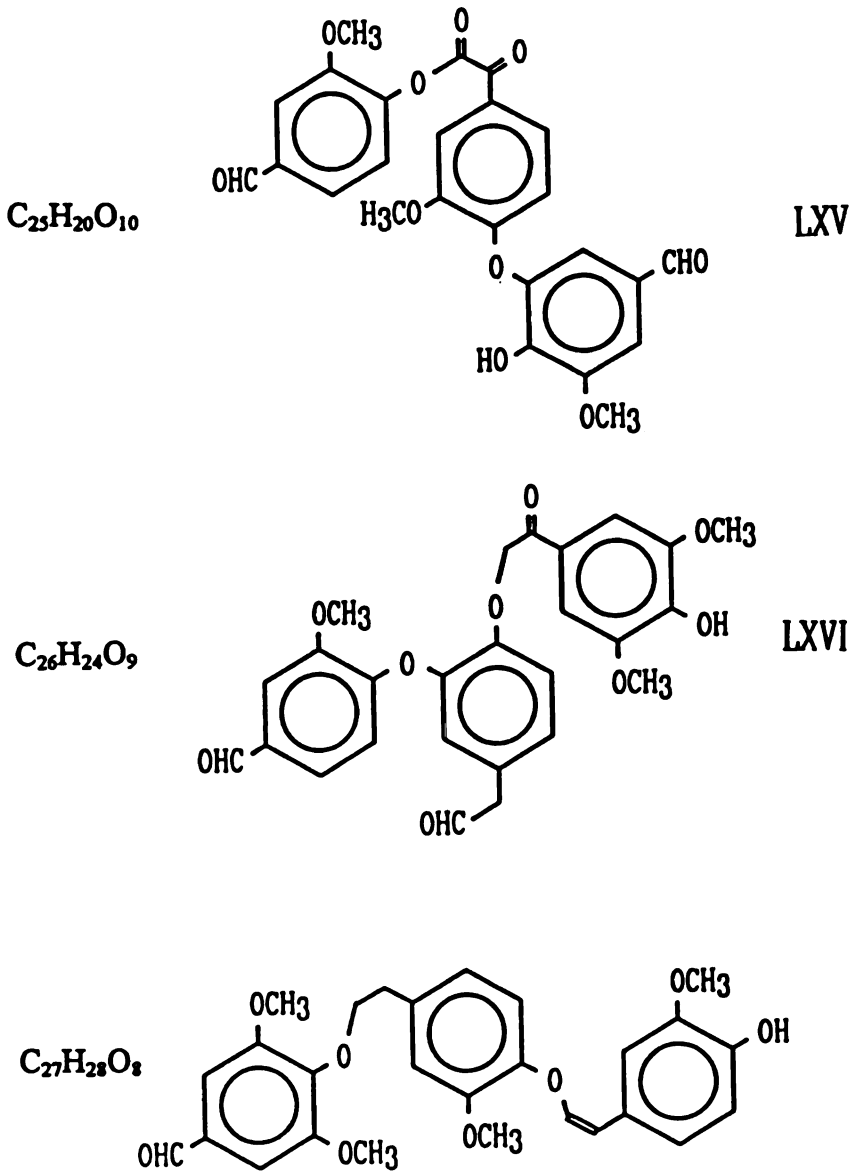

Figure 5.86: Proposed lignin-derived structures for the compound with mass spectrum shown in Figure 5.85. (a.) Structures which form mono-TMS derivatives.

2 TMS

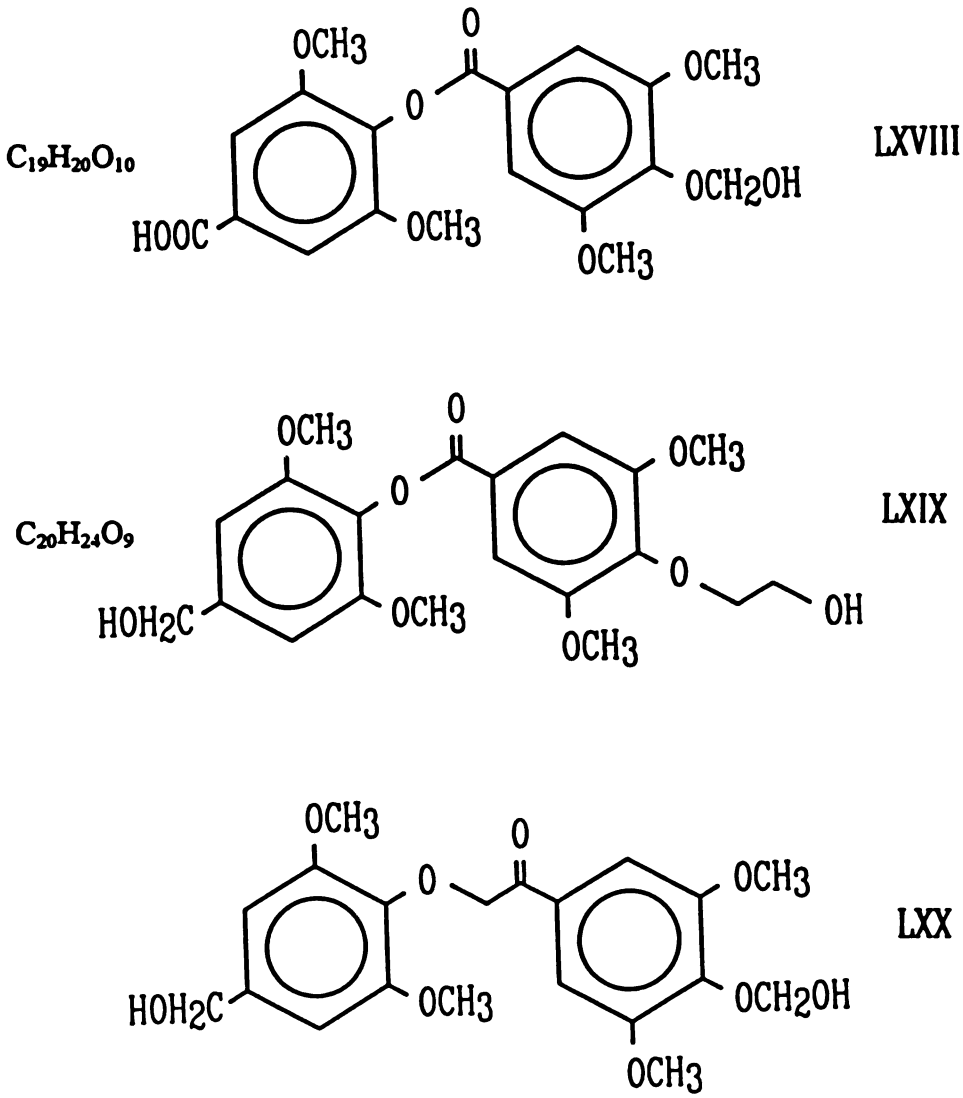

Figure 5.86: Proposed lignin-derived structures for the compound with mass spectrum shown in Figure 5.85. (b.) Structures which form di-TMS derivatives.

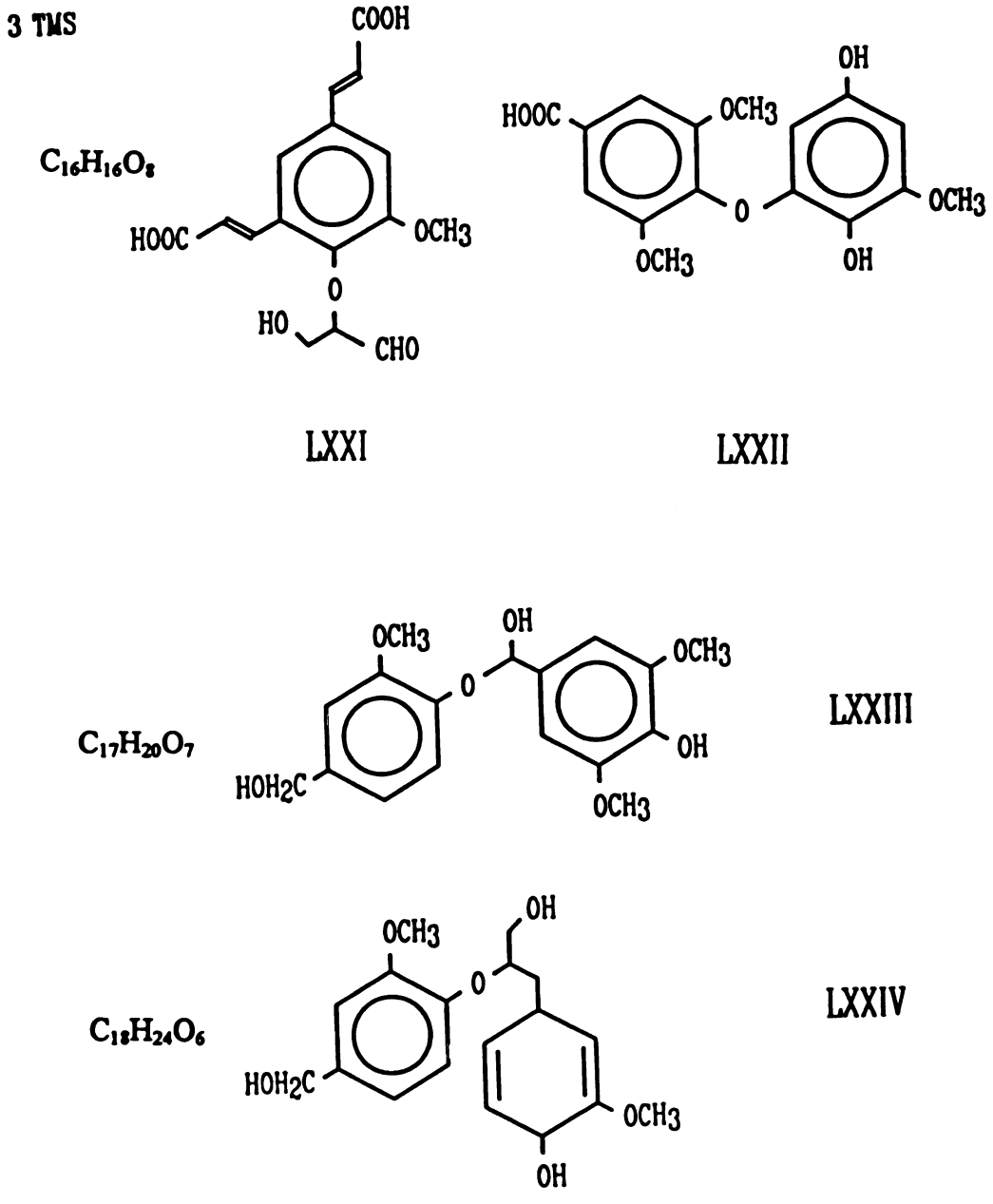

Figure 5.86: Proposed lignin-derived structures for the compound with mass spectrum shown in Figure 5.85. (c.) Structures which from tri-TMS derivatives.

cleavage of the side chain of ring 2. Finally, Structure LXXIV looks reasonable; however, formation of ring 2 may not be energetically favorable (see analysis of structures VII and VIII above). Thus, only structures LXVII and LXXIV, and probably LXXI are excluded.

5.13.4.4 Peaks In The MNP Alone BC S-EA Extract

a. Scan 437

The mass spectrum for the peak in the S-EA extract at scan 437 (6'32") is presented in Figure 5.87; this compound was unique to the MNP Alone BC S-EA extract. This compound occurred in low concentration (0.0189 ng/μL), and so the mass spectrum contains a fair amount of noise. The compound may be molecular weight 318 (TMS-derivative), but this is unclear. No reasonable compounds were obtained for this compound using the non-ring-opened criterion for exclusion of possibilities. Therefore, it is very possible that this compound is a ring-opened product. Regardless, it will be treated here as an unidentifiable unknown.

b. Scan 1063

The mass spectrum for the peak in the S-EA extract at scan 1063 (15'55") is presented in Figure 5.70; it is identical to that found in the LIP + MNP BC L-EA extract in scan 987 (14'47"). This compound was found in the S-EA BC extract at 0.0902 ng/μL and in the ER$^-$ extract at 0.0179 ng/μL, but not in any other controls; it is again probable, based on the results for the LIP + MNP BC L-EA extract that it was present other controls also, but at levels too low to be detected. Refer to the treatment of scan 987 in the LIP + MNP BC L-EA extract for this peak.

5.13.5 Summary of GC/MS Analysis Results

Analysis of the extracts of the solid and liquid phases from the Base Case reactor runs indicates a number of unique peaks which can be attributed to release from the lignin by action of the enzymes, by virtue of their absence in the controls and in a separate sample of the internal standard. These controls (see Tables 4.6-4.8) were

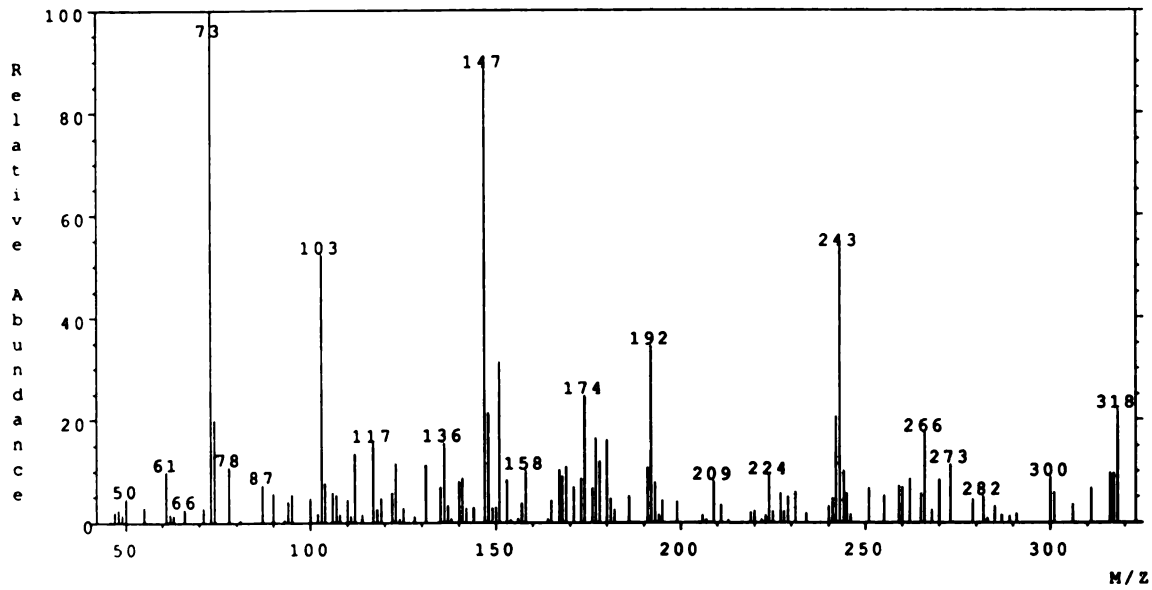

Figure 5.87: Electron-impact mass spectrum obtained from scan 437 (background average of scans 435 and 439) of the TIC from the MNP Alone BC S-EA extract.

carefully designed to eliminate any compounds not released from the lignin by the activities of the peroxidase enzymes when all necessary reagents were present, and thus any peak unique to a BC extract is almost certain to be a compound released from the lignin by the activities of the enzyme(s). Many structures are possible for these compounds which are consistent with the known mechanisms of both LIP and MNP on lignin model compounds. Summaries of the predicted structures (listed by structure number) are given in Tables 5.16-5.18 for the LIP Alone, MNP Alone, and LIP + MNP BC extracts, respectively. Note that any structures with unconjugated rings like that for structure I are not considered as probable products of free radical-mediated oxidation of lignin, since the loss of aromaticity and conjugation are not likely to occur with this type of reaction. In the case of peaks for which these types of structures are the only possibilities (given the assumption that the ring itself was intact), it is possible that the compounds are ring-opened products. Loss of the ring would allow a greater degree of freedom in prediction of oxidized structures consistent with lignin-derived ring-opened products. These peaks are indicated in Tables 5.16-5.18 as ring-opened products.

While it is impossible to verify most of the structures without the aid of other techniques better suited to that task, such as ^{13}C-NMR, when the GC/MS results are combined with the lignin recoveries and the FTIR/PLS results for the base case runs versus the controls (see Figure 5.88), it seems clear that some degradation did occur due to enzyme activity, at least when both LIP and MNP were present. The presence of unique, probable lignin-derived compounds in both the LIP Alone and MNP Alone BCs may indicate a very limited release of soluble fragments from the lignin, too small to be detected merely by weight loss or by the FTIR/PLS technique. There is also the possibility that, in the case of MNP Alone, more modification of the solid occurred than weight loss, causing a net increase in the mass of the solid even though compounds were solubilized. In any event, the presence of unique soluble lignin-derived compounds in both the LIP Alone and MNP Alone BCs does not contradict the results from the mass

Table 5.16: Summary of probable lignin-derived structures for peaks in the LIP Alone BC extracts which were selected for structural analysis. The structures are indicated by number; the identity of the compound is listed if verified by an authentic standard. Peaks for which only structures that contain a saturated carbon in an otherwise conjugated ring (ie. like structure I) are listed as probable ring-opened products.

Extract	RT+	Est. Conc. (ng/μL)	Derivatized M.W. (g/mole)	No. TMS Groups	Possible Formula	Probable Structures or Identity
L-C	16'00"	0.0256	370?	2?		Unknown
L-EA	8'08"	0.1656	182	0	$C_9H_{10}O_4$	Ring-opened
					$C_{10}H_{14}O_3$	Ring-opened
L-EA	8'59"	0.8820	226	1		3,4-dimethoxyphenol
L-EA	10'04"	0.1209	284	2		2-methoxyhydroquinone*
L-EA	11'10"	0.0925	282	2		p-hydroxybenzoic acid**
L-EA	11'15"	0.9226	256	0	$C_9H_{12}O_4$	Ring-opened

+ Retention time with DB-1 GC column and 3.75 min solvent hold.

* Identified by comparison with spectrum of Valli et al. (1992b).

** Identified by comparison with spectrum in NIST database.

Table 5.17: Summary of probable lignin-derived structures for peaks in the MNP Alone BC extracts which were selected for structural analysis. The structures are indicated by number; the identity of the compound is listed if verified by an authentic standard. Peaks for which only structures that contain a saturated carbon in an otherwise conjugated ring (ie. like structure I) are listed as probable ring-opened products.

Extract	RT+	Est. Conc. (ng/μL)	Derivatized M.W. (g/mole)	No. TMS Groups	Possible Formula	Probable Structures or Identity
L-C*	13'36"	0.0249	372	— see Table 5.18 —		
L-C	15'25"	0.0445	342	2	$C_9H_{10}O_5$	XLIX
				2	$C_{10}H_{14}O_4$	LII
				3	$C_6H_6O_3$	None
L-C	21'37"	0.0498	526	1	$C_{24}H_{22}O_9$	None
				2	$C_{20}H_{14}O_8$	LIX
				3	$C_{15}H_{18}O_7$	LXI
				3	$C_{16}H_{22}O_6$	LXII
L-EA	10'12"	0.0358	298?	2?	Unknown**	
L-EA***	15'54"	0.1499	400	— see Table 5.18 —		
S-C	22'26"	0.0988	552	1	$C_{25}H_{20}O_{10}$	LXV
				1	$C_{26}H_{24}O_9$	LXVI
				2	$C_{19}H_{20}O_{10}$	LXVIII
				2	$C_{20}H_{24}O_9$	LXIX, LXX
				3	$C_{16}H_{16}O_8$	LXXII
				3	$C_{17}H_{20}O_7$	LXXIII
S-EA	6'32"	0.0189	318	1	Unknown**	
S-EA***	15'55"	0.0902	400	— see Table 5.18 —		

+ Retention time with DB5-MS GC column and 2.00 min solvent hold.A32

* This compound is identical to that in scan 834 (12'29") of the S-C BC extract for the LIP + MNP enzyme case.

** The noise level in the mass spectrum for this peak is too high to identify the molecular ion with a high degree of certainty.

*** This compound is identical to that in scan 987 (14'47") of the L-EA BC extract for the LIP + MNP enzyme case.

Table 5.18: Summary of probable lignin-derived structures for peaks in the LIP + MNP BC extracts which were selected for structural analysis. The structures are indicated by number; the identity of the compound is listed if verified by an authentic standard. Peaks for which only structures that contain a saturated carbon in an otherwise conjugated ring (ie. like structure I) are listed as probable ring-opened products.

Extract	RT[+]	Est. Conc. (ng/μL)	Derivatized M.W. (g/mole)	No. TMS Groups	Possible Formula	Probable Structures or Identity
L-EA	6'22"	0.0235	280	1	$C_{10}H_8O_5$	XV, XVI, XVII
				1	$C_{11}H_{12}O_4$	XVIII
L-EA	14'47"	0.1933	400	1	$C_{17}H_{12}O_7$	XXII
				1	$C_{18}H_{16}O_6$	XXIII
				1	$C_{19}H_{20}O_5$	XXIV
				2	$C_{11}H_{12}O_7$	XXVI
				2	$C_{12}H_{16}O_6$	XXVII
				2	$C_{13}H_{20}O_5$	XXVIII
				3	$C_8H_8O_5$	XXIX
				3	$C_9H_{12}O_4$	XXX
S-C	9'17"	0.0532	308	1	$C_{13}H_{16}O_4$	XXXIII
				2	$C_9H_8O_3$	XXXV, XXXVI
S-C	12'29"	0.0450	372	2	$C_{11}H_{16}O_5$	XXXIX
				2	$C_{14}H_{12}O_5$	XL, XLI
				3	$C_7H_8O_4$	XLII
S-EA	12'07"	0.0252	356	2	$C_{10}H_{12}O_5$	XLIV
				2	$C_{11}H_{16}O_4$	XLVI
				3	$C_7H_8O_3$	XLVIII
S-EA[*]	14'46"	0.0551	400	--- see above ---		

+ Retention time with DB-1 GC column and 3.75 min solvent hold.

* This compound is identical to that in scan 987 (14'47") of the L-EA BC extract for this enzyme case.

SUMMARY OF RESULTS

	LIP	MNP	LIP + MNP
Color Change ?	**NO**	**YES**	**TRANSIENT**
Loss of Mass ?	**(NO)**	**GAIN**	**YES (11 %)**
Loss of Lignin ?	**(NO)**	**NO**	**YES (8 %)**
Unique Products Solubilized ?	**YES**	**YES**	**YES**

Figure 5.88: Summary of the general results for color changes, residual solid mass losses, lignin contents, and formation of unique lignin-derived products for the treatment of isolated insoluble poplar lignin in aqueous media by LIPs Alone, MNPs Alone, and LIPs + MNPs.

recoveries or those from the FTIR. This is because the release of small amounts of soluble products would represent release of only a very small percentage of the total mass of the solid and of the lignin; given the relatively wide uncertainty ranges for both measurements for the LIP Alone and MNP Alone BCs, then, solubilization of a small fraction of the lignin cannot be ruled out. In the case of the LIP + MNP BC extracts, however, the GC/MS results are completely consistent with the prior measurements (solid recovery and lignin content), indicating degradation of the lignin when both LIPs and MNPs are present.

IN VITRO DEPOLYMERIZATION OF NATURAL INSOLUBLE LIGNIN IN AQUEOUS MEDIA BY THE EXTRACELLULAR PEROXIDASES OF *PHANEROCHAETE CHRYSOSPORIUM*

Volume II

by

David Neil Thompson

A DISSERTATION

Submitted to
Michigan State University
in partial fulfillment of the requirements
for the degree of

DOCTOR OF PHILOSOPHY

Department of Chemical Engineering

1994

CHAPTER VI: DISCUSSION

6.1 Substrate

The preferred substrate for use in *in vitro* lignin depolymerization studies with extracellular peroxidases is an insoluble, unmodified, carbohydrate-free lignin which is not chemically or structurally different from lignin as it occurs in wood (Tien, 1987). The isolated lignin substrate which was used in this study approaches this goal, in that it has a high lignin content, is low in carbohydrates, and does not appear to be very highly condensed versus the unmodified native poplar lignin before isolation, based on the results of the thioacidolysis tests performed by Dr. John R. Obst at the USDA Forest Products Laboratory. The substrates most used in both mechanistic studies and in general depolymerization studies have been lower molecular weight, water- or aqueous organic solvent-soluble lignin model dimers and synthetic lignins, because of the apparent lack of activity of both LIPs and MNPs on high molecular weight, completely insoluble lignin (Tien, 1987). The lignin used in this study is of a very high molecular weight, as evidenced by its complete insolubility in conventional lignin solvents, even after acetylation (Dr. John R. Obst, Personal Communication). It is also highly polymeric, as evidenced by the extremely low phenolic hydroxyl content determined by FTIR/PLS (B. Hames, Personal Communication). Finally, only a small amount of the β-O-4 intermonomer linkages, the most common linkage type in lignin, are condensed (thioacidolysis results) and therefore the lignin is likely to be structurally similar to natural lignin. Thus, while it may not be identical in every way to unmodified lignin as it occurs in wood, the substrate used in this study is not substantially different from natural lignin, and represents a marked improvement in choice of substrate for this type of peroxidase study. Note that native (untreated) poplar lignin was not used in this study because the large amount of carbohydrates present would interfere with the FTIR/PLS analysis.

6.2 Reactor and Model

The lignin depolymerization system developed in this study is simple, inexpensive, and provides a basis for the development of more complicated on-line systems which would maintain concentrations in a similar manner. The system provides good mixing, high O_2 concentrations, and when combined with the model, provides a simple method for maintaining high enzyme activities and low, controllable reagent concentrations in contact with the enzymes. The apparent success of lignin depolymerization by LIPs and MNPs in this system underscores the importance of maintaining concentrations of H_2O_2 and VA within optimal ranges for peroxidative activity on high molecular weight insoluble lignins (Olsen *et al.*, 1991; Hammel *et al.*, 1993). With soluble substrates, this consideration is not as important, because reaction rates are higher due to the proximity of the substrate molecules to the enzyme (and therefore free radicals released from the active site). Thus, the need for control of the concentrations of H_2O_2 and VA can be attributed indirectly to the increased rate limitations imposed by free radical diffusion and stability combined with the need for protection of the enzyme against inactivation by H_2O_2.

The control scheme devised for the reactor using the model of the system appears to maintain the concentrations of both H_2O_2 and VA within ranges in which *in vitro* degradation can occur, since previous *in vitro* attempts at degradation of insoluble lignin in aqueous media without control of these concentrations have invariably failed (Hammel *et al.*, 1993). It is unfortunate that it was not possible to test the model predictions with measured time courses of $[H_2O_2]_B$, $[VA]_B$, $[Mn(II)]_B$, $[Mn(III)\text{-}tart_2]_B$, $[LIP]_B$, and $[MNP]_B$, but the cost to the enzyme stocks would simply have been too high given the difficulty in obtaining large amounts of the LIPs and MNPs. To verify that control was obtained and that it was necessary for degradation to occur, in light of limited enzyme supplies, a "negative" control in which the reactor runs are started at the same initial conditions as the BCs but no pulses are added, will be necessary. A lack of lignin

degradation would indicate that control of $[H_2O_2]_B$, $[VA]_B$, $[LIP]_B$, and $[MNP]_B$ is required for lignin degradation to occur.

The terms in the model which are most likely to cause errors in predictions are the terms dealing with [Mn(III)-$tart_2$] diffusion, stability, and reaction with oxidizable lignin bonds to recycle Mn(II). The stability and diffusion questions can be answered with the application of on-line systems for measurement of the decay constants and effective diffusion coefficient; however, given the complexity of lignin and its oxidizable bonds, it is not likely that values of k_s can be determined which will be anything more than first-order estimates (which is exactly what was done here).

The stability of the model predictions is most sensitive to errors in the [Mn(III)-$tart_2$]-related parameters, followed by the measured diffusion coefficients and the volume of Side B (reaction chamber). The model predictions are relatively insensitive to measured kinetic constants and to enzyme decay constants. It should be noted here that after the model was completed and the LIP kinetic constants were determined, a newer mechanism for the oxidation of aromatic substrates by LIP was published (Gold *et al.*, 1989; Wariishi *et al.*, 1991; Cai and Tien, 1993), indicating that oxidation of aromatic alcohols, etc., by LIP follows essentially the same pathway as oxidation of Mn(II) by MNP, ie.

$$LIP + H_2O_2 \xrightarrow{k_1} LIPI + H_2O \qquad (6\text{-}1)$$

$$H_2O_2 + LIPI \underset{k_{-2}}{\overset{k_2}{\rightleftharpoons}} LIPI\text{-}H_2O_2 \qquad (6\text{-}2)$$

$$LIPI + AH \xrightarrow{k_3} LIPII + A\cdot \qquad (6\text{-}3)$$

$$LIPII + AH \xrightarrow{k_4} LIP + A\cdot \qquad (6\text{-}4)$$

where AH is the oxidizable substrate, and $A\cdot$ is the free radical species formed. This is

the LIP catalytic mechanism presented in Figure 2.5. If this mechanism is correct for the oxidation of VA by LIP, the new rate equation for the formation of veratraldehyde by LIP would be

$$\frac{d[A\cdot]}{dt} = v = \frac{2k_1k_3k_4[LIP]_o[H_2O_2][AH]}{k_3k_4[AH]+k_1k_3[H_2O_2]+k_1k_4[H_2O_2](1+\frac{[H_2O_2]}{K_I})} \quad (6\text{-}5)$$

Again, AH represents VA. Veratraldehyde would be formed in this scheme from the addition of an activated oxygen species to free radical A·, and subsequent loss of $\cdot O_2^-$ anion + H^+. Comparison of this equation with equation (C-11) (derived in Appendix C) indicates that the equations are quite similar, except for the appearance of [VA] in the second term of the denominator, and with the different stoichiometry indicated by the factor of 2 in the numerator. However, it is known that in the oxidation of VA to veratraldehyde by LIP/H_2O_2, formation of free radical species during the reaction does occur (Tien *et al.*, 1986). It is also known that the stoichiometry for VA oxidation by LIP is one VA consumed and one veratraldehyde formed per H_2O_2 consumed, and that the oxidation of VA to veratraldehyde occurs in two consecutive one-electron oxidations by the LIP heme (Tien *et al.*, 1986; Haemmerli *et al.*, 1987; Bono *et al.*, 1990). Therefore, the mechanism used to derive the kinetic rate equation for LIP/VA kinetics is supported by the available literature, while the mechanism above, with 2 substrate molecules oxidized per H_2O_2 consumed, is not. It should be noted, though, that the above mechanism is correct for other substrates such as methoxybenzenes and other lignin model compounds (Tien *et al*, 1986). In any event, the original kinetic equation used is valid for use in the model, since the rate constants were determined from kinetic data -- in effect, an empirical equation could have been used just as effectively, as long as its coefficients were determined accurately from rate data. It is doubtful that any change in the kinetic equations would affect the model predictions, given the relative

insensitivity of the model to the accuracy of the rate constants.

The control scheme for the dialysis reactor system provides a starting point for the development of an on-line system for *in vitro* degradation of insoluble lignin in aqueous media by LIPs and MNPs. The apparent success of the reactor and control scheme in achieving *in vitro* lignin degradation by the peroxidases may in some measure verify that control is necessary, but it does not indicate anything about the accuracy of the predictions or the relative length of time that non-prohibitive concentrations of H_2O_2 and VA were maintained. Time courses of the reagent concentrations and enzyme levels will be absolutely necessary before any on-line system is developed, since verification that the predictions are accurate is necessary in order to maintain precise concentration ranges so that maximum lignin depolymerization can be achieved in the minimum length of time.

6.3 Enzyme Production

Regulation of the production of LIP and MNP by excluding Mn(II) and by adding high concentrations of Mn(II), respectively, to the *P. chrysosporium* cultures had the desired effect of producing LIP stocks which were essentially free of MNP, and vice versa, as shown by the FPLC profiles of the two stocks. The isoenzyme profile for the D5NoMn stock was typical of production of peroxidases by *P. chrysosporium* in acetate buffered culture with low Mn(II). The D4HiMn culture produced higher than expected levels of H3 relative to H4; H4 is normally the major isoenzyme when the fungus is grown in acetate buffered cultures, whereas H3 is the major isoenzyme in the D4HiMn stock. Bonnarme and Jeffries (1990) obtained higher levels of H3 relative to H4 in tartrate buffer after 6 days of cultivation in agitated cultures, using basal levels of Mn(II) (11.15 ppm), but H4 was still the major isoenzyme produced when no Mn(II) was added. It is unknown why the production of H3 exceeded that of H4 in this study (100 ppm Mn(II) added); however, this question is beyond the scope of this study and will not be addressed further.

The enzyme solutions used for the reactor studies were also as desired, with LIP essentially free of MNP, MNP essentially free of LIP, and a mixture of the two with approximately equal amounts of both LIPs and MNPs (equal amounts of protein from each enzyme class, as measured by FPLC peak areas). That some MNP activity was present in the D5NoMn EF was not surprising, as low levels of MNP are produced even if no Mn(II) is added (Bonnarme and Jeffries, 1990), probably partially due to low concentrations of Mn(II) present in the water used for the culture media. The presence of LIP in the D4HiMn EF was a little surprising, however, since no LIP activity was detected in the concentrated, dialyzed EF (no dilution of the sample for LIP activity measurement). Evidently the production of LIP was not completely shut down by 100 ppm Mn(II) addition; it is probable that harvesting the cultures on day 3 instead of day 4 would have resulted in even less LIP in the EF, since LIP peaks between days 5 and 6.

6.4 *In vitro* Treatment of Lignin in the Reactor

The evidence supplied by the various techniques used to characterize the solid and liquid phases recovered from the Base Case runs versus the controls indicate that lignin modification and perhaps some very limited degradation occurred with MNP alone, that very limited degradation may have occurred with LIP alone, and that definite degradation of the lignin occurred in the LIP + MNP Base Case. Each independent line of evidence will be discussed, in turn, below.

6.4.1 Lignin Color Change

Comparison of the color of the lignin from the MNP Alone BC with that of its controls indicates that MNP activity caused a modification of the lignin, since the color of the lignin from all of the controls is identical, while that of the BC lignin is darker. The conversion of aromatic nuclei to quinones in lignin by oxidation with metal oxides is a well known reaction in lignin chemistry (Sarkanen and Ludwig, 1971); perhaps the [Mn(III)-$tart_2$] complex, which is also an oxidizing agent, oxidizes the lignin in a similar

manner. In addition, quinone formation in lignin can make the color of the lignin darker (B. Hames, Personal Communication; Dr. K.E. Hammel, Personal Communication; Dr. J.R. Obst, Personal Communication), although this color change alone does not provide proof that quinones were formed.

The color of the lignin after treatment with LIP alone is not much different from that of the controls, indicating that LIP may not modify the solid lignin to any extent. When both LIP and MNP are present, however, the lignin color darkens initially and then lightens back to near its original color over time, suggesting that the modified groups in the lignin are either being changed back to their original forms or released from the lignin polymer. In addition, this indicates that MNP performs the modification and that LIP is responsible for the return of the color to its original state, since the lignin from the MNP Alone treatment remained dark, while the lignin from the LIP + MNP treatment lightened after initially darkening.

6.4.2 Lignin Recovery from the Reactor Runs

A change of color cannot by itself be used to indicate lignin degradation, but can be used to indicate modification. The solids recoveries for the BCs versus the controls, however, provides more direct evidence that degradation and modification occurred in certain cases. Within the error of the measurement, the mass of solid recovered from the MNP Alone BC increased over the initial amount added to the reactor; no change was seen in the controls. This result is consistent with the observed color change and with oxidation and modification of the solid lignin polymer due to the activity of MNP, since addition of oxygen to the solid would increase its mass. The result says nothing about the putative release of lignin fragments, since an increase in solid mass due to the addition of oxygen to the polymer would increase the mass, while release of fragments would cause a decrease. The increase in mass does suggest, however, that the main activity of the MNP on the solid lignin is to oxidatively modify it.

The mass of solid recovered from the LIP Alone BC, within the error of the

measurement, indicates that little or no modification or release of lignin fragments occurs when LIP is used alone. This result is consistent with the lack of color change for the LIP Alone case, and indicates that LIP has no role in the modification of the lignin as MNP seems to. With LIP and MNP present, however, there is a measurable decrease in the mass of the solid in the BC versus the controls, even taking into account the uncertainties in the weight measurements, the solid recovery measurements (average recovery of solids from several reactor trial runs in which only lignin and buffer were added to the reactor), and the dry weight analyses of the initial lignin (the lignin was added to the reactor as a wet cake to prevent any collapse of the lignin matrix due to drying). It is possible that over the course of the sample handling, much more mass was lost from this sample than the others, but the chance that this would happen in only one sample and not any of the 14 others is slim. The loss of mass in the LIP + MNP BC is consistent with the color change of the solid from light to dark, and back to light, and suggests that the color lightened because the MNP-modified groups were released from the lignin.

6.4.3 FTIR/PLS Analysis of Solid Lignin

Determination of the lignin content of the MNP Alone BC versus its controls by FTIR/PLS indicates that on a per unit mass basis, MNP alone and LIP alone did not alter the lignin content of the substrate, but together, the two enzymes significantly decreased the lignin content. While there is question as to the validity of comparing absolute predictions of the values of the lignin contents between samples run at widely differing times, the predictions are useful with a high degree of confidence within a set of samples measured closely together in time (B. Hames, Personal Communication). This is another independent verification that release of lignin fragments occurred, and only when both enzymes and the reagents necessary for their activity were present. The results of the lignin content analysis are completely consistent with those of both the lignin color observations and the solid mass recoveries for the BCs versus the controls. The

carbohydrate analyses were simply too variable to be of much use, in addition to the fact that the spectral information used with the carbohydrate predictions was outside of the calibration range for the carbohydrates (B. Hames, Personal Communication). It is interesting to note, however, that the predicted carbohydrate content for the LIP + MNP BC is significantly higher than that of its controls (which are close together), and is nearly outside of the uncertainty range for the controls; a higher carbohydrate content relative to lignin would be expected if mass was lost due to lignin release.

The lack of any differences in the methoxyl contents of any of the samples indicates that any degradation which took place was homogeneous with respect to syringyl and guaiacyl units, since syringyl-units contain two methoxyls and guaiacyl units contain only one. This result also indicates that no significant demethoxylation of the solid lignin occurred, which is a known activity of LIP with lignin models and synthetic lignins (Boominathan and Reddy, 1992). Finally, the very low phenolic hydroxyl contents for all samples indicate only that the lignin samples are highly polymeric; ie., that there are few phenolic hydroxyls which are not in intermonomer bonds. This result suggests that intermonomer bond cleavage did not occur to any significant degree in the interior of the polymer, but must have occurred near the end units where the free phenolic hydroxyl content is highest (Sarkanen and Ludwig, 1971).

6.4.4 GC/MS Analysis of Soluble Products

The presence of unique products in the Base Case extracts for all three enzyme cases versus their controls, which were carefully designed to eliminate compounds which could not have been released from the lignin by the enzymes, suggests that there was a release of lignin fragments catalyzed by both enzymes over the course of the 12 hour reaction, alone (although to a limited degree, as evidenced by the mass recovery data and the FTIR) and in combination. Consideration of the mass spectra and molecular formulas possible for each compound indicates that reasonable structures that could be lignin-derived are possible for all unique products found in the extracts of all three

enzyme cases. In the case of LIP alone, the presence of relatively substantial amounts of *p*-hydroxybenzoic acid (a known *in vivo* lignin degradation product; Chen and Chang, 1982) in the BC extracts but not in the controls suggests than some depolymerization occurred, notwithstanding the mass recovery data and the FTIR/PLS predictions of lignin content. The presence of 2,6-dimethoxyhydroquinone in both the MNP Alone and LIP + MNP extracts in concentrations too high to be accounted for solely by extractable syringaldehyde, and the absence of the quinone form (Dr. M.H. Gold, Personal Communication; see Chapter V) suggests that some depolymerization occurred in both the MNP and LIP + MNP enzyme cases. It is well known that quinones and hydroquinones are often present during the biodegradation of lignin (Chung *et al.*, 1993), which provides additional support for the presumption that some of the 2,6-dimethoxyhydroquinone and its quinone form may have originated through release by MNP from the solid lignin polymer. For peaks for which only questionable structures were found, such as partially-formed quinone-like structures in which there is an oxo-group at position 4 of the ring and a saturated carbon-carbon bond at position 1 (these structures most likely would not be formed from an aromatic ring), it should be noted that one of the first assumptions made in the structural analysis was that the products had to have an intact ring with one or more double bonds within the ring structure. This assumption precludes any ring-opened structures, which might account for the difficulty in assigning lignin-like structures to some of these products. It is interesting that the peaks for which the great majority of these types of structures were proposed eluted the GC columns at or below scans 500-600 (corresponding to retention times earlier than about 7.3 minutes to about 9 minutes for the DB-1 GC column). It was noted during analysis of the GC/MS data that compounds in which the molecular ion was also the base peak (100 % abundance), which are likely to be aromatic because of the stability afforded by the conjugated ring, did not tend to elute the GC columns until around scan 600 or after, unless they were quite volatile (such as the internal standard, 2-chloro-5-

trifluoromethylbenzoic acid, which is more volatile due to the fluorine atoms).

It is possible that the unique products observed are enzyme oxidation products of soluble lignin extractives, such as syringaldehyde, which were not completely removed during the exhaustive solvent extractions of the C-AH residue to produce the EC-AH lignin substrate; a control to eliminate this sort of product was not forthcoming. It is entirely possible, then, that the products seen in the LIP Alone and MNP Alone BC extracts are this type of product since the mass recovery data and the FTIR/PLS analyses do not support that significant lignin degradation occurred; however, in the case of the LIP + MNP BC extracts, both of the aforementioned analyses indicated loss of mass as lignin, and so it is reasonable to expect that the unique products identified in the extracts are lignin-derived and are released by enzyme activity.

Another interesting result of the GC/MS analysis, but one which cannot be used as proof of lignin degradation, is the multiple simultaneous peaks in the TICs at or below the level of the noise, of various combinations of the mass fragments 107, 137, 151, 167, and 181, which are typical electron-impact ion fragments of lignin-derived products. These occurrences were more frequent in the base case extracts than in the controls, suggesting that there were many possible lignin-derived compounds present that were simply at too low of a concentration to be detected. This suggestion is supported by the fact that the baseline in the TICs of the solid extracts of the BCs for all three enzyme cases ramped up at later retention times, suggesting the presence of higher molecular weight, low concentration compounds; many simultaneous peaks of the fragments listed above were present, especially in this region. While this phenomenon occurred to some extent in the controls as well, the effect was more pronounced in the BC extracts.

It is quite clear that more information will be necessary before any of the products found can be attributed to release from the lignin. It will certainly be necessary to use tools such as ^{13}C NMR to characterize the compounds, since GC/MS is only suited to that task if authentic standards are available. It might have been better to use ^{13}C-ring-

labelled VA in the reactor runs to aid in the exclusion of VA derived products -- this approach was initially considered, but the ring-labelled compound would have been simply too expensive to justify the cost; it was decided instead to use a system of controls to exclude VA products.

6.5 Significance

It is unquestionable that both LIP and MNP can cleave lignin model dimers in aqueous media and release fragments from synthetic lignins dispersed in organic solvents (Hammel *et al.*, 1985; Hammel and Moen, 1991; Hammel *et al.*, 1993; Perez and Jeffries, 1993; Tuor *et al.*, 1992; Boyle *et al.*, 1992). Because depolymerization of a high molecular weight lignin in an aqueous system has not previously been demonstrated (Tien, 1987; Boominathan and Reddy, 1992), this brings into question whether these enzymes are actually involved in the *in vivo* degradation of lignin (Sarkanen *et al.*, 1991). Indeed, Dordick *et al.* (1986) clearly demonstrated that both horseradish peroxidase and milk lactoperoxidase, while unable to degrade either synthetic or natural lignins in aqueous media, were able to depolymerize polyconiferyl alcohol, milled wood lignin, and Kraft pine lignin in dioxane, DMF, or methylformate containing 5 % aqueous buffer. This suggests that the inability of peroxidases to degrade the lignin in aqueous media is most probably due to simple inaccessibility of the enzymes or the active oxidizing species to close proximity of the insoluble lignin; it is probable that LIPs and MNPs would behave similarly when in aqueous media versus nonaqueous media (Ryu and Dordick, 1992).

The significance of this study to the lignin biodegradation field is clear, since it has not been proven that LIPs or MNPs possess the ability to take an active role in the *in vivo* degradation of lignin by white rot fungi. This is the first direct *in vitro* evidence with an insoluble natural lignin in aqueous media that these enzymes do take part in the depolymerization of lignin. While each separate piece of evidence does not prove that lignin was depolymerized, when considered as a whole, it seems clear that lignin was

degraded when both enzymes were present, but not to any significant extent when each enzyme was used singly. MNP appeared to modify the lignin (color change combined with increase in mass), and when LIP was also present, the color initially changed but later returned to normal and lignin was released. These results support the conclusions of Perez and Jeffries (1992) that MNP performs the initial stages of depolymerization, but that LIP performs the bulk of the depolymerization. The results of this study also support the conclusions of Tuor *et al.* (1992), namely that LIP and MNP act synergistically to degrade lignin. The results do not, however, support the conclusions of Sarkanen *et al.* (1991) that the role of LIP in lignin degradation is to detoxify aromatics released by other enzymes, by polymerizing the compounds into high molecular weight, insoluble molecules.

6.6 Conclusions

The results of this study indicate that both the LIPs and MNPs of *P. chrysosporium* take part in the depolymerization of lignin. MNPs appear to catalyze the initial steps of the degradation through modification of the lignin, perhaps introducing functional groups into the lignin which make it a more suitable substrate for the LIPs. It is unclear whether singly these enzymes released any soluble fragments from the lignin at all, since the mass recovery data and FTIR/PLS results did not show any loss of solid mass or decrease in lignin content, while the GC/MS data suggested that some fragments might have been released. From the complexity of the GC/MS analysis, it is also clear that no soluble products are released at high enough concentrations to be accurately used singly as an indicator of the extent of lignin depolymerization for use in enzyme accessibility studies, but that simple lignin content measurements would probably suffice.

6.7 Future Directions

The next direction that a continuation of this work must take is in direct proof that the unique compounds identified by GC/MS are indeed lignin fragments, and that they are released by enzyme activity and are not merely products of the oxidation of soluble

lignin extractives by the enzymes. A variety of approaches might be used for this task, such as the addition of a control in which the lignin is first run in the reactor as an ER$^-$ control, and then the liquid phase recovered is subjected to enzyme activity. Simpler methods for the exclusion of VA derived products should be developed, such as the use of nonlabelled VA and ^{13}C-ring-labelled lignin to exclude peaks, or by using ^{14}C-ring-labelled lignin with radioactivity measurements coupled with GC to verify that the products came from the lignin. The use of milled wood lignin, either labelled or unlabelled, in the reactor in aqueous media could provide information on decreases in molecular weight of the polymer, since milled wood lignins are insoluble in water but are soluble in lignin solvents. Finally, purified LIPs and MNPs will eventually have to be used in the system in order to completely exclude the possibility that unique products present are not the products of other enzyme activities present.

APPENDICES

APPENDIX A

Assays

A.1 LIP Assay

This assay measures lignin peroxidase activity as described by Tien and Kirk (1984). This is done spectrophotometrically at room temperature (23 °C) by measuring the rate of veratraldehyde formation from veratryl alcohol in the presence of H_2O_2. One U/L of LIP activity is then defined as one μmole of veratraldehyde formed per liter per minute at these conditions, using an extinction coefficient (Tien *et al.*, 1986) of 9300 M^{-1} cm^{-1}. Stock solutions are as follows: (A.) 125 mM Tartaric Acid, pH 2.50; (B.) 40 mM Veratryl Alcohol (VA); and (C.) 8 mM H_2O_2 (make fresh daily). Reaction mix for 50 assays is prepared by mixing 20 mL of Stock A, 2.5 mL of Stock B, and 2.5 mL of Stock C.

The assay is performed as follows: (1.) blank the spectrophotometer at 310 nm with water in quartz cuvets; (2.) add 0.5 mL of sample containing lignin peroxidase to an empty quartz cuvet; (3.) add 0.5 mL of reaction mix and quickly mix by placing a piece of parafilm over the cuvet and inverting several times; (4.) measure the absorbance change with a chart recorder for at least 1 minute. Typical chart recorder settings are 100 mV and 5 cm/min for an activity range of 50 to 500 U/L. The slope of the recorder trace in (OD/min) is then measured and the LIP activity is calculated as:

$$[LIP](U/L) = \frac{slope(\frac{OD}{min}) \times (1000\mu L/500\mu L) \times (10^6 \mu mol/mol)}{9300\ M^{-1}cm^{-1} \times (1\ cm)} \qquad \text{(A-1)}$$

A.2 MNP Assay #1

This assay measures manganese peroxidase activity by following the oxidation of phenol red dye as described by Kuwahara *et al.* (1984) and Michel *et al.* (1991). Reaction takes place at 30 °C for 4 minutes in test tubes. Extent of reaction after 4 minutes is measured spectrophotometrically at 610 nm. One U/L of MNP activity is then

defined as one μmole of phenol red oxidized per liter per minute, using an extinction coefficient of 4460 M^{-1} cm^{-1} (Michel *et al.*, 1991). Stock solutions are as follows: (A.) 500 mM Na-Lactate, pH 4.50; (B.) 400 mM Na-Succinate, pH 4.50; (C.) 2 % (w/v) Egg albumin (discard every month); (D.) 0.2 % (w/v) Sodium salt of Phenol Red dye; (E.) 20 mM $MnSO_4$; and (F.) 20 mM H_2O_2 (make fresh daily). Reagent I is prepared (99.5 mL) by adding 5 mL of Stocks A, B, C, and D, 0.5 mL of Stock E, and 79 mL of distilled water. Reaction mix (Reagent II) for 50 assays is prepared by mixing 49.75 mL of Reagent I and 0.25 mL of solution F. Reagent II should be prepared fresh daily.

The assay is performed as follows: (1.) add 20 to 40 μL of sample containing manganese peroxidase to a test tube (also prepare two blanks by adding 20 to 40 μL of distilled water (same volume as sample) to two test tubes); (2.) add 1 mL of Reagent II to each tube and incubate for 4 minutes in a water bath at 30 °C; (3.) when the reaction has proceeded for 4 minutes, add 40 μL of 2 N NaOH to stop the reaction, and quickly mix the tubes; (4.) transfer the samples to cuvets (quartz cuvets are not necessary) and blank the spectrophotometer at 610 nm with the two sample blanks; (5.) measure the absorbance of the sample at 610 nm. The MNP activity (eg. for a 20 μL sample) is then calculated as:

$$[MNP](U/L) = \frac{\Delta A_{610} \times (1060 \mu L/20 \mu L) \times (10^6 \mu mol/mol)}{(4 \text{ min}) \times 4460\ M^{-1}cm^{-1} \times (1\ cm)} \quad \text{(A-2)}$$

A.3 MNP Assay #2

This assay measures manganese peroxidase activity as described by Olsen *et al.* (1991). This is done spectrophotometrically at room temperature (23 °C) by measuring the rate of oxidation of phenol red dye in the presence of H_2O_2. One U/L of MNP activity is then defined as an increase of one absorbance unit at 530 nm per minute per liter of sample (Olsen *et al.*, 1991). Stock solutions are as follows: (A.) 0.11 g/L sodium salt of phenol red dye, 1.1 g/L Ovalbumin, 2.5 mL/L of 85 % Lactic Acid, in

20 mM Na-Succinate, pH 4.50; (B.) 10 mM $MnSO_4$ in 20 mM Na-Succinate, pH 4.50; and (C.) 9.8 mM H_2O_2 (prepared fresh daily).

The assay is performed as follows: (1.) add 900 μL of Stock A to a quartz cuvet; (2.) add 100 μL of sample/distilled water to the cuvet; (3.) add 10 μL of Stock B to the cuvet; (4.) mix the contents of the cuvet by placing a piece of parafilm over the cuvet and inverting several times; (5.) blank the spectrophotometer with this cuvet at 530 nm; (6.) add 10 μL of Stock C to the cuvet; (7.) immediately mix the contents of the cuvet by placing a piece of Parafilm over the cuvet and inverting several times; and (8.) record the absorbance at 530 nm for 30 seconds at room temperature (23 °C) on a chart recorder. The absorbance change is linear within a range of 0.05 to 0.20 OD/min (samples should be kept within this range). Typical chart recorder settings are 10 mV and 5 cm/min. The absorbance change is then measured from the slope of the recorder trace in (OD/min) and the MNP activity (eg. for a 100 μL sample) is calculated as:

$$[MNP](U/L) = \frac{\Delta A_{530} \times (10^3 mL/L)}{(0.5\ \text{min}) \times (0.100\ mL)} \qquad \text{(A-3)}$$

A.4 H_2O_2 Assay

This assay measures H_2O_2 by following the decolorization of Remazol Brilliant Blue R dye as described by Muheim *et al.* (1990). This is done spectrophotometrically at room temperature (23 °C) by measuring the overall absorbance change at 585 nm when Remazol Brilliant Blue R dye is decolorized by Horseradish Peroxidase in the presence of H_2O_2. Stock solutions are as follows: (A.) 400 μg/mL Horseradish peroxidase Type II (HRP) in phosphate buffer, pH 7.00, frozen in 101 μL aliquots in Eppendorf tubes; (B.) 0.1 % (w/v) Remazol Brilliant Blue R dye; (C.) 200 mM 2,2-dimethyl succinic acid (DMS), pH 7.00, and (D.) H_2O_2 standards ranging in concentration from 5 to 60 μM (make fresh daily). Before preparing the reaction mix, the frozen HRP is thawed and 899 μL of distilled water is added and the tube mixed.

Reaction mix for 20 assays is then prepared by mixing the diluted contents of the HRP tube with 0.5 mL of Stock B, 5 mL of Stock C, and 3.5 mL of distilled water.

The assay is performed as follows: (1.) blank the spectrophotometer at 585 nm with 0.5 mL of reaction mix and 0.5 mL of water (quartz cuvets are not necessary); (2.) place a cuvet containing 0.5 mL of reaction mix into the sample cell; (3.) add 0.5 mL of sample containing H_2O_2 in the range 3 to 30 μM; (4.) quickly close the spectrophotometer lid and measure the absorbance change with a chart recorder until no there is further decrease in absorbance. Typical chart recorder settings are 50 mV and 5 cm/min for an H_2O_2 concentration range of 3 to 30 μM. The H_2O_2 standards are also measured in this manner and the absorbance changes fit versus H_2O_2 concentration using linear regression. Sample concentrations are then calculated from this relationship.

A.5 Veratryl Alcohol (VA) Assay

This assay measures veratryl alcohol concentrations using lignin peroxidase to catalyze its oxidation to veratraldehyde, with a method similar to that of Leisola *et al.* (1986). This is done spectrophotometrically at room temperature (23 °C) by measuring the overall absorbance change at 310 nm when veratryl alcohol is oxidized to veratraldehyde by lignin peroxidases from *P. chrysosporium* in the presence of H_2O_2. Stock solutions are as follows: (A.) Dialyzed crude extracellular fluid from a Day 6 culture of *P. chrysosporium* in 10 mM acetate buffer, pH 6.00, containing 100 to 200 U/L of LIP activity as measured by the LIP Assay above, and frozen in 10 mL aliquots in test tubes; (B.) 125 mM Tartaric Acid, pH 2.50; (C.) 8 mM H_2O_2 ; and (D.) VA standards ranging in concentration from 0.1 to 1.6 mM (make fresh weekly). Before preparing the reaction mix, the frozen extracellular fluid is thawed. Reaction mix for 10 assays is prepared by mixing 4 mL of Stock B with 0.5 mL of Stock C.

The assay is performed as follows: (1.) blank the spectrophotometer at 310 nm with water in quartz cuvets; (2.) add 450 μL of reaction mix to an empty quartz cuvet; (3.) add 50 μL of sample containing VA in the range 0.1 to 1.6 mM; (4.) mix by placing

a piece of parafilm over the cuvet and inverting several times; (5.) place the cuvet into the sample cell; (6.) add 0.5 mL of the thawed dialyzed extracellular fluid; (4.) quickly close the spectrophotometer lid and measure the absorbance change with a chart recorder until no there is further increase in absorbance. Typical chart recorder settings are 100 mV and 2 cm/min for a sample concentration range of 0.1 to 1.6 mM. The VA standards are also measured in this manner and the absorbance changes fit versus VA concentration using linear regression. Sample concentrations are then calculated from this relationship.

APPENDIX B

Derivation of H_2O_2 and VA Transport Equations

For simple diffusion across a membrane from Side A to Side B, the mass balances may be written as

$$V_A \frac{dC_A}{dt} = -Aj \tag{B-1}$$

and

$$V_B \frac{dC_B}{dt} = Aj \tag{B-2}$$

The flux j is given by

$$j = \frac{D^{eff} H}{l}(C_A - C_B) \tag{B-3}$$

where H is a partition coefficient between the bulk fluid and the membrane. Letting H = 1, we see that

$$\frac{dC_A}{dt} = -\frac{D^{eff} A}{l V_A}(C_A - C_B) \tag{B-4}$$

and

$$\frac{dC_B}{dt} = \frac{D^{eff} A}{l V_B}(C_A - C_B) \tag{B-5}$$

These are the transport equations used directly in the derivation of the unsteady state model for the reactor (for H_2O_2 and Mn(II)). Experiment showed (see Results) that D^{eff} for VA depended on VA concentration, due to increasing solution viscosity with increasing VA concentration; this dependence was found to be exponential. It was also found (see Results) that the VA concentration versus time data were approximated best when an additional exponential term was included; this additional exponential dependence was interpreted as being the result of VA aggregation in water (VA is relatively insoluble

in water). Combining these exponential relationships with the Stokes-Einstein equation (Bird *et al.*, 1960) gives

$$D = \frac{kT}{6\pi r\mu} = \frac{kT}{6\pi r^{\circ} e^{\frac{a_1}{[VA]}} \mu^{\circ} e^{\alpha[VA]}} \qquad \text{(B-6)}$$

where α and μ° are from the fit of the viscosity data, and r° and a_1 are empirical constants. In the Stokes-Einstein equation, k is the Boltzmann constant, T is absolute temperature, r is molecular radius, and μ is solution viscosity. It should be noted that the Stokes-Einstein equation os only valid for dilute solutions (Bird *et al.*, 1960). Since the concentrations of VA to be used in the reactor runs were low, the high VA concentration data from the diffusion experiments wer edropped when the effective diffusion coefficient parameters for VA were calculated (see below). Combining constants (T is kept constant in the experiments at 37 °C) into D°, and combining the exponential terms gives

$$D = D^{\circ}_{VA} e^{-\beta[VA]}$$
$$D^{\circ}_{VA} = \frac{kT}{6\pi r^{\circ}\mu^{\circ}}; \quad \beta = \left(\alpha + \frac{1}{a_1}\right) \qquad \text{(B-7)}$$

For pseudo steady state diffusion across a membrane,

$$\frac{d[VA]_B}{dt} = -\frac{A}{lV_B}\int_{[VA]_A}^{[VA]_B} D(c)dt \qquad \text{(B-8)}$$

Inserting the expression for the effective diffusion coefficient for VA and integrating gives

$$\frac{d[VA]_B}{dt} = \frac{D^{\circ}_{VA}A}{\beta lV_B}\left(e^{-\beta[VA]_B} - e^{-\beta[VA]_A}\right) \qquad \text{(B-9)}$$

This is the form of the VA transport used in the derivation of the reactor model. Combining equations (B-4 through B-9) we get

$$\frac{d}{dt}(C_A - C_B) = -\gamma D^{eff}(C_A - C_B)$$
$$\gamma = \frac{A}{l}\left(\frac{1}{V_A} + \frac{1}{V_B}\right) \qquad \text{(B-10)}$$

Solution of this equation gives

$$\ln\left(\frac{C_A - C_B}{C_{A_o} - C_{B_o}}\right) = -\gamma D^{eff} t \qquad \text{(B-11)}$$

Knowledge of the cell measurements, initial concentrations, and concentrations at a certain time into the experiment allows calculation of D^{eff} (for H_2O_2 and Mn(II)). For VA, it was necessary to solve equation (B-9) for $[VA]_B$ and fit the solution to the data by trial and error since the values of D° and a_1 were unknown (α was known from the viscosity data). The solution to equation (B-9) is

$$[VA]_B = \frac{1}{\beta}\ln\left(\tanh\left(e^{-\frac{1}{2}\beta([VA]_A^\circ + [VA]_B^\circ)}\left(\frac{D_{VA}^\circ A}{lV_B}\right)t + \tanh^{-1}\left(e^{\frac{1}{2}\beta([VA]_B^\circ - [VA]_A^\circ)}\right)\right)\right)$$
$$+ \frac{1}{2}([VA]_A^\circ + [VA]_B^\circ) \qquad \text{(B-12)}$$

This equation was used in a trial and error shooting method the find the best values of the unknown parameters.

APPENDIX C

Derivation of Enzyme Kinetic Equations

C.1 Kinetics of Veratryl Oxidation by LIP

The reactions proposed by Tien *et al.* (1986) for the oxidation of veratryl alcohol to veratraldehyde by LIP, namely, two substrate ping-pong kinetics with competitive inhibition by H_2O_2 and two-step oxidation of veratryl alcohol are

$$H_2O_2 + Cpd0 \xrightarrow{k_1} CpdI + H_2O \tag{4-6}$$

$$H_2O_2 + CpdI \underset{k_{-2}}{\overset{k_2}{\rightleftharpoons}} CpdI\text{-}H_2O_2 \tag{4-7}$$

$$VA + CpdI \xrightarrow{k_3} CpdII\text{-}VA\cdot \tag{4-8}$$

$$CpdII\text{-}VA\cdot \xrightarrow{k_4} VA_{ox} + Cpd0 \tag{4-9}$$

where Cpd0, CpdI and CpdII represent the different oxidation states of the LIP heme, and VA_{ox} is veratraldehyde (Tien *et al.*, 1986). The rates of consumption of H_2O_2 and VA, and the rate of production of veratraldehyde are

$$\frac{d[H_2O_2]}{dt} = -k_1[H_2O_2][Cpd0] - k_2[H_2O_2][CpdI] + k_{-2}[CpdI\text{-}H_2O_2] \tag{C-1}$$

$$\frac{d[VA]}{dt} = -k_3[VA][CpdI] \tag{C-2}$$

$$\frac{d[VA_{ox}]}{dt} = k_4[CpdII\text{-}VA\cdot] \tag{C-3}$$

The rates of change of the LIP intermediates are

$$\frac{d[CpdI]}{dt} = k_1[H_2O_2][Cpd0] - k_2[H_2O_2][CpdI] + k_{-2}[CpdI\text{-}H_2O_2] - k_3[VA][CpdI] \quad \text{(C-4)}$$

$$\frac{d[CpdI\text{-}H_2O_2]}{dt} = k_2[H_2O_2][CpdI] - k_{-2}[CpdI\text{-}H_2O_2] \quad \text{(C-5)}$$

$$\frac{d[CpdII\text{-}VA^{\cdot}]}{dt} = k_3[VA][CpdI] - k_4[CpdII\text{-}VA^{\cdot}] \quad \text{(C-6)}$$

Applying the Steady State Assumption (SSA) to each of these equations and using an overall enzyme balance:

$$[LIP]_o = [Cpd0] + [CpdI] + [CpdI\text{-}H_2O_2] + [CpdII\text{-}VA^{\cdot}] \quad \text{(C-7)}$$

we get

$$[Cpd0] = \frac{[LIP]_o}{1 + \frac{k_1[H_2O_2]}{k_3[VA]}\left(1+\frac{[H_2O_2]}{K_I}\right) + \frac{k_1[H_2O_2]}{k_4}} \quad \text{(C-8)}$$

where

$$K_I = \frac{k_{-2}}{k_2} \quad \text{(C-9)}$$

We also find that

$$v = \frac{d[VA_{ox}]}{dt} = -\frac{d[H_2O_2]}{dt} = -\frac{d[VA]}{dt} \quad \text{(C-10)}$$

Combining equations (C-2), (C-4), (C-8), and (C-10), after rearrangement, gives the kinetic rate equation

$$v=\frac{k_1k_3k_4[LIP]_o[H_2O_2][VA]}{k_3k_4[VA]+k_1k_3[H_2O_2][VA]+k_1k_4[H_2O_2](1+\frac{[H_2O_2]}{K_I})} \qquad \text{(C-11)}$$

C.2 Kinetics of Mn(II) Oxidation by MNP

The reactions for the oxidation of Mn(II) to Mn(III) by MNP, namely, two substrate peroxidase ping-pong kinetics (Wariishi *et al.*, 1989a) are

$$MNP + H_2O_2 \xrightarrow{k_5} MNPI + H_2O \qquad \text{(4-15)}$$

$$MNPI + Mn(II) \xrightarrow{k_6} MNPII + Mn(III) \qquad \text{(4-16)}$$

$$MNPII + Mn(II) \xrightarrow{k_7} MNP + Mn(III) \qquad \text{(4-17)}$$

$$Mn(III) + AH \xrightarrow{k_8} Mn(II) + A\cdot \qquad \text{(4-18)}$$

where MNP, MNPI and MNPII represent the different oxidation states of the MNP heme, and AH is oxidizable lignin bonds. Since the kinetic experiments to be performed with MNP only encompassed the first three reactions, the fourth reaction is left out of these derivations. The form of the rate equation containing the term for this reaction is presented at the end of the derivation. The rates of consumption of H_2O_2 and Mn(II), and the rate of production of Mn(III) are

$$\frac{d[H_2O_2]}{dt} = -k_5[H_2O_2][MNP] \qquad \text{(C-12)}$$

$$\frac{d[Mn(II)]}{dt} = k_6[MNPI][Mn(II)] - k_7[MNPII][Mn(II)] \qquad \text{(C-13)}$$

$$\frac{d[Mn(III)]}{dt} = k_6[MNPI][Mn(II)] + k_7[MNPII][Mn(II)] \qquad \text{(C-14)}$$

The rates of change of the MNP intermediates are

$$\frac{d[MNPI]}{dt} = k_5[H_2O_2][MNP] - k_6[MNPI][Mn(II)] \qquad \text{(C-15)}$$

$$\frac{d[MNPII]}{dt} = k_6[MNPI][Mn(II)] - k_7[MNPII][Mn(II)] \qquad \text{(C-16)}$$

Applying the Steady State Assumption (SSA) to each of these equations and using an overall enzyme balance:

$$[MNP]_o = [MNP] + [MNPI] + [MNPII] \qquad \text{(C-17)}$$

we get

$$[MNP] = \frac{[MNP]_o}{1 + \frac{k_5[H_2O_2]}{k_6[Mn(II)]} + \frac{k_5[H_2O_2]}{k_7[Mn(II)]}} \qquad \text{(C-18)}$$

We also find that

$$v = \frac{d[Mn(III)]}{dt} = -\frac{d[Mn(II)]}{dt} - 2\frac{d[H_2O_2]}{dt} \qquad \text{(C-19)}$$

Combining equations (C-13), (C-15), (C-18), and (C-19), after rearrangement, gives the kinetic rate equation

$$v = \frac{2k_5k_6k_7[MNP]_o[H_2O_2][Mn(II)]}{k_5k_6[Mn(II)] + k_5(k_6 + k_7)[H_2O_2]} \qquad \text{(C-20)}$$

Since k_6 and k_7 appear both as a product and as a sum in this rate equation, neither can be determined from simple kinetic experiments encompassing the first three reactions. Thus, a parameter, Ψ, was defined to remove them from the equation and allow the ratio of the sum and the product of k_6 and k_7 to be calculated from the intercept of a double reciprocal plot of rate versus inverse concentration data. The parameter Ψ is defined, then, as

$$\Psi = \frac{k_6 + k_7}{k_6k_7} \qquad \text{(C-21)}$$

Solving this relationship for k_6k_7 and inserting the solution into the above rate equation gives

$$v = \frac{2k_5[MNP]_o[H_2O_2][Mn(II)]}{[Mn(II)] + 4k_5\Psi[H_2O_2]} \qquad \text{(C-22)}$$

This is the form of the rate equation used for the kinetic studies for MNP. Note that the "4" in the denominator comes from the use of 2 mM $MnSO_4$ in the kinetic experiments (see Chapter IV). The form of the rate equation used in the reactor model included the fourth (non-MNP dependent) reaction. With this reaction included, the rate equation becomes

$$v_{total} = \frac{2k_5[MNP]_o[H_2O_2][Mn(II)]}{[Mn(II)] + 4k_5\Psi[H_2O_2]} - k_8[Mn(III)][AH] \qquad \text{(C-23)}$$

APPENDIX D

FORTRAN PROGRAMS

D.1 FORTRAN Simulation of Reactor

D.1.1 Variables Used In FORTRAN Program RKG.FOR

a. Double Precision Variables

Variable	Units	Description
aa	mM/(U/L)	Temporary value of alp
aah	mM	Temporary value of ah(2)
ah(2)	mM	Concentration of oxidizable lignin bonds
ahconc	mM	Variable used in dilution calculations for oxidizable lignin bonds
alp	mM/(U/L)	Ratio of maximum [H2O2]B to maximum [LIP]
apvol	mL	Volume pulsed to Side A
arange	%/100	Fraction over minimum [H2O2]B for pulse
area	cm^2	Cross-sectional area for transport
a1	mM	Radius exponent from Deff(VA)
a2	mM	Viscosity exponent from Deff(VA)
bb	mM/(U/L)	Temporary value of bta
bpvol	mL	Volume pulsed to Side B
brange	%/100	Fraction under maximum [VA]B for pulse
bta	mM/(U/L)	Ratio of maximum [VA]B to maximum [LIP]
delta	%/100	Fractional correction to transport rates
dfpv	---	Derivative of function for Newton's Method
dm	cm^2/min	Effective diffusion coefficient for Mn(II)
dm3	cm^2/min	Effective diffusion coefficient for [Mn(III)-(tart)2] complex
dp	cm^2/min	Effective diffusion coefficient for H2O2
dv	cm^2/min	Diffusion coefficient for VA at infinite dilution
convrt	(Uo/L)/(Up/L)	Conversion factor from the Patent U/L MNP to our U/L MNP
ee	mM/(U/L)	Temporary value of eps
eps	mM/(U/L)	Ratio of maximum Mn(II) to maximum MNP
fpv	---	Function for Newton's Method
frac1	---	Fraction of g2/(f2/f1) to make g1
frac2	---	Fraction of f2 to make g2
fr1pct	%/100	Increase of g1 per consecutive pulse
fr2pct	%/100	Decrease of g2 per consecutive pulse
fr3pct	%/100	Decrease of g3 per consecutive pulse
f1	---	Ratio of initial rates of VA transport to VA consumption
f2	---	Ratio of initial rates of peroxide transport to peroxide consumption
f2ovf1	---	Ratio of f2 to f1
f3	---	Ratio of [H2O2]A after pulse to initial [H2O2]A (no enzyme added)
f4	---	Additional fraction of f3 (enzyme added)
g	mL	Guess used in Newton's Method

gma	mM^{-1}	Exponent in VA diffusion coefficient ($= 1/a_1 + 1/a_2$)
gt	mL	Temporary value of g
g1	---	Ratio of rates of VA transport to VA consumption after pulse
g2	---	Ratio of rates of peroxide transport to peroxide consumption after pulse (LIP pulsed alone)
g3	---	Ratio of rates of peroxide transport to peroxide consumption after pulse (LIP and MNP pulsed together)
h	min	Time step size
initlo	U/L	Initial [LIP] activity
inimo1	U/L	Initial D5NoMn [MNP] activity
inimo2	U/L	Initial D4HiMn [MNP] activity
kah(4)	mM	Runge-Kutta-Gill approximation constants for oxidizable lignin bonds
kdl1	U/L/hr	Zero-order decay constant for LIP
kdl2	hr^{-1}	First-order decay constant for LIP
kdma	hr^{-1}	First-order decay constant for D5NoMn MNP
kdmb	hr^{-1}	First-order decay constant for D4HiMn MNP
ki	mM	Inhibition constant for peroxide in LIP/VA kinetics
kma(4)	---	Runge-Kutta-Gill approximation constants for Side A Mn(II)
kmb(4)	---	Runge-Kutta-Gill approximation constants for Side B Mn(II)
km3a(4)	---	Runge-Kutta-Gill approximation constants for Side A [Mn(III)-(tart)2] complex
km3b(4)	---	Runge-Kutta-Gill approximation constants for Side B [Mn(III)-(tart)2] complex
kpa(4)	---	Runge-Kutta-Gill approximation constants for Side A peroxide
kpb(4)	---	Runge-Kutta-Gill approximation constants for Side B peroxide
kva(4)	---	Runge-Kutta-Gill approximation constants for Side A VA
kvb(4)	---	Runge-Kutta-Gill approximation constants f8or Side A VA
k1	$[min(U/L)]^{-1}$	Rate constant for 1st step in LIP/VA kinetics
k3	$[min(U/L)]^{-1}$	Rate constant for 2nd step in LIP/VA kinetics
k4	$mM[min(U/L)]^{-1}$	Rate constant for 3rd step in LIP/VA kinetics
k5a	$[min(U/L)]^{-1}$	Rate constant for 1st step in MNP/MN(II) kinetics (for D5NoMn MNP)
k5b	$[min(U/L)]^{-1}$	Rate constant for 1st step in MNP/Mn(II) kinetics (for D4HiMn MNP)
k8	$[min\ mM]^{-1}$	Rate constant for oxidation of lignin bonds by [Mn(III)-(tart)2] complex
lip	U/L	[LIP] activity at time t
lo	U/L	[LIP] activity at reference time zero
lotmp	U/L	Temporary value of lo
lrange	%/100	Ratio of minimum [LIP] to initial [LIP]
lth	cm	Wet membrane thickness

ma(2)	mM	Concentration of Mn(II) in Side A
maconc	mM	Variable used in dilution calculations for Mn(II) in Side A
m3acnc	mM	Variable used in dilution calculations for [Mn(III)-(tart)2] complex in Side A
mb(2)	mM	Concentration of Mn(II) in Side B
mma	mM	Temporary value of Mn(II) in Side A, used in Runge-Kutta-Gill solution
mmb	mM	Temporary value of Mn(II) in Side B, used in Runge-Kutta-Gill solution
mm3a	mM	Temporary value of [Mn(III)-(tart)2] complex in Side A, used in Runge-Kutta-Gill solution
mm3b	mM	Temporary volue of [Mn(III)-(tart)2] complex in Side A, used in Runge-Kutta-Gill solution
mnp	U/L	Total [MNP] activity at time t
mnp1	U/L	D5NoMn [MNP] activity at time t
mnp2	U/L	D4HiMn [MNP] activity at time t
mo	U/L	Total [MNP] activity at reference time zero
mo1	U/L	D5NoMn [MNP] activity at reference time zero
mo2	U/L	D4HiMn [MNP] activity at reference time zero
mo1tmp	U/L	Temporary value of mo1
mo2tmp	U/L	Temporary value of mo2
mrange	%/100	Ratio of minimum [MNP] to initial [MNP]
m3a(2)	mM	Concentration of [Mn(III)-(tart)2] complex in Side A
m3b(2)	mM	Concentration of [Mn(III)-(tart)2] complex in Side B
pao	mM	Initial value of pa(2)
pa(2)	mM	Concentration of peroxide in Side A
paconc	mM	Variable used in pulse concentration calculations for H2O2 in Side A
pastnd	mM	Temporary value of patemp
patemp	mM	Standard (repetitive) H2O2 pulse concentration for pulses to Side A
pb(2)	mM	Concentration of peroxide in Side B
pbmax	mM	Maximum concentration of H2O2 in Side B
pbmin	mM	Minimum concentration of H2O2 in Side B
plconc	U/L	[LIP] pulse concentration for Side B
pltemp	U/L	Temporary value of plconc
pmconc	U/L	Total [MNP] pulse concentration for Side B
pm1cnc	U/L	D5NoMn [MNP] pulse concentration for Side B
pm2cnc	U/L	D4HiMn [MNP] pulse concentration for Side B
pm1tmp	U/L	Temporary value of pm1cnc
pm2tmp	U/L	Temporary value of pm2cnc
ppa	mM	Temporary value of H2O2 in Side A, used in Runge-Kutta-Gill solution
ppb	mM	Temporary value of H2O2 in Side B, used in Runge-Kutta-Gill solution
psia	---	Ratio of (k6 + k7)/(k6k7) for D5NoMn MNP
psib	---	Ratio of (k6 + k7)/(k6k7) for D4HiMn MNP
ptemp	μL	Output pulse concentration of peroxide

		for Side A
ptemp2	μL	Temporary value of ptemp
pvol	mL	Standard pulse volume multiple (0.010 mL) for enzyme pulses
ratep	μmol/hr	Rate of peroxide transport
raterp	μmol/hr	Rate of peroxide consumption
raterv	μmol/hr	Rate of VA transport
ratev	μmol/hr	Rate of VA consumption
rka	---	Runge-Kutta-Gill derivative approximation weighting constant
rkb	---	Runge-Kutta-Gill derivative approximation weighting constant
rkc	---	Runge-Kutta-Gill derivative approximation weighting constant
rkd	---	Runge-Kutta-Gill derivative approximation weighting constant
rrange	%/100	Ratio of rate of transport of peroxide to rate of transport of VA before pulse
sig	mM/(U/L)	Ratio of maximum H2O2 to maximum MNP
tact	min	Actual cumulative time
tart	mM	Concentration of tartrate in both sides
tdelay	min	Counter for pulse time delay
temp	---	Temporary calculation variable
temp2	---	Temporary calculation variable
tpls	min	Time at which pulse is added to either side
tref	min	Enzyme activity reference time
va(2)	mM	Concentration of VA in Side A
vaconc	mM	Variable used in pulse concentration calculations and dilution calculations for VA in Side A
vb(2)	mM	Concentration of VA in Side B
vbmax	mM	Maximum concentration of VA in Side B
vbmin	mM	Minimum concentration of VA in Side B
vol	mL	Volume of Side B
vola	mL	Volume of Side A
volbt	mL	Temporary value of vol
vtemp	μL	Output pulse concentration of VA for Side A
vtemp2	μL	Temporary value of vtemp
vva	mM	Temporary value of VA in Side A, used in Runge-Kutta-Gill solution
vvb	mM	Temporary value of VA in Side B, used in Runge-Kutta-Gill solution

b. Integer Variables

Variable	Units	Description
delay	---	Variable used in counting pulse time delay
flag	---	Flag which indicates enzymes present
flag2	---	Flag which differentiates between pulse types
flag3	---	Flag which differentiates between pulse types
flag4	---	Flag which differentiates between pulse types

flag5	---	Flag which indicates that a pulse has just occurred (and does not allow another)
i	---	Loop counter
j	---	Loop counter
n	---	Main time step loop counter
nprint	---	Data output step increment
ntotal	---	Total number of time steps
tcount	---	Pulse delay time step counter
pcount	---	Temporary value of tcount
x	---	Loop counter for Newton's Method

D.1.2 FORTRAN Program RKG.FOR

```
C ***************************************************************************
C
C  PROGRAM RKG.FOR
C
C    Reactor Model Simulation Program
C
C ***************************************************************************
      double precision aa, aah, ah(2), ahconc, alp, apvol
      double precision arange, area, a1, a2
      double precision bb, bpvol, brange, bta
      double precision delta, dfpv, dm, dm3, dp, dv
      double precision convrt
      double precision ee, eps
      double precision fpv, frac1, frac2, fr1pct, fr2pct, fr3pct
      double precision f1, f2, f2ovf1, f3, f4
      double precision g, gma, gt, g1, g2, g3
      double precision h
      double precision initlo, inimo1, inimo2
      double precision kah(4), kdl1, kdl2, kdma, kdmb, ki, kma(4)
      double precision kmb(4), km3a(4), km3b(4), kpa(4), kpb(4)
      double precision kva(4), kvb(4), k1, k3, k4, k5a, k5b, k8
      double precision lip, lo, lotmp, lrange, lth
      double precision ma(2), maconc, m3acnc, mb(2), mma, mmb, mm3a
      double precision mm3b, mnp, mnp1, mnp2, mo, mo1, mo2, mo1tmp
      double precision mo2tmp, mrange, m3a(2), m3b(2)
      double precision pao, pa(2), paconc, pastnd, patemp, pb(2)
      double precision pbmax, pbmin, plconc, pltemp, pltmp2, pmconc
      double precision pm1cnc, pm2cnc, pm1tmp, pm2tmp, pm1tp2, pm2tp2
      double precision ppa, ppb, psia, psib, ptemp, ptemp2, pvol
      double precision ratep, raterp, raterv, ratev, rka, rkb, rkc
      double precision rkd, rrange
      double precision sig
      double precision tact, tart, tdelay, temp, temp2
      double precision tpls, tref
      double precision va(2), vaconc, vb(2), vbmax, vbmin, vol, vola
      double precision volbt, vtemp, vtemp2, vva, vvb
      integer delay, flag, flag2, flag3, flag4, flag5, flag6, i, j, n
      integer nprint, ntotal, tcount, pcount, x
      common /lipkin/ k1, k3, k4, ki
      common /mnpkin/ k5a, psia, k5b, psib, k8
```

```
      common /trans/ dp, dv, dm, dm3, a1, a2, gma
      common /stable/ kdl1, kdl2, kdma, kdmb
      common /rxtr/ lth, vol, vola, area, lo, mo1, mo2, h
      common /conc1/ pa, pb, va, vb, ma, mb
      common /conc2/ m3a, m3b, ah, lip, mnp
      common /conc3/ pbmin, pbmax, vbmax
      common /rate/ ratep, ratev, raterp, raterv
      common /apulse/ apvol, ptemp, vtemp
      common /bpulse/ bpvol, ptemp2, vtemp2
      common /epulse/ plconc, pm1cnc, pm2cnc
      flag=0
      flag2=0
      flag3=0
      flag4=0
      flag5=0
      flag6=0
      g3=0.d0
      convrt=16.679d0
      rka=(2.d0**0.5d0-1.d0)/2.d0
      rkb=(2.d0-2.d0**0.5d0)/2.d0
      rkc=-(2.d0**.5d0)/2.d0
      rkd=1.d0+(2.d0**0.5d0)/2.d0
C
C *** SET MODEL PARAMETERS ***
C
      area=0.2206d0
      lth=6.136d-3
      vol=1.0d0
      vola=1.d0
      dp=1.7000d-4
      dv=4.4935d-5
      dm=1.319d-4
      dm3=2.020d-5
      a1=600.d0
      a2=1807.68d0
      gma=1.d0/a1+1.d0/a2
C
C *** SET KINETIC CONSTANTS ***
C
      k1=2.147d-2
      k3=8.101d-3
      k4=1.246d-3
      ki=4.918d0
      k5a=6.566d-3
      k5b=5.089d-3
      k8=7.2d-3
      psia=2983.2d0
      psib=2336.8d0
C
C *** SET STABILITY CONSTANTS ***
C
      kdl1=19.16d0
      kdl2=1.867d-2
```

```
      kdma=5.168d-2
      kdmb=2.535d-2
      tart=20.d0
      pao=0.d0
      ptemp=0.d0
      vtemp=0.d0
      ptemp2=0.d0
      vtemp2=0.d0
      pastnd=0.d0
      paconc=0.d0
      pmconc=0.d0
      pbconc=0.d0
      maconc=0.d0
      m3acnc=0.d0
      ahconc=0.d0
      arange=0.d0
      brange=0.d0
      patemp=0.d0
C
C *** INPUT STEP SIZE, RATE CORRECTION FRACTIONS, ETC. ***
C
      write(*,*) 'INPUT DATA:'
      write(*,*) 'Step Size h, # of Steps, Pr. Inc'
      read(*,*) h, ntotal, nprint
      write(*,*) '[LIP]o, [MNP]o (D5NoMn), [MNP]o (D4HiMn)'
      write(*,*) '  *** Enter -1.0 if none is present ***'
      read(*,*) initlo, inimo1, inimo2
      if (initlo .eq. -1.d0) then
         write(*,*) '[H2O2]Ap, f3, f4'
         read(*,*) patemp, f3, f4
         write(*,*) 'Input [H2O2]Bmin Range and [MNP] Range:'
         read(*,*) arange, mrange
         write(*,*) 'Input MNP Pulse Concentration (U/L):'
         read(*,*) pm2tmp
         write(*,*) 'Input pa(1):'
         read(*,*) pa(1)
         pao=pa(1)
         write(*,*) 'Input Pct Decrease of f3:'
         read(*,*) fr2pct
         lrange=0.d0
         rrange=0.d0
         f2ovf1=1.d0
         f2=1.d0
      else
         write(*,*) 'f2/f1, f2'
         read(*,*) f2ovf1, f2
         if (inimo2 .eq. -1.d0) then
            write(*,*) 'Input Rate Range and [LIP] Range:'
            read(*,*) rrange, lrange
            write(*,*) 'Input [VA]Bmax Range:'
            read(*,*) brange
            write(*,*) 'Input Fractions of g2 and g1:'
            read(*,*) frac2, frac1
```

```
      write(*,*) 'Input LIP Pulse Concentration (U/L):'
      read(*,*) pltemp
      write(*,*) 'Input H2O2 Pulse (Alone) Concentration (mM):'
      read(*,*) patemp
    else
      write(*,*)'Input Rate Range, [LIP] Range, & [MNP] Range:'
      read(*,*) rrange, lrange, mrange
      write(*,*) 'Input [VA]Bmax Range:'
      read(*,*) brange
      write(*,*) 'Input H2O2 Pulse (Alone) Concentration (mM):'
      read(*,*) patemp
      write(*,*) 'Input Fractions of g2 and g1:'
      read(*,*) frac2, frac1
      write(*,*) 'Input g3 & Pct decrease of g3:'
      read(*,*) g3, fr3pct
      write(*,*) 'Input Pct Increase of g1, & Decrease of g2:'
      read(*,*) fr1pct, fr2pct
      write(*,*) 'Input Enzyme Pulse Concentrations (U/L):'
      write(*,*) '{ [LIP]p, [MNP]p (D5NoMn), [MNP]p (D4HiMn) }'
      write(*,*) '  1.) For LIP Alone and MNP Alone Pulses:'
      read(*,*) pltemp, pm1tmp, pm2tmp
      write(*,*) '  2.) For LIP + MNP Pulses:'
      read(*,*) pltmp2, pm1tp2, pm2tp2
      flag6=999
    endif
  endif
  if (initlo .eq. -1.d0) then
    initlo=0.d0
    inimo1=0.d0
    pltemp=0.d0
    pm1tmp=0.d0
    flag=999
  elseif (inimo2 .eq. -1.d0) then
    inimo1=0.d0
    inimo2=0.d0
    pm1tmp=0.d0
    pm2tmp=0.d0
    flag=1001
  endif
  delta=(1.d0+(1.d0-rrange))
  lo=initlo
  mo1=inimo1
  mo2=inimo2
  lip=lo
  mnp1=mo1
  mnp2=mo2
  mnp=mnp1+mnp2
  pmconc=pm1tmp+pm2tmp
  pvol=0.01d0
  if (flag .ne. 999) then
    alp=0.1d0/lip
    bta=0.6d0/lip
  else
```

```
      alp=1.d0
      bta=1.d0
    endif
    if (flag .ne. 1001) then
      eps=0.1d0/(mnp1+mnp2)
      sig=0.1d0/(mnp1+mnp2)
    else
      eps=1.d0
      sig=1.d0
    endif
    f1=f2/f2ovf1
    if (flag .ne. 1001) then
      g2=f2*frac2
      g1=g2/f2ovf1*frac1
    else
      g2=f2*frac2
      g1=f1*frac1
    endif
    open(2,file='data1.prn',status='new')
    open(8,file='data2.prn',status='new')
    open(3,file='data3.prn',status='new')
    open(6,file='data4.prn',status='new')
    open(4,file='apulses.prn',status='new')
    open(5,file='bpulse1.prn',status='new')
    open(7,file='bpulse2.prn',status='new')
    open(9,file='initial.prn',status='new')
C
C *** SET INITIAL CONDITIONS BASED ON PATENT RANGES ***
C
    tref=0.d0
    tact=0.d0
    tcount=0
    tdelay=0.d0
    pcount=0
    if (flag .eq. 1001) then
      pa(1)=dp*area*(k1*alp*lo*(k3*bta+k4*alp/ki)+k4*(k1*alp
   +          +k3*bta))
      pa(1)=(k1*k3*k4*alp*bta*lth*vol*lo**2)/pa(1)
      temp2=k5a*alp*eps*lth*vol*lo*mo1*(mo1+mo2)
      temp2=temp2/(dp*area*(eps*(mo1+mo2)+k5a*alp*psia*lo))
      pa(1)=pa(1)+temp2
      temp2=k5b*alp*eps*lth*vol*lo*mo2*(mo1+mo2)
      temp2=temp2/(dp*area*(eps*(mo1+mo2)+k5b*alp*psib*lo))
      pa(1)=f2*(pa(1)+temp2)+alp*lo
      pb(1)=alp*lo
      pbmax=pb(1)
      pbmin=5.0d-3/lo*lo
    elseif (flag .eq. 0) then
      pa(1)=dp*area*(k1*alp*lo*(k3*bta+k4*alp/ki)+k4*(k1*alp
   +          +k3*bta))
      pa(1)=(k1*k3*k4*alp*bta*lth*vol*lo**2)/pa(1)
      pa(1)=f2*pa(1)+alp*lo
      pb(1)=alp*lo
```

```
      pbmax=pb(1)
      pbmin=5.0d-3/lo*lo
    elseif (flag .eq. 999) then
      pb(1)=sig*mo2
      pbmax=pb(1)
      pbmin=5.0d-3/mo2*mo2
    endif
    va(1)=dv*area*(k1*alp*lo*(k3*bta+k4*alp/ki)+k4*(k1*alp+k3*bta))
    va(1)=(f1*k1*k3*k4*alp*bta*gma*lth*vol*(lo**2))/va(1)
    va(1)=-1.d0/gma*dlog(dexp(-bta*gma*lo)-va(1))
    vb(1)=bta*lo
    vbmax=vb(1)
    if (flag .ne. 999) then
      vbmin=5.0d-3/lo*lo
    else
      vbmin=0.d0
    endif
    mb(1)=0.d0
    ma(1)=0.d0
    m3a(1)=0.d0
    m3b(1)=eps*(mo1+mo2)
    ah(1)=0.02d0*2.d0/206.9d0*1.d6
    call rates(tact,pa(1),pb(1),va(1),vb(1),mb(1),ratep,
   +       ratev,raterp,raterv)
C
C *** OPEN OUTPUT FILES AND INITIALIZE ***
C
    write(2,*) 't (min), Pa, Pb, Va, Vb (all in mM)'
    write(8,*) 't (min), M2a, M2b, M3a, M3b, AH (all in mM)'
    write(3,*) 't (min), Camin, Pbmax, Vbmax (all in mM); [LIP],
   +          [MNP] (U/L)'
    write(4,*) '         REAGENT PULSES TO SIDE A'
    write(4,*)
    write(4,*)'t (min)  Pvol (uL) Paconc (mM)  Vaconc (mM) VolA(mL)'
    write(5,*) '         REAGENT PULSES TO SIDE B'
    write(5,*)
    write(5,*)'t (min) Pvol (uL) Pbconc (mM) Vbconc (mM) VolB(mL)'
    write(7,*) '         ENZYME PULSES TO SIDE B'
    write(7,*)
    write(7,*)'                    P(LIP)      P(MNP1)     P(MNP2)'
    write(7,*)'t (min) Pvol (uL) Conc (U/L) Conc (U/L) Conc (U/L)'
    write(6,*)'t (min), and R(H2O2), R(VA), RP(RXN), & RV(RXN) (
   +          umol/min)'
    write(9,*) '          INITIAL REACTOR CONDITIONS'
    write(9,*)
    write(9,*) 'REAGENT & ENZYME CONCENTRATIONS:'
    write(9,*)
    write(9,*) '   Side A:'
    write(9,*)
    write(9,*) '[H2O2]Ao     = ',pa(1),' mM'
    write(9,*) '[VA]Ao       = ',va(1),' mM'
    write(9,*) '[Mn(II)]Ao   = ',ma(1),' mM'
    write(9,*) '[Mn(III)]Ao  = ',m3a(1),' mM'
```

```
write(9,*) '[Tartrate]Ao = ',tart,' mM'
write(9,*)
write(9,*) '   Side B:'
write(9,*)
write(9,*) '[H2O2]Bo     = ',pb(1),' mM'
write(9,*) '[VA]Bo       = ',vb(1),' mM'
write(9,*) '[Mn(II)]Bo   = ',mb(1),' mM'
write(9,*) '[Mn(III)]Bo  = ',m3b(1),' mM'
write(9,*) '[AH]Bo       = ',ah(1),' mM'
write(9,*) '  { or [Lignin]Bo = ',20.d0,' mg }'
write(9,*) '[Tartrate]Bo = ',tart,' mM'
write(9,*)
write(9,*) 'D5NoMn [LIP]Bo = ',lo,' U/L'
write(9,*) 'D5NoMn [MNP]Bo = ',mo1,' U/L'
write(9,*) 'D4HiMn [MNP]Bo = ',mo2,' U/L'
write(9,*) ' Total [MNP]Bo = ',mo1+mo2,' U/L'
write(9,*)
write(9,*)
write(9,*) 'MODEL PARAMETERS:'
write(9,*)
write(9,*) 'h (Step Size) = ',h
write(9,*) 'f2/f1 =',f2ovf1
write(9,*) 'f1      =',f1
write(9,*) 'f2      =',f2
write(9,*) 'f3      =',f3
write(9,*) 'f4      =',f4
write(9,*) 'frac1   =',frac1
write(9,*) 'frac2   =',frac2
write(9,*) 'g3      =',g3
write(9,*) 'fr1pct  =',fr1pct
write(9,*) 'fr2pct  =',fr2pct
write(9,*) 'fr3pct  =',fr3pct
write(9,*) 'Rrange  = ', rrange
write(9,*) 'Lrange  = ', lrange
write(9,*) 'Mrange  = ', mrange
write(9,*) 'Arange  = ', arange
write(9,*) 'Brange  = ', brange
write(9,*)
write(9,*) 'PULSE CONCENTRATIONS:'
write(9,*)
write(9,*) 'patemp ',patemp,' mM'
if (flag6 .eq. 999) then
   write(9,*) 'FOR LIP ALONE AND MNP ALONE PULSES:'
   write(9,*)
endif
write(9,*) 'patemp = ',patemp,' mM'
write(9,*) 'D5NoMn LIP =',pltemp,' U/L'
write(9,*) 'D5NoMn MNP =',pm1tmp,' U/L'
write(9,*) 'D4HiMn MNP =',pm2tmp,' U/L'
if (flag6 .eq. 999) then
   write(9,*)
   write(9,*) 'FOR LIP + MNP PULSES ONLY:'
   write(9,*)
```

```
        write(9,*) 'D5NoMn LIP =', pltmp2,' U/L'
        write(9,*) 'D5NoMn MNP =', pm1tp2,' U/L'
        write(9,*) 'D4HiMn MNP =', pm2tp2,' U/L'
      endif
      close(9)
      flag6=0
      pa(1)=dnint(pa(1)*1.d4)/1.d4
      va(1)=dnint(va(1)*1.d4)/1.d4
      write(2,100) tact, pa(1), pb(1), va(1), vb(1)
      write(3,101) tact, pbmin, pbmax, vbmax, lip, mnp
      write(8,102) tact, ma(1), mb(1), m3a(1), m3b(1), ah(1)
      write(6,103) tact, ratep, ratev, raterp, raterv
C
C *** MAIN LOOP - SOLVES BY 4TH ORDER RUNGE-KUTTA-GILL ***
C
      j=0
      do 10 n = 1, ntogwl
        j=j+1
        ppa=pa(1)
        ppb=pb(1)
        vva=va(1)
        vvb=vb(1)
        mma=ma(1)
        mmb=mb(1)
        mm3a=m3a(1)
        mm3b=m3b(1)
        aah=ah(1)
        temp=tref
        do 20 i = 1, 4
          call func1h(temp,ppa,ppb,kpa(i))
          call func2h(temp,vva,vvb,kva(i))
          call func3h(temp,ppb,ppa,vvb,mmb,kpb(i))
          call func4h(temp,vvb,vva,ppb,kvb(i))
          call func5h(temp,mma,mmb,kma(i))
          call func6h(temp,mma,mmb,mm3b,aah,ppb,kmb(i))
          call func7h(temp,mm3a,mm3b,km3a(i))
          call func8h(temp,mm3a,mm3b,ppb,mmb,aah,km3b(i))
          call func9h(temp,aah,mm3b,kah(i))
          if (i .eq. 1) then
            temp=tref+0.5d0*h
            ppa=pa(1)+0.5d0*kpa(i)
            ppb=pb(1)+0.5d0*kpb(i)
            vva=va(1)+0.5d0*kva(i)
            vvb=vb(1)+0.5d0*kvb(i)
            mma=ma(1)+0.5d0*kma(i)
            mmb=mb(1)+0.5d0*kmb(i)
            mm3a=m3a(1)+0.5d0*km3a(i)
            mm3b=m3b(1)+0.5d0*km3b(i)
            aah=ah(1)+0.5d0*kah(i)
          elseif (i .eq. 2) then
            temp=tref+0.5d0*h
            ppa=pa(1)+rka*kpa(i-1)+rkb*kpa(i)
            ppb=pb(1)+rka*kpb(i-1)+rkb*kpb(i)
```

```
            vva=va(1)+rka*kva(i-1)+rkb*kva(i)
            vvb=vb(1)+rka*kvb(i-1)+rkb*kvb(i)
            mma=ma(1)+rka*kma(i-1)+rkb*kma(i)
            mmb=mb(1)+rka*kmb(i-1)+rkb*kmb(i)
            mm3a=m3a(1)+rka*km3a(i-1)+rkb*km3a(i)
            mm3b=m3b(1)+rka*km3b(i-1)+rkb*km3b(i)
            aah=ah(1)+rka*kah(i-1)+rkb*kah(i)
          elseif (i .eq. 3) then
            temp=tref+h
            ppa=pa(1)+rkc*kpa(i-1)+rkd*kpa(i)
            ppb=pb(1)+rkc*kpb(i-1)+rkd*kpb(i)
            vva=va(1)+rkc*kva(i-1)+rkd*kva(i)
            vvb=vb(1)+rkc*kvb(i-1)+rkd*kvb(i)
            mma=ma(1)+rkc*kma(i-1)+rkd*kma(i)
            mmb=mb(1)+rkc*kmb(i-1)+rkd*kmb(i)
            mm3a=m3a(1)+rkc*km3a(i-1)+rkd*km3a(i)
            mm3b=m3b(1)+rkc*km3b(i-1)+rkd*km3b(i)
            aah=ah(1)+rkc*kah(i-1)+rkd*kah(i)
          endif
   20   continue
        tref=tref+h
        tact=tact+h
        if ((flag2 .eq. 999) .or. (flag3 .eq. 999) .or.
     +       (flag3 .eq. 1000)) then
C            *** INCREMENT PULSE DELAY COUNTER ***
          tcount=tcount+1
        endif
        tdelay=h*dble(tcount)
        delay=idnint(tdelay*100.d0)
        pa(2)=pa(1)+(kpa(1)+kpa(4))/6.d0+(rkb*kpa(2)+rkd*kpa(3))/3.d0
        pb(2)=pb(1)+(kpb(1)+kpb(4))/6.d0+(rkb*kpb(2)+rkd*kpb(3))/3.d0
        va(2)=va(1)+(kva(1)+kva(4))/6.d0+(rkb*kva(2)+rkd*kva(3))/3.d0
        vb(2)=vb(1)+(kvb(1)+kvb(4))/6.d0+(rkb*kvb(2)+rkd*kvb(3))/3.d0
        ma(2)=ma(1)+(kma(1)+kma(4))/6.d0+(rkb*kma(2)+rkd*kma(3))/3.d0
        mb(2)=mb(1)+(kmb(1)+kmb(4))/6.d0+(rkb*kmb(2)+rkd*kmb(3))/3.d0
        m3a(2)=m3a(1)+(km3a(1)+km3a(4))/6.d0+(rkb*km3a(2)+
     +              rkd*km3a(3))/3.d0
        m3b(2)=m3b(1)+(km3b(1)+km3b(4))/6.d0+(rkb*km3b(2)+
     +              rkd*km3b(3))/3.d0
        ah(2)=ah(1)+(kah(1)+kah(4))/6.d0+(rkb*kah(2)+rkd*kah(3))/3.d0
        if (ma(2) .lt. 0.d0) then
          ma(2)=0.d0
        elseif (mb(2) .lt. 0.d0) then
          mb(2)=0.d0
        elseif (m3a(2) .lt. 0.d0) then
          m3a(2)=0.d0
        elseif (m3b(2) .lt. 0.d0) then
          m3b(2)=0.d0
        elseif (ah(2) .lt. 0.d0) then
          ah(2)=0.d0
        endif
C
C *** CALCULATE NEW MAXIMA AND MINIMA; CHECK RATE CRITERIA ***
```

```
C
      lip=(kdl1/kdl2+lo)*dexp(-kdl2*tref/60.d0)-kdl1/kdl2
      if (lip .lt. 0.d0) then
        lip=0.d0
      endif
      mnp1=mo1*dexp(-kdma*tref/60.d0)
      mnp2=mo2*dexp(-kdmb*tref/60.d0)
      mnp=mnp1+mnp2
      if (flag .eq. 999) then
        pbmax=0.1d0/mnp2*mnp2
        pbmin=5.0d-3/mnp2*mnp2
      else
        pbmax=0.1d0/lip*lip
        pbmin=5.0d-3/lip*lip
      endif
      if (flag .ne. 999) then
        vbmax=0.60/lip*lip
        vbmin=5.0d-3/lip*lip
      else
        vbmax=0.d0
        vbmin=0.d0
      endif
      call rates(tref,pa(2),pb(2),va(2),vb(2),mb(2),
     +     ratep,ratev,raterp,raterv)
      if (j .eq. nprint) then
        call out1(tact)
        j=0
      endif
C
C *** DETERMINE PULSES NEEDED AND THEIR CONCENTRATIONS ***
C
      if (flag .eq. 1001) then
        paconc=0.d0
        vaconc=0.d0
      endif
      maconc=0.d0
      m3acnc=0.d0
      ahconc=0.d0
      plconc=0.d0
      pmconc=0.d0
      pm1cnc=0.d0
      pm2cnc=0.d0
      if (flag .eq. 1001) then
C       *** LIP IS PRESENT, SO PULSE BY LIP METHOD ***
        if ((flag2 .eq. 0) .and. (flag3 .eq. 0)) then
          if (flag5 .gt. 0) then
            flag5=flag5+1
          endif
          if (flag5 .gt. 50) then
            flag5=0
          endif
           if ((vb(2) .ge. brange*vbmax) .and.
     +          (flag5 .eq. 0) .and. (tact .gt. 20.d0)) then
```

```
C                *** H2O2 IN SIDE A NEEDS PULSED ***
                 flag5=flag5+1
                 tpls=tact
                 apvol=0.d0
                 bpvol=0.d0
                 if (lip .gt. lrange*initlo) then
C                  *** LIP DOES NOT NEED PULSED ***
C                  ***   PULSE A WITH PEROXIDE  ***
                   paconc=patemp
                   ptemp=paconc
                   vtemp=0.d0
C
C *** SOLVE FOR PULSE VOLUME USING NEWTON'S METHOD ***
C
                   g=pvol
                   do 1 x = 1, 100000
                     fpv=dv*delta/dp*dexp(-gma*va(2)*((vol-g)
     +                     /vol))
                     fpv=fpv/gma+(paconc-pa(2))*g/vol+pa(2)-pb(2)
                     fpv=fpv-dv*delta/dp/gma*dexp(-gma*vb(2))
                     dfpv=dv*delta/dp*dexp(-gma*va(2)*((vol-g)
     +                     /vol))
                     dfpv=dfpv*va(2)/vol+(paconc-pa(2))/vol
                     gt=g
                     g=g-fpv/dfpv
                     if (dabs(g-gt) .lt. 1.d-5) then
                       goto 2
                     endif
   1                 continue
   2                 apvol=g
                     apvol=dnint(apvol*1.d5)/1.d5
                     vola=vola-apvol
                     call rates(tref,pa(2),pb(2),va(2),vb(2),
     +                    mb(2),ratep,ratev,raterp,raterv)
                     mnp=mnp1+mnp2
                     call out1(tact)
C                      *** SET PULSE DELAY FLAG ***
                     flag2=999
                     tcount=0
                   elseif (lip .le. lrange*initlo) then
C                    *** PULSE A WITH PEROXIDE AND VA ***
                     vola=vola-2.d0*pvol
                     call rates(tref,pa(2),pb(2),va(2),vb(2),
     +                     mb(2),ratep,ratev,raterp,raterv)
                     mnp=mnp1+mnp2
                     call out1(tact)
C                      *** SET PULSE DELAY FLAG ***
                     flag3=999
                     tcount=0
                   endif
                 endif
               elseif ((flag2 .eq. 999) .and. (delay .eq. 30)) then
C                *** ADD DELAYED H2O2 PULSE (NO LIP PULSE LATER) ***
```

```
            vola=vola+apvol
            pa(2)=(pa(2)*(vola-apvol)+ptemp*apvol)/vola
            va(2)=va(2)*(vola-apvol)/vola
            ma(2)=ma(2)*(vola-apvol)/vola
            m3a(2)=m3a(2)*(vola-apvol)/vola
            apvol=apvol*1000.d0
            call rates(tref,pa(2),pb(2),va(2),vb(2),mb(2),
     +           ratep,ratev,raterp,raterv)
            mnp=mnp1+mnp2
            call out1(tact)
            call out2(tpls)
            flag2=0
            tcount=0
          elseif ((flag3 .eq. 999) .and. (delay .eq. 30)) then
C             *** ADD DELAYED H2O2/VA PULSE (LIP PULSE LATER) ***
            vola=vola+4.d0*pvol
            paconc=pa(2)*(vola-4.d0*pvol)
            maconc=ma(2)*(vola-4.d0*pvol)
            m3acnc=m3a(2)*(vola-4.d0*pvol)
            vaconc=va(2)*(vola-4.d0*pvol)
            plconc=pltemp
            pm1cnc=pm1tmp
            pm2cnc=pm2tmp
            volbt=vol+2.d0*pvol
            lotmp=(lip*vol+pltemp*2.d0*pvol)/volbt
            mo1tmp=(mnp1*vol+pm1tmp*2.d0*pvol)/volbt
            mo2tmp=(mnp2*vol+pm2tmp*2.d0*pvol)/volbt
            aa=0.1d0/lotmp
            bb=0.6d0/lotmp
            if (flag .ne. 1001) then
              ee=0.1d0/(mo1tmp+mo2tmp)
            else
              ee=1.d0
            endif
            pa(2)=dp*area*(k1*aa*lotmp*(k3*bb+k4*aa/ki)+k4*(k1*aa
     +           +k3*bb))
            pa(2)=(k1*k3*k4*aa*bb*lth*volbt*lotmp**2)/pa(2)
            temp2=k5a*aa*ee*lth*volbt*lotmp*mo1tmp*(mo1tmp+mo2tmp)
            temp2=temp2/(dp*area*(ee*(mo1tmp+mo2tmp)+
     +                 k5a*aa*psia*lotmp))
            pa(2)=pa(2)+temp2
            temp2=k5b*aa*ee*lth*volbt*lotmp*mo2tmp*(mo1tmp+mo2tmp)
            temp2=temp2/(dp*area*(ee*(mo1tmp+mo2tmp)+
     +                 k5b*aa*psib*lotmp))
            pa(2)=g2*(pa(2)+temp2)+aa*lotmp
            va(2)=k1*aa*lotmp*(k3*bb+k4*aa/ki)
            va(2)=dv*area*(va(2)+k4*(k1*aa+k3*bb))
            va(2)=g1*k1*k3*k4*aa*bb*gma*lth*volbt*lotmp**2/va(2)
            va(2)=-1.d0/gma*dlog(dexp(-bb*gma*lotmp)-va(2))
            ma(2)=(maconc/vola)
            m3a(2)=(m3acnc/vola)
            paconc=(pa(2)*vola-paconc)/(4.d0*pvol)
            vaconc=(va(2)*vola-vaconc)/(4.d0*pvol)
```

```
            ptemp=paconc
            ptemp=dnint(ptemp*1.d3)/1.d3
            vtemp=vaconc
            vtemp=dnint(vtemp*1.d3)/1.d3
            apvol=4.d0*pvol
            apvol=apvol*1000.d0
            apvol=dnint(apvol*100.d0)/100.d0
            call rates(tref,pa(2),pb(2),va(2),vb(2),mb(2),
     +                  ratep,ratev,raterp,raterv)
            mnp=mnp1+mnp2
            call out1(tact)
          elseif ((flag3 .eq. 999) .and. (delay .eq. 70)) then
C             *** ADD DELAYED LIP PULSE ***
            tref=0.d0
            plconc=pltemp
            pm1cnc=pm1tmp
            pm2cnc=pm2tmp
            lo=(lip*vol+pltemp*2.d0*pvol)/(vol+2.d0*pvol)
            mo1=(mnp1*vol+pm1tmp*2.d0*pvol)/(vol+2.d0*pvol)
            mo2=(mnp2*vol+pm2tmp*2.d0*pvol)/(vol+2.d0*pvol)
            vol=vol+2.d0*pvol
            lip=lo
            mnp1=mo1
            mnp2=mo2
            alp=0.1d0/lo
            bta=0.6d0/lo
            if (flag .ne. 1001) then
              eps=0.1d0/(mo1+mo2)
            else
              eps=1.d0
            endif
            pbmax=alp*lip
            vbmax=bta*lip
            pbmin=5.0d-3/lip*lip
            vbmin=5.0d-3/lip*lip
            pb(2)=pb(2)*(vol-2.d0*pvol)/vol
            vb(2)=vb(2)*(vol-2.d0*pvol)/vol
            mb(2)=mb(2)*(vol-2.d0*pvol)/vol
            m3b(2)=m3b(2)*(vol-2.d0*pvol)/vol
            ah(2)=ah(2)*(vol-2.d0*pvol)/vol
            bpvol=2.d0*pvol
            bpvol=bpvol*1000.d0
            bpvol=dnint(bpvol*100.d0)/100.d0
            call rates(tref,pa(2),pb(2),va(2),vb(2),mb(2),
     +                  ratep,ratev,raterp,raterv)
            mnp=mnp1+mnp2
            call out1(tact)
            call out2(tpls)
            flag3=0
            tcount=0
          endif
        elseif (flag .eq. 0) then
C   *** LIP AND MNP ARE PRESENT, SO PULSE BY LIP+MNP METHOD ***
```

```
            mnp=mnp1+mnp2
            initmo=inimo1+inimo2
            if ((flag2 .eq. 0) .and. (flag3 .eq. 0)
     +           .and. (flag4 .eq. 0)) then
              temp2=raterp-raterv
              if (flag5 .gt. 0) then
                flag5=flag5+1
              endif
              if (flag5 .gt. 500) then
                flag5=0
              endif
              if ((vb(2) .ge. brange*vbmax) .and.
     +             (flag5 .eq. 0) .and. (tact .gt. 20.d0)) then
C                  *** H2O2 IN SIDE A NEEDS PULSED ***
                flag5=flag5+1
C               *** H2O2 IN SIDE A NEEDS PULSED ***
                tpls=tact
                apvol=0.d0
                bpvol=0.d0
                mnp=mnp1+mnp2
                mo=mo1+mo2
                if ((lip .lt. 0.97d0*initlo) .and.
     +               (mnp .lt. mrange*initmo)) then
                  flag6=999
                endif
                if ((lip .gt. lrange*initlo) .and.
     +               (mnp .gt. mrange*initmo)) then
C                 *** LIP DOES NOT NEED PULSED ***
C                 *** MNP DOES NOT NEED PULSED ***
C                 ***   PULSE A WITH PEROXIDE  ***
                  paconc=patemp
                  ptemp=paconc
                  vtemp=0.d0
C
C *** SOLVE FOR PULSE VOLUME USING NEWTON'S METHOD ***
C
                  g=pvol
                  do 3 x = 1, 100000
                    fpv=dv*delta/dp*dexp(-gma*va(2)*((vol-g)
     +                   /vol))
                    fpv=fpv/gma+(paconc-pa(2))*g/vol+pa(2)
                    fpv=fpv-lth*vola/dp/area*temp2/vol/60.d0
                    fpv=fpv-dv*delta/dp/gma*dexp(-gma*vb(2))
                    fpv=fpv-pb(2)
                    dfpv=dv*delta/dp*dexp(-gma*va(2)*((vol-g)
     +                   /vol))
                    dfpv=dfpv*va(2)/vol+(paconc-pa(2))/vol
                    gt=g
                    g=g-fpv/dfpv
                    if (dabs(g-gt) .lt. 1.d-5) then
                      goto 4
                    endif
   3                continue
```

```
   4            apvol=g
                apvol=dnint(apvol*1.d5)/1.d5
                vola=vola-apvol
                call rates(tref,pa(2),pb(2),va(2),vb(2),
     +              mb(2),ratep,ratev,raterp,raterv)
                mnp=mnp1+mnp2
                call out1(tact)
C                  *** SET PULSE DELAY FLAG ***
                flag2=999
                tcount=0
              elseif ((lip .le. lrange*initlo) .and.
     +                (mnp .gt. mrange*initmo)) then
C                *** PULSE A WITH PEROXIDE AND VA ***
C                *** LIP NEEDS PULSED ALSO ***
                vola=vola-2.d0*pvol
                mnp=mnp1+mnp2
                call rates(tref,pa(2),pb(2),va(2),vb(2),
     +              mb(2),ratep,ratev,raterp,raterv)
                call out1(tact)
C                  *** SET PULSE DELAY FLAG ***
                flag3=999
                flag4=999
                tcount=0
              elseif (((lip .gt. lrange*initlo) .and.
     +                (flag6 .eq. 0)) .and.
     +                (mnp .le. mrange*initmo)) then
C                *** PULSE A WITH PEROXIDE ONLY ***
C                ***   MNP NEEDS PULSED ALSO    ***
C                ***   ADD DELAYED H2O2 PULSE   ***
C                ***     MNP PULSE LATER        ***
                paconc=pa(2)*vola
                plconc=0.d0
                pm1cnc=0.d0
                pm2cnc=pm2tmp
                vola=vola+2.d0*pvol
                apvol=2.d0*pvol
                temp2=raterp-raterv
                va(2)=va(2)*(vola-apvol)/vola
                ma(2)=ma(2)*(vola-apvol)/vola
                m3a(2)=m3a(2)*(vola-apvol)/vola
                pa(2)=dv*delta/dp/gma*(dexp(-gma*vb(2))-dexp(-gma
     +              *va(2)))+lth*vola/dp/area*temp2/vol/60.d0
                pa(2)=pa(2)+pb(2)
                apvol=apvol*1000.d0
                paconc=(pa(2)*vola-paconc)/(2.d0*pvol)
                ptemp=paconc
                vtemp=0.d0
                mnp=mnp1+mnp2
                call rates(tref,pa(2),pb(2),va(2),vb(2),
     +              mb(2),ratep,ratev,raterp,raterv)
                call out1(tact)
C                  *** SET PULSE DELAY FLAG ***
                flag3=999
```

```
                flag4=1001
                tcount=0
              elseif (((lip .le. lrange*initlo) .and.
     +             (mnp .le. mrange*initmo)) .or.
     +             (((lip .gt. lrange*initlo) .and.
     +             (flag6 .eq. 999)) .and.
     +             (mnp .le. mrange*initmo))) then
C               *** PULSE A WITH PEROXIDE AND VA ***
C               *** LIP NEEDS PULSED ALSO ***
C               *** MNP NEEDS PULSED ALSO ***
C
C               *** ADD DELAYED H2O2/VA PULSE ***
C               ***     LIP PULSE LATER       ***
                vola=vola-1.d0*pvol
                mnp=mnp1+mnp2
                call rates(tref,pa(2),pb(2),va(2),vb(2),
     +                mb(2),ratep,ratev,raterp,raterv)
                call out1(tact)
C                 *** SET PULSE DELAY FLAG ***
                flag3=1000
                if (flag6 .eq. 999) then
                  flag6=0
                endif
                tcount=0
              endif
            endif
          elseif ((flag2 .eq. 999) .and. (delay .eq. 30)) then
C             *** ADD DELAYED H2O2 PULSE ***
C             *** NO LIP OR MNP PULSES LATER ***
            vola=vola+apvol
            pa(2)=(pa(2)*(vola-apvol)+ptemp*apvol)/vola
            va(2)=va(2)*(vola-apvol)/vola
            ma(2)=ma(2)*(vola-apvol)/vola
            m3a(2)=m3a(2)*(vola-apvol)/vola
            apvol=apvol*1000.d0
            call rates(tref,pa(2),pb(2),va(2),vb(2),mb(2),
     +             ratep,ratev,raterp,raterv)
            mnp=mnp1+mnp2
            call out1(tact)
            call out2(tpls)
            flag2=0
            tcount=0
          elseif ((flag3 .eq. 999) .and. (delay .eq. 30) .and.
     +          (flag4 .eq. 999)) then
C             *** ADD DELAYED H2O2/VA PULSE ***
C             ***     LIP PULSE LATER       ***
            vola=vola+4.d0*pvol
            paconc=pa(2)*(vola-4.d0*pvol)
            maconc=ma(2)*(vola-4.d0*pvol)
            m3acnc=m3a(2)*(vola-4.d0*pvol)
            vaconc=va(2)*(vola-4.d0*pvol)
            plconc=pltemp
            pm1cnc=pm1tmp
```

```
            pm2cnc=0.d0
            volbt=vol+2.d0*pvol
            lotmp=(lip*vol+pltemp*2.d0*pvol)/volbt
            mo1tmp=(mnp1*vol+pm1tmp*2.d0*pvol)/volbt
            mo2tmp=mnp2*vol/volbt
            aa=0.1d0/lotmp
            bb=0.6d0/lotmp
            ee=mb(2)*vol/volbt
            pa(2)=dp*area*(k1*aa*lotmp*(k3*bb+k4*aa/ki)
     +             +k4*(k1*aa+k3*bb))
            pa(2)=(k1*k3*k4*aa*bb*lth*volbt*lotmp**2)/pa(2)
            temp2=0.d0
            pa(2)=g2*(pa(2)+temp2)+aa*lotmp
            va(2)=k1*aa*lotmp*(k3*bb+k4*aa/ki)
            va(2)=dv*area*(va(2)+k4*(k1*aa+k3*bb))
            va(2)=g1*k1*k3*k4*aa*bb*gma*lth*volbt*lotmp**2/va(2)
            va(2)=-1.d0/gma*dlog(dexp(-bb*gma*lotmp)-va(2))
            ma(2)=(maconc/vola)
            m3a(2)=(m3acnc/vola)
            paconc=(pa(2)*vola-paconc)/(4.d0*pvol)
            temp2=(va(2)*vola-vaconc)/(4.d0*pvol)
            if (temp2 .lt. 0.d0) then
              va(2)=vaconc/(vola-4.d0*pvol)
              vtemp=0.d0
            else
              vtemp=temp2
            endif
            ptemp=paconc
            ptemp=dnint(ptemp*1.d3)/1.d3
            vtemp=dnint(vtemp*1.d3)/1.d3
            apvol=4.d0*pvol*1000.d0
            apvol=dnint(apvol*100.d0)/100.d0
            mnp=mnp1+mnp2
            call rates(tref,pa(2),pb(2),va(2),vb(2),mb(2),
     +           ratep,ratev,raterp,raterv)
            call out1(tact)
          elseif ((flag3 .eq. 1000) .and. (delay .eq. 30)) then
C             *** ADD DELAYED H2O2/VA PULSE ***
C             ***     LIP PULSE LATER       ***
C             ***   MNP PULSE LATER YET     ***
            vola=vola+4.d0*pvol
            paconc=pa(2)*(vola-4.d0*pvol)
            maconc=ma(2)*(vola-4.d0*pvol)
            m3acnc=m3a(2)*(vola-4.d0*pvol)
            vaconc=va(2)*(vola-4.d0*pvol)
            plconc=pltmp2
            pm1cnc=pm1tp2
            pm2cnc=pm2tp2
            volbt=vol+3.d0*pvol
            lotmp=(lip*vol+pltmp2*3.d0*pvol)/volbt
            mo1tmp=(mnp1*vol+pm1tp2*3.d0*pvol)/volbt
            mo2tmp=(mnp2*vol+pm2tp2*3.d0*pvol)/volbt
            aa=0.1d0/lotmp
```

```
            bb=0.6d0/lotmp
            ee=mb(2)*vol/volbt
            pa(2)=dp*area*(k1*aa*lotmp*(k3*bb+k4*aa/ki)
     +                +k4*(k1*aa+k3*bb))
            pa(2)=(k1*k3*k4*aa*bb*lth*volbt*lotmp**2)/pa(2)
            temp2=0.d0
            pa(2)=g3*(pa(2)+temp2)+aa*lotmp
            va(2)=k1*aa*lotmp*(k3*bb+k4*aa/ki)
            va(2)=dv*area*(va(2)+k4*(k1*aa+k3*bb))
            va(2)=g1*k1*k3*k4*aa*bb*gma*lth*volbt
     +                  *lotmp**2/va(2)
            va(2)=-1.d0/gma*dlog(dexp(-bb*gma*lotmp)-va(2))
            ma(2)=(maconc/vola)
            m3a(2)=(m3acnc/vola)
            paconc=(pa(2)*vola-paconc)/(4.d0*pvol)
            temp2=(va(2)*vola-vaconc)/(4.d0*pvol)
            if (temp2 .lt. 0.d0) then
              va(2)=vaconc/(vola-4.d0*pvol)
              vtemp=0.d0
            else
              vtemp=temp2
            endif
            ptemp=paconc
            ptemp=dnint(ptemp*1.d3)/1.d3
            vtemp=dnint(vtemp*1.d3)/1.d3
            apvol=4.d0*pvol*1000.d0
            apvol=dnint(apvol*100.d0)/100.d0
            mnp=mnp1+mnp2
            call rates(tref,pa(2),pb(2),va(2),vb(2),mb(2),
     +           ratep,ratev,raterp,raterv)
            call out1(tact)
          elseif ((flag3 .eq. 999) .and. (delay .eq. 40) .and.
     +        (flag4 .eq. 1001)) then
C           *** ADD DELAYED MNP PULSE ***
            plconc=0.d0
            pm1cnc=0.d0
            pm2cnc=pm2tmp
            lo=lip*vol/(vol+2.d0*pvol)
            mo1=mnp1*vol/(vol+2.d0*pvol)
            mo2=(mnp2*vol+pm2tmp*2.d0*pvol)/(vol+2.d0*pvol)
            lip=lo
            mnp1=mo1
            mnp2=mo2
            tref=0.d0
            vol=vol+2.d0*pvol
            alp=0.1d0/lip
            bta=0.6d0/lip
            if (flag .ne. 1001) then
              eps=0.5d0/(mnp1+mnp2)
            else
              eps=1.d0
            endif
            pbmax=alp*lip
```

```
            vbmax=bta*lip
            pbmin=5.0d-3/lip*lip
            vbmin=5.0d-3/lip*lip
            pb(2)=pb(2)*(vol-2.d0*pvol)/vol
            vb(2)=vb(2)*(vol-2.d0*pvol)/vol
            mb(2)=mb(2)*(vol-2.d0*pvol)/vol
            m3b(2)=m3b(2)*(vol-2.d0*pvol)/vol
            ah(2)=ah(2)*(vol-2.d0*pvol)/vol
            bpvol=2.d0*pvol*1000.d0
            bpvol=dnint(bpvol*100.d0)/100.d0
            mnp=mnp1+mnp2
            call rates(tref,pa(2),pb(2),va(2),vb(2),mb(2),
     +                  ratep,ratev,raterp,raterv)
            call out1(tact)
            call out2(tpls)
            flag3=0
            flag4=0
            tcount=0
          elseif ((flag3 .eq. 999) .and. (delay .eq. 70) .and.
     +           (flag4 .eq. 999)) then
C             *** ADD DELAYED LIP PULSE ***
            plconc=pltemp
            pm1cnc=pm1tmp
            pm2cnc=0.d0
            lo=(lip*vol+pltemp*2.d0*pvol)/(vol+2.d0*pvol)
            mo1=(mnp1*vol+pm1tmp*2.d0*pvol)/(vol+2.d0*pvol)
            mo2=mnp2*vol/(vol+2.d0*pvol)
            lip=lo
            mnp1=mo1
            mnp2=mo2
            tref=0.d0
            vol=vol+2.d0*pvol
            alp=0.1d0/lip
            bta=0.6d0/lip
            if (flag .ne. 1001) then
              eps=0.5d0/(mnp1+mnp2)
            else
              eps=1.d0
            endif
            pbmax=alp*lip
            vbmax=bta*lip
            pbmin=5.0d-3/lip*lip
            vbmin=5.0d-3/lip*lip
            pb(2)=pb(2)*(vol-2.d0*pvol)/vol
            vb(2)=vb(2)*(vol-2.d0*pvol)/vol
            mb(2)=mb(2)*(vol-2.d0*pvol)/vol
            m3b(2)=m3b(2)*(vol-2.d0*pvol)/vol
            ah(2)=ah(2)*(vol-2.d0*pvol)/vol
            bpvol=2.d0*pvol*1000.d0
            bpvol=dnint(bpvol*100.d0)/100.d0
            mnp=mnp1+mnp2
            call rates(tref,pa(2),pb(2),va(2),vb(2),mb(2),
     +                  ratep,ratev,raterp,raterv)
```

```
            call out1(tact)
            call out2(tpls)
            frac2=frac2*(1.d0-fr2pct)
            g2=f2*frac2
            g1=g2/f2ovf1*(1.d0+fr1pct)
            flag3=0
            flag4=0
            tcount=0
          elseif ((flag3 .eq. 1000) .and. (delay .eq. 70)) then
C           *** ADD DELAYED LIP/MNP PULSE ***
            plconc=pltmp2
            pm1cnc=pm1tp2
            pm2cnc=pm2tp2
            lo=(lip*vol+pltmp2*3.d0*pvol)/(vol+3.d0*pvol)
            mo1=(mnp1*vol+pm1tp2*3.d0*pvol)/(vol+3.d0*pvol)
            mo2=(mnp2*vol+pm2tp2*3.d0*pvol)/(vol+3.d0*pvol)
            lip=lo
            mnp1=mo1
            mnp2=mo2
            tref=0.d0
            vol=vol+3.d0*pvol
            alp=0.1d0/lip
            bta=0.6d0/lip
            if (flag .ne. 1001) then
              eps=0.5d0/(mnp1+mnp2)
            else
              eps=1.d0
            endif
            pbmax=alp*lip
            vbmax=bta*lip
            pbmin=5.0d-3/lip*lip
            vbmin=5.0d-3/lip*lip
            pb(2)=pb(2)*(vol-3.d0*pvol)/vol
            vb(2)=vb(2)*(vol-3.d0*pvol)/vol
            mb(2)=mb(2)*(vol-3.d0*pvol)/vol
            m3b(2)=m3b(2)*(vol-3.d0*pvol)/vol
            ah(2)=ah(2)*(vol-3.d0*pvol)/vol
            bpvol=3.d0*pvol*1000.d0
            bpvol=dnint(bpvol*100.d0)/100.d0
            mnp=mnp1+mnp2
            call rates(tref,pa(2),pb(2),va(2),vb(2),mb(2),
     +                 ratep,ratev,raterp,raterv)
            call out1(tact)
            call out2(tpls)
            frac2=frac2*(1.d0-fr2pct)
            g2=f2*frac2
            g1=g2/f2ovf1*(1.d0+fr1pct)
            g3=g3*(1.d0-fr3pct)
            flag3=0
            tcount=0
          endif
        elseif (flag .eq. 999) then
C         *** LIP IS NOT PRESENT, SO PULSE BY MNP METHOD ***
```

```
      if ((flag2 .eq. 0) .and. (flag3 .eq. 0)) then
        mnp1=mo1*dexp(-kdma*tref/60.d0)
        mnp2=mo2*dexp(-kdmb*tref/60.d0)
        mnp=mnp1+mnp2
        initmo=inimo1+inimo2
        if (flag5 .gt. 0) then
          flag5=flag5+1
        endif
        if (flag5 .gt. 500) then
          flag5=0
        endif
         if ((pb(2) .le. (pbmin+arange*(pbmax-pbmin))) .and.
     +       (flag5 .eq. 0)) then
C              *** H2O2 IN SIDE A NEEDS PULSED ***
          flag5=flag5+1
          tpls=tact
          apvol=0.d0
          bpvol=0.d0
          if (mnp .gt. mrange*initmo) then
C              *** MNP DOES NOT NEED PULSED ***
C              ***     H2O2 NEEDS PULSED    ***
C              ***   PULSE A WITH PEROXIDE  ***
            temp2=pao*f3
            apvol=(temp2-pa(2))/(patemp-pa(2))*vola
            apvol=dnint(apvol*1.d5)/1.d5
            vola=vola-apvol
            call rates(tref,pa(2),pb(2),va(2),vb(2),
     +          mb(2),ratep,ratev,raterp,raterv)
            call out1(tact)
C              *** SET PULSE DELAY FLAG ***
            flag2=999
            tcount=0
          elseif (mnp .le. mrange*initmo) then
C              ***     MNP NEEDS PULSED    ***
C              ***     H2O2 NEEDS PULSED   ***
C              *** ADD DELAYED H2O2 PULSE ***
C              ***     MNP PULSE LATER     ***
            paconc=pa(2)*vola
            apvol=2.d0*pvol
            vola=vola+2.d0*pvol
            mnp1=mo1*dexp(-kdma*tref/60.d0)
            mnp2=mo2*dexp(-kdmb*tref/60.d0)
            va(2)=va(2)*(vola-apvol)/vola
            ma(2)=ma(2)*(vola-apvol)/vola
            m3a(2)=m3a(2)*(vola-apvol)/vola
            pa(2)=pao*f3*f4
            apvol=apvol*1000.d0
            apvol=dnint(apvol*100.d0)/100.d0
            paconc=(pa(2)*vola-paconc)/(2.d0*pvol)
            ptemp=paconc
            vtemp=0.d0
            ptemp=dnint(ptemp*1.d3)/1.d3
            vtemp=dnint(vtemp*1.d3)/1.d3
```

```
                mnp=mnp1+mnp2
                call rates(tref,pa(2),pb(2),va(2),vb(2),
     +                mb(2),ratep,ratev,raterp,raterv)
                call out1(tact)
C                  *** SET PULSE DELAY FLAG ***
                flag3=999
                tcount=0
              endif
            endif
          elseif ((flag2 .eq. 999) .and. (delay .eq. 30)) then
C             *** ADD DELAYED H2O2 PULSE ***
C             ***   NO MNP PULSE LATER   ***
            vola=vola+apvol
            paconc=patemp
            ptemp=paconc
            vtemp=0.d0
            pa(2)=(pa(2)*(vola-apvol)+ptemp*apvol)/vola
            va(2)=va(2)*(vola-apvol)/vola
            ma(2)=ma(2)*(vola-apvol)/vola
            m3a(2)=m3a(2)*(vola-apvol)/vola
            apvol=apvol*1000.d0
            apvol=dnint(apvol*100.d0)/100.d0
            call rates(tref,pa(2),pb(2),va(2),vb(2),mb(2),
     +              ratep,ratev,raterp,raterv)
            call out1(tact)
            call out2(tpls)
            flag2=0
            tcount=0
            f3=f3*(1.d0-fr2pct)
          elseif ((flag3 .eq. 999) .and. (delay .eq. 40)) then
C             *** ADD DELAYED MNP PULSE ***
            tref=0.d0
            plconc=0.d0
            pm1cnc=0.d0
            pm2cnc=pm2tmp
            lo=lip*vol/(vol+2.d0*pvol)
            mo1=mnp1*vol/(vol+2.d0*pvol)
            mo2=(mnp2*vol+pm2tmp*2.d0*pvol)/(vol+2.d0*pvol)
            vol=vol+2.d0*pvol
            lip=lo
            mnp1=mo1
            mnp2=mo2
            if (flag .ne. 1001) then
              eps=0.1d0/(mnp1+mnp2)
              sig=0.1d0/(mnp1+mnp2)
            else
              eps=1.d0
              sig=1.d0
            endif
            pbmax=sig*mnp2
            pbmin=5.0d-3/(mnp1+mnp2)*(mnp1+mnp2)
            pb(2)=pb(2)*(vol-2.d0*pvol)/vol
            vb(2)=vb(2)*(vol-2.d0*pvol)/vol
```

```
            mb(2)=mb(2)*(vol-2.d0*pvol)/vol
            m3b(2)=m3b(2)*(vol-2.d0*pvol)/vol
            ah(2)=ah(2)*(vol-2.d0*pvol)/vol
            bpvol=2.d0*pvol*1000.d0
            bpvol=dnint(bpvol*100.d0)/100.d0
            mnp=mnp1+mnp2
            call rates(tref,pa(2),pb(2),va(2),vb(2),mb(2),
     +                  ratep,ratev,raterp,raterv)
            call out1(tact)
            call out2(tpls)
            flag3=0
            tcount=0
            f3=f3*(1.d0-fr2pct)
          endif
        endif
        pa(1)=pa(2)
        pb(1)=pb(2)
        va(1)=va(2)
        vb(1)=vb(2)
        ma(1)=ma(2)
        mb(1)=mb(2)
        m3a(1)=m3a(2)
        m3b(1)=m3b(2)
        ah(1)=ah(2)
   10 continue
      close(2)
      close(3)
      close(4)
      close(5)
      close(6)
      close(7)
      close(8)
  100 format(f8.3,2(1x,f8.4),1x,f10.4,1x,f8.4)
  101 format(f8.3,3(1x,f8.4),1x,f8.2,1x,f10.2)
  102 format(f8.3,4(1x,f8.6),1x,f8.4)
  103 format(f8.3,4(1x,f7.3))
      stop
      end
C
C *** OUTPUT SUBROUTINE #1 ***
C
      subroutine out1(ta)
      double precision ta, pa(2), pb(2), va(2), vb(2), ma(2)
      double precision mb(2), m3a(2), m3b(2), ah(2), l, m
      double precision pmn, pmx, vmx, rp, rv, rrp, rrv
      common /conc1/ pa, pb, va, vb, ma, mb
      common /conc2/ m3a, m3b, ah, l, m
      common /conc3/ pmn, pmx, vmx
      common /rate/ rp, rv, rrp, rrv
      write(2,1) ta, pa(2), pb(2), va(2), vb(2)
      write(3,2) ta, pmn, pmx, vmx, l, m
      write(8,3) ta, ma(2), mb(2), m3a(2), m3b(2), ah(2)
      write(6,4) ta, rp, rv, rrp, rrv
```

```
    1 format(f8.3,2(1x,f8.4),1x,f10.4,1x,f8.4)
    2 format(f8.3,3(1x,f8.4),1x,f8.2,1x,f10.2)
    3 format(f8.3,4(1x,f8.6),1x,f8.4)
    4 format(f8.3,4(1x,f7.3))
      return
      end
C
C *** OUTPUT SUBROUTINE #2 ***
C
      subroutine out2(tp)
      double precision tp, apv, ptmp, vtmp, bpv, ptmp2
      double precision vtmp2, plc, pm1c, pm2c, lth, vol
      double precision vola, area, lo, mo1, mo2, h
      common /rxtr/ lth, vol, vola, area, lo, mo1, mo2, h
      common /apulse/ apv, ptmp, vtmp
      common /bpulse/ bpv, ptmp2, vtmp2
      common /epulse/ plc, pm1c, pm2c
      write(4,1) tp, apv, ptmp, vtmp, vola
      write(5,2) tp, bpv, ptmp2, vtmp2, vol
      write(7,3) tp, bpv, plc, pm1c, pm2c
    1 format(10x,f8.3,5x,f5.2,5x,f8.3,4x,f10.3,5x,f5.2)
    2 format(10x,f8.3,5x,f5.1,5x,f8.3,4x,f8.3,5x,f5.2)
    3 format(10x,f8.3,3x,f5.1,3x,f10.3,2(3x,f10.3))
      return
      end
C
C ***** RUNGE-KUTTA-GILL DERIVATIVE EVALUATION SUBROUTINES *****
C *** CALCULATE RATE OF H2O2 SUPPLY TO SIDE B AT TIME T ***
C
      subroutine func1h(t,pa,pb,k)
      double precision t, pa, pb, k, f, h
      double precision dp, dv, dm, a1, a2, gma, dm3
      double precision lth, vol, vola, area, lo, mo1, mo2
      common /trans/ dp, dv, dm, dm3, a1, a2, gma
      common /rxtr/ lth, vol, vola, area, lo, mo1, mo2, h
      f=-dp*area/(lth*vola)*(pa-pb)
      k=h*f
      return
      end
C
C *** CALCULATE RATE OF VA SUPPLY TO SIDE B AT TIME T ***
C
      subroutine func2h(t,va,vb,k)
      double precision t, va, vb, k, f, h
      double precision dp, dv, dm, a1, a2, gma, dm3
      double precision lth, vol, vola, area, lo, mo1, mo2
      common /trans/ dp, dv, dm, dm3, a1, a2, gma
      common /rxtr/ lth, vol, vola, area, lo, mo1, mo2, h
      f=-dv*area/(gma*lth*vola)*(dexp(-gma*vb)-dexp(-gma*va))
      k=h*f
      return
      end
C
```

```
C *** CALCULATE RATE OF ACCUMULATION OF H2O2 IN SIDE B ***
C ***                  AT TIME T                        ***
C
      subroutine func3h(t,pb,pa,vb,mb,k)
      double precision t, pb, pa, vb, mb, k, f, h
      double precision dp, dv, dm, a1, a2, gma, dm3
      double precision lth, vol, vola, area, lo, mo1, mo2
      double precision k1, k3, k4, ki
      double precision k5a, psia, k5b, psib, k8
      double precision kdl1, kdl2, kdma, kdmb
      double precision lip, mnp1, mnp2
      common /lipkin/ k1, k3, k4, ki
      common /mnpkin/ k5a, psia, k5b, psib, k8
      common /trans/ dp, dv, dm, dm3, a1, a2, gma
      common /stable/ kdl1, kdl2, kdma, kdmb
      common /rxtr/ lth, vol, vola, area, lo, mo1, mo2, h
      lip=(kdl1/kdl2+lo)*dexp(-kdl2*t/60.d0)-kdl1/kdl2
      if (lip .lt. 0.d0) then
        lip=0.d0
      endif
      mnp1=mo1*dexp(-kdma*t/60.d0)
      mnp2=mo2*dexp(-kdmb*t/60.d0)
      f=k3*k4*vb+k1*k3*pb*vb+k1*k4*pb*(1.d0+pb/ki)
      f=k1*k3*k4*pb*vb*lip/f
      f=f+k5a*mnp1*pb*mb/(mb+k5a*psia*pb)
      f=f+k5b*mnp2*pb*mb/(mb+k5b*psib*pb)
      f=dp*area/(lth*vol)*(pa-pb)-f
      k=h*f
      return
      end
C
C *** CALCULATE RATE OF ACCUMULATION OF VA IN SIDE B ***
C ***                  AT TIME T                        ***
C
      subroutine func4h(t,vb,va,pb,k)
      double precision t, vb, va, pb, k, f, h
      double precision dp, dv, dm, a1, a2, gma, dm3
      double precision lth, vol, vola, area, lo, mo1, mo2
      double precision k1, k3, k4, ki
      double precision kdl1, kdl2, kdma, kdmb
      double precision lip
      common /lipkin/ k1, k3, k4, ki
      common /trans/ dp, dv, dm, dm3, a1, a2, gma
      common /stable/ kdl1, kdl2, kdma, kdmb
      common /rxtr/ lth, vol, vola, area, lo, mo1, mo2, h
      lip=(kdl1/kdl2+lo)*dexp(-kdl2*t/60.d0)-kdl1/kdl2
      if (lip .lt. 0.d0) then
        lip=0.d0
      endif
      f=k3*k4*vb+k1*k3*pb*vb+k1*k4*pb*(1.d0+pb/ki)
      f=k1*k3*k4*pb*vb*lip/f
      f=dv*area/(gma*lth*vol)*(dexp(-gma*vb)-dexp(-gma*va))-f
      k=h*f
```

```
      return
      end
C
C *** CALCULATE RATE OF Mn(II) SUPPLY TO SIDE B AT TIME T ***
C
      subroutine func5h(t,ma,mb,k)
      double precision t, ma, mb, k, f, h
      double precision dp, dv, dm, a1, a2, gma, dm3
      double precision lth, vol, vola, area, lo, mo1, mo2
      common /trans/ dp, dv, dm, dm3, a1, a2, gma
      common /rxtr/ lth, vol, vola, area, lo, mo1, mo2, h
      f=-dm*area/(lth*vola)*(ma-mb)
      k=h*f
      return
      end
C
C *** CALCULATE RATE OF ACCUMULATION OF Mn(II) IN SIDE B ***
C ***                AT TIME T                    ***
C
      subroutine func6h(t,ma,mb,m3b,ah,pb,k)
      double precision t, ma, mb, pb, k, f, h
      double precision dp, dv, dm, a1, a2, gma, dm3
      double precision lth, vol, vola, area, lo, mo1, mo2
      double precision k5a, psia, k5b, psib, k8
      double precision kdl1, kdl2, kdma, kdmb
      double precision mnp1, mnp2
      double precision m3b, ah
      common /mnpkin/ k5a, psia, k5b, psib, k8
      common /trans/ dp, dv, dm, dm3, a1, a2, gma
      common /stable/ kdl1, kdl2, kdma, kdmb
      common /rxtr/ lth, vol, vola, area, lo, mo1, mo2, h
      mnp1=mo1*dexp(-kdma*t/60.d0)
      mnp2=mo2*dexp(-kdmb*t/60.d0)
      f=-2.d0*k5a*mnp1*pb*mb/(mb+k5a*psia*pb)
      f=f-2.d0*k5b*mnp2*pb*mb/(mb+k5b*psib*pb)
      f=dm*area/(lth*vol)*(ma-mb)+f+k8*m3b*ah
      k=h*f
      return
      end
C
C *** CALCULATE RATE OF Mn(III) TRANSPORT FROM SIDE B AT TIME T ***
C
      subroutine func7h(t,m3a,m3b,k)
      double precision t, m3a, m3b, k, f, h
      double precision dp, dv, dm, a1, a2, gma, dm3
      double precision lth, vol, vola, area, lo, mo1, mo2
      common /trans/ dp, dv, dm, dm3, a1, a2, gma
      common /rxtr/ lth, vol, vola, area, lo, mo1, mo2, h
      f=-dm3*area/(lth*vola)*(m3a-m3b)
      k=h*f
      return
      end
C
```

```
C *** CALCULATE RATE OF ACCUMULATION OF Mn(III) IN SIDE B ***
C ***                  AT TIME T                          ***
C
      subroutine func8h(t,m3a,m3b,pb,mb,ah,k)
      double precision t, ah, m3a, m3b, mb, pb, k, f, h
      double precision dp, dv, dm, a1, a2, gma, dm3
      double precision lth, vol, vola, area, lo, mo1, mo2
      double precision k5a, psia, k5b, psib, k8
      double precision kdl1, kdl2, kdma, kdmb
      double precision mnp1, mnp2
      common /mnpkin/ k5a, psia, k5b, psib, k8
      common /trans/ dp, dv, dm, dm3, a1, a2, gma
      common /stable/ kdl1, kdl2, kdma, kdmb
      common /rxtr/ lth, vol, vola, area, lo, mo1, mo2, h
      mnp1=mo1*dexp(-kdma*t/60.d0)
      mnp2=mo2*dexp(-kdmb*t/60.d0)
      f=-2.d0*k5a*mnp1*pb*mb/(mb+k5a*psia*pb)
      f=f-2.d0*k5b*mnp2*pb*mb/(mb+k5b*psib*pb)
      f=f+k8*m3b*ah
      f=dm3*area/(lth*vol)*(m3a-m3b)-f
      k=h*f
      return
      end
C
C *** CALCULATE RATE OF ACCUMULATION OF LIGNIN BONDS IN SIDE B
***
C ***                      AT TIME T                      ***
C
      subroutine func9h(t,ah,m3b,k)
      double precision t, ah, m3b, k, f, h
      double precision lth, vol, vola, area, lo, mo1, mo2
      double precision k5a, psia, k5b, psib, k8
      common /mnpkin/ k5a, psia, k5b, psib, k8
      common /rxtr/ lth, vol, vola, area, lo, mo1, mo2, h
      f=-k8*m3b*ah
      k=h*f
      return
      end
C
C *** CALCULATE RATES FOR OUTPUT TO FILE ***
C
      subroutine rates(t,pa,pb,va,vb,mb,rp,rv,rrp,rrv)
      double precision t, pa, pb, va, vb, mb, rp, rv
      double precision rrp, rrv
      double precision dp, dv, dm, a1, a2, gma, dm3
      double precision lth, vol, vola, area, lo, mo1, mo2, h
      double precision k1, k3, k4, ki
      double precision k5a, psia, k5b, psib, k8
      double precision kdl1, kdl2, kdma, kdmb
      double precision lip, mnp1, mnp2
      common /lipkin/ k1, k3, k4, ki
      common /mnpkin/ k5a, psia, k5b, psib, k8
      common /trans/ dp, dv, dm, dm3, a1, a2, gma
```

```
common /stable/ kdl1, kdl2, kdma, kdmb
common /rxtr/ lth, vol, vola, area, lo, mo1, mo2, h
lip=(kdl1/kdl2+lo)*dexp(-kdl2*t/60.d0)-kdl1/kdl2
if (lip .lt. 0.d0) then
  lip=0.d0
endif
mnp1=mo1*dexp(-kdma*t/60.d0)
mnp2=mo2*dexp(-kdmb*t/60.d0)
rp=dp*area/(lth*vola)*(pa-pb)*vola*60.d0
rv=dv*area/(gma*lth*vola)*(dexp(-gma*vb)-dexp(-gma*va))
rv=rv*vola*60.d0
rrp=k3*k4*vb+k1*k3*pb*vb+k1*k4*pb*(1.d0+pb/ki)
rrp=k1*k3*k4*pb*vb*lip/rrp
rrp=rrp+k5a*mnp1*pb*mb/(mb+k5a*psia*pb)
rrp=(rrp+k5b*mnp2*pb*mb/(mb+k5b*psib*pb))*vol*60.d0
rrv=k3*k4*vb+k1*k3*pb*vb
rrv=rrv+k1*k4*pb*(1.d0+pb/ki)
rrv=k1*k3*k4*pb*vb*lip*vol*60.d0/rrv
return
end
```

D.2 Perturbation Program for Reactor Model Simulation

D.2.1 Variables Used In FORTRAN Program PERTURB.FOR

a. Double Precision Variables

Variable	Units	Description
aah	mM	Temporary value of ah(2)
ah(2)	mM	Concentration of oxidizable lignin bonds
apvol	mL	Volume pulsed to Side A
area	cm^2	Cross-sectional area for transport
a1	mM	Radius exponent from Deff(VA)
a2	mM	Viscosity exponent from Deff(VA)
bpvol	mL	Volume pulsed to Side B
const(2,25)	(---)	Array containing model parameters
data(16,8)	(---)	Array containing pulse profile data
delay	---	Pulse delay variable
dm	cm^2/min	Effective diffusion coefficient for Mn(II)
dm3	cm^2/min	Effective diffusion coefficient for [Mn(III)-(tart)2] complex
dp	cm^2/min	Effective diffusion coefficient for H2O2
dv	cm^2/min	Diffusion coefficient for VA at infinite dilution
gma	mM^{-1}	Exponent in VA diffusion coefficient ($= 1/a_1 + 1/a_2$)
h	min	Time step size
ilo	U/L	Initial LIP activity flag (-1 if none)
imo1	U/L	Initial D5NoMn MNP activity flag (-1 if none)
imo2	U/L	Initial D4HiMn MNP activity flag (-1 if none)
initlo	U/L	Initial [LIP] activity
inimo1	U/L	Initial D5NoMn [MNP] activity

inimo2	U/L	Initial D4HiMn [MNP] activity
kah(4)	mM	Runge-Kutta-Gill approximation constants for oxidizable lignin bonds
kdl1	U/L/hr	Zero-order decay constant for LIP
kdl2	hr^{-1}	First-order decay constant for LIP
kdma	hr^{-1}	First-order decay constant for D5NoMn MNP
kdmb	hr^{-1}	First-order decay constant for D4HiMn MNP
ki	mM	Inhibition constant for peroxide in LIP/VA kinetics
kma(4)	---	Runge-Kutta-Gill approximation constants for Side A Mn(II)
kmb(4)	---	Runge-Kutta-Gill approximation constants for Side B Mn(II)
km3a(4)	---	Runge-Kutta-Gill approximation constants for Side A [Mn(III)-(tart)2] complex
km3b(4)	---	Runge-Kutta-Gill approximation constants for Side B [Mn(III)-(tart)2] complex
kpa(4)	---	Runge-Kutta-Gill approximation constants for Side A peroxide
kpb(4)	---	Runge-Kutta-Gill approximation constants for Side B peroxide
kva(4)	---	Runge-Kutta-Gill approximation constants for Side A VA
kvb(4)	---	Runge-Kutta-Gill approximation constants for Side A VA
k1	$[min(U/L)]^{-1}$	Rate constant for 1st step in LIP/VA kinetics
k3	$[min(U/L)]^{-1}$	Rate constant for 2nd step in LIP/VA kinetics
k4	$mM[min(U/L)]^{-1}$	Rate constant for 3rd step in LIP/VA kinetics
k5a	$[min(U/L)]^{-1}$	Rate constant for 1st step in MNP/MN(II) kinetics (for D5NoMn MNP)
k5b	$[min(U/L)]^{-1}$	Rate constant for 1st step in MNP/Mn(II) kinetics (for D4HiMn MNP)
k8	$[min\ mM]^{-1}$	Rate constant for oxidation of lignin bonds by [Mn(III)-(tart)2] complex
lip	U/L	[LIP] activity at time t
lo	U/L	[LIP] activity at reference time zero
lth	cm	Wet membrane thickness
ma(2)	mM	Concentration of Mn(II) in Side A
mb(2)	mM	Concentration of Mn(II) in Side B
mma	mM	Temporary value of Mn(II) in Side A, used in Runge-Kutta-Gill solution
mmb	mM	Temporary value of Mn(II) in Side B, used in Runge-Kutta-Gill solution
mm3a	mM	Temporary value of [Mn(III)-(tart)2] complex in Side A, used in Runge-Kutta-Gill solution
mm3b	mM	Temporary volue of [Mn(III)-(tart)2] complex in Side A, used in Runge-Kutta-Gill solution
mnp	U/L	Total [MNP] activity at time t
mnp1	U/L	D5NoMn [MNP] activity at time t
mnp2	U/L	D4HiMn [MNP] activity at time t
mo1	U/L	D5NoMn [MNP] activity at reference time zero

mo2	U/L	D4HiMn [MNP] activity at reference time zero
m3a(2)	mM	Concentration of [Mn(III)-(tart)2] complex in Side A
m3b(2)	mM	Concentration of [Mn(III)-(tart)2] complex in Side B
npt	min	Pulse time
pa(2)	mM	Concentration of peroxide in Side A
paconc	mM	Variable used in pulse concentration calculations for H2O2 in Side A
pb(2)	mM	Concentration of peroxide in Side B
plconc	U/L	[LIP] pulse concentration for Side B
pm1cnc	U/L	D5NoMn [MNP] pulse concentration for Side B
pm2cnc	U/L	D4HiMn [MNP] pulse concentration for Side B
ppa	mM	Temporary value of H2O2 in Side A, used in Runge-Kutta-Gill solution
ppb	mM	Temporary value of H2O2 in Side B, used in Runge-Kutta-Gill solution
psia	---	Ratio of (k6 + k7)/(k6k7) for D5NoMn MNP
psib	---	Ratio of (k6 + k7)/(k6k7) for D4HiMn MNP
pulse(1,16)	min	Array containing pulse times
pvol	mL	Standard pulse volume multiple (0.010 mL) for enzyme pulses
pz1	%	Percent under measured parameter value to vary
pz2	%	Percent over measured parameter value to vary
rka	---	Runge-Kutta-Gill derivative approximation weighting constant
rkb	---	Runge-Kutta-Gill derivative approximation weighting constant
rkc	---	Runge-Kutta-Gill derivative approximation weighting constant
rkd	---	Runge-Kutta-Gill derivative approximation weighting constant
tact	min	Actual cumulative time
tdelay	min	Counter for pulse time delay
temp	---	Temporary calculation variable
temp2	---	Temporary calculation variable
tref	min	Enzyme activity reference time
va(2)	mM	Concentration of VA in Side A
vaconc	mM	Variable used in pulse concentration calculations and dilution calculations for VA in Side A
vb(2)	mM	Concentration of VA in Side B
vol	mL	Volume of Side B
vola	mL	Volume of Side A
vva	mM	Temporary value of VA in Side A, used in Runge-Kutta-Gill solution
vvb	mM	Temporary value of VA in Side B, used in Runge-Kutta-Gill solution

b. Integer Variables

Variable	Units	Description

flag	---	Flag which indicates enzymes present
i	---	Loop counter
j	---	Loop counter
k	---	Loop counter
l	---	Loop counter
n	---	Main time step loop counter
nprint	---	Data output step increment
npulse	---	Counts number of pulses already done
ntotal	---	Total number of time steps
tcount	---	Pulse delay time step counter
y	---	Number indication choice of enzyme mixtures
z	---	Number indicating choice of parameter to vary

D.2.2 FORTRAN Program PERTURB.FOR

```
C ***************************************************************************
C
C   PROGRAM PERTURB.FOR
C
C     Reactor Model Perturbation Program
C
C ***************************************************************************
      double precision aah, ah(2), apvol, area, a1, a2
      double precision bpvol, const(2,25), data(16,8)
      double precision delay, dm, dm3, dp, dv, gma, h
      double precision ilo, imo1, imo2, initlo, inimo1, inimo2
      double precision kah(4), kdl1, kdl2, kdma, kdmb, ki, kma(4)
      double precision kmb(4), km3a(4), km3b(4), kpa(4), kpb(4)
      double precision kva(4), kvb(4), k1, k3, k4, k5a, k5b, k8
      double precision lip, lo, lth
      double precision ma(2), mb(2), mma, mmb, mm3a, mm3b, mnp, mnp1
      double precision mnp2, mo1, mo2, m3a(2), m3b(2), npt
      double precision pa(2), paconc, pb(2), plconc, pm1cnc
      double precision pm2cnc, ppa, ppb, psia, psib, pulse(1,16)
      double precision pvol, pz1, pz2, rka, rkb, rkc, rkd
      double precision tact, tdelay, temp, temp2, tref
      double precision va(2), vaconc, vb(2), vol, vola, vva, vvb
      integer flag, i, j, k, l, n, nprint, npulse
      integer ntotal, tcount, y, z
      common /trans/ dp, dv, dm, dm3, a1, a2, gma
      common /rxtr/ lth, vol, vola, area, lo, mo1, mo2, h
      common /lipkin/ k1, k3, k4, ki
      common /mnpkin/ k5a, psia, k5b, psib, k8
      common /stable/ kdl1, kdl2, kdma, kdmb
      rka=(2.d0**0.5d0-1.d0)/2.d0
      rkb=(2.d0-2.d0**0.5d0)/2.d0
      rkc=-(2.d0**.5d0)/2.d0
      rkd=1.d0+(2.d0**0.5d0)/2.d0
C
C *** INPUT STEP SIZE & ENZYME MIXTURE ***
C
      write(*,*) 'INPUT # OF INITIAL ENZYME MIXTURE:'
      write(*,*)
```

```
      write(*,*) '1. LIP alone'
      write(*,*) '2. LIP + MNP'
      write(*,*) '3. MNP alone'
      write(*,*)
      read(*,*) y
      if (y .eq. 1) then
        ilo=1000.d0
        imo1=-1.d0
        imo2=-1.d0
      elseif (y .eq. 2) then
        ilo=1000.d0
        imo1=1200.d0
        imo2=54800.d0
      else
        ilo=-1.d0
        imo1=-1.d0
        imo2=56000.d0
      endif
      open(2,file='sideb.prn',status='new')
      write(2,*) 'BASE CASE MINUS VARIANCE'
      open(4,file='const.prn',status='old')
      do 5 j = 0, 4
        read(4,*) (const(1,k), k=(1+5*j),(5+5*j))
    5 continue
      close(4)
      do 6 k = 1, 25
        const(2,k)=const(1,k)
    6 continue
      write(*,*) 'ENTER THE NUMBER OF THE CONSTANT TO VARY:'
      write(*,*)
      write(*,*) '1. area    6. dv    11. k1    16. k5b    21. kdl2'
      write(*,*) '2. lth     7. dm    12. k3    17. k8     22. kdma'
      write(*,*) '3. vol     8. dm3   13. k4    18. psia   23. kdmb'
      write(*,*) '4. vola    9. a1    14. ki    19. psib   24.     '
      write(*,*) '5. dp     10. a2    15. k5a   20. kdl1   25.     '
      write(*,*)
      read(*,*) z
      write(*,*)
      write(*,*) 'ENTER [- %] and [+ %] (with signs) TO VARY:'
      write(*,*)
      read(*,*) pz1, pz2
      l=1
    7 if (l .eq. 1) then
        const(1,z)=const(1,z)*(1.d0+pz1/100.d0)
      else
        const(1,z)=const(2,z)*(1.d0+pz2/100.d0)
      endif
      flag=0
      npulse=1
C
C *** SET INITIAL CONDITIONS ***
C
      if (ilo .eq. -1.d0) then
```

```
      open(5,file='mnp.prn',status='old')
      initlo=0.d0
      inimo1=0.d0
      inimo2=imo2
      h=0.01d0
      ntotal=72000
      nprint=500
    elseif (imo2 .eq. -1.d0) then
      open(5,file='lip.prn',status='old')
      initlo=ilo
      inimo1=0.d0
      inimo2=0.d0
      h=0.1d0
      ntotal=7200
      nprint=50
    else
      open(5,file='lipmnp.prn',status='old')
      initlo=ilo
      inimo1=imo1
      inimo2=imo2
      h=0.01d0
      ntotal=72000
      nprint=500
    endif
    read(5,*) pa(1), va(1), ma(1), m3a(1)
    read(5,*) pb(1), vb(1), mb(1), m3b(1)
    read(5,*) (pulse(1,k), k=1,8)
    read(5,*) (pulse(1,k+8), k=1,8)
C
C *** SET MODEL PARAMETERS ***
C
    area=const(1,1)
    lth=const(1,2)
    vol=const(1,3)
    vola=const(1,4)
    dp=const(1,5)
    dv=const(1,6)
    dm=const(1,7)
    dm3=const(1,8)
    a1=const(1,9)
    a2=const(1,10)
    gma=1.d0/a1+1.d0/a2
C
C *** SET KINETIC CONSTANTS ***
C
    k1=const(1,11)
    k3=const(1,12)
    k4=const(1,13)
    ki=const(1,14)
    k5a=const(1,15)
    k5b=const(1,16)
    k8=const(1,17)
    psia=const(1,18)
```

```
      psib=const(1,19)
C
C *** SET STABILITY CONSTANTS ***
C
      kdl1=const(1,20)
      kdl2=const(1,21)
      kdma=const(1,22)
      kdmb=const(1,23)
      ah(1)=0.02d0*2.d0/206.9d0*1.d6
      lo=initlo
      mo1=inimo1
      mo2=inimo2
      lip=lo
      mnp1=mo1
      mnp2=mo2
      mnp=mnp1+mnp2
      pvol=0.01d0
      tref=0.d0
      tact=0.d0
      tcount=0
      tdelay=0.d0
C
C *** OPEN OUTPUT FILES AND INITIALIZE ***
C
      write(2,*) 't (min), Pb, Vb (all in mM)'
      write(2,100) tact, pb(1), vb(1)
C
C *** MAIN LOOP - SOLVES BY 4TH ORDER RUNGE-KUTTA-GILL ***
C
      j=0
      do 10 n = 1, ntotal
        j=j+1
        ppa=pa(1)
        ppb=pb(1)
        vva=va(1)
        vvb=vb(1)
        mma=ma(1)
        mmb=mb(1)
        mm3a=m3a(1)
        mm3b=m3b(1)
        aah=ah(1)
        temp=tref
        do 20 i = 1, 4
          call func1h(temp,ppa,ppb,kpa(i))
          call func2h(temp,vva,vvb,kva(i))
          call func3h(temp,ppb,ppa,vvb,mmb,kpb(i))
          call func4h(temp,vvb,vva,ppb,kvb(i))
          call func5h(temp,mma,mmb,kma(i))
          call func6h(temp,mma,mmb,mm3b,aah,ppb,kmb(i))
          call func7h(temp,mm3a,mm3b,km3a(i))
          call func8h(temp,mm3a,mm3b,ppb,mmb,aah,km3b(i))
          call func9h(temp,aah,mm3b,kah(i))
          if (i .eq. 1) then
```

```
            temp=tref+0.5d0*h
            ppa=pa(1)+0.5d0*kpa(i)
            ppb=pb(1)+0.5d0*kpb(i)
            vva=va(1)+0.5d0*kva(i)
            vvb=vb(1)+0.5d0*kvb(i)
            mma=ma(1)+0.5d0*kma(i)
            mmb=mb(1)+0.5d0*kmb(i)
            mm3a=m3a(1)+0.5d0*km3a(i)
            mm3b=m3b(1)+0.5d0*km3b(i)
            aah=ah(1)+0.5d0*kah(i)
          elseif (i .eq. 2) then
            temp=tref+0.5d0*h
            ppa=pa(1)+rka*kpa(i-1)+rkb*kpa(i)
            ppb=pb(1)+rka*kpb(i-1)+rkb*kpb(i)
            vva=va(1)+rka*kva(i-1)+rkb*kva(i)
            vvb=vb(1)+rka*kvb(i-1)+rkb*kvb(i)
            mma=ma(1)+rka*kma(i-1)+rkb*kma(i)
            mmb=mb(1)+rka*kmb(i-1)+rkb*kmb(i)
            mm3a=m3a(1)+rka*km3a(i-1)+rkb*km3a(i)
            mm3b=m3b(1)+rka*km3b(i-1)+rkb*km3b(i)
            aah=ah(1)+rka*kah(i-1)+rkb*kah(i)
          elseif (i .eq. 3) then
            temp=tref+h
            ppa=pa(1)+rkc*kpa(i-1)+rkd*kpa(i)
            ppb=pb(1)+rkc*kpb(i-1)+rkd*kpb(i)
            vva=va(1)+rkc*kva(i-1)+rkd*kva(i)
            vvb=vb(1)+rkc*kvb(i-1)+rkd*kvb(i)
            mma=ma(1)+rkc*kma(i-1)+rkd*kma(i)
            mmb=mb(1)+rkc*kmb(i-1)+rkd*kmb(i)
            mm3a=m3a(1)+rkc*km3a(i-1)+rkd*km3a(i)
            mm3b=m3b(1)+rkc*km3b(i-1)+rkd*km3b(i)
            aah=ah(1)+rkc*kah(i-1)+rkd*kah(i)
          endif
   20   continue
        tref=tref+h
        tact=tact+h
        if (flag .eq. 999) then
C           *** INCREMENT PULSE DELAY COUNTER ***
          tcount=tcount+1
        endif
        tdelay=h*dble(tcount)
        delay=idnint(tdelay*100.d0)
        pa(2)=pa(1)+(kpa(1)+kpa(4))/6.d0+(rkb*kpa(2)+rkd*kpa(3))/3.d0
        pb(2)=pb(1)+(kpb(1)+kpb(4))/6.d0+(rkb*kpb(2)+rkd*kpb(3))/3.d0
        va(2)=va(1)+(kva(1)+kva(4))/6.d0+(rkb*kva(2)+rkd*kva(3))/3.d0
        vb(2)=vb(1)+(kvb(1)+kvb(4))/6.d0+(rkb*kvb(2)+rkd*kvb(3))/3.d0
        ma(2)=ma(1)+(kma(1)+kma(4))/6.d0+(rkb*kma(2)+rkd*kma(3))/3.d0
        mb(2)=mb(1)+(kmb(1)+kmb(4))/6.d0+(rkb*kmb(2)+rkd*kmb(3))/3.d0
        m3a(2)=m3a(1)+(km3a(1)+km3a(4))/6.d0+(rkb*km3a(2)+
     +              rkd*km3a(3))/3.d0
        m3b(2)=m3b(1)+(km3b(1)+km3b(4))/6.d0+(rkb*km3b(2)+
     +              rkd*km3b(3))/3.d0
        ah(2)=ah(1)+(kah(1)+kah(4))/6.d0+(rkb*kah(2)+rkd*kah(3))/3.d0
```

```
      if (ma(2) .lt. 0.d0) then
        ma(2)=0.d0
      elseif (mb(2) .lt. 0.d0) then
        mb(2)=0.d0
      elseif (m3a(2) .lt. 0.d0) then
        m3a(2)=0.d0
      elseif (m3b(2) .lt. 0.d0) then
        m3b(2)=0.d0
      elseif (ah(2) .lt. 0.d0) then
        ah(2)=0.d0
      endif
C
C *** CALCULATE NEW MAXIMA AND MINIMA; CHECK RATE CRITERIA ***
C
      lip=(kdl1/kdl2+lo)*dexp(-kdl2*tref/60.d0)-kdl1/kdl2
      if (lip .lt. 0.d0) then
        lip=0.d0
      endif
      mnp1=mo1*dexp(-kdma*tref/60.d0)
      mnp2=mo2*dexp(-kdmb*tref/60.d0)
      mnp=mnp1+mnp2
      if (j .eq. nprint) then
        write(2,100) tact, pb(2), vb(2)
        j=0
      endif
      temp2=dble(idnint(tact*100.d0))/100.d0
      if (temp2 .eq. pulse(1,npulse)) then
        read(5,*) (data(npulse,k), k=1,8)
        flag=999
        npt=data(npulse,1)
        if (npt .eq. -1.d0) then
          npulse=npulse-1
        endif
        apvol=data(npulse,2)
        paconc=data(npulse,3)
        vaconc=data(npulse,4)
        bpvol=data(npulse,5)
        plconc=data(npulse,6)
        pm1cnc=data(npulse,7)
        pm2cnc=data(npulse,8)
      endif
      if (flag .eq. 999) then
        if ((apvol .ne. 40.d0) .and. (apvol .ne. 20.d0) .and.
     +          (temp2 .eq. npt)) then
          write(2,100) tact, pb(2), vb(2)
          vola=vola-apvol/1.d3
          tcount=0
        elseif ((apvol .eq. 40.d0) .and. (temp2 .eq. npt)) then
          vola=vola-2.d0*pvol
          write(2,100) tact, pb(2), vb(2)
          tcount=0
        elseif ((apvol .eq. 20.d0) .and. (temp2 .eq. npt)) then
          pa(2)=(pa(2)*vola+paconc*apvol/1.d3)/(vola+apvol/1.d3)
```

```
            va(2)=va(2)*(vola/(vola+apvol/1.d3))
            ma(2)=ma(2)*(vola/(vola+apvol/1.d3))
            m3a(2)=m3a(2)*(vola/(vola+apvol/1.d3))
            write(2,100) tact, pb(2), vb(2)
            vola=vola+apvol/1.d3
            tcount=0
          elseif ((delay .eq. 30) .and. (apvol .ne. 20.d0)) then
            pa(2)=(pa(2)*vola+paconc*apvol/1.d3)/(vola+apvol/1.d3)
            va(2)=(va(2)*vola+vaconc*apvol/1.d3)/(vola+apvol/1.d3)
            ma(2)=ma(2)*(vola/(vola+apvol/1.d3))
            m3a(2)=m3a(2)*(vola/(vola+apvol/1.d3))
            write(2,100) tact, pb(2), vb(2)
            vola=vola+apvol/1.d3
            if (apvol .ne. 40.d0) then
              flag=0
              tcount=0
              npulse=npulse+1
            endif
          elseif (((delay .eq. 40) .and. (apvol .eq. 20.d0)) .or.
     +            ((delay .eq. 70) .and. (apvol .eq. 40.d0))) then
            tref=0.d0
            lo=(lip*vol+plconc*bpvol/1.d3)/(vol+bpvol/1.d3)
            mo1=(mnp1*vol+pm1cnc*bpvol/1.d3)/(vol+bpvol/1.d3)
            mo2=(mnp2*vol+pm2cnc*bpvol/1.d3)/(vol+bpvol/1.d3)
            lip=lo
            mnp1=mo1
            mnp2=mo2
            pb(2)=pb(2)*(vol/(vol+bpvol/1.d3))
            vb(2)=vb(2)*(vol/(vol+bpvol/1.d3))
            mb(2)=mb(2)*(vol/(vol+bpvol/1.d3))
            m3b(2)=m3b(2)*(vol/(vol+bpvol/1.d3))
            ah(2)=ah(2)*(vol/(vol+bpvol/1.d3))
            write(2,100) tact, pb(2), vb(2)
            vol=vol+bpvol/1.d3
            flag=0
            tcount=0
            npulse=npulse+1
          endif
        endif
        pa(1)=pa(2)
        pb(1)=pb(2)
        va(1)=va(2)
        vb(1)=vb(2)
        ma(1)=ma(2)
        mb(1)=mb(2)
        m3a(1)=m3a(2)
        m3b(1)=m3b(2)
        ah(1)=ah(2)
10    continue
      close(5)
      write(2,*) 'BASE CASE PLUS VARIANCE'
      l=l+1
      if (l .gt. 2) then
```

```
        goto 8
      else
        goto 7
      endif
    8 close(2)
  100 format(f8.3,2(1x,f8.4))
      stop
      end
C
C ***** RUNGE-KUTTA-GILL DERIVATIVE EVALUATION SUBROUTINES *****
C *** CALCULATE RATE OF H2O2 SUPPLY TO SIDE B AT TIME T ***
C
      subroutine func1h(t,pa,pb,k)
      double precision t, pa, pb, k, f, h
      double precision dp, dv, dm, a1, a2, gma, dm3
      double precision lth, vol, vola, area, lo, mo1, mo2
      common /trans/ dp, dv, dm, dm3, a1, a2, gma
      common /rxtr/ lth, vol, vola, area, lo, mo1, mo2, h
      f=-dp*area/(lth*vola)*(pa-pb)
      k=h*f
      return
      end
C
C *** CALCULATE RATE OF VA SUPPLY TO SIDE B AT TIME T ***
C
      subroutine func2h(t,va,vb,k)
      double precision t, va, vb, k, f, h
      double precision dp, dv, dm, a1, a2, gma, dm3
      double precision lth, vol, vola, area, lo, mo1, mo2
      common /trans/ dp, dv, dm, dm3, a1, a2, gma
      common /rxtr/ lth, vol, vola, area, lo, mo1, mo2, h
      f=-dv*area/(gma*lth*vola)*(dexp(-gma*vb)-dexp(-gma*va))
      k=h*f
      return
      end
C
C *** CALCULATE RATE OF ACCUMULATION OF H2O2 IN SIDE B ***
C ***                  AT TIME T                    ***
C
      subroutine func3h(t,pb,pa,vb,mb,k)
      double precision t, pb, pa, vb, mb, k, f, h
      double precision dp, dv, dm, a1, a2, gma, dm3
      double precision lth, vol, vola, area, lo, mo1, mo2
      double precision k1, k3, k4, ki
      double precision k5a, psia, k5b, psib, k8
      double precision kdl1, kdl2, kdma, kdmb
      double precision lip, mnp1, mnp2
      common /lipkin/ k1, k3, k4, ki
      common /mnpkin/ k5a, psia, k5b, psib, k8
      common /trans/ dp, dv, dm, dm3, a1, a2, gma
      common /stable/ kdl1, kdl2, kdma, kdmb
      common /rxtr/ lth, vol, vola, area, lo, mo1, mo2, h
      lip=(kdl1/kdl2+lo)*dexp(-kdl2*t/60.d0)-kdl1/kdl2
```

```
      if (lip .lt. 0.d0) then
        lip=0.d0
      endif
      mnp1=mo1*dexp(-kdma*t/60.d0)
      mnp2=mo2*dexp(-kdmb*t/60.d0)
      f=k3*k4*vb+k1*k3*pb*vb+k1*k4*pb*(1.d0+pb/ki)
      f=k1*k3*k4*pb*vb*lip/f
      f=f+k5a*mnp1*pb*mb/(mb+k5a*psia*pb)
      f=f+k5b*mnp2*pb*mb/(mb+k5b*psib*pb)
      f=dp*area/(lth*vol)*(pa-pb)-f
      k=h*f
      return
      end
C
C *** CALCULATE RATE OF ACCUMULATION OF VA IN SIDE B ***
C ***                AT TIME T                       ***
C
      subroutine func4h(t,vb,va,pb,k)
      double precision t, vb, va, pb, k, f, h
      double precision dp, dv, dm, a1, a2, gma, dm3
      double precision lth, vol, vola, area, lo, mo1, mo2
      double precision k1, k3, k4, ki
      double precision kdl1, kdl2, kdma, kdmb
      double precision lip
      common /lipkin/ k1, k3, k4, ki
      common /trans/ dp, dv, dm, dm3, a1, a2, gma
      common /stable/ kdl1, kdl2, kdma, kdmb
      common /rxtr/ lth, vol, vola, area, lo, mo1, mo2, h
      lip=(kdl1/kdl2+lo)*dexp(-kdl2*t/60.d0)-kdl1/kdl2
      if (lip .lt. 0.d0) then
        lip=0.d0
      endif
      f=k3*k4*vb+k1*k3*pb*vb+k1*k4*pb*(1.d0+pb/ki)
      f=k1*k3*k4*pb*vb*lip/f
      f=dv*area/(gma*lth*vol)*(dexp(-gma*vb)-dexp(-gma*va))-f
      k=h*f
      return
      end
C
C *** CALCULATE RATE OF Mn(II) SUPPLY TO SIDE B AT TIME T ***
C
      subroutine func5h(t,ma,mb,k)
      double precision t, ma, mb, k, f, h
      double precision dp, dv, dm, a1, a2, gma, dm3
      double precision lth, vol, vola, area, lo, mo1, mo2
      common /trans/ dp, dv, dm, dm3, a1, a2, gma
      common /rxtr/ lth, vol, vola, area, lo, mo1, mo2, h
      f=-dm*area/(lth*vola)*(ma-mb)
      k=h*f
      return
      end
C
C *** CALCULATE RATE OF ACCUMULATION OF Mn(II) IN SIDE B ***
```

```
C ***                AT TIME T                    ***
C
      subroutine func6h(t,ma,mb,m3b,ah,pb,k)
      double precision t, ma, mb, pb, k, f, h
      double precision dp, dv, dm, a1, a2, gma, dm3
      double precision lth, vol, vola, area, lo, mo1, mo2
      double precision k5a, psia, k5b, psib, k8
      double precision kdl1, kdl2, kdma, kdmb
      double precision mnp1, mnp2
      double precision m3b, ah
      common /mnpkin/ k5a, psia, k5b, psib, k8
      common /trans/ dp, dv, dm, dm3, a1, a2, gma
      common /stable/ kdl1, kdl2, kdma, kdmb
      common /rxtr/ lth, vol, vola, area, lo, mo1, mo2, h
      mnp1=mo1*dexp(-kdma*t/60.d0)
      mnp2=mo2*dexp(-kdmb*t/60.d0)
      f=-2.d0*k5a*mnp1*pb*mb/(mb+k5a*psia*pb)
      f=f-2.d0*k5b*mnp2*pb*mb/(mb+k5b*psib*pb)
      f=dm*area/(lth*vol)*(ma-mb)+f+k8*m3b*ah
      k=h*f
      return
      end
C
C *** CALCULATE RATE OF Mn(III) TRANSPORT FROM SIDE B AT TIME T ***
C
      subroutine func7h(t,m3a,m3b,k)
      double precision t, m3a, m3b, k, f, h
      double precision dp, dv, dm, a1, a2, gma, dm3
      double precision lth, vol, vola, area, lo, mo1, mo2
      common /trans/ dp, dv, dm, dm3, a1, a2, gma
      common /rxtr/ lth, vol, vola, area, lo, mo1, mo2, h
      f=-dm3*area/(lth*vola)*(m3a-m3b)
      k=h*f
      return
      end
C
C *** CALCULATE RATE OF ACCUMULATION OF Mn(III) IN SIDE B ***
C ***                AT TIME T                    ***
C
      subroutine func8h(t,m3a,m3b,pb,mb,ah,k)
      double precision t, ah, m3a, m3b, mb, pb, k, f, h
      double precision dp, dv, dm, a1, a2, gma, dm3
      double precision lth, vol, vola, area, lo, mo1, mo2
      double precision k5a, psia, k5b, psib, k8
      double precision kdl1, kdl2, kdma, kdmb
      double precision mnp1, mnp2
      common /mnpkin/ k5a, psia, k5b, psib, k8
      common /trans/ dp, dv, dm, dm3, a1, a2, gma
      common /stable/ kdl1, kdl2, kdma, kdmb
      common /rxtr/ lth, vol, vola, area, lo, mo1, mo2, h
      mnp1=mo1*dexp(-kdma*t/60.d0)
      mnp2=mo2*dexp(-kdmb*t/60.d0)
      f=-2.d0*k5a*mnp1*pb*mb/(mb+k5a*psia*pb)
```

```
      f=f-2.d0*k5b*mnp2*pb*mb/(mb+k5b*psib*pb)
      f=f+k8*m3b*ah
      f=dm3*area/(lth*vol)*(m3a-m3b)-f
      k=h*f
      return
      end
C
C *** CALCULATE RATE OF ACCUMULATION OF LIGNIN BONDS ***
C ***          IN SIDE B AT TIME T                  ***
C
      subroutine func9h(t,ah,m3b,k)
      double precision t, ah, m3b, k, f, h
      double precision lth, vol, vola, area, lo, mo1, mo2
      double precision k5a, psia, k5b, psib, k8
      common /mnpkin/ k5a, psia, k5b, psib, k8
      common /rxtr/ lth, vol, vola, area, lo, mo1, mo2, h
      f=-k8*m3b*ah
      k=h*f
      return
      end
```

D.3 Linear Regression Program for Confidence Intervals

D.3.1 Variables Used In FORTRAN Program LINREG.FOR

a. Double Precision Variables

Variable	Description
b(ncolx,ncoly)	Vector of model coefficients
bt(ncoly,ncolx)	Transpose of vector b = (xtinv*xty)
e(numpt,ncoly)	Vector containing residual errors
mse	Mean square residual error
rel	Relative error
s(1,1)	Total sum of squares
sm(1,1)	Model sum of squares
sum	Temporary variable used to add residual errors
y(numpt,ncoly)	Vector of responses
ypred(numpt,ncoly)	Vector of predicted responses
yt(ncoly,numpt)	Transpose of vector y
x(numpt,ncolx)	Matrix of indpendent variables/factors
xt(ncolx,numpt)	Transpose of matrix x
xtinv(ncolx,ncolx)	Inverse of matrix xtx
xtx(ncolx,ncolx)	Matrix xt * Matrix x
xty(ncolx,ncoly)	Matrix xt * Matrix y

b. Integer Variables

Variable	Description
i	Loop counter
j	Loop counter
ncolx	Number of columns in matrix x

ncoly	Number of columns in vector y
numpt	Number of (x,y) data pairs

D.3.2 FORTRAN Program LINREG.FOR

```
C ***************************************************************************
C
C  PROGRAM LINREG.FOR
C
C    Linear Regression Program
C
C ***************************************************************************

      integer numpt, ncolx, ncoly, i, j
      parameter(numpt=249, ncolx=11,ncoly=1)
      double precision x(numpt,ncolx), y(numpt,ncoly), xt(ncolx,numpt)
      double precision xtx(ncolx,ncolx), xty(ncolx,ncoly)
      double precision xtinv(ncolx,ncolx), b(ncolx,ncoly)
      double precision bt(ncoly,ncolx), yt(ncoly,numpt)
      double precision s(1,1), sm(1,1), e(numpt,ncoly)
      double precision ypred(numpt,ncoly), sum, rel, mse
      open(2,file='data.csv',status='old')
      open(1,file='results',status='new')
      do 10 i = 1, numpt
        read(2,*) (x(i,j),j=1,ncolx)
   10 continue
      do 20 i = 1, numpt
        read(2,*) y(i,ncoly)
   20 continue
      close(2)
      call trans(x,xt,numpt,ncolx)
      call mult(xt,x,xtx,ncolx,numpt,numpt,ncolx,ncolx,ncolx)
      call invers(xtx,xtinv,ncolx)
      call mult(xt,y,xty,ncolx,numpt,numpt,ncoly,ncolx,ncoly)
      call mult(xtinv,xty,b,ncolx,ncolx,ncolx,ncoly,ncolx,ncoly)
      call trans(b,bt,ncolx,ncoly)
      call trans(y,yt,numpt,ncoly)
      call mult(yt,y,s,ncoly,numpt,numpt,ncoly,1,1)
      call mult(bt,xty,sm,ncoly,ncolx,ncolx,ncoly,1,1)
      call mult(x,b,ypred,numpt,ncolx,ncolx,ncoly,numpt,ncoly)
      sum=0.d0
      do 30 i = 1, numpt
        e(i,1)=abs(y(i,1)-ypred(i,1))/y(i,1)
        sum=sum+e(i,1)
   30 continue
      sum=sum/numpt*100.d0
      mse=((s(1,1)-sm(1,1))/(numpt-ncolx))**.5d0
      rel=((s(1,1)-sm(1,1))/s(1,1))**.5d0
      write(1,*) 'b='
      call print(b,ncolx,ncoly)
      write(1,*)
      write(1,*) ' S = ', s(1,1)
      write(1,*) 'Sm = ', sm(1,1)
```

```
      write(1,*) 'MSE= ', mse
      write(1,*) 'REL= ', rel
      write(1,*) '% DIFF= ',sum
      close(1)
      stop
      end
c
c *** MULTIPLICATION SUBROUTINE ***
c
      subroutine mult(a,b,c,ra,ca,rb,cb,rc,cc)
      integer ra, rb, rc, ca, cb, cc, i, j, k
      double precision sum, a(ra,ca), b(rb,cb), c(rc,cc)
      do 10 i = 1, ra
        do 20 j = 1, cb
          sum=0.d0
          do 30 k = 1, ca
            sum=sum+(a(i,k)*b(k,j))
   30      continue
          c(i,j)=sum
   20   continue
   10 continue
      return
      end
c
c *** TRANSPOSE SUBROUTINE ***
c
      subroutine trans(a,b,ra,ca)
      integer ra, ca, i, j
      double precision a(ra,ca), b(ca,ra)
      do 10 i = 1, ra
        do 20 j = 1, ca
          b(j,i)=a(i,j)
   20   continue
   10 continue
      return
      end
c
c *** INVERSION SUBROUTINE ***
c
c  ** Note: If ncolx > 10, change the dimensions of the matrix r to:
c                    r(ncolx, 2*ncolx)
c
      subroutine invers(a,b,c)
      integer c, i, j, k
      double precision a(c,c), b(c,c), r(20,40), const
      do 10 i = 1, c
        do 20 j = 1, c
          r(i,j)=a(i,j)
          if (i .eq. j) then
            r(i,j+c)=1.d0
          else
            r(i,j+c)=0.d0
          endif
```

```
   20    continue
   10 continue
        do 30 k = 1, c
          do 40 i = k, c
            do 50 j = 2*c, 1, -1
              r(i,j)=r(i,j)/r(i,k)
   50       continue
   40     continue
          if (k .eq. c) then
            goto 30
          endif
          do 60 i = k+1, c
            do 70 j = 1, 2*c
              r(i,j)=r(i,j)-r(k,j)
   70       continue
   60     continue
   30 continue
        do 80 k = 2, c
          do 90 i = 1, k-1
            if ((r(i,k)-r(i,k)*r(k,k)) .eq. 0.d0) then
              const=1.d0
            else
              const=-1.d0
            endif
            do 100 j = 2*c, k, -1
              r(i,j)=r(i,j)-const*r(i,k)*r(k,j)
  100       continue
   90     continue
   80 continue
        do 110 i = 1, c
          do 120 j = 1, c
            b(i,j)=r(i,j+c)
  120     continue
  110 continue
        return
        end
c
c *** PRINT SUBROUTINE ***
c
        subroutine print(a,ra,ca)
        integer ra, ca, i, j
        double precision a(ra,ca)
        do 10 i = 1, ra
          write(1,*) (a(i,j),j=1,ca)
   10 continue
        return
        end
```

APPENDIX E

TABULATED DATA

Table E.1: Data for Figure 5.4.

	[H2O2] in Membrane (mM)							
x/l	.002 min	.005 min	.010 min	.020 min	.040 min	.060 min	.080 min	.500 min
0.00	50.013	50.009	50.004	49.997	49.988	49.982	49.976	49.874
0.05	35.509	40.711	43.411	45.437	46.983	47.573	47.810	47.887
0.10	22.859	31.911	37.000	40.947	44.003	45.173	45.649	45.900
0.15	13.237	24.029	30.941	36.598	41.072	42.794	43.495	43.912
0.20	6.855	17.349	25.376	32.453	38.213	40.444	41.353	41.925
0.25	3.163	11.992	20.413	28.569	35.448	38.132	39.227	39.938
0.30	1.300	7.929	16.121	24.994	32.796	35.865	37.119	37.950
0.35	0.481	5.018	12.530	21.764	30.272	33.652	35.033	35.963
0.40	0.166	3.056	9.635	18.906	27.890	31.495	32.970	33.975
0.45	0.061	1.826	7.405	16.435	25.659	29.401	30.933	31.988
0.50	0.032	1.137	5.788	14.354	23.585	27.370	28.922	30.000
0.55	0.031	0.844	4.723	12.659	21.668	25.404	26.937	28.012
0.60	0.050	0.855	4.144	11.332	19.907	23.502	24.979	26.025
0.65	0.112	1.127	3.988	10.351	18.296	21.662	23.046	24.037
0.70	0.276	1.649	4.192	9.685	16.825	19.880	21.137	22.050
0.75	0.649	2.435	4.701	9.297	15.481	18.150	19.249	20.062
0.80	1.387	3.494	5.461	9.148	14.248	16.466	17.380	18.075
0.85	2.664	4.825	6.423	9.192	13.107	14.820	15.527	16.088
0.90	4.588	6.399	7.536	9.384	12.036	13.203	13.686	14.100
0.95	7.118	8.159	8.751	9.675	11.014	11.607	11.853	12.113
1.00	10.019	10.018	10.017	10.016	10.017	10.020	10.025	10.126

Table E.2: Data for Figure 5.5.

time (min)	Left-Hand-Side (lhs) for [H2O2]Ao of 50 mM	500 mM	1000 mM	2500 mM	5000 mM
0.0	0.000	0.000	0.000	0.000	0.000
0.0	0.000	0.000	0.000	0.000	0.000
0.0	0.000	0.000	0.000	0.000	0.000
0.0	0.000	0.000	0.000		0.000
1.0		1.613			
2.0	3.616	1.976	2.242	2.488	2.319
2.0		2.178	2.349	1.894	2.333
2.0		1.841	1.545	2.156	1.993
2.0		1.577	1.854		
4.0		4.188			
8.0	7.398	7.452	8.281	9.884	8.840
8.0		7.963	8.516	8.357	8.875
8.0	5.629	6.195	7.509	9.000	8.687
8.0		6.985	8.239		
12.0	9.555	11.341	13.234	15.452	14.466
12.0	10.904	11.589	12.594	14.586	15.192
12.0		9.123	12.019	14.837	14.076
12.0		10.687			14.093
24.0	28.079	24.232	26.145		

Table E.3: Data for Figure 5.6.

time (min)	lhs
0.00	0.00000
84.00	-0.01150
139.50	-0.01764
290.52	-0.03856
300.00	

Table E.4: Data for Figure 5.7.

[VA] (mM)	D^{eff} for VA (cm^2/min)	[VA] (mM)	D^{eff} for VA (cm^2/min)
48.0	4.520E-05	720.0	2.060E-05
48.0	4.850E-05	720.0	2.130E-05
48.0	3.270E-05	720.0	2.220E-05
48.0	4.490E-05	720.0	2.120E-05
48.0	4.290E-05	960.0	1.640E-05
48.0	4.030E-05	960.0	1.730E-05
48.0	4.750E-05	960.0	1.570E-05
96.0	3.370E-05	960.0	1.600E-05
96.0	3.570E-05	960.0	1.590E-05
96.0	3.840E-05	1440.0	1.030E-05
96.0	4.420E-05	1440.0	1.340E-05
96.0	3.500E-05	1440.0	1.320E-05
96.0	4.680E-05	1440.0	1.020E-05
240.0	2.850E-05	1440.0	1.130E-05
240.0	4.200E-05	1440.0	1.210E-05
480.0	2.860E-05	1440.0	1.120E-05
480.0	2.800E-05	1440.0	1.260E-05
480.0	2.990E-05	1440.0	1.260E-05
480.0	3.200E-05	1440.0	1.280E-05
480.0	3.380E-05	2400.0	1.080E-05
480.0	2.950E-05	2400.0	1.080E-05
480.0	3.330E-05	2400.0	5.600E-06
720.0	2.100E-05	2400.0	5.600E-06

Table E.5: Data for Figure 5.8.

	[VA] in Membrane (mM)							
x/l	.010 min	.020 min	.040 min	.060 min	.080 min	.100 min	.500 min	2.00 min
0.00	96.020	96.013	96.004	95.997	95.991	95.986	95.923	95.720
0.05	71.333	78.403	83.510	85.829	87.251	88.240	91.577	91.429
0.10	49.144	61.711	71.350	75.849	78.636	80.584	87.232	87.137
0.15	31.219	46.716	59.833	66.235	70.266	73.107	82.889	82.846
0.20	18.206	33.949	49.220	57.147	62.254	65.891	78.547	78.554
0.25	9.714	23.648	39.708	48.722	54.696	59.010	74.209	74.262
0.30	4.735	15.772	31.423	41.064	47.676	52.529	69.874	69.970
0.35	2.110	10.072	24.416	34.246	41.257	46.499	65.544	65.677
0.40	0.867	6.172	18.674	28.307	35.483	40.961	61.218	61.385
0.45	0.340	3.667	14.130	23.254	30.378	35.938	56.897	57.092
0.50	0.145	2.181	10.681	19.068	25.947	31.444	52.582	52.800
0.55	0.095	1.415	8.200	15.703	22.176	27.476	48.272	48.508
0.60	0.127	1.159	6.551	13.099	19.036	24.019	43.967	44.215
0.65	0.245	1.282	5.601	11.179	16.485	21.046	39.668	39.923
0.70	0.506	1.720	5.226	9.860	14.467	18.519	35.373	35.630
0.75	1.004	2.444	5.315	9.053	12.920	16.392	31.083	31.338
0.80	1.853	3.447	5.769	8.670	11.772	14.610	26.797	27.046
0.85	3.154	4.711	6.502	8.622	10.949	13.111	22.514	22.754
0.90	4.947	6.206	7.437	8.822	10.373	11.829	18.233	18.463
0.95	7.165	7.873	8.502	9.186	9.961	10.694	13.955	14.171
1.00	9.634	9.633	9.633	9.632	9.632	9.632	9.678	9.880

Table E.6: Data for Figure 5.9.

	[VA] in Membrane (mM)							
x/l	.010 min	.020 min	.040 min	.060 min	.080 min	.100 min	.500 min	2.00 min
0.00	96.028	96.025	96.021	96.017	96.014	96.012	95.983	95.928
0.05	47.332	60.281	70.259	74.848	77.622	79.531	88.788	91.561
0.10	16.360	31.901	47.329	55.264	60.276	63.803	81.667	87.195
0.15	3.836	14.012	29.165	38.507	44.845	49.484	74.692	82.831
0.20	0.618	5.060	16.359	25.242	31.900	37.045	67.931	78.471
0.25	0.094	1.503	8.323	15.530	21.658	26.736	61.445	74.116
0.30	0.039	0.382	3.835	8.952	14.017	18.588	55.289	69.766
0.35	0.036	0.101	1.605	4.832	8.646	12.451	49.507	65.424
0.40	0.036	0.046	0.619	2.448	5.094	8.058	44.133	61.090
0.45	0.036	0.037	0.231	1.180	2.897	5.083	39.192	56.764
0.50	0.036	0.036	0.099	0.574	1.650	3.209	34.696	52.446
0.55	0.036	0.036	0.071	0.346	1.047	2.158	30.646	48.137
0.60	0.036	0.037	0.098	0.351	0.884	1.715	27.032	43.837
0.65	0.036	0.042	0.193	0.541	1.050	1.733	23.834	39.545
0.70	0.036	0.070	0.416	0.936	1.499	2.118	21.022	35.261
0.75	0.042	0.182	0.864	1.588	2.224	2.814	18.557	30.984
0.80	0.094	0.538	1.668	2.557	3.232	3.786	16.394	26.713
0.85	0.416	1.433	2.949	3.883	4.520	5.002	14.479	22.448
0.90	1.668	3.222	4.765	5.559	6.061	6.421	12.756	18.187
0.95	4.765	6.060	7.058	7.517	7.795	7.988	11.162	13.929
1.00	9.635	9.635	9.634	9.634	9.634	9.633	9.633	9.672

Table E.7: Data for Figure 5.10.

[VA] (mM)	μ (cP)
0.000	0.6491
10.614	0.6522
46.853	0.6689
96.432	0.6760
480.058	0.8751
720.000	1.0000
961.920	1.0829
1440.000	1.4721
1915.392	1.8438
2395.008	2.4725

Table E.8: Data for Figure 5.11.

time (min)	Left-Hand-Side for $[VA]_{A_0}$ of 48 mM	96 mM	480 mM	720 mM
0.000	0.0000	0.0000	0.0000	0.0000
0.000	0.0000	0.0000	0.0000	0.0000
0.000	0.0000		0.0000	0.0000
0.000	0.0000		0.0000	
0.000	0.0000			
4.000			0.2190	0.1675
4.000	0.1003		0.1964	0.1805
4.000			0.2223	0.1994
4.000				
10.000			0.4603	0.4317
10.000	0.5085		0.4708	0.4257
10.000	0.2782		0.4854	0.4336
10.000				
23.083		0.8736		
23.750		1.1781		
30.000	1.0402			
30.000	1.2843			
40.000		1.7692		
40.000		1.6014		
45.000	2.3133			
45.000	2.0493			
60.000	2.8559	3.1546		
60.000	2.8766	2.5856		

Table E.9: Data for Figure 5.12.

[VA] (mM)	r/r°	[VA] (mM)	r/r°	[VA] (mM)	r/r°
0.0	1.0000	260.0	1.5424	520.0	2.3790
10.0	1.0168	270.0	1.5683	530.0	2.4189
20.0	1.0339	280.0	1.5947	540.0	2.4596
30.0	1.0513	290.0	1.6215	550.0	2.5009
40.0	1.0689	300.0	1.6487	560.0	2.5430
50.0	1.0869	310.0	1.6764	570.0	2.5857
60.0	1.1052	320.0	1.7046	580.0	2.6292
70.0	1.1237	330.0	1.7333	590.0	2.6734
80.0	1.1426	340.0	1.7624	600.0	2.7183
90.0	1.1618	350.0	1.7920	610.0	2.7640
100.0	1.1814	360.0	1.8221	620.0	2.8104
110.0	1.2012	370.0	1.8527	630.0	2.8577
120.0	1.2214	380.0	1.8839	640.0	2.9057
130.0	1.2419	390.0	1.9155	650.0	2.9545
140.0	1.2628	400.0	1.9477	660.0	3.0042
150.0	1.2840	410.0	1.9805	670.0	3.0547
160.0	1.3056	420.0	2.0138	680.0	3.1060
170.0	1.3275	430.0	2.0476	690.0	3.1582
180.0	1.3499	440.0	2.0820	700.0	3.2113
190.0	1.3725	450.0	2.1170	710.0	3.2652
200.0	1.3956	460.0	2.1526	720.0	3.3201
210.0	1.4191	470.0	2.1888		
220.0	1.4429	480.0	2.2255		
230.0	1.4672	490.0	2.2629		
240.0	1.4918	500.0	2.3010		
250.0	1.5169	510.0	2.3396		

Table E.10: Data for Figure 5.13.

$[LIP]_o/v$ (Umin/LmM)	$[H_2O_2]^{-1}$ (mM^{-1})
2052.4	25.896
1730.9	17.497
1466.0	17.497
1512.3	17.497
1512.3	12.952
1368.3	12.952
1368.3	12.952
1282.7	10.396
1271.4	10.396
1360.5	10.396
892.34	2.0767
884.65	2.0767
945.18	1.0634
1029.1	1.0634
1041.1	1.0634
1242.8	0.5250
1173.7	0.5250
1201.2	0.5250

Table E.11: Data for Figure 5.14.

$[LIP]_o/v$ (Umin/LmM)	$[VA]^{-1}$ (mM^{-1})
3218.3	17.267
3161.3	17.267
3161.3	17.267
2048.2	8.6334
2048.2	8.6334
2204.8	8.6334
1169.4	1.7267
1132.6	1.7267
1154.4	1.7267

Table E.12: Data for Figure 5.15.

1/[VA] (mM-1)	$[LIP]_o/v$ (Umin/LmM) for $[H_2O_2]$ at 544.7 µM	1093.1 µM	1547.9 µM	2179.5 µM
17.267	3122.6	3201.0	3307.6	
17.267	3090.2	3295.4	3370.1	
17.267	3069.0	3235.7		
8.6334	2152.2	2133.1	2152.2	2325.8
8.6334	2133.1	2184.8	2120.5	2253.1
8.6334	2060.0	2089.8	2253.1	2184.8
1.7267	1044.0	1053.2	1053.2	1084.9
1.7267	1084.9	1065.6	1059.4	1098.1
1.7267	1035.0	1065.6	1132.6	1132.6

Table E.13: Data for Figure 5.16.

$[H_2O_2]$ (μM)	Slope (min(U/L))
481.5	130.50
940.4	139.95
1428	145.65
1905	166.41

Table E.14: Data for Figure 5.17.

$[H_2O_2]^{-1}$ (mM^{-1})	$[MNP]_o/v$ (Umin/LmM)
25.896	2664.7
25.896	2779.6
25.896	2664.7
12.952	1798.5
12.952	1586.9
10.396	1541.6
10.396	1586.9
10.396	1586.9
2.0767	879.70

Table E.15: Data for Figure 5.18.

$[H_2O_2]^{-1}$ (mM^{-1})	$[MNP]_o/v$ (Umin/LmM)
94.473	10826
47.311	5843.2
47.311	4756.1
47.311	5087.4
23.401	2567.0
23.401	3383.0
23.401	2919.1
23.401	3317.1
15.706	2027.1
15.706	1824.4
11.662	1554.2
11.662	1554.2
11.662	1631.9
11.662	1652.6
9.3282	1231.6
9.3282	1388.9
1.8359	987.17
1.8359	987.17
1.8359	987.17

Table E.16: Data for Figures 5.19a and 5.19b.

	$[H_2O_2]$ (mM) for $[H_2O_2]_o$ equal to							
time (hr)	8.284 mM	58.02 mM	494.8 mM	1014 mM	2004 mM	2876 mM	3890 mM	4738 mM
0.000	8.284	58.02	494.8	1014	2004	2876	3890	4738
1.000	8.309	58.05	439.1	958.7	1924	2919	3866	4874
1.833	8.278	58.01	463.9	952.5	1961	2895	3909	4800
5.083	8.292	57.41	451.5	909.2	1955	2888	3909	4818
8.417	8.290	57.41	445.3	971.1	1967	2895	3915	4991
28.000	8.284	58.02	433.0	958.7	1979	2969	4076	5029

Table E.17: Data for Figure 5.20.

time (hr)	Left-Hand-Side (lhs) for $[LIP]_o$ at 795.7 U/L	1216 U/L	1587 U/L	2365 U/L
0.000	0.00000	0.00000	0.00000	0.00000
1.000	0.02631	0.02358	0.01760	0.01572
3.000	0.07092	0.06385	0.04649	0.05755
6.133	0.09295	0.1298	0.1124	0.1143

Table E.18: Data for Figure 5.21.

	[LIP] (U/L) for Average $[LIP]_o$ at			
time (hr)	795.7 (U/L)	1216 (U/L)	1587 (U/L)	2365 (U/L)
0.000	808.6	1206	1562	2348
0.000	782.8	1226	1612	2382
1.000	748.4	1141	1500	2297
1.000	748.4	1187	1583	2328
3.000	671.0	1071	1449	2126
3.000	671.0	1084	1488	2225
6.133	628.0	954.8	1265	1977
6.133	640.0	931.6	1354	2021

Table E.19: Data for Figure 5.22.

	[MNP] (U/L) for Average $[MNP_a]_o$ at			
time (hr)	1118 (U/L)	1889 (U/L)	2357 (U/L)	3668 (U/L)
0.000	1041	1892	2357	3544
0.000	1194	1886	2357	3791
1.000	1023	1775	2173	3633
1.000	1078	1731	2286	3369
3.000	965.5	1621	2108	3176
3.000	900.2	1582	1947	3084
6.133	821.4	1374	1747	2638
6.133	820.0	1332	1881	2582

Table E.20: Data for Figure 5.23.

	[MNP] (U/L) for Average $[MNP_b]_o$ at			
time (hr)	8905 (U/L)	16949 (U/L)	26292 (U/L)	48663 (U/L)
0.000	8793.7	17587	28342	52525
0.000	9016.5	16310	24242	44800
1.000	8392.7	15716	24108	41354
1.000	8556.1	15746		55020
3.000	7798.5	13577	24331	50980
3.000	8377.8	16815	24376	52287
6.133	7635.1	13161	22014	37789
6.133	7560.8	13220	24911	41235

APPENDIX F

FIGURES NOT SHOWN IN TEXT

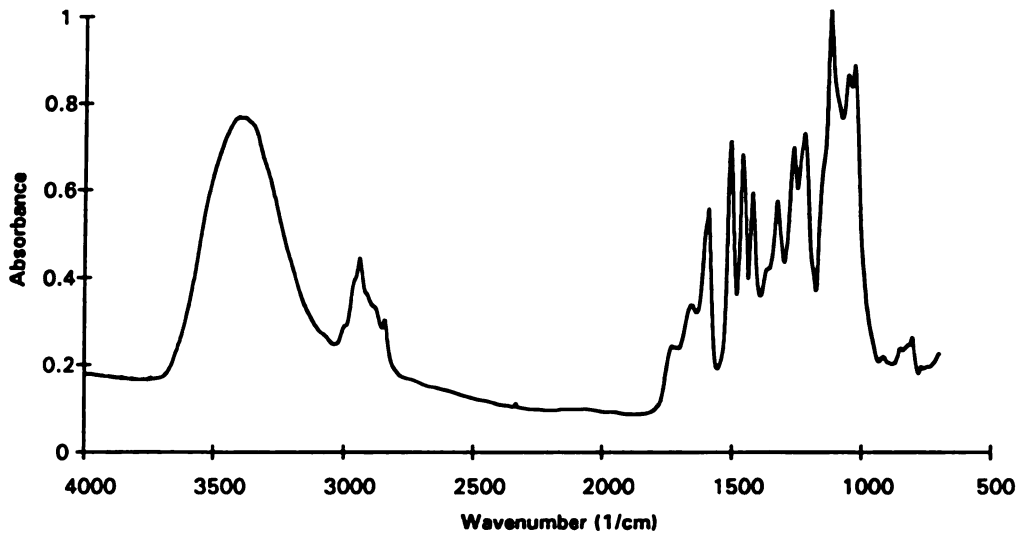

Figure F.1: FTIR absorbance spectrum of the LIP Alone, No reagent control (R^-) Lignin after treatment for 12 hours.

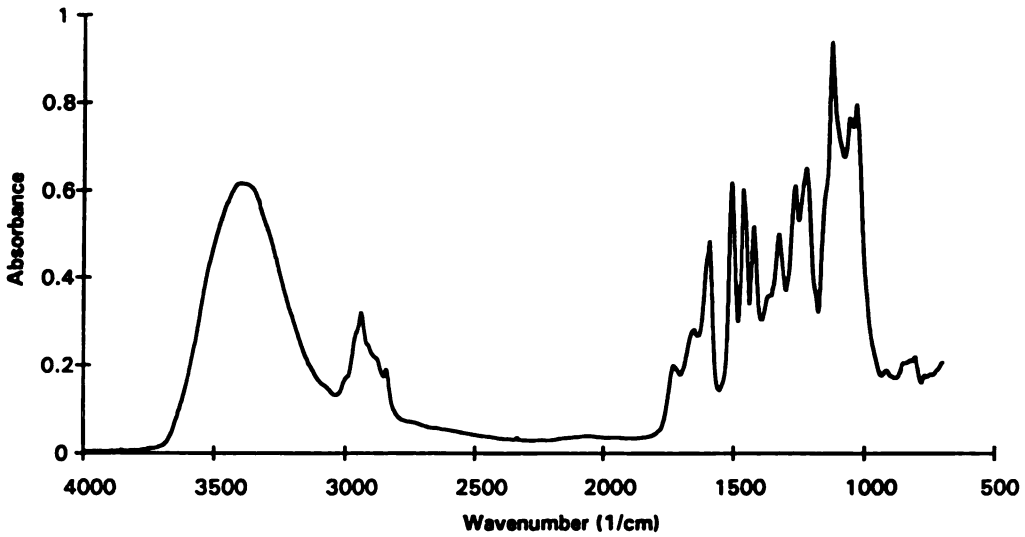

Figure F.2: FTIR absorbance spectrum of the LIP Alone, No LIP control (E^-) lignin after treatment for 12 hours.

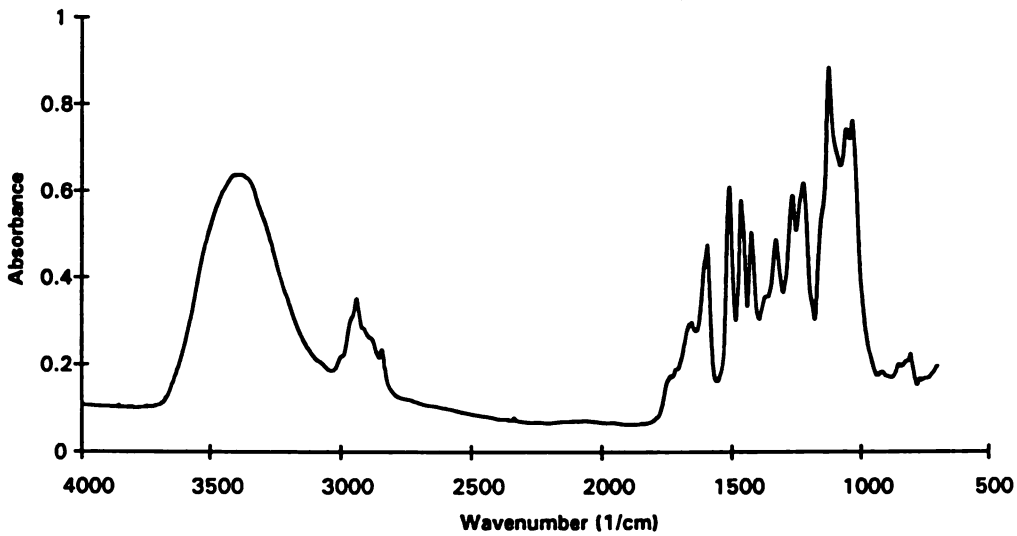

Figure F.3: FTIR absorbance spectrum of the LIP Alone, Autoclaved LIP control (AE) lignin after treatment for 12 hours.

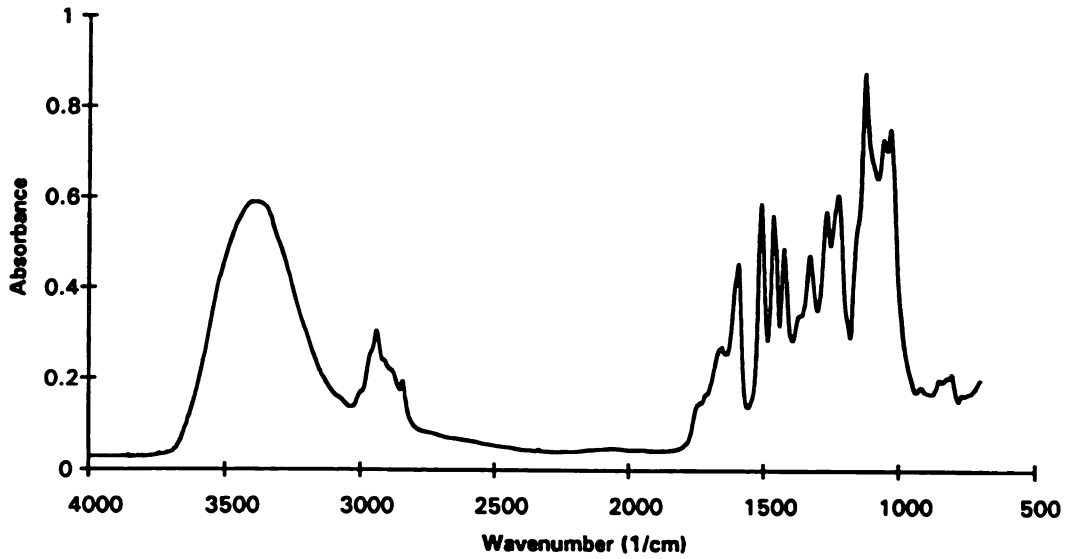

Figure F.4: FTIR absorbance spectrum of the LIP + MNP, No reagent control (R^-) lignin after treatment for 12 hours.

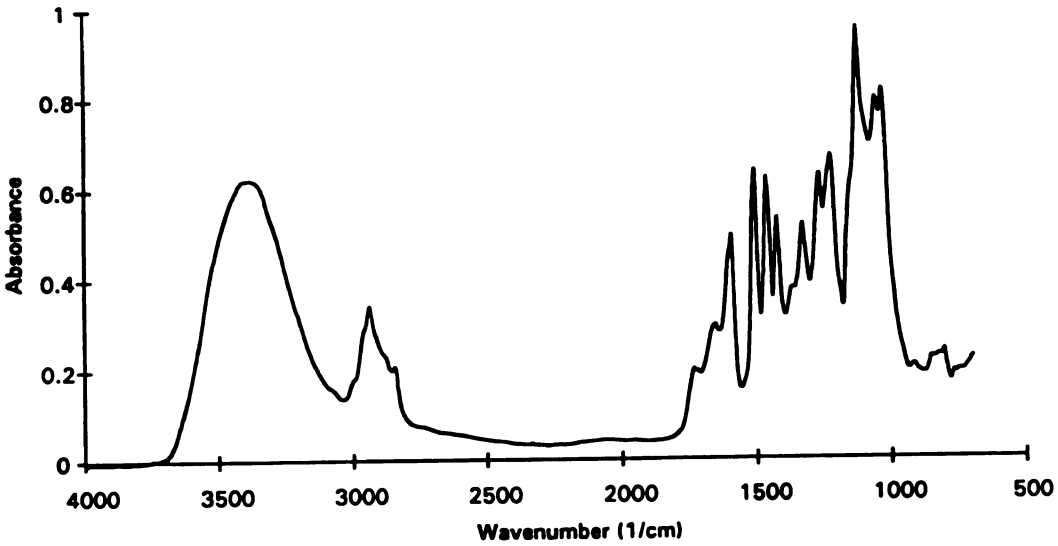

Figure F.5: FTIR absorbance spectrum of the LIP + MNP, No LIP, no MNP control (E˙) lignin after treatment for 12 hours.

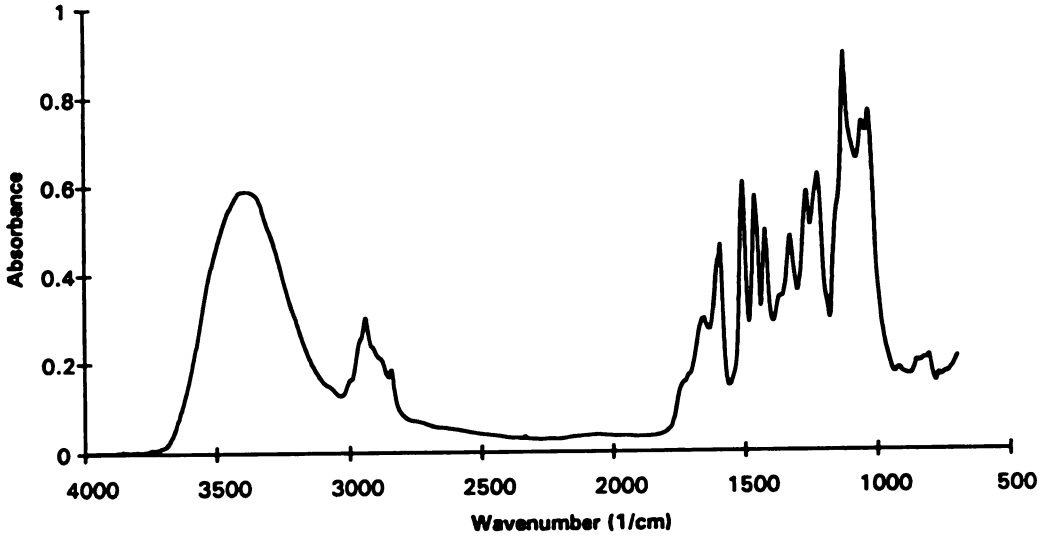

Figure F.6: FTIR absorbance spectrum of the LIP + MNP, Autoclaved LIP, autoclaved MNP control (AE) lignin after treatment for 12 hours.

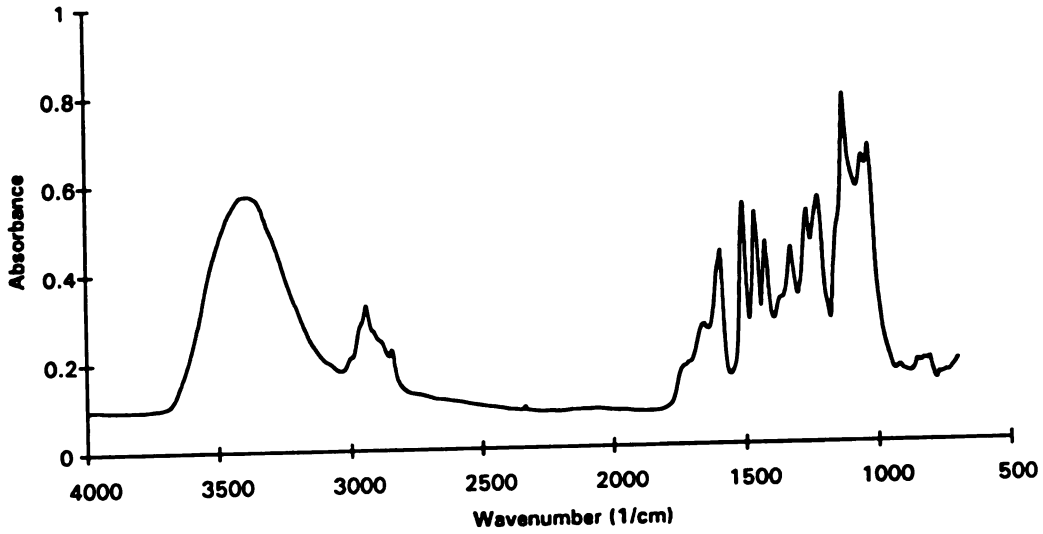

Figure F.7: FTIR absorbance spectrum of the MNP Alone, No reagent control (R^-) lignin after treatment for 12 hours.

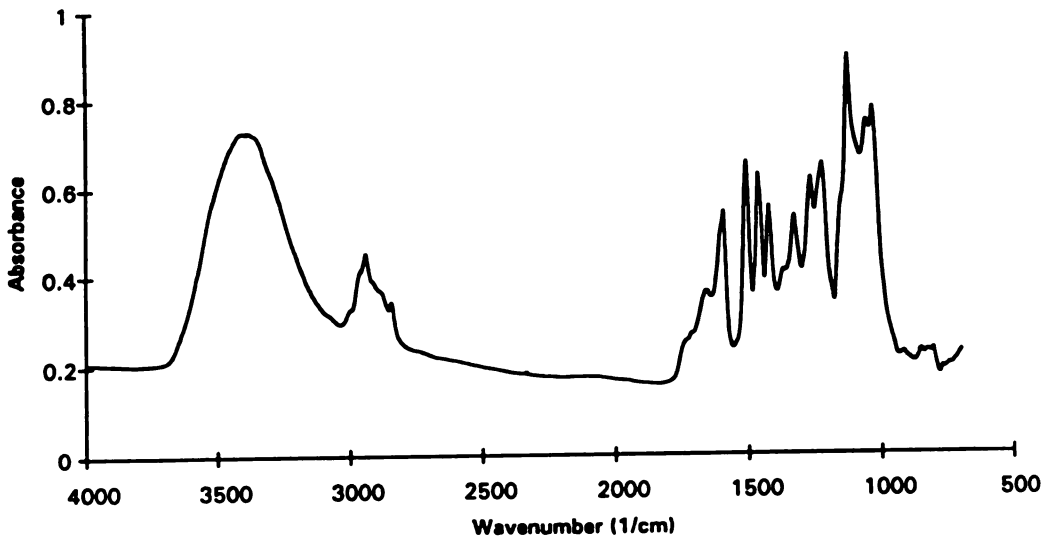

Figure F.8: FTIR absorbance spectrum of the MNP Alone, No MNP control (E^-) lignin after treatment for 12 hours.

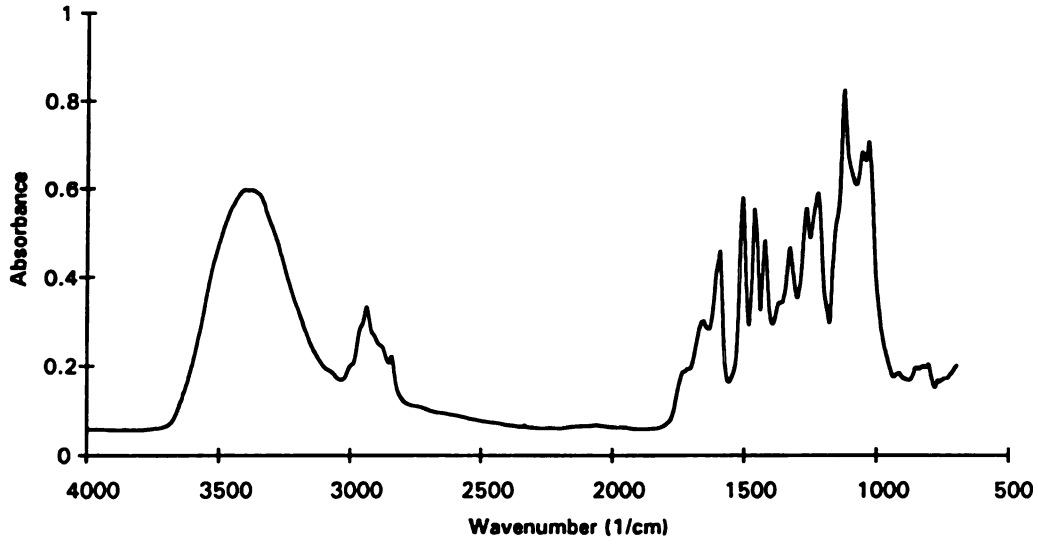

Figure F.9: FTIR absorbance spectrum of the MNP Alone, Autoclaved MNP control (AE) lignin after treatment for 12 hours.

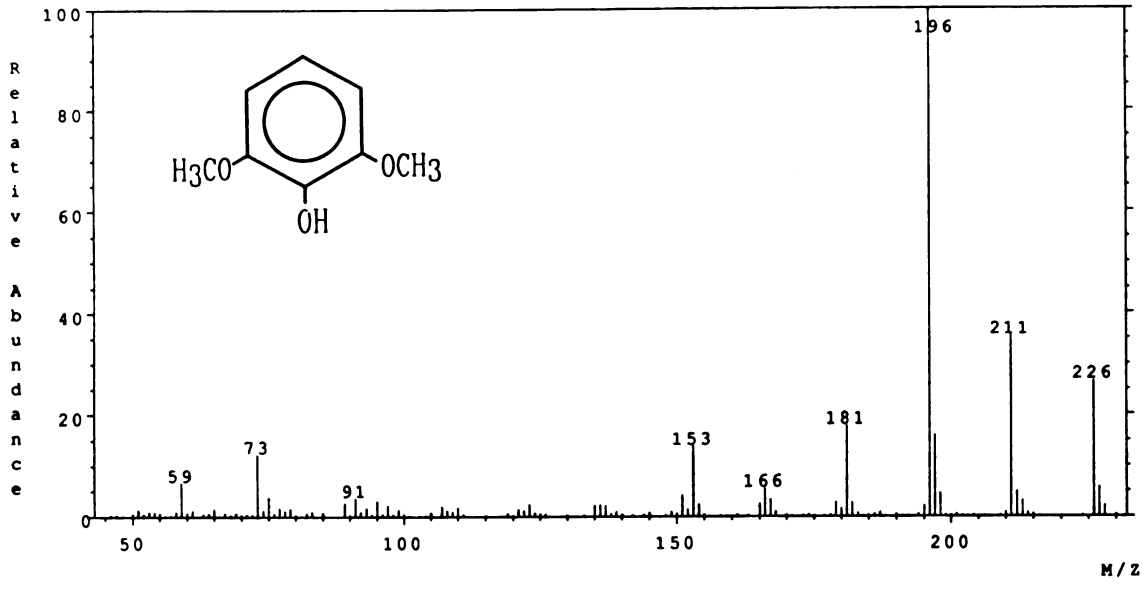

Figure F.10: Electron-impact mass spectrum of 2,6-dimethoxyphenol (Aldrich) obtained from scan 536 (background average of scans 533 and 538) of the TIC from an authentic standard analyzed with the DB-1 GC column.

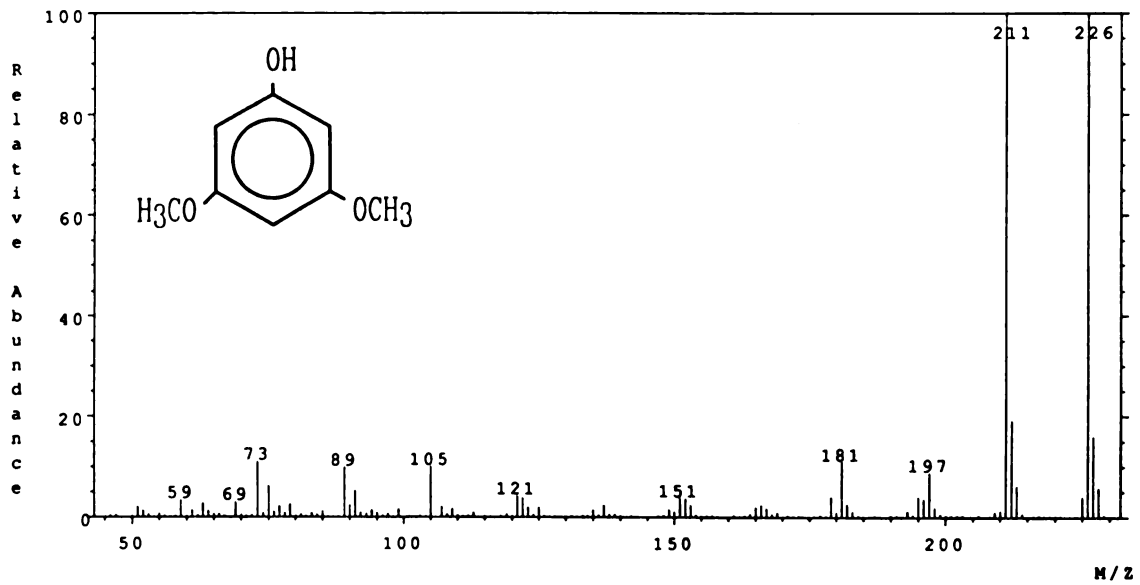

Figure F.11: Electron-impact mass spectrum of 3,5-dimethoxyphenol (Aldrich) obtained from scan 625 (background average of scans 623 and 627) of the TIC from an authentic standard analyzed with the DB-1 GC column.

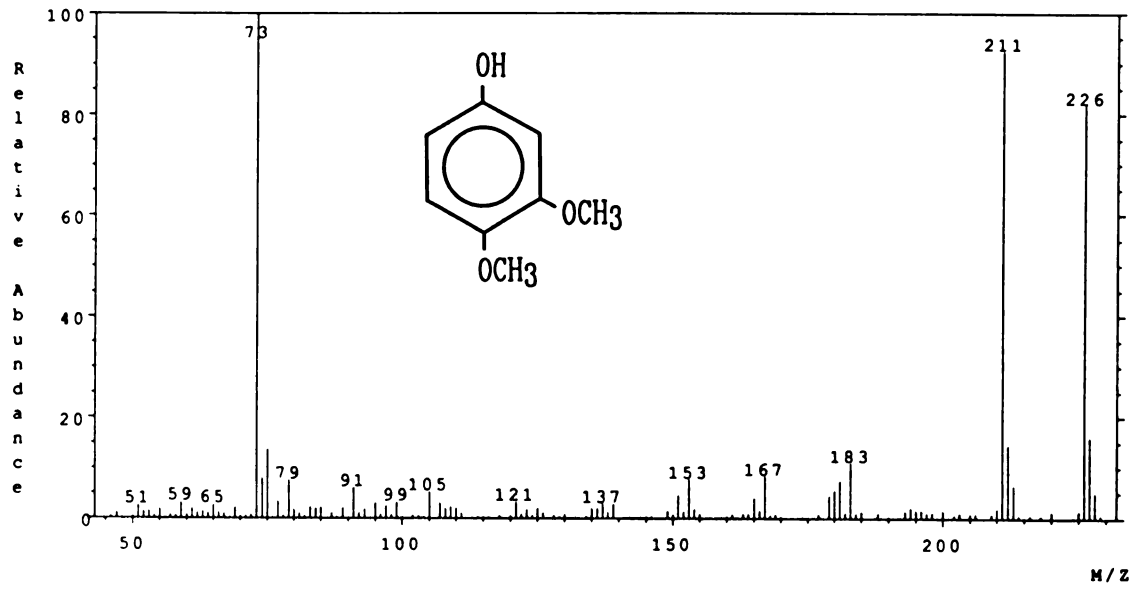

Figure F.12: Electron-impact mass spectrum of 3,4-dimethoxyphenol (Aldrich) obtained from scan 598 (background average of scans 596 and 600) of the TIC from an authentic standard analyzed with the DB-1 GC column.

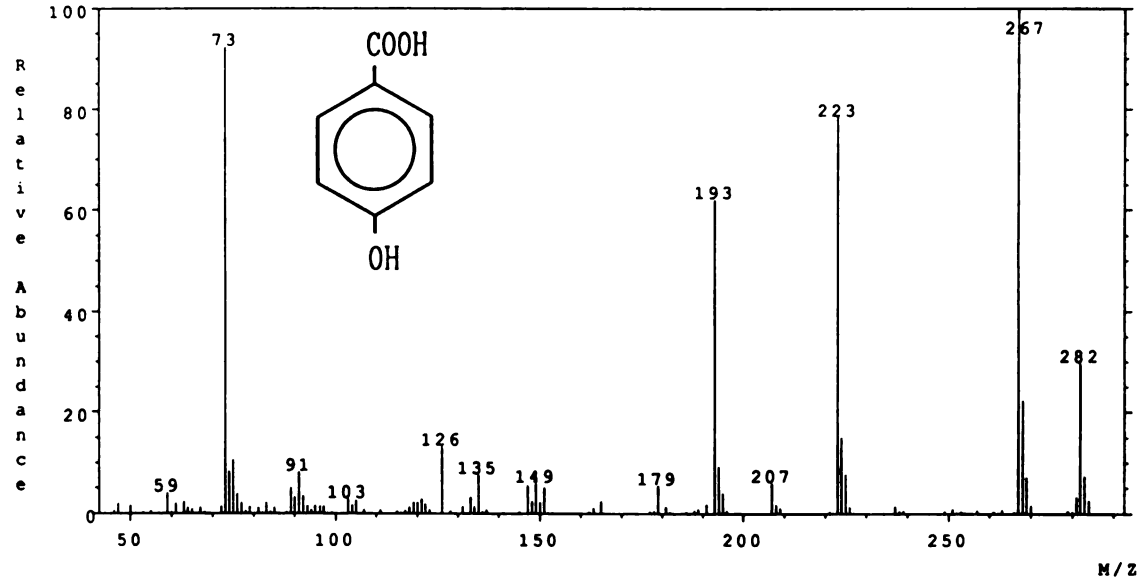

Figure F.13: Electron-impact mass spectrum of p-hydroxybenzoic acid (Aldrich) obtained from scan 744 (background scan 745) of the TIC from an authentic standard analyzed with the DB-1 GC column.

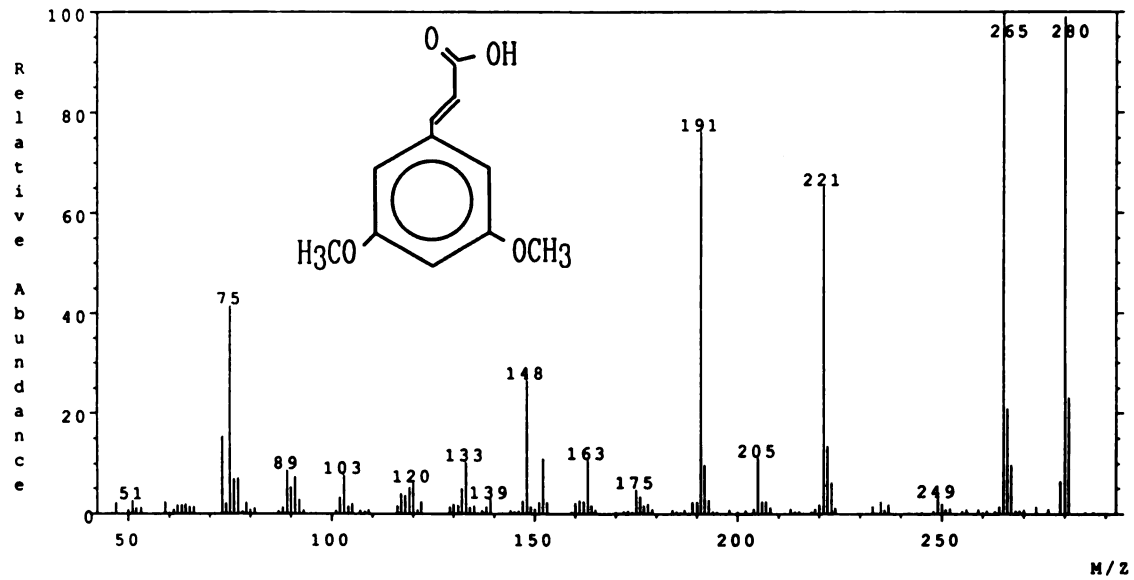

Figure F.14: Electron-impact mass spectrum of 3,5-dimethoxycinnamic acid (Aldrich) obtained from scan 1021 (background average of scans 1018 and 1022) of the TIC from an authentic standard analyzed with the DB-1 GC column.

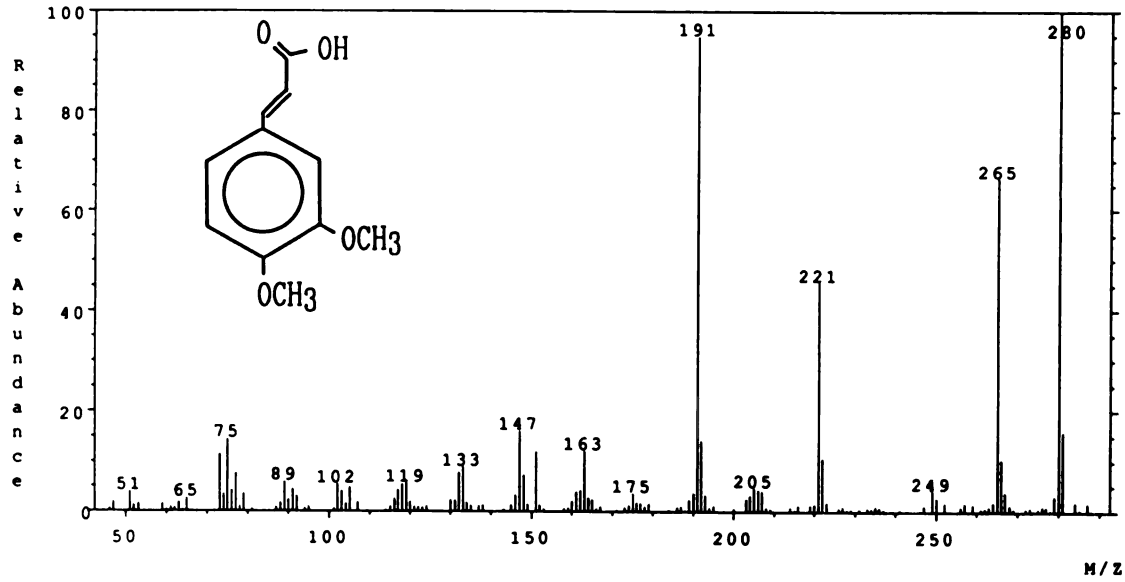

Figure F.15: Electron-impact mass spectrum of 3,4-dimethoxycinnamic acid (Aldrich) obtained from scan 1020 (background average of scans 1018 and 1022) of the TIC from an authentic standard analyzed with the DB-1 GC column.

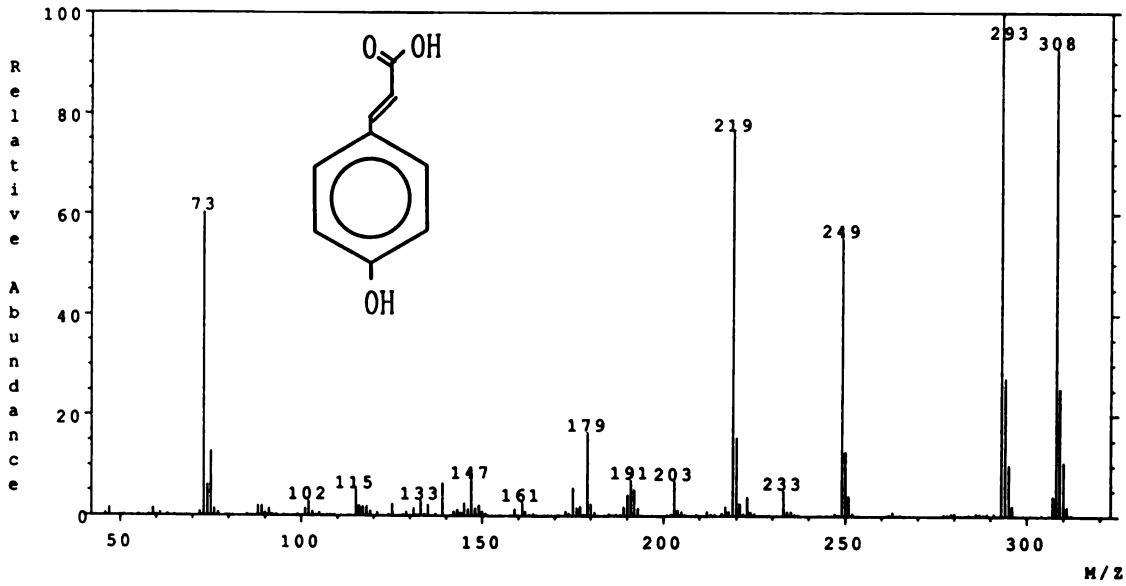

Figure F.16: Electron-impact mass spectrum of 4-coumaric acid (4-hydroxycinnamic acid; Aldrich) obtained from scan 975 (background average of scans 972 and 977) of the TIC from an authentic standard analyzed with the DB-1 GC column.

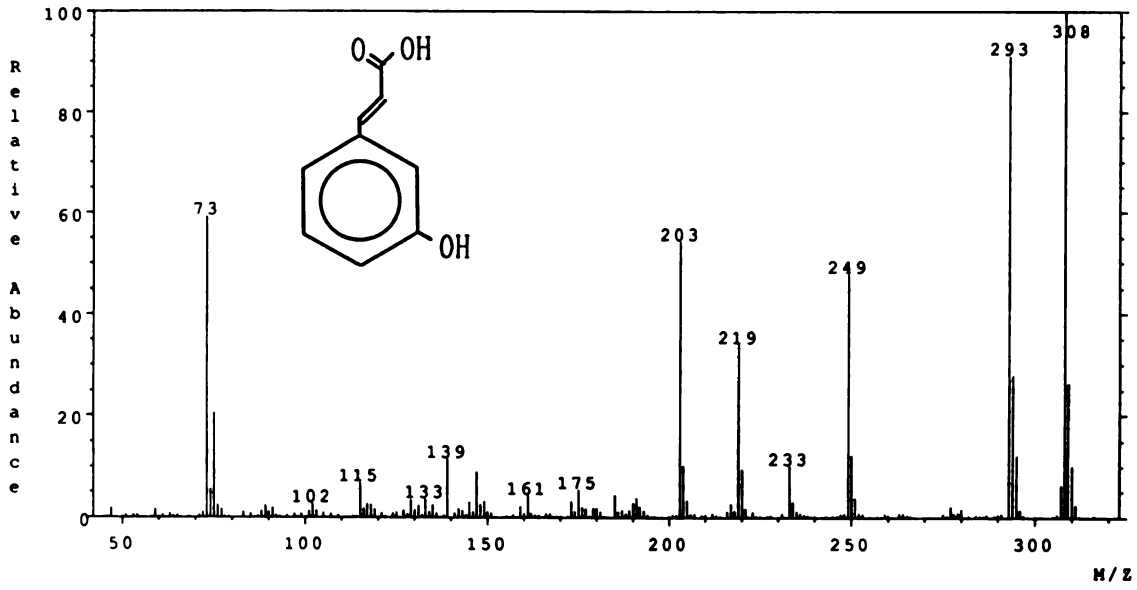

Figure F.17: Electron-impact mass spectrum of 3-coumaric acid (3-hydroxycinnamic acid; Aldrich) obtained from scan 926 (background average of scans 923 and 929) of the TIC from an authentic standard analyzed with the DB-1 GC column.

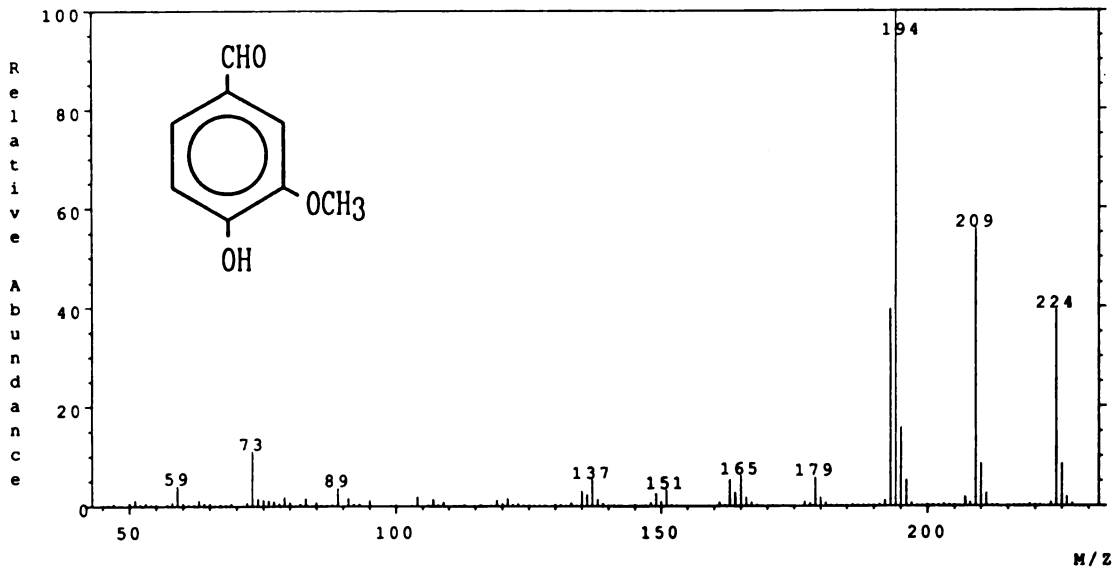

Figure F.18: Electron-impact mass spectrum of vanillin (vanillyl aldehyde; Aldrich) obtained from scan 649 (background average of scans 647 and 651) of the TIC from an authentic standard analyzed with the DB-1 GC column.

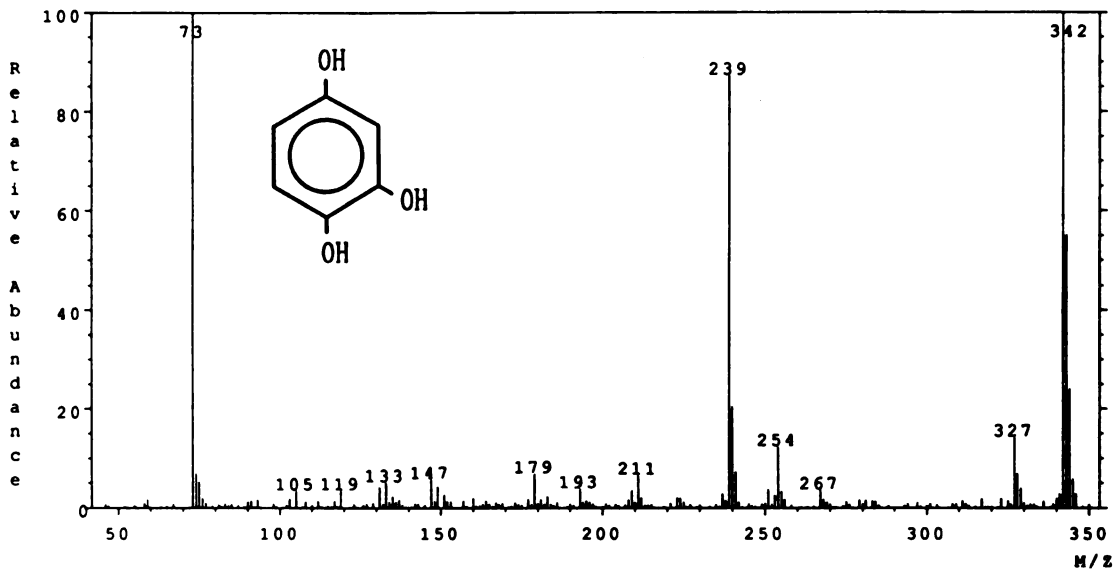

Figure F.19: Electron-impact mass spectrum of 1,2,4-benzenetriol (1,2,4-trihydroxybenzene; Aldrich) obtained from scan 732 (background average of scans 730 and 735) of the TIC from an authentic standard analyzed with the DB-1 GC column.

BIBLIOGRAPHY

Adler, E. 1977. Lignin chemistry- past, present, and future. **Wood Sci. Technol. 11**:169-218.

Aitken, M. D. and R. L. Irvine. 1990. Characterization of reactions catalyzed by manganese peroxidase from *Phanerochaete chrysosporium*. **Arch. Biochem. Biophys. 276**:405-414.

Allen, D. C., H. E. Grethlein and A. O. Converse. 1983. Process studies for enzymatic hydrolysis using high solids slurries of acid pretreated mixed hardwood. **Biotech. Bioeng. Symp. 13**:99.

Ander, P. and K. E. Eriksson. 1978. Lignin degradation and utilization by microorganisms. **Prog. Ind. Microbiol. 14**:1.

Andersson, L. A., V. Renganathan, A. A. Chiu, T. M. Loehr and M. H. Gold. 1985. Spectral characterization of a diarylpropane oxygenase, a novel peroxide-dependent, lignin degrading heme enzyme. **J. Biol. Chem. 260**:6080.

Antai, S. P. and D. L. Crawford. 1981. Degradation of softwood, hardwood, and grass lignocelluloses by two *Streptomyces* strains. **Appl. Environ. Microbiol. 42**:378-380.

Bagby, M. O., R. L. Cunningham and R. L. Maloney. 1973. Ultraviolet spectral determination of lignin. **Tappi. 56**:162-163.

Bailey, J. E. and D. F. Ollis. 1986. **Biochemical Engineering Fundamentals**, 2nd ed. McGraw-Hill, Inc., New York.

Bartuska, V. J., G. E. Maciel, H. I. Bolker and B. I. Fleming. 1980. Structural studies of lignin isolation procedures by ^{13}C NMR. **Holzforschung. 34**:214-217.

Bell, C. F. 1977. **Principles and Applications of Metal Chelation**. Atkins, P. W., J. S. E. Holker and A. K. Holliday. (eds.). Oxford University Press, New York.

Bird, R. B., W. E. Stewart, E. N. Lightfoot. 1960. **Transport Phenomena**. John Wiley and Sons, New York.

Blanchette, R. A. 1984. Screening wood decayed by white-rot fungi for preferential lignin degradation. **Appl. Environ. Microbiol. 48**:647-653.

Blanchette, R. A., A. R. Abad, R. L. Farrell and T. D. Leathers. 1989. Detection of lignin peroxidase and xylanase by immunocytochemical labelling in wood decayed by basidiomycetes. **Appl. Environ. Microbiol. 55**:1457-1465.

Blanchette, R. A. and I. D. Reid. 1986. Ultrastructural aspects of wood delignification by *Phlebia (Merulius) tremellosus*. **Appl. Environ. Microbiol. 52**:239-245.

Blau, K. and G. S. King (eds.). 1978. In **Handbook of Derivatives for Chromatography**. Heyden, and Son Inc., Philadelphia, PA.

Bonnarme, P. and T. W. Jeffries. 1990. Mn(II) regulation of lignin peroxidases and manganese-dependent peroxidass from liginin-degrading white rot fungi. **Appl. Environ. Microbiol. 56**: 210-217.

Boominathan, K. and C. A. Reddy. 1992. Fungal degradation of lignin: Biotechnological applications. In **Handbook of Applied Mycology**. Arora, D. K., R. P. Elander and K. G. Mukerji. (eds.). Marcel Dekker, New York. **4: Fungal Biotechnology**:763-822.

Bono, J.-J., P. Goulas, J.-F. Boe, N. Portet, and J.-L. Seris. 1990. Effect of Mn(II) on reactions catalyzed by lignin peroxidase from *Phanerochaete chrysosporium*. **Eur. J. Biochem. 192**:189-193.

Boon, J. J., A. D. Pouwels and G. B. Eijkel. 1987. Pyrolysis high-resolution gas chromatography-mass spectrometry studies on beech wood: capillary high-resolution mass spectrometry of a beech lignin fraction. **Biochem. Soc. Trans. 15**:170-174.

Boutelje, J. and I. Eriksson. 1984. Analysis of lignin in fragments from thermomechanical spruce pulp by ultraviolet microscopy. **Holzforschung. 38**:249-252.

Boutelje, J. and I. Eriksson. 1982. An UV-microscopy study of lignin in middle lamella fragments from fibers of mechanical pulp of spruce. **Svensk. Papperstidn. 85**:R39-R42.

Boyle, C. D., B. R. Kropp and I. D. Reid. 1992. Solubilization and mineralization of lignin by white rot fungi. **Appl. Environ. Microbiol. 58**:3217-3224.

Bradford, M. M. 1976. A rapid and sensitive method for the quantification of microgram quantities of protein using the principle of protein-dye binding. **Anal. Biochem. 72**:248-254.

Breneman, W. E., J. W. Westberg and R. W. Duerst. 1989. A rapid method for preparing KBr wafers for infrared spectroscopy. **Appl. Spectroscopy. 43**:726-727.

Brown, J. A., J. K. Glenn and M. H. Gold. 1990. Manganese regulates expression of manganese peroxidase by *Phanerochaete chrysosporium*. **J. Bacteriol. 172**:3125-3130.

Budde, W. L., T. D. Behymer, T. A. Bellar and J. S. Ho. 1990. Liquid chromatography-mass spectrometry: An emerging technology for nonvolatile compounds. **J. Am. Water Works Assoc. 82**:60-65.

Bumpus, J. A., M. Tien, D. Wright and S. D. Aust. 1985. Oxidation of persistent environmental pollutants by a white-rot fungus. **Science. 228**:1434-1436.

Buswell, J. A. 1991. Fungal degradation of lignin. In **Handbook of Applied Mycology Vol. 1: Soil and plants**. Arora, D. K., Bharat Rai, K. G. Mukerji and G. Knudsen. (eds.). Marcel Dekker, New York.

Buswell, J. A. and E. Odier. 1987. Lignin biodegradation. **CRC Crit. Rev. Biotechnol. 6**:1-60.

Cattlow, D. A. and M. E. Rose. 1989. Analysis of mixtures by mass spectrometry. Part I: Techniques other than gas chromatography/mass spectrometry. **Mass Spectrom. 10**:222-252.

Chen, C. L. 1988. Characterization of lignin by oxidative degradation: Use of gas chromatography-mass spectrometry technique. In **Methods in Enzymology**. Colowick, S. P. and N. O. Kaplan. (eds.). Academic Press, New York. **161**:110-136.

Chen, C. L. and H. M. Chang. 1982. Aromatic acids produced druing degradation of lignin in spruce wood by *Phanerochaete chrysosporium*. **Holzforschung. 36**:3-9.

Chen, C. L., M. G. S. Chua, J. Evans and H. M. Chang. 1982. ^{13}C NMR spectroscopic study of spruce lignin degraded by *Phanerochaete chrysosporium*: II. Synthesis and chemical shifts of model compounds. **Holzforschung. 36**:239-247.

Chua, M. G. S., C. L. Chen and H. M. Chang. 1982. ^{13}C NMR spectroscopic study of spruce lignin degraded by *Phanerochaete chrysosporium*: I. New structures. **Holzforschung. 36**:165-172.

Chung, N., M. M. Shah, T. A. Grover, and S. D. Aust. 1993. Reductive activity of a manganese-dependent peroxidase from *Phanerochaete chrysosporium*. **Arch. Biochem. Biophys. 306**:70-75.

Clesceri, L. S., A. E. Greenberg, R. R. Trussell and M. A. H. Franson (eds.). 1989. EDTA Titrimetric Method. In **Standard Methods for the Examination of Water and Wastewater**. Port City Press, Baltimore, MD. 3-85 to 3-87.

Concin, R., P. Burtscher, E. Burtscher and O. Bobleter. 1983. Separation and identification of monomeric lignin degradation products by G.L.C.-mass spectrometry. **Int. J. Mass Spectrom. Ion Phys. 48**:63-66.

Connors, W. J., S. Sarkanen and J. L. McCarthy. 1980. Gel chromatography and association complexes of lignin. **Holzforschung. 34**:80-85.

Crawford, D. L., M. J. Barder, A. L. Pometto, III and R. L. Crawford. 1982. Chemistry of softwood lignin degradation by *Steptomyces viridosporus*. **Arch. Microbiol. 131**:140-145.

Crawford, R. L. **Lignin biodegradation and transformation**. Wiley-Interscience, New York.

Cui, F. and D. Dolphin. 1991. Veratryl alcohol as a mediator in lignin model compound biodegradation. **Holzforschung. 45**:31-35.

Cussler, E. L. 1986. **Diffusion: Mass Transfer in Fluid Systems**. Cambridge University Press, New York.

Daniel, G., T. Nilsson and B. Pettersson. 1989. Intra- and extracellular localization of lignin peroxidase during the degradation of solid wood and wood fragments by *Phanerochaete chrysosporium* by using transmission electron microscopy and immuno-gold labeling. **Appl. Environ. Microbiol. 55**:871-881.

Dass, S. B. and C. A. Reddy. 1990. Characterization of extracellular peroxidases produced by acetate-buffered cultures of the lignin-degrading basidiomycete, *Phanerochaete chrysosporium*. **FEMS Microbiol. Lett. 69**:221-224.

de Jong, E., F. P. de Vries, J. A. Field, R. P. Van der Zwan and J. A. M. de Bont. 1992. Isolation and screening of basidiomycetes with high peroxidative activity. **Mycol. Res. 96**: 1098-1104.

de Jong, E., J. A. Field and J. A. M. de Bout. 1994. Aryl alcohols in the physiology of ligninolytic fungi. **FEMS Microbiol. Rev. 13**:153-188.

Dordick, J. S., M. A. Marletta and A. M. Klibanov. 1986. Peroxidases depolymerize lignin in organic media but not in water. **Proc. Natl. Acad. Sci. USA. 83**:6255-6257.

Dosoretz, C. G. and H. E. Grethlein. 1991. Physiological aspects of the regulation of extracellular enzymes of *Phanerochaete chrysosporium*. **Appl. Biochem. Biotechnol. 28/29**:253-265.

Drawert, F. and G. Leupold. 1976. Gas-chromatographische analyse der trimethylsilyl-derivative phenolischer verbindungen. **Chromatographia. 9**:605-610.

Eriksson, K. E. L. 1994. Where do we stand and where are we going? Lignin biodegradation and pratical utilization. **FEMS Microbiol. Rev. 13**:149-158.

Eriksson, K. E. and T. K. Kirk. 1985. Biopulping, biobleaching and treatment of kraft bleaching effluents with white-rot fungi. In **Comprehensive Biotechnology**. Cooney, C. L. and A. E. Humphrey. (eds.). Pergamon Press, 3:271-294.

Evans, C. S., M. V. Dutton, F. Guillen and R. G. Veness. 1994. Enzymes and small molecular mass agents involved with lignocellulose degradation. **FEMS Microbiol. Rev. 13**:235-240.

Evershed, R. P. 1989. Analysis of mixtures by mass spectrometry. Part I: Developments in gas chromatography-mass spectrometry. **Mass Spectrom. 10**:181-221.

Evliya, H. 1989. C-13 NMR studies of a dehydropolymer (DHP) from isoeugenol; comparison with spruce lignin. **Holzforschung. 43**:61- 64.

Faison, B. D., T. K. Kirk and R. L. Farrell. 1986. Role of veratryl alcohol in regulating ligninase activity in *Phanerochaete chrysosporium*. **Appl. Environ. Microbiol. 52**:251- 254.

Faix, O. 1992. Fourier transform infrared spectroscopy. In **Methods in Lignin Chemistry**. Lin, S. Y. and C. W. Dence. (eds.). Springer-Verlag, New York. 83-109.

Faix, O., D. Meier and I. Fortmann. 1988. Pyrolysis-gas chromatography-mass spectrometry of two trimeric lignin model compounds with alkyl-aryl ether structure. **J. Anal. Appl. Pyrol. 14**:135-148.

Faix, O., D. Meier and I. Grobe. 1987. Studies on isolated lignins and lignins in woody materials by pyrolysis-gas chromatography-mass spectrometry and off-line pyrolysis-gas chromatography with flame ionization detection. **J. Anal. Appl. Pyrol. 11**:403-416.

Faix, O., D. Meier and I. Fortmann. 1990a. Thermal degradation products of wood: Gas chromatographic separation and mass spectrometric characterization of monomeric lignin derived products. **Holz Als Roh-und Werkstoff. 48**:281-285.

Faix, O., D. Meier and I. Fortmann. 1990b. Thermal degradation products of wood: A collection of electron-impact (EI) mass spectra of monomeric lignin derived products. **Holz als Roh-und Werkstoff. 48**:351-354.

Fergus, B. J., A. R. Procter, J. A. N. Scott and D. A. I. Goring. 1969. The distribution of lignin in sprucewood as determined by ultraviolet microscopy. **Wood Sci. Technol. 3**:117-138.

Ferrer, I., M. Dezotti and N. Duran. 1991. Decolorization of kraft effluent by free and immobilized lignin peroxidases and horseradish peroxidase. **Biotechnol Lett. 13**:577-582.

Fiechter, A. 1993. Function and synthesis of enzymes involved in lignin degradation. **J. Biotechnol. 301**:49-55.

Finlayson, B. A. 1980. **Nonlinear Analysis in Chemical Engineering**. McGraw-Hill, Inc., New York.

Fleming, B. I. and H. I. Bolker. 1980. Carbon-13 NMR spectra of solid lignin preparations. **Pulp and paper reports; Pulp and paper research institute of Canada. PPR 293**:.

Freudenberg, K., A. Janson, E. Knopf and A. Haag. 1936. Zur Kenntnis des lignins. **Chem. Ber. 69**:1415-1425.

Freudenberg, K., W. Lautsch and K. Engler. 1940. **Chem. Ber. 73**: 167.

Fritz, J. O. and K. J. Moore. 1987. Separation and quantification of lignin-derived phenolic monomers using high-resolution gas chromatography. **J. Agric. Food Chem. 35**:710-713.

Fuller, M. P., G. L. Ritter and C. S. Draper. 1988a. Partial least squares quantitative analysis of infrared spectroscopic data. Part I. Algorithm implementation. **Appl. Spectroscopy. 42**: 217-227.

Fuller, M. P., G. L. Ritter and C. S. Draper. 1988b. Partial least squares quantitative analysis of infrared spectroscipic data. Part II. Application to detergent analysis. **Appl. Spectroscopy**. **42**:228-236.

Fullerton, T. J. and R. A. Franich. 1983. Lignin analysis by pyrolysis-GC-MS: characterisation of ethanol lignin pyrolysates and identification of syringyl units in *Pinus radiata* milled wood lignin. **Holzforschung**. **37**:267-269.

Gaskell, J. and D. Cullen. 1993. Recent advances in the organization and regulation of lignin peroxidase genes of *Phanerochaete chrysosporium*. **J. Biotechnol. 30**:109-114.

Gellerstedt, G. 1992. Chemical degradation methods: Permanganate oxidation. In **Methods in Lignin Chemistry**. S. Y. Lin and C. W. Dence. (eds.). Springer-Verlag, New York. 322-333.

Genuit, W., J. J. Boon and O. Faix. 1987. characterization of beech milled wood lignin by pyrolysis-gas chromatography- photoionization mass spectrometry. **Anal. Chem. 59**:508-513.

Glenn, J. K., L. Akileswaran and M. H. Gold. 1986. Mn(II) oxidation is the principal function of extracellular Mn- peroxidase from *Phanerochaete chrysosporium*. **Arch. Biochem. Biophys. 251**:688-696.

Glenn, J. K. and M. H. Gold. 1985. Purification and characterization of an extracellular Mn(II)-dependent peroxidase from the lignin-degrading basidiomycete *Phanerochaete chrysosporium*. **Arch. Biochem. Biophys. 242**:329-346.

Gold, M. H. and M. Alic. 1993. Molecular biology of the lignin-degrading basidiomycete *Phanerochaete chrysosporium*. **Microbiol. Rev. 57**:605-622.

Gold, M. H., H. Wariishi and K. Valli. 1989. Extracellular peroxidases involved in lignin degradation by the white rot basidiomycete *Phanerochaete chrysosporium*. In **Biocatalysis and Agricultural Biotechnology**. Whitaker, J. and P. E. Sonnet. (eds.). A. C. S., Washington D. C. 127-140.

Griffiths, P. R. and J. A. de Haseth. 1986. Fourier transform infrared spectrometry. In **Chemical Analysis**. Elving, P. J., J. D. Winefordnev and I. M. Kolthoff. (eds.). John Wiley and Sons, New York. **83**:

Grous, W. R., A. O. Converse and H. E. Grethlein. 1986. The effect of steam explosion pretreatment on pore size and enzymatic hydrolysis of poplar. **Enzyme Microb. Technol. 8**:274-280.

Hadar, Y., Z. Kerem and B. Borodecki. 1993. biodegradation of lignocellulosic agricultural wastes by *Pleurotus ostreatus*. **J. Biotechnol. 30**:133-139.

Haemmerli, S. D., M. S. A. Leisola and A. Feichter. 1986. Polymerisation of lignin by ligninases from *Phanerochaete chrysosporium*. **FEMS Microbiol. Lett. 35**:33-36.

Haemmerli, S. D., H. E. Schoemaker, H. W. H. Schmidt and M. S. A. Leisola. 1987. Oxidation of veratryl alcohol by the lignin peroxidase of *Phanerochaete chrysosporium*. **FEBS Lett. 220**:149- 154.

Haider, K. and J. Trojanowski. 1980. A comparison of the degradation of ^{14}C labeled DHP and corn stalk lignin by micro- and macrofungi and bacteria. In **Lignin Biodegradation: Microbiology, Chemistry, and Potential Applications**. Kirk, T. K., T. Higuchi and H. M. Chang. (eds.). CRC Press, Boca Raton, FL. **1**: 111-134.

Hames, B., S. K. Black, F. Agbleuor, R. Evans, D. K. Johnson and H. L. Chum. 1910, April 25. Measurement of the functional group contents of lignins using FTIR and partial least squares regression. Paper presented at the 45th APPITA General Conference and Exhibition, 6th International Symposium on Wood and Pulping Chemistry. Melbourne, Australia.

Hammel, K. E., K. A. Jr Jensen, M. D. Mozuch, L. L. Landucci, M. Tien and E. A. Pease. 1993. Ligninolysis by a purified lignin peroxidase. **J. Biol. Chem. 268**:12274-12281.

Hammel, K. E. and M. A. Moen. 1991. Depolymerization of a synthetic lignin *in vitro* by lignin peroxidase. **Enzyme Microb. Technol. 13**:15-18.

Hammel, K. E., M. Tien, B. Kalyanaraman and T. K. Kirk. 1985. Mechanisms of oxidative C_{α}-C_{β} cleavage of a lignin model dimer by *Phanerochaete chrysosporium* ligninase. **J. Biol. Chem. 260**:8348.

Hamming, M. C. and N. G. Foster. 1972. **Interpretation of Mass Spectra of Organic Compounds**. Academic Press, New York.

Harris, D. C. 1982. EDTA Titrations. In **Quantitative Chemical Analysis**. Vapnek, P. C. and D. J. Cross. (eds.). W. H. Freeman and Co., San Francisco, CA. **Chapter 14**:271-289.

Hartley, R. D. and H. Buchan. 1979. High-performance liquid chromatography of phenolic acids and aldehydes derived from plants or from the decomposition of organic matter in soil. **J. Chromatog. 180**:139-143.

Harvey, P. J., G. F. Gilardi, M. L. Goble and J. M. Palmer. 1993. Charge transfer reactions and feedback control of lignin peroxidase by phenolic compounds: Significance in lignin degradation. **J. Biotechnol. 30**:57-69.

Harvey, P. J., H. E. Schoemaker and J. M. Palmer. 1986. Veratryl alcohol as a mediator and the role of radical cations in lignin biodegradation by *Phanerochaete chrysosporium*. **FEBS Lett. 195**: 242-246.

Hatakka, A. 1994. Lignin-modifying enzymes from selected white-rot fungi: Production and role in lignin degradation. **FEMS Microbiol. Rev. 13**:125-135.

Higuchi, T. 1990. Lignin biochemistry: Biochemistry and biodegradation. **Wood Sci. Technol. 24**:23-63.

Higuchi, T. 1993. Biodegradation mechanism of lignin by white-rot basidiomycetes. **J. Biotechnol. 30**:1-8.

Higuchi, T., H. M. Chang and T. K. Kirk. 1983. **Recent advances in lignin biodegradation research**. Tokyo Univ.

Hoffmann, G. and L. Sweetman. 1987. O-(2,3,4,5,6-pentafluorobenzyl)oxime-trimethylsilyl ester derivatives for quantitative gas chromatographic and gas gas chromatographic-mass spectrometric studies of aldehydes, ketones, and oxoacids. **J. Chromatog. 421**:336-343.

Hyatt, J. A. 1989. Hydroxypropyl lignin and model compounds: Synthesis and characterization by electron-impact mass spectrometry. In **Lignin: Properties and Materials**. Glasser, W. G. and S. Sarkanen. (eds.). ACS Symp. Ser., **397**:425-435.

Janshekar, H., C. Brown and A. Fiechter. 1981. Determination of biodegraded lignin by ultraviolet spectrophotometry. **Anal. Chim. Acta. 130**:81-91.

Joshi, D. K. and M. H. Gold. 1993. Degradation of 2,4,5-trichlorophenol by the lignin-degrading basidiomycete *Phanerochaete chrysosporium*. **Appl. Environ. Microbiol. 59**:1779- 1785.

Katayama, Y., T. Nishida, N. Morohoshi and K. Kuroda. 1989. The metabolism of biphenyl structures in lignin by the wood-rotting fungus *Coriolus versicolor*. **FEMS Microbiol. Lett. 61** :307-314.

Kersten, P. J., M. Tien, B. Kalyanaraman and T. K. Kirk. 1985. The ligninase of *Phanerochaete chrysosporium* generates action radicals from methoxybenzenes. **J. Biol. Chem. 260**:2609.

Kim, K. R., M. K. Hahn, A. Zlatkis, E. C. Horning and B. S. Middleditch. 1989. Simultaneous gas chromatography of volatile and nonvolatile carboxylic acids as *tert*-butyldimethylsilyl derivatives. **J. Chromatog. 468**:289-301.

Kirk, T. K. 1984. Degradation of lignin. In **Microbial Degradation of Organic Compounds**. Gibson, D. T. (ed.). Dekker, New York. 399-437.

Kirk, T. K., W. J. Connors, R. D. Bleam, W. F. Hackett and J. G. Zeikus. 1975. Preparation and microbial decomposition of synthetic ^{14}C lignins. **Proc. Natl. Acad. Sci. USA. 72**:2515- 2519.

Kirk, T. K., W. J. Connors and J. G. Zeikus. 1976. Requirement of a growth substrate during lignin degradation by two wood rotting fungi. **Appl. Environ. Microbiol. 32**:192-196.

Kirk, T. K. and E. B. Cowling. 1984. Biological decomposition of solid wood. **Adv. Chem. Ser. 207**:455-487.

Kirk, T. K., S. Croan, M. Tien, K. E. Murtagh and R. L. Farrell. 1986a. Production of multiple ligninases by *Phanerochaete chrysosporium*: Effect of selected growth conditions and use of a mutant strain. **Enz. Microb. Technol. 8**:27-32.

Kirk, T. K. and R. L. Farrell. 1987. Enzymatic "combustion": The microbial degradation of lignin. **Ann. Rev. Microbiol. 41**:465-505.

Kirk, T. K., M. Tien, S. Croan, T. McDonagh and R. L. Farrell. 1986b. Production of multiple ligninases by *Phanerochaete chrysosporium*. Proc. 3rd Int. Congress on Biotechnology in the Pulp and Paper Industry. Stockholm. pp. 5-6.

Kolodziejski, W., J. S. Frye and G. E. Maciel. 1982. Carbon-13 nuclear magnetic resonance spectrometry with cross polarization and magic-angle spinning for analysis of lodgepole pine wood. **Anal. Chem. 54**:1419-1424.

Kreyszig, E. 1988. **Advanced Engineering Mathematics**, 6th ed. Pirtle, R. and J. Gazis. (eds.). John Wiley and Sons, New York.

Kringstad, K. P. and R. Morck. 1983. ^{13}C NMR spectra of kraft lignins. **Holzforschung. 37**:237-244.

Kuwahara, M., J. K. Glenn, M. A. Morgan and M. H. Gold. 1984. Separation and characterization of two extracellular H2O2-dependent oxidases from ligninolytic cultures of *Phanerochaete chrysosporium*. **FEBS Lett. 169**:247-250.

Lackner, R., E. Srebotnik and K. Messner. 1991. Oxidative degradation of high molecular weight chlorolignin by manganese peroxidase of *Phanerochaete chrysosporium*. **Biochem. Biophys Res. Commun. 178**:1092-1098.

Lapierre, C., J. Y. Lellemand and B. Monties. 1982. Evidence of poplar lignin heterogeneity by combination of ^{13}C and ^{1}H NMR spectroscopy. **Holzforschung. 36**:275-282.

Lapierre, C. and B. Monties. 1984. Photosynthetically ^{13}C-labelled poplar lignins: ^{13}C NMR experiments. **Holzforschung. 38**: 333-342.

Leary, G. J., J. A. Lloyd and K. R. Morgan. 1988. A ^{13}C CP/MAS NMR study of residual lignin in kraft pulps. **Holzforschung. 42**: 199-202.

Leisola, M. S. A., B. Kozulic, F. Meussdoerffer and A. Fiechter. 1987. Homology among multiple extracellular peroxidases from *Phanerochaete chrysosporium*. **J. Biol. Chem. 262**:419-424.

Leisola, M. S. A., B. Schmidt and A. Fiechter. 1986. Enzymatic determination of veratryl alcohol. **Anal. Biochem. 155**:108-111.

Liebeskind, M., H. Hocker, C. Wandrey and A. G. Jäger. 1990. Strategies for improved lignin peroxidase production in agitated pellet cultures of *Phanerochaete chrysosporium* and the use of a novel inducer. **FEMS Microbiol. Lett. 71**:325-330.

Lindstrom, K. and F. Osterberg. 1984. Characterization of the high molecular mass chlorinated matter in spent bleach liquors (SBL). Part I: Alkaline SBL. **Holzforschung. 38**:201-212.

Marsden, W. L. and P. P. Gray. 1986. Enzymatic hydrolysis of cellulose in lignocellulosic materials. In **Critical Reviews in Biotechnology.** Stewart, G. G. and I. Russel. (eds.). CRC Press, Boca Raton. 3:235-276.

Martin, F., C. Saiz-Jimenez and F. J. Gonzales-Vila. 1979. Pyrolysis-gas chromatography-mass spectrometry of lignins. **Holzforschung.** 33:210-212.

McCarthy, A. J. and P. Broda. 1984. Screening for lignin-degrading actinomycetes and characterization of their activity against [^{14}C]-lignin-labelled wheat lignocellulose. **J. Gen. Microbiol.** 130:2905-2913.

McLafferty, F. W. 1973. **Interpretation of Mass Spectra**, 2nd ed. W. A. Benjamin Inc., Reading, MA.

Mellor, D. P. 1979. Chemistry of chelation and chelating agents. In **The Chelation of Heavy Metals: International Encyclopedia of Pharmacology and Therapeutics.** Sartorelli, A. C. and W. G. Levine. (eds.). Pergamon Press, New York. 1-105.

Messner, K. and E. Srebotnik. 1994. Biopulping: An overview of developments in an environmentally safe paper-making technology. **FEMS Microbiol. Rev.** 13:351-364.

Michel, F. C. Jr. 1991. The peroxidases of *Phanerochaete chrysosporium*: Culture modelling and application. Doctoral Dissertation. Michigan State University, East Lansing, MI.

Michel, F. C. Jr, S. B. Dass, E. A. Grulke and C. A. Reddy. 1991. Role of manganese peroxidases and lignin peroxidases of *Phanerochaete chrysosporium* in the decolorization of kraft bleach plant effluent. **Appl. Environ. Micorbiol.** 57:2368.

Morck, R., H. Yoshida and K. P. Kringstad. 1986. Fractionation of kraft lignin by successive extraction with organic solvents: I. Functional groups, ^{13}C-NMR-spectra and molecular weight distribution. **Holzforschung.** 40(suppl.):51-60.

Muheim, A., R. Waldner, M. S. A. Leisola and A. Fiechter. 1990. An extracellular ary-alcohol oxidase from the white-rot fungus *Bjerkandera adusta*. **Enzyme Microb. Technol.** 12:204-209.

Nicholls, D. 1974. **Complexes and First-Row Transition Elements.** Sykes, P. (ed.). Macmillan Press LTD., London. 169-170.

Niemela, K. 1988a. GLC-MS studies on pine kraft black liquors. Part I: Identification of monomeric compounds. **Holzforschung.** 42:169-173.

Niemela, K. 1988b. GLC-MS studies on pine kraft black liquors. Part II: Identification of hydroxyacids with a stilbene structure. **Holzforschung.** 42:175-176.

Niemela, K. 1989. GLC-MS studies on pine kraft black liquors. Part V: Identification of catechol compounds. **Holzforschung. 43**:99- 103.

Nimz, H. H., D. Robert, O. Faix and M. Nemr. 1981. Carbon-13 NMR spectra of lignins, 8: Structural differences between lignins of hardwoods, softwoods, grasses and compression wood. **Holzforschung. 35**:16-26.

Obst, J. R. 1982. Guaiacyl and syringyl lignin composition in hardwood cell components. **Holzforschung. 36**:143-152.

Obst, J. R. and L. L. Landucci. 1986. Quantitative ^{13}C-NMR of lignins-methoxyl:aryl ratio. **Holzforschung. 40(suppl.)**:87-92.

Obst, J. R. and J. Ralph. 1983. characterization of hardwood lignin: Investigation of syringyl/guaiacyl composition by ^{13}C nuclear magnetic resoonance spectroscopy. **Holzforschung. 37**:297- 302.

Olsen, W. L., H. P. Gallagher, K. A. Burris, S. S. Bhattacharjee, J. P. Slocomb and D. M. Dewitt. 1991. Enzymatic deligninification of lignocellulosic material. European Patent Application No. 90111620.2. Publication No. 0 406 617 A2:.

Orth, A. B., D. J. Royse and M. Tien. 1993. Ubiquity of lignin- degrading peroxidases among various wood-degrading fungi. **Appl. Environ. Microbiol. 59**:4017-4023.

Osterberg, F. and K. Lindstrom. 1985a. Characterization of the high molecular mass chlorinated matter in spent bleach liquers (SBL). Part II: Acidic SBL. **Holzforschung. 39**:149-158.

Osterberg, F. and K. Lindstrom. 1985b. Characterization of the high molecular mass chlorinated matter in spent bleach liquers (SBL). 3-mass spectrometric interpretation of aromatic degradation products in SBL. **Org. Mass Spectrom. 20**:515-524.

Otjen, L. and R. A. Blanchette. 1986. A discussion of microstructural changes in wood during decomposition by white-rot basidiomycetes. **Can. J. Bot. 64**:905-911.

Paszczynski, A., R. L. Crawford and V. B. Huynh. 1988. Manganese peroxidase of *Phanerochaete chrysosporium*: Purification. In **Methods in Enzymology**. Colowick, S. P. and N. O. Kaplan. (eds.). Academic Press, New York. **161**:264-270.

Paszczynski, A., V. B. Huynh and R. L. Crawford. 1991. Enzymatic activities of an extracellular manganese-dependent peroxidase from *Phanerochaete chrysosporium*. **Biochem. Biophys. Res. Commun. 178**:1092-1098.

Perez, J. and T. W. Jeffries. 1990. Mineralization of ^{14}C-ring labeled synthetic lignin correlates with the production of lignin peroxidase not of manganese peroxidase or laccase. **Appl. Environ. Microbio. 56**:1806-1812.

Perez, J. and T. W. Jeffries. 1992. Roles of manganese and organic acid chelators in regulating lignin degradation and biosynthesis of peroxidases by *Phanerochaete chrysosporium*. **Appl. Environ. Microbiol. 58**:2402-2409.

Perez, J. and T. W. Jeffries. 1993. Roles of organic acid chelators in manganese regulation of lignin degradation by *Phanerochaete chrysosporium*. **Appl. Biochem. Biotechnol. 39/40**:227-238.

Philp, R. P., N. J. Russell, T. D. Gilbert and J. M. Friedrich. 1982. Characterization of victorian soft brown coal wood by microscopic techniques and Curie-point pyrolysis combined with gas chromatography-mass spectrometry. **J. Anal. Appl. Pyrol. 4**: 143-161.

Pick, E. and Y. Keisari. 1980. A simple colorimetric method for the measurement of hydrogen peroxide produced by cells in culture. **J. Immunol. Meth. 38**:161-170.

Pometto, A. L., III and D. L. Crawford. 1988a. Gas-liquid chromatography of aromatic fragments from lignin degradation. In **Methods in Enzymology**. Colowick, S. P. and N. O. Kaplan. (eds.). Academic Press, New York. **161**:175-183.

Pometto, A. L., III and D. L. Crawford. 1988b. High-performance liquid chromatography of aromatic fragments from lignin degradation. In **Methods in Enzymology**. Colowick, S. P. and N. O. Kaplan. (eds.). Academic Press, New York. **161**:183-190.

Ponwels, A. D. and J. J. Boon. 1987. Analysis of lignin and chlorolignin residues in a beech xylan fraction by pyrolysis gas chromatography mass spectrometry. **J. Wood Chem. Technol. 7**:197- 213.

Ramakrishnan, V. and J. M. T. Maroor. 1988. IR and raman studies of gel grown manganese tartrate. **Infrared Phys. 28**:201-204.

Reddy, C. A. and T. M. D'Souza. 1994. Physiology and molecular biology of the lignin peroxidase of *Phanerochaete chrysosporium*. **FEMS Microbiol. Rev. 13**:137-152.

Reid, I. D. and M. G. Paice. 1994. Biological bleaching of kraft pulps by white-rot fungi and their enzymes. **FEMS Microbiol. Rev. 13**:369-376.

Robert, D. 1989. Biodegradation of lignin in spruce wood by *Phanerochaete chrysosporium*: quantitative analysis of biodegraded spruce lignins by ^{13}C NMR spectroscopy. **Holzforschung. 43**:323-332.

Robert, D. R. and G. Grunow. 1984. Quantitative estimation of hydroxyl groups in milled wood lignin from spruce and in a dehydrogenation polymer from coniferyl alcohol using ^{13}C NMR spectroscopy. **Holzforschung. 38**:85-90.

Rolando, C., B. Monties and C. Lapierre. 1992. Thioacidolysis. In **Methods in Lignin Chemistry**. Lin, S. Y. and C. W. Dence. (eds.). Springer-Verlag, New York.

Ruel, K. and F. Barnoud. 1985. Degradation of wood by microorganisms. In **Biosynthesis and Biodegradation of Wood**. Higuchi, T. (eds.). Academic Press, San Diego, CA. 441-467.

Ryu, K. and J. S. Dordick. 1992. How do organic solvents affect peroxidase structure and function? **Biochemistry. 31**:2588-2598.

Saeman, J. F., J. L. Bubl and E. E. Harris. 1945. Quantitative saccarification of wood and cellulose. **Ind. Eng. Chem. 17**:35.

Saiz-Jimenez, C. and J. W. de Leeuw. 1984. Pyrolysis-gas chromatography-mass spectrometry of isolated, synthetic, and degraded lignins. **Org. Geochem. 6**:417-422.

Saka, S., P. Whiting, K. Fukazawa and D. A. I. Goring. 1982. Comparative studies on lignin distribution by UV microscopy and bromination combined with EDXA. **Wood Sci. Technol. 16**:269-277.

Salomonsson, A. C., O. Theander and P. Åman. 1978. Quantitative determination by GLC of phenolic acids as ethyl derivatives in cereal straws. **J. Agric. Food Chem. 26**:830-835.

Sanglard, D., M. S. A. Leisola and A. Fiechter. 1986. Role of extracellular ligninases in biodegradation of benzo(a)pyrene by *Phanerochaete chrysosporium*. **Enz. Microb. Technol. 8**:209-212.

Sarkanen, K. V. and C. H. Ludwig. 1971. **Lignins: Occurrence, formation, structure, and reactions**. Wiley-Interscience, New York.

Sarkanen, S., R. A. Razal, T. Piccariello, E. Yamamoto and N. G. Lewis. 1991. Lignin peroxidase: Toward a clarification of its role *in vivo*. **J. Biol. Chem. 266**:3636-3643.

Schoemaker, H. E., T. K. Lundell, A. I. Hatakka and K. Piontek. 1994. The oxidation of veratryl alcohol, dimeric lignin models and lignin by lignin peroxidase: The redox cycle revisited. **FEMS Microbiol. Rev. 13**:321-332.

Schmidt, H. W. H., S. D. Haemmerli, H. E. Schoemaker and M. S. A. Leisola. 1989. Oxidative degradation of 2,3-dimthoxybenzyl alcohol and its methyl ether by the lignin peroxidase of *Phanerochaete chrysosporium*. **Biochemistry. 28**:1776-1783.

Schultz, T. P. and W. G. Glasser. 1986. Quantitative structural analysis of lignin by diffuse reflectance infrared spectrometry. **Holzforschung. 40(suppl.)**:37-44.

Schultz, T. P., M. C. Templeton and G. D. McGinnis. 1985. Rapid determination of lignocellulose by diffuse reflectance fourier transform infrared spectrometry. **Anal. Chem. 57**:2867-2869.

Sedgwick, R. D. and D. M. Hindenlang. 1988. Mass Spectrometry. In **Materials Characterization and Chemical Analysis**. Siblia, J. P. (ed.). VCH, New York. **Chapter 3**:45-60.

Shimada, M. F., F. Nakatsubo, T. K. Kirk and T. Higuchi. 1981. Biosynthesis of the secondary metabolite veratryl alcohol in relation to lignin degradation in *Phanerochaete chrysosporium*. **Arch. Microbiol. 129**:321-324.

Sjöström, J. and M. Reunanen. 1990. Characterization of lignin and carbohydrates dissolved in groundwood pulping by pyrolysis-gas chromatography/mass spectrometry. **J. Anal. Appl. Pyrol. 17**: 305-318.

Susmel, P. and B. Stefanon. 1993. Aspects of lignin degradation by rumen microorganisms. **J. Biotechnol. 30**:141-148.

Tanahashi, M. and T. Higuchi. 1988. Chemical degradation methods for characterization of lignins. In **Methods in Enzymology**. Colowick, S. P. and N. O. Kaplan. (eds.). Academic Press, New York. **161**:101-109.

Taylor, J. R. 1982. **An Introduction to Error Analysis: The Study of Uncertainties in Physical Measurements**. Commins, E. D. (ed.). University Science Books, Mill Valley, CA.

Taylor, M. G., Y. Deslandes, T. Bluhm, R. H. Marchessault, M. Vincendon and J. Saint-Germain. 1983. Solid state ^{13}C-NMR characterization of wood. **Tappi J. 66**:92-94.

Thompson, D. N. 1989. The effects of physical and chemical constraints on the enzymatic hydrolysis of lignocellulosic materials. M. S. Thesis. Michigan State University, East Lansing, MI.

Thompson, D. N., H. C. Chen and H. E. Grethlein. 1992. Comparison of preteatment methods on the basis of available surface area. **Bioresource Technology. 39**:155-163.

Tien, M. 1987. Properties of ligninase from *Phanerochaete chrysosporium* and possible applications. **CRC Crit. Rev. Microbiol. 15**:141.

Tien, M. and T. K. Kirk. 1988. Lignin peroxidase of *Phanerochaete chrysosporium*. In **Methods in Enzymology**. Colowick, S. P. and N. O. Kaplan. (eds.). Academic Press, New York. **161**:238-249.

Tien, M. and T. K. Kirk. 1984. Lignin-degrading enzyme from *Phanerochaete chrysosporium*. Purification, characterization and catalytic properties of a unique H2O2-requiring oxygenase. **Proc. Natl. Acad. Sci. USA. 81**:2280-2284.

Tien, M., T. K. Kirk, C. Bull and J. A. Fee. 1986. Steady-state and transient-state kinetic studies on the oxidation of 3,4- dimethoxybenzyl alcohol catalyzed by the ligninase of *Phanerochaete chrysosporium* Burds. **J. Biol. Chem. 261**:1687-1693.

Tsao, G. T., M. R. Ladisch and H. R. Bungay. 1987. Biomass refining. In **Advanced Biochemical Engineering**. Bungay, H. R. and G. Belfort. (eds.). Wiley Interscience, New York. 79-101.

Tuor, U., H. Wariishi, H. E. Schoemaker and M. H. Gold. 1992. Oxidation of phenolic arylglycerol ß-aryl ether lignin model compounds by manganese peroxidase from *Phanerochaete chrysosporium*: Oxidative cleavage of a α-carbonyl model compound. **Biochemistry. 31**:4986-4995.

Umezawa, T. and T. Higuchi. 1988. Analysis of lignin degradation intermediates by thin-layer chromatography and gas chromatography-mass spectrometry. In **Methods in Enzymology**. Colowick, S. P. and N. O. Kaplan. (eds.). Academic Press, New York. **161**:200-211.

Valli, K., B. J. Brock, D. K. Joshi and M. H. Gold. 1992b. Degradation of 2,4-dinitrotoluene by the lignin-degrading fungus *Phanerochaete chrysosporium*. **Appl. Environ. Microbiol. 58**:1221- 1228.

Valli, K. and M. H. Gold. 1991. Degradation of 2,4-dichlorophenol by the lignin-degrading fungus *Phanerochaete chrysosporium*. **J. Bateriol. 173**:345-352.

Valli, K., H. Wariishi and M. H. Gold. 1992a. Degradation of 2,7-dichlorodibenzo-p-dioxin by the lignin-degrading basidiomycete *Phanerochaete chrysosporium*. **J. Bacteriol. 174**:2131-2137.

Van der Hage, E. R. E., M. M. Mulder and J. J. Boon. 1993. Structural characterization of lignin polymers by temperature-resolved in-source pyrolysis-mass spectrometry and Curie-point pyrolysis-gas chromatography/mass spectrometry. **J. Anal. Appl. Pyrol. 25**:149-183.

Van der Klashorst, G. H. 1988. Low Molecular weight mass lignin fragments present in industrial kraft pine spent liquor. **Holzforschung. 42**:65-66.

Wariishi, H., L. Akileswaran and M. H. Gold. 1988. Manganese peroxidase from the basidiomycete, *Phanerochaete chrysosporium*: Spectral characterization of the oxidized states and the catalytic cycle. **Biochemistry. 27**:5365-5370.

Wariishi, H., H. B. Dunford, I. D. MacDonald and M. H. Gold. 1989a. Manganese peroxidase from the lignin-degrading basidiomycete *Phanerochaete chrysosporium*: Transient state kinetics and reaction mechanism. **J. Biol. Chem. 264**:3335-3340.

Wariishi, H., K. Valli and M. H. Gold. 1991. *In vitro* depolymerization of lignin by manganese peroxidase of *Phanerochaete chrysosporium*. **Biochem. Biophys. Res. Commun. 176**: 269-275.

Wariishi, H., K. Valli and M. H. Gold. 1992. Manganese (II) oxidation by manganese peroxidase from the basidiomycete *Phanerochaete chrysosporium*: Kinetic mechanism and role of chelators. **J. Biol. Chem. 267**:23688-23695.

Wariishi, H., K. Valli, and M. H. Gold. 1989b. Oxidative cleavage of a phenolic diarylpropane lignin model dimer by manganese peroxidase from *Phanerochaete chrysosporium*. **Biochemistry. 28**:6017-6023.

Watson, J. T. 1985. **Introduction to Mass Spectrometry**, 2nd ed. Raven Press, New York. Chapter 9.

Yang, J. M. and D. A. I. Goring. 1980. The phenolic hydrozyl content of spruce wood. **Can. J. Chem. 58**:2411-2414.

Yannoni, C. S. 1982. High-resolution NMR in solids: The CPMAS experiment. **Acc. Chem. Res. 15**:201-208.